Coordination of AMPA and kainate receptor gating by the ligand-binding domain

By
G. BRENT DAWE

December 2016
INTEGRATED PROGRAM IN NEUROSCIENCE

McGill University
(Montreal, CANADA)

A thesis submitted to the Faculty of Graduate and Postdoctoral Studies in partial fulfillment of the requirement of the degree of
DOCTOR OF PHILOSOPHY

“We are the local embodiment of a Cosmos grown to selfawareness. We have begun to contemplate our origins: starstuff pondering the stars; organized assemblages of ten billion billion billion atoms considering the evolution of atoms; tracing the long journey by which, here at least, consciousness arose.”

-Carl Sagan

ABSTRACT

AMPA and kainate receptors (AMPARs and KARs) are members of a family of ion channel proteins known as the ionotropic glutamate receptors (iGluRs). AMPARs, which are ubiquitous throughout the central nervous system (CNS), facilitate the excitation of neurons, allowing signals to be transduced across synapses. Meanwhile, KARs have more restricted expression, though they serve as modulators of synaptic activity. The unique roles fulfilled by AMPARs and KARs are dependent upon the ability of each receptor class to rapidly activate (open their channel) in response to the binding of the chemical neurotransmitter glutamate. Also important is their fast desensitization, which curtails the prolonged excitation of neurons. Accordingly, there has been considerable investigation into the structural basis of iGluR channel gating, and in particular the molecular determinants activation and desensitization. Current models of AMPAR and KAR gating indicate that the assembly of the extracellular ligand-binding domain (LBD) in a dimer of dimers arrangement is critical for receptor activation, whereas the separation of subunits comprising each dimer underlies desensitization. However, the specific, atomic-level interactions contributing to the stability of LBD dimers, and by extension iGluR activation, have not been fully explored.

By employing a combination of outside-out patch-clamp electrophysiology, coupled with rapid solution exchange, as well as molecular dynamics simulations, protein crystallization, and atomic force microscopy, we explored the contribution of different sites in the LBD to AMPAR and KAR gating. We found that occupancy of a sodium-binding pocket at the apex of the KAR LBD is critical to maintain receptors in an activated state, and prevent desensitization, in the presence of glutamate. Specifically, the binding of sodium or the introduction of a positively

charged cross-dimer tether (by mutagenesis) into the GluK2 pocket sustained activation by holding together the upper portion of the LBD dimer.

Because of the importance of the LBD apex for KAR function, we asked whether this region governs AMPAR gating in a similar manner. In this instance we found that lithium can in fact play a similar role at GluA2 AMPARs as sodium had for KARs. Furthermore, the binding of lithium stabilized the GluA2 LBD dimer interface by strengthening interactions throughout a cross-dimer electrostatic network. When the electrostatic network was disrupted, GluA2 activation was severely inhibited, but the co-expression of AMPAR auxiliary subunits could rescue this deficit through interactions at the distal base of the LBD. As such, we determined that the activation of native AMPAR complexes is governed by intra- and inter-protein interactions that stabilize the LBD dimer at different positions.

We also studied how external anions regulate the gating of GluA2 AMPARs, in both a structural and functional context. Our experiments revealed that anion species regulates the height of GluA2 AMPARs, as well as their rate of desensitization in the presence of glutamate. Interestingly, we also identified a novel anion-binding site that was responsible for both of the aforementioned effects. Taken together, these findings are consistent with the idea that the binding of different anions can generate conformational rearrangements, which in turn dictate how AMPARs will later respond to glutamate.

Overall, three principal conclusions can be derived from my results. First, the apex of the LBD dimer interface is conserved as a critical region for AMPAR and KAR activation. Second, auxiliary proteins stabilize AMPAR LBD dimers by supporting the base of this domain, acting in a complementary manner to interactions across the apical dimer interface. Third and finally, conformational changes prior to agonist binding can affect the gating behaviour of AMPARs.

RÉSUMÉ

Les récepteurs AMPA et kaïnate (AMPARs et KARs) sont membres d'une famille de protéines de canaux ioniques connus comme les récepteurs ionotropes au glutamate (iGluRs). Les AMPARs, étant omniprésents dans le système nerveux central (SNC), facilitent l'excitation des neurones, permettant ainsi la transduction de signaux entre les synapses. Par contre, les KARs ont une expression plus restreinte et servent de modulateurs de l'activité synaptique. Les rôles uniques remplis par les AMPARs et les KARs dépendent de leur capacité à s'activer rapidement (ouvrir leur canal) en réponse à la liaison du glutamate, un neurotransmetteur. Leur désensibilisation rapide est également importante, car celle-ci limite l'excitation prolongée des neurones. Par conséquent, plusieurs groupes étudient la base structurale de l'ouverture des canaux iGluRs, en particulier les bases moléculaires responsables de l'activation et la désensibilisation des canaux. Les modèles structuraux actuels concernant l'activation des AMPARs et des KARs indiquent que l'assemblage des domaines extracellulaires de liaison du ligand (LBD) en dimères de dimères est essentiel pour leur activation, alors que la séparation des sous-unités faisant partie de chacun des dimères est à la base de leur désensibilisation. Cependant, les interactions atomiques spécifiques contribuant à la stabilité des dimères du LBD, et par extension, l'activation des iGluRs, n'ont pas été complètement explorées.

En combinant la technique d'électrophysiologie *patch-clamp*, couplée à un échange rapide de la solution, avec des simulations par dynamique moléculaire, la cristallisation des protéines et la microscopie à force atomique, nous avons exploré la contribution des différents sites du LBD dans l'activation des AMPARs et des KARs. Nous avons constaté que l'occupation d'une cavité d'interaction du sodium, au sommet du LBD des KARs, est essentielle pour maintenir les récepteurs dans un état activé et empêche leur désensibilisation en présence de

glutamate. Plus précisément, la liaison du sodium ou l'introduction d'une attache intra-dimérique chargée positivement (par mutagénèse) dans la cavité d'interaction de GluK2 soutient l'activation du canal en maintenant la partie supérieure du dimère LBD ensemble.

Étant donné l'importance de l'apex du LBD dans la fonction des KARs, nous avons postulé que cette région régissait l'activation des AMPARs d'une manière similaire. En effet, nous avons trouvé que le lithium peut jouer un rôle chez les AMPARs de type GluA2, similaire à celui du sodium chez les KARs. De plus, la liaison du lithium stabilise l'interface du dimère LBD de GluA2 en renforçant les interactions électrostatiques à travers un réseau intra-dimérique. Lorsque le réseau électrostatique est perturbé, l'activation de GluA2 est largement inhibée, mais la co-expression des sous-unités auxiliaires des AMPAR renverse ce déficit par des interactions à la base distale du LBD. Par conséquent, l'activation des complexes de AMPARs natifs est régie par des interactions intra- et inter-protéinaires qui stabilisent le dimère LBD à différentes positions.

Nous avons également étudié la façon dont les anions externes régulent le comportement structural et fonctionnel des récepteurs GluA2. Nos expériences ont montré que les espèces d'anions régulent la hauteur de ces récepteurs, ainsi que leur taux de désensibilisation en présence du glutamate. De plus, nous avons identifié un nouveau site de liaison des anions qui est responsable pour les effets mentionnés ci-dessus. L'ensemble de ces résultats est cohérent avec l'idée que la liaison des différents anions peut générer des réarrangements conformationnels, qui, à leur tour, dictent la réponse des AMPARs au glutamate.

Trois conclusions principales peuvent être tirées de mes résultats. Premièrement, le sommet de l'interface du dimère LBD est une région conservée et essentielle pour l'activation des AMPAR et des KAR. Deuxièmement, les protéines auxiliaires stabilisent les dimères LBD des

AMPARs en soutenant la base de ce domaine, agissant de manière complémentaire aux interactions intra-dimériques apicales. Enfin, des changements conformationnels précédant la liaison de l'agoniste peuvent affecter le comportement fonctionnel des récepteurs AMPA.

TABLE OF CONTENTS

Page

PART ONE: REVIEW OF THE LITERATURE

PART TWO: RESULTS

PART THREE: DISCUSSION AND CONCLUSIONS

PART FOUR: APPENDICES

LIST OF FIGURES AND TABLES

PART ONE: REVIEW OF THE LITERATURE

PART TWO: RESULTS

CHAPTER ONE

CHAPTER TWO

CHAPTER THREE

LIST OF ABBREVIATIONS

AFM	atomic force microscopy
AMPA	α-amino-3-hydroxy-5-methyl-4-isoxazolepropionic acid
AMPAR	AMPA receptor
APV	D-2-amino-5-phosphonopentanoate
ASIC	acid-sensing ion channel
ATD	amino-terminal domain
ATPA	(*RS*)-2-Amino-3-(3-hydroxy-5-*tert*-butylisoxazol-4-yl)propanoic acid
BN-PAGE	blue native-polyacrylamide gel electrophoresis
CAMKII	calcium/calmodulin-dependent protein kinase II
cDNA	complementary DNA
CKAMP	cystine-knot AMPA receptor modulating proteins
CNIH	cornichon homolog
CNQX	6-cyano-7-nitroquinoxaline-2,3-dione
CNS	central nervous system
CTD	C-terminal domain
CTZ	cyclothiazide
D1 & D2	upper (D1) and lower (D2) clamshell forming domains of the iGluR LBD
DCKA	5,7-dichlorokynurenic acid
DNA	deoxyribonucleic acid
DNQX	6,7-dinitroquinoxaline-2,3-dione
D-R	dose-response
EC_{50}	half-maximal effective concentration
EM	electron microscopy
EPSC	excitatory postsynaptic current
EPSP	excitatory postsynaptic potential
ER	endoplasmic reticulum
FRET	fluorescence resonance energy transfer
GABA	γ-aminobutyric acid
GlyR	glycine receptor
GlnBP	glutamine-binding protein
GPCR	G protein-coupled receptor
GRIP	glutamate receptor-interacting protein
GSG1L	germ cell-specific gene 1-like protein
GYKI	(described compounds from a class of 2,3-benzodiazepines)
HEK 293	human embryonic kidney 293, a human-derived cell line
IC_{50}	half-maximal inhibitory concentration
iGluR	ionotropic glutamate receptor
IP	inositol phosphate
IPSC	inhibitory postsynaptic current
I-V	current-voltage
KAR	kainate receptor
K_d	dissociation constant
LBD	ligand-binding domain
LGIC	ligand-gated ion channel

LIVBP	leucine/isoleucine/valine-binding protein
LRET	luminescence resonance energy transfer
LTD	long-term depression
LTP	long-term potentiation
L/Y	a well-known leucine to tyrosine mutant that blocks AMPAR desensitization
MD	molecular dynamics
mEPSC	miniature EPSC
mGluR	metabotropic glutamate receptor
mRNA	messenger RNA
MK-801	(5*S*,10*R*)-(+)-5-Methyl-10,11-dihydro-5*H*-dibenzo[*a*,*d*]cyclohepten-5,10-imine
NETO	neuropilin and tolloid-like protein
NMDA	N-methyl-D-aspartate
NMDAR	NMDA receptor
PDB	Protein Data Bank (archive of experimentally determined protein structures)
PDZ	motif mediating the association of many synaptic proteins
PEPA	2,6-difluoro-4-[2-(phenylsulfonylamino)ethylthio]phenoxyacetamide
PICK	protein interacting with C kinase
PKA	protein kinase A
PKC	protein kinase C
PSD-95	postsynaptic density protein 95
Q/R	glutamine/arginine RNA-edited site regulating AMPAR/KAR channel properties
RNA	ribonucleic acid
S1 & S2	LBD segments between the ATD and TM1 (S1) or between TM3 and TM4 (S2)
SUMO	small ubiquitin-like modifier
SynDIG	synapse differentiation induced gene 1
TARP	transmembrane AMPA receptor regulatory protein
TM1-4	transmembrane segment 1-4
TMD	transmembrane domain
VGIC	voltage-gated ion channel

Amino acid abbreviations

amino acid	3-letter code	1-letter code
Alanine	Ala	A
Arginine	Arg	R
Asparagine	Asn	N
Aspartate	Asp	D
Cysteine	Cys	C
Glutamate	Glu	E
Glutamine	Gln	Q
Glycine	Gly	G
Histidine	His	H
Isoleucine	Ile	I
Leucine	Leu	L
Lysine	Lys	K
Methionine	Met	M
Phenylalanine	Phe	F
Proline	Pro	P
Serine	Ser	S
Threonine	Thr	T
Tryptophan	Trp	W
Tyrosine	Tyr	Y
Valine	Val	V

ACKNOWLEDGMENTS

I will begin by thanking my supervisor Derek, who made the lab fun environment to practice science, whether in the Bellini or at meetings abroad. He has also been a great network builder and collaborator. First, he helped initiate the annual Glutamate Receptor Retreat, which has been an enjoyable and informative annual experience since 2013. More importantly for me personally, he has initiated collaborations that have been vital for my projects, and their successful outcomes can be seen on the author list of our publications. Derek has also never been afraid to aim high, even when it seemed unlikely to me that my work would be published in *Nature Structural & Molecular Biology* or *Neuron*. A necessary step for data to become a viable manuscript occurs when Derek, after some contemplation, says "it could go to *Nature*." Maybe sometime soon that will be borne out.

I must also thank Derek for continually filling the lab up with a great roster of trainees. I have enjoyed all my interactions with current lab-mates, alphabetically by last name, Ryan, Marika, Mark, Patricia, Erik, Hugo, Lois, Rafael, as well as past members Mike, Elizbaeth, Mabel, Bryan, Dave, Joe, and Ingrid. Special thanks should go to Patricia, who taught me patch-clamp, Mark, who refined my molecular biology skills, and Bryan, who was a mentor from across the hall. Another special recognition is owed to Mike, who was a lab-mate twice, starting at UOIT, but also a great roommate during my first two years in Montreal, though oddly we never intersected scientifically. An additional mention should go to Sandra and Felix, who were great co-occupants of the student room, despite not being part of the lab.

Not long after I joined the lab, the Friday happy hour became a routine occurrence, and over the years an evolving crew of 'regulars' would turn up to talk about science, politics, or

anything else that you could think of. Notably, from outside the Bowie lab, Filip, Jay, Mark J., and Behrang made Friday beers a great week-ending experience.

During the latter half of my time at McGill, I regularly took part in trivia, both at Thomson House and McKibbin's, with the team often consisting of some combination of Kristy, Andrew, Erik, Nikki, Sandra, Léa, and Julia. Perhaps all the exposure to trivia had an indirect effect on my thesis.

In all six years of my MSc/PhD studies I have served on the GSAN (Graduate Student Association of Neuroscience) Committee, and over that time volunteered with many great students, who were dedicated to making graduate school an enriching all-around experience for their colleagues. When I was on the 'executive' I was helped tremendously by working with presidents Rochelle and Julia, academic officers Jonathan and Anne, Marisa and Erik as PGSS council reps., and many others.

Furthermore, I want to thank members of my Advisory Committee, Dr. Charles Bourque and Dr. Ellis Cooper, as well as Dr. David Stellwagen. They could always be relied on to ask great questions, especially of a methodological nature, at annual committee meetings.

Returning to science for a moment, an important acknowledgment is owed to all of my collaborators, because without their contributions this thesis would not have been possible. First and foremost, Dr. Maria Musgaard has contributed data (i.e. computational simulations) toward all of my results chapters, and along with her supervisor, Dr. Philip Biggin, is responsible for bringing a structural interpretation to my electrophysiology data. Maria and I have remained in frequent contact for over four years, and I wish her a great career after she wraps up her postdoc at Oxford. Two of my projects have also relied upon collaborations with structural biologists, including Drs. Tim Green and Naushaba Nayeem from Liverpool, and later Drs. Jette Kastrup

and Raminta Venskutonyte from Copenhagen. Across the McGill campus, I also worked with the synthetic chemists Paolo Schiavini and Dr. Nicolas Moitessier. Hopefully, these partnerships illustrate the point that proteins are best studied using a variety of techniques.

Finally, before getting into the “business” of this thesis, a huge acknlowdgement is owed to family and friends for their continuous support throughout my educational trajectory, however obscure my studies may have seemed. That being said, I am endebted to my biggest supporter, Julia, for her encouragement, and many fond memories over the last four years.

CONTRIBUTION OF AUTHORS

This thesis is written in a manuscript-based format, as outlined in the McGill guidelines. The results section is composed of two published manuscripts (Chapters 1 and 2), and a third (Chapter 3) manuscript, which will likely be submitted in an altered form. All manuscripts are co-authored, with a description below of the authors' contributions, as required by Graduate and Postdoctoral Studies.

Chapter 1: "How allosteric ion binding is critical for KAR activation" was published in *Nature Structural & Molecular Biology* in September of 2013 as **Dawe, G.B., Musgaard, M., Andrews, E.D., Daniels, B.A., Aurousseau, M.R.P., Biggin, P.C., Bowie, D. (2013). Defining the structural relationship between kainate-receptor deactivation and desensitization.** ***Nat Struct Mol Biol*****, 20(9): 1054-61.** M. Musgaard and I are co-first authors.
For this work, I primarily generated and analyzed the data in Figures 1.1, 1.2, 1.4, 1.6, and 1.7, as well as Supplemental Figures S1.1, S1.3, and S1.5. M. Musgaard generated and analyzed the data in Figures 1.3, 1.5, S1.2, and S1.4. B.A. Daniels contributed data to Figure 1.2, while E.D. Andrews contributed data to Figures 1.6 and 1.7. M.R.P. Aurousseau generated and analyzed data in Figure S1.3, and prepared some cDNA constructs used throughout the manuscript. All authors who collected data also contributed to experimental design, along with P.C. Biggin and D. Bowie. Finally, D. Bowie and I conceived the project, drafted the manuscript, and responded to reviewers, though all authors helped with editing.

Chapter 2: "Intra- and inter-protein interactions determine the time course of AMPAR activation" was published in *Neuron* in March of 2016 as **Dawe, G.B., Musgaard,**

M., Aurousseau, M.R.P., Nayeem, N., Green, T., Biggin, P.C., Bowie, D. (2016). Distinct structural pathways coordinate the activation of AMPA receptor-auxiliary subunit complexes. ***Neuron*****, 89(6): 1264-76.** M. Musgaard, M.R.P. Aurousseau, and I are co-first authors.

For this work, I generated and analyzed the entirety of data presented in Figures 2.2, 2.5, 2.6, 2.7, and 2.8, as well as Supplemental Figures S2.1, S2.6, and S2.7. I also generated and analyzed some of the data in Figures 2.1, 2.3, 2.4, and S2.4. M. Musgaard generated and analyzed data in Figures 2.1, 2.3, 2.4., S2.3, and S2.4. M.R.P. Aurousseau generated and analyzed data in Figures S2.2 and S2.4, and prepared some cDNA constructs used throughout the manuscript. N. Nayeem and T. Green generated and analyzed data in Figures 2.4, S2.4, and S2.5. I helped to conceive the project, along with M.R.P. Aurousseau and D. Bowie. Meanwhile, D. Bowie and I drafted the manuscript and responded to reviewers, though all authors helped with editing.

Chapter 3: "External anions 'prime' the AMPAR response to glutamate" is a manuscript that remains to be submitted at the time of my thesis submission. In its present form, the author list would read **Dawe, G.B., Kadir, F., Venskutonyte, R., Musgaard, M., Aurousseau, M.R.P., Biggin, P.C., Kastrup, J.S., Edwardson, J.M., and Bowie, D.** Furthermore, F. Kadir, R. Venskutonyte, and I would be considered co-first authors.

For this work, I generated and analyzed the entirety of data presented in Figures 3.1 and 3.5, as well as Supplemental Figures S3.1, S3.3, and S3.6. F. Kadir generated and analyzed data in Figures 3.2 and 3.6, as well as Table 1. R. Venskutonyte generated and analyzed data in Figures 3.3 and S3.5, as well as Table 2. M. Musgaard generated and analyzed data in Figures 3.4. I

helped to conceive the project, along with R. Venskutonye, J.S. Kastrup, and D. Bowie. Meanwhile, D. Bowie and I drafted the manuscript, though all authors helped with editing.

In addition to these three chapters, I have included two other publications in the appendix. The first was a review article published in the *Journal of Physiology* in January of 2015 as **Dawe, G.B., Aurousseau, M.R.P., Daniels, B.A., Bowie, D. (2015). Retour aux sources: defining the structural basis of glutamate receptor activation. *J Physiol,* 593(1): 97-110.**

D. Bowie and I reviewed the literature and wrote the manuscript, but were helped by discussions with M.R.P. Aurousseau and B.A. Daniels.

The second work is outside the central topic in my thesis, as it concerns the development of novel glutamate receptor antagonists. It was published in *Bioorganic and Medicinal Chemistry Letters* as **Schiavini, P., Dawe, G.B., Bowie, D., Moitessier, N. (2015). Rational design of novel antagonists for GluK2. *Bioorg Med Chem Lett,* 25(11): 2416-20.** Here, I generated and analyzed the data presented in Figure 4, whereas chemical synthesis and structural data included in other figures came from P. Schiavini. However, I also helped to interpret data and edit the manuscript. The project had been conceived before I joined the lab, as a joint effort by both D. Bowie and N. Moitessier.

PREFACE

Before describing the history of ionotropic glutamate receptors (iGluRs) in more detail, I would like to quickly provide some general context to my thesis work. The year before I joined the Bowie lab, the first intact iGluR structure was published, and it became an unwritten requirement that every talk in my field must start with an image of the Y-shaped structure. More seriously though, the paper cemented a transition from function to structure. It was becoming increasingly rare to see significant, biophysically-oriented papers that did not include structural techniques. In other words, experienced electrophysiologists were beginning to integrate the interpretation of crystal structures and protein simulations into their work.

My research is an attempt to bridge structure and function. Specifically, I have sought out interactions within the ligand-binding domain (LBD) that dictate the gating behaviour of AMPA and kainate receptors (AMPARs and KARs). Prior work in the lab, spearheaded by Drs. David Maclean and Adrian Wong, has provided a great template to examine the allosteric regulation of iGluRs. In particular, they addressed how external ions affect KAR function. The projects I have been involved with ascribed a structural explanation to ionic regulation of kainate receptors, but then extended the same line of inquiry into AMPARs, and even explored their auxiliary proteins.

Accordingly, this thesis is separated into four parts. **PART ONE** is a review of the lieterature, written largely as a historical narrative, because I think it makes it easier to appreciate the landmark observations/discoveries in the glutamate receptor field, knowing how they were arrived at. **PART TWO** contains my experimental results, divided into three, manuscript-based chapters. First, Chapter I highlights the structural mechanism by which allosteric ions interact at the KAR LBD to regulate gating. Second, Chapter II identifies two discrete sites in the AMPAR LBD that coordinate the activation of receptor-auxiliary protein complexes. Third, Chapter III

examines a novel anion-binding site in the AMPAR LBD that regulates both the conformation of resting receptors and their subsequent gating behaviour. Finally, **PART THREE** is comprised of a discussion and some concluding statements, while **PART FOUR** is made up of appendices. These appendices are taken from other published articles I have been apart of, as well as reprints of articles described in the results chapters.

Ultimately, there is far more that can be written about glutamate receptors beyond what is included in this thesis. In an effort to streamline the literature review and discussion text, I have attempted to focus on AMPA and kainate receptors (where possible), sometimes omitting related ideas about NMDA or delta-type glutamate receptors. Not only does this decision stem from my research focus, but also because NMDA and delta receptors are quite different from AMPA and kainate receptors, despite belonging to the same protein family. Along the same lines, I have tried to avoid going too far into the vast realm of glutamate receptor physiology, limiting discussion to some key processes mediated by glutamatergic signaling. Moreover, I have steered clear of glutamate receptor regulation in disease states -it is a fascinating and extensively studied topic, but quite far removed from the biophysical world. Finally, I would just add that though you might wait awhile to see the translational relevance of my thesis, I do believe it to be “good science” and hope you are enlightened by the ideas within.

PART I:

REVIEW OF THE LITERATURE

1. DISCOVERY AND INITIAL CHARACTERIZATION OF GLUTAMATE RECEPTORS

1.1 Identifying glutamate as a neurotransmitter

The study of glutamate receptors was preceded by the study of glutamate. First isolated from wheat gluten in 1866, glutamate joined a growing list of amino acids that had come to be accepted as the chemical constituents of proteins (Perrett, 2007; Belitz et al., 2009). Apart from its presence in metabolic pathways responsible for protein synthesis, other physiological actions of glutamate were not anticipated in the early twentieth century. Interest was stoked, however, as new analytical techniques enabled more precise quantification of glutamate levels in animal tissue, revealing much higher concentrations in the brain versus other organs (Krebs et al., 1949). Furthermore, the diffuse application of sodium glutamate onto the cortex of animals -and humans- induced convulsions (Hayashi, 1954), suggesting a physiological effect on the nervous system. Several years later it was demonstrated that ionophoretic application of L-aspartate and L-glutamate could excite neurons (Curtis et al., 1960), yet the authors believed this action to be non-specific, and thus inconsistent with a synaptic neurotransmitter.

By the time glutamate was recognized for its excitatory effects, there were several agreed-upon criteria for a chemical to be classified as a neurotransmitter. In brief, the chemical must be released into the synaptic cleft upon activation of nerve terminals, producing a response in the postsynaptic cell that is mimicked by its exogenous application (McLennan, 1965). Whether glutamate adequately met all of these criteria was unclear into the 1970s (Lodge, 2009). In support of its role as a neurotransmitter, glutamate concentrations were known to be high throughout different subcellular fractions of the neuron (Mangan & Whittaker, 1966), but importantly, enough glutamate was present in isolated synaptosomal fractions to produce excitatory effects when applied to other cortical neurons (Krnjevic & Whittaker, 1965).

However, there was little evidence that neuronal activity elicited glutamate release from presynaptic vesicles (Krnjevic, 1974).

The most pervasive objection to amino acids as neurotransmitters was their lack of specificity, as it seemed that every cell type responded to them (McLennan, 1965). Along the same lines, it was unclear how glutamate could be removed from extracellular environment to regulate its presence in a temporal manner. The demonstration of high affinity glutamate uptake into brain tissue (Logan & Snyder, 1971) offered a plausible clearance mechanism, though other similar compounds (i.e. aspartate) competed with this uptake (Balcar & Johnston, 1972), implying that they too could be candidate neurotransmitters. It is now appreciated that neuronal glutamate is derived largely from astrocytic glutamine, as part of the glutamate-glutamine cycle, with a less significant role ascribed to presynaptic transporters (Marx et al., 2015). Forty years ago, however, it was quite difficult to conceptualize the movement of endogenous glutamate. Ultimately, there was no single breakthrough that solidified glutamate as a *bona fide* neurotransmitter, but the idea was gradually accepted following the discovery of selective agonists and antagonists that could pick apart its actions at neuronal receptors (Krnjevic, 2010).

1.2 Early studies of native glutamate receptors

The concept of a receptive substance, or receptor, through which drugs mediate their actions had been proposed by Langley (1905) long before chemical neurotransmission was known to occur at the synapse. Therefore, if the excitatory amino acids were acting as neurotransmitters, it was natural to assume that one or more receptors classes may exist. The observation that various structural analogs of glutamate -notably N-methyl-D-aspartate (NMDA), kainate, and quisqualate- excited neurons in a similar manner (Curtis & Watkins, 1963; Shinozaki & Konishi, 1970; Biscoe et al., 1975) provided a palette of compounds to

dissect the pharmacology of glutamatergic activity. Nevertheless, it was not until the discovery that magnesium ions (Mg^{2+}) acted as an "antagonist" of NMDA-evoked responses (Evans et al., 1977), and the later development of APV as a higher affinity selective antagonist (Davies & Watkins, 1982), that the segregation of glutamate receptors (GluRs) into NMDA and non-NMDA subfamilies solidified (Lodge, 2009).

A more thorough dissection and quantification of the different GluR subtypes was brought about by several technical advances that were implemented in the 1980s. To begin with, improvements in the voltage-clamp technique (i.e. single electrode penetration) facilitated its application to central neurons, where researchers could make more precise measurements of channel activity, while avoiding the confounds of voltage-dependent gating (Mayer & Westbrook, 1987). Interestingly, voltage-clamp experiments clearly demonstrated a voltage sensitivity of NMDA responses, marked by increasing conductance at more positive potentials, whereas kainate and quisqualate responses were voltage-insensitive (Mayer & Westbrook, 1984). This phenomenon was shown to be the consequence of channel block by physiological concentrations of extracellular magnesium (Nowak et al., 1984; Mayer et al., 1984). As a result, it was appreciated that relief of magnesium block through repetitive stimulation -which would increasingly depolarize the neuron- could explain the necessity for NMDA receptor activity in some forms of synaptic plasticity, particularly long-term potentiation, or LTP (Collingridge & Bliss, 1987).

In addition to voltage-clamp, the advanced analysis of channel activity linked to GluRs also required the delivery of fixed agonist concentration over a precise time interval. Pressure ejections from micropipettes could deliver "brief" agonist applications (as short as 10 ms), but because of diffusion it was unknown what agonist concentration was achieved at the plasma

membrane (Mayer and Westbrook, 1984). Therefore, if either the duration of channel activity is sensitive to agonist concentration, or channels desensitize on a fast (i.e. millisecond) timescale, one would observe a very biased representation of the glutamate response. As it turns out, faster agonist application techniques revealed that this was in fact the case. One such technique was "concentration-clamp," an example of which involved the placement of an isolated neuron into pressure-controlled tubing, where the external solution surrounding the cell was constant, and could be completely exchanged within 20 ms (Krishtal et al., 1983). An even more impressive, "ultra-fast" solution exchange was achieved by using the expansion/contraction in a piezoelectric crystal to drive the micrometre-scale movement of a liquid filament, such that excised membrane patches placed adjacent to the filament could transition between two solutions in hundreds of microseconds (Franke et al., 1987). Nevertheless, whole-cell recordings using the concentration-clamp technique still provided valuable insights, including the observation that current responses to sustained glutamate applications -at negative holding potentials, limiting NMDA receptor contribution- could completely desensitize within tens of milliseconds (Kiskin et al., 1986). This phenotype was mirrored with quisqualate, but not kainate, which was apparently non-desensitizing (Kiskin et al., 1986). Not long after, similar responses were elicited by ionophoretic agonist application, which revealed that NMDA responses did not undergo the same rapid desensitization of other agonists (Trussell et al., 1988). Moreover, because a conditioning pulse with glutamate could pre-desensitize a test response to kainate, both studies concluded that kainate and quisqualate are likely to act on the same receptor (Kiskin et al., 1986; Trussell et al., 1988). It was somewhat less clear whether the diverse array of GluR agonists all opened the same ion channel.

In theory, measurements of single-channel openings recorded in the presence of different GluR agonists could have resolved the receptor-channel ambiguity -in the era before GluR genes were cloned. Unfortunately, these agonists generally produce multiple conductance levels, and though NMDA conductances were typically larger than those of kainate or quisqualate, it appeared that they visited the same overall range of conductance levels (Jahr & Stevens 1987; Cull-Candy & Usowicz, 1987). It was therefore unclear whether one ion channel complex contained distinct binding sites for NMDA and kainate/quisqualate (favoured by Cull-Candy & Usowicz, 1987), or whether multiple complexes existed, permitting the possibility that their conductance levels might overlap (Jahr & Stevens, 1987). The discovery of MK-801 as a selective blocker of open NMDA-gated channels (Huettner & Bean, 1988) effectively ruled out the former possibility, as it could be demonstrated that channels opened by kainate and quisqualate were distinct. By this time, the hunt for DNA clones encoding a diverse family of GluR ion channels was well underway.

1.3 Cloning and initial characterization of iGluR subunits

1.3.1 Nomenclature

There are eighteen mammalian ionotropic glutamate receptor (iGluR) subunits (**Figure R1**), which are separated into α-amino-3-hydroxy-5-methyl-4-isoxazolepropionic acid, or AMPA (GluA1-4), kainate (GluK1-5), and NMDA (GluN1, GluN2A-D, GluN3A-B) selective subgroups, as well as an orphan/delta group (GluD1-2), which does not appear to form functional ion channels, either alone or co-expressed with other iGluR subunits (Traynelis et al., 2010). The current nomenclature was established relatively recently (Collingridge et al., 2009), though previously the AMPA receptors (AMPARs) were widely known as GluR1-4, the kainate receptors (KARs) as GluR5-7, KA-1, and KA-2, the NMDA receptors (NMDARs) as NR1,

NR2A-D, and NR3A-B, and the orphan/delta receptors as δ1-2 (Dingledine et al., 1999). Other, often confusing naming conventions were also used, especially in the early 1990s (Lodge, 2009). Though, in the interests of conveying a historical narrative, the pre-2009 nomenclature will be used throughout the next section.

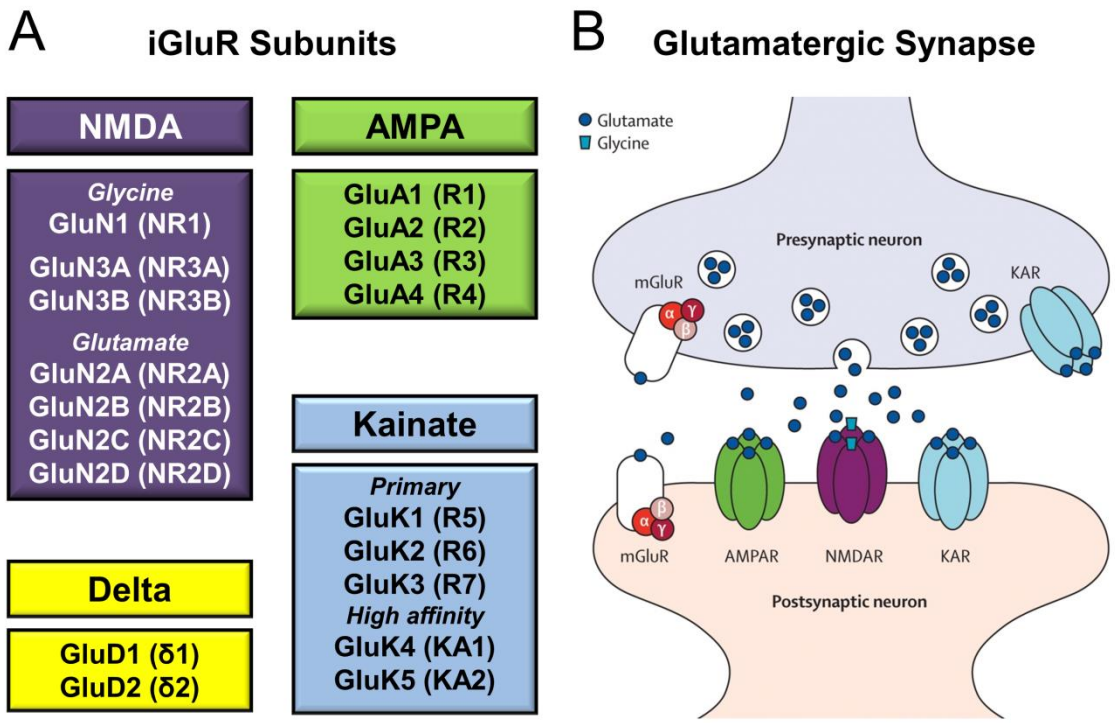

Figure R1. Nomenclature of ionotropic glutamate receptors (iGluRs).
(A) Division of subunits in the iGluR subfamilies, with old nomenclature in brackets. (B) Cartoon representation of a glutamatergic synapse. Note the glycine binding subunits of the NMDAR, as well as the mGluR, which is not an ion channel. Adapted from Kalia et al., 2008.

One additional point that must be mentioned here is the transition that led to quisqualate receptors being re-termed AMPARs. At the time AMPA was discovered, it was appreciated that the compound might act on different subsets of receptors from kainate (Krogsgaard-Larsen et al.,

1980). However, multiple other agonists, including quisqualate, yielded similar effects, and there was no initial reason to favour AMPA for naming purposes. The problem that arose with quisqualate was its high potency (relative to NMDA and kainate) generating inositol phosphate (IP) in neuronal preparations (Sladeczek et al., 1985). This function of quisqualate was later deemed to be mediated by a distinct class of metabotropic GluRs (mGluRs), since antagonists known to prevent glutamate-evoked ion channel activity were ineffective for inhibiting IP accumulation (Sugiyama et al., 1989). Even the quinoxalinediones CNQX and DNQX, which had recently been shown to selectively antagonize non-NMDA receptor responses, did not act in such a manner (Honore et al., 1988). The eventual outcome of these findings was that AMPA filled in to describe an emerging class of "ionotropic" receptors, whereas the mGluRs were appreciated as a distinct family of G protein-coupled receptors (GPCRs) following their initial cloning (Masu et al., 1991).

1.3.2 AMPA receptors

The cloning of the first iGluR subunit, rat GluR1, revealed that a single gene was capable of encoding a functional ion channel complex (Hollmann et al., 1989). Although four putative transmembrane segments were detected, the amino acid sequence of GluR1 diverged considerably from previously isolated ligand-gated ion channels (LGICs) in the Cys-loop superfamily (Hollmann et al., 1989). Shortly thereafter, other members of an AMPA-selective receptor family were cloned, including GluR2-3 from the lab of Stephen Heinemann (Boulter et al., 1990) and GluR2-4 from the lab of Peter Seeburg (Keinanen et al., 1990), two groups which published frequently in this "cloning era." The latter group also detected two variants of each AMPAR, named flip and flop, which are produced from alternative splicing of mRNA in the region prior to that encoding the fourth transmembrane segment (Sommer et al., 1990). Another

form of AMPAR regulation appeared to come from a glutamine to arginine substitution near the putative channel pore of GluR2, which accounted for its linear current-voltage (I-V) relation - whereas GluR1, 3, and 4 were strongly inwardly rectifying, unless forming heteromers with GluR2 (**Figure R2**; Verdoorn et al., 1991)- as well as its reduced calcium permeability (Hume et al., 1991; Burnashev et al., 1992). The residue found at what is now termed the Q/R site is under the control of RNA editing, which occurs in GluR2, but not other AMPAR subunits, and to an intermediate extent in KAR subunits (Sommer et al., 1991).

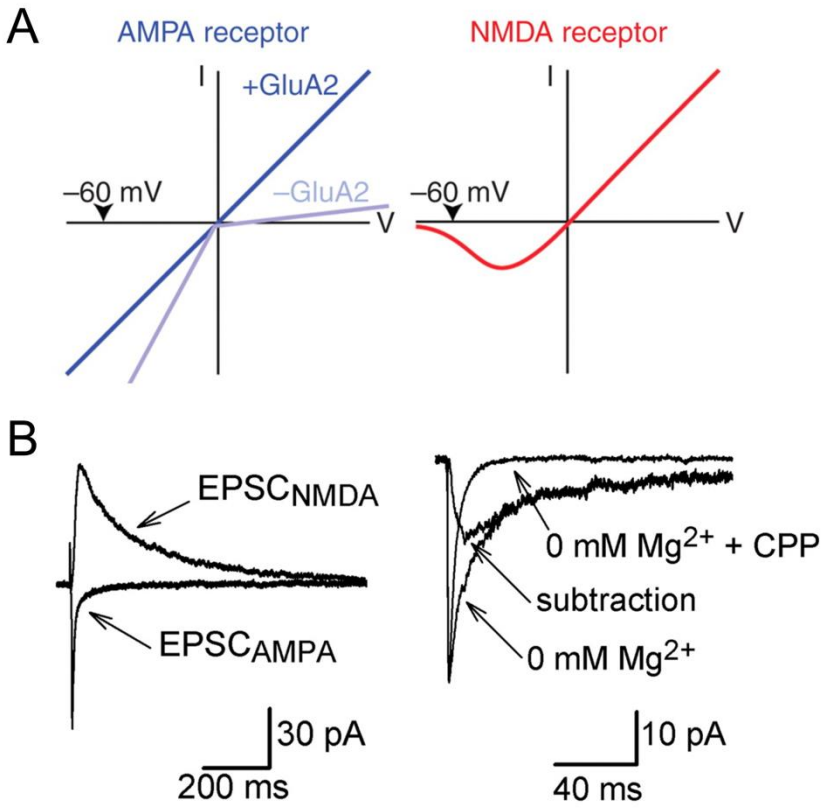

Figure R2. Biophysical properties of AMPARs and NMDARs shape postsynaptic current responses. (A) GluA2 AMPARs are uniquely edited at the Q/R site flanking the pore, which prevents channel block by intracellular polyamines, giving rise to a linear I-V relation (left). Meanwhile, NMDAR channels are blocked by extracellular magnesium ions, which reduce currents at negative membrane potentials, leading to an inverted, bell-shaped I-V relation (right). (B) As a result of the properties described above, glutamatergic EPCSs are predominantly mediated by AMPARs at negative membrane potentials and NMDARs at positive membrane potentials. The NMDAR component of an EPSC can be isolated by

comparing the response in magnesium-free solution before and after an antagonist (i.e. CPP) is applied. Adapted from Savic et al., 2003; Luscher & Malenka, 2012.

1.3.3 Kainate receptors

At the time that members of the AMPAR subfamily were cloned, they were often referred to as AMPA/kainate receptors, since AMPA, kainate, and quisqualate -but not NMDA- evoked current responses from recombinantly expressed subunits (Keinanen et al., 1990; Boulter et al., 1990). Shortly thereafter, the gene encoding a glutamate-responsive subunit known as GluR5 was isolated; however it retained only forty percent amino acid sequence homology with the AMPARs (Bettler et al., 1990). The cloning and expression of the GluR6 and GluR7 subunits, which exhibited seventy-five percent amino acid sequence identity with GluR5 (Egebjerg et al., 1991; Bettler et al., 1992), supported the idea of at least two distinct subfamilies of iGluRs. Eventually, several experimental observations justified the separation of GluR5-7 (now GluK1-3) as kainate-selective receptors. Amongst these observations were GluR6 current responses elicited by kainate, but not AMPA (Egebjerg et al., 1991), and the absence of detectable AMPA or NMDA binding at GluR6 or GluR7 (Bettler et al., 1992). Furthermore, co-expression experiments suggested that GluR5-7 subunits did not co-assemble into heteromeric complexes with GluR1-4 subunits, based on a lack of emergent properties (Bettler et al., 1990; Sommer et al., 1992). In particular, the co-expression of GluR2(R) did not alleviate the inward rectification of GluR5(Q) I-V relations (Sommer et al., 1992), as it would for other, Q/R unedited AMPAR subunits.

Two “high affinity” KAR subunits were also cloned, and termed KA-1 (Werner et al., 1991) and KA-2 (Sakimura et al., 1992; Herb et al., 1992). These receptors bound radiolabelled [^{3}H]kainate with nanomolar affinity, such that K_d = 5 nM and 15 nM for KA-1 and KA-2, respectively (Werner et al., 1991; Herb et al., 1992). In contrast, the much lower affinity kainate-

binding sites on GluR5-7, where K_d = 67 nM, 95 nM, and 77 nM, respectively (Sommer et al., 1992; Bettler et al., 1992), earned them the designation of low affinity KAR subunits. This discrepancy accounted for earlier observations of distinct, low and high affinity kainate-binding sites in the rat brain (London and Coyle, 1979). Nevertheless, it was initially unclear whether the high affinity kainate subunits should be classified as a unique subfamily or somewhere within the pantheon of AMPA/kainate receptors, because their amino acid sequence identity was only marginally higher when compared to GluR5-7 (43%) versus GluR1-4 (37%) (Hollmann & Heinemann, 1994). The KA-1 and KA-2 subunits did not exhibit agonist-evoked currents when expressed alone (Werner et al. 1991; Herb et al., 1992), though the latter could assemble with GluR5 or GluR6 to form heteromeric channels with unique properties, such as GluR6/KA-2 becoming responsive to AMPA (Herb et al., 1992). It was only much later that recombinantly expressed KA-2 subunits were shown to be confined within the endoplasmic reticulum, due to the presence of multiple retention motifs common to the KA-1 and KA-2 sequences that prevent their trafficking to the plasma membrane (Ren et al., 2003; Nasu-Nishimura et al., 2006). Consequently, KA-1 and KA-2 (GluK4 and GluK5) are now designated as secondary KAR subunits, as they must obligately heteromerize with one or more of the GluK1-3 primary subunits to form functional receptor complexes.

2. GATING PROPERTIES OF AMPARs & KARS

2.1 Overview and theory of LGIC gating

In order to properly communicate ideas that will arise later within this thesis, some terminology relating to the function of ion channels will be formalized here. Many of these terms were initially used in regard to voltage-gated ion channels (VGICs) before being applied to

ligand-gated ion channels (LGICs), so some mention of the former is warranted. To begin with, "gating" describes processes that open and close channels, while "permeation" reflects the transport of ions through an open channel (Horn, 1990). For VGICs, the energy required for opening the channel pore (activation) is derived from the movement of electrical charge across the cell membrane, while for LGICs this energy is supplied by the binding of one or more agonist molecules (Andersen & Koeppe, 1992). Through pioneering voltage-clamp experiments on the sodium conductance of the squid giant axon, Hodgkin and Huxley noted that a depolarizing step rapidly elicited membrane currents, but then gave rise to a more slowly arising inactive period, from which recovery was also slow (1952). In other words, the current passing through activated sodium channels -as we now know their molecular identity- can be suppressed by two distinct processes. The first, repolarization of the membrane, involves the removal of the stimulus that initially produced channel gating, and is generally referred to as deactivation. The second, inactivation, coincides with prolonged depolarization, and can manifest as a relaxation of the current response, or as a reduction in the amplitude of a test response from a depolarized membrane. As such, a channel need not open prior to inactivation (French & Horn, 1983).

Hodgkin and Huxley's investigations of the sodium current were later paralleled at the frog neuromuscular junction by their former collaborator Bernard Katz. Although it was known that the release of acetylcholine produced electrical events at this junction, Katz was the first to properly dissect the behaviour of acetylcholine receptors, assigning a mechanism that would serve as a prototype for future studies of LGICs (Nicholls & Hill, 2003). Notably, through ionophoretic application of acetylcholine he showed that following an initial pulse of the chemical, subsequent pulses yielded smaller responses (Katz & Thesleff, 1957). Concurrent with these experiments he developed kinetic models of acetylcholine receptors, including the idea of a

"non-reactive" or desensitized state to account for the attenuated depolarization observed while the agonist was present (Del Castillo & Katz, 1957). As a result, desensitization at LGICs can be simply described as a "progressive reduction in (elicitable) ionic flux in the prolonged presence of agonist" (Keramidas & Lynch, 2013). Though alternatively, at the molecular level, desensitization can be defined as a transition into a non-conducting desensitized state, while deactivation represents the transition from an open to a closed (though non-desensitized) state (Hinard et al., 2016).

The conceptualization of LGIC gating processes as transitions/reactions between states was inspired by earlier work on enzymes, which exist in multiple conformational states that are differentially occupied following the binding of a chemical substrate (Andersen & Koeppe, 1992). In this context, the binding of an agonist does not directly open the channel, but rather reduces the energetic barrier for another state transition that corresponds to opening -indeed, in exceptionally rare instances LGIC currents have been observed without any agonist present (Auerbach, 2015). The separation of binding from gating has in fact been appreciated for some time, allowing the response induced by a particular agonist, its potency, to be categorized in terms of both affinity and efficacy (Stephenson, 1956). Although definitions vary, one can reasonably say that affinity is determined by the initial agonist-binding reaction, whereas efficacy is the sum of all other gating transitions (Colquhoun, 1998). Accordingly, partial agonists are chemicals compounds that -at saturating concentrations- display reduced efficacy compared to some maximally efficacious compound (i.e. glutamate at iGluRs; Jin et al., 2003), while competitive antagonists possess no efficacy (Stephenson, 1956). An additional category of ligands known as non-competitive antagonists reduce receptor responsiveness by interacting somewhere distinct from the agonist-binding site, and are thus said to act in an "allosteric"

manner (Colquhoun, 1998). Over the last fifty years, the terminology used above has provided an adequate framework for describing the functional responses of LGICs, though the behaviour of individual receptor-channel complexes was a rather abstract matter until the first single channels were recorded using the patch-clamp technique (Neher and Sakmann, 1976).

2.2 Fast gating of AMPARs and KARs

AMPARs and KARs are said to have fast gating kinetics, particularly in comparison to NMDARs, and also GABA receptors at inhibitory synapses, but what exactly is considered fast? Generally, AMPAR state transitions occur on a scale of 10 ms or less (Baranovic & Plested, 2016), and this could be considered a good threshold to divide fast and slow for most gating processes. An exception to this rule of thumb is recovery from desensitization, a typically slower process, since the desensitized state is thought to be quite energetically stable (Armstrong et al., 2006). Nevertheless, in an effort to provide a more precise sense of the timescale of AMPAR and KAR gating, several examples will be included in the following section from GluA2 (**Figure R3**) and GluK2 receptors. These receptors have been utilized to obtain a great number of "precise" measurements, owing to their excellent expression in recombinant systems (i.e. HEK 293 cells). The cited values below are taken from channels expressed in outside-out patches - with fast agonist exchange- where the decay of the population response in (near) saturating glutamate is fit with an exponential function. In other recording systems (i.e. whole cell) where solution exchange times are slower, approaching the scale of the process being observed, less accurate measurements are taken (Jonas, 1993). For the other iGluR subunits, values of gating time constants can be easily gleaned from comprehensive reviews (e.g Traynelis et al., 2010).

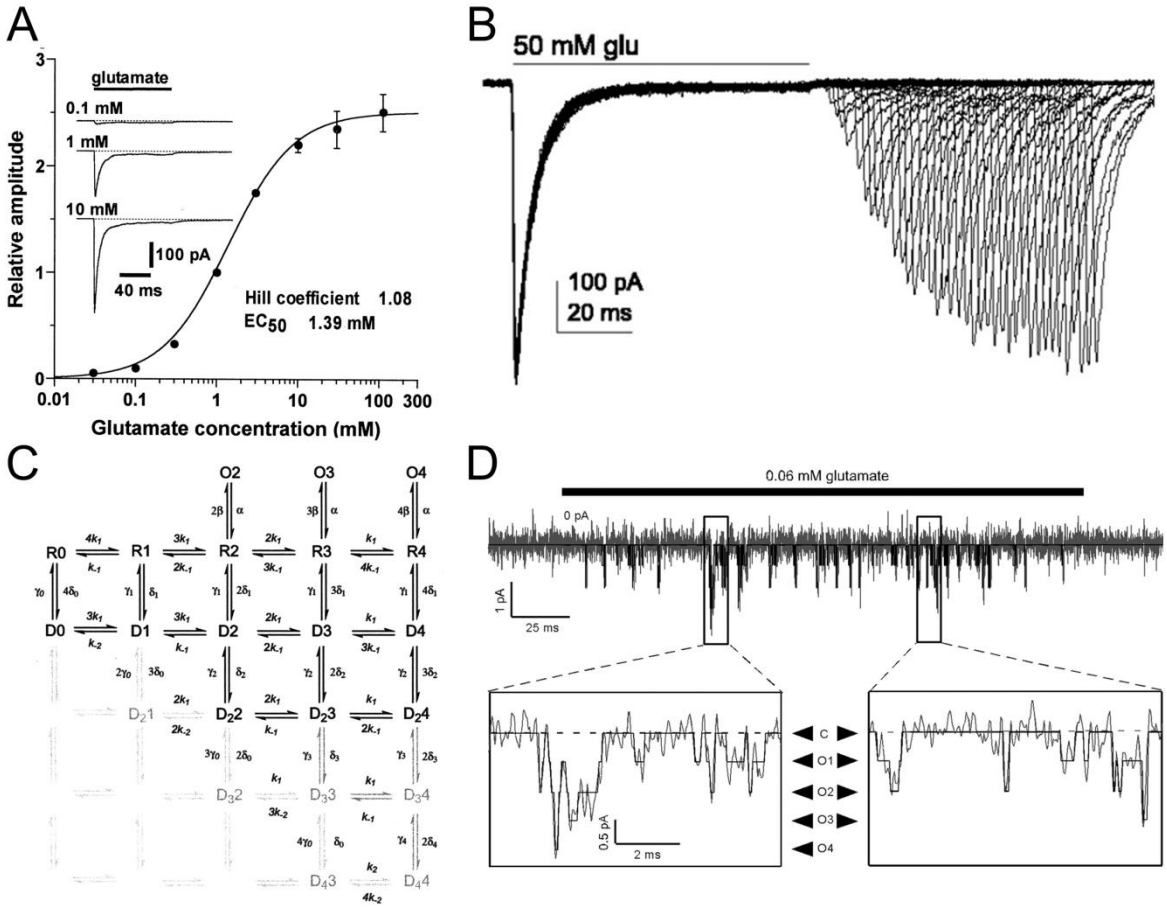

Figure R3. Gating and single-channel behaviour of recombinant AMPARs.
(A) D-R curve constructed by exposing an AMPAR-containing patch to various concentrations of glutamate. During a long pulse of glutamate (inset), current decay, reflecting the rate of entry into desensitization, can be measured. (B) Likewise, the time course of recovery from desensitization can be assessed by measuring the relative amplitude of test pulse responses, given at various time intervals after an initial, desensitizing pulse of glutamate. (C) Data from experiments like those shown in panels A and B can be used to create kinetic models that describe the rates of receptor transitions between resting (*R*), open (*O*), and desensitized (*D*) states with 0-4 bound agonist molecules. (D) Response of a single channel to sub-saturating glutamate with CTZ present in the background to attenuate desensitization. All traces in this figure come from GluA2 flip, Q/R unedited receptors. Adapted from Koike et al., 2000; Robert & Howe, 2003; Robert et al., 2005; Prieto & Wollmuth, 2010.

For the GluA2(Q) flip isoform, time constants of entry into desensitization range between 5 and 10 ms, while the ratio of the equilibrium current to the peak response -reflecting the extent of desensitization- is approximately 1-4% (Robert et al., 2005; Priel et al., 2005). The time constant of deactivation is meanwhile much faster at 0.3-0.8 ms (Sun et al., 2002; Carbone &

Plested, 2012). A caveat to such values is that biexponential functions can achieve a better fit of most current decay data (Robert et al., 2005; Zhang et al., 2006), although single exponential functions are adequate in most circumstances for homomeric AMPARs and KARs, where a fast component of decay is dominant (>90%).

The kinetic parameters above result in relatively little detectable GluA2 desensitization following a single 1 ms pulse of glutamate, based on the response amplitude of subsequent pulses (e.g. Koike et al., 2000). However, it is critical to note that during agonist applications of any length, desensitization still occurs at the same rate, but the process can be hidden to some extent by occurring from closed states after the apparent removal of the agonist (Raman & Trussell, 1995). Therefore, when 1ms glutamate pulses are delivered at high frequencies (i.e. > 100 Hz) GluA2 desensization is more evident (Rozov et al., 1998; Carbone & Plested, 2016), because a fraction of desensitized receptors accumulate without having time to recover from their inactive state(s). Recovery itself has a time constant of roughly 20-25 ms (Robert et al., 2005; Carbone & Plested, 2012).

Full dose-response (D-R) curves of AMPAR peak responses have seldom been attempted, likely owing to the low apparent affinity of receptors for full agonists. From the few published results of this protocol on GluA2 receptors, it seems that saturation occurs above 100 mM, with the EC_{50} estimated at 1 - 2 mM in glutamate (Koike et al., 2000; Robert et al., 2005). This estimate is also consistent with the fast time course of deactivation, which in part reflects agonist unbiding.

GluK2(Q) receptors desensitize over a similar time scale to GluA2 AMPARs, with a decay time constant of 5-8 ms, culminating in an equilibrium response that is between 0.3-0.4% of the peak current (Heckmann et al., 1996; Bowie et al., 2003). In contrast, the time constant of

deactivation is slower at 2.5-3.0 ms (Heckmann et al., 1996; Bowie, 2002), while that of recovery from desensitization is about 100-fold slower at roughly 2-3 s (Heckmann et al., 1996; Bowie & Lange, 2002). These discrepancies between GluA2 and GluK2 suggest that the KAR subunit has a higher apparent affinity for glutamate, and indeed its EC_{50} value is around 0.5 mM (Heckmann et al., 1996; Bowie et al., 2003), somewhat lower than its AMPAR counterpart. An explanation for the slower deactivation and recovery behaviour of KARs was recently provided by the extensive mutation of several non-conserved residues below the glutamate-binding pocket, which could convert each receptor phenotype to the other (Carbone & Plested, 2012).

2.3 Single-channel properties of AMPARs and KARs

Single-channel analysis is an incredible tool that offers insight into the molecular mechanisms governing the activity of ion channels. For instance, if an antagonist inhibits the response of an ion channel, it could be reducing open probability or channel conductance. To know for certain, some knowledge of single-channel behaviour would be required. Typically, such knowledge is obtained either by direct inspection of resolvable single-channel records, or stationary and non-stationary fluctuation (i.e. noise) analysis (Mortensen & Smart, 2007). The latter technique does not require resolution of single channels, because estimates of conductance and open probability are derived from the current variance of the entire channel population, which is comprised of a variable number of individual channel openings and closures, depending on the extent of agonist saturation (Traynelis & Jaramillo, 1998). Before single-channel recording became a possibility, it was known that noise analysis could provide information about individual neurotransmitter-membrane interactions, or even single-channel conductance (Stevens, 1972). However, there are still instances where noise analysis can be useful, including when single channels cannot be isolated, or if the conductance is too small to be resolved

(Traynelis & Jaramillo, 1998). Some of the single-channel properties of recombinant KAR and AMPAR receptors, obtained from noise analysis and direct observation, will be described over the next paragraphs.

Both AMPAR and KAR (Q/R unedited) subunits possess conductance levels of approximately 8, 16, and 24 pS (Swanson et al., 1996; Swanson et al., 1997) that have been thought to correlate the number of bound agonist molecules (2, 3, or 4) at the tetrameric receptor complex (Rosenmund et al., 1998). When the Q/R site is edited, however, unitary channel openings have typically been too small to directly resolve, and noise analysis has estimated femtosiemens-range (i.e. 0.2-0.5 pS) weighted conductances for GluK2(R) and GluA2(R) receptors (Howe, 1996; Swanson et al., 1997). Many studies have therefore focussed on the single-channel behaviour of GluA2(Q) (see **Figure R3**), given that single channels are measureable, and can be linked to structural data, which is most prevalent for that particular subunit (Pohlsgaard et al., 2011). In this regard, a comparison of GluA2 single-channel behaviour in different AMPAR agonists demonstrated a relationship between agonist efficacy and occupancy of higher conductance levels (Jin et al., 2003). More recent examinations of GluA2(Q) channels in saturating glutamate have still found low and intermediate subconductance levels to be the most prevalent, though they identified a fourth, larger conductance level above 30 pS that is rarely visited (Zhang et al., 2008; Prieto & Wollmuth, 2010). How this open state relates to agonist occupancy is presently unclear, though association with auxiliary subunits generally increases the frequency of AMPAR channel openings above 30 pS (Howe, 2015).

Another aspect of single-channel behaviour conserved among non-NMDAR iGluRs is their short open periods. Estimates of mean open time for the various subconductance levels of

GluA2(Q) and GluK2(Q) range between 0.3 and 0.9 ms in glutamate (Zhang et al., 2008; Zhang et al., 2009). Zhang and colleagues also monitored single-channel openings during the onset of glutamate application, and found "bursts" of channel activity typically persisted no more than a few milliseconds before channels desensitized, after which openings were rarely if ever seen again during the same agonist application (Zhang et al., 2008; Zhang et al., 2009). In theory, one can also estimate peak open probability from such recordings, if the number of channels in the membrane is known. Unfortunately, because of the multiple subconductance levels of AMPARs and KARs, as well as the tendency of such channels to open simultaneously in response to glutamate, it is very difficult to know the number of active channels. One way around this problem is to study channels in non-desensitizing conditions, where open probability is high (i.e. ~ 1) and it is clear that one channel is active (Rosenmund et al., 1998; Smith & Howe, 2000; Prieto & Wollmuth, 2010).

3. PHYSIOLOGICAL IMPORTANCE OF AMPARs & KARS

3.1 Overview

The statement "AMPARs mediate the majority of excitatory transmission in the CNS" is often used as a justification for their importance in the introduction of many scientific articles. Beyond the fact that there is no excitatory neurotransmitter in the brain comparable to glutamate, what lines of evidence support an important role for AMPAR and KAR subunits? Numerous neurological disorders are associated with an imbalance of iGluR activity, but notable among them is epilepsy, which can manifest as a result of AMPAR/KAR hyperactivity (Bowie, 2008). Conversely, the genetic removal of certain AMPAR or KAR subunits can limit basal synaptic activity, along with different types of synaptic plasticity associated with learning and memory

(Lerma, 2003; Kessels & Malinow, 2009). The next sections will address the expression of AMPAR and KAR subunits in the CNS, as well as delve deeper into their physiological contributions, using LTP to exemplify AMPAR involvement in synaptic regulation.

3.2 Spatiotemporal expression of AMPAR and KARs

With the cloning of the iGluRs in the early 1990s it became possible to use *in situ* hybridization to visualize the expression of their mRNA throughout the brain (e.g. Keinanen et al., 1990). These observations were later expanded upon with single-cell polymerase chain reaction (PCR) (Geiger et al., 1995) and quantitative mass spectrometry to assess the local or regional prevalence of particular subunits (Schwenk et al., 2014). Generally speaking, AMPAR mRNA has a widespread distribution that slowly increases from birth to adulthood, though the predominant subunits differ from region to region (Hollmann & Heinemann, 1994). At the protein level, GluA2 is typically the most prevalent subunit, while GluA4 is the least prevalent, except in the cerebellum and brainstem, where it has the highest expression. Meanwhile, GluA1 and GluA3 have intermediate expression, with the former more common in the hippocampus and the latter more common in the cortex (Schwenk et al., 2014). The subcellular distribution of AMPARs has been analyzed using receptor-specific antibodies that could localize them to somatodendritic sites (Craig et al., 1993), while higher resolution immunogold labeling placed them at the postsynaptic density, directly across from presynaptic vesicular release sites (Nusser et al., 1994). Estimates of the time individual receptor complexes remain at the plasma membrane vary, though an approximation of 24 hours has been suggested, depending on the developmental stage of a neuron (Mammen et al., 1997). However, even at the membrane, AMPARs exhibit dynamic behaviour, as they can be “trapped” at the synapse in response to

activity (Ehlers et al., 2007), or diffuse throughout the postsynaptic density following desensitization (Heine et al., 2008).

In terms of development, the overall expression of each AMPAR subunit exhibits little change from birth to adulthood (Schwenk et al., 2014), but this does not preclude changes in localization. For instance, "silent" glutamatergic synapses exhibit EPSCs comprised entirely of NMDAR-mediated responses, but they also possess a complement of AMPARs that becomes electrophysiologically detectable following plasticity-inducing stimulation protocols (Isaac et al., 1995; Liao et al., 1995). There is also evidence from cultured hippocampal neurons of newborn rats that the expression of synaptic AMPARs changes over time, with GluA2 upregulation into previously GluA1-dominated synapses (Pickard et al., 2000).

When compared to AMPARs, the expression of KAR mRNA is generally more constrained and prone to developmental regulation (Hollmann & Heinemann, 1994), though GluK5 is a notable exception for its ubiquity (Herb et al., 1992). Amongst the mRNA for primary KARs, all sequences are present to some extent in the cortex, GluK2 and GluK3 occur equally in the hippocampus, and in other regions expression is highly localized, usually including only one predominant subunit (Wisden & Seeburg, 1993). Assessment of subcellular localization using electron microscopy (EM) showed that KARs are found on postsynaptic spines, as well as presynaptic terminals (Darstein et al., 2003).

3.3 AMPARs in neuronal signaling

Under what conditions are synaptic AMPARs typically activated, and what does their activity mean for a neuron? Experiments designed to recreate the phenotype of the AMPAR/KAR EPSC on outside-out hippocampal membrane patches -where the concentration and duration of agonist application can be precisely controlled- suggested that 1 mM glutamate is

present for approximately 1 ms in the synaptic cleft (Colquhoun et al., 1992). A similar result was in fact estimated from the displacement of competitive antagonists by glutamate during NMDAR-mediated EPSCs (Clements et al., 1992). Because of the rapid clearing of glutamate, the excitatory synapse would seem ready to face high-frequency afferent activity, provided that receptors are "tuned" to keep pace.

Not surprisingly, AMPARs have several kinetic properties that impart them with an ability to yield fast, repetitive responses. To begin with, the low apparent affinity for glutamate amongst recombinant GluA1-4 subunits (EC_{50} ~ 1-2 mM; Koike et al., 2000; Robert & Howe, 2003) means that during EPSCs, native AMPARs deactivate within milliseconds (Colquhoun et al., 1992), after which they are ready to generate a similar-sized response to the next release of neurotransmitter. Moreover, the effect of desensitization to attenuate AMPAR EPSCs is limited, because receptors exhibit slow desensitization and fast recovery from desensitization -meaning desensitization is short-lived after a 1 ms synaptic glutamate release (Trussell et al., 1993). These traits are especially beneficial at synapses like the calyx of Held, which contributes to the localization of high-frequency sounds. Within the calyx, AMPARs mediate postsynaptic action potential firing that matches afferent fiber stimulation at frequencies up to nearly 1 kHz (Taschenberger & von Gersdorff, 2000). However, the development of action potentials following AMPAR activation is not such a trivial occurrence.

As with EPSCs at negative potentials, unitary EPSPs in hippocampal interneurons display a similarly rapid time course, due to the contribution of fast-gating AMPARs (Geiger et al., 1997). The occurrence of EPSPs is critical for the development of action potentials, either through their passive summation in the axon initial segment, or by the generation of dendritic spikes, which eventually trigger action potentials upon reaching the axon (Stuart & Spruston,

2015). As such, AMPARs allow neurons to detect simultaneous activity at several synapses, since fast EPSPs must occur within a strict temporal window to enable their integration (Geiger et al., 1997). More recent work has utilized two-photon photo-uncaging of glutamate at discrete sites on CA1 pyramidal neurons to quantify the number of synapses that must be stimulated within a specific time interval (~20 synapses, < 5 ms) to produce dendritic spikes (Losonczy & Magee, 2006). Of course, these values vary between cell types, but AMPARs are usually an important factor in the excitability of neurons.

3.4 KARs in neuronal signaling

For many years, most native KARs were unable to be studied in isolation. After kainate was shown to activate all recombinant AMPAR subunits (i.e. Keinanen et al., 1990), it became clear that the KAR receptor population was not pharmacologically separable. Fortunately, the discovery that 2,3-benzodiazepine (GYKI) compounds act as non-competitive antagonists, selective for AMPARs over KARs (Wilding & Huettner, 1995; Bleakman et al., 1997), paved over this roadblock, spurring many researchers to study KAR-mediated synaptic responses. The first studies focused on hippocampal CA3 neurons, where the KAR EPSC exhibited a much smaller amplitude than its AMPAR-mediated counterpart, as well as a much slower decay rate (τ ~100 ms) (Castillo et al., 1997; Vignes & Collingridge, 1997). Although decay was about ten-fold faster in CA1 interneurons (Cossart et al., 2002), KAR-mediated EPSC responses are generally slow throughout the CNS (Contractor et al., 2011).

The slow phenotype of KARs was particularly puzzling, because of the much faster gating behaviour (i.e. deactivation) of recombinant KAR subunits like GluK2 (Heckmann et al., 1996). Initially, it was speculated that this slow decay was due to perisynaptic localization, where receptors would exposed to lower glutamate concentrations on a delayed timescale

(Jaskolski et al., 2005). However, an alternate explanation that came into favour involved the emergent properties of synaptic KAR complexes, namely heteromerization and auxiliary protein association, which imparted them with the slow phenotype. It was already known that postsynaptic KARs in the hippocampus were likely comprised of both GluK2 and GluK5 subunits (Darstein et al., 2003), yet heteromeric receptors had been studied under a limited set of recombinant conditions, typically featuring a long agonist application (e.g. Swanson et al., 2002). When the same subunits were probed under conditions mimicking synaptic glutamate release (i.e. 1 mM concentration, 1 ms duration) it was found that deactivation slowed substantially (Barberis et al., 2008). Moreover, the KAR-specific auxiliary subunits neuropilin and tolloid-like (or NETO) 1 and 2, single-pass transmembrane proteins that associate with native KARs in brain tissue, further slow receptor deactivation -including that of GluK2/GluK5 heteromers- when expressed recombinantly (Zhang et al., 2009; Straub et al., 2011, a; Straub et al., 2011, b). The NETO subunits also slow desensitization (Zhang et al., 2009), which likely contributes to the summation of KAR EPSCs at many synapses in response to rapid, repetitive stimulations (Straub et al., 2011, b).

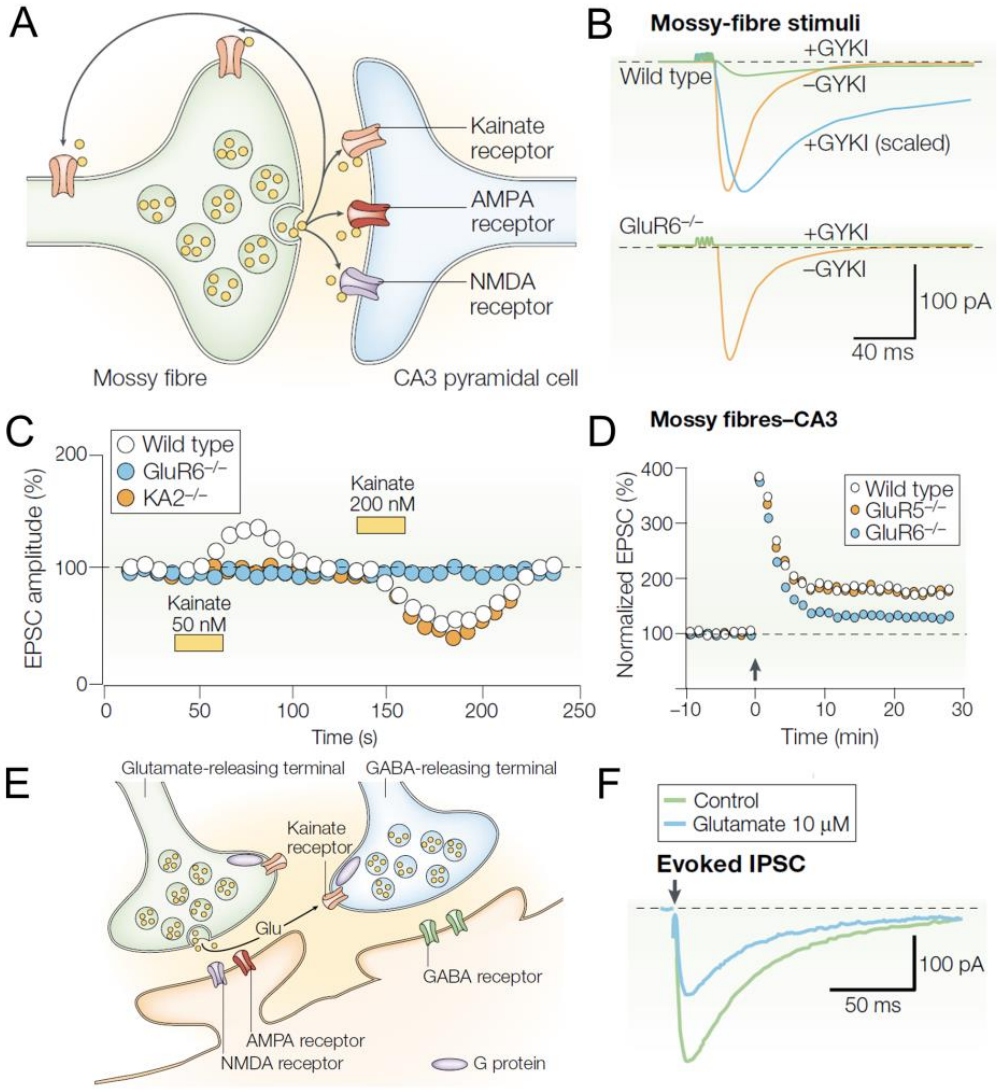

Figure R4. Physiological roles of KARs in synaptic transmission.
(A) Cartoon representation of the hippocampal mossy fiber-CA3 synapse, which contains both presynaptic and postsynaptic KARs. (B) At this synapse, a small, but slowly decaying KAR-mediated component of the EPSC can be isolated following application of the AMPAR-selective antagonist GYKI. (C) Bi-directional facilitation and inhibition of ESPC amplitude by the application of low and high concentrations of kainate, respectively. (D) The amplitude of LTP is reduced in GluK2 knockout mice, indicating a role for the KAR subunit in the process. (E) Illustration of the mechanism by which presynaptic KARs act metabotropically to suppress GABA release onto inhibitory synapses. (F) The application of glutamate reduces IPSC amplitude at the CA3-CA1 synapse by acting on presynaptic KARs, as depicted in the previous panel. Adapted from Lerma, 2003.

3.5 KARs as neuromodulators

Based on the size of their EPSCS, KARs simply cannot compete with AMPARs for the championship of basal synaptic transmission. Rather, native KARs seem to excel at modulating synaptic activity (**Figure R4**), working on both sides of the synapse, and signaling through ionotropic and metabotropic modes (Lerma & Marques, 2013). Several of these unexpected, modulatory roles of synaptic KARs were discovered by the application of kainate in the presence of GYKI, removing the possibility that the agonist was acting on AMPARs (Contractor et al., 2011). For example, at the oft-studied CA3-CA1 synapse, prolonged kainate application (i.e. over minutes) had the paradoxical effect of reducing NMDAR-mediated EPSC amplitudes, an action that could only seem to be reconciled if the agonist acted presynaptically (Chittajallu et al., 1996).

The nearby (hippocampal) mossy fiber synapse also proved to be a fertile ground to observe novel behaviours from presynaptic KARs. At this synapse, an NMDAR-independent form of LTP was found to be blocked by the KAR-selective antagonist LY382884 (Bortolotto et al., 1999). Meanwhile, a kainate-induced, bi-directional regulation of the NMDAR-mediated EPSC amplitude was attributed to presynaptic KARs by measuring presynaptic action potential 'volleys' alongside postsynaptic currents (Schmitz et al., 2000; Schmitz et al., 2001). In part because the presynaptic facilitation of EPSCs was occluded by KAR-mediated LTP, this form of potentiation was concluded to have a presynaptic origin (Lauri et al., 2001). Schmitz and colleagues also argued that the reversible modulation they observed could be achieved with synaptically-released glutamate acting on presynaptic KARs (Schmitz et al., 2000), but this interpretation has since been questioned. An alternative view is that mGluRs mediate some

effects attributed to endogenous glutamate acting on presynaptic KARs, since they also suppress glutamate release at the mossy fiber synapse (Kwon & Castillo, 2008).

Inhibitory neurotransmission and neuronal excitability are also subject to regulation by KARs. The earliest reports of this modulation again relied upon CA1 neurons, where it was found inhibitory postsynaptic current (IPSC) amplitude decreased following application of kainate or the GluK1 selective agonist ATPA (Clarke et al., 1997; Rodriguez-Moreno et al., 1997). Because kainate application alone did not cause postsynaptic depolarization -and for other, more complicated reasons- presynaptic KARs were thought to be the culprits (Clarke et al., 1997). In addition, G protein and protein kinase C (PKC) inhibitors prevented the kainate-mediated change in IPSC behaviour, strongly suggesting a metabotropic mechanism of action (Rodriguez-Moreno & Lerma, 1998). Since this observation, other metabotropic actions of KARs have been postulated, including the inhibition of a potassium current responsible for action potential after-hyperpolarization, an effect that ultimately increases CA1 neuronal firing (Melyan et al., 2002).

3.6 iGluRs in synaptic plasticity

3.6.1 The case of LTP at the CA3-CA1 synapse

Plasticity is a fundamental property of the brain. It allows us to commit new ideas to memory, and recall them periodically when useful, or forget them when of no use. How such neurological plasticity is manifest at the cellular and molecular level has been studied to a considerable extent. Although some details remain unknown, it has become increasingly clear that glutamate receptors are integral to many forms of synaptic plasticity, some of which have been shown to underlie learning and memory *in vivo* (Sweatt, 2016). In this regard, the most carefully examined plasticity mechanism involves a prolonged potentiation (LTP) of synaptic

transmission between hippocampal pyramidal cells projecting from the CA3 to CA1 region (**Figure R5**; Malenka & Bear, 2004). To exemplify the central role of iGluRs in an important neurophysiological process, a brief explanation of their contributions to the induction and expression of CA3-CA1 LTP will be provided. Since other synapses potentiate via different pathways, the details described hereafter refer to the CA3-CA1 synapse, unless otherwise stated.

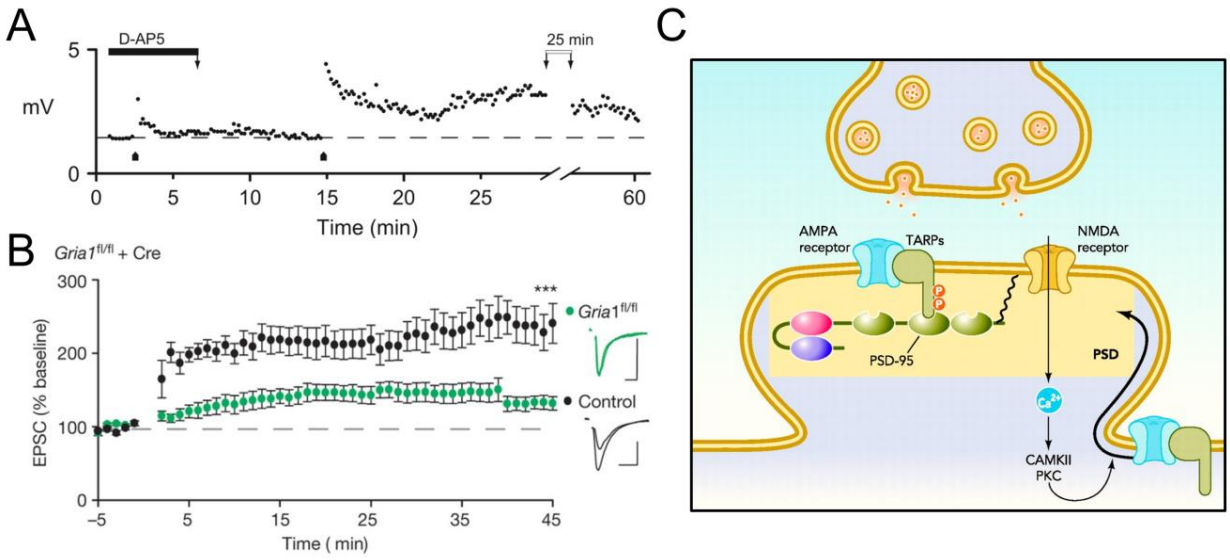

Figure R5. Mechanism of NMDAR-dependent LTP at the CA3-CA1 hippocampal synapse.
(A) Application of the NMDAR-selective antagonist D-AP5 (or APV) prevents the induction of LTP during high-frequency stimulation of the synapse. (B) The conditional knockout of *Gria1*, the gene encoding GluA1, results in severely attenuated LTP expression. (C) Cartoon summary of LTP at the CA3-CA1 synapse, including calcium entry through NMDARs leading to CAMKII activation and resulting in translocation of TARP-associated AMPARs to the postsynaptic density. Adapted from Tomita, 2010; Granger et al., 2013; Volianskis et al., 2015.

3.6.2 LTP induction

Hippocampal LTP was first described in anesthetized rabbits, where repetitive high-frequency stimulation over several seconds induced an increase in the synaptic response (i.e. EPSP) that persisted for hours (Bliss & Lomo, 1973). Ten years later, some mechanistic insight was gained from the discoveries that LTP could be blocked, either by application of the NMDAR-selective antagonist APV (Collingridge et al., 1983), or inclusion of the calcium

chelator ethylenediaminetetraacetic acid (EDTA) in the recording pipette (Lynch et al., 1983). These observations were clarified after it was demonstrated that NMDAR activation raises intracellular calcium concentration (MacDermott et al., 1986). In conjunction with experiments showing that the AMPAR/KAR selective antagonist DNQX did not prevent EPSP potentiation (Muller et al., 1988), pharmacological evidence had helped create a model wherein NMDARs induce LTP and AMPARs mediate its expression. An addition to this model came from studies reporting that the inhibition of protein kinases, and specifically calcium/calmodulin-dependent protein kinase II (CAMKII), also blocked LTP induction (Malenka et al., 1989; Malinow et al., 1989). CAMKII was plausible as the first downstream step in NMDAR-dependent LTP, given its ability to sense and respond to NMDAR-mediated calcium entry -in fact, CAMKII was later found to associate directly with the GluN1 and GluN2B subunits (Leonard et al., 1999). Nevertheless, the exact nature of LTP expression downstream of this point became an incredibly complicated matter, owing to the identification of multiple kinase targets and AMPAR interacting proteins.

3.6.3 LTP expression

Apart from experiments described in the last paragraph, few interventions have been able to entirely prevent hippocampal LTP. At the same time, there is expanding list of proteins considered to be important for its expression, often stemming from the observation of LTP impairment in knockout mice. For example, mice lacking the GluA1 subunit do not exhibit LTP at the CA3-CA1 synapse (Zamanillo et al., 1999). In contrast, knocking out GluA2, or both GluA2 and GluA3 together results in enhanced potentiation (Jia et al., 1996; Meng et al., 2003). This discrepancy has led to the idea that GluA2 and GluA3 may be important for basal synaptic transmission, while GluA1 is deployed to strengthen synapses during plasticity, settling into new

"slots" made available by some other protein(s) (Kessels & Malinow, 2009). In support of this idea, the overexpression of GluA1 in CA1 neurons resulted in greater inward rectification of the I-V plot after LTP, consistent with more polyamine-sensitive GluA1 subunits getting into the synapse (Hayashi et al., 2000).

Initially, it was suspected that phosphorylation might be the key driver to get GluA1 into newly formed synaptic slots. Corroborating this idea, a mouse possessing two phospho-null mutations at known phosphorylated residues in the GluA1 intracellular C-terminus had greatly reduced LTP (Lee et al., 2003). However, a more radical intervention involving a conditional knockout of the GluA1-3 subunits -rendering the AMPAR-mediated EPSC non-existent- and transfection of various iGluR subtypes into cultured neurons determined that the GluA1 C-terminal domain (CTD) is not required for LTP. For that matter, any one of the AMPAR subunits, and even the GluK2 KAR subunit, was shown to be capable of mediating LTP expression (Granger et al., 2013). Accordingly, LTP expression does not depend on C-terminal interactions unique to GluA1, or absolutely require AMPARs, but there may be preferential incorporation of certain subunits under normal conditions (Huganir & Nicoll, 2013).

AMPAR auxiliary proteins have also been considered as key intermediates in the LTP expression pathway (Herring & Nicoll, 2016). The transmembrane AMPAR regulatory proteins (TARPs), which constitute the most well studied AMPAR auxiliary protein family (see Jackson & Nicoll, 2011), are phosphorylated in the brain, and the viral infection of phospho-null TARP mutants abolished LTP in neuronal cultures (Tomita et al., 2005). Furthermore, knocking out the most abundant TARP subunit in the hippocampus (γ8) greatly reduced EPSC amplitude and almost eliminated LTP at the CA3-CA1 synapse (Rouach et al., 2005). This data fits with an earlier interpretation that the PDZ-binding motif of TARPs provides a hook to install AMPAR

complexes in the postsynaptic density (Chen et al., 2000). Additional investigation of mice with truncated γ8 subunits lacking the PDZ motif revealed an impairment of EPSC amplitude, though normal LTP expression (Sumioka et al., 2011), suggesting other TARP-related factors mediate plasticity. On the whole, TARPs appear important, but not essential, for LTP expression, though the exact mechanism by which they deliver additional AMPARs to the synapse is still unresolved. Because of the redundancy provided by six modulatory TARP subunits, with multiple subunits occurring together in many brain regions (Jackson & Nicoll, 2011), it has been difficult to study their net effect. Combinations of triple TARP gene knockouts -and presumably complete TARP elimination- are lethal (Menuz et al., 2009), meaning some aspects of TARP physiology may remain hidden without better genetic tools.

3.6.4 LTP as a correlate of learning and memory

Because LTP is traditionally studied *in vitro*, most findings related to the process cannot be explicitly linked to behaviour. Pioneering experiments showed that APV inhibited the ability of rodents to learn escape routes from a water-filled chamber (Morris et al., 1986), but the previously described blockade of LTP by the NMDAR antagonist (Collingridge et al., 1983) could not be causally linked with impaired spatial learning. Rather, it was hoped that the involvement of the hippocampus in memory-based navigation (Morris et al., 1982) and the extensive plasticity of hippocampal synapses were not coincidental. An excellent investigation into the causality of LTP found that completion of a spatial learning task -avoiding foot shocks associated with a specific location- resulted in a LTP-like phenotype at the CA3-CA1 synapse, while further potentiation was occluded (Whitlock et al., 2006). More recent experiments have found that memories can be “inactivated” and “reactivated” by the *in vivo* optogenetic induction

of long-term depression (LTD) and LTP, respectively (Nabavi et al., 2014), confirming a bi-directional role of plasticity in shaping behaviour.

4. A STRUCTURAL TOUR OF THE GLUTAMATE RECEPTOR

4.1 Survey of the iGluR domains

All iGluR subunits are comprised of four structural domains: the extracellular amino-terminal domain (ATD) and ligand-binding domain (LBD), the transmembrane domain (TMD), and an intracellular C-terminal domain (CTD) (**Figure R6**; Mayer & Armstrong, 2004). The sizes of the ATD and LBD are largely conserved, with each containing around 400 and 300 amino acids, respectively (Mayer, 2011). Likewise, each TMD is comprised of multiple, short membrane-spanning segments (TM 1, 3, and 4), as well as the pore loop (TM2), which does not cross the entire membrane, but provides the selectivity filter for ion permeation (Huettner, 2015). At the end of iGluR proteins, the CTD forms a less organized arrangement (Ryan et al., 2008) that varies between 20 and 500 amino acids (Mayer & Armstrong, 2004). When all domains are combined to calculate the total length of the longest splice variant of each subunit, AMPARs are approximately 900 amino acids, KARs range between 900 to 1000 amino acids, and NMDARs are generally much longer (900-1500 amino acids), owing to the extensive variability in the CTD of GluN2 subunits (Traynelis et al., 2010). However, an important consideration in the length and residue numbering of iGluR subunits is the inclusion of the signal peptide, a hydrophobic segment preceding the ATD that directs membrane insertion (Hollmann & Heinemann, 1994). Throughout this thesis, the signal peptide is included in residue numbering, but it is common in the AMPAR and KAR literature to refer to the length of the "mature" protein, from which the signal peptide has been cleaved.

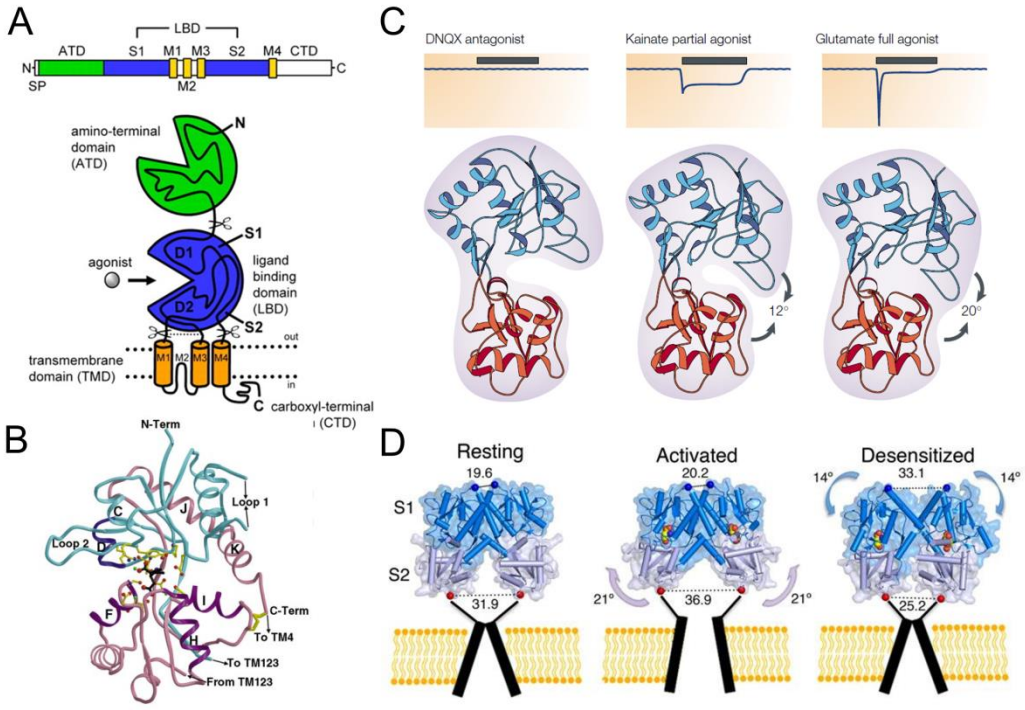

Figure R6. Insights into AMPAR/KAR gating from structures of the isolated LBD.
(A) Colour-coded representation of each iGluR domain, relative to the length of the protein as a whole (top), as well as a cartoon depiction of the overall topology (bottom). (B) Image of the first high-resolution crystal structure of an iGluR domain, namely the kainate-bound GluA2 LBD. (C) A structural model of agonist efficacy, indicating progressively greater closure of the agonist-binding cleft from an antagonist (DNQX) to partial agonist (kainate) to full agonist (glutamate). (D) A structural model of activation and desensitization. Notably, during activation the D2 lobes swing upward pulling on the linkers to the channel pore, while during desensitization the D1-D1 dimer interface comes apart. However, it should be noted that desensitization is not thought to occur directly from open states, and that multiple kinetic transitions would be expected in between each state (see Robert & Howe, 2003). Adapted from Traynelis et al., 2010; Armstrong et al., 1998; Madden, 2002; Kumar & Mayer, 2013.

4.2 Early structural insights

4.2.1 The topology of iGluRs

Concurrent with the initial cloning of an iGluR subunit, four putative TM segments were identified from its polypeptide sequence, though the topology and stoichiometry of assembled proteins were still highly speculative (Hollmann et al., 1989). Unlike other LGICs

known at the time, the region prior to the initial TMD was extremely long, and contained sequences that were homologous with both glutamine-binding proteins (GlnBPs) and leucine/isoleucine/valine-binding proteins (LIVBPs), two classes of periplasmic-binding protein found in bacteria (Nakanishi et al., 1990). Furthermore, it possessed several consensus sites for asparagine, or N-linked glycosylation (Boulter et al., 1990; Keinanen et al., 1990), which characteristically occurs on the extracellular face of membrane and secretory proteins (Standley & Beaudry, 2000). Together, the evidence for N-terminal ligand binding and glycosylation strongly suggested that this end of the protein was extracellular, though some confirmation came from deglycosylation assays (Rogers et al., 1991; Blackstone et al., 1992). Soon after, the first solid evidence for an intracellular C-terminal came from membrane permeabilization assays, which greatly increased antibody labeling at epitopes on the C-terminal end of the AMPAR (Craig et al., 1993; Molnar et al., 1994). This result stood in contrast to contemporary models that placed both termini on the extracellular side of the mmebrane (summarized in Hollmann & Heinemann, 1994). Part of this confusion stemmed from the four identified TM segments, since having N and C-termini on different sides of the membrane would be somewhat paradoxical.

Much of the mystery involving iGluR topology was resolved in 1994, with further exploration of N-glycosylation. The identification of a KAR-specific glycosylation site in the proposed intracellular loop between TM3 and TM4 suggested that this area was in fact extracellular (Roche et al., 1994). Moreover, the mutagenesis of native AMPAR glycosylation sites revealed two discontinuous extracellular segments, and led to the (correct) speculation that TM2 partially enters the membrane before returning out the same side (Hollmann et al., 1994). At the same time, this knowledge was used to generate AMPAR/KAR chimeras to demonstrate that the LBD is formed from both extracellular segments, which together define agonist

selectivity (Stern-Bach et al., 1994). These segments were named S1 (between the ATD and TM1) and S2 (between TM3 and TM4) (Stern-Bach et al., 1994).

Fortunately, it was possible to construct a soluble LBD from the S1 and S2 segments, which were joined by a linker segment (Kuusinen et al., 1995), a manipulation that was later used with great success for crystallographic analysis of GluA2 (reviewed in Dawe et al., 2015). In the meantime, insights into the tertiary structure of iGluR domains depended on homology modeling from atomic structures of periplasmic-binding proteins (Quiocho & Higgins, 1990; Kang et al., 1991). Due to the bi-lobed structure of these proteins, it was proposed that the iGluR LBD might respond to glutamate by acting like a venus flytrap (Mano et al., 1996).

4.2.2 The stoichiometry of iGluRs

The tetrameric subunit arrangement of the first intact AMPAR structure (Sobolevsky et al., 2009) could be considered the definitive proof of iGluR stoichiometry. Nevertheless, a great deal of indirect evidence had previously settled much of the debate regarding how many subunits comprise iGluR complexes. Some of the earliest insights came from NMDARs, where it was known that both glutamate and glycine must be bound for activation to occur (Johnson & Ascher, 1987; Kleckner & Dingledine, 1988). Using kinetic analysis of current responses, it was possible to derive a better fit from models with two -rather than one- binding steps for both glutamate and glycine (Benveniste & Mayer, 1991; Clements & Westbrook, 1991). Accordingly, it was proposed that NMDARs must have at least four subunits, assuming one subunit contained one agonist-binding site (Clements & Westbrook, 1991). The single binding site model was later validated, as both GluN1 and GluN2 subunits were shown to be required for functional expression of recombinant NMDARs (Monyer et al., 1992), and their respective mutation could reduce apparent affinity for glycine and glutamate (Kuryatov et al, 1994; Laube et al., 1997).

Subsequently, these mutations were brilliantly employed to demonstrate a tetrameric stoichiometry of NMDARs. By co-transfecting cDNA encoding lower affinity GluN1 or GluN2 mutants with wildtype receptors, a triphasic dose-response curve emerged, indicating zero, one, or two mutant subunits were incorporated into the functional complex -and by extrapolation an upper limit of two of each subunit would reflect four subunits in total (Laube et al., 1998). This stoichiometry has not been challenged, but following the isolation of what are now termed the GluN3A and B subunits (Sucher et al., 1995; Chatterton et al., 2002), it has been appreciated that NMDARs are not simply composed of two GluN1 and two GluN2 subunits. Rather, they can assemble as GluN1/GluN2 di- or triheteromers (i.e. GluN1, GluN2A, and GluN2B) (Hatton & Paoletti, 2005; Tovar et al., 2013), as well as GluN1/GluN3 receptors, which are responsive to glycine, and not glutamate (Chatterton et al., 2002). There is also some biochemical evidence that GluN3 subunits can incorporate into the same complex as GluN2, forming GluN1/GluN2/GluN3 triheteromers (Perez-Otano et al., 2001). Whether such triheteromers form functional channels remains to be conclusively demonstrated, since co-transfected subunits can also form two diheteromeric (N1/2, or N1/3) receptor populations.

At the same time as the NMDAR studies mentioned above, other experiments on homomeric AMPARs helped the field reach a consensus on tetrameric stoichiometry. For example, the addition of crosslinking reagents to brain tissue allowed AMPAR complexes to be isolated at molecular weights of up to four times that of the single subunit (Wu et al., 1996). Alternatively, the responsiveness of wild-type and mutant -with altered quisqualate sensitivity- GluA1 receptors, co-expressed at various ratios, was best fit with a four binding site model (Mano & Teichberg, 1998). These studies were then largely overshadowed by work from a non-desensitizing, chimeric GluA3/GluK2 receptor, from which the single-channel conductance was

found to increase incrementally as antagonists were replaced by agonist molecules at each binding site. The rate of appearance of the three subconductance levels for the chimeric channel was used to argue in favour of a tetrameric complex (Rosenmund et al., 1998). It was thus proposed that one agonist molecule is unable to open the AMPAR channel, whereas two, three, and four bound molecules corresponded to the low, medium, and high subconductance levels (Rosenmund et al., 1998). A concern with this interpretation -not appreciated until later- is that native and recombinant (e.g. GluA2) AMPARs possesses up to four subconductance levels, which can occur at both saturating and sub-saturating agonist concentrations (Smith & Howe, 2000; Zhang et al., 2008; Prieto et al., 2010), implying that other factors apart from agonist occupancy may dictate conductance level.

4.3 The ligand-binding domain (LBD)

4.3.1 Atomic structure of the LBD and agonist efficacy

The first high resolution structure of an iGluR domain was achieved in 1998, when the kainate-bound GluA2 flop LBD was crystallized using an S1-S2 linked construct (**Figure R6**; Armstrong et al., 1998). In a sense, this structure brought the study of iGluRs out of the dark, and was the first of many key contributions made by the lab of Eric Gouaux to the field. Consistent with earlier homology modeling, the LBD was determined to be "kidney-shaped," containing upper and lower domain 1 (D1) and domain 2 (D2) lobes that both form contacts with the agonist molecule (Armstrong et al., 1998). Moreover, comparison with the glutamine-bound GlnBP structure (Sun et al., 1998) suggested that the wide-open GluA2 agonist-binding cleft was capable of much more extensive closure between D1 and D2. Consistent with this prediction, a follow-up investigation of the GluA2 LBD found that -relative to the apo state- the binding of full agonists AMPA and glutamate induced a further 20° closure of the agonist-binding cleft,

based on the angle between the D1 and D2 domains. Meanwhile, the partial agonist kainate and the competitive antagonist CNQX only induced 12° and 5° of additional cleft closure, respectively (Armstrong & Gouaux, 2000). This spectrum of cleft closure led to a structural model of agonist efficacy, whereby more efficacious agonists could induce greater closure, which in turn facilitated gating of the channel pore (**Figure R6**; Armstrong & Gouaux, 2000). Validation of this model was dependent on studies linking the cleft closure induced in various agonist-bound structures to the relative efficacy of these agonists in electrophysiological assays (Hogner et al., 2002; Jin et al., 2003). The most compelling example involved the incorporation of increasingly bulky halide groups into a willardiine (an AMPAR partial agonist) chemical backbone. These chemical substitutions incrementally reduced cleft closure, alongside the maximal current response of GluA2 AMPARs (Jin et al., 2003), in agreement with the idea that more closure correlates with greater efficacy. Importantly, such currents were recorded from receptors containing a well-studied point mutation that blocks desensitization (see next section), removing that potential confound from the assignment of relative efficacy. An additional piece of evidence favouring the cleft closure paradigm came from a GluA2 mutant with reduced cross-cleft hydrogen bonding, as glutamate efficacy was lowered, relative to quisqualate, another full agonist (Robert et al., 2005).

Beyond AMPARs, the initial, isolated LBD structures from the NMDAR and KAR subfamilies were also in good agreement with closure dictating efficacy. The arrangement of the GluN1 agonist-binding cleft was more closed with the agonist glycine than the competitive antagonist DCKA (Furukawa & Gouaux, 2003). Likewise, the “co-first” GluK2 LBD structure was bound by the partial agonist domoate, and through comparison to existing GluA2 structures it was found to have intermediate cleft closure between the apo and glutamate-bound forms

(Nanao et al., 2005). At the same time, the GluK1 and GluK2 LBD structures reported by Mark Mayer all displayed a much larger agonist-binding cleft than that of GluA2, with greater domain closure relative to the GluA2 apo state. The kainate-bound GluK2 cleft was only 3° more open than the glutamate-bound cleft (Mayer, 2005), but that could have reflected that kainate is a much more efficacious agonist at recombinant GluK2 (MacLean et al., 2011) versus GluA2 receptors (Plested & Mayer, 2009).

4.3.2 Refining the model of agonist efficacy

Since the initial structural survey of GluA2 agonists and antagonists by Armstrong and Gouaux, an immense number of ligands have been crystallized in the agonist-binding cleft of various iGluR subunits. Even as of 2011, over eighty structures were reported for the GluA2 LBD alone (Pohlsgaard et al., 2011). It is clear that not all of the bound agonists have induced a degree of LBD cleft closure commensurate with their agonist activity (reviewed in Dawe et al., 2015). To highlight a few examples, two GluN1 partial agonists induced a similar cleft closure as the full agonist glycine (Inanobe et al., 2005), while kainate was reported to induce a similar degree of cleft closure in GluK1 and GluA2 (relative to glutamate), despite it being a much poorer agonist at the latter (Venskutonyte et al., 2012). A somewhat related finding was that kainate efficacy may be governed by a twisting motion of the LBD, rather than cleft closure (Birdsey-Benson et al., 2010). This corroborated previous molecular dynamics (MD) simulations of the GluA2 LBD, which predicted a capability of the structure to undergo discrete "hinge-bending" (cleft closure), twisting, and rocking motions (Bjerrum & Biggin, 2008). As more intact receptor complexes are solved in different states (i.e. Durr et al., 2014) it will be appropriate to refine explanations of agonist efficacy to complement the observed changes in quaternary structure. Nevertheless, considering the one-dimensional nature of the cleft closure

paradigm, the measurement exhibits a strong correlation with agonist efficacy (Pohlsgaard et al., 2011), and has provided a great structural starting point for thinking about how the iGluR LBD regulates channel gating.

4.3.3 AMPAR modulators and the molecular basis of desensitization

Prior to the crystallization of the AMPAR LBD, a great deal of electrophysiological evidence had pinpointed this domain as a molecular determinant of receptor desensitization. Toward this end, the characterization of compounds that modulate AMPAR desensitization was an important first step. Fortuitously, the cognition-enhancing drug aniracetam was identified early as a potentiator of neuronal AMPAR/KAR responses (Ito et al., 1990), though more detailed experiments showed it slows desensitization and EPSC decay (Vyklicky et al., 1991). Likewise, cyclothiazide (CTZ), a benzothiadiazide compound originally developed as a diuretic (Yamada & Tang, 1993), was also found to positively modulate non-NMDAR responses. However, CTZ almost completely blocks glutamate-induced desensitization, with little effect on deactivation kinetics (Patneau et al., 1993; Yamada & Tang, 1993). In recombinant expression systems, CTZ acts selectively on AMPARs, but not KARs (Partin et al., 1993). Furthermore, because of its greater modulation of the flip versus flop AMPAR variant -which differ in some S2 residues- it was possible to identify a single site in the LBD (S/N in GluA2 flip and flop at position 775) that imparts sensitivity to both CTZ and aniracetam (Partin et al., 1995; Partin et al., 1996).

Even without allosteric modulators bound, the alternative splicing of the AMPAR flip/flop exons affects the time course of desensitization, as flop variants generally desensitize faster (Mosbacher et al., 1994). An additional, complicating factor is RNA editing at the so-called “R/G” site immediately preceding the flip/flop region, which converts arginine to glycine

in flip and flop variants of GluA2-4, producing a modest slowing of entry into desensitization and acceleration of recovery from desensitization (Lomeli et al., 1994). Together, the genetic regulation of AMPARs and their response to allosteric modulators both suggested the end of the LBD S2 segment was important in the mechanism of desensitization.

4.3.4 The LBD dimer interface and AMPAR desensitization

The S1 segment of the LBD was also implicated in AMPAR desensitization by the discovery of a point mutation, known as L/Y (at residue 504 in GluA2), which prevented receptors from desensitizing (Stern-Bach et al., 1998). The L/Y site was identified using GluA3/GluK2 chimeras (Stern-Bach et al., 1994), from which the tyrosine of GluK2 conferred the non-desensitizing phenotype (Stern-Bach et al., 1998). Curiously, the L/Y site was positioned on the external face of the LBD, opposite to the agonist-binding cleft (Armstrong et al., 1998), so its role in gating was not immediately clear. With the crystallization of a modified GluA2 ligand-binding core (S1S2J) as dimers (Armstrong & Gouaux, 2000), it was then appreciated that both the S/N and L/Y sites were located in the "dimer interface," formed between the oppositely directed clefts. Applying the ultracentrifugation technique of sedimentation equilibrium to CTZ-bound or L/Y mutant GluA2 LBDs revealed that in both cases, protein dimerization was enhanced. This result, combined with crystal structures of the LBD dimer in each condition, enabled the first structural model of iGluR desensitization. According to this model, the dimer interface must rupture for desensitization to proceed (**Figure R6**; Sun et al., 2002).

Despite a large number of papers reporting altered desensitization kinetics through the mutation of various sites along the AMPAR and KAR dimer interface (e.g. Horning & Mayer, 2004; Zhang et al., 2006), two notable concerns with the dimer interface model have persisted. The first is its applicability in NMDARs, which are much less conserved with AMPARs, and the

second is whether it could be extrapolated to full-length receptors, rather than isolated LBDs. Regarding NMDARs, the first crystal structure of the LBD heterodimer, comprised of GluN1 and GluN2A subunits, showed a similar overall organization to that of GluA2 (Furukawa et al., 2005). However, analytical ultracentrifugation of isolated NMDAR LBDs suggests that both co-agonists must be present to facilitate heterodimer formation (Cheriyan et al., 2015). This contrasts with the idea that agonist binding promotes desensitization and dimer separation of AMPARs and KARs. In addition, agonist-bound intact NMDAR structures published recently (Zhu et al., 2016; Tajima et al., 2016) did not exhibit the same broken-dimer LBD arrangement seen in intact GluK2 (Meyerson et al., 2014) and GluA2 (Durr et al., 2014) structures that were deemed to be desensitized. For these non-NMDAR structures, captured in apo, "pre-activated," and desensitized states, the transitions observed in the LBD layer have been in agreement with the initial activation (Armstrong & Gouaux, 2000) and desensitization (Sun et al., 2002) mechanisms put forward by the Gouaux lab.

4.3.5 The LBD dimer interface and KAR desensitization

As an additional functional test for the role of the LBD dimer in iGluR gating, it was thought that the introduction of a disulfide bridge across the dimer interface would prevent the conformational transition accompanying desensitization. For the KAR subfamily, for which there were no mutations or modulatory compounds yet identified (as of 2006) that could severely attenuate desensitization, this was an attractive prospect. Indeed, two groups published cysteine crosslinking mutations at different positions in the GluK2 dimer interface that imparted the receptor with nondecaying responses to glutamate (Weston et al., 2006; Priel et al., 2006). Subsequent analysis of the Y512C/L783C mutation first described by Weston and colleagues revealed that single-channel openings were sporadic, despite occurring with equal probability

during saturating agonist applications (Daniels et al., 2013). Thus, although it seems likely that access to certain desensitized conformations is prevented, this does not equate with receptors remaining in an open-channel state. Such an interpretation is consistent with the original characterization of the equivalent GluA2 crosslinked mutant (L504C/L783C), for which current amplitudes were potentiated several fold by CTZ, indicating a relatively low open probability at equilibrium (Weston et al., 2006).

Around the same time that the dimer interface was first being explored in AMPAR desensitization, a coincidental finding in the GluK2 KAR pointed to its interface as an important allosteric regulator of gating. Specifically, the substitution of different cations and anions (beside sodium and chloride) in the external recording solution accelerated desensitization and reduced peak response amplitudes (Bowie, 2002). A more drastic perturbation involved the substitution of external sodium chloride with sucrose, which entirely abolished GluK2, but not GluA1 functional responses -mediated by ions in the pipette solution (Wong et al., 2006). Meanwhile, increasing the overall concentration of sodium chloride slowed desensitization (Bowie & Lange, 2002). The protein region responsible for ion sensitivity was isolated with the help of chimeric GluK2/GluA3 receptors -as AMPARs were insensitive to cation substitution- and pinpointed at the apex of the LBD, where mutations to key residues negated the modulatory effects of ion species (Paternain et al., 2003). Eventually, crystallographic analysis of KAR LBDs resolved two sodium-binding sites and one chloride-binding site at the respective margins and centre of the apical dimer interface, leading to the hypothesis that ions somehow stabilize the KAR dimer for efficient gating (Plested & Mayer, 2007; Plested et al., 2008). A similar structural role is thought to be played by the zinc ion, which binds at a lower position in the GluK3 LBD dimer interface, leading to current potentiation (Veran et al., 2012).

Prior to structural information concerning the position of ions in the GluK2 LBD, it was proposed that sodium and chloride might form a dipole (Wong et al., 2007), though subsequent investigations have suggested that allosteric anions might play a separable and secondary role to cations. For example, the substitution of cations, but not anions, can alter the relative efficacy of specific agonists (MacLean et al., 2011). Likewise, a point mutation introduced at the LBD apex (GluK2 D776K) apparently disrupted desensitization (Nayeem et al., 2009) by introducing a positively charged, cross-dimer tether into the sodium-binding pocket, all the while perturbing the chloride-binding site (Nayeem et al., 2011). Yet given the complicated nature of single channels recorded from cysteine-crosslinked KAR mutants, the ability of the D776K mutation to retain GluK2 in an activated state (without sodium binding) remained a valid concern.

4.4 The amino terminal domain (ATD)

4.4.1 Overview

The ATD is arguably the most perplexing iGluR domain. It comprises roughly half of the entire protein (Mayer, 2011), yet it is not required for assembly or channel gating, since NMDARs (Fayyazuddin et al., 2000; Meddows et al., 2001), AMPARs (Pasternack et al., 2002), and KARs (Plested & Mayer, 2007) lacking their respective ATDs can all retain channel function. Despite this apparent irrelevance, it has long been known that NMDAR gating is uniquely regulated at multiple sites within the ATD (Hansen et al., 2010). Moreover, a great deal of attention has been paid to the role of the ATD in facilitating the preferential assembly of non-NMDAR subunits (Greger et al., 2007). There may even be an important role for the ATD in iGluR association with other synaptic proteins (Garcia-Nafria et al., 2016). For these reasons the determination of ATD structures -either alone or within intact receptor complexes- has still been met with great interest, and merits some elaboration in an otherwise LBD-focused thesis.

4.4.2 The ATD in NMDAR gating

Early work on recombinant GluN2 receptors showed that the region prior to TM1 (Krupp et al., 1998), or specifically a motif within in the ATD (Villarroel et al., 1998), accounted for subunit differences in desensitization. It also offered an explanation for the progressively slower desensitization of the A to D subunits during a prolonged glutamate pulse (Vicini et al., 1998). An identical relationship exists in terms of the deactivation rates amongst GluN2 subunits, with D being slowest again (Monyer et al., 1994), but the molecular basis of this variability remained unclear for quite some time. Two concurrent studies published in 2009 revealed the origin of these gating properties by swapping the GluN2A ATD with that of GluN2B or GluN2D. In essence, the gating behaviour of the donor subunit was conferred to the recipient subunit, including its deactivation rate, glutamate and glycine EC_{50}, and channel open probability, all of which are normally highest in GluN1/GluN2A receptors (Gielen et al., 2009; Yuan et al., 2009).

In addition to governing channel gating, the NMDAR ATD also contains binding sites for several allosteric modulators, some of which appear to have physiological significance (Hansen et al., 2010). The first such modulator to be characterized, the divalent ion zinc, was observed to exogenously inhibit NMDA responses from neurons (Peters et al., 1987), in a manner that was not entirely voltage-dependent, and thus distinct from the channel block mediated by magnesium ions (Westbrook & Mayer, 1987). Later, with the help of recombinant expression, it was found that zinc had much greater affinity for GluN2A (IC_{50} < 100 nM) than other GluN2 subunits (Williams, 1996; Paoletti et al., 1997), and its effects were linked by mutagenesis to a cluster of histidine residues in the ATD (Choi & Lipton, 1999; Fayyazuddin et al., 2000). Although zinc binding has been frequently exploited for selective inhibition of GluN2A-containing NMDARs, there is also evidence that this action may have physiological relevance. Synaptic vesicles are

thought to contain varying concentrations of zinc and following vesicular release the ion may reach micromolar-range concentrations in the synaptic cleft -although measurements are quite tricky due to the transient nature of this process (Sensi et al., 2011). More compellingly, knockin mice lacking one of the zinc-coordinating histidine residues showed enhanced pain sensitivity, implying that zinc binding at NMDARs may prompt an analgesic effect (Nozaki et al., 2011).

Similar to zinc, extracellular acidification (i.e. protons) also causes voltage-independent inhibition of neuronal NMDAR responses (Giffard et al., 1990; Traynelis & Cull-Candy, 1990). This inhibition is regulated to some extent by the alternate splicing of an exon encoding part of the GluN1 ATD (Traynelis et al., 1995). However, mutations in the LBD dimer interface also augment both zinc and proton sensitivity (Gielen et al., 2008), raising the possibility that this region transduces their inhibitory actions downstream of the more distal binding sites. Given the low sequence conservation between NMDARs and other iGluR subunits (Hollmann & Heinemann, 1994), it is interesting that KARs also exhibit proton sensitivity, regulated by residues in the ATD (Mott et al., 2003). In AMPARs, proton inhibition occurs to a small extent (Ihle & Patneau, 2000), but the structural basis is unclear. Ultimately, it is unknown if proton inhibition of the various iGluR subtypes has a common mechanism, but given the NMDAR IC_{50} is around physiological pH (~7.4), slight changes in extracellular acidity brought about by conditions such as ischemia (Yuan et al., 2015) can have profound effects on NMDAR signaling in the brain.

On a related note, the anti-ischemic drug ifenprodil is another potent NMDAR antagonist (Carter et al., 1988). As with zinc, its effects are voltage-independent, and the inhibition curve displays both high and low-affinity components in neurons (Legendre & Westbrook, 1991). This observation was better understood following the discovery that ifenprodil is much more selective

for GluN2B-containing NMDARs (versus GluN2A), which yield a sub-micromolar IC_{50} (Williams, 1993). A screen of various mutations later identified the ATD as the binding site for ifenprodil, and it was proposed to act in a manner analogous to zinc at GluN2A (Perin-Dureau et al., 2002), though their binding sites were later shown to be non-equivalent in crystal structures. Due to the largely exclusive effects of zinc and ifenprodil at GluN2A and Glu2NB, respectively, researchers have had access to great pharmacological tools that can identify whether one or both NMDAR subunits are present in their system of interest. Nevertheless, these molecules have intermediate effects on triheteromeric receptors (Hansen et al., 2014), meaning interpretations of subunit composition in native receptor complexes should be made cautiously.

4.4.3 The ATD in receptor assembly

The first structures of isolated AMPAR (GluA2), KAR (GluK2), and NMDAR (GluN2B) ATDs were all reported within a short span in 2009 (Jin et al., 2009; Kumar et al., 2009; Karakas et al., 2009). The AMPAR and KAR ATDs both crystallized as dimers, with each subunit displaying a bi-lobed, or clamshell-shaped organization (Jin et al., 2009; Kumar et al., 2009). The bi-lobed form was not entirely surprising, given that earlier homology modeling had suggested the iGluR ATD resembles the mGluR and LIVBP ligand-binding sites (O'Hara et al., 1993). At the same time, there was little support for conserved ligand recognition, because of poor sequence conservation at key amino acid-binding residues, as well as several structural features hindering domain closure (Jin et al., 2009; Kumar et al., 2009). Consequently, the most interesting property of the ATD became its knack for dimerization. Consistent with earlier centrifugation experiments showing the GluA4 ATD and LBD formed dimers and monomers, respectively (Kuusinen et al., 1999), sedimentation analysis of the GluA2 and GluK2 ATDs indicated their monomer-dimer dissociation constants were orders of magnitude lower than

LBDs of the same subunits (Jin et al., 2009; Kumar et al., 2009). It has therefore been hypothesized that the ATD might facilitate the initial dimerization step during assembly of the tetrameric receptor complex (Gan et al., 2015). That being said, the structural template for tetramerization is likely elsewhere (i.e. the TMD, see Gan et al., 2016), since the ATD cannot tetramerize on its own (Zhao et al., 2012).

A more refined interpretation of the ATD is that it biases AMPAR assembly in favour of specific subunit combinations, explaining the predominance of heteromeric receptors at the synapse (Henley & Wilkinson, 2016). This interpretation originated from investigation of AMPAR/KAR chimeras, from which it was concluded that a mismatched ATD region can prevent co-assembly of otherwise similar subunits (Lueschner & Hoch, 1999; Ayalon & Stern Bach, 2001). However, much more clarity was provided by the sedimentation analysis of numerous isolated ATDs from AMPARs and KARs. Amongst single AMPAR subtypes, the K_d values of ATD dimerization differ considerably between GluA1 (~100 nM), GluA2 (< 10 nM), and GluA3 (> 1 μM) (Rossmann et al., 2011; Zhao et al., 2012). However, the K_d for heterodimerization is reduced to around 1 nM for both GluA1/GluA2 and GluA2/GluA3 heteromers (Rossmann et al., 2011), implying that neither GluA1 or GluA3 would be likely to assemble as a homomer in the presence of GluA2 subunits. Perhaps not coincidentally, it has been argued that most, if not all, AMPARs at the CA1 hippocampal synapse are GluA1/GluA2 (80%) or GluA2/GluA3 (15%) heteromers (Lu et al., 2009). Similarly, GluK2/GluK5 heteromers have been described as the most common KAR complex in the brain (Petralia et al., 1994), and the ATD heterodimer comprised of GluK2 and GluK5 has a lower K_d value than homodimers of either subunit (Kumar et al., 2011).

Looking beyond the formation of pore-forming subunits, a few studies have found that the iGluR ATD might also influence assembly of multi-protein complexes at excitatory synapses. In one case, the ATD of GluA2, but not GluA1, directly bound to N-cadherin, an interaction which promoted spine formation in cultured hippocampal neurons -even if the region following the ATD was replaced by another transmembrane protein (Saglietti et al., 2007). Likewise, neuronal pentraxin, a lectin (carbohydrate-binding) protein expressed on axons, colocalized with and clustered neuronal GluA4 AMPARs, unless the ATD was truncated (Sia et al., 2007). A similar role has been proposed for galectins (another lectin-family member), based on their slowing of AMPAR and KAR desensitization (Copits et al., 2014). In these cases, galectin modulation appears to be proportional to the number of N-glycosylation sites, which introduce oligosaccharides to the ATD of AMPARs and KARs (Garcia-Nafria et al., 2016).

4.4.4 Mechanism of allosteric inhibition of NMDARs by the ATD

The initial GluN2B ATD structure was equally closed in the apo and zinc-bound forms (Karakas et al., 2009). However, the differential accessibility of crosslinking reagents to the GluN2A ATD cleft in the presence of zinc was previously used to propose an ion-induced closure of the ATD lobes (Paoletti et al., 2000). Corroborating this idea, luminescence resonance energy transfer (LRET) experiments (Sirrieh et al., 2013) and MD simulations (Dutta et al., 2012) have reported ATD cleft closure with zinc present.

A similar structural mechanism is also thought to account for ifenprodil inhibition. The first dimeric crystal structures of the NMDAR ATD were comprised of GluN1 and GluN2B subunits, and included inhibitory molecules (i.e. ifenprodil) bound at the dimer interface -as it turned out, ATD dimerization only occurred when both GluN1 and GluN2 subunits were present (Karakas et al., 2011). Because there was not yet an open ATD structure, it was difficult to

confirm that ifenprodil caused cleft closure, though LRET studies again concluded the molecule reduced the distance between the ATD lobes (Sirrieh et al., 2015). Only recently have non-inhibited, though intact, structures been obtained using cryo-EM, and reiterated the lobe-closing effects of ifenprodil and related compounds (Zhu et al., 2016; Tajima et al., 2016).

4.5 Insights from intact iGluR structures

4.5.1 The first intact AMPAR and NMDAR structures

The first nearly full-length or "intact" iGluR crystal structure was published as a twelve (in-text) figure *Nature* article in 2009, and provided a wealth of new information regarding the arrangement of subunits, while offering hints at the structural basis of activation. The structure itself was a GluA2 tetramer, captured at 3.6 Å resolution in a closed-channel state, bound by a competitive antagonist -though it also had a truncated ATD-LBD linker, a deleted CTD, and many individual mutations. Notably, the receptor is tall (180 Å) and Y-shaped, with asymmetry above the level of the TMD. The A/B and C/D subunit pairs form ATD dimers, but the B and D subunits "cross-over" to form closely packed pairs of LBD dimers comprised of A/D and B/C subunits. To recover radial symmetry at the pore, the LBD-TMD linkers differ considerably between subunits, especially in the TM3-S2 linker, which is extended to reach the distal B and D subunit LBDs, but compressed to connect with the more proximal A and C subunit LBDs (Sobolevsky et al., 2009).

For several years, no additional atomic resolution structures were available, indicative of the difficulty in purifying and crystallizing intact membrane proteins. Yet in 2014, two intact diheteromeric NMDARs were reported in agonist-bound, though allosterically-inhibited states. These receptors contained GluN1 and GluN2B subunits, arranged in the respective A/C and B/D positions of the GluA2 tetramer. The ATD and LBD layers were also more compressed relative

to GluA2, taking on a "hot-air balloon" shape (Karakas & Furukawa, 2014; Lee et al., 2014). At this point there was a reference structure for both the AMPAR and NMDAR subfamilies, but not much indication of the conformational changes accompanying activation and/or desensitization. The next steps forward were made largely with the help of cryo-EM imaging.

4.5.2 Comparison of intact structures in distinct conformational states

The earliest images of the tetrameric iGluR were actually obtained using single particle cryo-EM, but above 20 Å resolution they were sufficient only to resolve a "dimer of dimers" architecture for the apo state (Safferling et al. 2001; Tichelaar et al. 2004). Native AMPAR complexes were also imaged in multiple conditions, distinguishing unliganded and glutamate-bound conformations to develop the idea that the compact organization of the ATD is lost during desensitization (Nakagawa et al. 2005; Nakagawa et al., 2006). In contrast, some cryo-EM derived models of unliganded GluA2 receptors suggested a compact ATD, yet separate LBD dimers (Midgett & Madden, 2008; Midgett et al. 2012), which seemed to be at odds with the first Y-shaped crystal structure (Sobolevsky et al., 2009). For GluK2 KARs, cryo-EM mapping of its resting and desensitized states suggested the LBD layer is formed from two, closely situated dimer pairs that separate into isolated subunits as desensitization proceeds (Schauder et al., 2013). A higher resolution of this process (~ 10 Å) was achieved in a follow-up study, combining GluA2 and GluK2 cryo-EM structures (Meyerson et al., 2014). This work coincided with two similar papers from the lab of Eric Gouaux (Durr et al., 2014; Chen et al., 2014), which together put forward a relatively consistent activation and desensitization mechanism for intact (non-NMDAR) iGluRs (**Figure R7**).

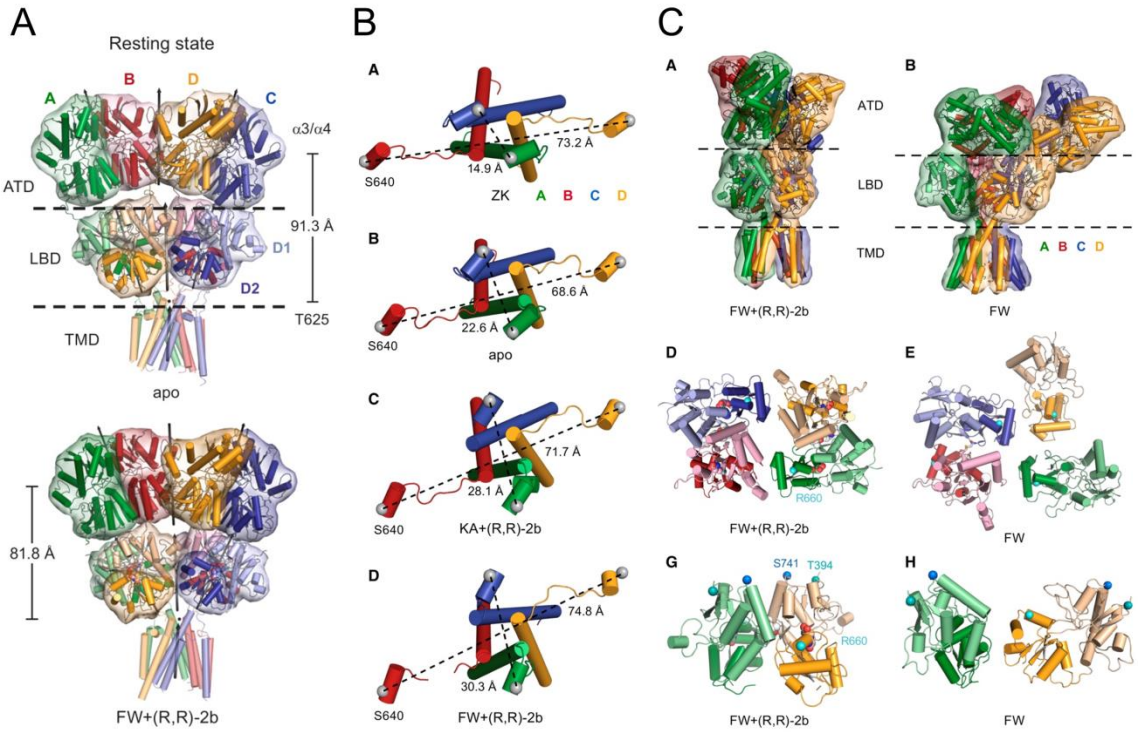

Figure R7. Insights into AMPAR/KAR gating from intact receptor structures.
(A) Structures of GluA2 in the apo state (top), as well as a "pre-open" state, with the partial agonist fluorowillardiine (FW) and a modulator (R,R-2b) that reduces desensitization (bottom). The height of the extracellular layers is compressed in the pre-open state. (B) Top view of the LBD-TMD (S2-TM3) linkers from antagonist-bound (ZK), apo, and pre-open structures. The separation distance increases between the A/C and B/D subunit linkers in the pre-open state, suggesting a means to pull open the channel pore. (C) Side view of FW-bound pre-open (with modulator) and desensitized (without modulator) structures (top), as well as a top view (middle) and side view (bottom) of their LBD layers. Note the extreme rotation of subunit D in the desensitized conformation. Adapted from Durr et al., 2014.

In brief, agonist-bound AMPAR structures exhibited closure of the agonist-binding cleft, as well as 5 - 20 Å of vertical compression in the ATD and LBD layers, when compared to apo or antagonist-bound states. Structures that included allosteric modulators -to inhibit desensitization- together with agonists (referred to as "pre-open" or active) featured an expansion of the LBD-TMD linkers (Durr et al., 2014; Chen et al., 2014), thought to generate the mechanical force that pulls open the channel pore (Kazi et al., 2014). Meanwhile, structures bound by agonists without modulators were classified as desensitized, and they featured variable

LBD dimerization. In the GluK2 desensitized state, both dimers were ruptured, with an extreme 125° rotation of the distal B/D subunits relative to the active state (Meyerson et al., 2014). Likewise, for GluA2, a similar 105° rotation was seen in one desensitized dimer, though the other dimer was less disrupted, having only moderate separation of the D1-D1 interface (Durr et al., 2014). No such rotations occurred for the ATD, as intact dimers were present in both desensitized GluA2 and GluK2 receptors. Yet in GluA2 the ATD dimers appeared able to bend downward and visit multiple conformations, while in GluK2 they remained rigidly upright (Durr et al., 2014; Meyerson et al., 2014). Of course, to become accepted mechanisms these structural rearrangements must be corroborated by additional evidence, such as functional tests on receptors where dynamic motifs are mutated or restricted from movement. Some headway has been made in this regard, as crosslinks introduced at the LBD "dimer-dimer interface" have supported the closely packed arrangement seen in the original Y-shaped AMPAR tetramer (Sobolevsky et al., 2009), but also suggest a lack of flexibility induced by such crosslinking can affect both activation and desensitization (Yelshanskaya et al., 2016; Baranovic et al., 2016).

More recent structures of intact AMPARs have painted a more complex picture of gating than was suggested from the initial studies of 2014. Specifically, another agonist-bound crystal structure showed only 2 Å vertical compression compared to the antagonist-bound state (Yelshanskaya et al., 2014). In addition, cryo-EM structures of the first AMPAR heteromers (in the apo state) more frequently adopted an O-shaped conformation (Herguedas et al., 2016), featuring separated LBD dimers that were reminiscent of earlier EM reconstructions (i.e. Midgett et al., 2012), rather than the Y-shaped crystal form. Perhaps more puzzling was that one model of the apo state contained a single subunit that swung outward from the LBD layer, in a manner reminiscent of the rotation seen in "desensitized" structures (Herguedas et al., 2016). Despite

these unexplained discrepancies, much was learned from the 2:2 subunit stoichiometry of the heteromer, for which GluA2 subunits resided in the A/C positions, while GluA3 subunits were in the B/D positions (Herguedas et al., 2016). More insight into the gating contribution of specific subunit positions (i.e. A/C vs B/D) may be gained from recent cryo-EM structures of active and non-active, agonist-bound NMDARs (Zhu et al., 2016; Tajima et al., 2016). It appears from these GluN1/GluN2B structures that the opening of the ATD cleft and rotation of subunits along the LBD dimer-dimer interface occur in a concerted manner to produce activation (Tajima et al., 2016). The latter movement is somewhat distinct from the rolling apart of the dimer-dimer interface measured during AMPAR activation (Durr et al., 2014).

As the structural study of iGluRs approaches the twenty year anniversary of the first crystallized LBD, several hurdles remain to be overcome. An obvious initial step involves the elucidation of a confirmed, open-channel structure, which might exhibit additional conformational changes beyond those already described for “pre-open” states. Equally clear is the need to obtain more structures of existing states to resolve inconsistencies in the published literature, and help formulate a refined interpretation of the gating mechanism for intact receptors. Whether such inconsistencies represent genuine variability in structure or stem from artifacts caused by protein processing should be resolved. Finally, as of yet there are no atomic resolution structures of iGluR-auxiliary protein complexes, other than those containing TARPs. It will be difficult to fully appreciate the numerous ways in which different auxiliary proteins modulate gating without structurally clarified pictures of their association.

4.6 The transmembrane region (TMD)

4.6.1 Overview

The TMD is comprised of four transmembrane regions, of which TM1 and TM4 reside on the outside of the pore, the TM2 re-entrant loop forms the pore, and TM3 lines the upper segment of the permeation pathway (Sobolevsky et al., 2009). The precise location of the selectivity filter is the segment immediately following the Q/R site, from which TM2 bends back toward the intracellular face of the membrane (Kuner et al., 2001), though structurally it is unresolved, except through homology modelling. The filter was identified, in part, because cysteine mutagenesis around the Q/R site rendered channel currents vulnerable to reduction by cysteine-reactive methanethiosulfonate compounds. In addition, at the residue suspected as the narrowest segment of the pore -two positions after the Q/R site- mutation greatly reduced the permeability of large organic cations (Kuner et al., 2001). Interestingly, iGluRs are permeable to a range of different-sized monovalent cations from lithium to cesium, though non-NMDARs can even pass some organic cations like tris(hydroxymethyl)aminomethane (Tris), resulting in estimates of minimal pore diameter of 5.5 Å for NMDARs (Villaroel et al., 1995) and 7.5 to 8.0 Å for AMPARs and KARs (Burnashev et al., 1996). These diameters are somewhat counter-intuitive, because NMDARs generally have a greater single-channel conductance (~ 40-50 pS, Paoletti et al., 2013) than AMPAR and KAR pore-forming subunits (< 30 pS, i.e. Swanson et al., 1996; Swanson et al., 1997). By the same token, NMDAR permeability to divalent calcium ions is about three-fold greater (~10% fractional current) than for AMPARs, even when the Q/R site is unedited (Burnashev et al., 1995). The molecular basis of this high permeability is unclear, though one hypothesis argues for additional divalent ion-binding sites in the NMDAR pore,

rather than greater pore diameter or the presence of an asparagine at the Q/R site (Wollmuth & Sakmann, 1998).

4.6.2 The Q/R site: polyamine block, and lipid inhibition

An additional role for the Q/R site was discovered in 1995, when a number of papers reported that the inward rectification of Q/R unedited (non-GluA2) AMPARs and KARs (Verdoorn et al., 1991) was due to channel block by intracellular polyamines (Kamboj et al., 1995; Koh et al., 1995; Bowie & Mayer, 1995; Donevan & Rogawski, 1995). The extent of rectification in whole-cell recordings was also consistent with estimates of free spermine and spermidine from other mammalian cells (~ 10-100 μM, Watanabe et al., 1991). Through further analysis of polyamine interactions at iGluRs it was found that the compounds could bind to receptors in a closed state (Bowie et al., 1998), but that activation -especially repetitive activation- would relieve this closed-channel block (Rozov et al., 1998). The second observation proved to be important in cortical neurons, where polyamine unblock was found to counteract the reduction in AMPAR-mediated EPSC amplitude typically observed during a paired-pulse protocol (Rozov & Burnashev, 1999). Though the co-expression of several auxiliary subunits has since been shown to reduce AMPAR and KAR polyamine block in recombinant systems (i.e. Soto et al., 2007), there is certainly abundant evidence that the profile of synaptic glutamate-evoked currents is still affected by polyamines at relevant physiological potentials.

As with internal polyamines, externally applied fatty acids have also been shown to inhibit neuronal AMPARs and KARs, depending on their Q/R editing status (Huettner, 2015). The first reports of this effect described how arachidonic acid, a constituent of cell membranes, could attenuate neuronal AMPAR responses, though inhibition had a relatively slow onset over several minutes (Kovalchuk et al., 1994). A similar, delayed reduction of KAR responses was

also observed, though it could be "washed out" by the application of bovine serum albumin (BSA) to bind fatty acids (Wilding et al., 1998). Given that KAR inhibition occurs in a voltage-independent manner (Wilding et al., 1998), it is noteworthy that increased susceptibility to inhibition occurs for both Q/R edited receptors (Wilding et al., 2005) and mutant receptors with a lipid-facing arginine residue introduced elsewhere in the pore-lining region (Wilding et al., 2008). The observations above suggest that fatty acids are not likely to act as channel blockers, but perhaps integrate into the membrane, altering the lipid environment around the TMD (Huettner, 2015). How the composition of endogenous membrane lipids alters iGluR activity is an area ripe for future investigation.

4.6.3 Role in assembly and trafficking

Similar to how the ATD is perceived as a "dimerization domain," an accumulating body of evidence indicates the TMD is important for the tetramerization of AMPARs. This idea was spurred by biochemical experiments suggesting that Q/R editing hinders endoplasmic reticulum (ER) exit and tetramerization (Greger et al., 2002; Greger et al., 2003). However, functional currents can be obtained from GluA2(R) receptors (i.e. Burnashev et al., 1992; Kato et al., 2008), meaning the Q/R site is not a critical factor for assembly on its own. A more drastic manipulation involving the truncation of GluA1 just prior to TM4 revealed that the final transmembrane segment -but not the CTD that follows- must be present for detectable surface expression (Salussolia et al., 2011). Because TM4 does not form the channel pore, and is actually absent in some functional, prokaryotic iGluRs (Chen et al., 1999), the idea of removing it was not such a crazy one. Moreover, TM4-lacking GluA1and GluA2 complexes were each detected as dimers, and not tetramers, using blue native-polyacrylamide gel electrophoresis (BN-PAGE) (Salusollia et al., 2013). To address whether the TMD alone is sufficient for tetramerization, a recent study

utilized a GluA1 construct without the ATD, LBD, and CTD some cases, leaving only the TM segments with a short linker between TM3 and TM4. Remarkably, even without the extracellular domains the truncated receptor still arrived at the plasma membrane, and inserted correctly, while tetramers were detected from the TMD portion alone (Gan et al., 2016). Assessed together, these experiments suggest that the "directions" for iGluR tetramerization are embedded in the TMD structure, and that regions such as the ATD merely facilitate the oligomerization process in full-length proteins.

4.7 The carboxyl terminal domain (CTD)

4.7.1 Overview

The fact that the CTD has the most sequence divergence between iGluR subunits (Traynelis et al., 2010) is likely related to the absence of highly conserved gating machinery and transmembrane regions. On this point, the observation of current responses from several iGluR subtypes with a deleted C-terminal tail (GluA1, Salussolia et al., 2011; GluK2, Yan et al., 2004; GluN1, Krupp et al., 1999; GluN2A, Kohr & Seeburg, 1996) has established that the CTD is largely non-essential for channel activity. However, CTD truncation also results in reduced surface expression for AMPAR (GluA1; Shen et al., 2000; GluA2 and GluA4, Coleman et al., 2003), as well as KAR (GluK2, Yan et al., 2004) subunits in heterologous cells. The CTD can therefore be described as a regulatory region that controls receptor trafficking and mediates association with a diverse set of scaffolding and signaling proteins on the intracellular side of the membrane (Mayer & Armstrong, 2004). This regulation begins with a number of splice variants that uniquely alter the C-terminal sequences of various AMPAR, KAR, and NMDAR subunits (reviewed in Traynelis et al., 2010). For the most part, these variants are not even mentioned when describing the cDNAs used for recombinant experiments, though for the results chapters

contained in this thesis, it should be noted that the common, short form of GluA2 (Kohler et al., 1994) and long form of GluK2 (Gregor et al., 1993) were studied. The role that CTD structure, protein interactions, and post-translational modifications play in receptor expression and signaling will be summarized in the following paragraphs.

4.7.2 Structural insights

What little is known about CTD arrangement in the cytoplasm has been learned from NMDARs, possibly because they have a more extensive intracellular domain to work with. Analysis of a soluble fragment from the distal GluN2B CTD reaffirmed that the region was intrinsically disordered (Choi et al., 2011a), matching the prediction of prior sequence analysis (Ryan et al., 2008). Moreover, single molecule fluorescence resonance energy transfer (smFRET) has allowed detection of conformational switching in the GluN2B CTD (Choi et al., 2011a), with the polypeptide achieving a more extended conformation after phosphorylation (Choi et al., 2011b). Whether these dynamics occur in intact receptors is unclear, as the CTD has been cut from crystallized constructs of "intact" AMPARs (Sobolevsky et al., 2009) and NMDARs (Karakas & Furukawa, 2014; Lee et al., 2014), on account of its disordered nature. The only atomic resolution fragment of the CTD is a calmodulin-bound motif from the GluN1 CTD (Ataman et al., 2007). Based on such scant information, iGluR CTDs have often been illustrated as long, winding strings with many associated proteins.

4.7.3 Protein-protein interactions

Too many CTD-interacting partners have been identified for iGluR subunits to mention them all here, but a few different subsets of proteins that interact with AMPARs and KARs are worth noting. A major class of iGluR binding partners includes the PDZ proteins, so named for their PDZ domains, which facilitate interactions with C-terminal motifs (PDZ ligands) on other

proteins, often in the postsynaptic density of excitatory synapses (Kim & Sheng, 2004). Multiple AMPAR subunits interact with PDZ proteins known as *protein interacting with C kinase* (PICK1) (Dev et al., 1999) and *glutamate receptor-interacting protein* (GRIP) (Dong et al., 1997). PICK1 is thought to modulate AMPAR recycling, leading to different subunit compositions at the synapse, whereas GRIP is thought to anchor AMPARs at the synapse (Henley & Wilkinson 2016). Another PDZ protein, postsynaptic density protein 95 (PSD-95), is a postsynaptic scaffold, within the membrane-associated guanylate kinase (MAGUK) family (Kim & Sheng, 2004). PSD-95 interacts directly with KARs (Garcia et al., 1998), but not AMPARs, though it forms interactions with TARPs that are critical for delivering AMPARs to the synapse (Schnell et al., 2002). Through additional binding partners, PSD-95 can link iGluR complexes to the actin cytoskeleton (Zheng et al., 2011), though AMPAR and KAR subunits can also interact directly with cytoskeletal-binding proteins like 4.1N, which enhance their surface expression (Shen et al., 2000; Copits & Swanson, 2013). More broadly, AMPAR subunits can even associate with enzymes like N-ethylmaleimide-sensitive factor (NSF) (Nishimune et al., 1998; Osten et al., 1998), which increases EPSC amplitude through yet unknown mechanisms when coupled to GluA2 (Henley & Wilkinson, 2016).

4.7.4 Post-translational modifications

A number of post-translation manipulations, including phosphorylation, palmitoylation, and SUMOylation, also regulate iGluRs via their CTDs. AMPAR and KAR CTDs generally possess multiple phosphorylation sites that are the targets of different kinases, such as protein kinases A and C (PKA and PKC), as well as CAMKII (Traynelis et al., 2010). Considering only the GluA1 subunit, which has a relatively long intracellular C-terminal (for an AMPAR), phosphorylation can promote interactions with other proteins, or have direct functional effects on

the channel itself. For example, PKC phosphorylation increases association with the binding partner 4.1N, to drive membrane insertion during plasticity (Lin et al., 2009), whereas CAMKII phosphorylation increases the conductance of receptors expressed recombinantly (Derkach et al., 1999) and in cultured neurons (Kristensen et al., 2011). All AMPAR subunits can also undergo palmitoylation, the covalent attachment of palmitic acid (a saturated fatty acid) to a cysteine residue, which negatively regulates plasma membrane expression by decreasing association with 4.1N (Hayashi et al., 2005). Another process known as SUMOylation similarly regulates GluK2 KARs. SUMOylation occurs when a substrate binds the small ubiquitin-like modifier (SUMO) protein, and in the case of GluK2, this protein reduces KAR-mediated EPSC amplitudes by promoting endocytosis (Martin et al., 2007).

5. AMPAR AUXILIARY PROTEINS

5.1 Definition of auxiliary subunits

What exactly is an iGluR auxiliary subunit? It has been appreciated for some time that VGICs generally consist of pore-forming α subunits, co-assembled with modulatory β subunits (Isom et al., 1994). Yet the first protein to be categorized as an LGIC auxiliary subunit was actually the TARP subunit γ2, a regulator of AMPAR trafficking and gating (Vandenberghe et al., 2005). As more iGluR interacting proteins were identified (**Figure R8**), it became important to clarify which ones serve as *bona fide* auxiliary subunits, as opposed to simply residing in the same signaling complex. In 2012, Susumu Tomita, who along with David Bredt was integral to the initial investigation of AMPAR-TARP complexes, defined criteria to assist in this regard. Proteins are considered auxiliary subunits if they cannot form a channel pore on their own (1), but interact directly with a pore-forming subunit (2) and modulate its trafficking and/or gating

properties in heterologous cells (3), as well as have some effect *in vivo* (4) (Yan & Tomita, 2012). During the last decade, there has been extensive investigation into the modulation of AMPARs by several classes of auxiliary proteins (described in this section), as well as KARs by NETO1 and NETO2 (Howe, 2015). In contrast, proteins proposed as "candidate" NMDAR auxiliary subunits (i.e. NETO1, see Ng et al., 2009) do not appear to form direct interactions with pore-forming subunits (Cousins et al., 2013), and as such their status is doubtful.

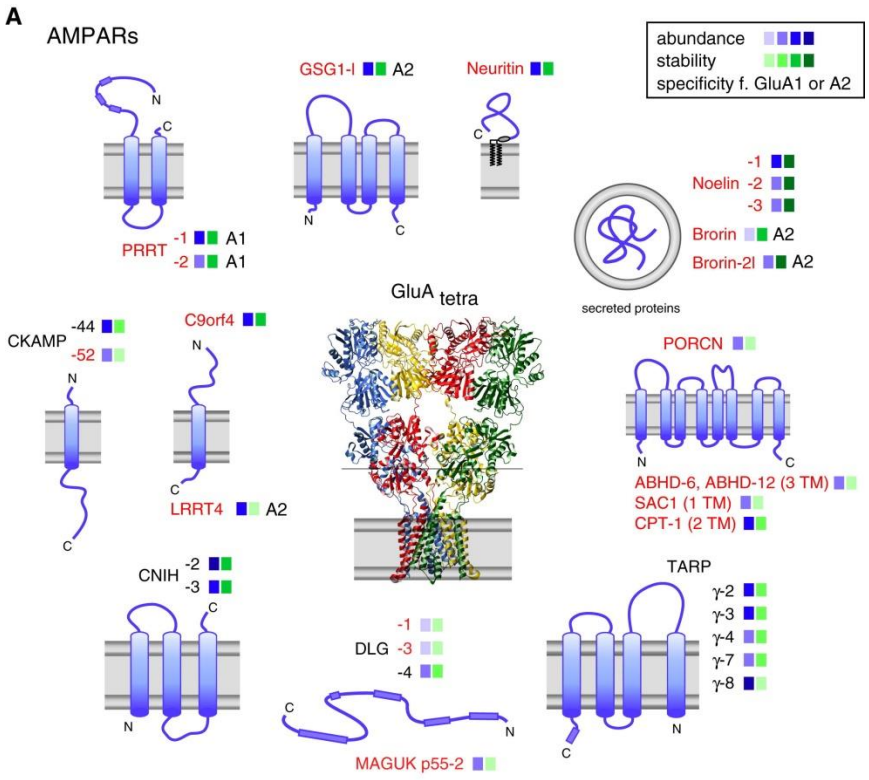

Figure R8. Protein constituents of native AMPAR complexes.
(A) The topology of numerous AMPAR-interacting proteins is shown, along with their relative abundance and stability in receptor complexes. Unlike the AMPAR itself (centre), there are no atomic resolution structures yet available for any AMPAR auxiliary subunit apart from TARP γ2. Adapted from Schwenk et al., 2012.

5.2 Transmembrane AMPA receptor regulatory proteins (TARPs)

5.2.1 The stargazer mouse and stargazin protein

The first known auxiliary protein of AMPARs was originally referred to as stargazin, a name derived from the *stargazer* mutant mouse, noted for its absence seizures -during which it seemingly stared into space- and ataxia (Noebels et al.. 1990). The gene disrupted in the stargazer mouse was later isolated (Letts et al., 1998), and deemed to belong within the same family as the gamma (γ1) modulatory subunit of voltage-gated calcium channels (Jay et al., 1990; Singer et al., 1991). Supporting this classification, both amino acid sequences displayed a similar topology, comprised of four transmembrane segments (Letts et al., 1998). Furthermore, recombinantly expressed stargazin protein (γ2) was found to produce a leftward shift the inactivation curve of calcium channels (Letts et al., 1998). The discovery of genes encoding additional γ subunits (Burgess et al., 1999; Burgess et al., 2001) led to the grouping of γ2, 3, 4, and 8 based on a conserved TTPV amino acid motif at the intracellular C-terminal, while two smaller subgroups of γ1 and γ6, as well as γ5 and γ7 were formed. These divisions would later prove to be important, but for AMPARs, rather than calcium channels.

5.2.2 Reclassification of γ subunits

The first observation linking stargazin to iGluRs came from recordings of cerebellar interneurons in stargazer mice, where evoked responses from synaptic AMPARs were almost entirely absent (Hashimoto et al., 1999). Though, intriguingly, AMPAR mRNA expression was preserved throughout the cerebellum (Hashimoto et al., 1999) and somatic AMPAR responses were later shown to remain intact (Jackson & Nicoll, 2011). This functional deficit could be restored by transfecting stargazin into neurons, and combined with evidence for the synaptic colocalization and co-immunoprecipitation of GluA4 with stargazin (Chen et al., 2000),

suggested a role for the γ2 subunit in AMPAR trafficking. In contrast, there was no obvious impairment in calcium channel activity in stargazer cerebellar granule neurons (Chen et al., 2000). At around the same time, further investigation of recombinant calcium channels revealed that most gating parameters exhibited little or no change upon co-expression with γ2-4 subunits (Kang et al., 2001; Rousset et al., 2001; Moss et al., 2003), despite some biochemical evidence for the association of stargazin with pore-forming α subunits *in vivo* (Kang et al., 2001).

Following reports that stargazin dramatically increased GluA1 and GluA2 surface expression and current responses in oocytes (Chen et al., 2003; Yamazaki et al., 2004), it became clear that the protein had a special role in AMPAR biogenesis. In addition, those γ subunits most closely conserved with stargazin (γ3, 4, and 8) were also shown to rescue AMPAR currents in the stargazer mouse (Tomita et al., 2003), leading to their recognition as a full-fledged family of *transmembrane AMPAR regulatory proteins*, or TARPs. Protein expression of these "Type-I" TARP subunits was found to occur throughout the brain, with a predominance of γ2 in the cerebellum, γ3 in the cerebral cortex, and γ8 in the hippocampus (Tomita et al., 2003). Thus, an argument could be made that TARPs are of universal importance for native AMPARs, which are expressed ubiquitously in the CNS.

5.2.3 Functional modulation of AMPARs by TARPs

Any doubts about the primary role of stargazin were erased in 2005, when a flurry of papers officially established the protein as an auxiliary subunit of AMPARs. To begin with, stargazin co-migrated with a majority of native AMPAR complexes on BN-PAGE gels, unlike other synaptic proteins known to associate with iGluRs (Vandenberghe et al., 2005). The first cryo-EM images of native AMPAR complexes also possessed a broader TMD than expected, due to the association of TARPs in that layer (Nakagawa et al., 2005). Perhaps more

convincingly, numerous gating and permeation properties of recombinant AMPARs have been shown to be modulated by stargazin and other Type-I TARPs (**Figure R9**). Notably, deactivation and desensitization are slower, the relative efficacy of kainate versus glutamate is increased, the D-R curve is leftward shifted, and single-channel properties like conductance and burst length are increased (Priel et al., 2005; Tomita et al., 2005; Turetsky et al., 2005). More nuanced effects have since been reported, such as the conversion of quinoxalinedione antagonists (i.e. CNQX and DNQX) into weak partial agonists (Menuz et al., 2007), "resensitization" during long agonist pulses (Kato et al., 2007), a partial relief of polyamine block (Soto et al., 2007), a decrease in peak current potentiation by CTZ (Cho et al., 2007), channel entry into a high open probability gating mode during single-channel recordings (Zhang et al., 2014), and even recovery from desensitization that surpasses the initial response amplitude, or "superactivation" (Carbone & Plested, 2016). Importantly, these TARP-mediated effects are generally consistent with the biophysical properties of native AMPARs (reviewed in Kato et al., 2010).

On the whole, there is minor variability in the functional phenotype imparted onto AMPARs by the Type-I TARP subunits (Kott et al., 2007; Milstein et al., 2007), and they all generally modulate surface trafficking and the duration of channel gating in a positive manner (summarized in Jackson & Nicoll, 2011). For the Type-II subunits γ5 and γ7, which possess a shorter intracellular C-terminus, less modulation of AMPAR gating occurs, despite the fact that both can immunoprecipitate with AMPAR subunits from brain tissue (Kato et al., 2007). The γ5 subunit in particular was found to accelerate the deactivation and desensitization of recombinant GluA2 receptors (with no effect on GluA1), despite simultaneously increasing the current response (Kato et al., 2008).

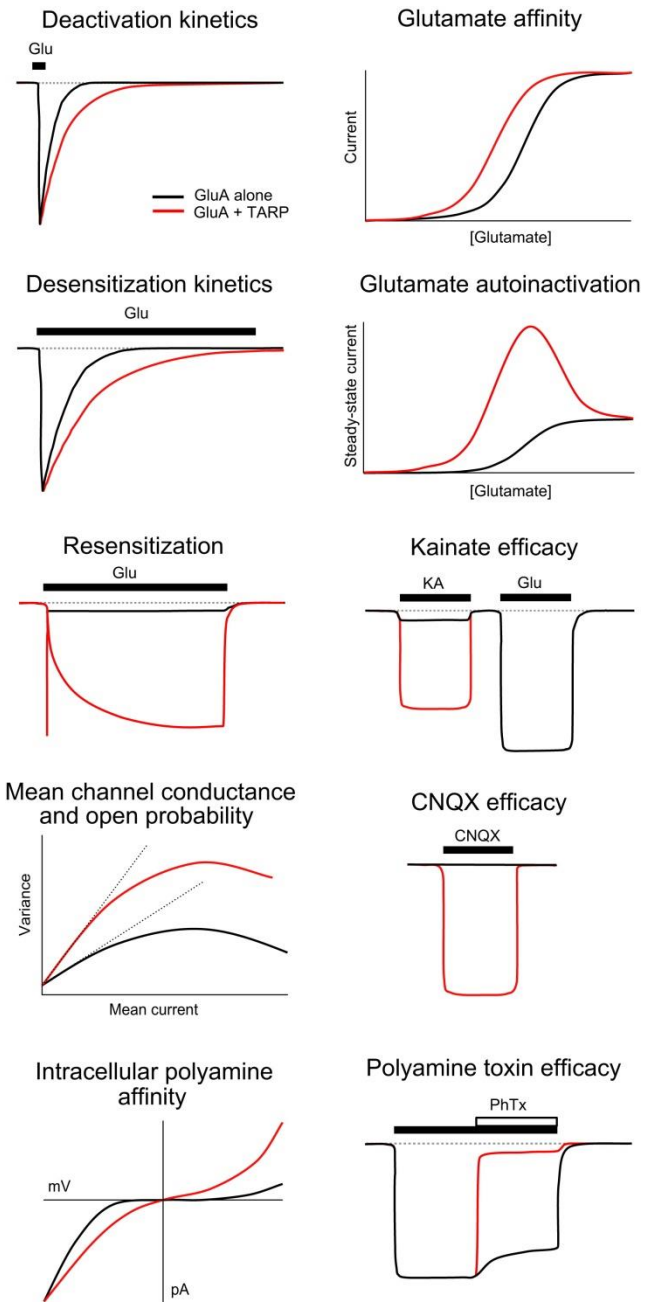

Figure R9. The effects of TARP association on AMPAR gating and permeation.
(A) The functional phenotype of various AMPAR gating and permeation properties, representative of pore-forming subunits expressed alone (black) or co-expressed with TARPs (red). These phenotypes can vary depending on the combination of AMPAR and TARP subunits expressed together. Adapted from Jackson & Nicoll, 2011.

5.2.4 AMPAR-TARP assembly and stoichiometry

One problem with the TARP subunit comparisons above is that much of variability in their modulation of AMPARs could be confounded by different affinities and/or stoichiometries between specific AMPAR and TARP subunits. The issue of subunit stoichiometry was clarified somewhat by the demonstration that AMPAR-TARP fusion proteins retain the same altered biophysical properties as observed during co-expression (Shi et al., 2009; Morimoto-Tomita et al., 2009), supporting the idea that one TARP subunit can associate for every pore-forming AMPAR subunit. Without the constraint of protein fusion, multiple techniques have suggested a variable stoichiometry of TARPs. Specifically, the molecular weights of purified AMPAR complexes detected on BN-PAGE gels (Kim et al., 2010) and the counting of fluorescent-tagged TARP subunits from single receptor complexes (Hastie et al., 2013) have led to estimates of between one and four TARPs per AMPAR tetramer. Such estimates have also been supported with new cryo-EM images of the GluA2-stargazin complex, as one group has reported one or two TARPs per receptor (Twomey et al., 2016), while the other has resolved a saturating load of four TARPs (Zhao et al., 2016).

Recent investigations of TARPs have started to provide insight into the structural basis by which they modulate AMPAR gating. The immunolabelling of TARP-bound AMPAR fragments from peptide arrays has suggested many extracellular locations, in both the ATD and LBD, may participate in their association (Cais et al., 2014). However, removal of the AMPAR ATD still permits functional modulation by stargazin (Tomita et al., 2007; Cais et al., 2014), meaning the LBD is likely to be the principal domain mediating extracellular interactions, if they occur. In agreement with this idea, stargazin was shown to induce domain closure of the

AMPAR agonist-binding cleft -presumably through some extracellular contact point- accounting for the increased efficacy of partial agonists (MacLean et al., 2014).

Whether AMPAR-TARP contact is maintained over time or more transient in nature remains to be fully resolved. It has been proposed that high concentrations of glutamate cause an "autoinactivation" effect, whereby TARPs dissociate from flop variant AMPARs following agonist binding/activation -producing a bell-shaped D-R curve at equilibrium- except when they are fused (Morimoto-Tomita et al., 2009). Alternatively, another group observed that AMPAR-TARP fusion did not affect autoinactivation, but that GluA2 flip receptors uniquely lacked the property (Semenov et al., 2012). Nonetheless, for synaptic AMPARs, tracked at the single-molecule level, glutamate appears to induce greater mobility, and the effect can be prevented by fusion to TARPs -suggesting that TARP uncoupling occurs (Constals et al., 2015). The spatiotemporal dynamics of the iGluR signaling complex -and its component proteins- will certainly be an interesting research area in the coming years.

5.3 Cornichons

The genetic locus of cornichon was originally identified from a screen of lethal mutations in *Drosophila* (Ashburner et al., 1990), and as such most early research on the protein was conducted in flies. The cornichon gene regulates anterior-posterior and dorsal-ventral pattern formation in developing fly embryos (Roth et al., 1995), though the protein product mediates export of the transmembrane growth factor *Gurken* from the ER (Bokel et al., 2006). The mammalian/human cornichon homolog (CNIH) and a related protein (CNIH-2) also assist the ER-mediated export of proteins in the transforming growth factor α (TGF-α) and epidermal growth factor families, respectively, during recombinant expression (Castro et al., 2007; Hoshino et al., 2007). Yet, despite these roles, and a topology including three transmembrane segments,

CNIH was not detected at the cell surface (Castro et al., 2007). As with stargazin, there were no initial reasons to implicate CNIH proteins in AMPAR biogenesis or signalling.

Mammalian CNIH-2 and CNIH-3 were eventually identified as AMPAR auxiliary subunits using high resolution mass spectrometry of AMPAR complexes that were purified from the rat brain (Schwenk et al., 2009). Remarkably, when recombinantly co-expressed with AMPAR subunits, CNIH-2 and CNIH-3 not only enhance receptor surface expression, but also slow desensitization and deactivation to a greater extent than the prototypical TARP subunit γ2 (Schwenk et al., 2009; Coombs et al., 2012). This effect on gating kinetics appears to be relevant at synapses, since the transfection or viral injection of CNIH-2 into cultured neurons can slow miniature EPSC (mEPSC) decay (Kato et al., 2010; Boudkkazi et al., 2014), while the viral infection of short hairpin RNA (shRNA) targeting CNIH-2 can accelerate the decay of EPSCs for some neuronal cell types (Herring et al., 2013; Boudkkazi et al., 2014). Moreover, a conditional knockout of both CNIH-2 and CNIH-3 greatly reduced the AMPAR-mediated EPSC amplitude and expression of LTP at the CA3-CA1 synapse, an effect that was linked to reduced GluA1 trafficking (Herring et al., 2013). As such, cornichon subunits play an important role in glutamatergic signaling in the brain, despite having a lower relative abundance than TARPs in AMPAR complexes (Schwenk et al., 2012).

Other TARP effects on AMPARs that are mimicked by cornichon co-expression include increased single-channel conductance and reduced channel block by polyamines (Coombs et al., 2012). In contrast, CNIH-2 is not as efficacious in increasing the kainate/glutamate current ratio (Shi et al., 2010), a trait that was exploited to demonstrate that CNIH subunits can reduce TARP stoichiometry in AMPAR complexes -a similar conclusion was reached from the molecular weight of migrating AMPAR complexes containing TARPs and/or CNIHs (Gill et al., 2011).

These observations suggest that TARP and cornichon subunits compete for the same association site on AMPARs, though it has been postulated that hippocampal AMPAR complexes contain four γ8 subunits with additional CNIH-2 or CNIH-3 subunits (Herring et al., 2013). Until precise sites of interaction on the AMPAR structure are pinpointed for each auxiliary subunit family, this matter may remain unresolved.

The regions of cornichon subunits responsible for regulating AMPAR activity are better understood than the motifs that they target. In the initial study linking AMPARs and cornichon subunits, the other two cornichon homologs, CNIH (or CNIH-1) and CNIH-4, were not detected in AMPAR complexes (Schwenk et al., 2009). Their reduced association with AMPARs was found to be the result of a missing peptide segment, found in the first extracellular loop of CNIH-2 and CNIH-3, which mediates both AMPAR interaction and gating modulation (Shanks et al., 2014). Consistent with its distinct secondary structure, CNIH-4 is now known to regulate the ER export of GPCRs (Sauvageau et al., 2014), a role more similar to that of CNIH-1.

5.4 Other auxiliary protein families

Germ cell-specific gene 1-like (GSG1L) is another four-pass transmembrane protein found in native AMPAR complexes (Schwenk et al., 2012; Shanks et al., 2012), and shown to associate with multiple AMPAR subunits *in vitro* (Shanks et al., 2012). When co-expressed with GluA2, GSG1L slows desensitization and recovery from desensitization (Shanks et al., 2012), though interestingly, unlike TARPs and cornichons it reduces single-channel conductance and enhances polyamine block (McGee et al., 2015). In neurons, GSG1L impairs membrane trafficking to reduce the amplitude of AMPAR-mediated EPSCs and mEPSCs (McGee et al., 2015; Gu et al., 2016).

The protein encoded by *synapse differentiation-induced gene 1* (SynDIG1) localizes at excitatory synapses and co-immunoprecipitates with GluA2 *in vitro* (Kalashnikova et al., 2010), though recombinant co-expression was found to have no effect on AMPAR response amplitudes or gating kinetics (Lovero et al., 2013). In neurons, the overexpression and shRNA knockdown of SynDIG1 respectively increase and decrease AMPAR EPSC amplitude. This appears to be a reflection of SynDIG1 regulating synapse number, because there was a much greater effect of the shRNA to reduce mEPSC frequency versus amplitude (Kalashnikova et al., 2010; Lovero et al., 2013).

Another class of AMPAR auxiliary proteins contains members interchangeably known as *cystine-knot AMPA receptor-modulating proteins* (CKAMPs) or Shisa proteins (Haering et al., 2014). So far, four CKAMP members have been shown to associate with AMPARs and/or influence their gating. CKAMPs 39, 44, 52, and 59 are all expressed in the brain, and possess a single-pass transmembrane topology with an intracellular PDZ domain-binding motif (Farrow et al., 2015). Two members (CKAMPs 44 and 52) have been specifically identified as co-localizing with AMPARs at excitatory synapses (von Engelhardt et al., 2010; Klaassen et al., 2016). Moreover, these CKAMPSs bind directly to both AMPAR subunits, as well as PSD-95, through which CKAMP44 is thought to promote the membrane trafficking of synaptic AMPARs, and CKAMP52 is thought to stabilize AMPARs in the postsynaptic density (Khodosevch et al., 2014; Klaassen et al., 2016). Biophysical investigation in recombinant systems has revealed variable effects on current amplitude, deactivation, desensitization, and recovery from desensitization, depending on the AMPAR and CKAMP subunits being expressed (Khodosevich et al., 2014; Farrow et al., 2015; Klaassen et al., 2016). Consistent with its effect to slow deactivation, the mEPSCs of CKAMP52 knockout mice had accelerated decay kinetics, but

amplitude and frequency were preserved (Klaassen et al., 2016). Meanwhile for CKAMP44, the first of its class to be characterized as an AMPAR auxiliary protein, no significant changes in mEPSC and EPSC properties, or LTP expression were seen in knockout mice (von Engelhardt et al., 2010; Khodosevich et al., 2014). Accordingly, more investigation will be needed to determine if any CKAMPs play a fundamental role in AMPAR physiology.

6. RATIONALE AND OBJECTIVES

The aim of my thesis research is to understand what structural interactions facilitate the activation of AMPARs and KARs in response to glutamate binding. In particular, I have focussed on the LBD as an important location for such interactions. When I first started my MSc/PhD studies, the lab had been exploring the functional consequences of KAR modulation by external ions, but there was less insight into their structural mechanism. After uncovering new details about the structural basis of KAR gating, I decided to explore whether similar rules governed the gating processes of AMPARs, the most closely related iGluR family member.

For the three results chapters that follow, a common approach was taken by my colleagues and me to explore structural influences on the function of KARs and AMPARs. Homomeric receptors were expressed recombinantly in mammalian cells to study them in isolation and minimize external factors that might affect their gating. The two subunits we selected for electrophysiological investigation were GluK2 (KAR) and GluA2 (AMPAR), owing to their excellent expression in HEK 293 cells, and the fact that both are the most abundant subunits from their subfamilies in the mammalian brain (Hollmann & Heinemann, 1994; Schwenk et al., 2014). Recordings of ion channel currents were performed in the outside-out patch configuration, limiting the size of the membrane to accommodate rapid and complete external solution exchange within a fraction of a millisecond (i.e. Franke et al., 1987). The rapid application of agonists was critical for studying receptors prior to and during the onset of deactivation and desensitization, which occur within milliseconds for most AMPAR and KAR subunits (Traynelis et al., 2010). Moreover, the outside-out patch configuration enabled us to interrogate receptors with a variety of harsh ionic conditions, which would be poorly tolerated by whole cells.

Another reason for studying GluA2 and GluK2 is that they have been the most favoured subunits amongst AMPARs and KARs, respectively, for structural characterization at atomic resolution (Mayer, 2011).Using high-resolution structures as templates; it was possible for us to design and incorporate numerous point mutations with the intent to measure specific effects on channel gating. We then re-evaluated those effects in the context of how they might alter certain structural properties of the receptor. However, it was often not enough to rely on existing structural images to understand the mechanisms underlying our observations, and new structural data were frequently required. We therefore collaborated with specialists in computational biochemistry (Phil Biggin, Oxford), structural biology (Tim Green, Liverpool and Jette Kastrup, Copenhagen) and single-molecule imaging (Michael Edwardson, Cambridge) to augment our electrophysiological data.

Chapter 1:

How allosteric ion binding is critical for KAR activation

Despite its name, this study did not initially examine allosteric ions, but rather began out of a desire to explain discrepancies in the single-channel behaviour of crosslinked (i.e. Y521C/L783C) GluK2 receptors. Previously, our lab had found that the "double-cysteine" receptor exhibited only brief, sporadic openings in response to glutamate (Daniels et al., 2013), despite the fact that its LBD dimer was constrained in a manner thought to prevent desensitization (Weston et al., 2006). We therefore set out with two objectives. First, we wanted to determine whether GluK2 D776K, another non-desensitizing mutant that forms cross-dimer interactions (Nayeem et al., 2009; Nayeem et al., 2011), behaved in a similar manner to Y521C/L783C at the single-channel level. Second, if D776K did exhibit a unique phenotype, what structural explanation could account for the differences between the mutants?

As it turned out, D776K and Y521C/L783C had very distinct single-channel phenotypes. Yet, because the mutant lysine of D776K occupies the GluK2 sodium-binding pocket (Nayeem et al., 2011), while the same pocket in the Y521C/L783C structure is vacant (Weston et al., 2006), we wondered whether this vacancy could account for the low open probability of the double-cysteine mutant. The question was appropriate, given the prior demonstration that removal of external sodium chloride rendered GluK2 receptors unable to activate (Wong et al., 2006). Through a combination of electrophysiology and MD simulations of other mutant receptors, we explored the relationship between occupancy of the sodium-binding pocket and the occurrence of GluK2 desensitization. This led us to develop a structurally inspired definition for the role of sodium in the KAR gating pathway.

Chapter 2:

Intra- and inter-protein interactions determine the time course of AMPAR activation

When the results in Chapter 1 were being written up for publication, we began a series of experiments to engineer a mutation into GluA2 that would have the same structural and functional phenotype as D776K did in GluK2. Namely, we wanted the mutant to form an electrostatic, cross-dimer tether and yield non-desensitizing current responses. Since the electronegative pocket where sodium binds to the GluK2 LBD is conserved in GluA2 (and other AMPARs), it seemed plausible that a positively charged amino group could be accommodated there as well. Of course, interactions at an allosteric site cannot be directly measured using electrophysiology, so we relied upon collaborators for structural and computational data to support our inferences in this regard. Once these experiments were underway, a crystal structure was published with a lithium ion bound in the GluA2 pocket (Assaf et al., 2013). It therefore became obvious to study whether external cations modulate GluA2 receptors as they do GluK2

receptors. Broadly speaking, the first objective of Chapter 2 was to characterize the role of the LBD apex in GluA2 gating, with an emphasis on the electronegative pocket.

In the first part of Chapter 2, we report mutations at the GluA2 LBD apex region that had severe negative consequences on receptor function. This result was not too surprising, given that the separation of subunits at the LBD dimer interface has been shown to underlie the structural transition to desensitization (Sun et al., 2002; Meyerson et al., 2014; Durr et al., 2014). However, we then explored this structural process in relation to AMPAR auxiliary proteins. Multiple classes of auxiliary proteins, notably TARPs and cornichons, are known to slow AMPAR desensitization, but the structural mechanism of this modulatory action was unknown. Taking advantage of mutant GluA2 receptors that lack key interactions across the LBD dimer interface and display accelerated desensitization, we asked whether their functional deficits could be rescued by co-expression with auxiliary proteins. We also searched for structural motifs where TARPs might associate with the extracellular domains of AMPARs to prolong channel activation, or otherwise oppose their structural inclination to desensitize.

Chapter 3:

External anions 'prime' the AMPAR response to glutamate

The final study contained in this thesis concerns the transitions that receptors undergo prior to agonist binding, as well as after. This focus on "pre-gating" came about in a rather different manner from the subjects of the previous two studies. Prior work from the lab had demonstrated that GluA1 gating (i.e. desensitization) was modulated by external anions (Bowie, 2002), though no structural explanation had ever been attributed to this effect. Interestingly, our collaborators had structural data identifying a novel anion-binding site in the GluA2 LBD that

could perhaps explain some of these functional effects. We therefore used mutagenesis to attempt to link the binding site with the phenotype.

By chance, we were also beginning to collaborate with a group that practiced atomic-force microscopy (AFM) imaging to study global changes in the conformation of intact iGluRs. We were curious whether ions, as allosteric modulators, might affect the conformational state of GluA2 in the absence of agonists or antagonists, something we could not measure electrophysiologically. Part of this interest stemmed from recent cryo-EM images of GluA2 receptors, which captured different conformations in the absence of any agonists or antagonists (Herguedas et al., 2016). The relevance of these apo state conformations, as well as how transitions between them might be brought about, remained unclear. Accordingly, we used AFM to test whether the substitution of external anion species could induce measureable changes in GluA2 quaternary structure, either in the presence or absence of glutamate. We were also interested if such changes might be related to the anion-binding site that had been unmasked in our novel crystal structure.

PART II:

RESULTS

CHAPTER ONE

How allosteric ion binding

is critical for KAR activation

FOREWORD TO CHAPTER ONE

As alluded to in the "rationale" section, the data included in this chapter were meant to follow-up a similar study by Bryan Daniels and Elizabeth Andrews (joint first authors) on the GluK2 mutant Y521C/L783C, which covalently bonds both sides of the LBD dimer interface. This time, the GluK2 mutant D776K would be the focus, as it had been shown to bridge the dimer interface by forming an electrostatic tether. Both studies were ground-breaking for our lab in that they contained (and emphasized) single-channel recordings, a technique rarely used to study KARs, owing to their low conductance. However, an advantage of this chapter coming along after the initial study was that the unique behaviour of Y521C/L783C and D776K channels could be contrasted. An important, though understated message within this chapter is that these mutant receptors have a similar functional phenotype in electrophysiological recordings of large channel "populations," but entirely different phenotypes at the level of single channels. This narrative was ultimately softened in order to emphasize how allosteric ions shape the gating of wildtype and mutant GluK2 receptors. As a manuscript, there was more strength in pairing electrophysiology and MD simulations to provide a structural interpretation for our data. Specifically, we conclude that sodium binding at the apex of the LBD dimer holds subunits together in an activated conformation, whereas mutations that hinder sodium binding lead to poorly activating receptors.

This chapter was submitted as a manuscript to *Nature Structural & Molecular Biology* in March of 2013, and rejected following peer review, though with an offer to consider a revised submission. The reviewers' concerns were in fact easily addressed by some experiments that had already been performed, as well as a more tempered interpretation of the data. After a second round of review the manuscript was accepted in July of 2013, published online in August, and

appeared in print in September. At the time of writing this thesis, the paper has been cited over twenty times, according to *Google Scholar*.

Article Title:

Defining the structural relationship between kainate-receptor deactivation and desensitization

ABSTRACT

Desensitization is an important mechanism that curtails the activity of ligand-gated ion-channels (LGICs). Although the structural basis of desensitization is not fully resolved, it is thought to be governed by the physicochemical properties of the bound ligand. Here, we show the importance of an allosteric cation binding pocket in controlling transitions between activated and desensitized states of rat kainate-type (KAR) ionotropic glutamate receptors (iGluRs). Tethering a positive charge to this pocket sustains KAR activation, preventing desensitization, whereas mutations that disrupt cation binding eliminate channel gating. These different outcomes explain the structural distinction between deactivation and desensitization. Deactivation occurs when the ligand unbinds before the cation, whereas desensitization proceeds if a ligand is bound without cation pocket occupancy. This sequence of events is absent from AMPA-type iGluRs, identifying cations as gatekeepers of KAR gating, a role unique among even closely-related LGICs.

INTRODUCTION

Structural and functional biologists have long sought to understand the mechanisms by which ligand-gated ion-channels (LGICs) respond to small chemical ligands and modulators. Seminal work established the general principle that LGICs are not only activated by biologically-derived molecules, such as the neurotransmitter acetylcholine (Katz & Thesleff, 1957), but they are also inactivated by prolonged exposure to these molecules through a process universally known as desensitization (Shelley & Cull-Candy, 2010). Since this work, almost all LGICs have been shown to desensitize. For example, desensitization is thought to shape signaling within the vertebrate central nervous system (CNS) by impacting fast chemical transmission mediated by ionotropic glutamate receptors (iGluRs), along with $GABA_A$ and glycine receptors (Jones & Westbrook, 1996). From all of this work, it has been concluded that the conformational events that lead to the occurrence of deactivation and the onset of desensitization are governed by the physicochemical properties of the bound ligand (Hille, 2001). In support of this, pioneering work on native AMPA-type iGluRs (AMPARs) has shown that even modest changes to the ligand structure have profound effects on the rates and degree of desensitization (Patneau et al., 1992).

During the last decade, structural and functional analyses of LGICs have revealed that the molecular basis of channel gating may be quite distinct for different ion-channel families (Flynn et al., 2001; Traynelis et al., 2010; Corringer et al., 2012). For the iGluR family, numerous mechanistic details of activation and desensitization have been identified and extensively commented upon (Madden, 2002; Wollmuth & Sobolevsky, 2004; Hansen et al., 2007). Following the elucidation of the ligand-binding domain (LBD) structure (Armstrong et al., 1998), a mechanism of iGluR desensitization was proposed, involving the separation of subunits that are assembled as dimers at the LBD (Sun et al., 2002). This mechanism has been supported

by additional crystal structures, which captured AMPARs in different functional states (Armstrong et al., 2006). Accordingly, efforts to engineer iGluR receptors that lack desensitization have focussed on constraining movement at the LBD dimer interface. From this, covalent crosslinking of the dimer interface has been shown to generate AMPAR and kainate-type iGluRs (KARs) that yield non-decaying currents upon sustained agonist application (Priel et al., 2006; Weston et al., 2006). Similar experiments on NMDA-type iGluRs have offered a more nuanced explanation of LBD function by studying the structural (Gielen et al., 2008) and single-channel effects (Borschel et al., 2011) of dimer crosslinking. Specifically, they propose that constricting the dimer interface primarily affects open-channel probability and not desensitization (Borschel et al., 2011). This observation suggests that a more in depth single-channel analysis of the mechanism of AMPAR and KAR desensitization is warranted.

Here, we set out to study the molecular basis of KAR desensitization by evaluating mutants that are proposed to block it (Weston et al., 2006; Nayeem et al., 2009). In both cases, the mutations are located in the GluK2 KAR LBD dimer interface, which not only is implicated in receptor desensitization, but also harbours binding pockets for both sodium and chloride ions (Plested & Mayer, 2007; Plested et al., 2008). Prior work from our lab shows that external ions are an absolute requirement for GluK2 receptor activation (Wong et al., 2006) yet their precise role in desensitization is unresolved (Plested et al., 2008; Bowie, 2010). Our present data identify that desensitization of KARs only proceeds if a ligand is bound without cation pocket occupancy, whereas deactivation occurs when the ligand unbinds before the cation. This sequence of events identifies external cations as pivotal in directing KARs into active states or long-lived desensitized states.

RESULTS

KARs desensitize with or without prior channel activation

To observe the microscopic behaviour of KAR desensitization, we excised outside-out patches from transfected mammalian cells expressing homomeric GluK2 receptors (see Methods). Using an ultrafast agonist perfusion system, we recorded single-channel events and then selected, for analysis, recordings where most responses corresponded to the conductance expected of a single channel (Zhang et al., 2009). Although the actual number of active receptors per patch is not known, these single-channel recordings nevertheless reveal the different routes taken by KARs before entering into desensitization. In most cases, rapid application of saturating glutamate (10 mM L-Glu) activated GluK2 receptors, which open to one of several conductance levels (**Figures 1.1A-1.1C**). Once in the open state, KAR channels typically closed within tens of milliseconds, and did not re-open for any measurable duration of time afterwards indicating that the receptor desensitized. Since desensitization is not thought to occur directly from the open state, it presumably proceeded shortly after channel closure. In agreement with this latter point, ensemble averages of single-channel sweeps exhibited decay times constants (6.49 ± 0.41 ms, n = 6) (**Figures 1.1D and 1.1E**) which were statistically indistinguishable from decay rates of macroscopic responses (6.28 ± 0.43 ms, n = 9, p = 0.74), re-affirming that the onset of KAR desensitization is approximated by the duration of channel activity.

In some cases, 10 mM L-Glu failed to elicit a measurable response during the entire 250 ms application (**Figure 1.1A**) corresponding to about 31.7 ± 5.5 % of the 525 total sweeps from five patches (**Figure 1.1E**). The apparent failure to respond to the agonist may reflect an intrinsic inability of L-Glu to reliably convert its energy of binding to activation. If this was the case, however, channel opening would eventually be observed, as the continued presence of L-Glu

would ensure that the energy threshold for activation would be overcome. Consequently, the inability of L-Glu to activate GluK2 receptors must represent the onset of desensitization without prior passage through the open state(s).

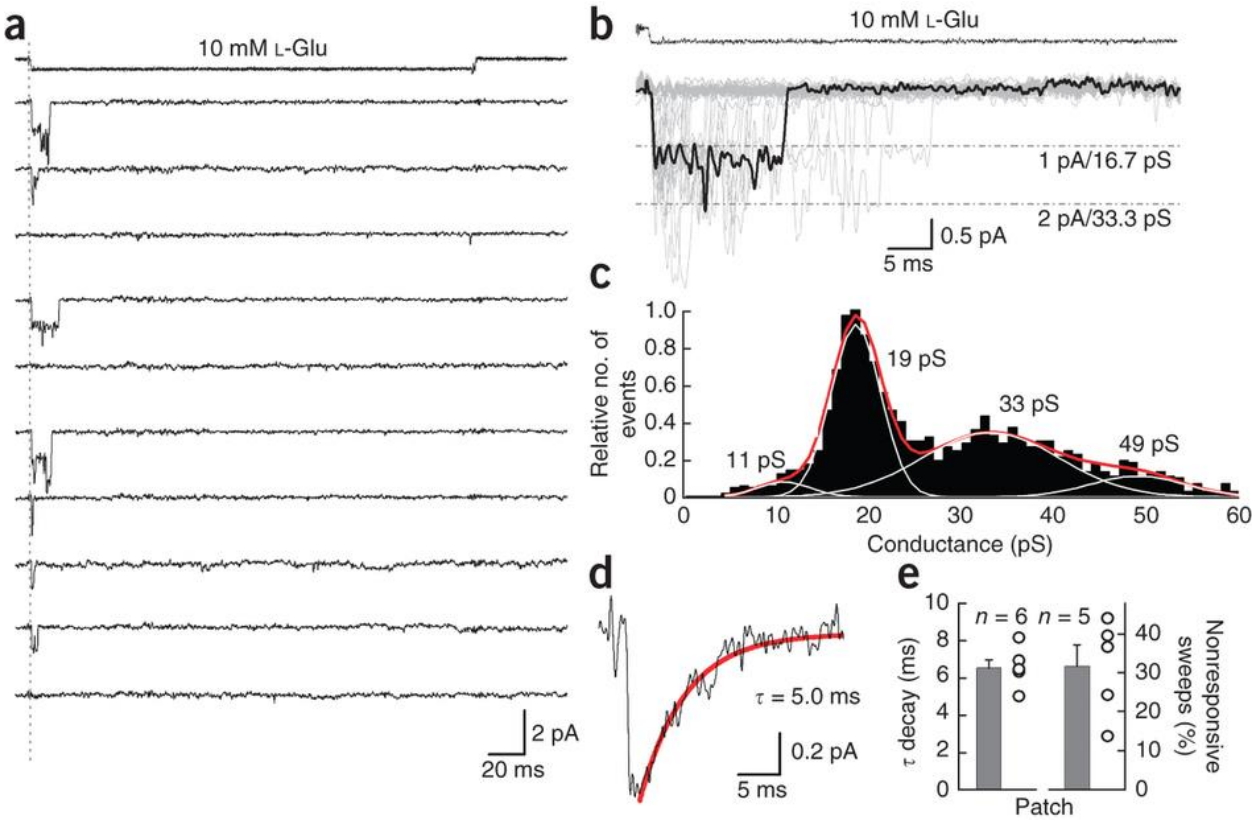

Figure 1.1 Kainate receptor desensitization occurs with or without channel activation
(**A**) Typical GluK2 receptor unitary current events elicited by 10 mM L-Glu (250 ms pulse duration) in an outside-out patch recording (Patch # 12212p1, -60 mV).
(**B**) Overlay of forty-five individual current records from the same patch as depicted in panel A. A typical opening elicited by L-Glu is shown in bold.
(**C**) GluK2 conductance distributions plotted following time course fitting.
(**D**) Averaging individual current records from the patch shown in panels A and B generated an ensemble response with a decay that could be fit by a single exponential function.
(**E**) Decay time constants of ensemble responses from several patches and (left) the fraction of L-Glu applications that did not elicit a measureable response from receptors (right).
Data are mean ± SEM from five or six independent patch experiments.

The discrete molecular events that bring about desensitization are currently unresolved. Several studies, however, identify the ligand-binding domain (LBD) dimer interface (Weston et al., 2006) and the cation binding site (Nayeem et al., 2009; Nayeem et al., 2011) in the conformational events that initiate KAR macroscopic desensitization. Whether one site or the other has a more direct effect on desensitization has yet to be directly studied. As discussed below, we examined this by studying the single-channel properties of two apparently non-desensitizing GluK2 receptors, namely the mutants D776K and Y521C/L783C.

The D776K mutation abolishes GluK2 receptor desensitization

The LBD dimer interface of wildtype GluK2 receptors contains binding sites for two sodium ions (purple) and a single chloride ion (green) (**Figure 1.2A**) (Plested & Mayer, 2007; Plested et al., 2008). Both GluK2 receptor mutations (D776K and Y521C/L783C) are also located at the LBD dimer interface (**Figures 1.2B and 1.2C**) where they are proposed to eliminate desensitization by constraining subunit movement. The positively-charged lysine of D776K establishes new inter-protomer contacts by tethering to the cation binding pocket (**Figure 1.2B**) (Nayeem et al., 2011), whereas the cysteine residues of Y521C/L783C are thought to achieve this through the formation of covalent disulfide bridges between subunits (**Figure 1.2C**) (Weston et al., 2006). Since both mutant receptors are expected to affect the functional properties of KARs similarly, we were surprised to observe that their single-channel behaviour was quite different.

Like wildtype receptors, 10 mM L-Glu rapidly activated single D776K channels. However, instead of opening only briefly prior to desensitization, agonist binding led to sustained activation of the 21-22 pS main open state (i.e. most-frequented) (**Figure 1.2D**). In support of this, repetitive applications of 10 mM L-Glu to patches containing a single D776K

receptor elicited activity in every case, demonstrating that this mutant GluK2 receptor displays close to the maximum probability of opening. Averaged ensemble responses were non-decaying in nature with rapid off-kinetics of about 2-3 ms due to L-Glu removal (**Figure 1.2D**). These persistent openings were nevertheless interrupted by transient closures too brief to represent long-lived desensitized states and, consequently, must represent sojourns to lower conductance levels, or closed or unliganded states.

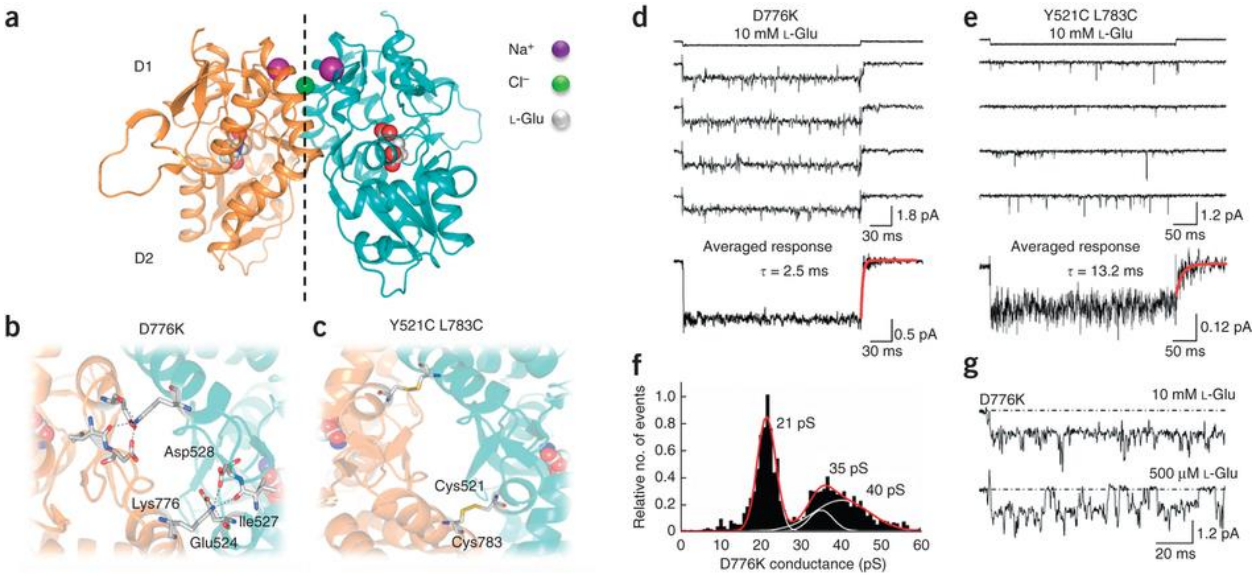

Figure 1.2 Mutation of Asp 776 to a Lys residue eliminates GluK2 receptor desensitization
(**A**) Crystal structure of the wildtype GluK2 LBD dimer (PDB: 3G3F; Chaudhry et al., 2009).
(**B**) Top view of the GluK2 D776K LBD dimer interface showing electrostatic interactions between Lys 776 and the adjacent subunit (PDB: 2XXX; Nayeem et al., 2011).
(**C**) Top view of the GluK2 Y521C/L783C LBD dimer interface showing covalent crosslinking between subunits (PDB: 2I0C; Weston et al., 2006).
(**D**) Typical current responses elicited by L-Glu acting on a single D776K channel (Patch # 12127p2, -60 mV).
(**E**) Unitary current events elicited by L-Glu acting on Y521C/L783C channels (Patch # 12322p3, -100 mV). In panels D and E, averaged ensemble responses were taken from 20 or 95 individual current records, respectively. Time constants of deactivation were obtained by fitting agonist-off current responses with a single exponential function.
(**F**) GluK2 D776K conductance distributions plotted following time course fitting.
(**G**) Individual current responses of a single GluK2 D776K receptor to 10 mM and 500 μM L-Glu (Patch # 12124p1).

Unlike the D776K receptor, the double cysteine mutant did not yield persistent channel activity in saturating L-Glu. Instead, recordings were dominated by sub-millisecond openings that were separated by longer apparent closures (**Figure 1.2E**) (Daniels et al., 2013). Given the infrequent nature of gating, we concluded that responses observed in the excised patches were likely to originate from multiple channels. Despite the transient openings, averaging sweeps from many agonist applications generated a non-decaying ensemble response. The decay kinetics of the ensemble average current of Y521C/L783C receptors were nevertheless at least five times slower (14.8 ± 2.9 ms, n = 4) than those of D776K receptors (**Figure 1.2E**).

For GluK2 D776K, its consistent gating behaviour allowed us to make additional inferences. Time-course fitting of resolvable single-channel events estimated conductance levels of 21, 35, and 40 pS which were calculated using a measured reversal potential of 0 mV (**Figure 1.2F**). The open level most frequently visited was 21-22 pS, closely matching the predominant 19 pS conductance level of wildtype receptors, with the two largest conductance levels corresponding to brief sojourns from this state (i.e. 35 and 40 pS). Fitting Gaussian functions to an all-points histogram of D776K data further shows that more than 90 % of the analyzed records corresponded to the main open state (**Figure S1.1**). These conductance levels are likely to originate from single channels, rather than several channels opening simultaneously, as lowering the concentration of L-Glu interrupted openings to the 21-22 pS state with clear closures to baseline (**Figure 1.2G**).

In summary, our single-channel data reveal that GluK2 D776K exhibits all the hallmarks expected of a non-desensitizing KAR: sustained activation, high unitary conductance, and an absence of long duration closures. GluK2 Y521C/L783C responds quite differently and therefore, we could conclude that the structural basis of its functional behaviour must be

different. Since the Lys 776 residue is proposed to act as a tethered cation (Nayeem et al., 2011) we reasoned that occupancy of the ion binding pocket may be the key structural event that prevents the onset of desensitization. If true, cation interactions at the Y521C/L783C receptor might therefore be unstable which would account for differences observed at the single-channel level. As explained below, we tested this hypothesis using molecular dynamic (MD) simulations to estimate the residency time of sodium bound to the cation binding pockets of both D776K and Y521C/L783C receptors.

Lys 776 substitutes for sodium at the cation binding pocket

MD simulations were employed to explore how electrostatic interactions affect occupancy of the cation binding pocket, which cannot be achieved using X-ray crystal structures or electrophysiology. Over the course of each of two 100 ns simulations, the cation pockets of the D776K receptor first released both sodium ions and then formed new contact points with the amino groups of Lys 776 (**Figures 1.3A-1.3D**). Consequently, the cation binding pocket was nearly continuously occupied by a positive charge during the entire simulation period, which is consistent with previous structural data (Nayeem et al., 2011). In contrast, simulations of the Y521C/L783C receptor predict that these mutations destabilize sodium and chloride ion binding, facilitating rapid ion release in both simulations performed (**Figure S1.2**). There was also a tendency for water molecules to more readily occupy the cation pockets of Y521C/L783C, which may explain the instability in sodium and chloride ion binding. Measurements of the surface area accessible to solvent indicated a much higher propensity for water molecules to interact with residues lining the cation pocket in the double cysteine mutant compared to wildtype GluK2 receptors (**Figure S1.2**). If these simulations reflect the physiological behaviour of kainate

receptors, then activation could depend on occupancy of the cation pocket, while cation unbinding would promote channel closure and/or desensitization.

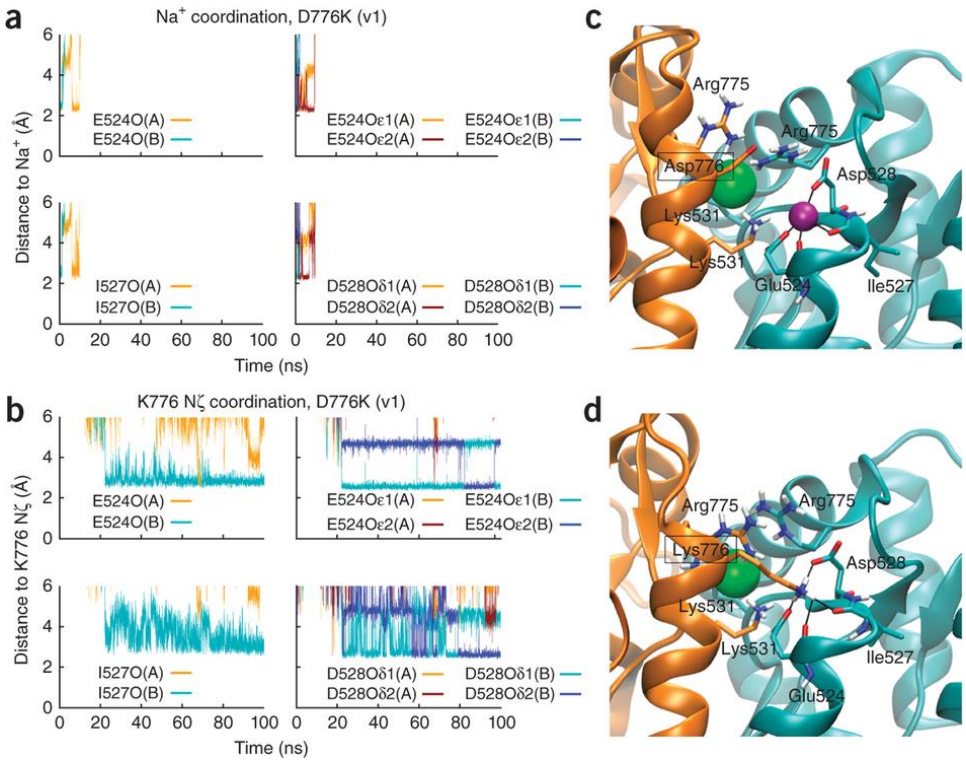

Figure 1.3 Lys 776 can act as a tethered ion at the GluK2 cation binding pocket
(**A**) Coordination distances between sodium ions (bound to chains A and B) and several oxygen atoms found on residues lining the cation binding pocket (E524, I527, D528) during a 100 ns MD simulation of the D776K mutant.
(**B**) Coordination distances for the positively charged Nζ of Lys 776. Distances were measured from oxygen atoms normally involved in sodium ion coordination.
(**C**) Sodium ion coordination in the crystal structure of the wildtype GluK2 LBD.
(**D**) Snapshot after 100 ns of MD simulation of the D776K mutant. Chain A and its residues are shown in orange, while chain B and its residues are shown in cyan. The sodium ion is shown in purple and the chloride ion in green. Coordination distances are indicated with black lines for the sodium ion (C) and the Lys 776 amine (D). Water molecules and non-polar hydrogen atoms are omitted.

GluK2 D776K receptors activate without external cations

If occupancy of the cation binding pocket is a prerequisite for wildtype KAR activation, removal of all external ions should result in the absence of any detectable current. Although such recordings have already been shown to abolish wildtype KAR activity (Wong et al., 2006), this

original finding has been disputed by more recent work claiming residual channel activity in ion-free conditions (Plested et al., 2008). To re-examine this issue, we repeated experiments comparing GluK2 receptors in the presence and absence of external ions. If Lys 776 acts as a tethered cation, as suggested by MD simulations (**Figure 1.3**) and structural data (Nayeem et al., 2011), we reasoned that the GluK2 D776K would gate in the absence of external cations. In contrast, the instability of cation binding to GluK2 Y521C/L783C suggests that this mutant would fail to gate in the absence of ions unless crosslinking the LBD dimer interface permits activation via a different mechanism. Consistent with the above predictions, wildtype GluK2 receptor activity was completely abolished by the removal of external monovalent ions (**Figures 1.4A and 1.4B**) whereas the D776K receptor continued to gate (**Figures 1.4C and 1.4D**) demonstrating that the wildtype GluK2 receptor gating mechanism has an absolute requirement for external cations. These data also further support the idea that the Lys 776 residue acts as a tethered cation, accounting for the ability of the D776K receptor to gate in the absence of external ions.

Interestingly, the Y521C/L783C receptor was also able to gate in the absence of external cations (**Figures 1.4E and 1.4F**). This finding is in agreement with a prior study (Plested et al., 2008) but inconsistent with the lack of responsiveness of wildtype GuK2 receptors in ion-free conditions (**Figures 1.4A and 1.4B**), suggesting the need for an alternative explanation. With this in mind, we considered the possibility that crosslinking the dimer interface of the GluK2 receptor may eliminate the requirement of external cations for activation. We tested this possibility by identifying mutations in the LBD dimer interface that would disrupt cation binding without forming inter-protomer crosslinks.

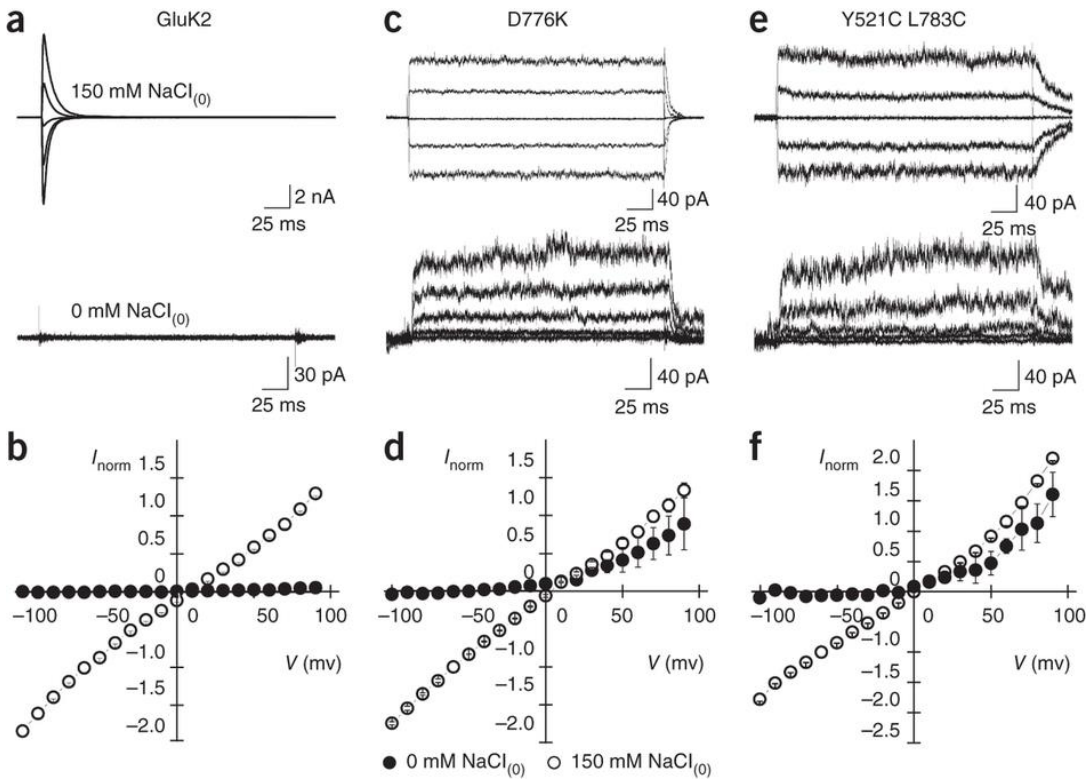

Figure 1.4 GluK2 D776K receptors gate in the absence of external ions
(**A, C, and E**) Membrane currents evoked by L-Glu acting on wildtype GluK2 (A), D776K (C), and Y521C/L783C (E) receptors, in either 150 mM NaCl (top) or in nominal ion-free (bottom) external solution (V_m = -60, -30, 0, 30, and 60 mV). For wildtype GluK2, the same patch was recorded in both ionic conditions to show the complete abolition of current (Patch # 121106p2), whereas mutant responses were taken from different patches (D776K ion, Patch # 11510 p1; ion-free, Patch # 12925 p5; Y521C/L783C ion, Patch # 121002 p2; ion-free, Patch # 121023 p2).
(**B**, **D, and F**) Averaged current-voltage plots in 0 mM (filled circles) and 150 mM (open circles) NaCl for wildtype GluK2 (B), D776K (D), and Y521C/L783C (F) receptors. Currents were normalized to responses at -60 mV in 150 mM NaCl.
Data are mean ± SEM from three independent experiments for each receptor.

Destabilizing cation binding impairs GluK2 activation

We studied disruption of the cation binding pocket by examining two mutant receptors, namely GluK2 E524G and L783C, which MD simulations suggest destabilize sodium binding to the cation binding pocket. Importantly, these mutations do not affect receptor surface expression (see **Figure S1.3**). For E524G, which has a less electronegative cation pocket, two simulations of sodium coordination both estimated that sodium is released within 5 ns, unlike the wildtype

receptor, which retained sodium for the duration of two, 100 ns simulations (**Figures 1.5A-1.5D**). In this respect, E524G mimics the Y521C/L783C receptor; however, it differs in that 10 mM L-Glu fails to elicit a measurable response in most excised patches (**Figure S1.3**). We did observe responses in 3 out of the 18 patches tested but they were small (> -10 pA) in amplitude and thus consistent with the E524G mutation acting to destabilize cation binding.

Interestingly, when only one of the crosslinking residues (i.e. L783C) was mutated, 10 mM L-Glu failed to elicit a response in all cases whether we examined whole-cell recordings (data not shown) or excised patches (n = 15) (**Figure S1.3**). MD simulations suggested that the L783C mutant has a less pronounced effect than E524G on sodium stability, yet the ions managed to dissociate from their binding pockets within 100 ns in one of two simulations (**Figures 1.5E and 1.5F**). One potential explanation for the sodium dissociation is that the L783C mutant permits access of additional water molecules into the cation binding pocket, as observed in simulations of Y521C/L783C. In comparison to the wildtype GluK2 receptor, the sodium ions in L783C interacted more frequently with water molecules, and less frequently with residues of the cation pocket (data not shown). In both mutants, our data point to the lack of responsiveness of E524G and L783C arising from their disruptive effects on the cation binding pocket, a condition that may be similar to desensitization in a wildtype receptor. Because mutant receptors that disrupt L-Glu binding are retained within mammalian cells (Mah et al., 2005), we do not think that an inability to bind agonists can account for the phenotypes of E524G and L783C. As a result, an explanation is required to account for an additional cysteine (Y521C) restoring channel gating when introduced atop the L783C mutation. We conclude that the cation-independent activation of GluK2 Y521C/L783C is due to its covalent crosslinking of the dimer interface, which circumvents normal gating requirements of the wildtype receptor.

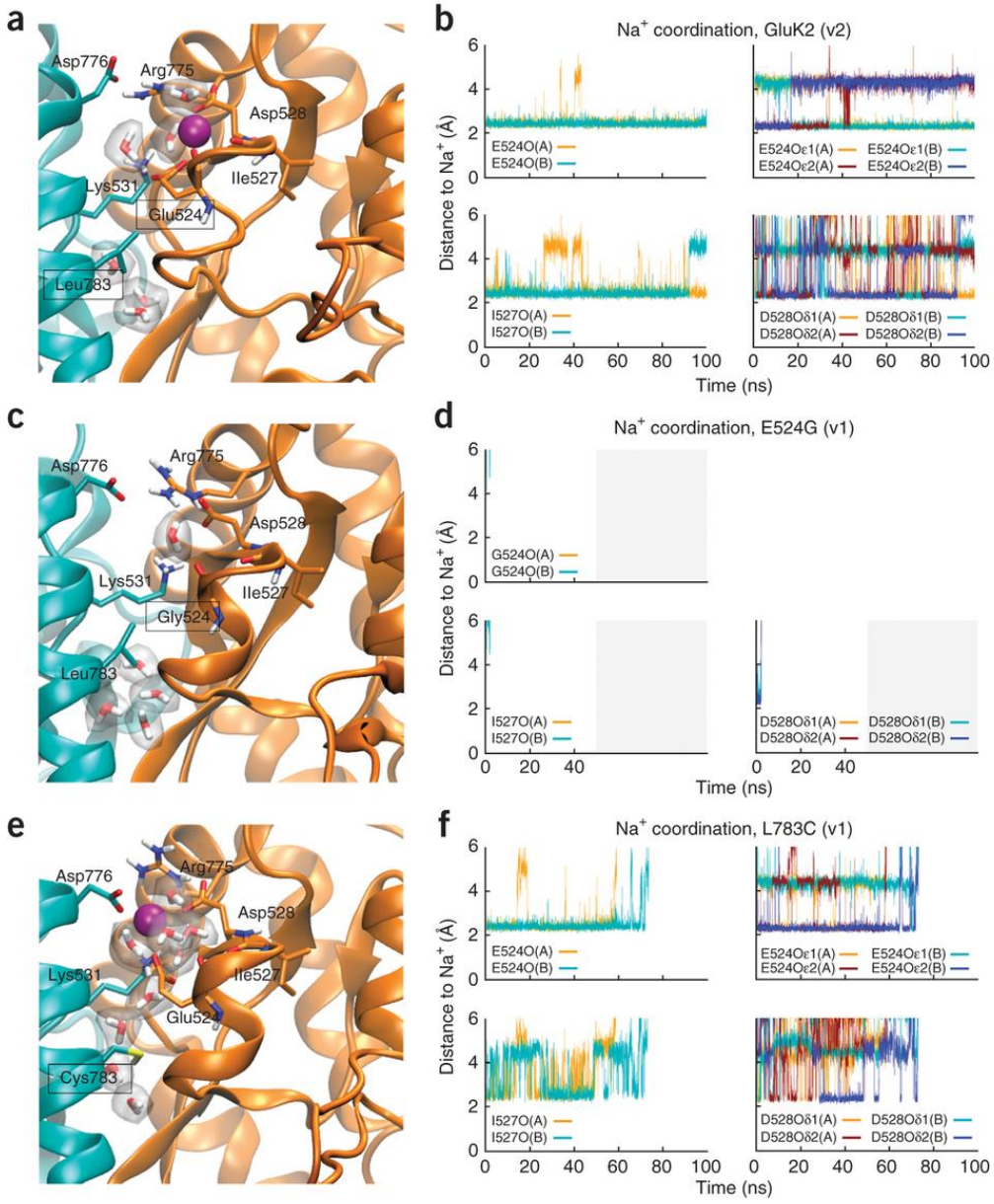

Figure 1.5 Occupancy of the GluK2 cation binding pocket is predicted to be disrupted by targeted mutation of the dimer interface
(**A, C, and E**) Snapshots of sodium coordination in the wildtype GluK2 receptor (A), as well as mutants E524G (C) and L783C (E), all taken approximately 15 ns after the start of the MD simulation.
(**B, D, and F**) Sodium coordination plotted from MD simulations of the LBD dimer in the wildtype GluK2 receptor (B), and mutants E524G (D) and L783C (F).

KAR desensitization proceeds after cation unbinding

MD simulations and single-channel data suggest that GluK2 D776K receptors are non-desensitizing because Lys 776 becomes tethered to the cation binding pocket. We therefore

conclude that cation binding primes KARs for activation by the agonist. We also conclude that cation-unbound states are not primed for activation and thus, agonist-binding promotes entry into desensitized states as observed with the L783C and E524G mutant receptors. These different outcomes are important because they will determine the degree to which desensitization, and by implication cation unbinding, contributes to the *wildtype* KAR response. For example, during long agonist applications routinely used to measure desensitization rates, most receptors should desensitize because cations will eventually unbind with the agonist still bound. In contrast, with brief applications of L-Glu used to measure deactivation rates, fewer GluK2 receptors should desensitize because the agonist will unbind before the cation. Importantly, this sequence of events can be tested experimentally. Specifically, we predict that deactivation rates estimated with a brief agonist application should be minimally affected by the presence or absence of desensitization because decay from the peak response corresponds to agonist unbinding from the cation-bound state(s).

To examine the impact of desensitization on deactivation rates, we compared the relaxation kinetics observed following a brief application (i.e. 1 ms) of 10 mM L-Glu onto wildtype and non-desensitizing D776K KARs (**Figure 1.6A**). For comparison, we also performed a similar analysis of wildtype and a mutant GluA1 AMPA receptor (i.e. L497Y) where single-channel desensitization is strongly inhibited (Stern-Bach et al., 1998) (**Figure 1.6B**). Wildtype GluK2 receptors exhibited a fast exponential time constant of deactivation of 2.3 ± 0.1 ms (n = 7) (**Figure 1.6A**) which was statistically indistinguishable from the off-kinetics of D776K receptors regardless of whether 1 ms (2.0 ± 0.2 ms, n=9) (p = 0.63) or 250 ms agonist pulses (2.4 ± 0.2 ms, n = 12) (p = 0.82) were applied (**Figures 1.6A and 1.6C**). These observations support our assertion that KAR desensitization proceeds after cation unbinding.

Accordingly, deactivation and desensitization can therefore be viewed as being structurally-distinct and separable processes. In contrast, the decay time constant observed following a 1 ms application of 10 mM L-Glu to GluA1 AMPARs had a fast exponential time constant of 1.0 ± 0.1 ms (n = 6) (**Figure 1.6B**), which was about 10 times faster than the off-kinetics of the non-desensitizing L497Y mutant (12.4 ± 1.6 ms, n=5) (**Figures 1.6B and 1.6C**). This finding is consistent with the effect of the allosteric modulator, cyclothiazide, which also attenuates AMPAR desensitization (Mitchell & Fleck, 2007).

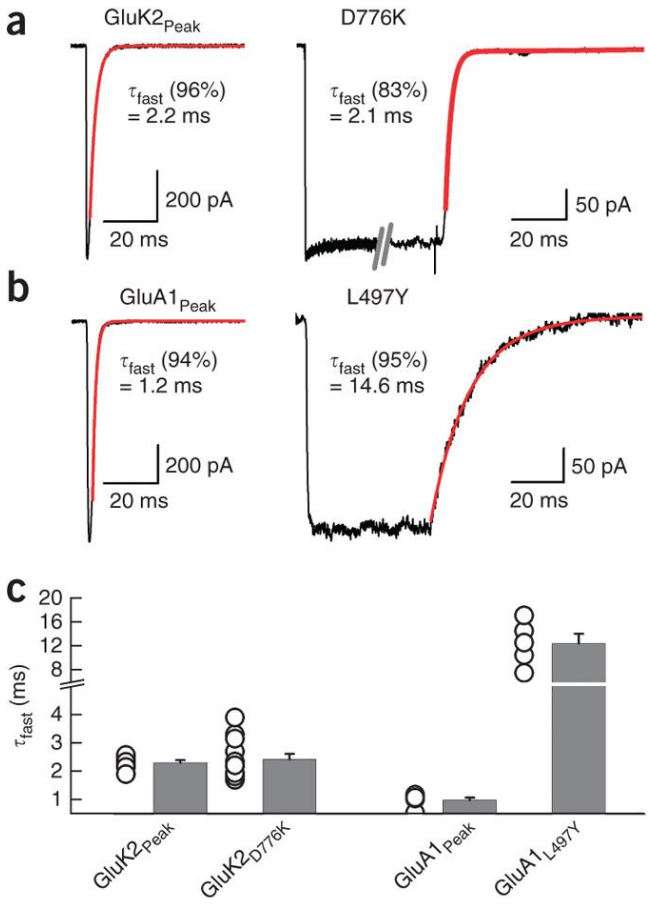

Figure 1.6 Desensitization and deactivation are uncoupled in GluK2 KARs
(**A**) Typical current decay observed following removal of 10 mM L-Glu from wildtype GluK2 (1 ms application, Patch # 00327p3) and GluK2 D776K (250 ms application, Patch # 11506p1) receptors.
(**B**) Typical current decay observed following removal of 10 mM L-Glu from wildtype GluA1 (1 ms application, Patch # 00404p1, -55mV) and GluA1 L497Y (50 ms application, Patch # 99608p1, -55mV)

receptors. For panels A and B, decay kinetics from saturating L-Glu were fit with a second-order exponential function (red) with representative values of the fast, dominant component displayed.
(**C**) Distribution of off-kinetic rates show that the τ_{fast} values for the GluK2 peak response and D776K were statistically indistinguishable (P = 0.68), whereas the values for the GluA1 peak response and L497Y were statistically different (P < 0.001). Two-tailed Student's *t* test performed (a = 0.05).
Data are mean ± SEM from five to twelve independent experiments.

To further test the impact of desensitization on the activation process, we compared the dose-response relationships of GluK2 D776K and wildtype receptors. We reasoned that because the absence of desensitization had little to no effect on GluK2 deactivation kinetics, rates of L-Glu unbinding should be high relative to rates of cation unbinding, which equate with desensitization. Under such circumstances, receptors would tend to enter desensitized states only during sustained L-Glu application. As such, the dose-response relationship of the peak response, occurring less than 1 ms after L-Glu exposure, should exhibit little change in the absence of desensitization.

In agreement with our predictions, the EC_{50} (and n_H) estimated from peak dose-response curves to L-Glu acting on wildtype GluK2 receptors were 652 ± 47 μM (n_H = 0.87, n = 7), which closely matched that of D776K receptors, where the EC_{50} value was estimated to be 520 ± 91 μM (n_H = 1.6, n = 8) (**Figures 1.7A and 1.7B**). These data differ from past work on AMPARs which has shown that mutations and allosteric modulators that reduce or eliminate desensitization cause progressive leftward shifts in the wildtype dose-response curve (Stern-Bach et al., 1998; Mitchell & Fleck, 2007). For example, one study noted a leftward shift of over an order of magnitude in the wildtype EC_{50} when studying GluA1 L497Y AMPARs (Mitchell & Fleck, 2007) (**Figure 1.7B**). Our observations comparing wildtype and D776K receptors support the idea that desensitization has little impact on the time GluK2 receptors remain activated. This is, of course, to be expected if desensitization can only proceed after cation unbinding. Indeed, MD simulations reported here suggest that LBD dimer separation, a structural correlate of

desensitization, is promoted for wildtype receptors in the absence of bound sodium ions (**Figure S1.4**). Our findings also suggest that desensitization impacts the time course of AMPAR activation which explains the effect of desensitization on both deactivation kinetics and agonist potency.

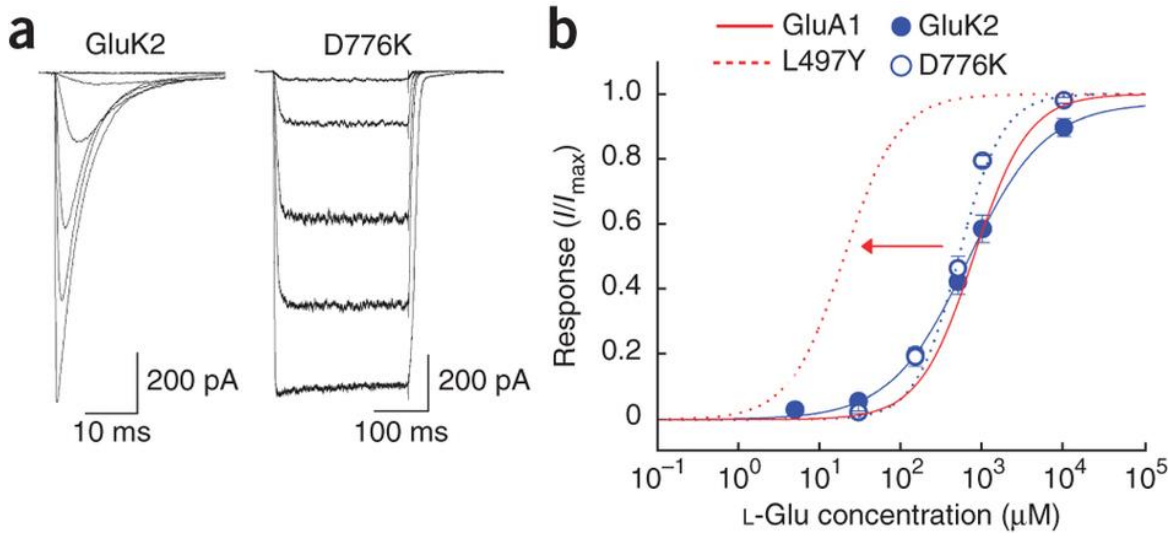

Figure 1.7 Desensitization does not substantially shift peak agonist potency of GluK2 KARs
(**A**) Typical current responses elicited by L-Glu (10 μM - 10 mM) acting on wildtype GluK2 (Patch # 091204p2) and GluK2 D776K (Patch # 11610p1) receptors.
(**B**) L-Glu dose-response relationships for KARs, normalized to the maximal current (I_{max}) of each patch, as well as simulated dose-response curves of wildtype and GluA1 L497Y receptors taken from previously reported values (Mitchell & Fleck, 2007).
Data are mean ± SEM from seven and eight independent experiments.

DISCUSSION

The present study advances our understanding of iGluR gating in several substantial ways. First, we show that cation occupancy is the central requirement in keeping agonist-bound KARs in the activated state and out of desensitization. Second, we propose a structural model for the sequence of events that give rise to deactivation and desensitization. Deactivation is observed when the ligand unbinds from cation-bound states, whereas desensitization proceeds when the ligand is bound to cation-unbound states. Third and finally, closely-related AMPARs do not share this reliance on cation-dependent gating, as a result; desensitization appears able to curtail AMPAR channel activation. As discussed below, this unique property of KARs may provide clues to how subunit composition and/or auxiliary proteins affect native receptors at glutamatergic synapses.

The KAR dimer interface is a multi-faceted structure

It is remarkable that subunit crosslinking at two neighbouring sites (residues 776 and 783) along the GluK2 LBD dimer interface produces very different functional consequences. The Y521C/L783C mutation bridges opposing subunits, yet the crystal structure of its LBD suggests a separation of the upper D1 segment of the dimer interface (Weston et al., 2006). Although separation of the dimer interface is thought to underlie both KAR and AMPAR desensitization (Sun et al., 2002), it is not clear how much separation would be tolerable before channel activation could no longer be maintained. Given microscopic recordings showing that Y521C/L783C channels cannot stably access the main open state of wildtype GluK2 (Daniels et al., 2013), we propose that this mutant is a mostly desensitized receptor typified by an open interface and/or a poorly activating receptor by virtue of its sporadic channel openings.

Targeted slightly higher along the LBD interface, the mutant residue Lys 776 occupies the GluK2 cation binding pocket and has two related consequences on receptor function; it increases open-channel probability to such an extent that no failures are observed and it sustains activation for the duration of agonist application. The latter effect supports the idea that the molecular events leading to desensitization are triggered at the apex of the interface, rather than being coordinated through the interface as a whole. Whether these interactions are further complicated by an emerging idea that KAR subunits desensitize with a tetrameric symmetry and not as a dimer of dimers (Bowie & Lange, 2002; Schauder et al., 2013) awaits future study.

The cation binding pocket and its relation to gating events

Although structural rearrangements of the LBD accompany iGluR desensitization (Sun et al., 2002), it is presently unknown how such conformational changes are initiated. The matter is further complicated in KARs, where bound ions have been proposed to stabilize the LBD dimer interface (Plested & Mayer, 2007). Here, we establish a framework to specify when KARs activate and desensitize by identifying the cation binding pocket as the molecular switch between these processes. In short, cation pocket occupancy maintains KAR activation, and by implication desensitization cannot occur until cations unbind. The link between cation binding and activation is based on several key observations reported above: the sustained single-channel activation observed in the GluK2 D776K mutation (**Figure 1.2**), where the cation binding pocket is thought to be continuously occupied, the inability of GluK2 to activate in the absence of external ions (**Figure 1.4**), and the gating deficiencies amongst mutants designed to disrupt cation binding (**Figures 1.5 and S1.3**). Furthermore, the assertion that cation unbinding precedes desensitization can be deduced from other observations we reported. Specifically, we showed that deactivation kinetics of wildtype KARs were unaffected by desensitization confirming our

assertion that the decay of the KAR peak response corresponds to agonist unbinding from the cation-bound state(s) (see **Figures 1.6A and 1.6C**). This conclusion is consistent with previous work showing that GluK2 deactivation kinetics are made faster by lowering the external cation concentration or by replacing sodium with another cation (Bowie, 2002). With long agonist applications (i.e. 250 ms), we propose that the decline in KAR activity is due cation unbinding since, besides the presence of the agonist, the only other known requirement of KARs to activate is allosteric ions (Wong et al., 2006). Given this, we concluded that their departure was the most plausible explanation to trigger the onset of desensitization. In accordance with this notion, MD simulations reported here (**Figure S1.4**) predict that removal of cations from the LBD dimer interface can induce structural changes associated with the desensitized state(s).

An alternative explanation for the observations above is that KAR desensitization is triggered by intrinsic rearrangements to the LBD structure, which are countered through the occupancy of bound cations. From this perspective, the relation between bound cations and decay kinetics is attributable to a direct modulation of the intrinsic rate of desensitization (by stabilizing LBD dimers) as has been suggested previously (Plested et al., 2008). This interpretation, however, is difficult to reconcile with several observations. To begin with, if desensitization is merely opposed, but not blocked by the presence of bound cations, some residual activation should be detected in solutions lacking external ions; which is not the case. Furthermore, from this perspective, the effect of cation species on deactivation kinetics would have to be explained by desensitization rates overlapping with those of deactivation. Experiments reported in this manuscript show that deactivation kinetics are unaffected by desensitization (i.e. comparing D776K to wildtype GluK2 receptors) (**Figure 1.6**), which must

therefore occur on a slower time scale. Thus, the two processes do not overlap, meaning activation must be directly regulated by cations.

Ion channels employ different strategies to desensitize

Desensitization of LGICs has been classically thought to arise from agonist molecules converting receptor complexes into non-reactive forms (Del Castillo & Katz, 1957) in much the same way that even earlier work linked changes in membrane potential to voltage-gated ion-channel inactivation (Hodgkin & Huxley, 1952). Since then, structural explanations have emerged to account for how the processes of inactivation and desensitization occur at the amino acid level. Some of the first insights came from work on voltage-gated sodium and potassium channels, which were shown to possess intracellular inactivation gates (Stuhmer et al., 1989; Hoshi et al., 1990), whereas work on Cys-loop LGICs hinted at a broader re-arrangement of quaternary structure (Unwin et al., 1998). Pioneering studies also identified coupling between activation and inactivation of voltage-gated channels (Armstrong & Bezanilla, 1977), which has been more difficult to establish at LGICs. Such coupling might be expected to occur at iGluRs since closure in the agonist-binding domain initiated by ligand binding is thought to bring about both activation and then desensitization, as the agonist becomes entrapped in a stable, yet inactive conformation (Mano et al., 1996; Armstrong et al., 1998). In keeping with this, data presented in this study suggest a tight coupling between these structural events in AMPARs. Interestingly, this is not the case for KARs, which uncouple the process of activation from desensitization through cation-dependent gating. This unique aspect of KAR gating provides an ideal target by which native receptor responses could be modulated at central synapses. For example, alterations in cation-affinity through protein-protein interactions could explain how heteromeric subunits (Barberis et al., 2008) and/or auxiliary proteins (Zhang et al., 2009)

regulate the duration of synaptic KAR activity (Copits & Swanson, 2012). Clearly, much still remains to be examined in future studies and how this allosteric cation binding pocket might be exploited to regulate KAR signaling within the vertebrate CNS.

METHODS

Cell culture and transfection

HEK293T cells were transiently co-transfected with cDNA encoding wildtype or mutant GluK2(Q) KAR or GluA1(Q) AMPAR subunits and enhanced green fluorescent protein ($eGFP_{S65T}$) as previously described (Bowie, 2002), or transfected with iGluR subunit cDNA on plasmids also encoding eGFP behind an internal ribosomal entry site. The cDNA for the mutant receptors was generated in two steps from wildtype plasmid using Quickchange II XL site-directed mutagenesis (Stratagene, LaJolla, CA). After transfection for 4 - 8 hrs using the calcium phosphate precipitation method, cells were washed twice with divalent-containing PBS and maintained in fresh medium (MEM containing Glutamax and 10% FBS). Electrophysiological recordings were performed 24 - 48 hrs later.

GluK2 receptor surface expression

To test for possible trafficking defects in mutants used in this study, we measured the fluorescence emitted by an ecliptic $_{pH}$GFP genetically fused to the extracellular N-terminal of mutant or wildtype GluK2 receptors (**Figure S1.3**). Unlike eGFP, the fluorescence emission of $_{pH}$GFP is almost entirely quenched at pH 5.45 (Miesenbock et al., 1998), which we used to evaluate the cellular location of the fluorophores (Khiroug et al., 2009). Using this approach, a substantial but reversible attenuation in the fluorescence signal emitted by wildtype $_{pH}$GFP-GluK2 was observed (n = 17 cells) following acidification of the external milieu (**Figure S1.3**) demonstrating that most of the fluorescence signal was emitted by tagged GluK2 receptors on the plasma membrane. In contrast, acidification of the external solution had little effect on the weak fluorescence emitted by $_{pH}$GFP-GluK2 R523A receptors (n = 6 cells) (**Figure S1.3**), consistent with previous work showing that this mutant has poor surface expression (Mah et al., 2005).

Fluorescence emitted by $_{pH}$GFP-GluK2 E524G and L783C receptors (n = 10 and 6 cells respectively) was robust, much like wildtype GluK2, and was reversibly attenuated by acidification (**Figure S1.3**) suggesting that trafficking to the plasma membrane is not substantially perturbed for either mutant.

Electrophysiological solutions & recordings

External recording solutions typically contained (in mM): 150 NaCl, 5 HEPES, 0.1 $CaCl_2$, 0.1 $MgCl_2$, 2% phenol red. The internal recording solution contained (mM): 115 NaCl, 10 NaF, 5 HEPES, 5 Na_4BAPTA, 0.5 $CaCl_2$, 1 $MgCl_2$, and 10 Na_2ATP to chelate endogenous polyamines. The osmotic pressure was set to 295-300 mOsm using sucrose and the pH adjusted to 7.35 with 5 N NaOH. Agonist solutions were prepared by dissolving the agonist in external solution and adjusting the pH appropriately. In the case of recordings conducted in nominal external ions, the solution contained 100 μM of $CaCl_2$ and $MgCl_2$ to improve patch stability, sucrose to maintain the osmotic pressure at 295-300 mOsm, and 5 mM Tris to buffer pH. The pH was adjusted to 7.3-7.4 using 10 N HCl. To optimize recording stability in solutions of nominal ions, quartz electrodes were used to excise some outside-out patches. The outward current conveyed by receptors in such conditions was due to the efflux of sodium ions from the patch pipette. The lack of inward current in response to L-Glu confirmed that all cations were removed from the external milieu of the membrane patch.

All experiments were performed on excised membrane patches in the outside-out configuration. We used thin-walled borosilicate glass pipettes (3-5 MΩ, King Precision Glass, Inc.) coated with dental wax for macroscopic experiments. To obtain low noise or single-channel recordings, we used quartz glass (3-15 MΩ, King Precision Glass, Inc.) coated with Sylgard (Dow Corning). Agonist solutions were rapidly applied to outside-out patches for 250 ms at -60

mV (unless otherwise stated) using a piezo-stack driven perfusion system. Sufficient time between applications of L-Glu was allowed for complete recovery from macroscopic desensitization. Solution exchange time was determined routinely at the end of each experiment by measuring the liquid junction current (10-90 % rise-time = 100-400 μs). Series resistances (3-15 MΩ) were routinely compensated by 95%. For microscopic recordings, the headstage was set to the capacitive feedback recording mode. All recordings were performed at room temperature using an Axopatch 200B amplifier (Axon Instruments Inc., Foster City, CA, USA). Current records were filtered at 5 kHz for macroscopic responses and digitized at 25-50 kHz. Single-channel currents were all acquired at 50-100 kHz, low-pass filtered by an 8-pole Bessel filter at 10 kHz and digitally filtered offline at 1-3 kHz. The reference electrode was connected to the bath via an agar bridge of 3M KCl. Data were acquired using pClamp9 software (Axon Instruments Inc., Foster City, CA, USA), and illustrated using Origin 7 (OriginLab Corp., Northampton, MA, USA).

Macroscopic response analysis

Data were analyzed using Clampfit 9.0 and tabulated using Microsoft Excel. Curve fittings for determining the off-kinetic rates were performed using 1^{st} or 2^{nd} order exponential functions: $y = A_i * \exp(-x/t_i)$. Dose-response data to L-Glu were normalized, pooled across patches, and fit with the logistic equation of the following form: $I = I_{max}/(1+(EC_{50}/[Glu])^{nH})$, where I is the normalized current at any agonist concentration, I_{max} is the interpolated maximal response, EC_{50} is the concentration of L-Glu that elicits the half-maximal response, and n_H is the slope or Hill coefficient.

Single-channel analysis

For wildtype GluK2 receptors, analysis was conducted on patches (n = 5) from which fifty or more agonist applications were made at 15 s intervals. For GluK2 D776K, which displayed uniform current responses, analysis was limited to 58 agonist applications, which were divided among four patches. Single-channel data were subjected to digital low-pass filtering at 3 kHz (or 1kHz for presentation in figures), which resulted in root mean square baseline noise values that averaged 0.22 ± 0.024 pA (n = 5) and 0.22 ± 0.043 pA (n = 4) for wildtype and D776K receptors, respectively. These noise values corresponded to less than fifty percent of the smallest difference between adjacent conductance levels in the wildtype receptor. The 3kHz frequency was chosen on account of our data containing many rapid transitions between conductance levels, as described previously for AMPARs (Zhang et al., 2008). Accordingly, a resolution of two filter rise times (2 x 111 μs) was imposed to detect and account for brief events, while maintaining resolution of small conductances. Digitally-filtered data were exported to Signal 5.0 (Cambridge Electronic Design) to perform time-course fitting analysis with the program SCAN (Colquhoun & Sigworth, 1995). The idealized records were then used to provide information on response amplitudes, which could be fit with Gaussian functions, whose peaks reflect discrete conductance levels: $y = \sum_{i=1...n} (A_i/w_i*\mathrm{sqrt}(\pi/2)))*\exp(-2*((x-xc_i)/w_i)2$ where A = area, xc = centre of the peak, w = error associated with xc. From this analysis, the distribution and amplitude of single-channel events observed in patches containing a few channels (**Figure 1.2F**) were similar to events measured at equilibrium in multichannel patches (**Figure S1.5**).

Molecular dynamics simulations

All crystal structures used in this manuscript were obtained from the Research Collaboratory for Structural Bioinformatics (RCSB) protein data bank. Two protein structures were used for building models for the MD simulations; an L-Glu-bound GluK2 LBD dimer (PDB: 3G3F; Chaudhry et al., 2009) and an L-Glu-bound GluK2 Y521C/L783C LBD dimer (PDB: 2I0C; Weston et al., 2006), respectively, which was used only for simulations concerning the double-cysteine mutant. Together with the crystallographically resolved water molecules, L-Glu ligands and ions were retained in the simulation setup, whereas two bound isopropyl alcohol molecules were deleted. In simulations of GluK2 without bound sodium ions (**Figure S1.4**), these were removed before system setup. The protein was solvated in water in a $(90\ \text{Å})^3$ box using the TIP3P water model (Jorgensen et al., 1983), whereafter the system was neutralized and 150 mM NaCl was added. Mutations, except for Y521C/L783C, were imposed manually prior to simulation setup, either by editing/deleting atoms in the pdb-file or by using the mutate function of PyMOL (The PyMOL Molecular Graphics System, Version 1.3, Schrödinger, LLC) and adjusting the side chain rotamer. For the double cysteine mutant, the GluK2 double-cysteine (Y521C/L783C) mutant structure was employed. This structure had no ions bound, so the interface-bound ions from the wildtype structure were added and rotamers for side chains surrounding the ion sites were optimised in PyMOL before solvation, neutralization and ionization as described above.

The MD simulations were performed in Gromacs 4.5 (Hess et al., 2008) with the OPLS all-atom force field (Jorgensen et al., 1996; Kaminski et al., 2001). The systems were first energy minimized until the maximum force on an atom was less than 100 kJ/mol/nm. Following energy minimization, a 200 ns restrained simulation with position restraints on protein heavy-atoms and

on bound ions with a force constant of 1000 kJ mol^{-1} nm^{-2} was performed in the NVT ensemble with a temperature of 300 K maintained by a Berendsen thermostat (Berendsen et al., 1984). Periodic boundary conditions were utilized and van der Waals interactions were cut off at 10 Å. Long-range electrostatics were accounted for by the Particle-Mesh Ewald method (Darden et al., 1993). All bonds were treated as constraints using the LINCS algorithm, allowing a time step of 2 fs. Subsequently, 100 ns of production run were performed (only 30-50 ns for E524G). The NPT ensemble was employed with the temperature retained at 300 K and the pressure at 1 bar by using the Berendsen thermostat and barostat, respectively (Berendsen et al., 1984). Two repeats for each mutational variant were produced. Analyses were performed using VMD (Humphrey et al., 1996) and analysis tools of Gromacs (Hess et al., 2008).

Statistical methods

Results are expressed as mean ± s.e.m. Statistical analyses of sample means were performed using two-tailed Student's *t* tests. $P < 0.05$ was considered to be statistically significant.

ACKNOWLEDGMENTS

This work was supported by operating grants from the Canadian Institutes of Health Research (CIHR) FRN-82804 (D.B.) and by the Leverhulme Trust RPG-059 (P.C.B.). G.B.D. and E.D.A. were supported by Natural Sciences and Engineering Research Council of Canada (NSERC) graduate fellowships, B.A.D. by a Chemical Biology CIHR postdoctoral award and M.R.P.A. by a CIHR Best & Banting doctoral award. D.B. is the recipient of a Canada Research Chair award. We thank the Oxford Supercomputing Centre for computer time. Finally, we wish to thank Dr. Jon Johnson for comments on the manuscript and Dr. Mark Fleck for discussions on AMPA receptors.

SUPPLEMENTAL FIGURES

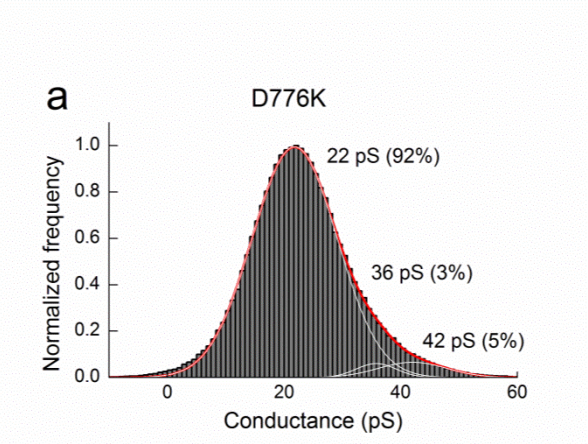

Figure S1.1 The non-desensitizing receptor GluK2 D776K primarily activates to an approximately 20 pS conductance level. Supplemental data associated with Figure 1.2.
(A) An all-points histogram detailing the conductance distribution of D776K single channels. Conductance levels were identified by fitting the distribution with three Gaussian functions (see Methods). The distribution was generated by compiling segments of channel activity from the same patches and sweeps for which time course fitting was carried out, following digital low-pass filtering at 3 kHz.

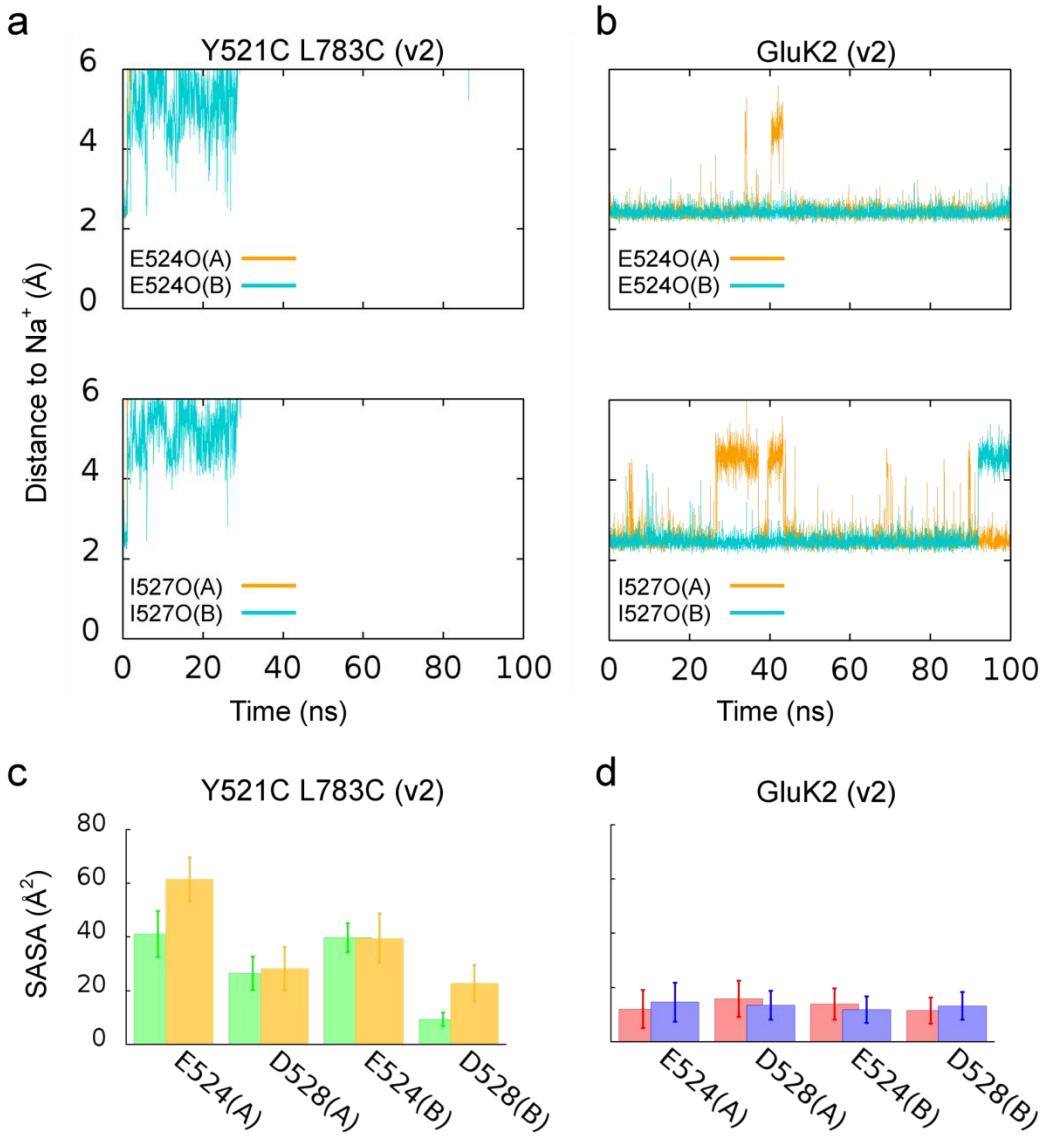

Figure S1.2 Cation binding is predicted to be disrupted in the GluK2 Y521C/L783C receptor. Supplemental data associated with Figure 1.3.

(A and B) Coordination of bound sodium ions by the backbone oxygen atoms of Glu 524 and Ile 527 in Y521C/L783C (A) and wildtype GluK2 (B), respectively, as predicted by MD simulations.

(C and D) Solvent-accessible surface area (SASA) for the sodium-coordinating residues Glu 524 and Asp 528 of Y521C/L783C (C) and wildtype GluK2 (D). Mutant simulations are denoted by green (v1), orange (v2), and wildtype simulations by red (v1) and blue (v2) to distinguish different simulation versions.

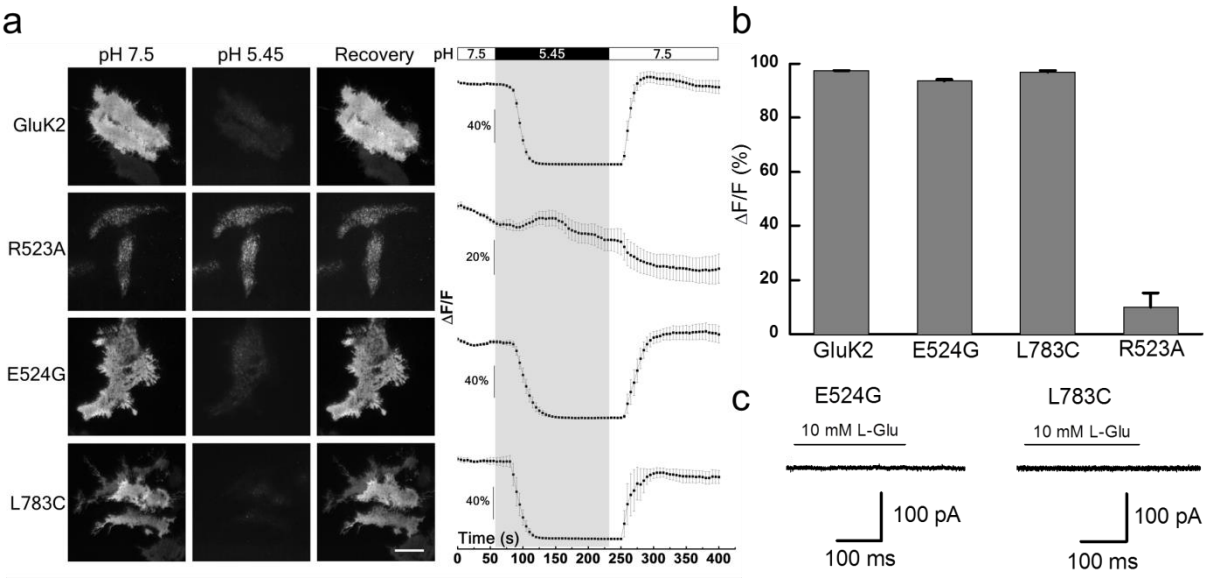

Figure S1.3 Mutations at the GluK2 cation binding pocket interfere with channel gating, but not receptor surface expression. Supplemental data associated with Figure 1.5.

(A) TIRF images of HEK293T cells transfected with wildtype and mutant GluK2 receptors reveal reversible changes in the eGFP fluorescence signal between pH 7.5 and 5.45 when proteins are expressed on the plasma membrane (scale bar = 10 μm).

(B) Bar graph tabulating the changes in fluorescent signal observed when expressing wildtype and mutant GluK2 receptors. Error bars, s.e.m. from six to seventeen independent imaging experiments for each receptor.

(C) Outside-out patch recordings taken from cells expressing GluK2 E524G (Patch # 12619p3) and L783C (Patch # 13114p5) receptors where 10 mM L-Glu failed to elicit a measurable current response.

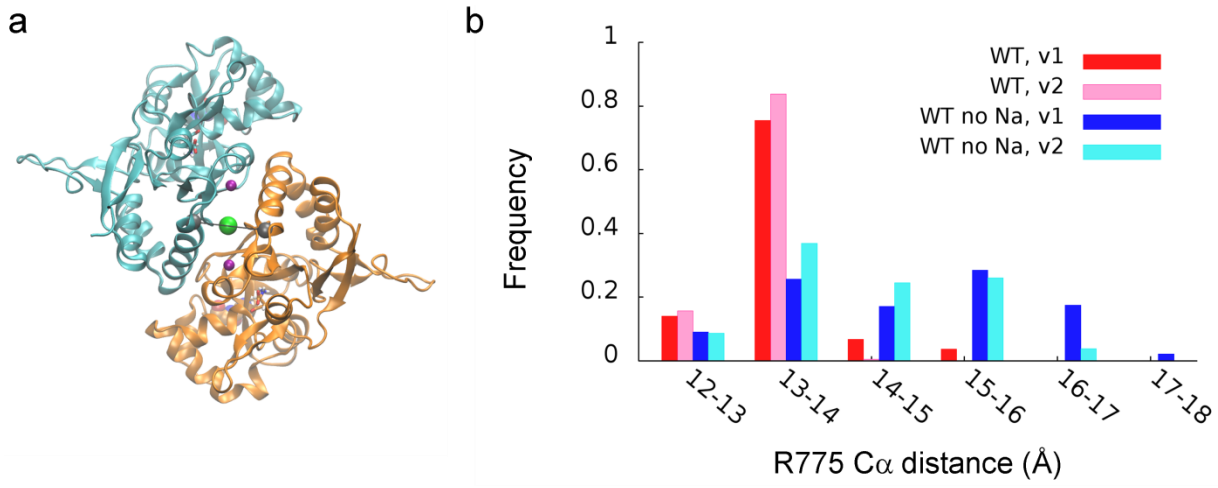

Figure S1.4 Sodium unbinding initiates rearrangements of the LBD dimer interface that are associated with desensitization. Supplemental data associated with Figures 1.6 and 1.7.
(A) Top view of the crystal structure of the wildtype GluK2 LBD dimer showing two sodium ions (purple), one chloride ion (green), and the alpha carbons of both R775 residues (grey) adjacent to the dimer interface. The distance of the line connecting these carbons reflects the separation of the upper lobes of subunits.
(B) Inter-subunit R775 alpha carbon distance during 100 ns MD simulations in which the two bound sodium ions are either left in place or removed prior to the simulation.

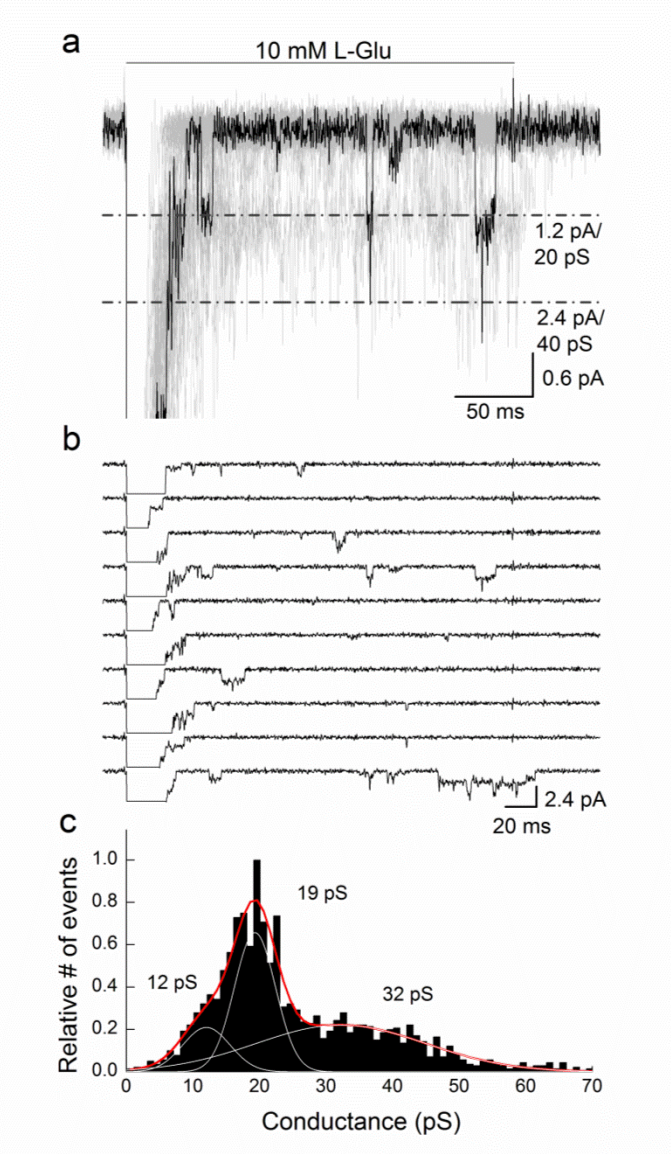

Figure S1.5 GluK2 channels activate to the same conductance levels before and after the onset of desensitization. Supplemental data associated with methods.

(A) Overlay of forty individual current records from a patch expressing GluK2 receptors that produced a peak response of approximately 100 pA in 10 mM L-Glu (Patch # 12309p2, -60 mV). A typical opening elicited by L-Glu is shown in bold.

(B) Typical GluK2 receptor unitary current events recorded from ten consecutive sweeps from the same patch, elicited by saturating L-Glu following the onset of desensitization. (c) GluK2 conductance distributions were fit following time-course fitting analysis of records from five patches (271 sweeps total).

CHAPTER TWO

Intra- and inter-protein interactions determine the time course of AMPAR activation

FOREWORD TO CHAPTER TWO

The data that comprise this chapter were originally meant to form two separate studies. The first study would have included what are now figures one to six, focusing on the critical role of the LBD apex in GluA2 AMPAR activation, and concluding on a surprising note -that auxiliary protein co-expression can compensate for the disruption of electrostatic interactions across the LBD dimer interface. Around the time that the first manuscript was written, I began to embark on a new project, involving the identification of sites on the AMPAR LBD that auxiliary proteins act upon to modulate receptor gating. This second project yielded some positive results, and in an effort to improve the first manuscript, it was wrapped up quickly to contribute what are now figures seven and eight.

Originally, the first portion of this chapter was submitted as a manuscript to *Nature Structural & Molecular Biology* in July of 2015, but it was quickly passed over for peer review. A month later we submit the manuscript to *Neuron* after receiving a positive response to our pre-submission inquiry. Following an initial round of peer review the manuscript was rejected, but a resubmission was allowed. At this point, we added what would become figures seven and eight -most new data had already been collected- to tie up some loose ends, explaining how auxiliary subunits (e.g. TARPs) can rescue poorly functioning AMPARs. The reviewers were generally much more pleased with the revised manuscript, and by this stage, only a few minor revisions were required. We submit the final revision just before the end of the year, meaning the manuscript was accepted in January of 2016, published online in February, and appeared in print in March.

During the writing of this thesis, two papers reported cryo-EM visualization (at <10 Å resolution) of intact AMPAR-stargazin complexes (Twomey et al., 2016; Zhao et al., 2016).

Interestingly, the antagonist-bound structure in the manuscript by Twomey and colleagues features the "KGK motif," described in figure seven of this chapter, as coming into contract with the extracellular, acidic lip of a γ2 subunit. The authors indeed concurred that this motif governs functional modulation of AMPARs by TARPs in activated states, based on the movements expected during AMPAR activation. Accordingly, this new structural research corroborates ideas about the "functional interactions" between AMPARs and their auxiliary proteins, first put forward in the results chapter that follows.

Article Title:

Distinct structural pathways coordinate the activation of AMPA receptor-auxiliary subunit complexes

ABSTRACT

Neurotransmitter-gated ion-channels adopt different gating modes to fine-tune signaling at central synapses. At glutamatergic synapses, high and low activity of AMPA receptors (AMPARs) is observed when pore-forming subunits co-assemble with or without auxiliary subunits, respectively. Whether a common structural pathway accounts for these different gating modes is unclear. Here, we identify two structural motifs that determine the time course of AMPAR channel activation. A network of electrostatic interactions at the apex of the AMPAR ligand-binding domain (LBD) is essential for gating by pore-forming subunits, whereas a conserved motif on the lower, D2 lobe of the LBD prolongs channel activity when auxiliary subunits are present. Accordingly, channel activity is almost entirely abolished by elimination of the electrostatic network, but restored via auxiliary protein interactions at the D2 lobe. In summary, we propose that activation of native AMPAR complexes is coordinated by distinct structural pathways, favoured by the association/dissociation of auxiliary subunits.

INTRODUCTION

Voltage- and ligand-gated ion-channels are signalling complexes that are often assembled from both regulatory and pore-forming subunits (Catterall et al., 2006; Jackson & Nicoll, 2011; Trimmer, 2015). AMPA-type (AMPAR) ionotropic glutamate receptors (iGluRs) are composed of pore-forming GluA1-4 subunits (Dingledine et al., 1999) that co-assemble with a variety of auxiliary proteins, including the transmembrane AMPAR receptor regulatory protein (TARP) and cornichon (CNIH) families (Tomita et al., 2003; Schwenk et al., 2009; Jackson & Nicoll, 2011), as well as CKAMP44 (von Engelhardt et al., 2010) and SynDIG1 (Kalashnikova et al., 2010), amongst others (Haering et al., 2014). Each pore-forming subunit possesses four principal domains, with the extracellular amino-terminal domain (ATD) controlling assembly and trafficking (Greger et al., 2007; Gan et al., 2015), and the ligand-binding domain (LBD) providing a bi-lobed agonist-binding pocket (Dawe et al., 2015). Meanwhile, the three transmembrane helices and re-entrant loop form the central pore domain, which governs cation selectivity and channel block (Huettner, 2015), and connects to the short, intracellular carboxyl-terminal domain (CTD). Once assembled, the native AMPAR is a homo- or heteromeric tetramer (Sobolevsky et al., 2009) with a variable stoichiometry of TARPs (Hastie et al., 2013) that may include additional CNIH subunits (Jackson & Nicoll, 2011; Herring et al., 2013). Understanding these interactions has been an area of intense study in recent years, especially as TARPs and CNIHs have been shown to directly affect the functional behaviour of native AMPARs as well as synaptic plasticity mechanisms (Jackson & Nicoll, 2011). Exactly how pore-forming and auxiliary subunits work together to achieve this, however, remains to be established.

Since TARPs and CNIHs are transmembrane proteins, interactions with AMPARs are expected to rely upon their proximity in the plasma membrane. Interestingly, protein-protein

interactions of this nature can be short- and long-lived. Autoinactivation of neuronal AMPARs is thought to reflect the rapid, millisecond-scale dissociation of AMPAR-TARP complexes mediated by receptor desensitization (Morimoto-Tomita et al., 2009; Constals et al., 2015). In contrast, single-channel analysis of AMPAR-TARP fusion proteins has revealed less frequent transitions between distinct gating modes of high and low open-channel probability (P_{open}) (Zhang et al., 2014) that are also thought to represent TARP-coupled and TARP-uncoupled forms of the receptor complex, respectively (Howe, 2015). The occurrence of distinct gating behaviour raises the question as to how auxiliary subunits mediate their effects on AMPAR gating. One possibility is that agonist-binding triggers channel activation through a single set of structural interactions that is modulated when pore-forming subunits are associated with auxiliary subunits. Alternatively, auxiliary subunits may integrate other allosteric sites into the activation process, depending on how they are functionally coupled to AMPAR complexes.

Here, we have designed experiments to delineate between these two possibilities. Our data identify a network of inter-subunit atomic bonds at the apex of the LBD that are critical to channel activation with pore-forming AMPAR subunits. This network can be stabilized by occupancy of an electronegative pocket that is conserved between AMPARs and kainate-type iGluRs (KARs). Disruption of the apical network abolishes almost all AMPAR gating, though co-assembly with auxiliary subunits rescues function because of interactions relayed through the lower, D2 lobe of the LBD. Thus, while it is likely that a common mechanism ultimately triggers opening of the channel pore, we propose that channel activation of native AMPAR complexes is coordinated by pathways originating from distinct structural interactions. One interaction is LBD apex-dependent and contained within pore-forming subunits, while the other is apex-independent, stemming from the association of AMPARs and auxiliary subunits.

RESULTS

A conserved cation pocket at the AMPAR and KAR LBD dimer interface

The topology of the iGluR tetramer is highly conserved between the AMPAR and KAR subfamilies, including the LBD, whose upper (D1) and lower (D2) lobes form the agonist-binding cleft (**Figure 2.1A**). AMPARs and KARs also possess an extensive network of electrostatic and hydrophobic interactions along the D1-D1 interface between subunits (Horning & Mayer, 2004) (**Figures 2.1B and 2.1C**) raising the question of their role in iGluR gating. In addition, KARs possess both sodium and chloride ion binding pockets at the apex of this interface, which are critical for channel gating (Bowie, 2010). In GluK2 KARs, occupancy of the cation-binding pocket (**Figure 2.1C**) is required for activation (Wong et al., 2006), with the time course of channel activity regulated by the residence time of bound sodium (Dawe et al., 2013). Curiously, although AMPARs have been considered cation-independent (Bowie, 2002), lithium has been modelled at this site in two X-ray crystal structures of the GluA2 LBD, including one determined at 1.24 Å resolution (**Figure 2.1B**) (Assaf et al., 2013) that exhibits many of the structural hallmarks of the KAR cation binding pocket (**Figure 2.1C**). Because lithium is frequently present in crystallization buffers for the GluA2 LBD (Green & Nayeem, 2015), we sought to determine if the lithium site is artifactual, with little impact on AMPAR gating, or whether lithium binding under experimental conditions can modulate gating behaviour.

To determine whether occupancy of the putative cation pocket affects AMPAR gating, molecular dynamic (MD) simulations were first performed to determine the residence time of lithium ions at wildtype GluA2 AMPARs (**Figure 2.1D**). Simulations were performed in either 150 mM NaCl or LiCl without initial occupancy of the pocket, enabling a prediction of whether cations readily bind to the site. When the distance between Glu507 (**Figure 2.1B**) and the closest

sodium or lithium ion was monitored over a 100 ns simulation, little meaningful interaction occurred (**Figure 2.1D**). The average frequency of interactions below 4 Å, taken as the cut-off value for intermolecular electrostatic interactions, was 0.4 % in NaCl and 5.2 % in LiCl, when the two binding sites of the dimer were considered. One factor that might explain the low propensity for cation binding is the contribution of Lys759 (**Figure 2.1B**), which often makes an intra-subunit projection toward the pocket and may compete with lithium ions for contact with electronegative residues. We therefore repeated the MD simulations, incorporating a mutation that replaced the positively charged Lys with a Met residue, as found in GluK2 KARs. As anticipated, lithium resided in the putative cation pocket for much longer periods of time (**Figure 2.1E**), confirming that removal of Lys759 impacts the ability of lithium to bind. Contact frequency between lithium and Glu507 averaged 52.1 % of simulation time, while sodium binding remained infrequent at 1.9 %. Together, these data make the prediction that lithium binding to the apex of the GluA2 LBD would have measurable consequences on AMPAR gating, which would be more pronounced for GluA2 K759M receptors.

Accordingly, we performed cation substitution experiments during patch-clamp recordings to determine whether lithium modulates the gating behaviour of wildtype and mutant GluA2 AMPARs. Membrane currents elicited by L-Glu in 150 mM NaCl at wildtype GluA2 and K759M receptors decayed rapidly with time constants of 6.9 ± 0.2 ms (n = 7; **Figure 2.1F**) and 9.9 ± 0.6 ms (n = 8; **Figure 2.1G**), consistent with MD simulations showing that sodium ions interact little with the electronegative residues of the cation pocket. The substitution of external NaCl with LiCl caused a dramatic slowing in the onset of desensitization (τ = 50.0 ± 3.4 ms; n = 7; $p < 0.0001$) for wildtype GluA2 (**Figure 2.1F**) and yielded a non-decaying phenotype (n = 6) in GluA2 K759M receptors (**Figure 2.1G**). In contrast, substitution with the larger monovalent

cation potassium had minimal effect on decay kinetics of both wildtype and mutant GluA2 receptors (**Figure S2.1)**. This suggests that access to the electronegative, "cation" pocket of AMPARs is restricted to ions of smaller ionic radius. Moreover, single-channel recordings revealed that external lithium prolongs the occurrence of channel openings prior to desensitization (**Figure S2.1**). Because the duration of this activity is affected by microscopic rates of channel opening and closing, as well as agonist unbinding and/or desensitization, we refer to channel activation/activity as the sum of these processes.

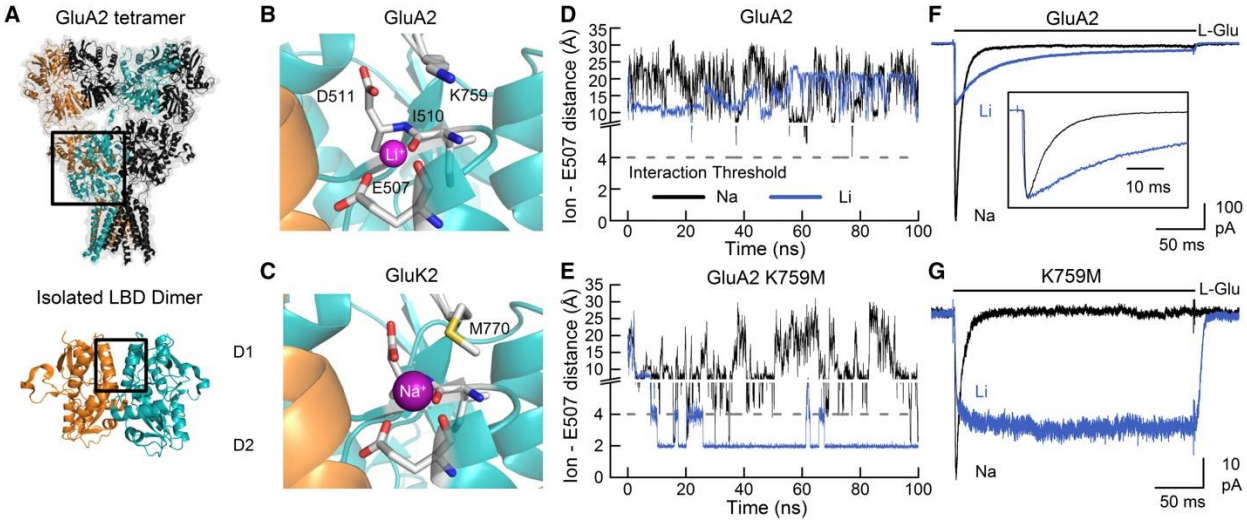

Figure 2.1 Lithium modulates GluA2 responses by binding at the LBD apex
(**A**) Crystal structure of the wildtype GluA2 tetramer (top, PDB: 3KG2; Sobolevsky et al., 2009) and isolated LBD dimer (bottom, PDB: 1FTJ; Armstrong & Gouaux, 2000).
(**B and C**) Illustration of the GluA2 (B) (PDB: 4IGT; Assaf et al., 2013) and GluK2 (C) (PDB: 2XXR; Nayeem et al., 2011) LBD dimer interfaces showing lithium and sodium ions, respectively, bound at a conserved electronegative pocket.
(**D and E**) Minimum distance between the nearest sodium or lithium ion and either sidechain oxygen atom found on residue Glu507 of chain A of wildtype GluA2 (D) or the K759M mutant (E). An interaction was deemed to occur when the cation was within 4 Å of an oxygen atom. In total, two 100 ns simulations were conducted in LiCl for each receptor, as well as three or four 100 ns simulations in NaCl for K759M and wildtype GluA2, respectively.
(**F and G**) Typical current responses elicited by 10 mM L-Glu on wildtype GluA2 (Patch # 140225p10) or K759M mutant (Patch # 140314p4) receptors in external solutions comprised of either NaCl or LiCl. Responses were also scaled to the same peak amplitude (inset).

Taken together, our observations corroborate the idea that in 150 mM LiCl external solution, lithium ions can bind to an electronegative pocket in wildtype and mutant GluA2 AMPARs, sustaining channel activity in an analogous manner to sodium binding at KARs (Dawe et al., 2013). However, unlike sodium, the presence of lithium in the nervous system is typically negligible, and even during lithium treatment for bipolar disorder, effective serum concentrations range from 0.4 -1.2 mM (Severus et al., 2008). When we supplemented our standard external recording solution with 1.5 mM LiCl there was no significant change in GluA2 decay kinetics ($p = 0.82$; $n = 5$; data not shown), meaning we could not ascribe a physiological role to cation binding at the GluA2 LBD. Instead, we used lithium as an experimental tool to interrogate the structural interactions modulated by its binding, and how these interactions shape the overall functional output of AMPARs.

GluA2 activation does not require electronegative pocket occupancy

One question not addressed by the cation substitution experiments is whether wildtype GluA2 or K759M AMPARs gate in the absence of external ions, as described previously for GluK2 KARs (Wong et al., 2006; Dawe et al., 2013). The issue is especially relevant for K759M receptors, where our data already establish that removal of the positively charged Lys provides a favourable binding site for external lithium ions (**Figures 2.1E and 2.1G**). The idea that AMPARs with the K-M mutation may be rendered cation-sensitive has been considered previously for GluA1 receptors, but it was not pursued further due to poor expression of the mutant (Wong et al., 2006). Using TIRF microscopy of GFP-tagged AMPARs, we confirmed that the equivalent K759M mutation in GluA2 did not prevent receptor expression at the plasma membrane (**Figure S2.2**). We therefore repeated experiments in external ion-free conditions for wildtype and mutant GluA2 receptors to determine their agonist responsiveness (**Figure 2.2**). In

agreement with observations on GluA1 receptors, GluA2 AMPARs continued to be activated by L-Glu, even in the absence of external NaCl, establishing that GluA2 AMPAR gating is not dependent on external cations, unlike GluK2 KARs (**Figures 2.2A and 2.2B**). GluA2 K759M also continued to elicit membrane currents when external NaCl was removed (**Figure 2.2C**), and in this condition both AMPARs produced outwardly rectifying current-voltage (I-V) plots that contrasted with the loss of the GluK2 response (**Figures 2.2D-2.2F**). These data demonstrate that while KARs require external cations to activate, GluA2 AMPARs require neither interactions with Lys759 in the wildtype receptor, nor occupancy by cations in the K759M mutant. As such, additional interactions modulated by lithium binding at the electronegative pocket must be able to profoundly affect GluA2 AMPAR activation.

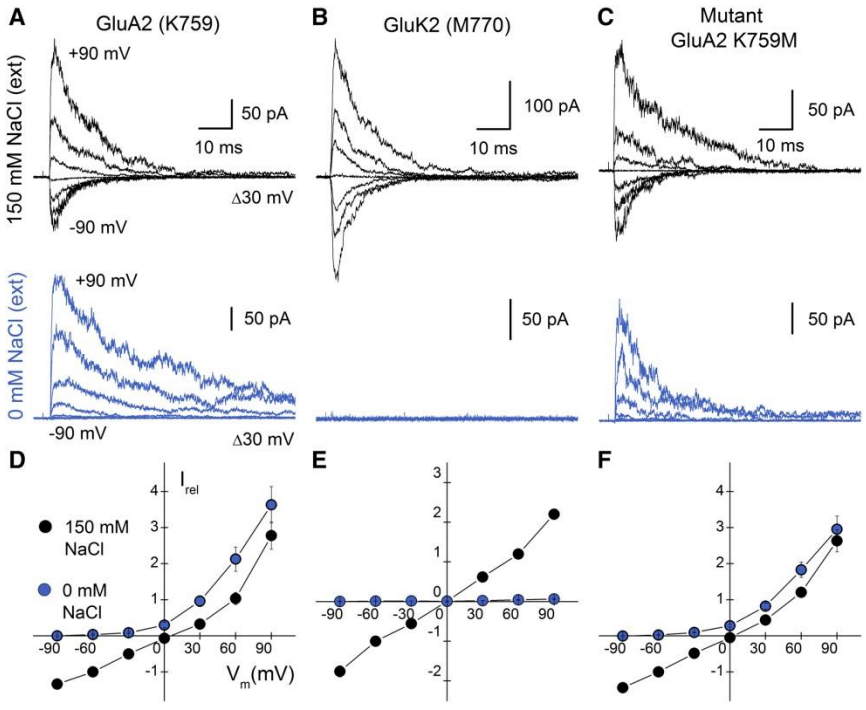

Figure 2.2 GluA2 K759M exhibits robust activation in the absence of external NaCl
(**A-C**) Membrane currents evoked by 1 (for KARs) or 10 mM (for AMPARs) L-Glu acting on wildtype GluA2 (A) and GluK2 (B), as well as GluA2 K759M mutant (C) receptors, in either 150 mM NaCl (top) or NaCl-free, sucrose-based (bottom) external solution (V_m = -90 to +90 mV, at 30 mV increments). For each receptor, the same patch was recorded in both ionic conditions. For wildtype GluA2 (Patch #

140417p4) and the K759M mutant (Patch # 140502p1) outward currents persisted at positive holding potentials, whereas GluK2 responses (Patch # 140904p3) were abolished.
(**D**-**F**) Current-voltage plots in 0 mM (blue) and 150 mM (black) NaCl for wildtype GluA2 (D), GluK2 (E), and GluA2 K759M (F) receptors. Currents were normalized to responses at -60 mV in 150 mM NaCl. Data are mean ± SEM, from four (GluA2), three (GluK2), or six (K759M) independent experiments for each receptor.

The electronegative pocket acts through inter-subunit contacts

Since the lithium binding site is quite distant from the channel pore, it remained unclear how lithium might influence LBD structure to stabilize the activated state of the receptor. To address this we used MD simulations, which revealed that cation binding promotes re-arrangements in the GluA2 K759M LBD dimer interface. Specifically, increasing the number of bound lithium ions shifted the distribution of predicted distances across the interface in a negative direction (**Figures 2.3A and 2.3B**). Because these distances were measured between two points at the apex of each D1 lobe, they are referred to as D1-D1 interface distances (**Figure 2.3B**). Nevertheless, lithium binding sites are fully contained within single subunits on each side of the interface, making it unlikely that lithium acts directly as an adhesive force between subunits. However, the ion is coordinated by Glu507, which forms electrostatic interactions across the interface with both Lys514 and Asn768 (**Figure 2.3A**). This prompted us to explore whether lithium modulates GluA2 current decay kinetics by stabilizing inter-subunit electrostatic interactions. We therefore removed these interactions in a K514M/N768T double mutant, where the mutated residues retain approximately the same bulkiness, but lose their charge or ability to form the same cross-dimer hydrogen bonds. This mutant exhibited currents that decayed with time constants of 8.4 ± 1.2 ms (n = 5) in NaCl and 6.9 ± 1.1 ms (n = 5) in LiCl (**Figures 2.3C and 2.3D**). The observation that decay kinetics were not significantly different between cation species (p = 0.26) stands in marked contrast to wildtype GluA2 (**Figure 2.3D**), and confirms that lithium modulation was abolished. Since it is possible that lithium binding was disrupted in

GluA2 K514M/N768T, we used MD simulations to evaluate this possibility. MD data revealed no gross conformational changes to the LBD dimer, and moreover, reported that lithium ions interact with the pocket with a frequency similar to or greater than with wildtype GluA2 (**Figure S2.3**). Taken together, our data indicate that experimental concentrations of external LiCl (i.e. 150 mM) influence inter-subunit electrostatic contacts at the apex of the LBD dimer interface, thereby stabilizing the activated conformation of the receptor. To explore this idea further, we investigated whether strengthening the apex of the LBD dimer interface could sustain AMPAR activation.

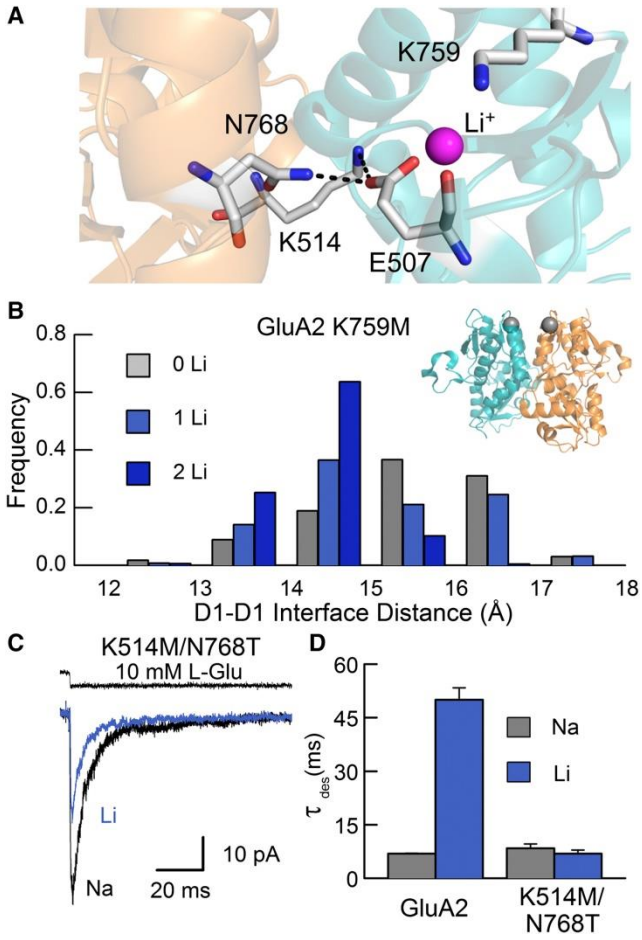

Figure 2.3 Lithium modulation is mediated by cross-dimer electrostatic contacts
(**A**) Image of an inter-subunit salt bridge and hydrogen bond adjacent to the lithium binding site (PDB: 4IGT; Assaf et al., 2013). Residues K514 and N768 are from chain A, while E507 and K759 are from chain B.
(**B**) Inter-subunit distance across the apex of the GluA2 LBD, relative to the number of lithium ions occupying the two cation pockets, measured during 100 ns MD simulations (two repeats) of GluA2 K759M in LiCl. Distances were measured between the grey spheres (inset, right), which represent a centre of mass for Cα atoms of residues 508-510 and 759-765.
(**C**) Typical current responses to L-Glu obtained from the GluA2 K514M/N768T mutant (Patch # 140718p4), recorded in external NaCl and LiCl. The top trace (black) shows the junction current, recorded with an open patch pipette after the experiment to monitor the profile of solution exchange.
(**D**) Plot of current decay time constants (τ_{des}) for wildtype GluA2 and K514M/N768T receptors. Data are mean ± SEM, from seven (wildtype GluA2), or five (K514M/N768T) independent patch experiments for each receptor.

Engineering an inter-subunit tether to sustain channel activation

In order to incorporate an additional electrostatic interaction across the D1-D1 interface, we used a Thr765 to Lys mutation to introduce a charged tether onto residues forming the opposing electronegative pocket (for additional rationale, see **Figure S2.4**). Alone, this mutation had little functional effect, but coupled with the K759M mutation (K759M/T765K) current decay slowed several fold, and the additional mutation N768T (creating K759M/T765K/N768T, or MKT) yielded non-decaying current responses (**Figure 2.4A**). Consistent with this, single-channel events of GluA2 MKT were sustained throughout the 250 ms period of agonist application, in contrast to wildtype channels (**Figures 2.4B and 2.4C**). In both cases, current records were fit with four conductance levels of approximately 6, 12, 24, and 40 pS, with the P_{open} of GluA2 MKT estimated to be 0.62 ± 0.14 (n = 4) (**Figure 2.4D**). The occurrence of MKT channel closures in these conditions could be explained by the failure of the mutant Lys residue to form a sustained, cross-dimer tether, enabling the LBD dimer to rupture.

In order to verify that a Lys tether had been introduced across the GluA2 LBD dimer, we attempted structural analysis of the MKT mutant. However, protein expression levels were too low to obtain diffracting crystals. In contrast, crystals of the GluA2 K759M/T765K LBD were

successfully grown in the presence of zinc, and a dataset was collected from a single crystal at 2.9 Å resolution (**Table S2.1**). Three protomers were present in the asymmetric unit, of which chains A and B formed a canonical dimer, and the third, C, formed a dimer with its symmetry-related counterpart. In each dimer (A:B and C:C') electron density was visible for both the mutant Met and Lys residues, and the latter residue was spanning the dimer interface as predicted (**Figure 2.4E; Figure S2.5**). Electrostatic interactions were formed between the amine group on residue 765 (i.e. T765K) and the sidechain carboxyl group of Asp511, as well as the backbone oxygen atom of Ile510 (**Figure 2.4E**). In addition to these contacts, there was also a general shift in the dimer conformation, with the apical residues having moved closer together relative to structures of wildtype GluA2, and forming a more extensive, contiguous interface (**Figure 2.4F**).

Consistent with functional recordings of GluA2 K759M/T765K (**Figure 2.4A**), our structural data also suggest that the cross-dimer tether does not persist indefinitely. First, an additional crystal structure grown in the presence of lithium (**Table S2.1**) revealed that the electronegative pocket was partially occupied by a lithium ion (**Figure S2.4; Figure S2.5**), and not the opposing Lys residue. Second, in MD simulations of both the double and triple mutant receptors, the T765K residue failed to make continuous contact with the electronegative pocket (**Figures 2.4G and 2.4H**). Overall, these structural and functional data support the premise that the Lys tether is not a permanent feature of the T765K mutant series. However, the MKT mutation makes tethering more favourable; likely because the replacement of Asn by the smaller Thr at position 768 reduces steric block, thereby allowing subunits within each LBD dimer to come closer together. As explained below, we explored the opposite effect of dimer cross-linking by determining if elimination of electrostatic interactions at the apex of the LBD dimer interface would disrupt GluA2 AMPAR functionality.

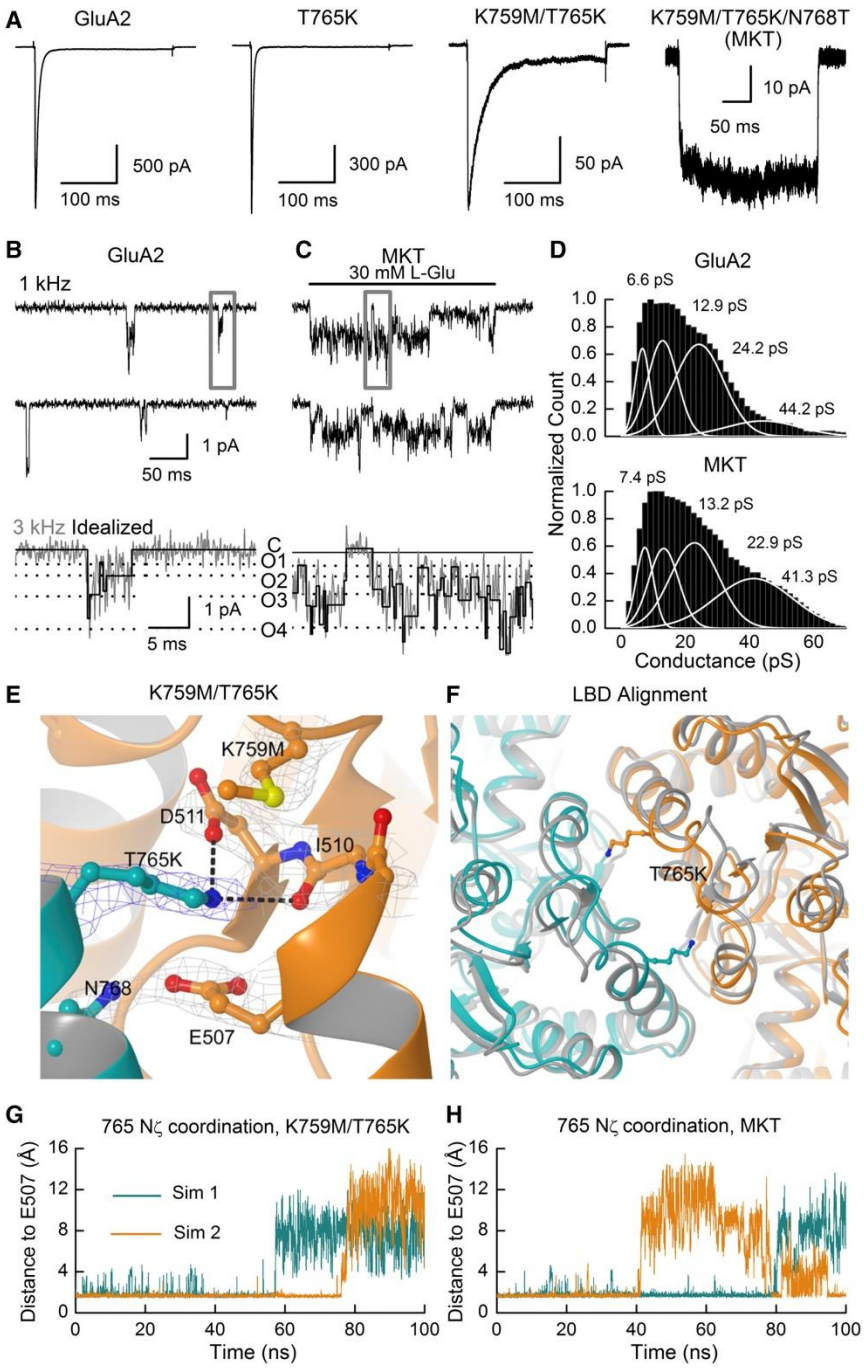

Figure 2.4 Structural and functional data show T765K can act as a cross-dimer tether

(**A**) Typical current responses to 10 mM L-Glu for a series of GluA2 mutants engineered to form a cross-dimer tether. Wildtype GluA2 (Patch # 130221p5), and mutants T765K (Patch # 130617p4), K759M/T765K (Patch # 130618p6), and K759M/T765K/N768T, or MKT (Patch # 130917p6) are shown left to right.

(**B and C**) Unitary channel activity evoked by 30 mM L-Glu for wildtype GluA2 receptors in equilibrium conditions (B) (Patch # 131212p7) and the triple mutant MKT (C) (Patch # 140124p1) during a 250 ms agonist application. Typical records are shown low-pass filtered at 1 kHz (top) or the 3 kHz threshold

used to fit channel openings (bottom), expanded from grey box above. Horizontal dotted lines correspond to the conductance levels of open states (O1-4) fit in panel D.
(**D**) Distributions of conductance levels from idealized records of wildtype GluA2 (top) or GluA2 MKT (bottom) fit with four Gaussian functions (white lines). Openings were analyzed using four patch recordings for each receptor.
(**E**) View of protomers A (orange) and B (teal) from the K759M/T765K structure, zinc-form, showing T765K tethering onto electronegative residues on the opposing subunit. Electron density ($|2F_{obs} - F_{calc}|\alpha_{calc}$, contoured at 1.3σ) is shown around the displayed side-chains only. Interactions between the amine group of 765 and atoms in protomer A are shown as dashed lines.
(**F**) Top view of an alignment between wildtype GluA2 (grey; PDB: 1FTJ; Armstrong & Gouaux, 2000) and K759M/T765K (orange / teal) LBD dimers.
(**G and H**) Minimum distance between the amine group nitrogen atom on the mutant Lys (introduced on chain B) and either sidechain oxygen atom found on residue Glu 507 (on chain A) for K759M/T765K (G) and the MKT mutant (H). Simulations were performed using the GluA2 K759M/T765K LBD dimer, while the N768T mutation was introduced atop this structure to simulate GluA2 MKT. Two repeats are shown for each mutant.

Removal of an electrostatic network disrupts gating by pore-forming subunits

Although the addition of new cross-dimer interactions (e.g. GluA2 MKT) can sustain GluA2 gating, the mutation of other interface residues has been shown to curtail channel activity. For example, the individual conversion of residues Glu507, Lys514, and Asn768 at the apex of the dimer interface (**Figure 2.5A**) to Ala speeds desensitization (Horning & Mayer, 2004). Of these residues, Glu507 and Lys514 form a salt bridge (**Figure 2.5A**). Interestingly, the two residues are conserved in AMPARs and KARs, but not NMDARs (**Figure S2.6**), suggesting that different sets of interactions regulate their slow time course of activation. However, because both Asn768 and Phe512 (via a backbone oxygen atom) can also contribute to the electrostatic network in GluA2, we evaluated the effect of completely disrupting this network using the triple mutant GluA2 E507A/K514A/N768A (i.e. GluA2 AAA). On this note, mean peak current responses elicited by GluA2 AAA (94.5 ± 28.5 pA; n = 7) were depressed by almost 10-fold compared to wildtype GluA2 receptors (928 pA ± 317 pA; n = 12) (**Figures 2.5B and 2.5C**). In addition, the onset of desensitization was almost ten-fold faster for GluA2 AAA (τ = 0.74 ± 0.06 ms; n = 7) versus wildtype GluA2 (τ = 6.1 ± 0.2 ms; n = 7) (**Figure 2.5D**). The diminished

functionality of the GluA2 AAA mutant demonstrates that the network of electrostatic interactions at the apex of the LBD dimer interface is a key structural element mediating channel gating by pore-forming AMPAR subunits.

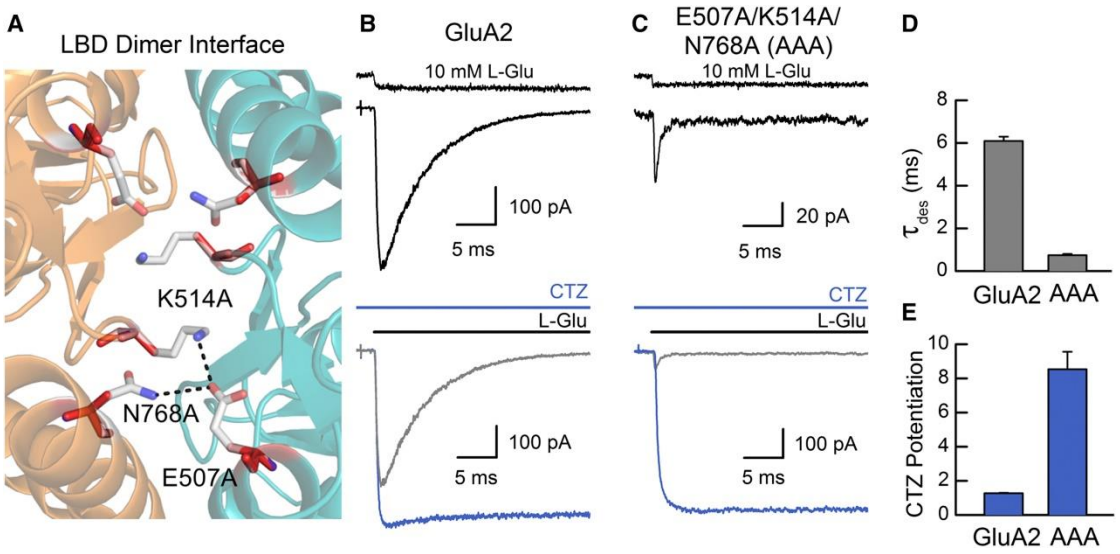

Figure 2.5 Truncation of key residues at LBD apex produces poorly functioning receptors
(**A**) Top view of the GluA2 LBD dimer interface (PDB: 1FTJ; Armstrong & Gouaux, 2000), showing charged and polar residues (faint grey) that were mutated to Ala (red). Labelled residues K514 and N768 are from chain A, while E507 is from chain B.
(**B and C**) Typical current responses of wildtype GluA2 (B) (Patch # 130305p7) and the E507A/K514A/N768A, or AAA mutant (C) (Patch # 151005p6) to L-Glu before (top, black; bottom, grey) and during (bottom, blue) exposure to cyclothiazide (CTZ), which attenuates desensitization. The uppermost trace (black) shows the junction current, recorded with an open patch pipette after the experiment to monitor the profile of solution exchange.
(**D**) Average time constants of current decay (τ_{des}) for wildtype GluA2 and the AAA mutant. Data are mean ± SEM, from seven (wildtype GluA2 and GluA2 AAA) independent patch experiments.
(**E**) CTZ potentiation of wildtype GluA2 and AAA mutant peak currents. Data are mean ± SEM, from eleven (wildtype GluA2) or seven (GluA2 AAA) independent patch experiments.

Appreciating that the positive allosteric modulator cyclothiazide (CTZ) binds to the bottom of the D1-D1 interface (Sun et al., 2002), we tested whether AMPAR functionality could be recovered when CTZ was present. CTZ restored the responsiveness of the GluA2 AAA mutant causing an 8.5 ± 1.0 fold (n = 7) increase in the peak response. In marked contrast, CTZ potentiated wildtype GluA2 currents to a significantly lesser extent of 1.3 ± 0.03 fold (n = 11; $p < 0.001$; **Figures 2.5B, 2.5C, and 2.5E**). However, since functionality can be restored by CTZ,

we conclude that, under certain circumstances, other interactions are capable of coordinating channel gating independent of the LBD apex region. To explore this further, we tested whether the functionality of GluA2 AAA could be rescued by co-expression with auxiliary subunits.

Auxiliary subunits rescue functionality of the GluA2 AAA mutant

To test the effect of TARP or CNIH protein association on GluA2 AAA, we co-expressed the mutant receptor with either γ2 or γ7 TARP subunits, or CNIH-3 (**Figure 2.6**). To control for the effect of TARPs and/or CNIHs on AMPAR trafficking (Jackson & Nicoll, 2011), we used the potentiation of peak L-Glu responses by CTZ as an estimate of P_{open} (Cho et al., 2007), or gating ability, in each condition. Large membrane currents were elicited from GluA2 AAA receptors when co-expressed with either TARP or CNIH subunits, contrasting with the AAA mutant expressed alone (**Figures 2.6A-2.6D**). Moreover, peak current potentiation of GluA2 AAA responses by CTZ was significantly reduced to 1.5- to 3-fold when receptors were co-expressed with γ2, γ7, or CNIH-3 subunits ($p < 0.002$ in all cases), though still higher than observed with wildtype receptors (**Figure 2.6E**). This finding reaffirms our hypothesis that auxiliary subunits are capable of coordinating channel gating of pore-forming subunits, independent of the network of electrostatic interactions at the LBD apex region. Also, desensitization kinetics of GluA2 AAA were also markedly faster than wildtype receptors when co-expressed with TARPs γ2 and γ7 (**Figures 2.6F and 2.6G**). Auxiliary subunits therefore do not fully rescue the gating deficits of GluA2 AAA, and most likely coordinate channel gating in synchrony with the apex region of the AMPAR LBD dimer interface. As a consequence, AMPAR channel gating is coordinated by apex-dependent and -independent interactions. The former are comprised of an intra-protein electrostatic network that mediates the activation of

pore-forming subunits, while the latter depends upon interactions that become available upon the association of auxiliary subunits.

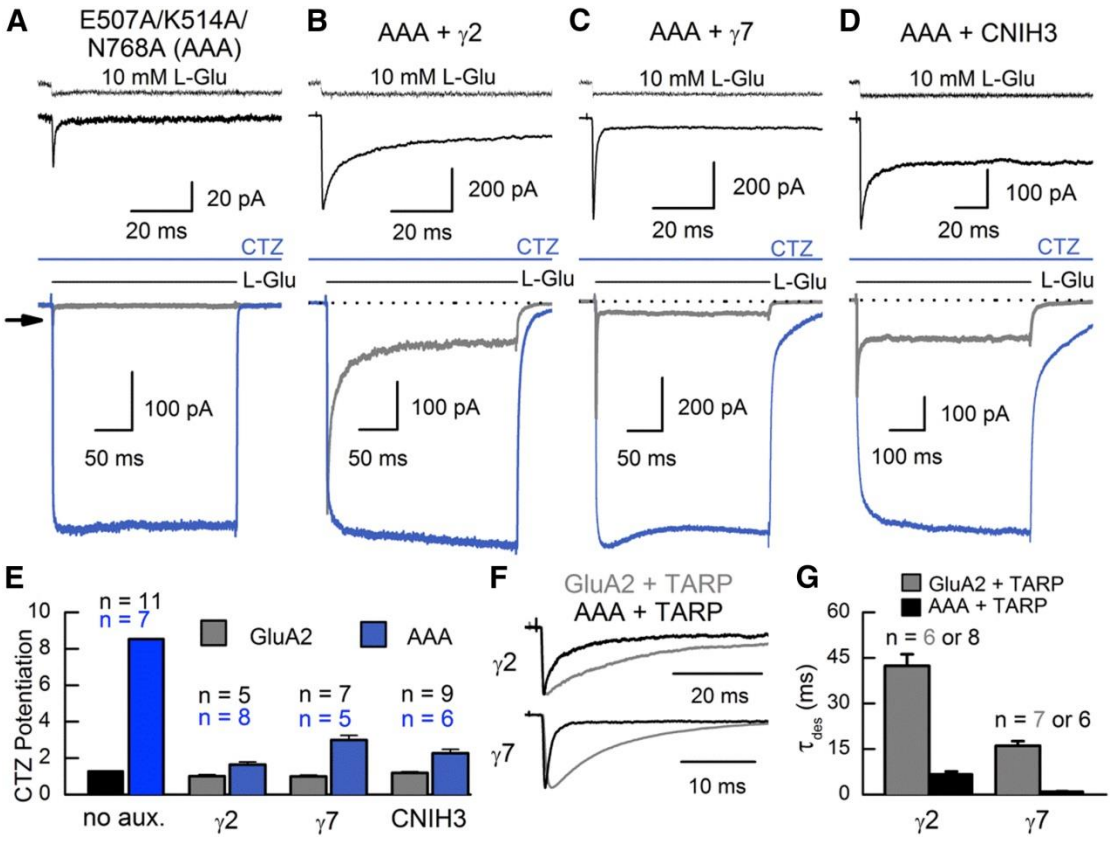

Figure 2.6 Co-expression of auxiliary subunits rescues function of the GluA2 AAA mutant
(**A-D**) Behaviour of GluA2 E507A/K514A/N768A, or AAA receptors when expressed alone (A) (Patch # 151008p10), or co-expressed with the TARP subunits γ2 (B) (Patch # 140731p3) or γ7 (C) (Patch # 141006p8), as well as the CNIH subunit CNIH-3 (D) (Patch # 140926p5). Traces correspond to L-Glu evoked responses prior to CTZ application (top, black; bottom, grey), or responses during (blue) CTZ exposure. The uppermost trace (black) shows the junction current, recorded with an open patch pipette after the experiment to monitor the profile of solution exchange. Arrow indicates the peak response of GluA2 AAA.
(**E**) CTZ potentiation of wildtype GluA2 and AAA mutant currents, tabulated in the presence or absence (no aux.) of different auxiliary subunits. Data are mean ± SEM, from the number of independent patch experiments indicated. Values with auxiliary subunits absent are as reported in Figure 2.5.
(**F**) Scaled comparison of wildtype GluA2 (grey) and AAA mutant (black) responses when co-expressed with TARP subunits γ2 (WT Patch # 141006p3, AAA Patch #140721p3) and γ7 (WT Patch # 141013p4, AAA Patch #141006p8).
(**G**) Time constants of current decay (τ_{des}) for wildtype GluA2 and GluA2 AAA co-expressed with TARP subunits γ2 or γ7. Data are mean ± SEM, from the number of independent patch experiments indicated.

TARPs modulate the duration of AMPAR gating by interactions on the D2 lobe

In order to pinpoint the site(s) where auxiliary proteins modulate AMPAR gating, we first compared the sequence of AMPAR and KAR LBDs. Since KARs do not bind TARPs (Chen et al., 2003), we reasoned that a sequence alignment would identify residues unique to AMPARs that may form functional interactions with auxiliary subunits. The most promising site was a Lys-Gly-Lys, or KGK motif (residues 718 – 720), situated on the lower D2 lobe of the GluA2 LBD, which is conserved amongst all AMPAR subunits (**Figures 2.7A and 2.7B**). The KGK motif faces outward, where an auxiliary subunit might be expected to reside, based on previous cryo-EM images of native AMPARs (Nakagawa et al., 2005). These three amino acids were therefore substituted with the single Asp residue (termed '3D' mutation) found in GluK1-3 KARs, where two residues are lost (**Figure 2.7B**). Importantly, the GluA2 3D mutant receptor had similar kinetic properties to wildtype GluA2, with deactivation and desensitization time constants of 0.53 ± 0.05 ms (n = 5) and 6.2 ± 0.5 ms (n = 5), respectively, demonstrating that this site has a minimal effect on channel gating mediated solely by pore-forming subunits.

To study the functional impact of the 3D mutant on TARP-dependent gating, we used a GluA2/γ2 fusion protein to constrain subunit stoichiometry and to also prevent any confounding effect of disrupting AMPAR-TARP association. We then evaluated the 3D mutant by investigating three sets of AMPAR properties known to be regulated by TARP association: the time course of channel activation (Priel et al., 2005), apparent agonist efficacy (Turetsky et al., 2005), and the degree of polyamine channel block (Soto et al., 2007). First, we examined the time course of L-Glu induced channel activation by measuring both deactivation and desensitization kinetics (**Figures 2.7C and 2.7D**). We also assessed the degree of equilibrium desensitization by measuring the equilibrium/peak response ratio (**Figure 2.7E**). Second, we

examined apparent agonist efficacy by using CTZ potentiation as an indicator of peak P_{open} (Cho et al., 2007) and measuring the KA/L-Glu current ratio (**Figure S2.7**). Finally, we analyzed the affinity and voltage-dependency of polyamine channel block, which was determined using 100 μM internal spermine (**Figure S2.7**).

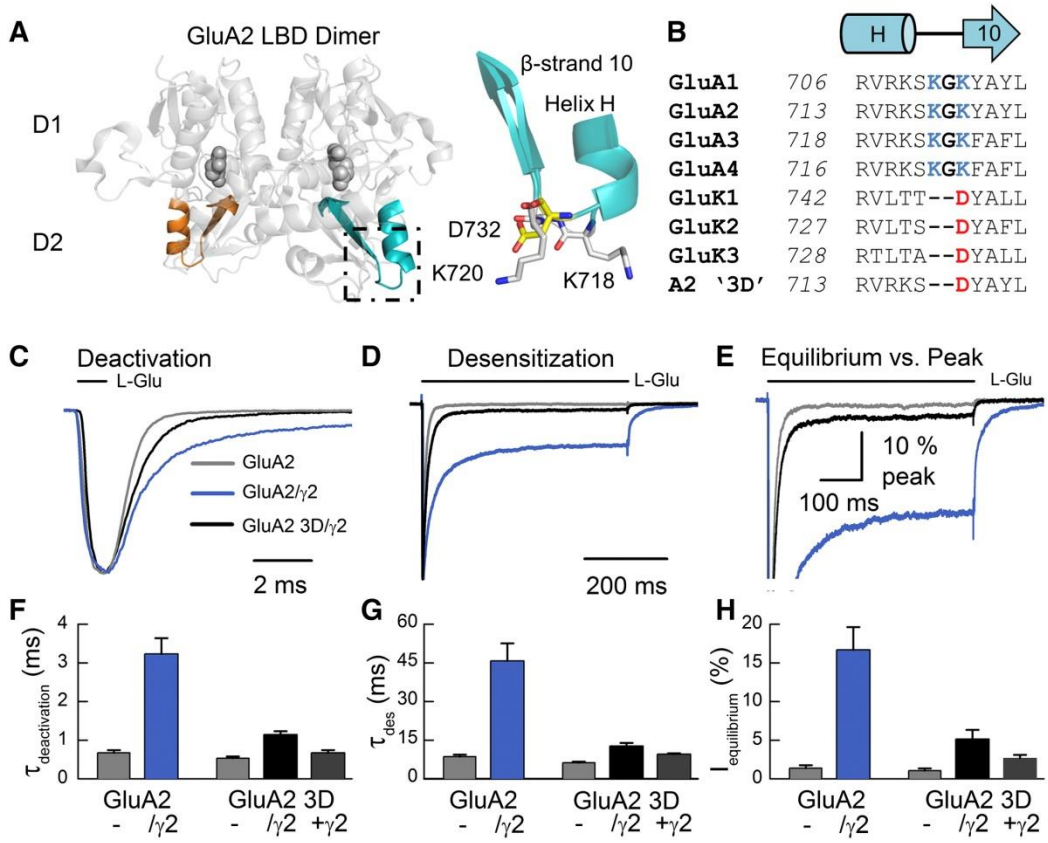

Figure 2.7 A single D2 mutation attenuates TARP γ2 modulation of GluA2 current decay
(**A**) View of the GluA2 LBD dimer (PDB: 1FTJ; Armstrong & Gouaux, 2000), highlighting the site of the 718-720 KGK to D (3D) mutation (in colour, at left), between helix H and β-strand 10 on the D2 lobe (at right). Mutated residues appear as in GluA2 (grey stick) or GluK2 (yellow stick) structures (PDB: 1FTJ or 2XXR; Nayeem et al., 2011).
(**B**) Sequence alignment of the 3D mutation site for rat AMPAR and KAR subunits.
(**C and D**) Scaled current responses of wildtype GluA2 (Patch # 150317p2, grey), as well as GluA2/γ2 (Patch # 150316p3, blue) and GluA2 3D/γ2 (Patch # 150511p6, black) AMPAR-TARP fusion proteins to 1 ms (C) and 500 ms (D) applications of 10 mM L-Glu.
(**E**) Scaled equilibrium responses of wildtype GluA2 (Patch # 150317p3, grey), as well as GluA2/γ2 (Patch # 150316p3, blue) and GluA2 3D/γ2 (Patch # 150511p6, black) AMPAR-TARP fusion proteins during a 500 ms L-Glu application.
(**F-H**) Mean time constants of current decay after a 1ms L-Glu application ($\tau_{deactivation}$) (F) or in the continued presence of L-Glu (τ_{des}) (G), as well as mean equilibrium current amplitude, as a percentage of the peak response (H). Data are mean ± SEM, from the number of independent patch experiments that

follows: eight (F) or nine (G and H) for GluA2, nine (F) or eleven (G and H) for GluA2/γ2, five (F-H) for GluA2 3D, eight (F-H) for GluA2 3D/γ2, and seven (F-H) for co-expressed GluA2 3D + γ2.

When incorporated into the wildtype GluA2/γ2 fusion receptor, the 3D mutation accelerated deactivation and desensitization kinetics from 3.2 ± 0.4 ms (n = 9) and 45.7 ± 6.8 ms (n = 11), respectively, to 1.1 ± 0.1 ms (n = 8) and 12.7 ± 1.2 ms (n = 8), respectively (**Figures 2.7C and 2.7D**). Notably, the deactivation (τ = 0.67 ± 0.07 ms; n = 7) and desensitization (τ = 9.5 ± 0.4 ms; n = 7) time constants of GluA2 3D co-expressed with γ2 were statistically indistinguishable from GluA2 expressed alone (p = 0.95 and p = 0.29, respectively; **Figures 2.7F and 2.7G**), suggesting that the 3D mutant almost completely abolishes the effects of γ2 on the time course of GluA2 channel activity. Likewise, the equilibrium/peak response (%) was also reduced from 16.7 ± 2.9 % (n = 11) with GluA2/γ2 to 5.1 ± 1.2 % (n = 8) with GluA2 3D/γ2 (**Figure 2.7E**), which was much closer to the equilibrium/peak response of GluA2 alone (**Figures 2.7E and 2.7H**). The reverse mutation in GluK2 KARs (i.e. Asp732 to Lys-Gly-Lys) produced no significant change in channel kinetics between the mutant receptor expressed alone or as a GluK2/γ2 fusion protein (data not shown), suggesting that these residues in the D2 lobe are not sufficient to confer functional TARP modulation of KARs. Taken together, our data identify the KGK motif as the critical structural element by which TARP γ2 prolongs the time course of AMPAR channel activation.

Interestingly, other functional properties of AMPARs modulated by TARPs such as CTZ potentiation, KA/L-Glu current ratio, and polyamine channel block were unchanged in the GluA2 3D/γ2 mutant receptor (for details see **Figure S2.7**). These findings demonstrate that TARPs are still able to associate with the 3D mutant GluA2 subunits, despite the reduced

modulation of channel decay kinetics. Importantly, these findings also show that the 3D site only accounts for a subset of all properties by which TARPs regulate AMPARs.

LBD dimer apex and the D2 lobes coordinate channel activation independently

Because the 3D site profoundly attenuates the prolongation of channel activation by TARPs, we examined whether functional coupling between the D2 lobe and the TARP γ2 could account for the rescue of GluA2 AAA receptors by auxiliary subunits (**Figure 2.6**). To do this, the time course of channel activation of the double-site mutant, GluA2 AAA/3D, was compared in the presence and absence of TARP γ2 (**Figure 2.8**). In the absence of TARP subunits, there was no significant difference between desensitization time constants for GluA2 AAA and GluA2 AAA/3D (τ = 0.68 ± 0.10 ms; n = 6; p = 0.56; **Figures 2.8A and 2.8B**). Consistent with the phenotype of GluA2 AAA, the mean peak response of GluA2 AAA/3D was also small in amplitude (29.8 ± 8.6 pA; n = 7) and greatly potentiated by CTZ (17.0 ± 2.2 fold; n = 7; **Figure 2.8B**). However, when co-expressed with the γ2 subunit, the time constant of desensitization was about 3-fold faster (τ = 2.4 ± 0.3 ms; n = 7) for GluA2 AAA/3D than GluA2 AAA (τ = 6.6 ± 0.9 ms; n = 8; p = 0.002; **Figures 2.8C-2.8E**). The attenuation in γ2 modulation of the AAA mutant demonstrates that the 3D site is largely responsible for rescuing the time course of channel activation. Figure 2.8E summarizes how the co-expression of γ2 affects desensitization rates of the AAA and/or 3D mutant GluA2 receptors. Whether LBD apex interactions are present (i.e. wildtype GluA2) or absent (i.e. GluA2 AAA) the 3D mutation reduces TARP modulation of desensitization kinetics approximately three fold (**Figure 2.8E**). This suggests an independence of the LBD apex and D2 lobe in regulating the gating behaviour of TARP-associated AMPARs. In summary, our data support a model where different sets of structural interactions determine the time course of activation of AMPAR-auxiliary subunit complexes (**Figure 2.8F**).

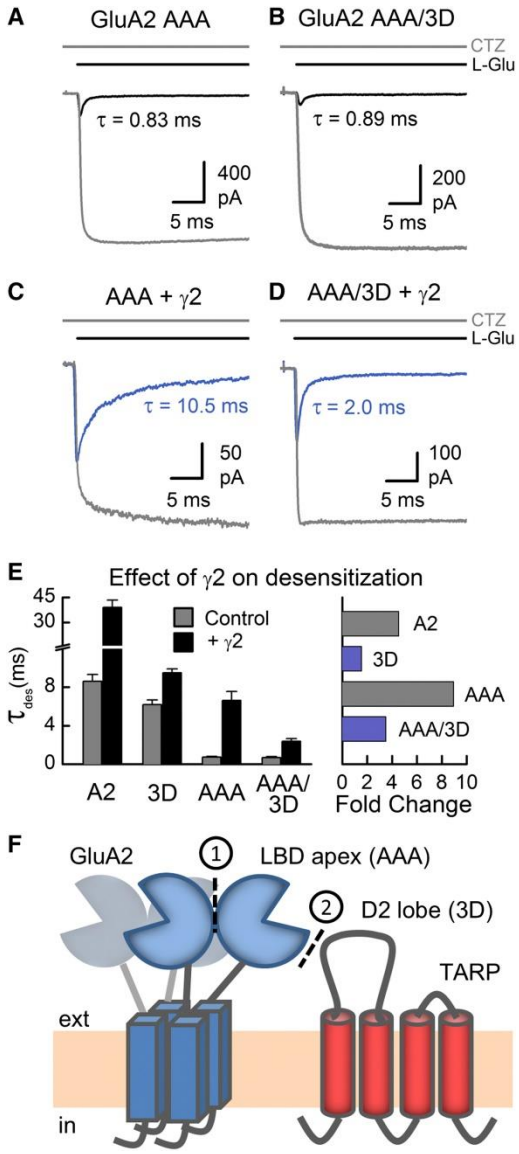

Figure 2.8 Intra- and inter-protein interactions independently regulate GluA2 gating
(**A-D**) Typical current responses of GluA2 AAA (A) (Patch # 151005p12), AAA/3D (B) (Patch #151001p11), AAA + γ2 (C) (Patch #140721p3), and AAA/3D + γ2 (D) (Patch #150924p11) mutant receptors to a 250 ms application of 10 mM L-Glu, shown before (black, or blue with γ2) and during (grey) CTZ exposure. Time constants of current decay during desensitization are indicated.
(**E**) Mean time constants of current decay (τ_{des}, left) for several GluA2 receptors, which were expressed alone (grey bar) or co-expressed with the TARP subunit γ2 (black bar). The ratio of the time constants for each receptor (γ2: no TARP) is also shown, expressed as a fold change (right). Data are mean ± SEM, from the number of independent patch experiments that follows: nine (GluA2), ten (GluA2 + γ2), five (GluA2 3D), seven (GluA2 3D + γ2), seven (GluA2 AAA), eight (GluA2 AAA + γ2), six (GluA2 AAA/3D), and seven (GluA2 AAA/3D + γ2).
(**F**) Illustration of two distinct LBD regions (apex and D2 lobe) critical for regulating the time course of GluA2 activation, which were disrupted by the AAA and 3D mutations, respectively.

DISCUSSION

This study advances our understanding of AMPARs in two fundamental ways. First, we demonstrate that an evolutionary-conserved electrostatic network within the LBD apex is critical for the activation of pore-forming AMPAR subunits, which use it to generate rapid, millisecond-scale gating at central synapses. This network can be stabilized by the occupancy of an adjacent cation pocket, sustaining channel activation by a similar mechanism to sodium binding at KARs (Dawe et al., 2013). Although physiological cation species do not appear to regulate the GluA2 LBD apex, the near loss of channel activity after elimination of the electrostatic network indicates this region is one of the most important structural determinants of AMPAR gating. Accordingly, our observations reveal that for both KA and AMPA receptor families, changes in only a few critical atomic interactions can drastically alter the time course of channel activation. Second, we show that pore-forming AMPAR subunits use different gating pathways when associated with and without auxiliary proteins. Although TARPs have been the focus of numerous studies in recent years, the structural interactions underpinning their modulation of AMPARs have remained largely unknown. Our data identify an important site at the D2 lobe of the GluA2 LBD, which mediates TARP prolongation of channel gating, independently of interactions at the LBD apex. Because this motif does not affect other properties modulated by TARPs (i.e. agonist efficacy and permeation), we conclude that several discrete sites must act together to bring about the ensemble behaviour of TARP-bound AMPARs.

An evolutionarily-conserved hotspot governing KAR and AMPAR activation

A key difference between KARs and other iGluRs subfamilies is that external cations are required for KAR activation, in addition to modulating their gating behaviour (Bowie, 2002;

Wong et al., 2006). Although AMPAR and KAR protein architecture is very similar, the ability of cations to modulate AMPARs has not been thoroughly studied. In part, this was due to the discrepancy between the KAR cation-binding pocket, which can bind monovalent cations of various sizes (Bowie, 2002; Plested et al., 2008), and the equivalent AMPAR site, where lithium binding was only recently observed (Assaf et al., 2013). Moreover, the gating kinetics of GluA1 AMPAR subunits lack modulation by cations (Bowie, 2002), and perhaps cannot bind lithium. It should be noted that a potentiation of GluA2 and GluA3 equilibrium currents by external lithium was reported in oocytes (Karkanias & Papke, 1999), and later experiments characterized an increase in native AMPAR P_{open} under similar conditions (Gebhardt & Cull-Candy, 2010). These observations are consistent with the behaviour we observed in outside-out patch recordings; however, no structural mechanism was then ascribed to them.

By combining recordings of full-length GluA2 receptors with simulations of the LBD dimer, we were able to show that high experimental concentrations of external LiCl permit lithium to occupy an electronegative pocket in the apical dimer interface, thereby sustaining channel activation. Furthermore, we identified an inter-subunit electrostatic bridge adjacent to the pocket that mediates lithium effects on gating. Because LBD dimer pairs appear to be intact in unliganded and pre-open, but not desensitized GluA2 structures (Durr et al., 2014; Meyerson et al., 2014), the rupture of this bridge might be a key trigger for desensitization. In this sense, lithium acts upon GluA2 as we proposed sodium does for GluK2, serving as a gatekeeper to prevent desensitization (Dawe et al., 2013).

Auxiliary subunits rewire the AMPAR gating pathway

There is a substantial body of literature describing to what extent TARP and CNIH proteins modulate or, typically, slow AMPAR desensitization and deactivation kinetics (e.g. Priel et al., 2005; Schwenk et al., 2009). Nevertheless, it is presently debated whether such effects are mediated primarily through increasing the rate of channel opening, pre-gating rearrangements of the agonist-binding cleft, or other kinetic transitions. Our observation that the co-expression of auxiliary subunits rescued gating deficits in the GluA2 AAA mutant receptor brings new perspective to how they modulate AMPAR behaviour. The Ala mutations were predicted to weaken affinity between individual LBDs, leading dimers to more readily move apart, as is proposed to occur during the structural transition to desensitization (Sun et al., 2002; Meyerson et al., 2014). Because the binding site for CTZ has been well characterized, its rescue of GluA2 AAA could be attributed to the molecule acting as an adhesive in the LBD dimer interface, interfering with the separation of subunits (Sun et al., 2002). In contrast, TARPs and CNIHs are large transmembrane proteins, and unlikely to brace the LBD dimer from within, meaning another mechanism should account for their rescue of the AAA mutant.

Cryo-EM experiments have resolved TARP and CNIH proteins situated beside the AMPAR transmembrane domain (TMD), tucked underneath the LBD (Nakagawa et al., 2005; Shanks et al., 2014). More recent assays using antibody-labelling of GluA2 peptide arrays have identified several discrete sites to which TARP γ2 may bind, within both the TMD and LBD, but also the more distal ATD (Cais et al., 2014). That being said, the LBD appears to be the principle extracellular site where TARPs modulate gating, since removal of the ATD still allows them to promote AMPAR trafficking and modulate decay kinetics (Cais et al., 2014). Specific sites of γ2 interaction identified at the GluA2 LBD include residues that comprise the LBD-TMD linker,

segments abutting the agonist-binding cleft, and helices along the D1 dimer interface (Cais et al., 2014). The linker region has been shown to regulate P_{open} of NMDAR channels (Kazi et al., 2014), and could mediate TARP-dependent increases in AMPAR P_{open} (Tomita et al., 2005; Cho et al., 2007). Likewise, more extensive closure of the agonist-binding cleft with γ2 (MacLean et al., 2014) may underlie changes in the relative efficacy of agonists such as KA. Nevertheless, the structural basis for TARP prolongation of channel gating has remained a matter of speculation.

Our identification of a site on the lower D2 lobe (i.e. the KGK motif) responsible for γ2 modulation of GluA2 deactivation and desensitization kinetics sheds new light on the functional interaction between TARP and AMPAR subunits. Specifically, we propose that TARP auxiliary subunits provide external stabilization at the base of the LBD dimer, interfering with the turning apart and/or separation of receptor subunits that characterizes desensitization (Meyerson et al., 2014; Durr et al., 2014). The low, outward facing orientation of the KGK motif is also consistent with the predicted location of TARP subunits in native AMPAR complexes (Nakagawa et al., 2005). Moreover, the continued importance of the KGK residues for γ2 co-expression to rescue gating of GluA2 AAA receptors demonstrates that inter-protein interactions relayed through the basal D2 lobe operate independently of the electrostatic interactions at the LBD apex. Given that the KGK motif did not affect TARP modulation of agonist efficacy or polyamine block it is likely that several other discrete interactions are required to achieve the full set of TARP effects. As such, auxiliary proteins add additional branches to the intrinsic gating machinery of pore-forming AMPAR subunits, coordinating receptor activation through distinct structural pathways.

METHODS

DNA constructs

The GluA2/γ2 and GluK2/γ2 TARP fusion constructs were generated by large-insert site-directed mutagenesis (see Geiser et al., 2001). The γ2 coding sequence was amplified as part of a megaprimer, and then subsequently incorporated into plasmids encoding either the GluA2 or GluK2 iGluR subunit. The forward primer used to amplify the megaprimer corresponded to the C-terminal of the GluA2 or GluK2 (without its stop codon), a seven amino acid linker sequence ELGTRGS (Semenov et al., 2012), and the N-terminal of γ2. Likewise, the reverse primer corresponded to a region downstream of the iGluR subunit coding region and the C-terminal of γ2. The primer sequences used to generate the megaprimer for the GluA2/γ2 fusion protein were 5'- GGC ATC GAG AGT GTT AAA ATT GAA CTG GGT ACA CGA GGT TCT ATG GGG CTG TTT GAT CGA GGT G -3' (forward primer) and 5'- GTA ATT GAC AGC CTT GCC TTG CTC CTC ATT TCT CAT ACG GGC GTG GTC CG -3' (reverse primer), while for the GluK2/γ2 fusion protein they were 5'- CCA GGT AAA GAA ACT ATG GCA GAA CTG GGT ACA CGA GGT TCT ATG GGG CTG TTT GAT CGA GGT G -3' (forward primer) and 5'- CGA CAG TTT GTG CTT GGG TGA TTG GCC TCT TCT CAT ACG GGC GTG GTC CG -3' (reverse primer). All new constructs were screened by restriction digestion and confirmed by sequencing.

Cell culture and transfection

HEK293T cells were used to recombinantly express KAR or AMPAR subunits for outside-out patch recordings and surface expression assays. For AMPARs, the Q/R unedited, flip variant of subunits was used. Mutant receptors were generated using site-directed mutagenesis. Auxiliary subunits and AMPARs were co-expressed at a 2:1 cDNA ratio. After transfection for 4

- 16 hours using the calcium phosphate precipitation method, cells were washed twice with divalent-containing PBS and maintained in fresh medium (MEM containing Glutamax and 10 % FBS), including 30 µM DNQX if auxiliary subunits were present. Electrophysiological recordings were performed 24 - 48 hours later. Residue numbering includes the signal peptide.

GluA2 receptor surface expression

To assess the membrane trafficking capabilities of AMPARs used in this study, we measured the fluorescence emitted by an ecliptic, pH-sensitive sfGFP genetically fused to the extracellular amino-terminal of wildtype or mutant AMPARs, as described previously for the KAR subunit GluK2 (see Dawe et al., 2013).

Electrophysiological recording and analysis

External recording solutions typically contained (in mM): 150 XCl, 5 HEPES, 0.1 $CaCl_2$, 0.1 $MgCl_2$, 2 % phenol red, where X was ordinarily Na, but replaced with other alkali metals in cation substitution experiments. The internal recording solution typically contained (mM): 115 NaCl, 10 NaF, 5 HEPES, 5 Na_4BAPTA, 0.5 $CaCl_2$, 1 $MgCl_2$, and 10 Na_2ATP or 135 CsF, 33 CsOH, 10 HEPES, 11 EGTA, 1 $CaCl_2$, and 2 $MgCl_2$ for single-channel recordings. The osmotic pressure was set to 300 mOsm using sucrose and the pH adjusted to 7.4 with alkali hydroxide solutions. In the case of recordings conducted without external NaCl, the solution contained 100 µM of $CaCl_2$ and $MgCl_2$ to improve patch stability, sucrose to maintain the osmotic pressure at 300 mOsm, and 5 mM Tris to buffer pH, while the pH was adjusted to 7.4 using 10 N HCl. For experiments involving spermine in the patch pipette the internal solution contained (in mM): 120 NaCl, 10 NaF, 5 HEPES, 5 Na_4BAPTA, and 0.5 $CaCl_2$ with 100 µM spermine added on the day of experiments. Agonist solutions were prepared by dissolving the agonist in external solution

and adjusting the pH appropriately. L-Glu was used at 10 mM, unless otherwise stated. CTZ was used at 100 µM to fully saturate GluA2 receptors.

All experiments were performed on excised membrane patches in the outside-out configuration. Agonist solutions were applied using a piezo-stack driven perfusion system, and measured solution exchange time was under 400 µs. Recording pipettes were composed of borosilicate glass (3-5 MΩ, King Precision Glass) coated with dental wax, or quartz glass (3-15 MΩ, King Precision Glass) coated with Sylgard (Dow Corning) to obtain recordings of single channels or for stable recordings in external solution without NaCl. The reference electrode was connected to the bath via an agar bridge of 3M KCl. The holding potential during recordings was -60 mV (unless otherwise stated). Series resistances (3-15 MΩ) were routinely compensated by 95 %. For single-channel recordings, the headstage was set to the capacitive feedback recording mode. All recordings were performed using an Axopatch 200B amplifier (Molecular Devices). Current records were low-pass filtered by an 8-pole Bessel filter at 10 kHz and sampled at 25-100 kHz for population responses or 100 kHz for single-channel responses. Data were acquired using pClamp9 software (Molecular Devices) and illustrated using Origin 7 (OriginLab).

Analysis of Electrophysiological Data

Electrophysiological data containing population and single-channel responses were analyzed using Clampfit 9.0 (Molecular Devices) and Signal 5.0 (Cambridge Electronic Design), respectively. Current decay rates were fit using 1^{st} or 2^{nd} order exponential functions: $y = A_i * \exp(-x/t_i)$, with the latter used when auxiliary subunits were present (see **Table S2.2**). Single-channel data were processed as described previously (Dawe et al., 2013). In brief, digital low-pass filtering at 3 kHz was performed prior to time-course fitting, which resulted in root mean square baseline noise values that averaged 0.22 ± 0.02 pA (n = 4) and 0.18 ± 0.01 pA (n = 4) for

wildtype GluA2 and MKT mutant receptors, respectively. These noise values corresponded to approximately fifty percent of the smallest conductance level. Idealized record response amplitudes were fit with Gaussian functions, whose peaks reflect discrete conductance levels: $y = \sum_{i=1...n} (A_i/(w_i*\mathrm{sqrt}(\pi/2)))*\exp(-2*((x-xc_i)/w_i)^2)$ where A = area, xc = centre of the peak, w = error associated with xc. Open probability was calculated for each patch containing GluA2 MKT as the percentage of open time in the idealized record.

Fitting of Conductance Voltage Relationships

Agonist-evoked membrane conductance (G) was calculated using the equation: $G = I / (V - V_{rev})$, where I is the current at V holding potential, and V_{rev} is the reversal potential. Conductance-voltage (G/V) relationships were fit using Origin 7 (OriginLab) with two different equations (Bowie et al., 1998). For recordings without internal polyamines, $y = (1 + (G_0 - 1)*\exp(x/V))$ was used, where G_0 is the minimal conductance and V is the holding potential. For recordings with internal polyamines, $y = G_{max} / (1 + [PA]/(g*\exp(x/h) + L*\exp(x/k)))$ was used, where G_{max} is the maximal conductance and [PA] is the concentration of polyamine (in µM), such that the polyamine dissociation constant, $K_d = g*\exp(V/h) + L*\exp(V/k)$ (see Bowie et al., 1998). For each receptor studied, the K_d(0 mV) and the voltage-dependent rates h an k are reported (**Table S2.3**). Conductance-voltage data from patch recordings with internal polyamines were corrected based on the average conductance profile of the same receptor without polyamines. In some cases, residual polyamine block was detected during outside-out patch recordings, despite the presence of 10 mM ATP to chelate polyamines in the patch pipette. To eliminate this block during control experiments, a train of L-Glu pulses at -80 mV were delivered prior to the test pulse, as described previously (Rozov et al., 1998).

Molecular dynamics simulations

The GluA2 flip, R/G unedited (PDB: 2UXA; Greger et al., 2006) and K759M/T765K mutant LBD dimers were used for constructing models for MD simulations. The wildtype structure was obtained from the Research Collaboratory for Structural Bioinformatics (RCSB) protein data bank (Berman et al., 2000). For the wildtype structure, chains A and C were used, and for the K759M/T765K mutant structure, chains A and B were used. Zinc ions were removed in both cases before simulation setup, and for all simulations based on the 2UXA structure, the R764G mutation was introduced. Missing atoms were added in PyMOL (The PyMOL Molecular Graphics System, Version 1.4, Schrödinger) and missing residues were added using Modeller Version 9.12 (Sali & Blundell, 1993). The LBD dimer was solvated in a cubic water box with dimensions $(100\ \text{Å})^3$ using the TIP3P water model (Jorgensen et al., 1983), and subsequently the system was neutralized and 150 mM NaCl or LiCl was added. Mutations were imposed manually prior to simulation setup, either by editing/deleting atoms in the pdb-file or by using the mutate function of PyMOL (The PyMOL Molecular Graphics System, Version 1.4, Schrödinger) and adjusting the side chain rotamer.

MD simulations were performed using Gromacs 4.6 (Hess et al., 2008) with the OPLS all-atom force field (Jorgensen et al., 1996; Kaminski et al., 2001). For MD simulations, the systems were first energy minimized until the maximum force on an atom was less than 100 kJ/mol/nm. Following energy minimization, a 200 ps restrained simulation with position restraints on protein heavy-atoms with a force constant of 1000 kJ mol^{-1} nm^{-2} was performed in the NVT ensemble with a temperature of 300 K maintained by a Berendsen thermostat (Berendsen et al., 1984). Periodic boundary conditions were employed and van der Waals interactions were cut off at 10 Å. Long-range electrostatics were accounted for by the Particle-

Mesh Ewald method (Essmann et al., 1995). All bonds were treated as constraints using the LINCS algorithm (Hess, 2008), allowing a time step of 2 fs. Subsequently, another 200 ps restrained simulation was performed as above but in the NPT ensemble at a pressure of 1 bar, maintained by a Berendsen barostat (Berendsen et al., 1984). Following this, 100 ns of production run were performed at 300 K and 1 bar pressure using the Berendsen thermostat and barostat, respectively (Berendsen et al., 1984). Two to four repeats for each wildtype or mutant dimer were produced. Analyses were performed using VMD (Humphrey et al., 1996) and Gromacs (Hess et al., 2008).

X-ray crystallography

The GluA2 (flip) K759M/T765K LBD construct was generated from the wildtype GluA2 LBD (provided by Ingo Greger, Cambridge, UK) using the Quikchange protocol (Stratagene). Induction and expression (1 mM IPTG, 20 h at 24°C) were followed by protoplast formation and freeze-thaw lysis. Briefly, cell pellets were incubated in high sucrose buffer (20 % (w/v) sucrose, 25 mM HEPES pH 8.0, 5 mM EDTA, 0.25 mg/ml lysozyme) for 45 min at room temperature, spun (2,000x g, 30 min, 4°C) and the pellets frozen at -80°C. These were thawed into 25 mM HEPES pH 7.5, 150 mM NaCl, 5mM L-Glu, 0.25 U/ml benzonase (Sigma), incubated (30 min at room temperature) and spun (18,500x g, 30 min, 4°C). Purification of the resulting supernatant on nickel-affinity and HiTrap-Q columns was performed as described previously (Nayeem et al., 2011). Crystals were grown in hanging-drops by mixing purified protein (5-10 mg/ml in 25mM HEPES, 150 mM NaCl, 5 mM L-Glu) in a 1:1 ratio with well solution containing either lithium (20-22 % PEG 4,000, 200 mM lithium sulfate, 100 mM acetate pH 5.0; grown at 6°C) or zinc ions (12-15 % PEG 8,000, 200 mM zinc acetate, 100 mM MES pH 6.0; grown at 23°C). Crystals

grew in 1-3 weeks and were cryo-protected by briefly soaking in well solution containing 20-22.5 % glycerol prior to plunge-freezing in liquid N_2.

Diffraction data were collected at 100 K on Diamond beamline I03 at an energy of 12,700 eV (Didcot, UK; Pilatus3 6M detector). Diffraction limits were chosen based on a combination of $I / \sigma I > 1$, CC(1/2) > 0.5, and completeness in the outer shell > 90%. Data processing was performed using either XDS/XSCALE (lithium form) or XDS/AIMLESS (zinc form). Molecular replacement in PHASER used the 2UXA GluA2i LBD structure as a model, modified with residues K759 and T765 truncated to alanine. Refinement was performed using a combination of REFMAC5 (Murshudov et al., 1997) and PHENIX.REFINE (Adams et al., 2002). For the zinc structure PHASER was used for SAD-MR to locate the five zinc ions, and for map generation either map sharpening (REFMAC5) or feature-enhanced maps (PHENIX.REFINE) were used. TLS groups were identified using the TLSMD server (Painter & Merritt, 2006). In all cases model visualisation and manipulation was done using COOT (Emsley et al., 2010), and figures were generated using CCP4MG (McNicholas et al., 2011). Ramachandran statistics were 99.2/0.8/0.0 (% favoured/allowed/outlier) for the zinc form and 99.0/1.0/0.0 for the lithium form.

Statistical methods

Results are expressed as mean ± SEM. Statistical analyses of sample means were performed using two-tailed paired or two sample (assuming unequal variance) *t* tests. $p < 0.05$ was considered to be statistically significant.

ACKNOWLEDGMENTS

This work was supported by operating grants from the Canadian Institutes of Health Research (FRN:82804, D.B.), the Leverhulme Trust (RPG-059, P.C.B and M.M.), and the Medical Research Council (MR/M0004331, P.C.B). G.B.D. is supported by a Canada Gradate Scholarship (CGS-D) from the Natural Sciences and Engineering Research Council of Canada. M.M. held a postdoctoral fellowship from the Alfred Benzon Foundation. D.B. was a Canada Research Chair. We thank the Advanced Research Computing (ARC) facility, the Blue Joule facility at the Hartree Centre, the National Service for Computational Chemistry Software, the IRIDIS High Performance Computing facility, and the HECTOR and ARCHER UK National Supercomputing Services for computer time through the EPSRC funded, HECBioSim consortium, as well as the Diamond Synchrotron for beam-time (provided through the Manchester/Liverpool BBSRC BAG). We also thank Jennifer Flemming for collecting the P2 21 21 dataset at Diamond, and Dr. Gergely Lukacs for use of his TIRF microscope. The authors declare no competing financial interests.

SUPPLEMENTAL FIGURES

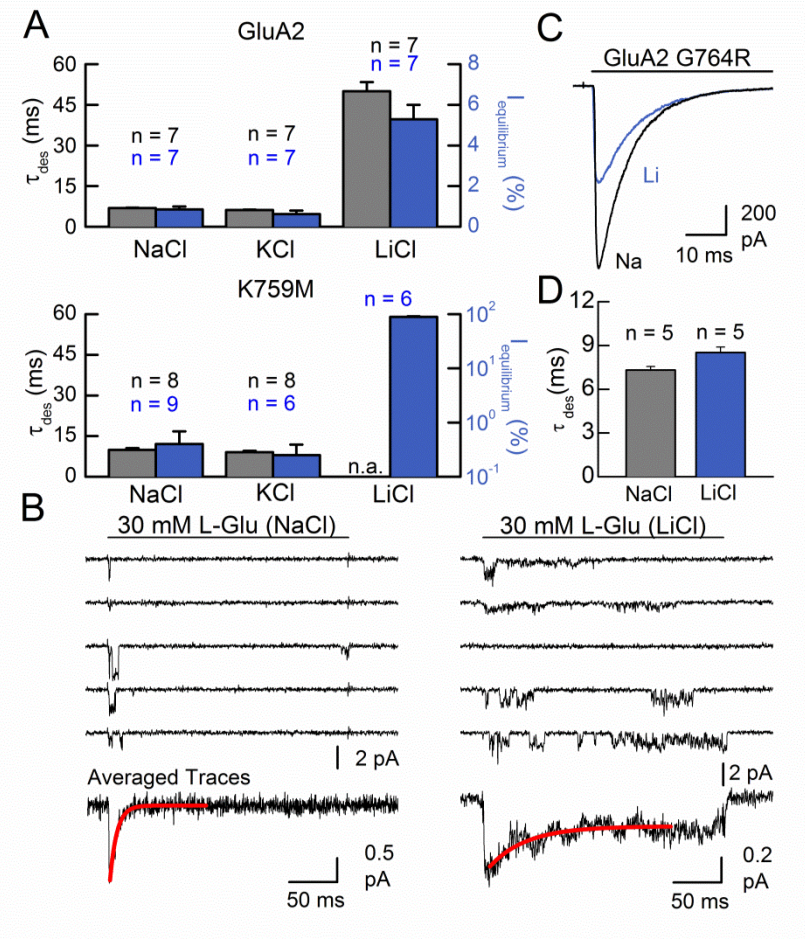

Figure S2.1 Functional properties of GluA2 receptors in different external ionic conditions. Supplemental data associated with Figure 2.1.

Since cation substitution experiments at GluA1 AMPARs do not affect the time course of channel activation (Bowie, 2002), we have explored whether GluA2 AMPARs are sensitive to other cation species beside lithium (i.e. potassium), and whether any structural features account for the difference in ion modulation between AMPAR subunits. One difference between GluA1 and GluA2 AMPARs is the R/G RNA editing site, located at the apex of the LBD, adjacent to the electronegative pocket on the same and opposing (across the dimer interface) subunits. This residue is edited (i.e. Gly) in GluA2, but unedited (i.e. Arg) in GluA1 (Lomeli et al., 1994). To determine whether the editing state of the R/G site affects lithium modulation of GluA2, we measured desensitization kinetics in the GluA2 G764R mutant.

(A) Current decay time constants (left, grey) and equilibrium to peak current ratios (right, blue) for wildtype GluA2 (top) and K759M (bottom) mutant receptors in the presence of different cation species. Data are mean ± SEM, from the number of independent patch experiments indicated.

(B) Typical GluA2 unitary current events elicited by 30 mM L-Glu in NaCl (left) (Patch #140128p7) and LiCl (right) (Patch # 140121p10) external solutions. Below is an average of several individual sweeps, including a single, exponential function fit (red) of the current decay.

(C) Typical current responses elicited by 10 mM L-Glu on GluA2 G764R mutant receptors in external NaCl and LiCl (Patch # 150203p3).

(D) Average current decay time constants for GluA2 G764R receptors. Consistent with the behaviour of GluA1 receptors, the slowing of wildtype GluA2 receptor decay kinetics observed with lithium was almost entirely eliminated in G764R mutant receptors, which exhibited desensitization time constants of 7.3 ± 0.2 ms (n = 5) in NaCl and 8.5 ± 0.4 ms (n = 5) in LiCl. Data are mean ± SEM, from the number of independent patch experiments indicated.

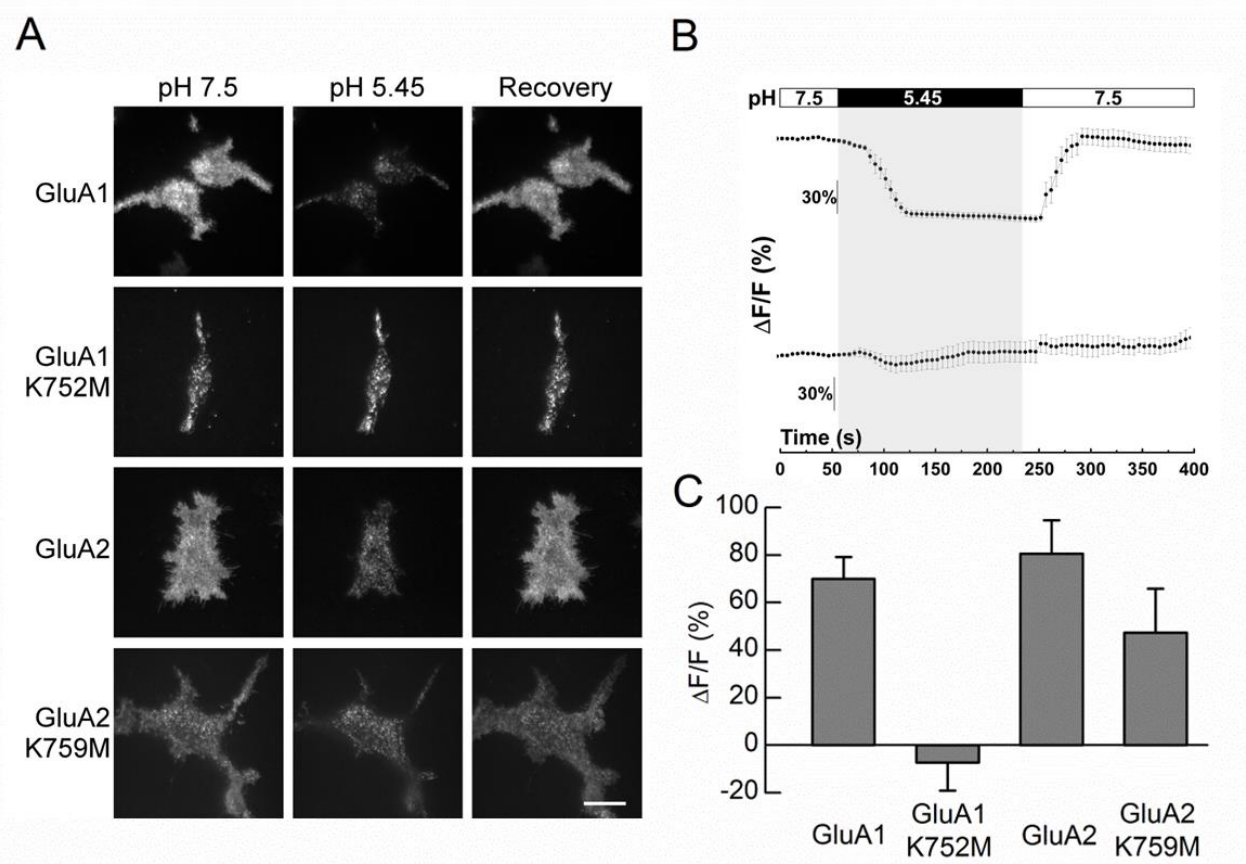

Figure S2.2 Surface expression of AMPAR subunits harbouring an equivalent Lys to Met mutation at the electronegative pocket. Supplemental data associated with Figure 2.2.

(A) TIRF images of HEK293T cells transfected with GFP-tagged wildtype and mutant GluA1 and GluA2 receptors exhibit reversible attenuation of the fluorescence signal between pH 7.5 and 5.45 when subunits are expressed on the plasma membrane (scale bar = 20 μm).

(B) Individual, time-resolved fluorescence profiles for single cells expressing either wildtype GluA1 (top) or the K752M mutant (bottom).

(C) Bar graph tabulating the change in fluorescent signal observed for cells expressing wildtype and mutant AMPARs. Data are mean ± SEM, from five (GluA1 K752M), ten (wildtype GluA1), thirteen (GluA2 K759M), or eighteen (wildtype GluA2) individual cell imaging experiments for each receptor.

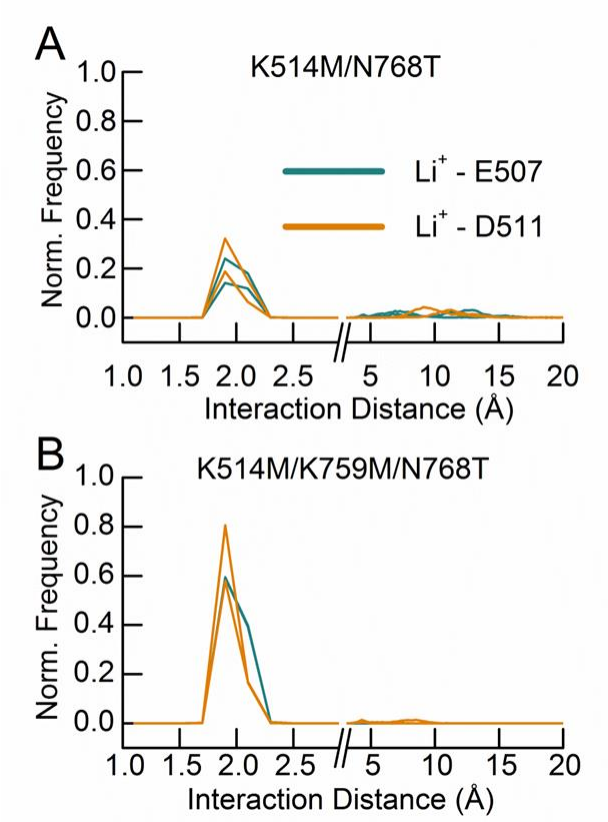

Figure S2.3 Lithium binding properties of the GluA2 K514M/N768T mutant receptor. Supplemental data associated with Figure 2.3.

(A and B) Data from MD simulations reporting the interaction distance between residue Glu507 or Asp511and the nearest lithium ion, for K514M/N768T (A) and K514M/K759M/N768T (B) mutant GluA2 receptors. Data from the triple mutant (i.e. K514M/N768T + K759M) was included to take advantage of the increased frequency of lithium binding measured in prior simulations following addition of the K759M mutation (Figure 1). Distance was measured from the sidechain oxygen atom closest to lithium on the residues indicated. Frequency is normalized (bin size = 0.2 Å, cumulative frequency = 1.0) and averaged from two simulation repeats of 100 ns for each receptor. Values for each chain (A and B) in the LBD dimer are shown.

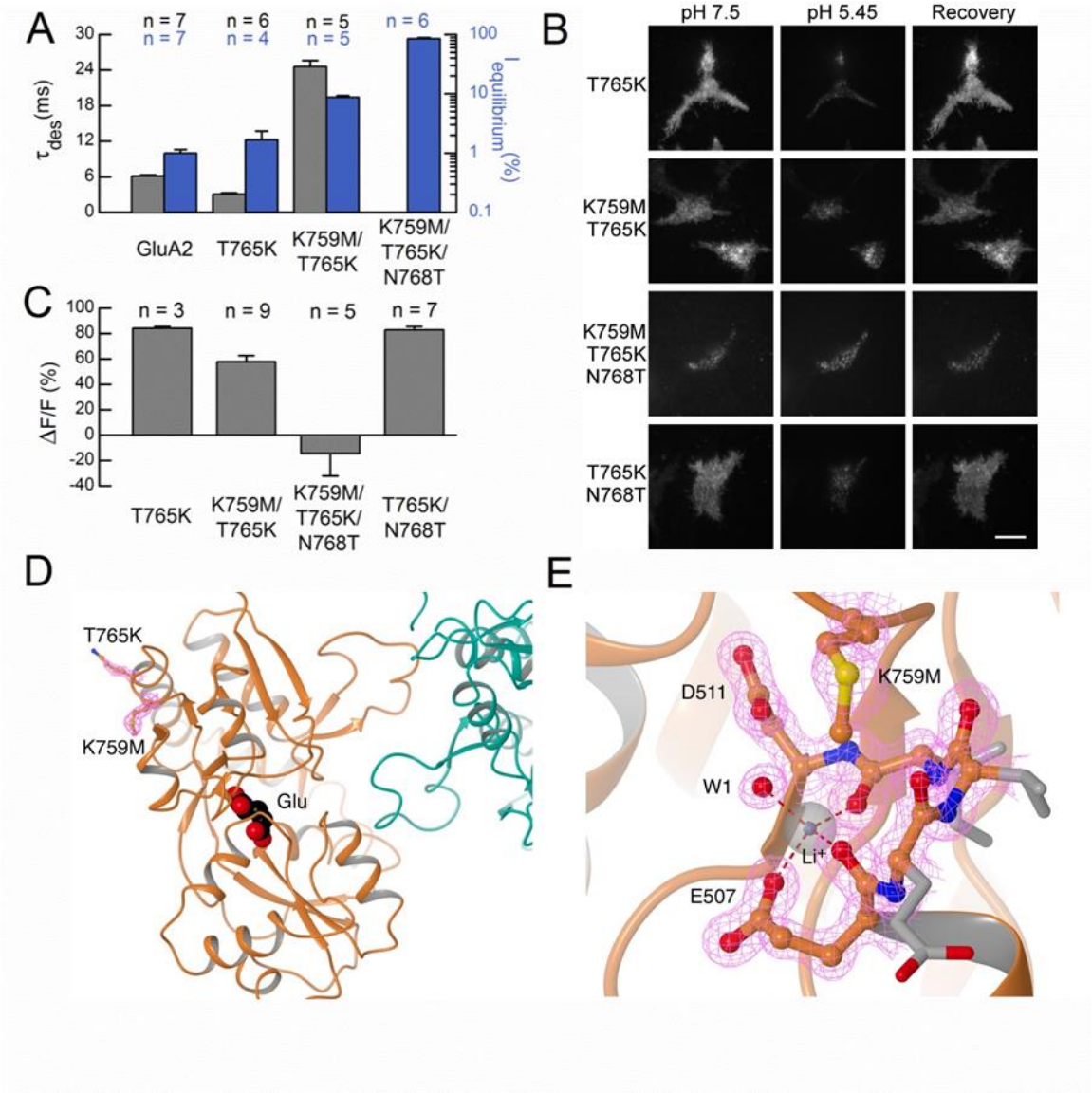

Figure S2.4 Structure, function, and surface expression of the GluA2 T765K mutant series of receptors. Supplemental data associated with Figure 2.4.

Our previous work has established that GluK2 KAR desensitization is abolished by the D776K mutation, which acts as a cross-dimer electrostatic tether onto the cation binding pocket (Nayeem et al., 2009; Nayeem et al., 2011; Dawe et al., 2013). We created a series of mutants incorporating the equivalent mutation in GluA2, namely T765K, in the hopes of achieving a similar tether between GluA2 subunits. Perhaps because Lys759 interferes with the tethering of the mutant lysine at the electronegative pocket of GluA2 (Figure 1), the addition of the K759M mutation was required atop T765K to prolong the time course of current responses. As such, we focussed our analysis on GluA2 K759M/T765K, for which we were able to crystalize a

crosslinked LBD dimer, and also GluA2 K759M/T765K/N768T (MKT), which showed little, if any, detectable current decay over 250 ms L-Glu applications. Nevertheless, kinetic analysis of GluA2 MKT was made difficult due to its greatly diminished surface expression.

(A) Time constants of current decay (left, grey) and equilibrium to peak current ratio (right, blue) for the GluA2 T765K series of mutants. Data are mean ± SEM, from the number of independent patch experiments indicated.

(B) TIRF images of HEK293T cells transfected with wildtype GluA2 or one of several mutant receptors possessing Lys at the 765 position. Reversible attenuation of the GFP fluorescence signal occurs between pH 7.5 and 5.45 when subunits are expressed on the plasma membrane (scale bar = 20 μm).

(C) Bar graph tabulating the change in fluorescent signal observed for cells expressing wildtype and mutant AMPARs. Data are mean ± SEM, from the number of independent patch experiments indicated.

(D) View of protomer A (orange), with the two mutated residues shown with associated electron density ($|2F_{obs} - F_{calc}|\alpha_{calc}$; pink mesh, contoured at 1.5σ). The L-Glu ligand is shown in black space-fill. Part of protomer B (teal) can be seen to the right, highlighting the absence of the biological dimer from this crystal form.

(E) Closer view of protomer A (orange) from approximately the viewpoint shown in Figure 4. The modeled lithium ion (grey sphere) is shown, along with an interacting water (W1) and other atoms within the electronegative pocket. Electron density ($|2F_{obs} - F_{calc}|\alpha_{calc}$) is shown contoured at 2σ around the displayed atoms (pink mesh) with the exception of the lithium ion, where it is displayed at 1σ (grey mesh). Contacts between the lithium ion and other atoms are shown as dashed lines.

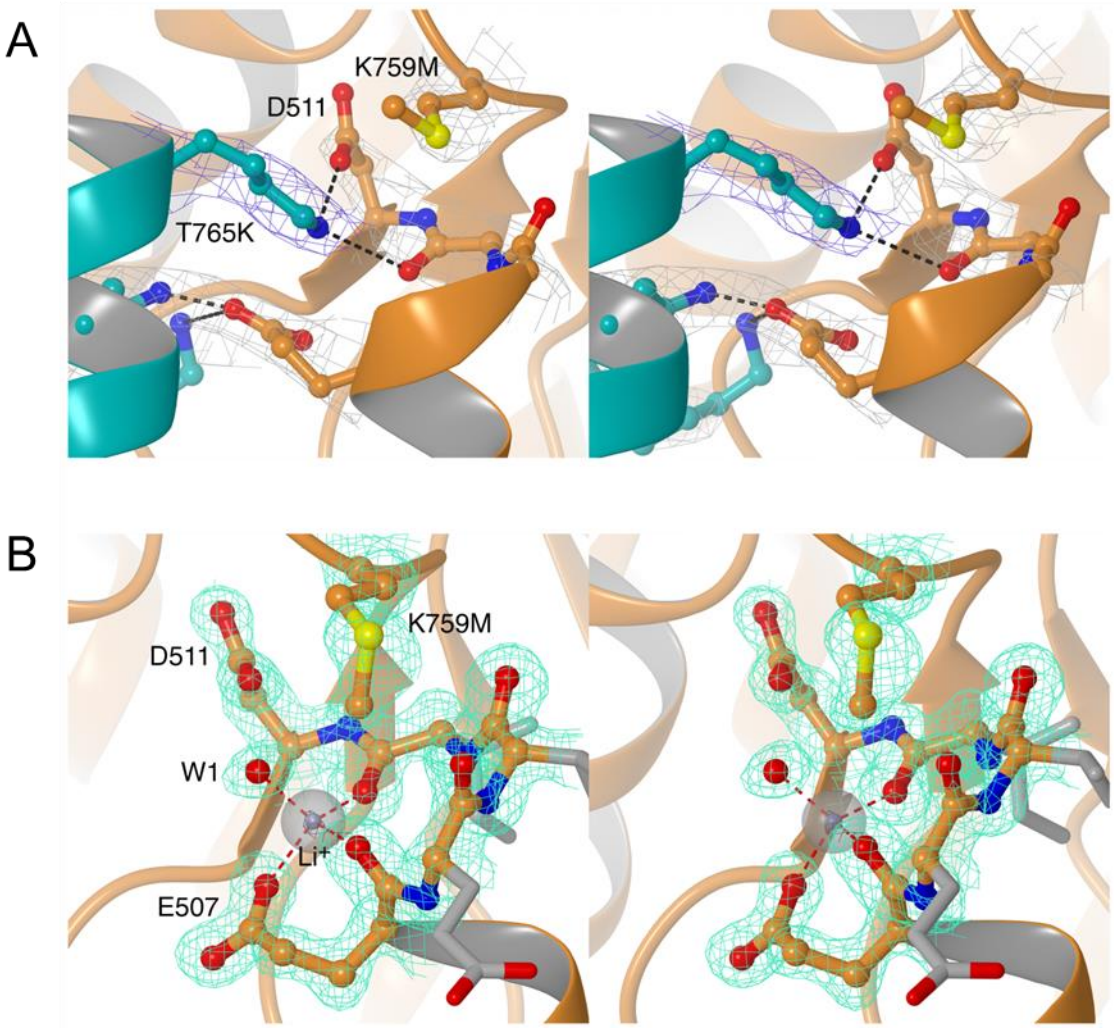

Figure S2.5 Stereo views of composite omit maps of the GluA2 K759M/T765K LBD, generated using PHENIX. Supplemental data associated with Figure 2.4.

(A) View of the mutant T765K residue on protomer B of the zinc crystal form, interacting with residues in the electronegative pocket of protomer A. Residue and density labelling is maintained as for Figure 4, with contours displayed at 1.2 σ.

(B) View of the electronegative binding pocket on protomer A of the lithium crystal form. Residue and density labelling is maintained as for Supplemental Figure 4, with contours displayed at 1.5 σ (or 0.8 σ around the lithium ion).

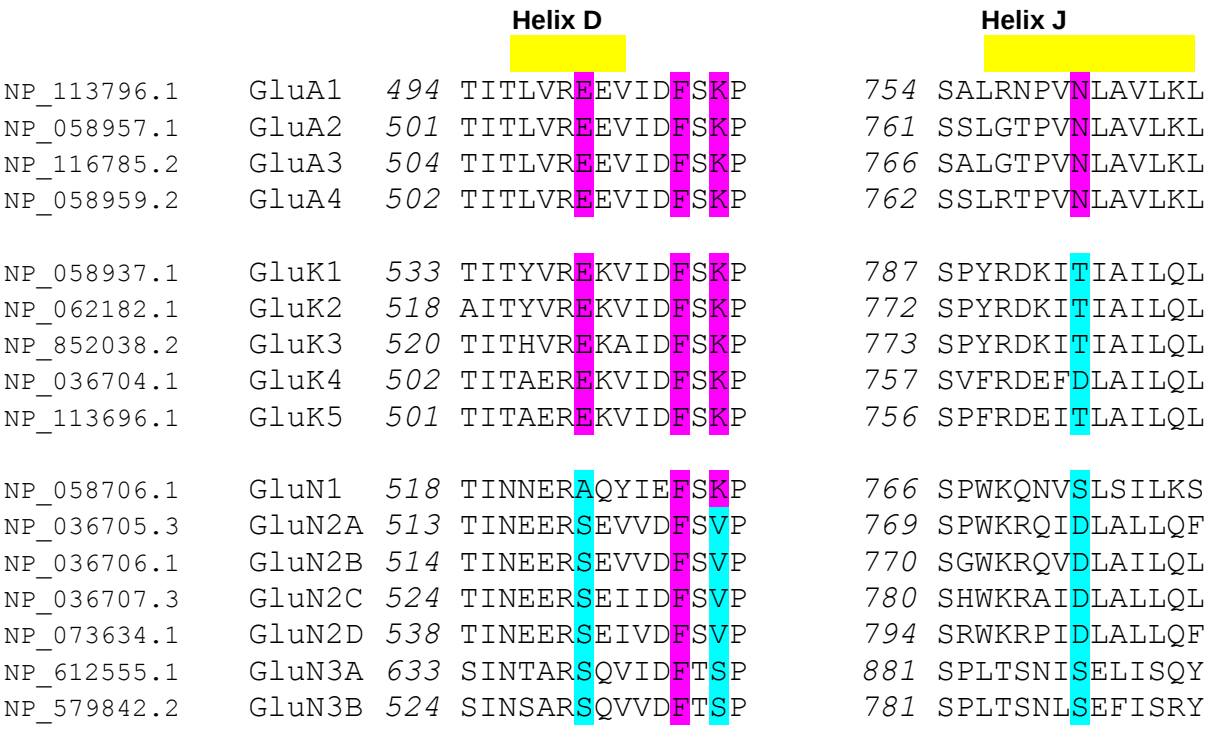

Figure S2.6 Amino acid sequence alignment of iGluRs at the apical LBD dimer interface. Supplemental data associated with Figure 2.5.

Amino acid sequences of iGluR subunits from *R. norvegicus*, aligned over two segments of the LBD. The NCBI accession code is shown at left. For AMPAR subunits, the flip isoform was selected. Residues participating in cross-dimer electrostatic interactions at the apex of the GluA2 LBD are highlighted magenta. When these residues are not conserved with the equivalent AMPAR residue they are highlighted cyan. The conserved Phe residue at position 512 could not be mutated alongside other resides in the GluA2 AAA mutant, since its contribution to the electrostatic network is from a backbone oxygen atom. Nevertheless, both residues across the dimer interface that would be expected to interact with Phe512, namely Lys514 and Asn768, were truncated.

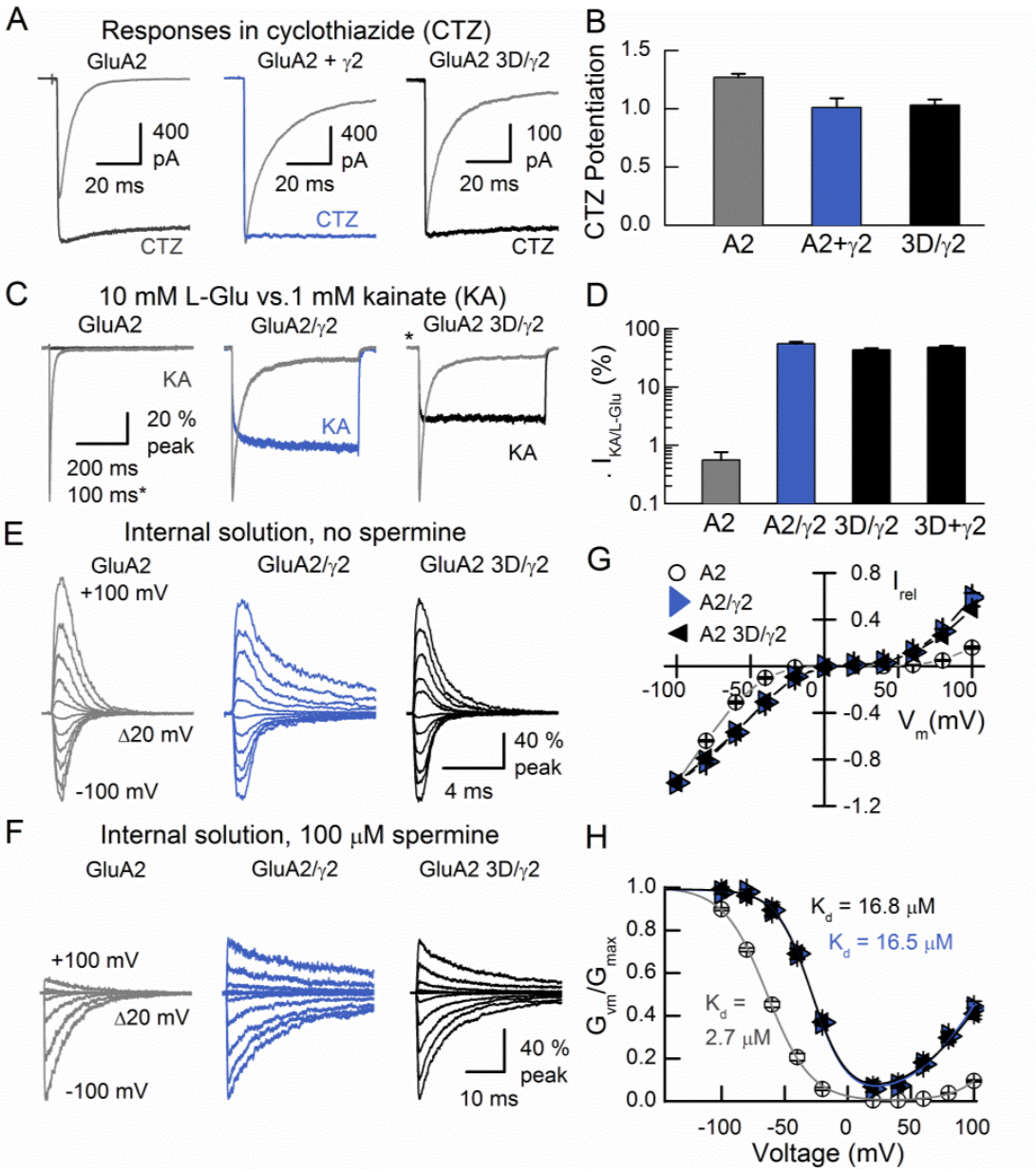

Figure S2.7 The GluA2 3D mutation does not attenuate TARP γ2 modulation of apparent agonist efficacy or channel block by spermine. Supplemental data associated with Figure 2.7.

(A) Typical current responses to 10 mM L-Glu before (grey) and during CTZ exposure for wildtype GluA2 (Patch # 130217p8, dark grey), as well as co-expressed GluA2 + γ2 (Patch # 150305p7, blue) and the GluA2 3D/γ2 (Patch # 150911p1, black) AMPAR-TARP fusion protein. (B) Mean CTZ potentiation of the receptors described in panel A. Values for GluA2 and GluA2 + γ2 correspond to those reported in Figures 5 and 6. Data are mean ± SEM, from eleven (GluA2), five (GluA2 + γ2), or six (GluA2 3D/γ2) independent patch experiments.

(C) Scaled current responses to 10 mM L-Glu (grey) and 1 mM KA for wildtype GluA2 (Patch # 150317p3, dark grey), as well as GluA2/γ2 (Patch # 150316p10, blue) and GluA2 3D/γ2 (Patch # 150511p6, black) AMPAR-TARP fusion proteins.

(D) Mean 1mM KA response, as a percentage of the peak current yielded by 10 mM L-Glu, for the receptors in panel C, as well as GluA2 3D + γ2 (TARP co-expressed). Data are mean ± SEM, from five (GluA2 and GluA2 3D/γ2), six (GluA2/γ2) and seven (GluA2 3D + γ2) independent patch experiments.

(E) Scaled current responses to 10 mM L-Glu at a range of membrane potentials (-100 to +100 mV, Δ20 mV) for wildtype GluA2 (Patch # 150716p10, grey), as well as GluA2/γ2 (Patch # 150723p11, blue) and GluA2 3D/γ2 (Patch # 150911p6, black) AMPAR-TARP fusion proteins.

(F) Scaled current responses to 10 mM L-Glu at a range of membrane potentials (-100 to +100 mV, Δ20 mV) with 100 μM spermine added to the internal recording solution for wildtype GluA2 (Patch # 150525p5, grey), as well as GluA2/γ2 (Patch # 150528p11, blue) and GluA2 3D/γ2 (Patch # 150910p7, black) AMPAR-TARP fusion proteins.

(G) Current-voltage plots with 100 μM internal spermine for wildtype GluA2 (white circles), as well as GluA2/γ2 (blue triangles) and GluA2 3D/γ2 (black triangles) AMPAR-TARP fusion proteins. Currents were normalized to the response at -100 mV (I_{rel} = -1). Data are mean ± SEM, from six (GluA2, GluA2/γ2, and GluA2 3D/γ2) independent patch experiments.

(H) Conductance-voltage plots with 100 μM internal spermine for wildtype GluA2 (white circles), as well as GluA2/γ2 (blue triangles) and GluA2 3D/γ2 (black triangles) AMPAR-TARP fusion proteins. Conductance is normalized to the fitted maximal conductance (G_{max}), and corrected to account for the average conductance-voltage relationship in recordings without internal spermine (see Supplemental Experimental Procedures). Data are mean ± SEM, from six independent patch experiments for each condition (GluA2, GluA2/γ2, and GluA2 3D/γ2) with 100μM spermine.

Table S2.1 Data collection and refinement statistics (molecular replacement) for GluA2 K759M/T765K LBD crystal structures. Supplemental data associated with Figure 2.4.

Data set	GluA2 K759M/T765K zinc-form	GluA2 K759M/T765K lithium-form
Data collection		
Space group	*P* 2 2_1 2_1	*P* 1 2 1
Cell dimensions		
a, *b*, *c* (Å)	46.38, 110.52, 167.26	67.32, 47.56, 96.75
α, β, γ (°)	90, 90, 90	90, 95.65, 90
Resolution (Å)	2.90-92.2 (2.90-3.08) [a]	1.35-67.0 (1.35-1.39)
R_{meas}	0.225 (1.68)	0.074 (1.11)
$I / \sigma I$	4.5 (1.1)	10.92 (1.88)
CC(1/2)	98.8 (73.9)	99.7 (62.2)
Completeness (%)	100 (100)	94.7 (92.5)
Redundancy	5.0 (5.1)	3.5 (3.6)
Refinement		
Resolution (Å)	2.90	1.35
No. reflections	36,525	126,864
R_{work} / R_{free} [b]	0.243 / 0.283	0.161 / 0.178
No. atoms		
Protein	5873	4143
Ligands (Glu only)	30 (30)	52 (20)
Ions	5	2
Water	0	688
B-factors		
Protein	97.1	23.2
Ligands (Glu only)	89.7 (89.7)	33.9 (15.4)
Ions	119.4	11.2
R.m.s. deviations		
Bond lengths (Å)	0.006	0.011
Bond angles (°)	1.035	1.391

Data were collected from single crystals in each case.
[a] Values in parentheses are for highest-resolution shell.
[b] Tests sets for R_{free} contained 5% (zinc-form) or 2% (lithium-form) of total reflections.

Table S2.2 Time course of desensitization and deactivation for wildtype and mutant GluA2 receptors expressed alone, with auxiliary subunits, or as GluA2/γ2 fusion proteins. Supplemental data associated with Figures 2.6, 2.7, and 2.8.

	τ_{fast}	τ_{slow}	% fast	$\tau_{weighted}$	$\tau_{monoexponential}$	n
AMPAR subunits						
GluA2						
desensitization	7.9 ± 0.7	36.8 ± 8.3	94 ± 1	**9.2 ± 0.8**	**8.7 ± 0.71**	9
deactivation	0.61 ± 0.07	6.2 ± 0.9	96 ± 1	**0.76 ± 0.08**	**0.67 ± 0.07**	8
3D mutant series						
GluA2/y2						
desensitization	22.4 ± 2.4	133.0 ± 17.3	79 ± 3	**45.7 ± 6.8**		11
deactivation	1.4 ± 0.3	13.8 ± 2.2	84 ± 3	**3.2 ± 0.4**		9
GluA2 3D/y2						
desensitization	7.9 ± 0.9	32.3 ± 3.1	80 ± 3	**12.7 ± 1.2**		8
deactivation	0.83 ± 0.05	6.6 ± 1.2	93 ± 2	**1.1 ± 0.1**		8
GluA2 3D + γ2						
desensitization	5.8 ± 0.6	25.5 ± 3.7	76 ± 6	**9.5 ± 0.4**		7
deactivation	0.69 ± 0.05	16.4 ± 3.3	100 ± 0	**0.74 ± 0.04**	**0.67 ± 0.07**	7
AAA mutant series						
GluA2 + γ2						
desensitization	20.5 ± 3.6	86.1 ± 15.8	65 ± 7	**39.0 ± 4.4**		10
GluA2 + γ7						
desensitization	9.8 ± 1.0	58.7 ± 8.3	87 ± 1	**16.0 ± 1.5**		7
GluA2 AAA + γ2						
desensitization	2.5 ± 0.3	16.9 ± 1.4	73 ± 4	**6.6 ± 0.9**		8
GluA2 AAA + γ7						
desensitization	0.91 ± 0.10	27.0 ± 8.5	99 ± 0	**1.1 ± 0.1**	**0.92 ± 0.10**	6
GluA2 AAA/3D + γ2						
desensitization	1.1 ± 0.1	14.6 ± 2.3	89 ± 2	**2.4 ± 0.3**		7

GluA2 receptors were activated by long application (250 or 500 ms) or short (1 ms) applications of 10 mM glutamate to measure desensitization and deactivation kinetics, respectively. In the presence of auxiliary subunits, current decay associated with desensitization and deactivation was fit using bi-exponential functions to obtain the components τ_{fast} and τ_{slow}. Weighted time constants ($\tau_{weighted}$) were calculated based on the relative area fit by the fast and slow components. In cases where the τ_{fast} accounted for 94 % or more of the total area, the decay was instead fit by a monoexponential function, as reported as the value in the $\tau_{monoexponential}$ column. The number of patches for each condition (n) is indicated, and all values are mean ± SEM.

Table S2.3 Spermine affinities of GluA2 receptors. Supplemental data associated with Figure 2.7.

Fit parameters of GluA2 G/V relationships

Receptor		Mean	SEM	n
GluA2	Kd (0 mV) (μM)	2.7	0.4	
100 μM spermine	h (mV)	-17.3	0.6	6
	k (mV)	16.5	0.2	
0 μM spermine	G_0	1.09		
	V	53.2		
GluA2/γ2	Kd (0 mV) (μM)	16.5	1.3	
100 μM spermine	h (mV)	-14.0	1.0	6
	k (mV)	21.5	0.9	
0 μM spermine	G_0	1.14		
	V	82.4		
GluA2 3D/γ2	Kd (0 mV) (μM)	16.8	2.1	
100 μM spermine	h (mV)	-14.2	1.1	6
	k (mV)	25.2	0.6	
0 μM spermine	G_0	1.09		
	V	74.0		

Affinities were obtained using responses evoked by 250 or 500 ms applications of 10 mM L-Glu. Values for ‘h’ and ‘k’ indicate the voltage dependency. The number of patches for each condition (n) is indicated, and all values are mean ± SEM.

CHAPTER THREE

External anions ‘prime’ the AMPAR response to glutamate

FOREWORD TO CHAPTER THREE

The final results chapter is the most collaborative study within my thesis. It combines electrophysiology, crystallography, AFM, and MD simulations to investigate how anions modulate the structure and function of GluA2 AMPARs. This manuscript could truly never have taken its current form without datasets from all these disciplines, as well as a few lucky breaks. Since AFM was not mentioned in the literature review, a point worth making here is that the technique has seldom been applied in the field of iGluR biophysics. From NMDARs it is known that the process of agonist binding -or likely desensitization, on the time scale of AFM measurement- induces an approximately 1 nm height reduction in GluN1/GluN2A (Suzuki et al., 2013) and GluN1/GluN3 (Balasuriya et al., 2013) complexes reconstituted in lipid bilayers. Otherwise, little else has been measured by AFM from the other iGluR subfamilies, except resting-state height (Baranovic et al., 2013).

This chapter remains unpublished at the time of my thesis submission. However, we are hoping to rectify the situation over the next few months…

Article Title:

Regulation of AMPA receptor gating by anion-induced vertical compression of the apo state

Reproduced with permission from G. Brent Dawe, Mohammad Fadim Kadir, Raminta Venskutonyte, Maria Musgaard, Mark R.P. Aurousseau, Philip C. Biggin, Jette Kastrup, J. Michael Edwardson, and Derek Bowie. 2016.
Regulation of AMPA receptor gating by anion-induced vertical compression of the apo state.
To be submitted to **Neuron**.

ABSTRACT

AMPA-type ionotropic glutamate receptors (AMPARs) undergo global, conformational changes when bound by agonist molecules, coinciding with activation and/or desensitization. Yet little is known about the conformational flexibility of apo, or resting state AMPARs. Specifically, it is unclear whether "resting" receptors transition between different conformations under physiological conditions and how such conformational states might influence channel gating after agonist binding occurs. Here, we used a combination of atomic force microscopy imaging and electrophysiology to demonstrate that halide ion exchange alters the height of apo state $GluA2_i$ (flip isoform) AMPARs, as well as desensitization kinetics in L-glutamate. We also report crystal structures of bromide-bound GluA2 ligand-binding domain dimers and identify a common mechanism for anion modulation of receptor height and gating. Both types of modulation were severely attenuated in $GluA2_o$ (flop) AMPARs. Accordingly, we propose that anion-induced, isoform-specific conformational changes "prime" apo state AMPARs to respond in a specific manner to agonists.

INTRODUCTION

Ionotropic glutamate receptors (iGluRs) constitute a major class of ligand-gated ion channels (LGICs) that mediates excitatory signaling in the vertebrate central nervous system (Traynelis et al., 2010). Though all iGluRs possess a tetrameric stoichiometry (Laube et al., 1998; Rosenmund et al., 1998), they can be divided into two functional groups: rapidly-gating AMPA and kainate-selective receptors (AMPARs and KARs) that mediate the initial postsynaptic response to neurotransmitter molecules (Henley and Wilkinson, 2016), as well as slower-gating NMDA-selective receptors (NMDARs) known to induce several forms of synaptic plasticity (Paoletti et al., 2013). Within the AMPAR subfamily, gating kinetics can be further regulated by subunit assembly, as well as the alternate splicing of flip and flop exons (Mosbacher et al., 1994). A number of studies have shed light on the structural mechanism of AMPAR activation and desensitization by reporting intact, high-resolution GluA2 structures in several, ligand-bound conformational states (i.e. (Durr et al., 2014; Meyerson et al., 2014; Yelshanskaya et al., 2014)). Nevertheless, structural information regarding the apo state remains scant and inconsistent, as the few published structures indicate an arrangement much like the antagonist-bound and "pre-activated" forms (Durr et al., 2014; Yelshanskaya et al., 2016), while LRET measurements suggest a more dynamic LBD layer with an open dimer interface. Accordingly, it has remained unclear whether AMPARs exhibit much conformational flexibility in the absence of bound agonists.

A recent study reported structures of the first intact, heteromeric AMPARs, obtained from single particle electron cryo-microscopy (cryo-EM) (Herguedas et al., 2016). Interestingly, the ligand-free GluA2/GluA3 structures could be segregated into distinct classes: a Y-shaped arrangement, consistent with the first tetrameric AMPAR crystal structure (Sobolevsky et al.,

2009), as well as two, O-shaped arrangements, each possessing a compact amino-terminal domain (ATD) layer and separate ligand-binding domain (LBD) dimers, similar to previous cryo-EM images (i.e. (Midgett and Madden, 2008)). However, one of the O-shaped models curiously displayed a ruptured LBD dimer, strikingly reminiscent of the extreme >100° rotation detected in the pore-distal 'B/D' subunits of agonist-bound, desensitized GluK2 (Meyerson et al., 2014) and GluA2 (Durr et al., 2014) structures. The idea that AMPARs can behave as though desensitized, but without agonist molecules bound, is not without precedent. Prior kinetic modeling of AMPARs has suggested such a state may account for incomplete recovery from desensitization (Robert and Howe, 2003), as some receptors recover on a much slower time scale than would be expected following agonist unbinding.

Here, we explore the extent to which GluA2 AMPARs undergo conformational change in the absence of bound agonists, as well as the effect of such changes on channel gating. Because anions have previously been shown to regulate GluA1 desensitization kinetics (Bowie, 2002), we used anion substitution in the context of electrophysiology, atomic force microscopy (AFM), X-ray crystallography, and molecular dynamics (MD) simulations to interrogate AMPAR behaviour in the presence and absence of the agonist L-Glu. Specifically, we report a relationship between halide radius and a compression of intact, apo state AMPARs that also correlates with the onset of desensitization. Furthermore, we isolate the site of action of anions to the LBD dimer interface. Mutations at this site, which corresponds to the flip/flop alternate splicing cassette, disrupt the structural and functional effects of halide ion substitution. Overall, our data identify a novel allosteric site that can "prime" AMPARs to respond in a specific manner upon agonist binding.

RESULTS

The structure and function of intact GluA2 AMPARs is modified by external anions

In light of recent evidence that apo state GluA2 AMPARs can alternate between resting and pseudo-desensitized conformations, we decided to re-evaluate the mechanism of allosteric modulators of AMPAR desensitization. Specifically, we asked whether such modulators solely influence state transitions following agonist binding, or also induce novel structural rearrangements prior to agonist binding. To address this question, we studied halide ions, as they have been previously demonstrated to weakly modulate GluA1 flip ($GluA1_i$) desensitization in a graded manner (Bowie, 2002). In fact, a correlation was found between the diameter of the halide ion comprising the external solution and the rate of $GluA1_i$ receptor desensitization (Bowie, 2002).

To confirm that anions modulate $GluA2_i$ receptors in a similar manner to $GluA1_i$ receptors, we substituted external NaCl with other halide salts, and assessed both the time constant and overall extent of desensitization in L-Glu (**Figures 3.1A and 3.1B**). As for $GluA1_i$, iodide and fluoride respectively yielded the fastest ($\tau = 1.6 \pm 0.1$ ms; n = 7) and slowest ($\tau = 9.2 \pm 0.4$ ms; n = 8) time constants of desensitization amongst the halides, with chloride ($\tau = 7.3 \pm 0.3$ ms; n = 15) and bromide ($\tau = 4.3 \pm 0.2$ ms; n = 7) kinetics residing in between (**Figure 3.1B**). The relationship between ionic diameter and desensitization rate was also mirrored by an increase in the overall extent of desensitization, as reflected in the equilibrium to peak current ratio (**Figure 3.1B**). Meanwhile, the substitution of propanoate resulted in a slower time constant of desensitization ($\tau = 10.4 \pm 0.8$ ms; n = 7) than occurred in fluoride (Figure 1B), suggesting that halides in general may facilitate desensitization.

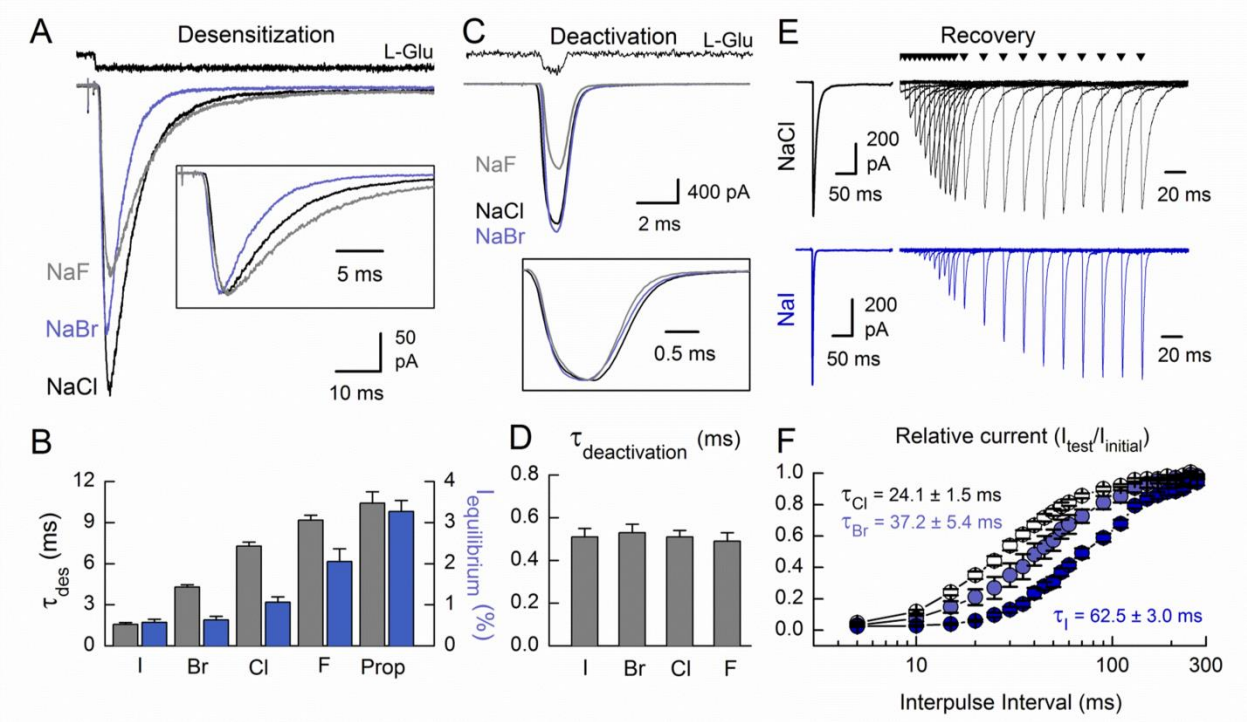

Figure 3.1 External anions modulate desensitization of GluA2 AMPARs in a graded manner

(**A**) Typical current responses of wild-type $GluA2_i$ receptors (patch number 140228p6) to a 250 ms application of 10 mM L-Glu in the presence of external NaCl (black), NaBr (light blue), and NaF (grey). The responses are also scaled to the same peak amplitude (inset). The uppermost trace (black) shows the junction current, recorded with an open patch pipette after the experiment to monitor the profile of solution exchange.

(**B**) Mean time constants of current decay after a 250 ms L-Glu application (τ_{des}) (left axis), as well as mean equilibrium current amplitude ($I_{equilibrium}$) as a percentage of the peak response (right axis), in the presence of different external anions. Data are mean ± SEM, from seven (NaI, NaBr, NaProp), eight (NaF), or fifteen (NaCl) independent patch experiments.

(**C**) Typical current response of wild-type $GluA2_i$ receptors (patch number 150825p10) to a 1 ms application of 10 mM L-Glu in the presence of external NaCl (black), NaBr (light blue), and NaF (grey). The responses are also scaled to the same peak amplitude (inset). The uppermost trace (black) shows the junction current, recorded with an open patch pipette after the experiment to monitor the profile of solution exchange.

(**D**) Mean time constants of current decay after a 1 ms L-Glu application ($\tau_{deactivation}$), in the presence of different external anions. Data are mean ± SEM, from five (NaI), seven (NaBr, NaF) or twelve (NaCl) independent patch experiments.

(**E**) Profile of recovery from desensitization for wild-type $GluA2_i$ receptors in external NaCl (top, black) and NaI (bottom, dark blue). The traces are from a two-pulse protocol, during which an initial 200 ms application of 10 mM L-Glu desensitized receptors and was then repeated (arrows) after allowing receptors to recover from desensitization for different time intervals. The amplitude of the second peak, or test response determines the time course of recovery from desensitization. Both conditions were recorded from the same patch experiment (patch number 151201p9).

(**F**) Mean current elicited by the test pulse from the recovery protocol described above, relative to the initial peak response. The results were fitted with a Hodgkin-Huxley-type equation, and the time constants of recovery derived from the fitting are indicated for each ionic condition. Data are mean ± SEM, from six (NaI), seven (NaBr), or thirteen (NaCl) independent patch experiments.

Because the effect of anion species on AMPAR deactivation and recovery from desensitization has not been reported previously, we analyzed those properties as well. The time constant of deactivation did not exhibit significant changes between chloride and any other halide species ($P > 0.65$ in all cases), occurring near 0.5 ms in all conditions (**Figures 3.1C and 3.1D**). However, the time constant of recovery from desensitization varied between anion species, becoming slower as ionic radius increased (**Figures 3.1E and 3.1F**). Accordingly, anions appear to selectively modulate $GluA2_i$ desensitization, rather than deactivation.

Given the topology of AMPAR subunits, modulation by external anions could occur at the level of the ATD or LBD layers (or both). We therefore performed similar anion substitution experiments on a truncated $GluA2_i$ receptor, which lacked the ATD region. Mimicking the behaviour of full-length receptors, $GluA2_i$ ΔATD receptors exhibited faster entry into desensitization and slower recovery from desensitization as ionic radius increased (**Figure S3.1**). Therefore, anions appear to target the LBD (or adjacent pore linker regions) to modulate the desensitization kinetics of $GluA2_i$ receptors.

Our next step was to investigate whether any structural perturbations were induced by external anion substitution. For this effort we used AFM to image to isolated receptor complexes that had been reconstituted in a lipid bilayer. AFM permitted reasonable temporal resolution of changes induced by agonists and/or allosteric modulators, specifically in regard to the height of bilayer-integrated receptors (**Table S3.1**). The selection of height as our measurement parameter was based on GluA2 crystal structures, which exhibit a vertical compression of the extracellular domains upon agonist binding (Durr et al., 2014), as well as previous AFM studies that reported the same behaviour in agonist-bound NMDARs (Balasuriya et al., 2014; Suzuki et al., 2013). HA-tagged $GluA2_i$ was isolated from detergent extracts of transfected HEK203T cells by anti-

HA immunoaffinity chromatography. SDS-PAGE, followed by silver staining or immunoblotting using an anti-HA antibody, detected a single band at ~ 105 kDa, indicating the purity of the sample (**Figure 3.2A**). Isolated $GluA2_i$ was integrated into liposomes, which were then used to generate supported lipid bilayers. In contrast to protein-free bilayers, which were featureless when visualized by AFM (**Figure 3.2B**), bilayers containing $GluA2_i$ contained numerous particles (arrows, **Figure 3.2C**). A frequency distribution of heights of these particles had two peaks, at 4.7 ± 0.1 nm and 7.2 ± 0.2 nm (**Figure 3.2D**). We have previously shown for NMDA receptors that the higher peak represents the extracellular region of assembled receptors (Balasuriya et al., 2014; Suzuki et al., 2013). We therefore selected particles with heights between 5.5 and 8.5 nm for analysis. When the external solution in the imaging chamber was changed from NaCl to either NaBr or NaI, $GluA2_i$ receptors exhibited a height reduction of 0.74 ± 0.06 nm (n = 12) or 0.87 ± 0.11 nm (n = 13), respectively (**Figures 3.2E and 3.2G**). A smaller height reduction was observed when the agonist L-Glu (10 mM) was added to NaBr (0.25 ± 0.05 nm; n = 14) or NaI (0.18 ± 0.06 nm; n = 12) solutions (**Figure 3.2G**). In contrast, the addition of L-Glu to NaCl led to a much greater reduction in receptor height (0.69 ± 0.11 nm; n = 11; **Figures 3.2F and 3.2H**).

To ensure that the final height of agonist-bound $GluA2_i$ receptors reflected that they were desensitized, rather than activated, we repeated the experiment in the presence of cyclothiazide (CTZ), a positive allosteric modulator of AMPARs. CTZ nearly completely eliminates AMPAR desensitization (Patneau et al., 1993; Yamada and Tang, 1993) by stabilizing receptors in an activated conformation (Sun et al., 2002). The L-Glu-induced compression of $GluA2_i$ was prevented by CTZ, as the mean change in height was -0.03 ± 0.07 nm (n = 14; **Figure 3.2I**). A similar lack of response to L-Glu was observed in the presence of the competitive antagonist

CNQX (-0.10 ± 0.07 nm; n = 12; not shown), suggesting that the height reductions observed in L-Glu correspond to receptors transitioning to desensitized states. Meanwhile, the height reductions induced by anion substitution (**Figure 3.2G**) indicate that apo state $GluA2_i$ receptors can undergo conformational changes of a similar amplitude to those that occur during gating.

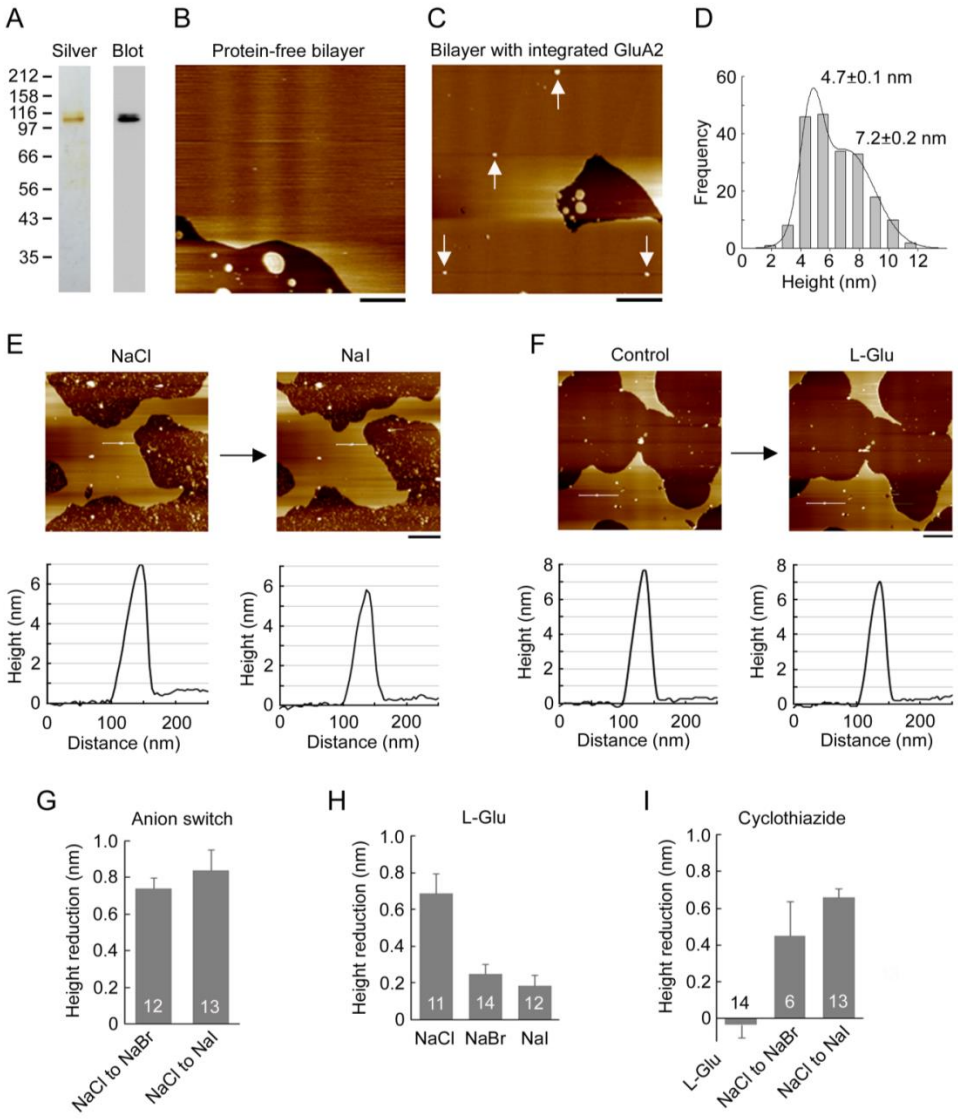

Figure 3.2 Effect of anions on $GluA2_i$ receptor height
(**A**) Silver stain and immunoblot (using an anti-HA antibody) of a sample of isolated $GluA2_i$ receptors. Representative AFM image of a protein-free supported lipid bilayer. Height range, 10 nm; scale bar, 400 nm.

(**B and C**) AFM images of supported lipid bilayers, either protein-free or containing $GluA2_i$ receptors (arrows). Height range, 10 nm; scale bar, 400 nm.
(**D**) Frequency distribution of heights of particles in supported lipid bilayers.
(**E**) Effect of a buffer switch from NaCl to NaI-containing solution on the height of an individual receptor. Top panels: AFM images of the same area of bilayer before and after buffer switch. The section taken through the receptor is indicated. Height range, 8.9 nm; scale bar, 400 nm Bottom panels: Height profiles through the section indicated in the AFM images.
(**F**) Effect of L-Glu on the height of an individual receptor. Top panels: AFM images of the same area of bilayer before and after buffer switch. The section taken through the receptor is indicated. Height range, 10.0 nm; scale bar, 400 nm. Bottom panels: Height profiles through the section indicated in the AFM images.
(**G**) Reductions in height of $GluA2_i$ receptors in response to anion switches. NaCl, NaBr and NaI were all at 100 mM. The numbers of individual receptor analysed are indicated.
(**H**) Height reductions in response to 10 mM L-Glu in the presence of different anions.
(**I**) Height reductions in response to L-Glu, as well as switching of solution to NaBr or NaI, in the presence of cyclothiazide (100 μM).
Data are mean ± SEM from the number of experiments indicated in Table S3.1.

Identification of anion interactions in the GluA2 LBD

Our functional data suggest that external anions modulate AMPAR gating via interactions with the LBD (**Figure S3.1**). Therefore, we sought to crystallize a soluble construct of the GluA2 LBD (GluA2-LBD) in complex with halide ions. Four X-ray structures of GluA2-LBD crystallized in presence of bromide ions were determined (**Table S3.2**), of which two were flop isoforms ($GluA2_o$-LBD in NaBr and RbBr) and the remaining two were flip-like ($GluA2_o$-LBD N775S in NaBr and RbBr). Anomalous scattering data clearly indicated the location of the bromide ions within the dimer interface (**Figures 3.3A and 3.3B**). Here, the $GluA2_o$-LBD N775S structure, which was crystallized with RbBr in space group C2 and solved at 1.8 Å resolution, will be used as a representative structure for detailed analysis of the $GluA2_i$ anion binding site. In this structure, one $GluA2_o$-LBD N775S molecule was found in the asymmetric unit of the crystal, though it formed a typical dimer with its symmetry mate.

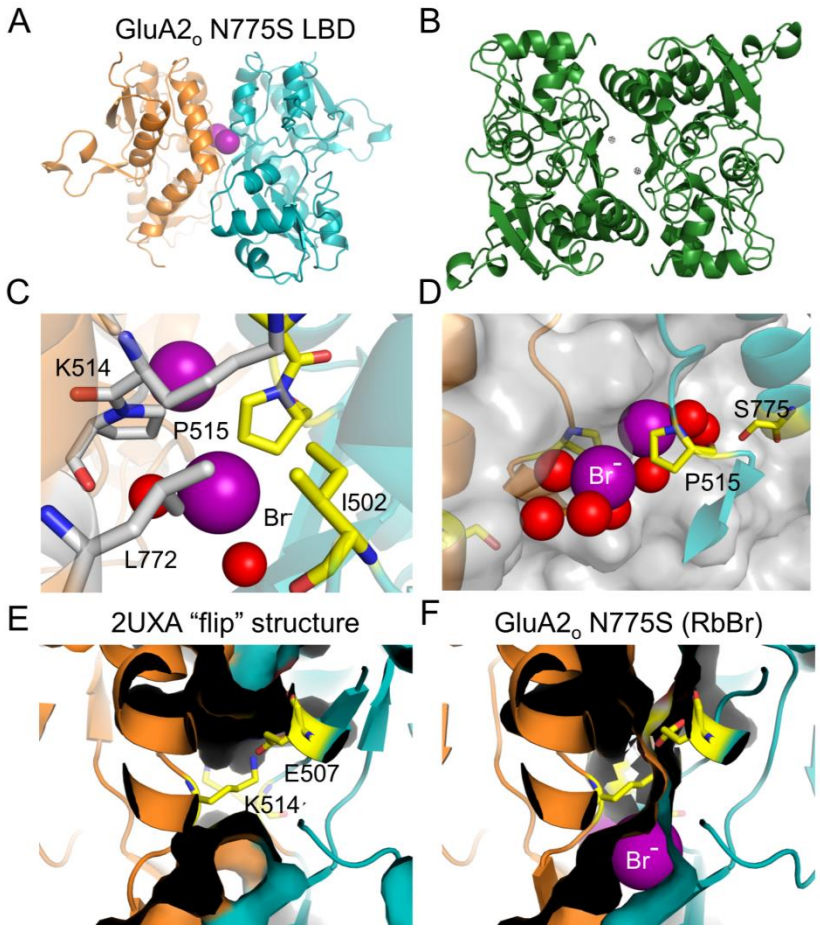

Figure 3.3 Detection of bromide ions in the GluA2-LBD dimer interface
(**A**) Side view of the GluA2$_o$-LBD N775S dimer, RbBr form. Bromide ions are shown as purple spheres.
(**B**) Anomalous difference electron density map from GluA2$_o$-LBD, contoured at 12σ for bromide ions.
(**C**) Close-up side view of the bromide binding sites in the GluA2$_o$-LBD N775S dimer interface. Bromide ions are shown as purple spheres, water molecules as red spheres, and amino acid residues surrounding the binding sites are different colours (yellow or grey sticks) based on their subunit of origin.
(**D**) The interior surface of the dimer interface is illustrated for one GluA2$_o$-LBD N775S subunit. The Ser775 residues point toward water molecules (red) that surround the bromide ions.
(**E and F**) The wild-type GluA2 flip structure (PDB: 2UXA; (Greger et al., 2006)) has a more intact dimer interface (E), compared with the GluA2$_o$-LBD N775S structure (RbBr form), where a "fissure" appears in the surface representation at the level of the Glu507-Lys514 salt bridge (F).

The anion binding site is located in a somewhat hydrophobic space, consisting of Pro515 and Leu772 from one subunit, as well as Ile502 and Pro515 from the partner subunit. Beside these hydrophobic residues, each bromide makes polar contacts to multiple water molecules, while a lysine residue (Lys514) caps the binding site, within 5 Å of bromide (**Figures 3.3C and**

3.3D). Interestingly, there is additional solvent-exposed surface, extending upward from bromide, along the midline of the dimer interface, in contrast with previous structures of $GluA2_i$ where bromide ions are not present (**Figures 3.3E and 3.3F**). This exposed area includes a salt bridge formed between Glu507 and Lys514, a key cross-dimer contact where mutations accelerate desensitization (Dawe et al., 2016; Horning and Mayer, 2004). As a result, it seems plausible that the binding of larger halide ions (i.e. bromide and iodide) could facilitate GluA2 desensitization by reducing dimer stability at the LBD apex.

It is also worth noting that LBD structures crystallized in both anions possessed additional electron density in the vicinity of the anion binding site (data not shown), perhaps corresponding to other anions inhabiting the dimer interface. This observation, coupled with the absence of a well-formed anion binding pocket, led us to suspect that anions might not reside at one, discrete site. Accordingly, we used MD simulations to augment our structural data, identifying regions of the $GluA2_i$ LBD which have a higher probability of interaction with anions (**Figure 3.4**). Numerous regions of chloride density were predicted on the outward-facing surface of the LBD, typically near basic amino acid residues (**Figures 3.4A and 3.4B**). In addition, a few residues in the LBD dimer interface also came into close proximity (i.e. within 4 Å) with chloride (**Figure 3.4C**), of which the only hydrophobic residue was Leu504. This position was particularly interesting, given that larger halide ions are known to participate in hydrophobic interactions, but also because AMPAR desensitization is strongly regulated by its sidechain composition. Notably, the introduction of tyrosine at the 504 position (or its equivalent in other AMPAR subunits) results in a non-desensitizing phenotype (Stern-Bach et al., 1998; Sun et al., 2002). In contrast to Leu504, no chloride interaction was predicted near Ser775 (**Figure 3.4C**), at odds with the bromide and chloride densities in the crystal structures. The inability of

MD simulation to reproduce the same anion binding sites in either additive or polarizable force fields could be due to the nature of the force fields themselves, which were unable to capture the hydrophobic properties of the halide ions.

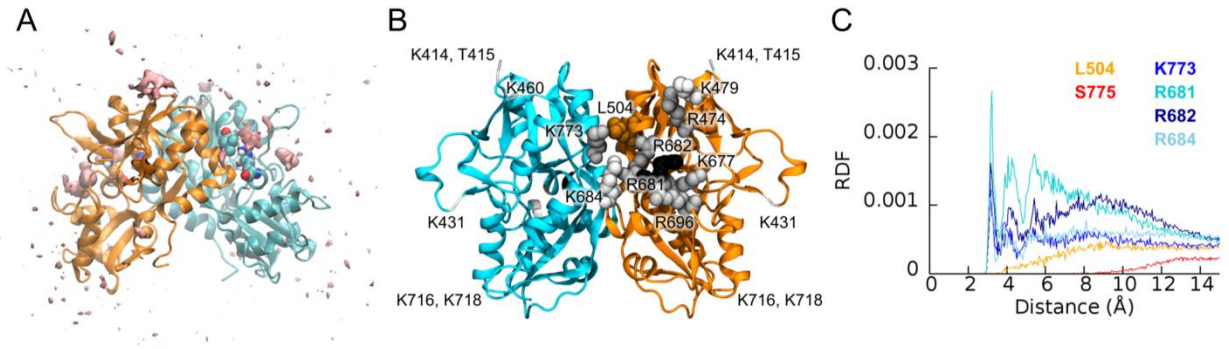

Figure 3.4 MD simulations predict anion interactions with several residues in the LBD dimer interface
(**A**) Isosurface representation of chloride ion density (pink), as predicted from an MD simulation of the $GluA2_i$ LBD dimer. The density is averaged from 200 ns of one simulation repeat.
(**B**) Side view of the dimer, highlighting residues (sphere form) that exhibited interactions with one or more chloride ions for over 10% of the total simulation time, which was comprised of 100 ns from each of four simulation repeats. Darker shading of residues indicates more prolonged anion interactions, while Leu504 is highlighted orange.
(**C**) Radial distribution function (RDF), indicating the probability of a chloride ion at various distances from specific residues in the LBD dimer interface. Values were calculated from the same set of simulation repeats as in panel B.

MD simulations may also have been hindered by the much weaker electron density of bromide ions in the flip-like $GluA2_o$-LBD N775S structure, despite both GluA2 isoforms having identical anion binding sites. Since the serine or asparagine residues at position 775 project toward water molecules, which in turn interact with bromide ions (**Figure 3.3D**), one possibility is that this position regulates anion binding. More commonly, position 775 is known for forming part of the CTZ binding pocket (**Figure S3.3**), as the modulator binds with higher apparent affinity and more profoundly attenuates desensitization of serine-containing (i.e. flip) AMPARs (Partin et al., 1995). In NaBr and NaI-based external solutions, CTZ produced the same functional effects on $GluA2_i$ current responses as in NaCl (**Figure S3.3**), suggesting that the

compound can out-compete anions, or that anions act at discrete sites. To resolve this issue, it was necessary to determine whether anion interactions in the dimer interface were in fact responsible for modulating receptor desensitization.

Allosteric anions "prime" GluA2 receptors for accelerated desensitization

Taken together, our crystallographic data and MD simulations indicate that anions may form multiple, electrostatic interactions throughout the GluA2 LBD dimer interface, and that anion stability may be regulated by flip/flop editing. In an effort to link the functional effects of anions to their putative binding sites in the dimer interface, we performed external anion substitution experiments on $GluA2_o$ receptors (**Figure 3.5**), as they contain a bulkier residue (asparagine) at position 775, close to the bromide density. We also assessed the mutation $GluA2_i$ L504A, as computational analysis predicted another region of anion density just below Leu504 (**Figure 3.4**). If these positions actually influence the anion binding environment, one would expect functional modulation of AMPARs by anions to be attenuated or enhanced, when they are alternately transcribed or mutated.

As opposed to $GluA2_i$ receptors, which had quite variable desensitization kinetics in different halide ion species (**Figure 3.5A**), $GluA2_o$ receptors exhibited a more consistent phenotype (**Figure 3.5B**), though the trend of faster desensitization in the presence of larger anions persisted (**Figures 3.5E and 3.5F**). Specifically, the time constant of $GluA2_o$ desensitization was 0.8 ± 0.05 ms (n = 6) in iodide and 1.7 ± 0.1 ms (n = 6) in fluoride, an approximately two-fold change. The same time constant for $GluA2_i$ in fluoride was about six-fold slower than that of iodide. To be sure that the reduced anion modulation of $GluA2_o$ was due to position 775, we tested the mutation $GluA2_i$ S775N (**Figure 3.5C**), since two other residues in the LBD dimer interface (Thr765 and Pro766) also differ in flip and flop isoforms. Consistent with the flop phenotype, the time constants of $GluA2_i$ S775N desensitization in iodide and

fluoride were, respectively, 3.6 ± 0.5 ms (n = 6) and 5.8 ± 0.4 ms (n = 6) (**Figure 3.5E**). Again, this equates to nearly a two-fold change. As a result, the reduction in anion modulation of desensitization rates moving from flip to flop-type GluA2 AMPARs is attributable to the presence of an asparagine residue at position 775.

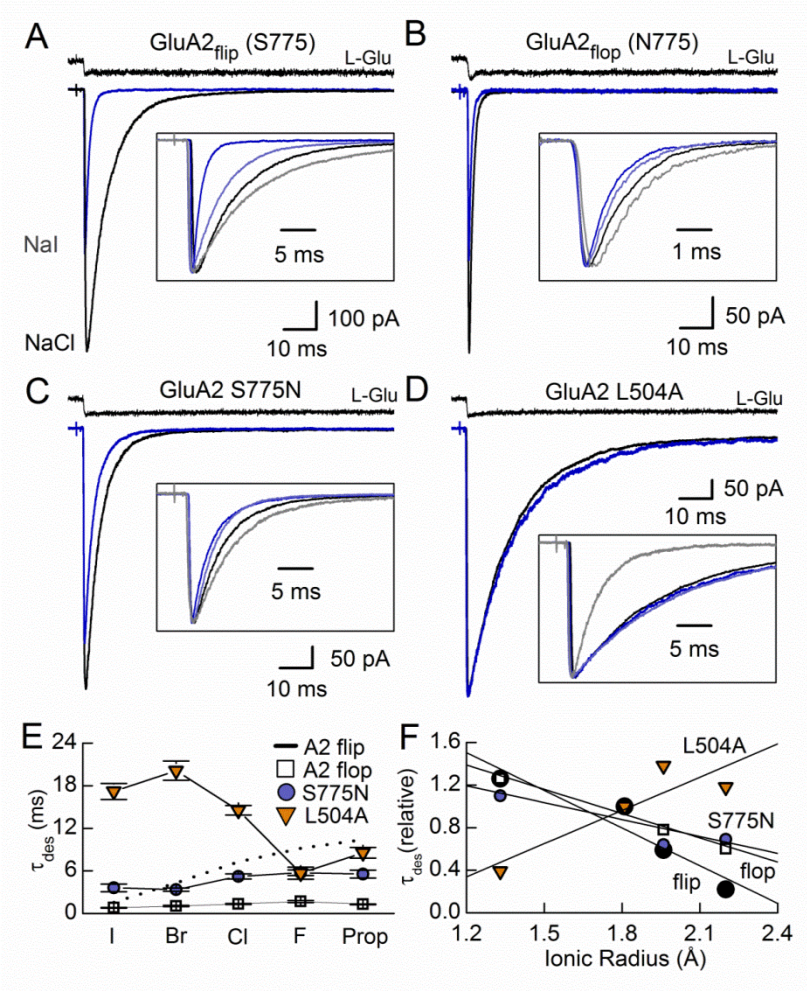

Figure 3.5 Flip/flop editing at LBD residues disrupts anion modulation of desensitization
(**A-D**) Typical current responses of wildtype $GluA2_i$ (A, patch number 151123p15) and wildtype $GluA2_o$ (B, patch number 160218p14), as well as $GluA2_i$ S775N (C, patch number 160119p3) and $GluA2_i$ L504A (D, 160215p10) mutant receptors to a 250 ms application of 10 mM L-Glu in the presence of external NaCl (black) and NaI (dark blue). The responses of the same receptors in NaI (dark blue), NaBr (light blue), NaCl (black), and NaF (grey) are also scaled to the same peak amplitude (inset). The responses in NaBr and NaF are from different patches, where the initial time constant of desensitization measured in NaCl was similar to those patches listed above. The uppermost trace (black) shows the junction current, recorded with an open patch pipette after the experiment to monitor the profile of solution exchange.
(**E**) Mean time constants of current decay after a 250 ms L-Glu application (τ_{des}) for the receptors described in panels A-D, in the presence of different external anions. Data are mean ± SEM, from the

number of independent patch experiments that follows: $GluA2_i$ NaCl (15), NaF (8), other anions (7); $GluA2_o$ NaCl (12), other anions (6); $GluA2_i$ S775N NaCl (12), other anions (6); $GluA2_i$ L504A NaCl (10), other anions (5).
(**F**) Relative values of τ_{des} (NaCl = 1) for the receptors described in panels A-D, plotted against the ionic radius of different halide ions, in which desensitization was measured.

It is not entirely clear why $GluA2_o$ receptors were less modulated by anions than their $GluA2_i$ counterparts, especially given the greater bromide density in the flop structures (**Figure 3.3**). One possible explanation is that a hydrogen bond formed between Asn775 and Ser750 (**Figure S3.5**), which cannot occur in flip receptors, counteracts the ability of halide ions to break apart the flop dimer interface. Alternatively, the bromide densities reported in the crystal structures may not represent the site of functional modulation by halide ions. For example, the ions may occupy a secondary site in a less stable manner (i.e. around Leu504), which in turn affects entry into desensitization.

A more unique phenotype was observed for $GluA2_i$ L504A receptors, as there was little deviation in the time course of desensitization between chloride, bromide, and iodide (τ ~ 15-20 ms), but fluoride substitution led to significantly faster desensitization ($\tau = 5.7 \pm 0.9$ ms; n = 5) (**Figures 3.5D and 3.5E**). Accordingly, the relationship between anion radius and desensitization rate was inverted for this mutant receptor (**Figure 3.5F**). The fact that two separate mutations (i.e. S775N or L504A) alter how anions regulate GluA2 desensitization supports the existence of multiple, discrete binding sites, or a large, individual site that is more diffuse in nature. In either case, both mutations are consistent with the functional interaction of anions at the LBD dimer interface. Yet the possibility of additional anion interactions is supported by the inability of either the S775N or L504A mutations to influence the relationship between halide ion size and the rate of recovery from desensitization (**Figure S3.6**). Given the numerous anion densities

predicted by MD simulations (**Figure 3.4**), any number of sites on the exterior surface of the GluA2 LBD may facilitate anion modulation of recovery kinetics.

Limiting our focus to the LBD dimer interface, which affected anion regulation of entry into desensitization, we next addressed whether this region also accounts for the vertical compression of receptors, observed in the absence of agonist molecules. If the same GluA2 receptors that exhibited reduced anion modulation of desensitization (i.e. $GluA2_o$ and $GluA2_i$ L504A) also exhibited smaller height reductions upon changing from NaCl to NaBr or NaI solutions, there would be a strong indication that the two effects are related. In this sense, the accelerated desensitization of $GluA2_i$ receptors that occurs in the presence of large halide ions would be a consequence of the vertical compression in the extracellular domains. However, the compression could also be mediated at another site in the ATD or LBD, and might have no influence over gating behaviour.

Consistent with the coupling of structural and functional effects induced by anion substitution, the height reductions in NaBr (0.06 ± 0.06 nm; n = 12) and NaI (0.12 ± 0.06 nm; n = 15) were almost entirely eliminated for $GluA2_o$ receptors that were purified and integrated into lipid bilayers (**Figures 3.6A and 3.6B**). At the same time, a greater $GluA2_o$ height reduction occurred when L-Glu was applied in the NaBr (0.70 ± 0.14 nm; n = 10) or NaI (0.59 ± 0.11 nm; n = 11) backgrounds, of a similar amplitude to that of agonist-bound $GluA2_i$ (~ 0.7 nm) and $GluA2_o$ (0.61 ± 0.07 nm; n = 10) receptors in NaCl (**Figure 3.6C**). Consequently, the combined height reductions caused by NaBr or NaI anion substitution and L-Glu application range from roughly 0.7 to 1.0 nm in flip and flop-type receptors. The main difference between the isoforms is that a majority of the total compression is due to anions in $GluA2_i$ receptors, and L-Glu in $GluA2_o$ receptors. Interestingly, the height profile of $GluA2_o$ receptors was mirrored by $GluA2_i$

L504A receptors, which displayed minimal compression in NaBr and NaI (< 0.1 nm), compared to that induced by L-Glu application in any of the ionic species tested (> 0.6 nm; **Figures 3.6D-3.6F**).

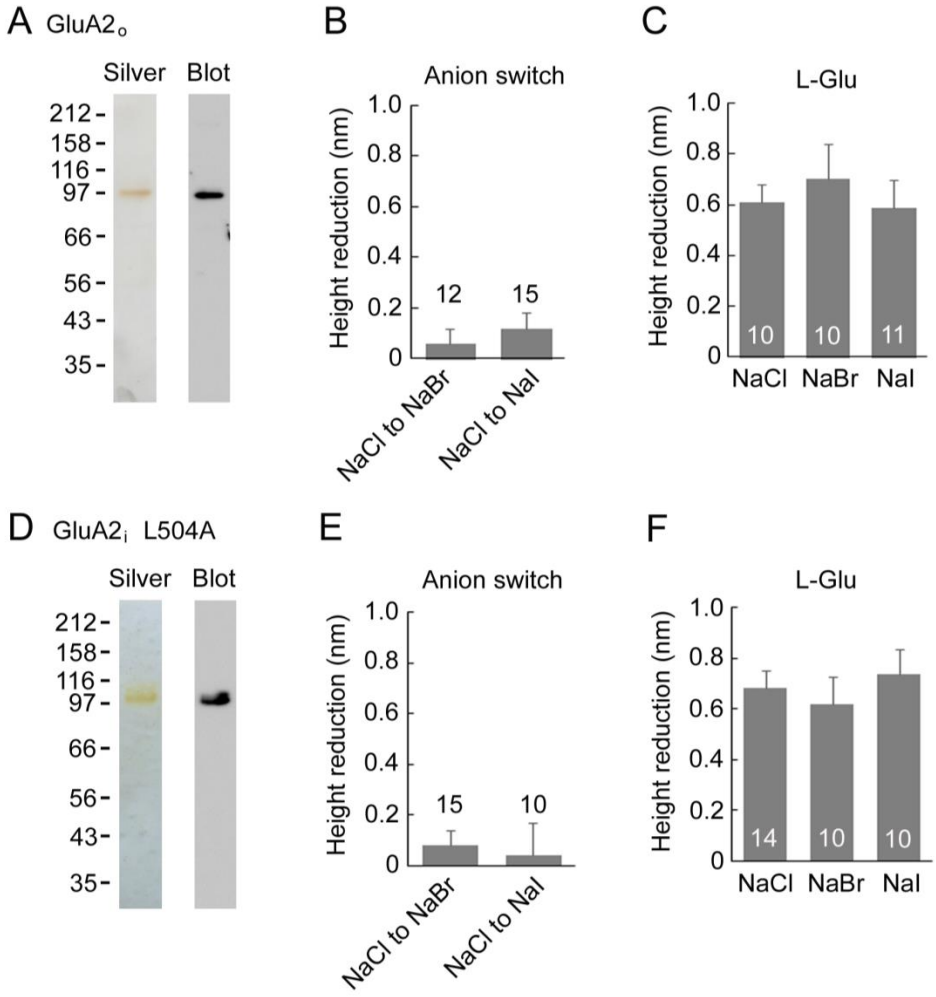

Figure 3.6 Effect of anions on GluA2$_o$ and GluA2$_i$ L504A receptor height
(**A**) Silver stain and immunoblot (using an anti-HA antibody) of a sample of isolated GluA2$_o$ receptors.
(**B**) Reductions in height of GluA2$_o$ receptors in response to anion switches. NaCl, NaBr and NaI were all at 100 mM. The numbers of individual receptor analyzed are indicated.
(**C**) Height reductions of GluA2$_o$ receptors in response to glutamate (10 mM) in the presence of different anions.
(**D**) Silver stain and immunoblot (using an anti-HA antibody) of a sample of isolated GluA2$_i$ 504A.
(**E**) Reductions in height of GluA2$_i$ 504A receptors in response to anion switches.
(**F**) Height reductions of GluA2$_i$ 504A receptors in response to glutamate (10 mM) in the presence of different anions.
Data are mean ± SEM from the number of experiments indicated in Table S3.1.

In conjunction, our electrophysiology and AFM data indicate that bromide and iodide ions selectively induce vertical compression in flip, but not flop-type GluA2 AMPARs, and that this conformational change results in accelerated desensitization, when compared to standard (i.e. NaCl) ionic conditions. This assertion is based on the fact that the same mutations, in the vicinity where we detected anion binding (**Figure 3.3**), can attenuate or eliminate both effects. We therefore propose that anions, as allosteric modulators, can "prime" certain AMPAR subtypes to respond in a specific manner upon agonist binding. Concurrent with this idea, distinct apo state conformations must exist, and the equilibrium between them must be altered by the anion composition of the external milieu.

DISCUSSION

This study advances our understanding of AMPARs in two fundamental ways. First, we demonstrate that intact, apo state $GluA2_i$ AMPARs can transition between discrete structural conformations, which in turn regulate their gating behaviour in the presence of agonist molecules. Specifically, we identified a common set of interactions between external halide ions and the LBD dimer interface that govern both the height of receptor complexes and the time course of entry into desensitization. The mutation of key residues in the dimer interface strongly attenuates both effects. As such, halide ions can be viewed as "priming" AMPARs to respond in a particular manner, once agonist molecules bind. Second, we show that the priming effect is present in flip, but not flop isoforms of GluA2 AMPARs. The reason why these two isoform exist simultaneously in the central nervous system is currently unknown. However, our data point toward a potential mechanism by which alternative splicing could shape glutamatergic signaling in the nervous system.

Understanding the functional modulation of AMPARs by external anions

Our electrophysiological data reveal that $GluA1_i$ (Bowie, 2002) and $GluA2_i$ AMPAR desensitization can be modulated in a bi-directional manner by different halide ion species. Bromide and iodide accelerate entry into desensitization (versus chloride), while fluoride slows this process. Therefore, the effect of anion binding in general could be to destabilize the LBD dimer, promoting the subunit separation that accompanies desensitization (Durr et al., 2014; Meyerson et al., 2014). In this case, iodide would be reasoned to have the strongest modulatory effect on the LBD. An alternative possibility we cannot entirely discount is that anions in fact stabilize the LBD dimer, with species of smaller ionic radius (i.e. fluoride) having the most profound effect. Nonetheless, several pieces of evidence support the former explanation. The fact

that electron density for bromide was readily observed in the NaBr and RbBr crystal structures suggests that larger halide ions can easily access the dimer interface. Furthermore, the addition of a negatively charged aspartate residue at position 775, which may mimic the electrostatic effect of a bound anion in the same region of the dimer interface, led to much faster desensitization in a previous study (Sun et al., 2002), and also when we tested the mutant (data not shown). Finally, an inter-subunit anion binding site has also been described for another LGIC family, namely the acid-sensing ion channels (ASICs) (Jasti et al., 2007). Interestingly, experiments on the ASIC1 subunit have revealed that larger anions in the external environment accelerate desensitization (Kusama et al., 2010), while deactivation is largely unaffected (MacLean and Jayaraman, 2016). In short, ASIC1 behaves quite similarly to the phenotype we observed in $GluA2_i$ AMPARs. It is tempting to speculate that, as a general rule, halide ions destabilize protein complexes, forming contacts with both polar and non-polar residues (Dauter and Dauter, 2001) that disrupt important endogenous interactions between subunits. However, KARs utilize the binding of a single chloride ion in the LBD dimer interface (Plested and Mayer, 2007) to help stabilize the dimer assembly (in conjunction with allosteric sodium ions), as both larger (i.e. NaI) and smaller (i.e. NaF) sodium-paired halides accelerate GluK2 desensitization (Bowie, 2002). Given that the distinct anion binding sites of AMPAR and KAR subunits produce quite different functional effects when occupied, mechanisms of anion modulation are likely to be highly dependent on the micro-environment surrounding an anion.

The occurrence of multiple apo states in AMPARs

A recent structural investigation of intact, apo state AMPARs revealed that (at least) two, distinct structural conformations are possible, while accompanying computational modelling suggested that receptors are capable of substantial vertical extension and compression

(Herguedas et al., 2016). Though such conformational flexibility is intriguing, a molecular mechanism that could account for structural transitions within the apo state has remained elusive. Here, we have identified that external anions (i.e. bromide and iodide), acting at the LBD dimer interface, can induce height changes in $GluA2_i$ receptors, without agonists or competitive antagonists present. Because AFM measurements cannot report more detailed structural rearrangements, it is unclear whether compressed $GluA2_i$ receptors adopt a pseudo-desensitized conformation (e.g. (Herguedas et al., 2016)), or retain an intact dimer arrangement in the LBD layer. If a rupture of one or more LBD dimers did coincide with height compression, would those receptors behave as though they were desensitized, and be unable to respond to L-Glu application? Within the total receptor population, L-Glu-evoked responses were still observed in NaBr and NaI, suggesting that this is not the case. More convincingly, CTZ potentiation, an indicator of AMPAR channel open probability (see (Cho et al., 2007)) was consistent across halide ion species (**Figure S3.3**), indicating that changes in the fraction of activation-capable receptors did not occur.

Different regulation of flip and flop AMPAR isoforms by anions

Despite the fact that flip and flop AMPAR isoforms differ by a mere ten amino acids, there are numerous instances of brain region-specific flip/flop expression for individual AMPAR subunits (Sommer et al., 1990), indicative that the transcription of one isoform over another is important for neuronal signaling. In addition, flip/flop alternate splicing is under developmental regulation, as flip isoforms can be detected from embryonic stages onward, whereas flop isoforms are upregulated postnatally (Monyer et al., 1991). The advantage conferred by possessing both flip and flop isoforms could be related to their different functional characteristics, such as faster desensitization in flop isoforms (Mosbacher et al., 1994), or

variability in their assembly and surface expression (Greger et al., 2006). Indeed, these factors appear to come together, as differences in alternative splicing have been proposed to alter AMPAR subunit composition and re-shape the profile of the AMPAR-mediated postsynaptic potentials following activity deprivation (Penn et al., 2012). Yet, there have been no clear illustrations of a property that is entirely unique to one isoform or another.

We found that the anion-induced regulation of receptor compression and accelerated desensitization occurs in $GluA2_i$, but much less so in $GluA2_o$ receptors. As a result, there is a means of selectively regulating the gating of flip isoform AMPARs. To what extent flip subunit-containing AMPARs may undergo vertical extension and compression *in vivo* is unclear, because the bromide and iodide ions we used to induce compression were not assessed at physiological concentrations. Typically, bromide is found at trace levels in serum, becoming toxic above 10 mM (Sourkes, 1991), while serum iodide concentrations are in the 50 nM range (Saller et al., 1998). At the same time, it is still feasible that some endogenous molecule may act in a manner similar to bromide and iodide ions. Bicarbonate, phosphate, and sulfate ions, along with organic anions, combine with chloride to dictate the ionic environment of the blood (Kraut and Madias, 2007), meaning several other charged molecules could act as modulators. Another possibility is that apo state $GluA2_i$ receptors did undergo dynamic rearrangements with chloride bound, but they were too brief to detect based on the AFM scan rate (~ 20 Hz), whereas the equilibrium between different states was altered in the presence of other anions. Ultimately, more investigation will be required to decipher the nature of distinct apo state conformations in AMPARs, and why they display isoform selectivity.

METHODS

Electrophysiology

HEK293 cells were used to recombinantly express GluA2 AMPAR subunits for outside-out patch recordings. Unless otherwise noted, the Q/R unedited, flip isoform of subunits was used, and residue numbering includes the signal peptide. Mutant receptors were generated using site-directed mutagenesis. External and internal recording solutions typically contained (in mM): 150 NaX (X = halide ion), 5 HEPES, 0.1 $CaCl_2$, 0.1 $MgCl_2$, and 2% phenol red at pH 7.4, and 115 NaCl, 10 NaF, 5 HEPES, 5 Na_4BAPTA, 0.5 $CaCl_2$, 1 $MgCl_2$, and 10 Na_2ATP at pH 7.4, respectively. Sucrose was supplemented to maintain the osmotic pressure at 300 mOsm. L-Glu was typically applied at 10 mM and CTZ at 100 µM.

Recording pipettes were comprised of borosilicate glass (3-5 MΩ, King Precision Glass, Inc.) coated with dental wax. The reference electrode was connected to the bath via an agar bridge of 3M KCl. Agonist solutions were applied using a piezo-stack driven perfusion system, and measured solution exchange time was under 400 µs. Series resistances (3-15 MΩ) were routinely compensated by 95%. All recordings were performed using an Axopatch 200B amplifier (Molecular Devices, LLC). Current records were low-pass filtered by an 8-pole Bessel filter at 10 kHz and sampled at 25-50 kHz. Data were acquired using pClamp9 software (Molecular Devices, LLC) and illustrated using Origin 7 (OriginLab Corp.).

Electrophysiological data were analyzed using Clampfit 10.5 (Molecular Devices, LLC). To measure deactivation and entry into desensitization, current decay rates were fitted using 1^{st} or 2^{nd} order exponential functions of the form $y = A_i * \exp(-x/\tau_i)$. Where two exponential components were used, time constants are expressed as a weighted mean. To measure recovery from desensitization, a two-pulse protocol was delivered using variable interpulse intervals, and

the peak amplitude of the second pulse was expressed as a fraction of the first peak. Recovery data were fitted with the Hodgkin-Huxley equation $y = N_0+(1-N_0)*(1-\exp(-k_{rec}*x))^n$, where N_0 is the equilibrium response at the end of the first pulse, k_{rec} is the recovery rate, and n is an exponent that reflects the number of kinetic transitions contributing to the recovery time course. The value of n was set to 2 (see (Robert et al., 2005)).

AMPA receptor purification and AFM imaging

GluA2 receptors ($GluA2_i$, $GluA2_o$, and $GluA2_i$ L504A) used in AFM imaging included a hemagglutinin (HA) tag, added by site-directed mutagenesis, to facilitate protein purification. The HA tag contained the residues YPYDVPDYA, located after the first amino acid following the signal peptide (i.e. between residues 22 and 32). GluA2-encoding cDNA was transfected into HEK293T cells using calcium phosphate precipitation. In all cases, 250 μg of DNA was used to transfect 5 x 162 cm^2 flasks. After transfection, cells were incubated for 48 h at 37 °C to allow protein expression, and then solubilized in 1% (v/v) Triton X-100 for 1 h at 4 °C before centrifugation at 62,000 g in order to remove all insoluble material. HA-tagged GluA2 was isolated using anti-HA immunoaffinity chromatography, and the isolated sample was analysed using SDS-PAGE followed by silver staining and immunoblotting with a mouse monoclonal anti-HA antibody (Covance).

Chloroform solutions of L-α-phosphatidylcholine (PC) and brain L-α-phosphatidylserine (PS; Avanti Polar Lipids) were mixed at a molar ratio of 3:1. The chloroform was then evaporated under a stream of nitrogen gas, and the lipids were mixed with 200 μl of purified receptor in 2% 3-[(3-cholamidopropyl) dimethylammonio] propanesulfonate (Sigma). The mixture was dialysed at 4 °C against HEPES-buffered saline (HBS; 100 mM NaCl; 20 mM HEPES-NaOH, pH 7.6) for 2 days, with several buffer changes. The resulting liposome

suspension was deposited onto freshly cleaved mica disks. After a 5-min adsorption, the sample was rinsed with HBS containing 1 mM $CaCl_2$ to remove unadsorbed liposomes, and then transferred to the atomic force microscope.

AFM imaging under fluid was carried out at room temperature (20 °C) using a Bruker-AXS FastScan Dimension atomic force microscope. The instrument was set to perform in micro-volume fluid mode to facilitate buffer exchanges while imaging. All images were collected in 'tapping' mode, using the B triangle of SNL-10 silicon nitride probes (Bruker). The cantilevers, with a typical spring constant of 0.25 N/m, were tuned to set a resonance frequency of 110-140 kHz. The microscope was engaged with a 2-μm scan area to allow for tuning. The setpoint was adjusted to the highest setting that allowed imaging with little noise, to minimize the force applied to the sample. Images were captured at a scan rate of 20 Hz, and with 512 scan lines per area. Individual particles in the images were identified, and particles with heights between 5.5 and 9.5 nm were taken to represent assembled AMPA receptors. Cross-sections were taken at the highest point of each receptor to generate height profiles. Data analysis was performed using the Nanoscope analysis 1.5 software.

Crystallization

Wildtype $GluA2_o$ and N775S (flip-like) mutant LBDs were expressed and purified as described previously (Krintel et al., 2014). Crystallization was performed using the vapour diffusion hanging drop method at 6 ^oC. The crystallization drop consisted of 1 μl $GluA2_o$-LBD solution (5-10 mg/ml) in a buffer containing 10 mM HEPES, 20 mM NaCl, 1 mM EDTA (pH 7.0), and 1 μl of reservoir solution. Before setting up the crystallization drops, the protein solution was mixed with L-Glu to a final concentration of 4 mM (RbBr) or 10 mM (NaBr and NaCl), and alkali halide salts to a final concentration of 300 mM. The $GluA2_o$-LBD N775S

mutant solution used for crystallization was 4-5 mg/ml and the same buffer contained 0.7 mM or 4 mM L-Glu accompanying 300 mM NaBr or RbBr, respectively. Crystals used for diffraction data collection were obtained at conditions consisting of 18-24.4% PEG4000, 0.2-0.3 M Li_2SO_4, and 0.1 M CH_3COONa, pH 5.5 ($GluA2_o$ LBD with NaBr or RbBr), 0.1 M cacodylate, pH 6.5 ($GluA2_o$-LBD N775S with NaBr or RbBr), or phosphate citrate, pH 4.5 ($GluA2_o$-LBD with NaCl).

Data collection and structure determination

All X-ray diffraction data on GluA2 LBD crystals were collected at Max-Lab beamline I911-3 (Lund, Sweden) (Ursby et al., 2013) at 100 K using the following wavelengths (Å): 0.91949 ($GluA2_o$ NaBr); 0.79999 ($GluA2_o$ RbBr); 0.91976 ($GluA2_o$-LBD N775S RbBr); 1.0000 ($GluA2_o$-LBD N775S NaBr and $GluA2_o$-LBD NaCl). Diffraction images were processed in XDS (Kabsch, 2010) or Mosflm within the CCP4 programme suite (Winn et al., 2011). Data were scaled and merged using SCALA (Evans, 2006) and the structures were solved by molecular replacement in Phaser (McCoy et al., 2007) within CCP4, using GluA2-LBD structures as search models (PDB: 3DP6, (Ahmed et al., 2009); and PDB: 4O3A, molA, (Krintel et al., 2014)). Initially, the structures were rebuilt in AutoBuild (Terwilliger et al., 2008) within Phenix (Adams et al., 2010). Structures were further improved using Coot (Emsley et al., 2010) and refinement in Phenix (Afonine et al., 2012). All three refined structures displayed good quality indicators as calculated by MolProbity (Chen et al., 2010) within Phenix, with over 98% of residues within Ramachandran favoured regions. Figures were prepared with the PyMOL Molecular Graphics System (Version 1.7.4, Schrödinger, LLC).

MD Simulations

The $GluA2_i$ (PDB: 2UXA; (Greger et al., 2006)) LBD dimer, comprised of chains A and C, was used for constructing models for MD simulations. Missing atoms were added in PyMOL (Version 1.4) and missing residues were added using Modeller Version 9.12 (Sali and Blundell, 1993). The R764G mutation was imposed prior to simulation. The LBD dimer was solvated in a cubic water box with dimensions $(100\ Å)^3$ using the TIP3P water model (Jorgensen et al., 1983), and subsequently the system was neutralized and 150 mM NaCl was added. MD simulations were performed using Gromacs 4.6 (Hess et al., 2008) with the OPLS all-atom force field (Jorgensen et al., 1996; Kaminski et al., 2001) as described previously (Dawe et al., 2016). Four simulation repeats were produced (a-d), with all being 100 ns, except repeat C, which was extended to 200 ns. Analyses were performed using VMD (Humphrey et al., 1996) and Gromacs (Hess et al., 2008). Atomic radial pair distribution functions were calculated over the two LBD chains for 2000 frames (500 frames from each simulation), using chloride ions as one selection and a specific residue (without hydrogen atoms) as the other selection.

Statistical Methods

Results are expressed as mean ± SEM. Statistical analyses of sample means were performed using unpaired two-sample t tests (assuming unequal variance). A p value < 0.05 was considered significant.

ACKNOWLEDGMENTS

This work was supported by operating grants from the Canadian Institutes of Health Research (D.B.), the Biotechnology and Biological Sciences Research Council (BB/J018236/1, J.M.E.), the Leverhulme Trust (RPG-059, P.C.B. and M.M.), and the Medical Research Council (MR/M0004331, P.C.B.). The Lundbeck foundation and Danscatt, are also acknowledged for financial support (J.S.K.). G.B.D. is supported by a Canada Graduate Scholarship (CGS-D) from the Natural Sciences and Engineering Research Council of Canada. M.F.K. is supported by the Islamic Development Bank and the Cambridge Commonwealth Trust. R.V. was supported by the Lundbeck Foundation. M.M. held a postdoctoral fellowship from the Alfred Benzon Foundation. D.B. was a Canada Research Chair. We thank the Advanced Research Computing (ARC) facility, the Blue Joule facility at the Hartree Centre, the National Service for Computational Chemistry Software, the IRIDIS High Performance Computing facility, and the HECTOR and ARCHER UK National Supercomputing Services for computer time through the EPSRC-funded HECBioSim consortium (www.hecbiosim.ac.uk). In additional MAX-lab, Lund, Sweden is thanked for providing beamtime and technical assistance. Heidi Peterson purified the $GluA2_o$ LBD protein and Anne Mette Kaern crystallized the $GluA2_o$-LBD with sodium bromide and sodium chloride.

SUPPLEMENTAL INFORMATION

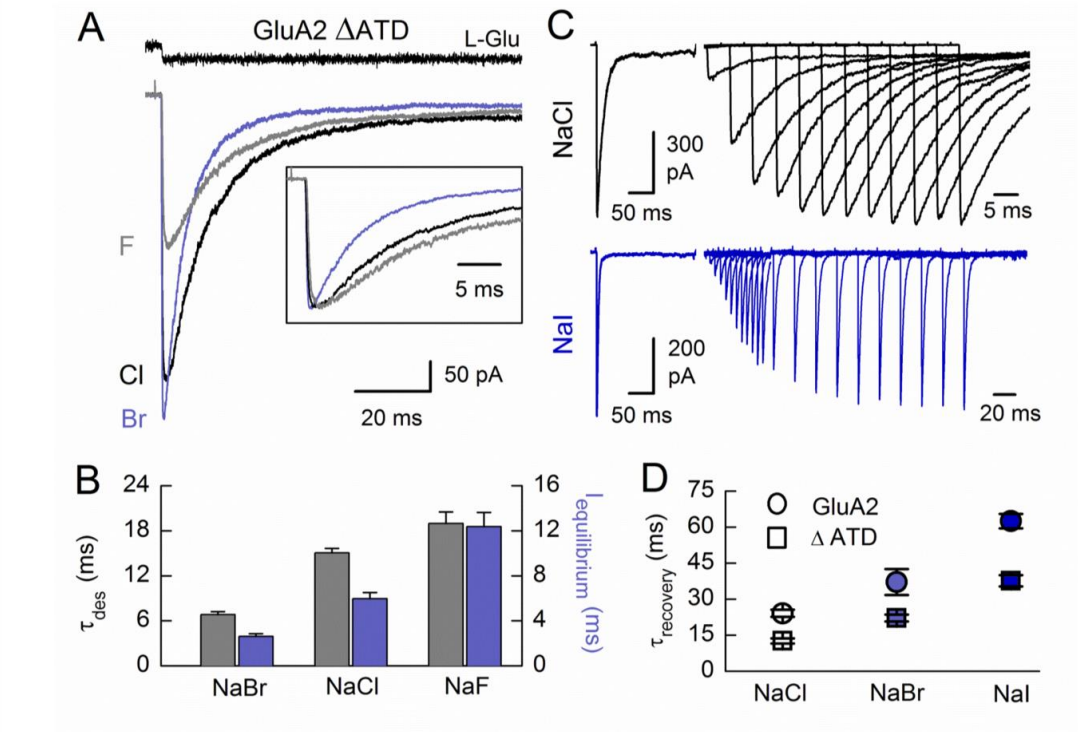

Figure S3.1 Functional modulation of GluA2 by external anions is mediated by the LBD. Supplemental data associated with Figure 3.1.
(A) Typical current responses of GluA2$_i$ ΔATD receptors (patch number 150825p1) to a 250 ms application of 10 mM L-Glu in the presence of external NaCl (black), NaBr (light blue), and NaF (grey). The responses are also scaled to the same peak amplitude (inset). The uppermost trace (black) shows the junction current, recorded with an open patch pipette after the experiment to monitor the profile of solution exchange.
(B) Mean time constants of current decay after a 250 ms L-Glu application (τ_{des}) (left axis), as well as mean equilibrium current amplitude ($I_{equilibrium}$) as a percentage of the peak response (right axis), in the presence of different external anions. Data are mean ± SEM, from six independent patch experiments.
(C) Profile of recovery from desensitization for GluA2$_i$ ΔATD receptors in external NaCl (top, black) and NaI (bottom, dark blue). The traces are from a two-pulse protocol, during which an initial 200 ms application of 10 mM L-Glu desensitized receptors and was then repeated after allowing receptors to recover from desensitization for different time intervals. The amplitude of the second peak, or test response determines the time course of recovery from desensitization. Both conditions were recorded from the same patch experiment (patch number 160428p11).
(D) Mean time constants of recovery from desensitization for wild-type GluA2$_i$ (circle) and GluA2$_i$ ΔATD (square) receptors, derived from the protocol described above after the relative amplitude of the test pulse was fitted with a Hodgkin-Huxley-type equation. Data are mean ± SEM, from six (NaI), seven (NaBr), or thirteen (NaCl) patch experiments for wild-type GluA2$_i$, or from four (NaI), six (NaBr), or ten (NaCl) independent patch experiments for GluA2$_i$ ΔATD.

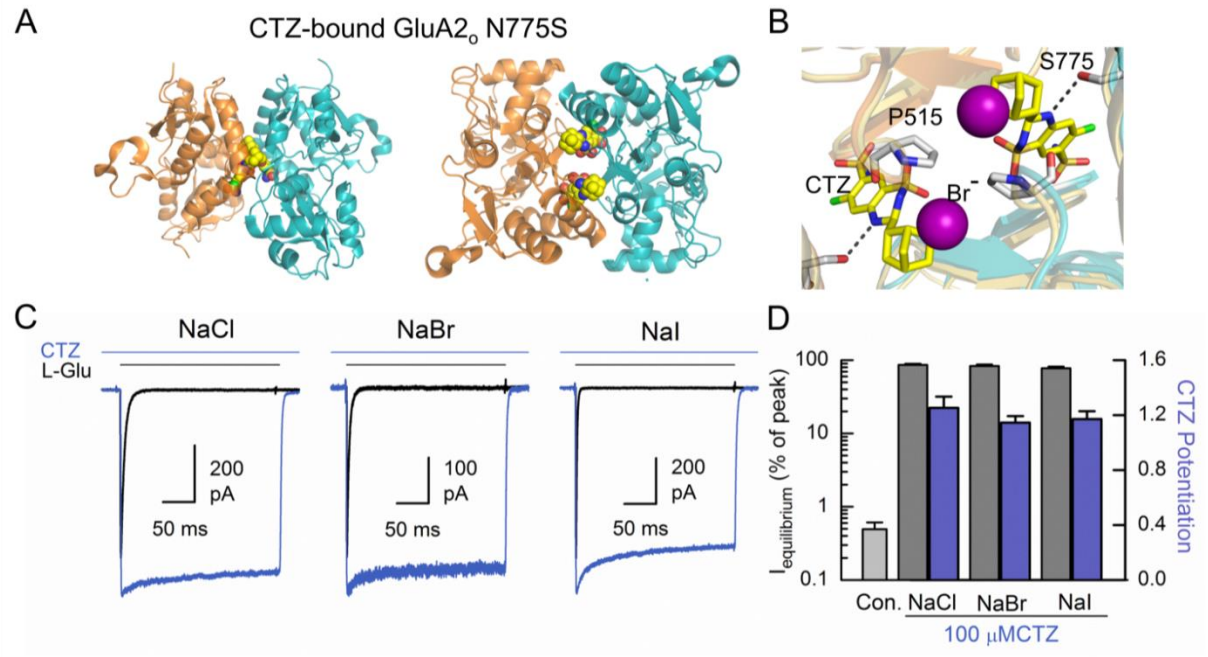

Figure S3.3 GluA2 sensitivity to cyclothiazide persists in different external anions. Supplemental data associated with Figure 3.3.
(A) Side (left) and top (right) views of the $GluA2_o$-LBD N775S dimer (PDB: 3H6T; (Hald et al., 2009)), showing two CTZ molecules (yellow spheres) bound in the dimer interface.
(B) Close-up view of an alignment between the CTZ-bound LBD shown in panel A (faint yellow) and the $GluA2_o$-LBD N775S crystallized in the presence of RbBr (orange/teal).
(C) Response of $GluA2_i$ receptors to a sustained (250 ms) application of 10 mM L-Glu in different external halide ions, prior to the application of CTZ (black) and during (blue) CTZ exposure. Responses in NaCl (patch number 160516p4), NaBr (patch number 160512p4), and NaI (patch number 160510p4) were obtained from separate patch experiments.
(D) Mean equilibrium current amplitude ($I_{equilibrium}$) of $GluA2_i$ receptors, as a percentage of the peak response (left axis, grey), in NaCl prior to CTZ application (Con.), or various halide ions in the presence of CTZ. The potentiation of the peak current response induced by CTZ in the same set of ionic conditions is also shown (right axis, blue). Data are mean ± SEM, from six (NaCl, NaI) or seven (NaBr) independent patch experiments.

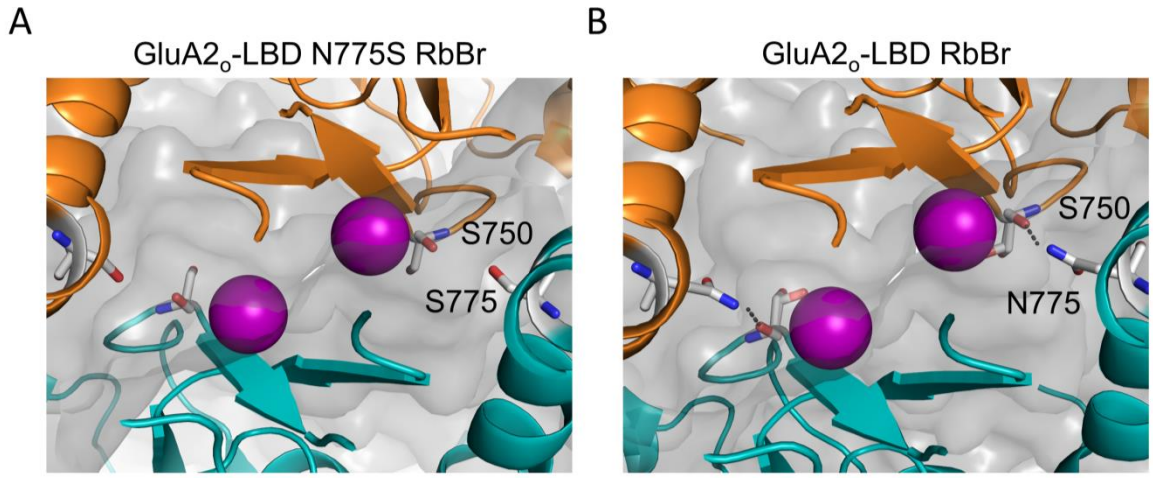

Figure S3.5 A hydrogen bond could account for reduced anion sensitivity in $GluA2_o$ receptors. Supplemental data associated with Figure 3.5.
(A and B) Top views of the $GluA2_o$-LBD N775S, or flip-like, dimer (A) and the $GluA2_o$-LBD (B) dimer are depicted, including a hydrogen bond between residues Ser750 and Asn775 in the latter structure. The two subunits are coloured as orange or teal with surface representation also shown (grey).

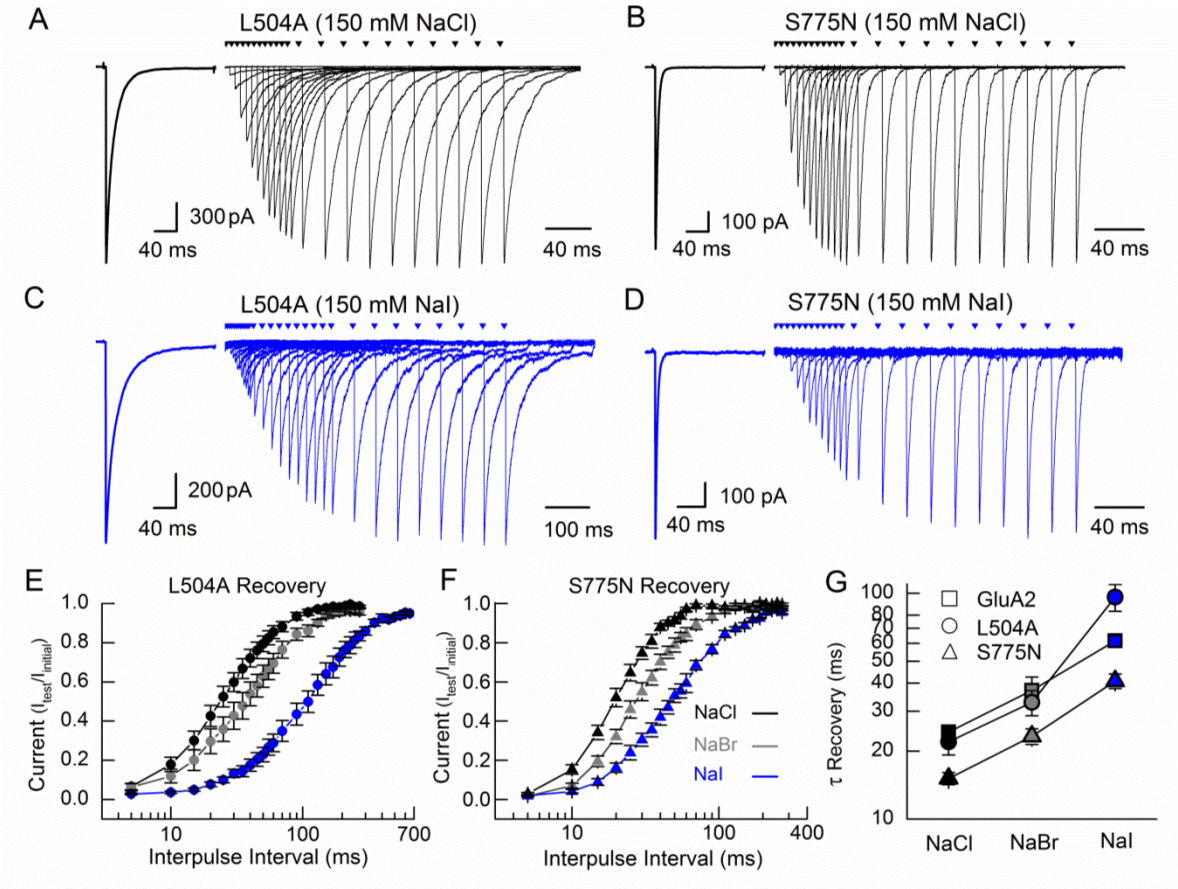

Figure S3.6 The GluA2$_i$ S775N and L504A mutations do not influence anion sensitivity of recovery from desensitization. Supplemental data associated with Figure 3.5.

(A-D) Profile of recovery from desensitization is shown for GluA2$_i$ L504A in external NaCl (A) and NaI (C, patch number 160331p9) as well as GluA2$_i$ S775N in external NaCl (B) and NaI (D, patch number 160401p15). The traces are from a two-pulse protocol, during which an initial 200 ms application of 10 mM L-Glu desensitized receptors and was then repeated (black arrows) after allowing receptors to recover from desensitization for different time intervals. The amplitude of the second peak, or test response determines the time course of recovery from desensitization.

(E and F) Mean current elicited by the test pulse from the recovery protocol described above, relative to the initial peak response, for GluA2$_i$ L504A (E) and GluA2$_i$ S775N (F) mutant receptors. The results were fitted with a Hodgkin-Huxley-type equation. Data are mean ± SEM, from six (NaI, NaBr) or twelve (NaCl) patch experiments for GluA2$_i$ L504A, or from five (NaI, NaBr), or nine (NaCl) independent patch experiments for GluA2$_i$ S775N.

(G) Mean time constants of recovery from desensitization for wild-type GluA2$_i$, as well as L504A and S775N mutant receptors, derived from the recovery protocol described above. Data are mean ± SEM, from the same number of independent patch experiments indicated for panels E and F.

Table S3.1 Changes in GluA2 receptor height measured by AFM.

		Height Reduction	N
$GluA2_i$	**Condition**		
Ion Substitution	NaBr	0.74 ± 0.06	12
	NaI	0.87 ± 0.11	13
L-Glu	NaCl	0.69 ± 0.11	11
	NaBr	0.25 ± 0.05	14
	NaI	0.18 ± 0.06	12
CTZ (background)	NaCl+L-Glu	-0.03 ± 0.07	14
	NaCl to NaBr	0.45 ± 0.19	6
	NaCl to NaI	0.66 ± 0.05	13
CNQX (background)	NaCl+L-Glu	-0.10 ± 0.07	12
$GluA2_o$			
Ion Substitution	NaBr	0.06 ± 0.06	12
	NaI	0.12 ± 0.06	15
L-Glu	NaCl	0.61 ± 0.07	10
	NaBr	0.70 ± 0.14	10
	NaI	0.59 ± 0.11	11
$GluA2_i$ L504A			
Ion Substitution	NaBr	0.08 ± 0.06	15
	NaI	0.04 ± 0.13	10
L-Glu	NaCl	0.69 ± 0.07	14
	NaBr	0.62 ± 0.11	10
	NaI	0.74 ± 0.10	10

Cyclothiazide (CTZ) was present at 100 μM in the background, while CNQX was present at 500 μM to ensure saturation of receptors. The number of receptors measured in each condition (N) is indicated, and values are reported as mean ± SEM.

Table S3.2 Data collection and refinement statistics for GluA2 LBD structures.

	$GluA2_o$ NaBr	**$GluA2_o$ RbBr**	**$GluA2_o$ NaCl***	**$GluA2_o$ N775S RbBr**	**$GluA2_o$ N775S NaBr***
Data collection					
Space group	P2	P 2_1 2_1 2	P2	C2	C2
Cell dimensions					
(a,b,c,β)	104.8, 47.6,	64.1,90.8,	67.0, 47.2,	123.0, 47.5,	122.7, 47.5,
(Å, °)	124.15, 113.4	47.8, 90.0	95.8, 95.6	49.8, 110.2	49.7, 110.1
Resolution (Å)	39.1-2.00 (2.11-2.00)	30.3-1.68 (1.77-1.68)	47.7-1.48 (1.56-1.48)	46.8-1.75 (1.84-1.75)	46.7-1.60 (1.69-1.60)
R_{merge} (%)	10.5 (29.0)	10.1 (38.2)	5.1 (35.5)	7.4 (37.3)	5.0 (41.4)
$I/\sigma I$	5.4 (2.3)	5.4 (1.9)	10.7 (2.1)	7.5 (1.8)	12.3 (1.9)
Completeness (%)	100 (100)	100 (100)	97.6 (83.6)	100 (100)	99.8 (98.5)
Redundancy	6.0 (6.0)	8.1 (8.2)	4.8 (2.5)	5.0 (4.7)	4.0 (2.9)
Refinement					
Resolution (Å)	37.97-2.00	30.21-1.68		34.35-1.75	
No. reflections	76965	32476		27413	
R_{work} / R_{free} (%)	17.25/22.47	11.49/16.60		12.16/19.87	
No. atoms					
Protein	8289	2130		2089	
Ligand/ion	116	43		30	
Water	734	383		323	
B-factors (Å^2)					
Protein	27.87	12.26		20.85	
Ligand/ions	51.80	40.21		55.29	
Water	30.02	29.78		35.65	
R.m.s. deviations					
Bond lengths (Å)	0.024	0.010		0.009	
Bond angles (°)	1.11	1.20		1.18	

Values in parentheses are for highest-resolution shell. *After data collection, the structure was solved by molecular replacement in PHASER and initially refined using AutoBuild in Phenix. After inspection of possible sodium in potential cation binding sites, no further refinements were carried out as the structures were considered redundant.

PART III:

DISCUSSION AND

CONCLUSIONS

DISCUSSION

A few topics pertaining to my research were too broad in scope to discuss in the manuscripts that comprise the results chapters of this thesis. I will attempt to address some of them here in three subsections. Moreover, at the end of each subsection, I will also suggest some experiments that could be done to shed light on the issues at hand. It is my hope that this broader discussion enagages readers who may not see the direct appeal of ion channel biophysics, but still appreciate the importance of studying the iGluR protein family.

First, underlying all of my electrophysiological measurements is the fast gating of AMPAR and KAR complexes. The ability of a protein to bind another molecule and open an ion channel within a fraction of a millisecond is no trivial feat. Of course, this speed has not always been present in iGluR progenitors, and it is worthwhile to consider how and why they evolved faster activation and desensitization. On a related subject, what are the consequences if AMPAR desensitization is attenuated or blocked entirely? In order to justify the study of desensitization in excruciating structural detail, I think it is useful to explain why the process is critical *in vivo*. As it turns out, there have also been interesting therapeutic benefits derived from synthetic molecules that modulate (i.e. inhibit) AMPAR desensitization. Finally, the use of ions as an experimental tool to investigate channel gating is prevalent throughout my thesis. Similar to AMPARs and KARs, many other membrane proteins are modulated by external ions. I will tour through several LGIC and GPCR families to explore this common mode of allosteric regulation, and how it fulfills unique functions to fine-tune protein activity.

1. The evolution of fast gating in AMPARs

All of the critical functions of the nervous system, including sensory perception, movement, learning, and memory, are dependent upon signal processing -usually of a chemical nature- at synaptic connections (Jessell & Kandel, 1993). As a functional unit, the chemical synapse can be thought of as a series of rapid reactions: the action potential, followed by calcium-mediated vesicular release, neurotransmitter receptor activation, and transmitter removal from the synaptic cleft. It is necessary for all of these steps to involve low-affinity interactions, or else the rapid cycle of neurotransmission, and by extension the function of the nervous system, would grind to a halt (Dunant & Bloc, 2003). If AMPAR affinity for glutamate was even ten-fold higher, receptors might still be agonist-bound at the time of the next vesicular release (due to slow deactivation or recovery from desensitization), rendering them unable to "sense" the second round of glutamate. As a result, some information relayed by presynaptic axons would either be lost or improperly integrated on the postsynaptic side, rendering high-frequency signal transduction ineffective.

Given the central importance of AMPARs for rapid information processing in mammalian neurons, it is interesting that iGluR genes encoding functional ion channels are also found in plants (Lam et al., 1998; Tapken et al., 2013), as well as prokaryotes (Chen et al., 1999). The occurrence of iGluRs prior to the evolution of the animal nervous system means that their ancestral versions likely had entirely different functions. For example, exogenous glutamate application modulates root growth in *Arabidopsis* (Walch-Liu et al., 2006), while the iGluRs of the primitive animal *Trichoplax* have been speculated to sense the amino acid as a nutrient signal in the surrounding environment (Jorgensen, 2014). Even if their physiological roles are unclear, a number of iGluRs from diverse animal and plant phyla have been functionally characterized;

illuminating the evolutionary changes these proteins have undergone to suit the modern, mammalian brain.

The first prokaryotic iGluR to be studied in isolation was "GluR0" from the cyanobacterium *Synechocystis*, and though it responds to glutamate, its pore is selective for potassium ions (Chen et al., 1999). This selectively is not entirely surprising, as earlier sequence analysis had been used to argue that iGluRs likely arose when the pore of a potassium channel precursor was incorporated into an amino acid-binding protein (Wo & Oswald, 1995). Perhaps more unexpected was the slow gating of GluR0, which activated and deactivated over an approximately ten-fold greater time scale than mammalian GluA2 (Chen et al., 1999). Since then iGluRs from other primitive animals, including the rotifer *Adineta vaga* (Lomash et al., 2013) and comb jelly *Mnemiopsis leidyi* (Alberstein et al., 2015), have been shown to possess extremely slow gating kinetics, with recovery from desensitization on the scale of minutes. Although rotifers possess a simple nervous system, *A. vaga* GluR1 is not thought to be a neurotransmitter receptor, because it exhibits little agonist specificity, activating in response to several polar and hydrophobic amino acids (Janovjak et al., 2011). In contrast, the nematode *Caenorhabditis elegans* possesses iGluRs with greater biophysical similarity to their mammalian counterparts, desensitizing in tens of milliseconds and recovering over several seconds (Mellem et al., 2002). Could these more rapid state transitions reflect the fact *C. elegans* uses glutamate as a *bona fide* neurotransmitter to mediate withdrawal movements in response to mechanical stimulation (Brockie & Maricq, 2006)?

A correlation appears to exist between the presence and/or utility of the nervous system in animals and the time scale of iGluR gating -though the number of species whose receptors have been examined recombinantly is still rather small. Since iGluRs were present in the

precursor species to modern animals, it is interesting that they have been subsequently lost in *Porifera* (sponges), which do not possess a nervous system (Srivastava et al., 2010). Alternatively, for more complex animals, it seems as though iGluRs were useful to keep around, especially for CNS signaling. Indeed, a sharp increase in the number of iGluR genes occurred between the common ancestor of chordates and that of vertebrates (Liebeskind et al., 2015), a subgroup that uniquely concentrates command of the nervous system at the brain. One can imagine that as the vertebrate brain evolved to house more complex neuronal circuitry, along with an expanding number of synapses, rapid neurotransmitter processing was required to maintain timely responses to incoming information. Not unrelated to that idea, there may also have been selective pressure to develop faster reactions to external stimuli as predator-prey interactions intensified and survival was at stake. In any case, ancestral iGluRs -or what would become AMPARs- seem to have been selected as an ion channel template though which evolution engineered faster chemical neurotransmission.

Because the LBD of several primitive iGluRs has been crystallized, it is possible to speculate on the structural changes that this domain has undergone to accommodate faster gating. For instance, it has been noted that within the agonist-binding cleft of mammalian AMPARs, cleft closure is mediated by a network of D1-D2 hydrogen bonds, involving either water molecules or direct interactions between amino acids (Zhang et al., 2008). Yet in the *M. leidyi* structure, a cross-cleft salt bridge that is absent from other iGluRs contributes to high apparent agonist affinity and slow recovery from desensitization (Yu et al., 2016). Accordingly, the replacement of fixed, chemical interactions with bonding to free water molecules could have served to reduce agonist affinity and permit rapid neurotransmitter unbinding at the synapse (Plested, 2016). A second adaptation for speed appears to be a modification of cross-dimer

interactions, which may in turn account for faster desensitization. Remarkably, *Synechocystis* GluR0 and *A.vaga* GluR1 both possess a lysine at the equivalent position of the mutant residue in GluK2 D776K, which does not exhibit desensitization (Nayeem et al., 2009; Dawe et al., 2013, results chapter 1). In all three cases, the lysine would be expected to form contacts with negatively charged groups on the opposing subunit, and based on the KAR mutant phenotype, the location of the lysine appears to be a very strong position from which to hold together the dimer. The electrostatic interactions that form interface of wildtype GluA2 and GluK2 are somewhat lower, and they are sufficiently unstable that a few key mutations (GluA2) or the removal of allosteric ions (GluK2) leaves little time for activation before the onset of desensitization (Dawe et al., 2016, results chapter 2). In this sense, the modern iGluR interfaces could be described cynically as "built to fail," at least after glutamate has bound for a few milliseconds.

Because a systematic structural comparison of iGluR LBDs across extant animal species is currently unavailable, it is useful to pinpoint some experiments that might corroborate the informal hypothesis above: less stable inter-domain and inter-subunit interactions have provided the structural flexibility to achieve the rapid iGluR gating cycle of modern mammals. One investigative approach might be to introduce mutations in the LBD dimer interface that convert mammalian residues to their more primitive counterparts, and simultaneously measure the consequences for channel function, as well as dimer assembly, via ultracentrifugation. If such perturbations produced lower dissociation constants of dimerization they would support an evolutionary path that relied on weakening of the dimer interface to achieve faster desensitization. Likewise, mutations that form stronger cross-cleft interactions and increase apparent agonist affinity (like the salt bridge in *M. leidyi*) would be interesting to examine in

recombinant systems and also *in vivo*. Presumably, there would be some deficit in high-frequency synaptic transmission, since agonist unbinding would be too slow to allow recovery to a resting state capable of response to further rounds of neurotransmitter release. In this regard, a link could be provided between the nature of the agonist-binding cleft and the suitability of iGluRs for fast neuronal signaling.

2. The role of AMPAR desensitization *in vivo*

The rate of desensitization is known to shape how iGluRs respond to high-frequency synaptic transmission (i.e. Raman & Trusell, 1995). At the same time, if neurotransmitter molecules can unbind from their receptors prior to the onset of desensitization, a greater proportion of receptors should remain in a naïve state that is capable of responding to the next vesicular release. For GluA2 AMPARs this scenario is indeed relevant, because desensitization occurs at a relatively slow rate, ensuring that sizeable responses to 1 ms glutamate pulses can be maintained, even at high (i.e. 100 Hz) frequencies (Rozov et al., 1998). In contrast, the time constant of GluA1 desensitization (~ 2.0-2.5 ms) is fast enough (Bowie, 2002) that a 1 ms glutamate pulse will desensitize many receptors, and responses to high-frequency stimulation are subject to the rate of recovery from desensitization (Rozov et al., 1998). As such, ESPC amplitudes become depressed when measured in quick succession (Trussell et al., 1993), probably due to the large contribution of heteromeric AMPARs. By (almost) eliminating desensitization, CTZ can drastically reduce this paired-pulse depression (Trussell et al., 1993), though the synaptic effects of such drugs are predictable. A more interesting problem arises from the consequences of attenuating AMPAR desensitization, when assessed at the level of the entire

nervous system. As it turns out, numerous groups have addressed this question using pharmacological agents that prevent desensitization, as well as genetic manipulations.

A relatively straight-forward intervention involving the injection of CTZ into the brains of freely moving rats produced seizure activity (Kong et al., 2010), as might be expected if neuronal excitation is totally unfettered. In spite of this observation, it is not clear if the removal of AMPAR desensitization was the culprit, because CTZ also directly inhibits GABA-A receptors (Deng & Chen, 2003), which could still cause greater net excitation. Another confounding action of CTZ is that it doubles the time constant of deactivation (after a 1 ms glutamate pulse) for recombinant AMPARs (Partin et al., 1996), and accordingly slows EPSC decay (Trussell et al., 1993). As mentioned above, the increase in apparent affinity of CTZ-bound AMPARs for glutamate could be detrimental for the maintenance of high-frequency glutamatergic signaling. However, an alternative to drug injection was realized with the creation of a heterozygous GluA2 L/Y mutant mouse -the homozygous mutation was lethal (Christie et al., 2010). Perhaps because the non-desensitizing L/Y mutation was only present in one AMPAR gene, its effects were attenuated, but importantly, basal synaptic transmission was relatively normal, including EPSC decay rate. Interestingly, these mice also displayed frequent seizures and died within a few weeks after birth (Christie et al., 2010). An even more extreme, constitutively active receptor, produced by the "Lurcher" mutation near the channel pore, can also be thought of as restricting desensitization (Klein & Howe, 2004), and results in lethality after birth because of excitotoxic cell death. As such, there seems to be a consistent, epileptic and/or excitotoxic phenotype associated with reduced AMPAR desensitization, though to what extent individual receptors resisted desensitization is unclear from these *in vivo* studies.

There has also been great interest in molecules that reduce AMPAR desensitization for therapeutic use. Just about any chemical will be toxic at a high enough dose, but that does not preclude such chemicals being beneficial under other conditions. CTZ itself does not readily cross the blood-brain barrier, preventing its use in neurological interventions (Black, 2005). Nevertheless, several compounds with similar binding sites and functional effects have been investigated as cognitive enhancers. Aniracetam has long been approved for clinical use in some jurisdictions, as there are numerous studies reporting its ability to alleviate cognitive deficits in conditions like Alzheimer's disease, at least to a moderate extent (Lee & Benfield, 1994). Based on the promise of finding a more potent and/or efficacious derivative of aniracetam, the CX class of molecules known as "ampakines" was developed. CX-516 acts by slowing the deactivation and desensitization of neuronal AMPARs (Arai et al., 1996), and its application can improve memory in rodents (Granger et al., 1996), as well as human subjects (i.e. Lynch et al., 1996). Unfortunately, its short half-life and low potency have suppressed interest in its therapeutic application (Black, 2005).

Around the same time that ampakines first appeared, two AMPAR modulators from other structural classes were also investigated as cognitive enhancers. Specifically, the benzothiadiazide IDRA-21 (related to CTZ) and the sulfonylamino compound PEPA both potentiate AMPAR current responses, as well as improve rodent performance on the water maze task (Zivkovic et al., 1995; Sekiguchi et al., 1997; Sekiguchi et al., 2001). More sensitive electrophysiological examination revealed that IDRA-21 has the dual effects of slowing deactivation and blocking desensitization of neuronal AMPARs (Yamada et al., 1998). Meanwhile, PEPA reduces the extent of desensitization of recombinant AMPARs, but not their rate of desensitization or deactivation (Sekiguchi et al., 2002). Though their biophysical and

behavioural effects are broadly similar to the ampakines, IDRA-21 and PEPA were not put into clinical trials (Black, 2005). As a result, the search for a miracle AMPAR modulator is ongoing.

From a drug discovery perspective, it is encouraging that IDRA-21, PEPA, and CX-516 were all crystallized in the LBD dimer interface of GluA2 AMPARs (Ptak et al., 2009; Ahmed et al., 2010; Krintel et al., 2013), where CTZ and aniracetam interact. One of the so-called "LY" compounds (created by Lilly), part of a class of biarylpropylsulfonamide AMPAR potentiators (Ornstein et al., 2000), binds in a similar manner to PEPA (Sobolevsky et al., 2009), and its companion molecules have exhibited diverse anti-depressant, neuroprotective, or cognitive effects in preclinical testing (Black, 2005). This suggests that the rational design of compounds targeting the LBD dimer interface may be a reasonable strategy to combat several neurological conditions. So far, four binding modes have been reported amongst AMPAR modulators that reside in the interface (Pohlsgaard et al., 2011), meaning many interactions could be exploited to engineer the ideal modulatory compound.

Returning to the original matter of the kinetics of AMPAR desensitization, it seems problematic that these receptors inactivate so rapidly, when there are many apparent benefits derived from synthetic molecules that hold together the LBD dimer interface and delay desensitization. Assuming that human AMPAR precursors evolved faster gating over time, why was a protein structure that maximized cognitive performance not selected for? It is possible that selective pressure for greater cognition was just not that great, or else achieved in other genes. Alternatively, the increased charge transfer gained by slowing AMPAR deactivation and desensitization might somehow occlude synaptic plasticity. Given the preservation of LTP and LTD in the presence of ampakines (Arai et al., 2004), as well as a normal LTP amplitude in the GluA2 L/Y mutant mouse (Christie et al., 2010), that possibility does not appear to be the case.

All the same, it is clear that AMPAR desensitization makes an important contribution to glutamatergic signaling, both *in vitro* and *in vivo*. In this regard, structural models of iGluR desensitization are relevant far outside the biophysical realm.

One area where desensitization has not been thoroughly explored *in vivo* concerns flip versus flop alternative splicing. The only clear biophysical difference between the two isoforms appears to be the faster desensitization of flop-type receptors, for GluA2-4 subunits at least (Mosbacher et al., 1994). Because the three amino acid residues that contribute to this phenotype are known (Quirk et al., 2004), it would be fascinating to genetically convert one form to the other and gauge what, if any, synaptic and behavioural effects might arise. Though the design of this experiment is complicated, owing to multiple alternatively spliced residues across multiple subunits, a rigorous approach is likely required to determine why both isoforms exist simultaneously, rather than only one.

Presumably, if mammals were to have only flip or flop AMPAR isoforms there would be negative consequences. In support of this idea, an increase in the ratio of flip versus flop mRNA has been associated with excitotoxic cell death in multiple studies (e.g. Pollard et al., 1993; Park et al., 2016). On a more functional level, changes in flip/flop mRNA expression coincided with an enhanced summation of EPSPs in response to neuronal activity deprivation (Penn et al., 2012). Though the latter results were intriguing, it appears as though altered splicing itself did not achieve synaptic plasticity, but instead provided a means to influence subunit assembly. At this juncture, it is unknown why the composition of AMPAR complexes might be regulated through differential alternative splicing, when numerous other postsynaptic proteins can directly regulate the trafficking and localization of specific subunits. However, the role of flip/flop splicing is likely to become better understood through big-data approaches like transcriptomics,

which can quantify the abundance of each isoform, as well as more powerful genetic tools (i.e. CRISPR) to manipulate the isoforms.

3. Allosteric ions as a tool to regulate agonist binding and gating

The occurrence of modulatory ion-binding sites outside the channel pore is by no means unique to iGluRs. In fact, there are far more known interactions between extracellular ions and membrane proteins than there is space to discuss them here -and probably many interactions still to be identified. The reason for this perhaps stems from the ubiquity of ions in the extracellular environment (i.e. sodium, chloride, and others), combined with the abundance of charged and polar amino acid residues on the solvent-facing surface of proteins. Because the ions are already present, and it is easy enough -in evolutionary terms, over millions of years- to engineer a protein surface or agonist-binding cavity, why not use them as an extra layer of regulation over protein signaling? In an attempt to provide a quick survey of the diverse mechanisms through which allosteric ions can influence protein behaviour, a few examples of their effects on agonist binding, as well as gating and signaling, at LGICs and GPCRs will be highlighted.

3.1 Examples of allosteric ions at LGICs

Multiple LGIC families have exploited extracellular zinc ions to regulate their responsiveness to agonists (i.e. NMDARs). Because zinc is released from synaptic vesicles at micromolar concentrations (Sensi et al., 2011) it could in theory be quite useful to tune receptor responses in conjunction with presynaptic activity. Along these lines, zinc potentiates ATP-induced currents in neurons (Li et al., 1993) by causing a leftward shift in the D-R curves of several P2X receptor subunits (i.e. Brake et al., 1994; Soto et al., 1996). A structural picture of this modulation is beginning to emerge, as subunit-specific zinc-binding sites have been

identified at the inter-subunit interface of $P2X_2$ (Nagaya et al., 2005), as well as the central cavity between the three subunits of $P2X_4$ (Kasuya et al., 2016). For the latter site, MD simulations predict that zinc binding promotes channel opening by increasing the pore radius (Kasuya et al., 2016). There is also a physiological importance of zinc in purinergic signaling, as P2X antagonists have been shown to prevent zinc-induced augmentation of LTP amplitude at the CA3-CA1 synapse (Lorca et al., 2011).

A second LGIC target of zinc is the glycine receptor (GlyR), where low (~ 1 μM) and high (~ 100 μM) concentrations of the cation respectively potentiate and inhibit current responses (Bloomenthal et al., 1994; Laube et al., 1995). As with the $P2X_2$ receptor, mutagenesis revealed a pair of N-terminal histidine residues on the GlyRα1 subunit to be responsible for coordinating zinc and mediating inhibition (Harvey et al., 1999), though other nearby residues have also been identified as forming a separate "potentiation site" (Laube et al., 2000). The inhibitory site is found at the inner subunit interface and thought to restrict multi-subunit rearrangements that coincide with activation (Miller et al., 2008). The potentiation site, meanwhile, faces outward (Miller et al., 2008). In order to assess the impact of GlyR potentiation by zinc *in vivo*, knockin mice with a point mutation at the potentiation site were generated. These mice turned out to be more prone to tremors and have an enhanced acoustic startle response, similar to hyperekplexia in humans (Hirzel et al., 2006).

A third LGIC family, comprised of the acid-sensing ion channels (ASICs), has been investigated recently as a target of anion modulation. This line of research was spurred by the first ASIC crystal structure (of ASIC1a), which placed a single chloride ion in the large, extracellular domain of each subunit (Jasti et al., 2007). Electrophysiological characterization of the ASIC1a subunit determined that substitution of external chloride with larger anions

(bromide, iodide, and methanesulfonate) accelerated current decay during concentration jumps to low pH, establishing a relationship between ionic radius and desensitization rate (Kusama et al., 2010). Moreover, the mutation of residues predicted to interact with chloride abolished the gating effect of anion substitution (Kusama et al., 2010). Despite this finding, anion modulation of the ASIC2a and ASIC3 subunits is largely insensitive to the same mutations, and does not follow the same size relationship as ASIC1a, perhaps accounting for the differential anion sensitivity of neuronal receptors, thought to be comprised of ASIC1a/ASIC3 heteromers (Kusama et al., 2013).

3.2 Examples of allosteric ions at GPCRs

Amongst class A GPCRs, there are numerous instances of agonist binding under allosteric regulation by sodium ions (Katrich et al., 2014). The phenomenon was first noted in native opioid receptors, for which agonist binding was inhibited at high sodium chloride concentrations (Pert et al., 1973). A similar effect occurs in adenosine receptors, but the sodium dependence of binding could be abolished through the mutation of a conserved aspartate residue in the second transmembrane helix (Barbhaiya et al., 1996). Interestingly, this site has been identified through mutagenesis as an important mediator of sodium regulation in many class A GPCRs (Katrich et al., 2014). Yet it was using the A_{2A} adenosine receptor that sodium was first crystallized within the central, water-filled cavity between the transmembrane helices, partially coordinated by the conserved aspartate (Liu et al., 2012). This A_{2A} receptor was also bound by a competitive antagonist, and comparison with a previously crystallized agonist-bound receptor revealed that the sodium pocket is collapsed in the active state (Liu et al., 2012). Additional computational analysis has since been used to propose that agonists and sodium ions bind to entirely distinct conformational states of the receptor (Gutierrez de Teran et al., 2013)

Ions also regulate agonist binding at mGluRs, a subfamily of class C GPCRS. For the group I mGluR subunit mGluR1, increasing extracellular calcium enhances the agonist response (EC_{50} $[Ca^{2+}]$ ~ 5 mM), and in some cases has been claimed as sufficient to activate the receptor (Saunders et al., 1998; Kubo et al., 1998). Site-directed mutagenesis and computational modelling from existing structures have suggested that calcium resides adjacent to the agonist-binding site, at the hinge of the extracellular domain (Kubo et al., 1998; Jiang et al., 2010). The assignment of this position is consistent with radioligand binding assays that have demonstrated quisqualate binding to mGluR1 is nearly eliminated, unless divalent ions are present in the buffer solutions (Kuang & Hampson, 2006).

3.3 Ion binding at GluK2 and GluA2 receptors in relation to other membrane proteins

Two themes seem to emerge from the brief, though by no means exhaustive, survey of allosteric ion binding at LGICs and GPCRs. The first is that ions are often found in the vicinity of LGIC subunit interfaces (e.g. Jasti et al., 2007; Miller et al., 2008; Kasuya et al., 2016). It could be that ions bound at inter-subunit interfaces are just more readily detectable, if they play a part in subunit assembly and stabilize protein interaction surfaces in a manner amenable to crystallization. An alternate view is that more ion-binding sites actually occur at interfaces, since they are better sites for allosteric modulation. Indeed, this should be the case for the dynamic LBD layer of AMPARs and KARs.

The second, notable facet of ion interactions is that they often appear to regulate agonist binding in a positive or negative manner. For the GluK2 KAR, which has been carefully scrutinized in response to ion modulation, it is unclear that such regulation occurs. The sodium-binding pocket of GluK2 is outside of the agonist-binding cleft (Plested et al., 2008), though the two sites are close to each other. Complicating this matter is that glutamate-evoked D-R curves

constructed in different external sodium chloride concentrations display a bell-shaped relationship between ion concentration and the EC_{50} value (Bowie, 2002). In other words, it is difficult to infer a simple cooperativity mechanism between agonists and allosteric ions from these data. To take a more extreme case, background glutamate can still desensitize wildtype GluK2 receptors in the absence of external monovalent ions, such that a concentration jump into 150 mM sodium chloride will not produce any current response (Wong et al., 2006). Consequently, ion binding does not appear to be a prerequisite for agonist binding.

As an alternative possibility, could sodium somehow facilitate agonist binding to GluK2 KARs, as zinc does for P2X receptors? Increasing external sodium chloride concentration does slow GluK2 deactivation (Bowie, 2002), evidence of a greater apparent affinity for glutamate. However, a more plausible explanation for such behaviour is that desensitization becomes faster at lower ion concentrations, dominating the phenotype of a 1ms agonist pulse where deactivation would normally be measured. Data from MD simulations suggest that the initial structural rearrangements corresponding to desensitization occur when sodium is removed from LBD environment (Dawe et al., 2013, results chapter 1). All the same, it is unclear exactly how much faster these transitions might occur as ion concentrations are dropped from physiological levels.

One experimental avenue that could provide more structural information about ion modulation of KAR gating is AFM. Since global conformational changes associated with AMPAR desensitization have been detected by AFM, as reported in this thesis (Dawe et al., 2016, results chapter 3), it seems feasible that the method could also measure whether similar changes are induced by ion exchange at GluK2 KARs. One might expect that solution exchange between sodium and another, poorly binding cation species would produce vertical compression if receptors are transitioning to some conformationally unique inactive state -assuming there is a

resemblance to the compressed desensitized states observed across iGluR subfamilies. Alternatively, structural sensitivity to ions may only occur once agonist molecules are also bound, or manifest in different forms that are not so easily detected on a single axis of measure.

For anions acting at GluA2 AMPARs, it is interesting that conformational changes occurred in the absence of agonists, while gating effects were specific to agonist-induced desensitization. Rather than being two unrelated phenomena, mutation of the same residues (produced by $GluA2_o$ splicing) attenuated both effects, suggesting that a single anion binding site is responsible for the structural and functional variation, even if desensitization kinetics are not causally related to receptor compression. Though bromide ions were crystallized in the GluA2 LBD dimer interface, there were no positively charged residues coordinating the anions, distinct from the chloride-bound ASIC structure (Jasti et al., 2007). Nevertheless, anion substitution has similar functional effects on certain subunits within these protein families. Notably, for ASIC1a and GluA2 receptors alike, larger halide ions accelerate desensitization, despite minimal effects on deactivation (MacLean et al., 2016; Dawe et al., 2016, results chapter 3). Because both anion sites are located at an inter-subunit interface (Jasti et al., 2007; Dawe et al., 2016, results chapter 3) it is possible that the anions act through a common mechanism to disrupt contacts that are critical for maintaining the activated subunit assembly. Of course, more will have to be learned about the structural mechanism of ASIC desensitization to pinpoint the precise role of anions in this process.

4. CONCLUSION

In **PART I** of this thesis, I have revisited the literature describing glutamate receptors, which spans from the early characterization of glutamate-evoked currents in the CNS to quite recent, atomic-resolution structural mechanisms of receptor activation. I have also tried to relay how the biophysical properties of isolated iGluRs can explain the functional phenotype of synaptic iGluRs. Within **PART II** of this thesis are three results chapters that contain my experimental observations. Using patch-clamp electrophysiology to measure currents from recombinantly expressed iGluR subunits, I have been able to demonstrate that interactions at the apex of the LBD are critical to keep glutamate-bound AMPARs and KARs in an activated (i.e. open-channel) conformation, defined by intact LBD dimers. For KARs, allosteric sodium ion binding fulfills this role, whereas in AMPARs an endogenous network of electrostatic interactions helps to stabilize dimers. I also identified a site of auxiliary protein interaction at the base of the AMPAR LBD, which helps to prolong receptor activation. Meanwhile, my final results chapter describes a novel mechanism, whereby anions can interact at the AMPAR LBD, inducing conformational changes in apo state (i.e. resting) receptors that shape the time course of channel gating after glutamate binds. It should be noted that my present interpretation of the results mentioned above would not have been possible without the structural and computational techniques of collaborators. Finally, in **PART III** of this thesis I have discussed several topics related to my results, including the evolution of rapid iGluR gating, the importance of AMPAR desensitization *in vivo,* and the occurrence of allosteric ion-binding sites amongst several families of ion channels.

As a “take home message” for readers of this thesis, I would like to relay the point there is always something to be learned from more in-depth exploration of an existing idea. It is easy

to look at the current set of intact iGluR crystal structures, conclude that they illustrate the structural basis of channel gating, and avoid the subject further. However, it is only through the painstaking manipulation (i.e. mutation) of various positions within a structural framework, and the electrophysiological measurement of those manipulated forms that one can advance the ideas of static, often heavily-modified structures toward physiological relevance. It has long been appreciated that the LBD plays in important role in iGluR gating, as it must transduce agonist binding into channel opening. What I hope to have done is introduced an extra degree of specificity to this idea, identifying individual amino acid residues that allow the LBD to coordinate activation. It is also my hope to have "broken down" the LBD, so it can be seen as a dynamic domain, comprised of many distinct sites that each plays a part to set the duration of channel activity.

5. SUMMARY OF ORIGINAL CONTRIBUTIONS

I. I found that the GluK2 D776K mutant receptor exhibited single-channel responses with a near-maximal open probability and a conductance matching that of the wildtype receptor. This contrasted with the unexpected behaviour of GluK2 Y521C/L783C channels that my colleagues had described previously (**PART II**, Chapter 1).

II. We found that the subunits comprising GluK2 LBD dimers come apart during MD simulations in the absence of NaCl, shedding light on the requirement of external ions to maintain KAR subunits in an activated conformation (**PART II**, Chapter 1).

III. We propose that for activated GluK2 KARs, the unbinding of agonist molecules results in deactivation, whereas the unbinding of allosteric sodium ions is a key trigger for desensitization (**PART II**, Chapter 1).

IV. I found that external lithium slows the desensitization of GluA2 AMPARs by binding at an electronegative pocket equivalent to the KAR sodium-binding site, at the apex of the LBD dimer interface (**PART II**, Chapter 2).

V. We found that the mutation of two residues (K759M and T765K) creates a cross-dimer charged tether that inhibits GluA2 AMPAR desensitization, similar to that of the GluK2 D776K mutation described in the first results chapter (**PART II**, Chapter 2).

VI. I found that a GluA2 triple mutant (i.e. E507A/K514A/N768A or AAA), which lacks endogenous interactions at the apex of the LBD dimer interface, is barely capable of activation, but can be “rescued” by the co-expression of either TARP or CNIH auxiliary subunits (**PART II**, Chapter 2).

VII. I found that the “KGK” motif at the base of the LBD, conserved across all AMPAR subunits (residues 718-720 of GluA2) mediates TARP modulation of GluA2 gating kinetics, including the

slowing of deactivation and desensitization. This motif also appears to be responsible, in part, for the rescue of the AAA mutant described in the previous item (**PART II**, Chapter 2).

VIII. I found that halide ions modulate the desensitization, but not deactivation, of GluA2 AMPARs, and that this modulation is much more pronounced in the flip, rather than flop, alternatively-spliced isoform (**PART II**, Chapter 3).

IX. We found that the substitution of external halide ion species induces height changes in apo state GluA2 AMPARs of the flip isoform (**PART II**, Chapter 3).

X. We found a novel anion-binding site in the GluA2 LBD dimer interface, through which ions can regulate both the height of apo state receptors and entry into desensitization (**PART II**, Chapter 3).

XI. We propose that allosteric anions can "prime" flip-type AMPARs to respond in a particular manner upon agonist binding (**PART II**, Chapter 3).

6. REFERENCES

Adams MD & Oxender DL. (1989). Bacterial periplasmic binding protein tertiary structures. The journal of biological chemistry 264, 15739-15742.

Adams PD, Afonine PV, Bunkoczi G, Chen VB, Davis IW, Echols N, Headd JJ, Hung LW, Kapral GJ, Grosse-Kunstleve RW, McCoy AJ, Moriarty NW, Oeffner R, Read RJ, Richardson DC, Richardson JS, Terwilliger TC & Zwart PH. (2010). PHENIX: a comprehensive Python-based system for macromolecular structure solution. Acta crystallographica Section D, Biological crystallography 66, 213-221.

Adams PD, Grosse-Kunstleve RW, Hung LW, Ioerger TR, McCoy AJ, Moriarty NW, Read RJ, Sacchettini JC, Sauter NK & Terwilliger TC. (2002). PHENIX: building new software for automated crystallographic structure determination. Acta crystallographica Section D, Biological crystallography 58, 1948-1954.

Afonine PV, Grosse-Kunstleve RW, Echols N, Headd JJ, Moriarty NW, Mustyakimov M, Terwilliger TC, Urzhumtsev A, Zwart PH & Adams PD. (2012). Towards automated crystallographic structure refinement with phenix.refine. Acta crystallographica Section D, Biological crystallography 68, 352-367.

Ahmed AH, Ptak CP & Oswald RE. (2010). Molecular mechanism of flop selectivity and subsite recognition for an AMPA receptor allosteric modulator: structures of GluA2 and GluA3 in complexes with PEPA. Biochemistry 49, 2843-2850.

Ahmed AH, Wang Q, Sondermann H & Oswald RE. (2009). Structure of the S1S2 glutamate binding domain of GLuR3. Proteins 75, 628-637.

Akaike N. (1995). Concentration clamp technique. In Neuromethods, Patch-clamp applications and protocols, ed. Boulton A, Baker, G., Walz, W., pp. 141-154. Humana Press Inc.

Alberstein R, Grey R, Zimmet A, Simmons DK & Mayer ML. (2015). Glycine activated ion channel subunits encoded by ctenophore glutamate receptor genes. Proc Natl Acad Sci U S A 112, E6048-6057.

Andersen OS & Koeppe RE, 2nd. (1992). Molecular determinants of channel function. Physiol Rev 72, S89-158.

Arai A, Kessler M, Rogers G & Lynch G. (1996). Effects of a memory-enhancing drug on DL-alpha-amino-3-hydroxy-5-methyl-4-isoxazolepropionic acid receptor currents and synaptic transmission in hippocampus. The journal of pharmacology and experimental therapeutics 278, 627-638.

Arai AC, Xia YF & Suzuki E. (2004). Modulation of AMPA receptor kinetics differentially influences synaptic plasticity in the hippocampus. Neuroscience 123, 1011-1024.

Armstrong CM & Bezanilla F. (1977). Inactivation of the sodium channel. II. Gating current experiments. The journal of general physiology 70, 567-590.

Armstrong N & Gouaux E. (2000). Mechanisms for activation and antagonism of an AMPA-sensitive glutamate receptor: crystal structures of the GluR2 ligand binding core. Neuron 28, 165-181.

Armstrong N, Jasti J, Beich-Frandsen M & Gouaux E. (2006). Measurement of conformational changes accompanying desensitization in an ionotropic glutamate receptor. Cell 127, 85-97.

Armstrong N, Mayer M & Gouaux E. (2003). Tuning activation of the AMPA-sensitive GluR2 ion channel by genetic adjustment of agonist-induced conformational changes. Proc Natl Acad Sci U S A 100, 5736-5741.

Armstrong N, Sun Y, Chen GQ & Gouaux E. (1998). Structure of a glutamate-receptor ligand-binding core in complex with kainate. Nature 395, 913-917.

Ascher P & Nowak L. (1988). Quisqualate- and kainate-activated channels in mouse central neurones in culture. J Physiol 399, 227-245.

Ashburner M, Thompson P, Roote J, Lasko PF, Grau Y, el Messal M, Roth S & Simpson P. (1990). The genetics of a small autosomal region of Drosophila melanogaster containing the structural gene for alcohol dehydrogenase. VII. Characterization of the region around the snail and cactus loci. Genetics 126, 679-694.

Assaf Z, Larsen AP, Venskutonyte R, Han L, Abrahamsen B, Nielsen B, Gajhede M, Kastrup JS, Jensen AA, Pickering DS, Frydenvang K, Gefflaut T & Bunch L. (2013). Chemoenzymatic synthesis of new 2,4-syn-functionalized (S)-glutamate analogues and structure-activity relationship studies at ionotropic glutamate receptors and excitatory amino acid transporters. Journal of medicinal chemistry 56, 1614-1628.

Ataman ZA, Gakhar L, Sorensen BR, Hell JW & Shea MA. (2007). The NMDA receptor NR1 C1 region bound to calmodulin: structural insights into functional differences between homologous domains. Structure 15, 1603-1617.

Auerbach A. (2015). Agonist activation of a nicotinic acetylcholine receptor. Neuropharmacology 96, 150-156.

Ayalon G & Stern-Bach Y. (2001). Functional assembly of AMPA and kainate receptors is mediated by several discrete protein-protein interactions. Neuron 31, 103-113.

Balasuriya D, Takahashi H, Srivats S & Edwardson JM. (2014). Activation-induced structural change in the GluN1/GluN3A excitatory glycine receptor. Biochemical and biophysical research communications 450, 1452-1457.

Balcar VJ & Johnston GA. (1972). The structural specificity of the high affinity uptake of L-glutamate and L-aspartate by rat brain slices. Journal of neurochemistry 19, 2657-2666.

Baranovic J, Ramanujan CS, Kasai N, Midgett CR, Madden DR, Torimitsu K, Ryan JF. (2013). Reconstitution of homomeric GluA2(flop) receptors in supported lipid membranes: functional and structural properties. The journal of biological chemistry 288, 8647-8657.

Baranovic J, Chebli M, Salazar H, Carbone AL, Faelber K, Lau AY, Daumke O & Plested AJ. (2016). Dynamics of the Ligand Binding Domain Layer during AMPA Receptor Activation. Biophysical journal 110, 896-911.

Baranovic J & Plested AJ. (2016). How to build the fastest receptor on earth. Biological chemistry 397, 195-205.

Barberis A, Sachidhanandam S & Mulle C. (2008). GluR6/KA2 kainate receptors mediate slow-deactivating currents. J Neurosci 28, 6402-6406.

Barbhaiya H, McClain R, Ijzerman A & Rivkees SA. (1996). Site-directed mutagenesis of the human A1 adenosine receptor: influences of acidic and hydroxy residues in the first four transmembrane domains on ligand binding. Molecular pharmacology 50, 1635-1642.

Belitz HD, Grosch W & Schieberle P. (2009). Food chemistry, 4th rev. and extended edn, pp. xliv, 1070 p. Springer, Berlin.

Benveniste M & Mayer ML. (1991). Kinetic analysis of antagonist action at N-methyl-D-aspartic acid receptors. Two binding sites each for glutamate and glycine. Biophysical journal 59, 560-573.

Berendsen HJC, Postma JPM, Vangunsteren WF, Dinola A & Haak JR. (1984). Molecular-Dynamics with Coupling to an External Bath. J Chem Phys 81, 3684-3690.

Berman HM, Westbrook J, Feng Z, Gilliland G, Bhat TN, Weissig H, Shindyalov IN & Bourne PE. (2000). The Protein Data Bank. Nucleic acids research 28, 235-242.

Bettler B, Boulter J, Hermans-Borgmeyer I, O'Shea-Greenfield A, Deneris ES, Moll C, Borgmeyer U, Hollmann M & Heinemann S. (1990). Cloning of a novel glutamate receptor subunit, GluR5: expression in the nervous system during development. Neuron 5, 583-595.

Bettler B, Egebjerg J, Sharma G, Pecht G, Hermans-Borgmeyer I, Moll C, Stevens CF & Heinemann S. (1992). Cloning of a putative glutamate receptor: a low affinity kainate-binding subunit. Neuron 8, 257-265.

Birdsey-Benson A, Gill A, Henderson LP & Madden DR. (2010). Enhanced efficacy without further cleft closure: reevaluating twist as a source of agonist efficacy in AMPA receptors. J Neurosci 30, 1463-1470.

Biscoe TJ, Evans RH, Headley PM, Martin M & Watkins JC. (1975). Domoic and quisqualic acids as potent amino acid excitants of frog and rat spinal neurones. Nature 255, 166-167.

Bjerrum EJ & Biggin PC. (2008). Rigid body essential X-ray crystallography: distinguishing the bend and twist of glutamate receptor ligand binding domains. Proteins 72, 434-446.

Black MD. (2005). Therapeutic potential of positive AMPA modulators and their relationship to AMPA receptor subunits. A review of preclinical data. Psychopharmacology 179, 154-163.

Blackstone CD, Moss SJ, Martin LJ, Levey AI, Price DL & Huganir RL. (1992). Biochemical characterization and localization of a non-N-methyl-D-aspartate glutamate receptor in rat brain. Journal of neurochemistry 58, 1118-1126.

Bleakman D, Ballyk BA, Schoepp DD, Palmer AJ, Bath CP, Sharpe EF, Woolley ML, Bufton HR, Kamboj RK, Tarnawa I & Lodge D. (1996). Activity of 2,3-benzodiazepines at native rat and recombinant human glutamate receptors in vitro: stereospecificity and selectivity profiles. Neuropharmacology 35, 1689-1702.

Bliss TV & Lomo T. (1973). Long-lasting potentiation of synaptic transmission in the dentate area of the anaesthetized rabbit following stimulation of the perforant path. J Physiol 232, 331-356.

Bloomenthal AB, Goldwater E, Pritchett DB & Harrison NL. (1994). Biphasic modulation of the strychnine-sensitive glycine receptor by Zn2+. Molecular pharmacology 46, 1156-1159.

Bokel C, Dass S, Wilsch-Brauninger M & Roth S. (2006). Drosophila Cornichon acts as cargo receptor for ER export of the TGFalpha-like growth factor Gurken. Development 133, 459-470.

Borschel WF, Murthy SE, Kasperek EM & Popescu GK. (2011). NMDA receptor activation requires remodelling of intersubunit contacts within ligand-binding heterodimers. Nature communications 2, 498.

Bortolotto ZA, Clarke VR, Delany CM, Parry MC, Smolders I, Vignes M, Ho KH, Miu P, Brinton BT, Fantaske R, Ogden A, Gates M, Ornstein PL, Lodge D, Bleakman D & Collingridge GL. (1999). Kainate receptors are involved in synaptic plasticity. Nature 402, 297-301.

Boudkkazi S, Brechet A, Schwenk J & Fakler B. (2014). Cornichon2 dictates the time course of excitatory transmission at individual hippocampal synapses. Neuron 82, 848-858.

Boulter J, Hollmann M, O'Shea-Greenfield A, Hartley M, Deneris E, Maron C & Heinemann S. (1990). Molecular cloning and functional expression of glutamate receptor subunit genes. Science 249, 1033-1037.

Bowie D. (2002). External anions and cations distinguish between AMPA and kainate receptor gating mechanisms. J Physiol 539, 725-733.

Bowie D. (2008). Ionotropic glutamate receptors & CNS disorders. CNS & neurological disorders drug targets 7, 129-143.

Bowie D. (2010). Ion-dependent gating of kainate receptors. J Physiol 588, 67-81.

Bowie D, Garcia EP, Marshall J, Traynelis SF & Lange GD. (2003). Allosteric regulation and spatial distribution of kainate receptors bound to ancillary proteins. J Physiol 547, 373-385.

Bowie D & Lange GD. (2002). Functional stoichiometry of glutamate receptor desensitization. J Neurosci 22, 3392-3403.

Bowie D, Lange GD & Mayer ML. (1998). Activity-dependent modulation of glutamate receptors by polyamines. J Neurosci 18, 8175-8185.

Bowie D & Mayer ML. (1995). Inward rectification of both AMPA and kainate subtype glutamate receptors generated by polyamine-mediated ion channel block. Neuron 15, 453-462.

Brake AJ, Wagenbach MJ & Julius D. (1994). New structural motif for ligand-gated ion channels defined by an ionotropic ATP receptor. Nature 371, 519-523.

Brockie PJ & Maricq AV. (2006). Building a synapse: genetic analysis of glutamatergic neurotransmission. Biochemical Society transactions 34, 64-67.

Burgess DL, Davis CF, Gefrides LA & Noebels JL. (1999). Identification of three novel Ca(2+) channel gamma subunit genes reveals molecular diversification by tandem and chromosome duplication. Genome research 9, 1204-1213.

Burgess DL, Gefrides LA, Foreman PJ & Noebels JL. (2001). A cluster of three novel Ca2+ channel gamma subunit genes on chromosome 19q13.4: evolution and expression profile of the gamma subunit gene family. Genomics 71, 339-350.

Burnashev N, Monyer H, Seeburg PH & Sakmann B. (1992). Divalent ion permeability of AMPA receptor channels is dominated by the edited form of a single subunit. Neuron 8, 189-198.

Burnashev N, Villarroel A & Sakmann B. (1996). Dimensions and ion selectivity of recombinant AMPA and kainate receptor channels and their dependence on Q/R site residues. J Physiol 496 (Pt 1), 165-173.

Burnashev N, Zhou Z, Neher E & Sakmann B. (1995). Fractional calcium currents through recombinant GluR channels of the NMDA, AMPA and kainate receptor subtypes. J Physiol 485 (Pt 2), 403-418.

Cais O, Herguedas B, Krol K, Cull-Candy SG, Farrant M & Greger IH. (2014). Mapping the interaction sites between AMPA receptors and TARPs reveals a role for the receptor N-terminal domain in channel gating. Cell reports 9, 728-740.

Carbone AL & Plested AJ. (2012). Coupled control of desensitization and gating by the ligand binding domain of glutamate receptors. Neuron 74, 845-857.

Carbone AL & Plested AJ. (2016). Superactivation of AMPA receptors by auxiliary proteins. Nature communications 7, 10178.

Carter C, Benavides J, Legendre P, Vincent JD, Noel F, Thuret F, Lloyd KG, Arbilla S, Zivkovic B, MacKenzie ET & et al. (1988). Ifenprodil and SL 82.0715 as cerebral anti-ischemic agents. II. Evidence for N-methyl-D-aspartate receptor antagonist properties. The journal of pharmacology and experimental therapeutics 247, 1222-1232.

Castillo PE, Malenka RC & Nicoll RA. (1997). Kainate receptors mediate a slow postsynaptic current in hippocampal CA3 neurons. Nature 388, 182-186.

Castro CP, Piscopo D, Nakagawa T & Derynck R. (2007). Cornichon regulates transport and secretion of TGFalpha-related proteins in metazoan cells. Journal of cell science 120, 2454-2466.

Catterall WA, Hulme JT, Jiang X & Few WP. (2006). Regulation of sodium and calcium channels by signaling complexes. J Recept Signal Transduct Res 26, 577-598.

Chatterton JE, Awobuluyi M, Premkumar LS, Takahashi H, Talantova M, Shin Y, Cui J, Tu S, Sevarino KA, Nakanishi N, Tong G, Lipton SA & Zhang D. (2002). Excitatory glycine receptors containing the NR3 family of NMDA receptor subunits. Nature 415, 793-798.

Chaudhry C, Weston MC, Schuck P, Rosenmund C & Mayer ML. (2009). Stability of ligand-binding domain dimer assembly controls kainate receptor desensitization. The EMBO journal 28, 1518-1530.

Chen GQ, Cui C, Mayer ML & Gouaux E. (1999). Functional characterization of a potassium-selective prokaryotic glutamate receptor. Nature 402, 817-821.

Chen GQ & Gouaux E. (1997). Overexpression of a glutamate receptor (GluR2) ligand binding domain in Escherichia coli: application of a novel protein folding screen. Proc Natl Acad Sci U S A 94, 13431-13436.

Chen L, Chetkovich DM, Petralia RS, Sweeney NT, Kawasaki Y, Wenthold RJ, Bredt DS & Nicoll RA. (2000). Stargazin regulates synaptic targeting of AMPA receptors by two distinct mechanisms. Nature 408, 936-943.

Chen L, Durr KL & Gouaux E. (2014). X-ray structures of AMPA receptor-cone snail toxin complexes illuminate activation mechanism. Science 345, 1021-1026.

Chen L, El-Husseini A, Tomita S, Bredt DS & Nicoll RA. (2003). Stargazin differentially controls the trafficking of alpha-amino-3-hydroxyl-5-methyl-4-isoxazolepropionate and kainate receptors. Molecular pharmacology 64, 703-706.

Chen VB, Arendall WB, 3rd, Headd JJ, Keedy DA, Immormino RM, Kapral GJ, Murray LW, Richardson JS & Richardson DC. (2010). MolProbity: all-atom structure validation for macromolecular crystallography. Acta crystallographica Section D, Biological crystallography 66, 12-21.

Cheriyan J, Mezes C, Zhou N, Balsara RD & Castellino FJ. (2015). Heteromerization of ligand binding domains of N-methyl-D-aspartate receptor requires both coagonists, L-glutamate and glycine. Biochemistry 54, 787-794.

Chittajallu R, Vignes M, Dev KK, Barnes JM, Collingridge GL & Henley JM. (1996). Regulation of glutamate release by presynaptic kainate receptors in the hippocampus. Nature 379, 78-81.

Cho CH, St-Gelais F, Zhang W, Tomita S & Howe JR. (2007). Two families of TARP isoforms that have distinct effects on the kinetic properties of AMPA receptors and synaptic currents. Neuron 55, 890-904.

Choi UB, McCann JJ, Weninger KR & Bowen ME. (2011). Beyond the random coil: stochastic conformational switching in intrinsically disordered proteins. Structure 19, 566-576.

Choi UB, Xiao S, Wollmuth LP & Bowen ME. (2011). Effect of Src kinase phosphorylation on disordered C-terminal domain of N-methyl-D-aspartic acid (NMDA) receptor subunit GluN2B protein. The journal of biological chemistry 286, 29904-29912.

Choi YB & Lipton SA. (1999). Identification and mechanism of action of two histidine residues underlying high-affinity Zn2+ inhibition of the NMDA receptor. Neuron 23, 171-180.

Christie LA, Russell TA, Xu J, Wood L, Shepherd GM & Contractor A. (2010). AMPA receptor desensitization mutation results in severe developmental phenotypes and early postnatal lethality. Proc Natl Acad Sci U S A 107, 9412-9417.

Clarke VR, Ballyk BA, Hoo KH, Mandelzys A, Pellizzari A, Bath CP, Thomas J, Sharpe EF, Davies CH, Ornstein PL, Schoepp DD, Kamboj RK, Collingridge GL, Lodge D & Bleakman D. (1997). A hippocampal GluR5 kainate receptor regulating inhibitory synaptic transmission. Nature 389, 599-603.

Clements JD, Lester RA, Tong G, Jahr CE & Westbrook GL. (1992). The time course of glutamate in the synaptic cleft. Science 258, 1498-1501.

Clements JD & Westbrook GL. (1991). Activation kinetics reveal the number of glutamate and glycine binding sites on the N-methyl-D-aspartate receptor. Neuron 7, 605-613.

Coleman SK, Cai C, Mottershead DG, Haapalahti JP & Keinanen K. (2003). Surface expression of GluR-D AMPA receptor is dependent on an interaction between its C-terminal domain and a 4.1 protein. J Neurosci 23, 798-806.

Collingridge GL, Kehl SJ & McLennan H. (1983). Excitatory amino acids in synaptic transmission in the Schaffer collateral-commissural pathway of the rat hippocampus. J Physiol 334, 33-46.

Collingridge GL & Lester RA. (1989). Excitatory amino acid receptors in the vertebrate central nervous system. Pharmacol Rev 41, 143-210.

Collingridge GL, Olsen RW, Peters J & Spedding M. (2009). A nomenclature for ligand-gated ion channels. Neuropharmacology 56, 2-5.

Collingridge GLB, T.V.P. (1987). NMDA receptors -their role in long-term potentiation. Trends Neurosci 10, 288-293.

Colquhoun D. (1998). Binding, gating, affinity and efficacy: the interpretation of structure-activity relationships for agonists and of the effects of mutating receptors. British journal of pharmacology 125, 924-947.

Colquhoun D, Jonas P & Sakmann B. (1992). Action of brief pulses of glutamate on AMPA/kainate receptors in patches from different neurones of rat hippocampal slices. J Physiol 458, 261-287.

Colquhoun DS, F. (1995). Fitting and statistical analysis of single-channel records. In Single-channel recording, 2 edn, ed. Sakmann BN, E., pp. 483-587. Plenum Press, London.

Constals A, Penn AC, Compans B, Toulme E, Phillipat A, Marais S, Retailleau N, Hafner AS, Coussen F, Hosy E & Choquet D. (2015). Glutamate-induced AMPA receptor desensitization increases their mobility and modulates short-term plasticity through unbinding from Stargazin. Neuron 85, 787-803.

Contractor A, Mulle C & Swanson GT. (2011). Kainate receptors coming of age: milestones of two decades of research. Trends Neurosci 34, 154-163.

Coombs ID, Soto D, Zonouzi M, Renzi M, Shelley C, Farrant M & Cull-Candy SG. (2012). Cornichons modify channel properties of recombinant and glial AMPA receptors. J Neurosci 32, 9796-9804.

Copits BA & Swanson GT. (2012). Dancing partners at the synapse: auxiliary subunits that shape kainate receptor function. Nature reviews Neuroscience 13, 675-686.

Copits BA & Swanson GT. (2013). Kainate receptor post-translational modifications differentially regulate association with 4.1N to control activity-dependent receptor endocytosis. The journal of biological chemistry 288, 8952-8965.

Copits BA, Vernon CG, Sakai R & Swanson GT. (2014). Modulation of ionotropic glutamate receptor function by vertebrate galectins. J Physiol 592, 2079-2096.

Corringer PJ, Poitevin F, Prevost MS, Sauguet L, Delarue M & Changeux JP. (2012). Structure and pharmacology of pentameric receptor channels: from bacteria to brain. Structure 20, 941-956.

Cossart R, Epsztein J, Tyzio R, Becq H, Hirsch J, Ben-Ari Y & Crepel V. (2002). Quantal release of glutamate generates pure kainate and mixed AMPA/kainate EPSCs in hippocampal neurons. Neuron 35, 147-159.

Cousins SL, Innocent N & Stephenson FA. (2013). Neto1 associates with the NMDA receptor/amyloid precursor protein complex. Journal of neurochemistry 126, 554-564.

Craig AM, Blackstone CD, Huganir RL & Banker G. (1993). The distribution of glutamate receptors in cultured rat hippocampal neurons: postsynaptic clustering of AMPA-selective subunits. Neuron 10, 1055-1068.

Cull-Candy SG, Howe JR & Ogden DC. (1988). Noise and single channels activated by excitatory amino acids in rat cerebellar granule neurones. J Physiol 400, 189-222.

Cull-Candy SG & Usowicz MM. (1987). Multiple-conductance channels activated by excitatory amino acids in cerebellar neurons. Nature 325, 525-528.

Cull-Candy SG & Usowicz MM. (1989). On the multiple-conductance single channels activated by excitatory amino acids in large cerebellar neurones of the rat. J Physiol 415, 555-582.

Curtis DR, Phillis JW & Watkins JC. (1960). The chemical excitation of spinal neurones by certain acidic amino acids. J Physiol 150, 656-682.

Curtis DR & Watkins JC. (1963). Acidic amino acids with strong excitatory actions on mammalian neurones. J Physiol 166, 1-14.

Daniels BA, Andrews ED, Aurousseau MR, Accardi MV & Bowie D. (2013). Crosslinking the ligand-binding domain dimer interface locks kainate receptors out of the main open state. J Physiol 591, 3873-3885.

Darden TY, D.; Pedersen, L. (1993). Particle mesh Ewald: an N·log(N) method for Ewald sums in large systems. J Chem Phys 98, 10089–10092.

Darstein M, Petralia RS, Swanson GT, Wenthold RJ & Heinemann SF. (2003). Distribution of kainate receptor subunits at hippocampal mossy fiber synapses. J Neurosci 23, 8013-8019.

Dauter Z & Dauter M. (2001). Entering a new phase: using solvent halide ions in protein structure determination. Structure 9, R21-26.

Davies J & Watkins JC. (1982). Actions of D and L forms of 2-amino-5-phosphonovalerate and 2-amino-4-phosphonobutyrate in the cat spinal cord. Brain research 235, 378-386.

Dawe GB, Aurousseau MR, Daniels BA & Bowie D. (2015). Retour aux sources: defining the structural basis of glutamate receptor activation. J Physiol 593, 97-110.

Del Castillo J & Katz B. (1957). Interaction at end-plate receptors between different choline derivatives. Proceedings of the Royal Society of London Series B, Biological sciences 146, 369-381.

Deng L & Chen G. (2003). Cyclothiazide potently inhibits gamma-aminobutyric acid type A receptors in addition to enhancing glutamate responses. Proc Natl Acad Sci U S A 100, 13025-13029.

Derkach V, Barria A & Soderling TR. (1999). Ca2+/calmodulin-kinase II enhances channel conductance of alpha-amino-3-hydroxy-5-methyl-4-isoxazolepropionate type glutamate receptors. Proc Natl Acad Sci U S A 96, 3269-3274.

Dev KK, Nishimune A, Henley JM & Nakanishi S. (1999). The protein kinase C alpha binding protein PICK1 interacts with short but not long form alternative splice variants of AMPA receptor subunits. Neuropharmacology 38, 635-644.

Dingledine R, Borges K, Bowie D & Traynelis SF. (1999). The glutamate receptor ion channels. Pharmacol Rev 51, 7-61.

Donevan SD & Rogawski MA. (1995). Intracellular polyamines mediate inward rectification of Ca(2+)-permeable alpha-amino-3-hydroxy-5-methyl-4-isoxazolepropionic acid receptors. Proc Natl Acad Sci U S A 92, 9298-9302.

Dong H, O'Brien RJ, Fung ET, Lanahan AA, Worley PF & Huganir RL. (1997). GRIP: a synaptic PDZ domain-containing protein that interacts with AMPA receptors. Nature 386, 279-284.

Dong H & Zhou HX. (2011). Atomistic mechanism for the activation and desensitization of an AMPA-subtype glutamate receptor. Nature communications 2, 354.

Dunant Y & Bloc A. (2003). Low- and high-affinity reactions in rapid neurotransmission. Neurochemical research 28, 659-665.

Durr KL, Chen L, Stein RA, De Zorzi R, Folea IM, Walz T, McHaourab HS & Gouaux E. (2014). Structure and Dynamics of AMPA Receptor GluA2 in Resting, Pre-Open, and Desensitized States. Cell 158, 778-792.

Dutta A, Shrivastava IH, Sukumaran M, Greger IH & Bahar I. (2012). Comparative dynamics of NMDA- and AMPA-glutamate receptor N-terminal domains. Structure 20, 1838-1849.

Egebjerg J, Bettler B, Hermans-Borgmeyer I & Heinemann S. (1991). Cloning of a cDNA for a glutamate receptor subunit activated by kainate but not AMPA. Nature 351, 745-748.

Ehlers MD, Heine M, Groc L, Lee MC & Choquet D. (2007). Diffusional trapping of GluR1 AMPA receptors by input-specific synaptic activity. Neuron 54, 447-460.

Emsley P, Lohkamp B, Scott WG & Cowtan K. (2010). Features and development of Coot. Acta crystallographica Section D, Biological crystallography 66, 486-501.

Essmann U, Perera L, Berkowitz ML, Darden T, Lee H & Pedersen LG. (1995). A Smooth Particle Mesh Ewald Method. J Chem Phys 103, 8577-8593.

Evans P. (2006). Scaling and assessment of data quality. Acta crystallographica Section D, Biological crystallography 62, 72-82.

Evans RH, Francis AA & Watkins JC. (1977). Selective antagonism by Mg2+ of amino acid-induced depolarization of spinal neurones. Experientia 33, 489-491.

Farrow P, Khodosevich K, Sapir Y, Schulmann A, Aslam M, Stern-Bach Y, Monyer H & von Engelhardt J. (2015). Auxiliary subunits of the CKAMP family differentially modulate AMPA receptor properties. eLife 4, e09693.

Fay AM, Corbeil CR, Brown P, Moitessier N & Bowie D. (2009). Functional characterization and in silico docking of full and partial GluK2 kainate receptor agonists. Molecular pharmacology 75, 1096-1107.

Fayyazuddin A, Villarroel A, Le Goff A, Lerma J & Neyton J. (2000). Four residues of the extracellular N-terminal domain of the NR2A subunit control high-affinity Zn2+ binding to NMDA receptors. Neuron 25, 683-694.

Fenwick MK & Oswald RE. (2008). NMR spectroscopy of the ligand-binding core of ionotropic glutamate receptor 2 bound to 5-substituted willardiine partial agonists. Journal of molecular biology 378, 673-685.

Fleck MW, Cornell E & Mah SJ. (2003). Amino-acid residues involved in glutamate receptor 6 kainate receptor gating and desensitization. J Neurosci 23, 1219-1227.

Flynn GE, Johnson JP, Jr. & Zagotta WN. (2001). Cyclic nucleotide-gated channels: shedding light on the opening of a channel pore. Nature reviews Neuroscience 2, 643-651.

Franke C, Hatt H & Dudel J. (1987). Liquid filament switch for ultra-fast exchanges of solutions at excised patches of synaptic membrane of crayfish muscle. Neuroscience letters 77, 199-204.

French RJ & Horn R. (1983). Sodium channel gating: models, mimics, and modifiers. Annual review of biophysics and bioengineering 12, 319-356.

Frydenvang K, Lash LL, Naur P, Postila PA, Pickering DS, Smith CM, Gajhede M, Sasaki M, Sakai R, Pentikainen OT, Swanson GT & Kastrup JS. (2009). Full domain closure of the ligand-

binding core of the ionotropic glutamate receptor iGluR5 induced by the high affinity agonist dysiherbaine and the functional antagonist 8,9-dideoxyneodysiherbaine. The journal of biological chemistry 284, 14219-14229.

Furukawa H & Gouaux E. (2003). Mechanisms of activation, inhibition and specificity: crystal structures of the NMDA receptor NR1 ligand-binding core. The EMBO journal 22, 2873-2885.

Furukawa H, Singh SK, Mancusso R & Gouaux E. (2005). Subunit arrangement and function in NMDA receptors. Nature 438, 185-192.

Gan Q, Dai J, Zhou HX & Wollmuth LP. (2016). The Transmembrane Domain Mediates Tetramerization of alpha-Amino-3-hydroxy-5-methyl-4-isoxazolepropionic Acid (AMPA) Receptors. The journal of biological chemistry 291, 6595-6606.

Gan Q, Salussolia CL & Wollmuth LP. (2015). Assembly of AMPA receptors: mechanisms and regulation. J Physiol 593, 39-48.

Garcia EP, Mehta S, Blair LA, Wells DG, Shang J, Fukushima T, Fallon JR, Garner CC & Marshall J. (1998). SAP90 binds and clusters kainate receptors causing incomplete desensitization. Neuron 21, 727-739.

Garcia-Nafria J, Herguedas B, Watson JF & Greger IH. (2016). The dynamic AMPA receptor extracellular region: A platform for synaptic protein interactions. J Physiol (in press).

Gates M, Ogden A & Bleakman D. (2001). Pharmacological effects of AMPA receptor potentiators LY392098 and LY404187 on rat neuronal AMPA receptors in vitro. Neuropharmacology 40, 984-991.

Gebhardt C & Cull-Candy SG. (2010). Lithium acts as a potentiator of AMPAR currents in hippocampal CA1 cells by selectively increasing channel open probability. J Physiol 588, 3933-3941.

Geiger JR, Lubke J, Roth A, Frotscher M & Jonas P. (1997). Submillisecond AMPA receptor-mediated signaling at a principal neuron-interneuron synapse. Neuron 18, 1009-1023.

Geiger JR, Melcher T, Koh DS, Sakmann B, Seeburg PH, Jonas P & Monyer H. (1995). Relative abundance of subunit mRNAs determines gating and Ca2+ permeability of AMPA receptors in principal neurons and interneurons in rat CNS. Neuron 15, 193-204.

Geiser M, Cebe R, Drewello D & Schmitz R. (2001). Integration of PCR fragments at any specific site within cloning vectors without the use of restriction enzymes and DNA ligase. BioTechniques 31, 88-90, 92.

Gielen M, Le Goff A, Stroebel D, Johnson JW, Neyton J & Paoletti P. (2008). Structural rearrangements of NR1/NR2A NMDA receptors during allosteric inhibition. Neuron 57, 80-93.

Gielen M, Siegler Retchless B, Mony L, Johnson JW & Paoletti P. (2009). Mechanism of differential control of NMDA receptor activity by NR2 subunits. Nature 459, 703-707.

Giffard RG, Monyer H, Christine CW & Choi DW. (1990). Acidosis reduces NMDA receptor activation, glutamate neurotoxicity, and oxygen-glucose deprivation neuronal injury in cortical cultures. Brain research 506, 339-342.

Gill MB, Kato AS, Roberts MF, Yu H, Wang H, Tomita S & Bredt DS. (2011). Cornichon-2 modulates AMPA receptor-transmembrane AMPA receptor regulatory protein assembly to dictate gating and pharmacology. J Neurosci 31, 6928-6938.

Gonzalez J, Du M, Parameshwaran K, Suppiramaniam V & Jayaraman V. (2010). Role of dimer interface in activation and desensitization in AMPA receptors. Proc Natl Acad Sci U S A 107, 9891-9896.

Gouaux E. (2004). Structure and function of AMPA receptors. J Physiol 554, 249-253.

Granger AJ, Shi Y, Lu W, Cerpas M & Nicoll RA. (2013). LTP requires a reserve pool of glutamate receptors independent of subunit type. Nature 493, 495-500.

Granger R, Deadwyler S, Davis M, Moskovitz B, Kessler M, Rogers G & Lynch G. (1996). Facilitation of glutamate receptors reverses an age-associated memory impairment in rats. Synapse 22, 332-337.

Green T & Nayeem N. (2015). The multifaceted subunit interfaces of ionotropic glutamate receptors. J Physiol 593, 73-81.

Greger IH, Akamine P, Khatri L & Ziff EB. (2006). Developmentally regulated, combinatorial RNA processing modulates AMPA receptor biogenesis. Neuron 51, 85-97.

Greger IH, Khatri L, Kong X & Ziff EB. (2003). AMPA receptor tetramerization is mediated by Q/R editing. Neuron 40, 763-774.

Greger IH, Khatri L & Ziff EB. (2002). RNA editing at arg607 controls AMPA receptor exit from the endoplasmic reticulum. Neuron 34, 759-772.

Greger IH, Ziff EB & Penn AC. (2007). Molecular determinants of AMPA receptor subunit assembly. Trends Neurosci 30, 407-416.

Gregor P, O'Hara BF, Yang X & Uhl GR. (1993). Expression and novel subunit isoforms of glutamate receptor genes GluR5 and GluR6. Neuroreport 4, 1343-1346.

Gu X, Mao X, Lussier MP, Hutchison MA, Zhou L, Hamra FK, Roche KW & Lu W. (2016). GSG1L suppresses AMPA receptor-mediated synaptic transmission and uniquely modulates AMPA receptor kinetics in hippocampal neurons. Nature communications 7, 10873.

Gutierrez-de-Teran H, Massink A, Rodriguez D, Liu W, Han GW, Joseph JS, Katritch I, Heitman LH, Xia L, Ijzerman AP, Cherezov V, Katritch V & Stevens RC. (2013). The role of a sodium ion binding site in the allosteric modulation of the A(2A) adenosine G protein-coupled receptor. Structure 21, 2175-2185.

Haering SC, Tapken D, Pahl S & Hollmann M. (2014). Auxiliary subunits: shepherding AMPA receptors to the plasma membrane. Membranes (Basel) 4, 469-490.

Hald H, Ahring PK, Timmermann DB, Liljefors T, Gajhede M & Kastrup JS. (2009). Distinct structural features of cyclothiazide are responsible for effects on peak current amplitude and desensitization kinetics at iGluR2. Journal of molecular biology 391, 906-917.

Hansen KB, Furukawa H & Traynelis SF. (2010). Control of assembly and function of glutamate receptors by the amino-terminal domain. Molecular pharmacology 78, 535-549.

Hansen KB, Ogden KK, Yuan H & Traynelis SF. (2014). Distinct functional and pharmacological properties of Triheteromeric GluN1/GluN2A/GluN2B NMDA receptors. Neuron 81, 1084-1096.

Hansen KB, Yuan H & Traynelis SF. (2007). Structural aspects of AMPA receptor activation, desensitization and deactivation. Current opinion in neurobiology 17, 281-288.

Harms JE, Benveniste M, Maclean JK, Partin KM & Jamieson C. (2013). Functional analysis of a novel positive allosteric modulator of AMPA receptors derived from a structure-based drug design strategy. Neuropharmacology 64, 45-52.

Harvey RJ, Thomas P, James CH, Wilderspin A & Smart TG. (1999). Identification of an inhibitory Zn2+ binding site on the human glycine receptor alpha1 subunit. J Physiol 520 (Pt 1), 53-64.

Hashimoto K, Fukaya M, Qiao X, Sakimura K, Watanabe M & Kano M. (1999). Impairment of AMPA receptor function in cerebellar granule cells of ataxic mutant mouse stargazer. J Neurosci 19, 6027-6036.

Hastie P, Ulbrich MH, Wang HL, Arant RJ, Lau AG, Zhang Z, Isacoff EY & Chen L. (2013). AMPA receptor/TARP stoichiometry visualized by single-molecule subunit counting. Proc Natl Acad Sci U S A 110, 5163-5168.

Hatton CJ & Paoletti P. (2005). Modulation of triheteromeric NMDA receptors by N-terminal domain ligands. Neuron 46, 261-274.

Hayashi T. (1954). Effects of sodium glutamate on the nervous system. Keio Journal of Medicine 3, 183-192.

Hayashi T, Rumbaugh G & Huganir RL. (2005). Differential regulation of AMPA receptor subunit trafficking by palmitoylation of two distinct sites. Neuron 47, 709-723.

Heckmann M, Bufler J, Franke C & Dudel J. (1996). Kinetics of homomeric GluR6 glutamate receptor channels. Biophysical journal 71, 1743-1750.

Heine M, Groc L, Frischknecht R, Beique JC, Lounis B, Rumbaugh G, Huganir RL, Cognet L & Choquet D. (2008). Surface mobility of postsynaptic AMPARs tunes synaptic transmission. Science 320, 201-205.

Henley JM & Wilkinson KA. (2016). Synaptic AMPA receptor composition in development, plasticity and disease. Nature reviews Neuroscience 17, 337-350.

Herb A, Burnashev N, Werner P, Sakmann B, Wisden W & Seeburg PH. (1992). The KA-2 subunit of excitatory amino acid receptors shows widespread expression in brain and forms ion channels with distantly related subunits. Neuron 8, 775-785.

Herguedas B, Garcia-Nafria J, Cais O, Fernandez-Leiro R, Krieger J, Ho H & Greger IH. (2016). Structure and organization of heteromeric AMPA-type glutamate receptors. Science (in press).

Herring BE & Nicoll RA. (2016). Long-Term Potentiation: From CaMKII to AMPA Receptor Trafficking. Annual review of physiology 78, 351-365.

Herring BE, Shi Y, Suh YH, Zheng CY, Blankenship SM, Roche KW & Nicoll RA. (2013). Cornichon proteins determine the subunit composition of synaptic AMPA receptors. Neuron 77, 1083-1096.

Hess B. (2008). P-LINCS: A parallel linear constraint solver for molecular simulation. J Chem Theory Comput 4, 116-122.

Hess B, Kutzner C, van der Spoel D & Lindahl E. (2008). GROMACS 4: Algorithms for highly efficient, load-balanced, and scalable molecular simulation. J Chem Theory Comput 4, 435-447.

Hille B. (2001). Ion channels of excitable membranes. Sinauer, Sunderland, Mass.

Hinard V, Britan A, Rougier JS, Bairoch A, Abriel H & Gaudet P. (2016). ICEPO: the ion channel electrophysiology ontology. Database: the journal of biological databases and curation (in press).

Hirzel K, Muller U, Latal AT, Hulsmann S, Grudzinska J, Seeliger MW, Betz H & Laube B. (2006). Hyperekplexia phenotype of glycine receptor alpha1 subunit mutant mice identifies Zn(2+) as an essential endogenous modulator of glycinergic neurotransmission. Neuron 52, 679-690.

Hodgkin AL & Huxley AF. (1952). The dual effect of membrane potential on sodium conductance in the giant axon of Loligo. J Physiol 116, 497-506.

Hogner A, Kastrup JS, Jin R, Liljefors T, Mayer ML, Egebjerg J, Larsen IK & Gouaux E. (2002). Structural basis for AMPA receptor activation and ligand selectivity: crystal structures of five agonist complexes with the GluR2 ligand-binding core. Journal of molecular biology 322, 93-109.

Hollmann M & Heinemann S. (1994). Cloned glutamate receptors. Annual review of neuroscience 17, 31-108.

Hollmann M, Maron C & Heinemann S. (1994). N-glycosylation site tagging suggests a three transmembrane domain topology for the glutamate receptor GluR1. Neuron 13, 1331-1343.

Hollmann M, O'Shea-Greenfield A, Rogers SW & Heinemann S. (1989). Cloning by functional expression of a member of the glutamate receptor family. Nature 342, 643-648.

Holm MM, Naur P, Vestergaard B, Geballe MT, Gajhede M, Kastrup JS, Traynelis SF & Egebjerg J. (2005). A binding site tyrosine shapes desensitization kinetics and agonist potency at GluR2. A mutagenic, kinetic, and crystallographic study. The journal of biological chemistry 280, 35469-35476.

Honore T, Davies SN, Drejer J, Fletcher EJ, Jacobsen P, Lodge D & Nielsen FE. (1988). Quinoxalinediones: potent competitive non-NMDA glutamate receptor antagonists. Science 241, 701-703.

Horn R. (1990). A primer of permeation and gating. In Sensory Transduction, ed. Borsellino AC, L.; Torre, V. Springer.

Horning MS & Mayer ML. (2004). Regulation of AMPA receptor gating by ligand binding core dimers. Neuron 41, 379-388.

Hoshi T, Zagotta WN & Aldrich RW. (1990). Biophysical and molecular mechanisms of Shaker potassium channel inactivation. Science 250, 533-538.

Hoshino H, Uchida T, Otsuki T, Kawamoto S, Okubo K, Takeichi M & Chisaka O. (2007). Cornichon-like protein facilitates secretion of HB-EGF and regulates proper development of cranial nerves. Molecular biology of the cell 18, 1143-1152.

Howe JR. (1996). Homomeric and heteromeric ion channels formed from the kainate-type subunits GluR6 and KA2 have very small, but different, unitary conductances. Journal of neurophysiology 76, 510-519.

Howe JR. (2013). CrossTalk proposal: TARPs modulate AMPA receptor gating transitions. J Physiol 591, 1581-1583; discussion 1589.

Howe JR. (2015). Modulation of non-NMDA receptor gating by auxiliary subunits. J Physiol 593, 61-72.

Hsiao CD, Sun YJ, Rose J & Wang BC. (1996). The crystal structure of glutamine-binding protein from Escherichia coli. Journal of molecular biology 262, 225-242.

Huettner JE. (1990). Glutamate receptor channels in rat DRG neurons: activation by kainate and quisqualate and blockade of desensitization by Con A. Neuron 5, 255-266.

Huettner JE. (2003). Kainate receptors and synaptic transmission. Progress in neurobiology 70, 387-407.

Huettner JE. (2015). Glutamate receptor pores. J Physiol 593, 49-59.

Huettner JE & Bean BP. (1988). Block of N-methyl-D-aspartate-activated current by the anticonvulsant MK-801: selective binding to open channels. Proc Natl Acad Sci U S A 85, 1307-1311.

Huganir RL & Nicoll RA. (2013). AMPARs and synaptic plasticity: the last 25 years. Neuron 80, 704-717.

Hume RI, Dingledine R & Heinemann SF. (1991). Identification of a site in glutamate receptor subunits that controls calcium permeability. Science 253, 1028-1031.

Humphrey W, Dalke A & Schulten K. (1996). VMD: Visual molecular dynamics. J Mol Graph Model 14, 33-38.

Ihle EC & Patneau DK. (2000). Modulation of alpha-amino-3-hydroxy-5-methyl-4-isoxazolepropionic acid receptor desensitization by extracellular protons. Molecular pharmacology 58, 1204-1212.

Inanobe A, Furukawa H & Gouaux E. (2005). Mechanism of partial agonist action at the NR1 subunit of NMDA receptors. Neuron 47, 71-84.

Isaac JT, Nicoll RA & Malenka RC. (1995). Evidence for silent synapses: implications for the expression of LTP. Neuron 15, 427-434.

Isom LL, De Jongh KS & Catterall WA. (1994). Auxiliary subunits of voltage-gated ion channels. Neuron 12, 1183-1194.

Ito I, Tanabe S, Kohda A & Sugiyama H. (1990). Allosteric potentiation of quisqualate receptors by a nootropic drug aniracetam. J Physiol 424, 533-543.

Jackson AC & Nicoll RA. (2011). The expanding social network of ionotropic glutamate receptors: TARPs and other transmembrane auxiliary subunits. Neuron 70, 178-199.

Jackson AC & Nicoll RA. (2011). Stargazin (TARP gamma-2) is required for compartment-specific AMPA receptor trafficking and synaptic plasticity in cerebellar stellate cells. J Neurosci 31, 3939-3952.

Jahr CE & Stevens CF. (1987). Glutamate activates multiple single channel conductances in hippocampal neurons. Nature 325, 522-525.

Janovjak H, Sandoz G & Isacoff EY. (2011). A modern ionotropic glutamate receptor with a K(+) selectivity signature sequence. Nature communications 2, 232.

Jaskolski F, Coussen F & Mulle C. (2005). Subcellular localization and trafficking of kainate receptors. Trends in pharmacological sciences 26, 20-26.

Jasti J, Furukawa H, Gonzales EB & Gouaux E. (2007). Structure of acid-sensing ion channel 1 at 1.9 A resolution and low pH. Nature 449, 316-323.

Jessell TM & Kandel ER. (1993). Synaptic transmission: a bidirectional and self-modifiable form of cell-cell communication. Cell 72 Suppl, 1-30.

Jia Z, Agopyan N, Miu P, Xiong Z, Henderson J, Gerlai R, Taverna FA, Velumian A, MacDonald J, Carlen P, Abramow-Newerly W & Roder J. (1996). Enhanced LTP in mice deficient in the AMPA receptor GluR2. Neuron 17, 945-956.

Jiang Y, Huang Y, Wong HC, Zhou Y, Wang X, Yang J, Hall RA, Brown EM & Yang JJ. (2010). Elucidation of a novel extracellular calcium-binding site on metabotropic glutamate receptor 1α (mGluR1α) that controls receptor activation. The journal of biological chemistry 285, 33463-33474.

Jin R, Banke TG, Mayer ML, Traynelis SF & Gouaux E. (2003). Structural basis for partial agonist action at ionotropic glutamate receptors. Nature neuroscience 6, 803-810.

Jin R, Horning M, Mayer ML & Gouaux E. (2002). Mechanism of activation and selectivity in a ligand-gated ion channel: structural and functional studies of GluR2 and quisqualate. Biochemistry 41, 15635-15643.

Jin R, Singh SK, Gu S, Furukawa H, Sobolevsky AI, Zhou J, Jin Y & Gouaux E. (2009). Crystal structure and association behaviour of the GluR2 amino-terminal domain. The EMBO journal 28, 1812-1823.

Johnson JW & Ascher P. (1987). Glycine potentiates the NMDA response in cultured mouse brain neurons. Nature 325, 529-531.

Johnston JM & Filizola M. (2011). Showcasing modern molecular dynamics simulations of membrane proteins through G protein-coupled receptors. Current opinion in structural biology 21, 552-558.

Jonas P. (1993). AMPA-type glutamate receptors--nonselective cation channels mediating fast excitatory transmission in the CNS. Exs 66, 61-76.

Jonas P. (1995). Fast application of agonists to isolated membrane patches. In Single-channel recording, ed. Sakmann B, Neher, E., pp. 231-243. Plenum Press, New York.

Jones MV & Westbrook GL. (1996). The impact of receptor desensitization on fast synaptic transmission. Trends Neurosci 19, 96-101.

Jorgensen EM. (2014). Animal evolution: looking for the first nervous system. Current biology: CB 24, R655-658.

Jorgensen WL, Chandrasekhar J, Madura JD, Impey RW & Klein ML. (1983). Comparison of Simple Potential Functions for Simulating Liquid Water. J Chem Phys 79, 926-935.

Jorgensen WL, Maxwell DS & TiradoRives J. (1996). Development and testing of the OPLS all-atom force field on conformational energetics and properties of organic liquids. J Am Chem Soc 118, 11225-11236.

Kaae BH, Harpsoe K, Kastrup JS, Sanz AC, Pickering DS, Metzler B, Clausen RP, Gajhede M, Sauerberg P, Liljefors T & Madsen U. (2007). Structural proof of a dimeric positive modulator bridging two identical AMPA receptor-binding sites. Chemistry & biology 14, 1294-1303.

Kabsch W. (2010). Xds. Acta crystallographica Section D, Biological crystallography 66, 125-132.

Kalashnikova E, Lorca RA, Kaur I, Barisone GA, Li B, Ishimaru T, Trimmer JS, Mohapatra DP & Diaz E. (2010). SynDIG1: an activity-regulated, AMPA- receptor-interacting transmembrane protein that regulates excitatory synapse development. Neuron 65, 80-93.

Kalia LV, Kalia SK & Salter MW. (2008). NMDA receptors in clinical neurology: excitatory times ahead. The Lancet Neurology 7, 742-755.

Kamboj SK, Swanson GT & Cull-Candy SG. (1995). Intracellular spermine confers rectification on rat calcium-permeable AMPA and kainate receptors. J Physiol 486 (Pt 2), 297-303.

Kaminski GA, Friesner RA, Tirado-Rives J & Jorgensen WL. (2001). Evaluation and reparametrization of the OPLS-AA force field for proteins via comparison with accurate quantum chemical calculations on peptides. J Phys Chem B 105, 6474-6487.

Kang CH, Shin WC, Yamagata Y, Gokcen S, Ames GF & Kim SH. (1991). Crystal structure of the lysine-, arginine-, ornithine-binding protein (LAO) from Salmonella typhimurium at 2.7-A resolution. The journal of biological chemistry 266, 23893-23899.

Kang MG, Chen CC, Felix R, Letts VA, Frankel WN, Mori Y & Campbell KP. (2001). Biochemical and biophysical evidence for gamma 2 subunit association with neuronal voltage-activated Ca2+ channels. The journal of biological chemistry 276, 32917-32924.

Karakas E & Furukawa H. (2014). Crystal structure of a heterotetrameric NMDA receptor ion channel. Science 344, 992-997.

Karakas E, Simorowski N & Furukawa H. (2009). Structure of the zinc-bound amino-terminal domain of the NMDA receptor NR2B subunit. The EMBO journal 28, 3910-3920.

Karakas E, Simorowski N & Furukawa H. (2011). Subunit arrangement and phenylethanolamine binding in GluN1/GluN2B NMDA receptors. Nature 475, 249-253.

Karkanias NB & Papke RL. (1999). Lithium modulates desensitization of the glutamate receptor subtype gluR3 in Xenopus oocytes. Neuroscience letters 277, 153-156.

Kasuya G, Fujiwara Y, Takemoto M, Dohmae N, Nakada-Nakura Y, Ishitani R, Hattori M & Nureki O. (2016). Structural Insights into Divalent Cation Modulations of ATP-Gated P2X Receptor Channels. Cell reports 14, 932-944.

Kato AS, Gill MB, Ho MT, Yu H, Tu Y, Siuda ER, Wang H, Qian YW, Nisenbaum ES, Tomita S & Bredt DS. (2010). Hippocampal AMPA receptor gating controlled by both TARP and cornichon proteins. Neuron 68, 1082-1096.

Kato AS, Gill MB, Yu H, Nisenbaum ES & Bredt DS. (2010). TARPs differentially decorate AMPA receptors to specify neuropharmacology. Trends Neurosci 33, 241-248.

Kato AS, Siuda ER, Nisenbaum ES & Bredt DS. (2008). AMPA receptor subunit-specific regulation by a distinct family of type II TARPs. Neuron 59, 986-996.

Kato AS, Zhou W, Milstein AD, Knierman MD, Siuda ER, Dotzlaf JE, Yu H, Hale JE, Nisenbaum ES, Nicoll RA & Bredt DS. (2007). New transmembrane AMPA receptor regulatory protein isoform, gamma-7, differentially regulates AMPA receptors. J Neurosci 27, 4969-4977.

Katritch V, Fenalti G, Abola EE, Roth BL, Cherezov V & Stevens RC. (2014). Allosteric sodium in class A GPCR signaling. Trends in biochemical sciences 39, 233-244.

Katz B & Thesleff S. (1957). A study of the desensitization produced by acetylcholine at the motor end-plate. J Physiol 138, 63-80.

Kazi R, Dai J, Sweeney C, Zhou HX & Wollmuth LP. (2014). Mechanical coupling maintains the fidelity of NMDA receptor-mediated currents. Nature neuroscience 17, 914-922.

Keinanen K, Wisden W, Sommer B, Werner P, Herb A, Verdoorn TA, Sakmann B & Seeburg PH. (1990). A family of AMPA-selective glutamate receptors. Science 249, 556-560.

Keramidas A & Lynch JW. (2013). An outline of desensitization in pentameric ligand-gated ion channel receptors. Cellular and molecular life sciences: CMLS 70, 1241-1253.

Kessels HW & Malinow R. (2009). Synaptic AMPA receptor plasticity and behavior. Neuron 61, 340-350.

Khiroug SS, Pryazhnikov E, Coleman SK, Jeromin A, Keinanen K & Khiroug L. (2009). Dynamic visualization of membrane-inserted fraction of pHluorin-tagged channels using repetitive acidification technique. BMC neuroscience 10, 141.

Khodosevich K, Jacobi E, Farrow P, Schulmann A, Rusu A, Zhang L, Sprengel R, Monyer H & von Engelhardt J. (2014). Coexpressed auxiliary subunits exhibit distinct modulatory profiles on AMPA receptor function. Neuron 83, 601-615.

Kim E & Sheng M. (2004). PDZ domain proteins of synapses. Nature reviews Neuroscience 5, 771-781.

Kim KS, Yan D & Tomita S. (2010). Assembly and stoichiometry of the AMPA receptor and transmembrane AMPA receptor regulatory protein complex. J Neurosci 30, 1064-1072.

Kiskin NI, Krishtal OA & Tsyndrenko A. (1986). Excitatory amino acid receptors in hippocampal neurons: kainate fails to desensitize them. Neuroscience letters 63, 225-230.

Klaassen RV, Stroeder J, Coussen F, Hafner AS, Petersen JD, Renancio C, Schmitz LJ, Normand E, Lodder JC, Rotaru DC, Rao-Ruiz P, Spijker S, Mansvelder HD, Choquet D & Smit AB. (2016). Shisa6 traps AMPA receptors at postsynaptic sites and prevents their desensitization during synaptic activity. Nature communications 7, 10682.

Kleckner NW & Dingledine R. (1988). Requirement for glycine in activation of NMDA-receptors expressed in Xenopus oocytes. Science 241, 835-837.

Klein RM & Howe JR. (2004). Effects of the lurcher mutation on GluR1 desensitization and activation kinetics. J Neurosci 24, 4941-4951.

Koh DS, Burnashev N & Jonas P. (1995). Block of native Ca(2+)-permeable AMPA receptors in rat brain by intracellular polyamines generates double rectification. J Physiol 486 (Pt 2), 305-312.

Kohler M, Kornau HC & Seeburg PH. (1994). The organization of the gene for the functionally dominant alpha-amino-3-hydroxy-5-methylisoxazole-4-propionic acid receptor subunit GluR-B. The journal of biological chemistry 269, 17367-17370.

Kohr G & Seeburg PH. (1996). Subtype-specific regulation of recombinant NMDA receptor-channels by protein tyrosine kinases of the src family. J Physiol 492 (Pt 2), 445-452.

Koike M, Tsukada S, Tsuzuki K, Kijima H & Ozawa S. (2000). Regulation of kinetic properties of GluR2 AMPA receptor channels by alternative splicing. J Neurosci 20, 2166-2174.

Kong S, Qian B, Liu J, Fan M, Chen G & Wang Y. (2010). Cyclothiazide induces seizure behavior in freely moving rats. Brain research 1355, 207-213.

Kott S, Werner M, Korber C & Hollmann M. (2007). Electrophysiological properties of AMPA receptors are differentially modulated depending on the associated member of the TARP family. J Neurosci 27, 3780-3789.

Kovalchuk Y, Miller B, Sarantis M & Attwell D. (1994). Arachidonic acid depresses non-NMDA receptor currents. Brain research 643, 287-295.

Kraut JA & Madias NE. (2007). Serum anion gap: its uses and limitations in clinical medicine. Clinical journal of the American Society of Nephrology: CJASN 2, 162-174.

Krebs HA, Eggleston LV & Hems R. (1949). Distribution of glutamine and glutamic acid in animal tissues. The Biochemical journal 44, 159-163.

Krintel C, Frydenvang K, Ceravalls de Rabassa A, Kaern AM, Gajhede M, Pickering DS & Kastrup JS. (2014). L-Asp is a useful tool in the purification of the ionotropic glutamate receptor A2 ligand-binding domain. The FEBS journal 281, 2422-2430.

Krintel C, Harpsoe K, Zachariassen LG, Peters D, Frydenvang K, Pickering DS, Gajhede M & Kastrup JS. (2013). Structural analysis of the positive AMPA receptor modulators CX516 and Me-CX516 in complex with the GluA2 ligand-binding domain. Acta crystallographica Section D, Biological crystallography 69, 1645-1652.

Krishtal OA, Marchenko SM & Pidoplichko VI. (1983). Receptor for ATP in the membrane of mammalian sensory neurones. Neuroscience letters 35, 41-45.

Kristensen AS, Jenkins MA, Banke TG, Schousboe A, Makino Y, Johnson RC, Huganir R & Traynelis SF. (2011). Mechanism of Ca2+/calmodulin-dependent kinase II regulation of AMPA receptor gating. Nature neuroscience 14, 727-735.

Krnjevic K. (1974). Chemical nature of synaptic transmission in vertebrates. Physiological Reviews 54, 418-540.

Krnjevic K. (2010). When and why amino acids? J Physiol 588, 33-44.

Krnjevic K & Whittaker VP. (1965). Excitation and depression of cortical neurones by brain fractions released from micropipettes. J Physiol 179, 298-322.

Krogsgaard-Larsen P, Honore T, Hansen JJ, Curtis DR & Lodge D. (1980). New class of glutamate agonist structurally related to ibotenic acid. Nature 284, 64-66.

Krupp JJ, Vissel B, Thomas CG, Heinemann SF & Westbrook GL. (1999). Interactions of calmodulin and alpha-actinin with the NR1 subunit modulate Ca2+-dependent inactivation of NMDA receptors. J Neurosci 19, 1165-1178.

Kuang D & Hampson DR. (2006). Ion dependence of ligand binding to metabotropic glutamate receptors. Biochemical and biophysical research communications 345, 1-6.

Kubo Y, Miyashita T & Murata Y. (1998). Structural basis for a Ca2+-sensing function of the metabotropic glutamate receptors. Science 279, 1722-1725.

Kumar J & Mayer ML. (2013). Functional insights from glutamate receptor ion channel structures. Annual review of physiology 75, 313-337.

Kumar J, Schuck P, Jin R & Mayer ML. (2009). The N-terminal domain of GluR6-subtype glutamate receptor ion channels. Nature structural & molecular biology 16, 631-638.

Kumar J, Schuck P & Mayer ML. (2011). Structure and assembly mechanism for heteromeric kainate receptors. Neuron 71, 319-331.

Kuner T, Beck C, Sakmann B & Seeburg PH. (2001). Channel-lining residues of the AMPA receptor M2 segment: structural environment of the Q/R site and identification of the selectivity filter. J Neurosci 21, 4162-4172.

Kuryatov A, Laube B, Betz H & Kuhse J. (1994). Mutational analysis of the glycine-binding site of the NMDA receptor: structural similarity with bacterial amino acid-binding proteins. Neuron 12, 1291-1300.

Kusama N, Gautam M, Harding AM, Snyder PM & Benson CJ. (2013). Acid-sensing ion channels (ASICs) are differentially modulated by anions dependent on their subunit composition. American journal of physiology Cell physiology 304, C89-101.

Kusama N, Harding AM & Benson CJ. (2010). Extracellular chloride modulates the desensitization kinetics of acid-sensing ion channel 1a (ASIC1a). The journal of biological chemistry 285, 17425-17431.

Kuusinen A, Abele R, Madden DR & Keinanen K. (1999). Oligomerization and ligand-binding properties of the ectodomain of the alpha-amino-3-hydroxy-5-methyl-4-isoxazole propionic acid receptor subunit GluRD. The journal of biological chemistry 274, 28937-28943.

Kuusinen A, Arvola M & Keinanen K. (1995). Molecular dissection of the agonist binding site of an AMPA receptor. The EMBO journal 14, 6327-6332.

Kwon HB & Castillo PE. (2008). Role of glutamate autoreceptors at hippocampal mossy fiber synapses. Neuron 60, 1082-1094.

Lam HM, Chiu J, Hsieh MH, Meisel L, Oliveira IC, Shin M & Coruzzi G. (1998). Glutamate-receptor genes in plants. Nature 396, 125-126.

Langley JN. (1905). On the reaction of cells and of nerve-endings to certain poisons, chiefly as regards the reaction of striated muscle to nicotine and to curari. J Physiol 33, 374-413.

Lau AY & Roux B. (2007). The free energy landscapes governing conformational changes in a glutamate receptor ligand-binding domain. Structure 15, 1203-1214.

Laube B, Hirai H, Sturgess M, Betz H & Kuhse J. (1997). Molecular determinants of agonist discrimination by NMDA receptor subunits: analysis of the glutamate binding site on the NR2B subunit. Neuron 18, 493-503.

Laube B, Kuhse J & Betz H. (1998). Evidence for a tetrameric structure of recombinant NMDA receptors. J Neurosci 18, 2954-2961.

Laube B, Kuhse J & Betz H. (2000). Kinetic and mutational analysis of Zn2+ modulation of recombinant human inhibitory glycine receptors. J Physiol 522 (Pt 2), 215-230.

Laube B, Kuhse J, Rundstrom N, Kirsch J, Schmieden V & Betz H. (1995). Modulation by zinc ions of native rat and recombinant human inhibitory glycine receptors. J Physiol 483 (Pt 3), 613-619.

Lauri SE, Bortolotto ZA, Bleakman D, Ornstein PL, Lodge D, Isaac JT & Collingridge GL. (2001). A critical role of a facilitatory presynaptic kainate receptor in mossy fiber LTP. Neuron 32, 697-709.

Lee CH, Lu W, Michel JC, Goehring A, Du J, Song X & Gouaux E. (2014). NMDA receptor structures reveal subunit arrangement and pore architecture. Nature 511, 191-197.

Lee CR & Benfield P. (1994). Aniracetam. An overview of its pharmacodynamic and pharmacokinetic properties, and a review of its therapeutic potential in senile cognitive disorders. Drugs & aging 4, 257-273.

Lee HK, Takamiya K, Han JS, Man H, Kim CH, Rumbaugh G, Yu S, Ding L, He C, Petralia RS, Wenthold RJ, Gallagher M & Huganir RL. (2003). Phosphorylation of the AMPA receptor GluR1 subunit is required for synaptic plasticity and retention of spatial memory. Cell 112, 631-643.

Legendre P & Westbrook GL. (1991). Ifenprodil blocks N-methyl-D-aspartate receptors by a two-component mechanism. Molecular pharmacology 40, 289-298.

Leonard AS, Lim IA, Hemsworth DE, Horne MC & Hell JW. (1999). Calcium/calmodulin-dependent protein kinase II is associated with the N-methyl-D-aspartate receptor. Proc Natl Acad Sci U S A 96, 3239-3244.

Lerma J. (2003). Roles and rules of kainate receptors in synaptic transmission. Nature reviews Neuroscience 4, 481-495.

Lerma J & Marques JM. (2013). Kainate receptors in health and disease. Neuron 80, 292-311.

Lerma J, Paternain AV, Naranjo JR & Mellstrom B. (1993). Functional kainate-selective glutamate receptors in cultured hippocampal neurons. Proc Natl Acad Sci U S A 90, 11688-11692.

Letts VA, Felix R, Biddlecome GH, Arikkath J, Mahaffey CL, Valenzuela A, Bartlett FS, 2nd, Mori Y, Campbell KP & Frankel WN. (1998). The mouse stargazer gene encodes a neuronal Ca2+-channel gamma subunit. Nature genetics 19, 340-347.

Leuschner WD & Hoch W. (1999). Subtype-specific assembly of alpha-amino-3-hydroxy-5-methyl-4-isoxazole propionic acid receptor subunits is mediated by their n-terminal domains. The journal of biological chemistry 274, 16907-16916.

Li C, Peoples RW, Li Z & Weight FF. (1993). Zn2+ potentiates excitatory action of ATP on mammalian neurons. Proc Natl Acad Sci U S A 90, 8264-8267.

Liao D, Hessler NA & Malinow R. (1995). Activation of postsynaptically silent synapses during pairing-induced LTP in CA1 region of hippocampal slice. Nature 375, 400-404.

Liebeskind BJ, Hillis DM & Zakon HH. (2015). Convergence of ion channel genome content in early animal evolution. Proc Natl Acad Sci U S A 112, E846-851.

Lin DT, Makino Y, Sharma K, Hayashi T, Neve R, Takamiya K & Huganir RL. (2009). Regulation of AMPA receptor extrasynaptic insertion by 4.1N, phosphorylation and palmitoylation. Nature neuroscience 12, 879-887.

Lipton SA. (2006). Paradigm shift in neuroprotection by NMDA receptor blockade: memantine and beyond. Nature reviews Drug discovery 5, 160-170.

Liu W, Chun E, Thompson AA, Chubukov P, Xu F, Katritch V, Han GW, Roth CB, Heitman LH, AP IJ, Cherezov V & Stevens RC. (2012). Structural basis for allosteric regulation of GPCRs by sodium ions. Science 337, 232-236.

Lodge D. (2009). The history of the pharmacology and cloning of ionotropic glutamate receptors and the development of idiosyncratic nomenclature. Neuropharmacology 56, 6-21.

Logan WJ & Snyder SH. (1971). Unique high affinity uptake systems for glycine, glutamic and aspartic acids in central nervous tissue of the rat. Nature 234, 297-299.

Lomash S, Chittori S, Brown P & Mayer ML. (2013). Anions mediate ligand binding in Adineta vaga glutamate receptor ion channels. Structure 21, 414-425.

Lomeli H, Mosbacher J, Melcher T, Hoger T, Geiger JR, Kuner T, Monyer H, Higuchi M, Bach A & Seeburg PH. (1994). Control of kinetic properties of AMPA receptor channels by nuclear RNA editing. Science 266, 1709-1713.

London ED & Coyle JT. (1979). Specific binding of [3H]kainic acid to receptor sites in rat brain. Molecular pharmacology 15, 492-505.

Lorca RA, Rozas C, Loyola S, Moreira-Ramos S, Zeise ML, Kirkwood A, Huidobro-Toro JP & Morales B. (2011). Zinc enhances long-term potentiation through P2X receptor modulation in the hippocampal CA1 region. Eur J Neurosci 33, 1175-1185.

Losonczy A & Magee JC. (2006). Integrative properties of radial oblique dendrites in hippocampal CA1 pyramidal neurons. Neuron 50, 291-307.

Lovero KL, Blankenship SM, Shi Y & Nicoll RA. (2013). SynDIG1 promotes excitatory synaptogenesis independent of AMPA receptor trafficking and biophysical regulation. PloS one 8, e66171.

Lu W, Shi Y, Jackson AC, Bjorgan K, During MJ, Sprengel R, Seeburg PH & Nicoll RA. (2009). Subunit composition of synaptic AMPA receptors revealed by a single-cell genetic approach. Neuron 62, 254-268.

Luscher C & Malenka RC. (2012). NMDA receptor-dependent long-term potentiation and long-term depression (LTP/LTD). Cold Spring Harbor perspectives in biology 4.

Lynch G, Kessler M, Rogers G, Ambros-Ingerson J, Granger R & Schehr RS. (1996). Psychological effects of a drug that facilitates brain AMPA receptors. International clinical psychopharmacology 11, 13-19.

Lynch G, Larson J, Kelso S, Barrionuevo G & Schottler F. (1983). Intracellular injections of EGTA block induction of hippocampal long-term potentiation. Nature 305, 719-721.

MacDermott AB, Mayer ML, Westbrook GL, Smith SJ & Barker JL. (1986). NMDA-receptor activation increases cytoplasmic calcium concentration in cultured spinal cord neurones. Nature 321, 519-522.

MacDonald JF & Nowak LM. (1990). Mechanisms of blockade of excitatory amino acid receptor channels. Trends in pharmacological sciences 11, 167-172.

MacLean DM. (2013). CrossTalk opposing view: TARPs modulate AMPA receptor conformations before the gating transitions. J Physiol 591, 1585-1586; discussion 1587.

MacLean DM & Jayaraman V. (2016). Acid-sensing ion channels are tuned to follow high-frequency stimuli. J Physiol 594, 2629-2645.

MacLean DM, Ramaswamy SS, Du M, Howe JR & Jayaraman V. (2014). Stargazin promotes closure of the AMPA receptor ligand-binding domain. The journal of general physiology 144, 503-512.

Maclean DM, Wong AY, Fay AM & Bowie D. (2011). Cations but not anions regulate the responsiveness of kainate receptors. J Neurosci 31, 2136-2144.

Madden DR. (2002). The structure and function of glutamate receptor ion channels. Nature reviews Neuroscience 3, 91-101.

Mah SJ, Cornell E, Mitchell NA & Fleck MW. (2005). Glutamate receptor trafficking: endoplasmic reticulum quality control involves ligand binding and receptor function. J Neurosci 25, 2215-2225.

Malenka RC & Bear MF. (2004). LTP and LTD: an embarrassment of riches. Neuron 44, 5-21.

Malenka RC, Kauer JA, Perkel DJ, Mauk MD, Kelly PT, Nicoll RA & Waxham MN. (1989). An essential role for postsynaptic calmodulin and protein kinase activity in long-term potentiation. Nature 340, 554-557.

Mammen AL, Huganir RL & O'Brien RJ. (1997). Redistribution and stabilization of cell surface glutamate receptors during synapse formation. J Neurosci 17, 7351-7358.

Mangan JL & Whittaker VP. (1966). The distribution of free amino acids in subcellular fractions of guinea-pig brain. The Biochemical journal 98, 128-137.

Mano I, Lamed Y & Teichberg VI. (1996). A venus flytrap mechanism for activation and desensitization of alpha-amino-3-hydroxy-5-methyl-4-isoxazole propionic acid receptors. The journal of biological chemistry 271, 15299-15302.

Mano I & Teichberg VI. (1998). A tetrameric subunit stoichiometry for a glutamate receptor-channel complex. Neuroreport 9, 327-331.

Martin S, Nishimune A, Mellor JR & Henley JM. (2007). SUMOylation regulates kainate-receptor-mediated synaptic transmission. Nature 447, 321-325.

Marx MC, Billups D & Billups B. (2015). Maintaining the presynaptic glutamate supply for excitatory neurotransmission. Journal of neuroscience research 93, 1031-1044.

Masu M, Tanabe Y, Tsuchida K, Shigemoto R & Nakanishi S. (1991). Sequence and expression of a metabotropic glutamate receptor. Nature 349, 760-765.

Mayer ML. (2005). Crystal structures of the GluR5 and GluR6 ligand binding cores: molecular mechanisms underlying kainate receptor selectivity. Neuron 45, 539-552.

Mayer ML. (2011). Emerging models of glutamate receptor ion channel structure and function. Structure 19, 1370-1380.

Mayer ML & Armstrong N. (2004). Structure and function of glutamate receptor ion channels. Annual review of physiology 66, 161-181.

Mayer ML & Westbrook GL. (1984). Mixed-agonist action of excitatory amino acids on mouse spinal cord neurones under voltage clamp. J Physiol 354, 29-53.

Mayer ML & Westbrook GL. (1987). The physiology of excitatory amino acids in the vertebrate central nervous system. Progress in neurobiology 28, 197-276.

Mayer ML, Westbrook GL & Guthrie PB. (1984). Voltage-dependent block by Mg2+ of NMDA responses in spinal cord neurones. Nature 309, 261-263.

McCoy AJ, Grosse-Kunstleve RW, Adams PD, Winn MD, Storoni LC & Read RJ. (2007). Phaser crystallographic software. Journal of applied crystallography 40, 658-674.

McGee TP, Bats C, Farrant M & Cull-Candy SG. (2015). Auxiliary Subunit GSG1L Acts to Suppress Calcium-Permeable AMPA Receptor Function. J Neurosci 35, 16171-16179.

McLennan H. (1965). Synoptic transmission in the central nervous system. In Physiological Pharmacology, ed. Root WSH, F.G. Academic Press.

McLennan H. (1983). Receptors for the excitatory amino acids in the mammalian central nervous system. Progress in neurobiology 20, 251-271.

McNicholas S, Potterton E, Wilson KS & Noble ME. (2011). Presenting your structures: the CCP4mg molecular-graphics software. Acta crystallographica Section D, Biological crystallography 67, 386-394.

Meddows E, Le Bourdelles B, Grimwood S, Wafford K, Sandhu S, Whiting P & McIlhinney RA. (2001). Identification of molecular determinants that are important in the assembly of N-methyl-D-aspartate receptors. The journal of biological chemistry 276, 18795-18803.

Mellem JE, Brockie PJ, Zheng Y, Madsen DM & Maricq AV. (2002). Decoding of polymodal sensory stimuli by postsynaptic glutamate receptors in C. elegans. Neuron 36, 933-944.

Melyan Z, Wheal HV & Lancaster B. (2002). Metabotropic-mediated kainate receptor regulation of IsAHP and excitability in pyramidal cells. Neuron 34, 107-114.

Meng Y, Zhang Y & Jia Z. (2003). Synaptic transmission and plasticity in the absence of AMPA glutamate receptor GluR2 and GluR3. Neuron 39, 163-176.

Menuz K, Kerchner GA, O'Brien JL & Nicoll RA. (2009). Critical role for TARPs in early development despite broad functional redundancy. Neuropharmacology 56, 22-29.

Menuz K, Stroud RM, Nicoll RA & Hays FA. (2007). TARP auxiliary subunits switch AMPA receptor antagonists into partial agonists. Science 318, 815-817.

Meyerson JR, Kumar J, Chittori S, Rao P, Pierson J, Bartesaghi A, Mayer ML & Subramaniam S. (2014). Structural mechanism of glutamate receptor activation and desensitization. Nature 514, 328-334.

Midgett CR, Gill A & Madden DR. (2012). Domain architecture of a calcium-permeable AMPA receptor in a ligand-free conformation. Frontiers in molecular neuroscience 4, 56.

Midgett CR & Madden DR. (2008). The quaternary structure of a calcium-permeable AMPA receptor: conservation of shape and symmetry across functionally distinct subunit assemblies. Journal of molecular biology 382, 578-584.

Miesenbock G, De Angelis DA & Rothman JE. (1998). Visualizing secretion and synaptic transmission with pH-sensitive green fluorescent proteins. Nature 394, 192-195.

Miller PS, Topf M, & Smart TG. (2008). Mapping a molecular link between allosteric inhibition and activation of the glycine receptor. Nature structural & molecular biology 15, 1084-1093.

Milstein AD, Zhou W, Karimzadegan S, Bredt DS & Nicoll RA. (2007). TARP subtypes differentially and dose-dependently control synaptic AMPA receptor gating. Neuron 55, 905-918.

Mitchell NA & Fleck MW. (2007). Targeting AMPA receptor gating processes with allosteric modulators and mutations. Biophysical journal 92, 2392-2402.

Molnar E, McIlhinney RA, Baude A, Nusser Z & Somogyi P. (1994). Membrane topology of the GluR1 glutamate receptor subunit: epitope mapping by site-directed antipeptide antibodies. Journal of neurochemistry 63, 683-693.

Monyer H, Burnashev N, Laurie DJ, Sakmann B & Seeburg PH. (1994). Developmental and regional expression in the rat brain and functional properties of four NMDA receptors. Neuron 12, 529-540.

Monyer H, Seeburg PH & Wisden W. (1991). Glutamate-operated channels: developmentally early and mature forms arise by alternative splicing. Neuron 6, 799-810.

Monyer H, Sprengel R, Schoepfer R, Herb A, Higuchi M, Lomeli H, Burnashev N, Sakmann B & Seeburg PH. (1992). Heteromeric NMDA receptors: molecular and functional distinction of subtypes. Science 256, 1217-1221.

Morimoto-Tomita M, Zhang W, Straub C, Cho CH, Kim KS, Howe JR & Tomita S. (2009). Autoinactivation of neuronal AMPA receptors via glutamate-regulated TARP interaction. Neuron 61, 101-112.

Moriyoshi K, Masu M, Ishii T, Shigemoto R, Mizuno N & Nakanishi S. (1991). Molecular cloning and characterization of the rat NMDA receptor. Nature 354, 31-37.

Morris RG, Anderson E, Lynch GS & Baudry M. (1986). Selective impairment of learning and blockade of long-term potentiation by an N-methyl-D-aspartate receptor antagonist, AP5. Nature 319, 774-776.

Morris RG, Garrud P, Rawlins JN & O'Keefe J. (1982). Place navigation impaired in rats with hippocampal lesions. Nature 297, 681-683.

Mortensen M & Smart TG. (2007). Single-channel recording of ligand-gated ion channels. Nature protocols 2, 2826-2841.

Mosbacher J, Schoepfer R, Monyer H, Burnashev N, Seeburg PH & Ruppersberg JP. (1994). A molecular determinant for submillisecond desensitization in glutamate receptors. Science 266, 1059-1062.

Moss FJ, Dolphin AC & Clare JJ. (2003). Human neuronal stargazin-like proteins, gamma2, gamma3 and gamma4; an investigation of their specific localization in human brain and their influence on CaV2.1 voltage-dependent calcium channels expressed in Xenopus oocytes. BMC neuroscience 4, 23.

Mott DD, Washburn MS, Zhang S & Dingledine RJ. (2003). Subunit-dependent modulation of kainate receptors by extracellular protons and polyamines. J Neurosci 23, 1179-1188.

Muller D, Joly M & Lynch G. (1988). Contributions of quisqualate and NMDA receptors to the induction and expression of LTP. Science 242, 1694-1697.

Murshudov GN, Vagin AA & Dodson EJ. (1997). Refinement of macromolecular structures by the maximum-likelihood method. Acta crystallographica Section D, Biological crystallography 53, 240-255.

Musgaard M & Biggin PC. (2016). Steered Molecular Dynamics Simulations Predict Conformational Stability of Glutamate Receptors. Journal of chemical information and modeling 56, 1787-1797.

Nabavi S, Fox R, Proulx CD, Lin JY, Tsien RY & Malinow R. (2014). Engineering a memory with LTD and LTP. Nature 511, 348-352.

Nagaya N, Tittle RK, Saar N, Dellal SS & Hume RI. (2005). An intersubunit zinc binding site in rat P2X2 receptors. The journal of biological chemistry 280, 25982-25993.

Nakagawa T. (2010). The biochemistry, ultrastructure, and subunit assembly mechanism of AMPA receptors. Molecular neurobiology 42, 161-184.

Nakagawa T, Cheng Y, Ramm E, Sheng M & Walz T. (2005). Structure and different conformational states of native AMPA receptor complexes. Nature 433, 545-549.

Nakagawa T, Cheng Y, Sheng M & Walz T. (2006). Three-dimensional structure of an AMPA receptor without associated stargazin/TARP proteins. Biological chemistry 387, 179-187.

Nakanishi N, Shneider NA & Axel R. (1990). A family of glutamate receptor genes: evidence for the formation of heteromultimeric receptors with distinct channel properties. Neuron 5, 569-581.

Nakanishi S. (1992). Molecular diversity of glutamate receptors and implications for brain function. Science 258, 597-603.

Nanao MH, Green T, Stern-Bach Y, Heinemann SF & Choe S. (2005). Structure of the kainate receptor subunit GluR6 agonist-binding domain complexed with domoic acid. Proc Natl Acad Sci U S A 102, 1708-1713.

Nasu-Nishimura Y, Hurtado D, Braud S, Tang TT, Isaac JT & Roche KW. (2006). Identification of an endoplasmic reticulum-retention motif in an intracellular loop of the kainate receptor subunit KA2. J Neurosci 26, 7014-7021.

Naur P, Hansen KB, Kristensen AS, Dravid SM, Pickering DS, Olsen L, Vestergaard B, Egebjerg J, Gajhede M, Traynelis SF & Kastrup JS. (2007). Ionotropic glutamate-like receptor delta2 binds D-serine and glycine. Proc Natl Acad Sci U S A 104, 14116-14121.

Nayeem N, Mayans O & Green T. (2011). Conformational flexibility of the ligand-binding domain dimer in kainate receptor gating and desensitization. J Neurosci 31, 2916-2924.

Nayeem N, Zhang Y, Schweppe DK, Madden DR & Green T. (2009). A nondesensitizing kainate receptor point mutant. Molecular pharmacology 76, 534-542.

Neher E & Sakmann B. (1976). Single-channel currents recorded from membrane of denervated frog muscle fibres. Nature 260, 799-802.

Ng D, Pitcher GM, Szilard RK, Sertie A, Kanisek M, Clapcote SJ, Lipina T, Kalia LV, Joo D, McKerlie C, Cortez M, Roder JC, Salter MW & McInnes RR. (2009). Neto1 is a novel CUB-domain NMDA receptor-interacting protein required for synaptic plasticity and learning. PLoS biology 7, e41.

Nicholls J & Hill O. (2003). Bernard Katz: his search for truth and beauty. Journal of neurocytology 32, 425-430.

Nishimune A, Isaac JT, Molnar E, Noel J, Nash SR, Tagaya M, Collingridge GL, Nakanishi S & Henley JM. (1998). NSF binding to GluR2 regulates synaptic transmission. Neuron 21, 87-97.

Niswender CM & Conn PJ. (2010). Metabotropic glutamate receptors: physiology, pharmacology, and disease. Annual review of pharmacology and toxicology 50, 295-322.

Noebels JL, Qiao X, Bronson RT, Spencer C & Davisson MT. (1990). Stargazer: a new neurological mutant on chromosome 15 in the mouse with prolonged cortical seizures. Epilepsy research 7, 129-135.

Nowak L, Bregestovski P, Ascher P, Herbet A & Prochiantz A. (1984). Magnesium gates glutamate-activated channels in mouse central neurones. Nature 307, 462-465.

Nozaki C, Vergnano AM, Filliol D, Ouagazzal AM, Le Goff A, Carvalho S, Reiss D, Gaveriaux-Ruff C, Neyton J, Paoletti P & Kieffer BL. (2011). Zinc alleviates pain through high-affinity binding to the NMDA receptor NR2A subunit. Nature neuroscience 14, 1017-1022.

Nusser Z, Mulvihill E, Streit P & Somogyi P. (1994). Subsynaptic segregation of metabotropic and ionotropic glutamate receptors as revealed by immunogold localization. Neuroscience 61, 421-427.

O'Hara PJ, Sheppard PO, Thogersen H, Venezia D, Haldeman BA, McGrane V, Houamed KM, Thomsen C, Gilbert TL & Mulvihill ER. (1993). The ligand-binding domain in metabotropic glutamate receptors is related to bacterial periplasmic binding proteins. Neuron 11, 41-52.

Ollivier JF, Shahrezaei V & Swain PS. (2010). Scalable rule-based modelling of allosteric proteins and biochemical networks. PLoS computational biology 6, e1000975.

Ornstein PL, Zimmerman DM, Arnold MB, Bleisch TJ, Cantrell B, Simon R, Zarrinmayeh H, Baker SR, Gates M, Tizzano JP, Bleakman D, Mandelzys A, Jarvie KR, Ho K, Deverill M & Kamboj RK. (2000). Biarylpropylsulfonamides as novel, potent potentiators of 2-amino-3- (5-methyl-3-hydroxyisoxazol-4-yl)- propanoic acid (AMPA) receptors. Journal of medicinal chemistry 43, 4354-4358.

Osten P, Srivastava S, Inman GJ, Vilim FS, Khatri L, Lee LM, States BA, Einheber S, Milner TA, Hanson PI & Ziff EB. (1998). The AMPA receptor GluR2 C terminus can mediate a reversible, ATP-dependent interaction with NSF and alpha- and beta-SNAPs. Neuron 21, 99-110.

Paas Y. (1998). The macro- and microarchitectures of the ligand-binding domain of glutamate receptors. Trends Neurosci 21, 117-125.

Painter J & Merritt EA. (2006). Optimal description of a protein structure in terms of multiple groups undergoing TLS motion. Acta crystallographica Section D, Biological crystallography 62, 439-450.

Paoletti P, Ascher P & Neyton J. (1997). High-affinity zinc inhibition of NMDA NR1-NR2A receptors. J Neurosci 17, 5711-5725.

Paoletti P, Bellone C & Zhou Q. (2013). NMDA receptor subunit diversity: impact on receptor properties, synaptic plasticity and disease. Nature reviews Neuroscience 14, 383-400.

Paoletti P, Perin-Dureau F, Fayyazuddin A, Le Goff A, Callebaut I & Neyton J. (2000). Molecular organization of a zinc binding n-terminal modulatory domain in a NMDA receptor subunit. Neuron 28, 911-925.

Park YH, Broyles HV, He S, McGrady NR, Li L & Yorio T. (2016). Involvement of AMPA Receptor and Its Flip and Flop Isoforms in Retinal Ganglion Cell Death Following Oxygen/Glucose Deprivation. Investigative ophthalmology & visual science 57, 508-526.

Partin KM, Bowie D & Mayer ML. (1995). Structural determinants of allosteric regulation in alternatively spliced AMPA receptors. Neuron 14, 833-843.

Partin KM, Fleck MW & Mayer ML. (1996). AMPA receptor flip/flop mutants affecting deactivation, desensitization, and modulation by cyclothiazide, aniracetam, and thiocyanate. J Neurosci 16, 6634-6647.

Partin KM, Patneau DK, Winters CA, Mayer ML & Buonanno A. (1993). Selective modulation of desensitization at AMPA versus kainate receptors by cyclothiazide and concanavalin A. Neuron 11, 1069-1082.

Pasternack A, Coleman SK, Jouppila A, Mottershead DG, Lindfors M, Pasternack M & Keinanen K. (2002). Alpha-amino-3-hydroxy-5-methyl-4-isoxazolepropionic acid (AMPA) receptor channels lacking the N-terminal domain. The journal of biological chemistry 277, 49662-49667.

Paternain AV, Cohen A, Stern-Bach Y & Lerma J. (2003). A role for extracellular Na+ in the channel gating of native and recombinant kainate receptors. J Neurosci 23, 8641-8648.

Patneau DK & Mayer ML. (1990). Structure-activity relationships for amino acid transmitter candidates acting at N-methyl-D-aspartate and quisqualate receptors. J Neurosci 10, 2385-2399.

Patneau DK & Mayer ML. (1991). Kinetic analysis of interactions between kainate and AMPA: evidence for activation of a single receptor in mouse hippocampal neurons. Neuron 6, 785-798.

Patneau DK, Mayer ML, Jane DE & Watkins JC. (1992). Activation and desensitization of AMPA/kainate receptors by novel derivatives of willardiine. J Neurosci 12, 595-606.

Patneau DK, Vyklicky L, Jr. & Mayer ML. (1993). Hippocampal neurons exhibit cyclothiazide-sensitive rapidly desensitizing responses to kainate. J Neurosci 13, 3496-3509.

Penn AC, Balik A, Wozny C, Cais O & Greger IH. (2012). Activity-mediated AMPA receptor remodeling, driven by alternative splicing in the ligand-binding domain. Neuron 76, 503-510.

Perez-Otano I, Schulteis CT, Contractor A, Lipton SA, Trimmer JS, Sucher NJ & Heinemann SF. (2001). Assembly with the NR1 subunit is required for surface expression of NR3A-containing NMDA receptors. J Neurosci 21, 1228-1237.

Perin-Dureau F, Rachline J, Neyton J & Paoletti P. (2002). Mapping the binding site of the neuroprotectant ifenprodil on NMDA receptors. J Neurosci 22, 5955-5965.

Perrett D. (2007). From 'protein' to the beginnings of clinical proteomics. Proteomics Clinical applications 1, 720-738.

Pert CB, Pasternak G & Snyder SH. (1973). Opiate agonists and antagonists discriminated by receptor binding in brain. Science 182, 1359-1361.

Peters S, Koh J & Choi DW. (1987). Zinc selectively blocks the action of N-methyl-D-aspartate on cortical neurons. Science 236, 589-593.

Petralia RS, Wang YX & Wenthold RJ. (1994). Histological and ultrastructural localization of the kainate receptor subunits, KA2 and GluR6/7, in the rat nervous system using selective antipeptide antibodies. The journal of comparative neurology 349, 85-110.

Pickard L, Noel J, Henley JM, Collingridge GL & Molnar E. (2000). Developmental changes in synaptic AMPA and NMDA receptor distribution and AMPA receptor subunit composition in living hippocampal neurons. J Neurosci 20, 7922-7931.

Pirotte B, Francotte P, Goffin E & de Tullio P. (2013). AMPA receptor positive allosteric modulators: a patent review. Expert opinion on therapeutic patents 23, 615-628.

Plested AJ. (2016). Structural mechanisms of activation and desensitization in neurotransmitter-gated ion channels. Nature structural & molecular biology 23, 494-502.

Plested AJ & Mayer ML. (2007). Structure and mechanism of kainate receptor modulation by anions. Neuron 53, 829-841.

Plested AJ, Vijayan R, Biggin PC & Mayer ML. (2008). Molecular basis of kainate receptor modulation by sodium. Neuron 58, 720-735.

Pohlsgaard J, Frydenvang K, Madsen U & Kastrup JS. (2011). Lessons from more than 80 structures of the GluA2 ligand-binding domain in complex with agonists, antagonists and allosteric modulators. Neuropharmacology 60, 135-150.

Pollard H, Heron A, Moreau J, Ben-Ari Y & Khrestchatisky M. (1993). Alterations of the GluR-B AMPA receptor subunit flip/flop expression in kainate-induced epilepsy and ischemia. Neuroscience 57, 545-554.

Priel A, Kolleker A, Ayalon G, Gillor M, Osten P & Stern-Bach Y. (2005). Stargazin reduces desensitization and slows deactivation of the AMPA-type glutamate receptors. J Neurosci 25, 2682-2686.

Priel A, Selak S, Lerma J & Stern-Bach Y. (2006). Block of kainate receptor desensitization uncovers a key trafficking checkpoint. Neuron 52, 1037-1046.

Prieto ML & Wollmuth LP. (2010). Gating modes in AMPA receptors. J Neurosci 30, 4449-4459.

Ptak CP, Ahmed AH & Oswald RE. (2009). Probing the allosteric modulator binding site of GluR2 with thiazide derivatives. Biochemistry 48, 8594-8602.

Purohit P, Gupta S, Jadey S & Auerbach A. (2013). Functional anatomy of an allosteric protein. Nature communications 4, 2984.

Qian A & Johnson JW. (2002). Channel gating of NMDA receptors. Physiology & behavior 77, 577-582.

Quiocho FA. (1990). Atomic structures of periplasmic binding proteins and the high-affinity active transport systems in bacteria. Philosophical transactions of the Royal Society of London Series B, Biological sciences 326, 341-351; discussion 351-342.

Quirk JC, Siuda ER & Nisenbaum ES. (2004). Molecular determinants responsible for differences in desensitization kinetics of AMPA receptor splice variants. J Neurosci 24, 11416-11420.

Raman IM & Trussell LO. (1995). The mechanism of alpha-amino-3-hydroxy-5-methyl-4-isoxazolepropionate receptor desensitization after removal of glutamate. Biophysical journal 68, 137-146.

Reiner A & Isacoff EY. (2014). Tethered ligands reveal glutamate receptor desensitization depends on subunit occupancy. Nature chemical biology 10, 273-280.

Ren Z, Riley NJ, Garcia EP, Sanders JM, Swanson GT & Marshall J. (2003). Multiple trafficking signals regulate kainate receptor KA2 subunit surface expression. J Neurosci 23, 6608-6616.

Robert A, Armstrong N, Gouaux JE & Howe JR. (2005). AMPA receptor binding cleft mutations that alter affinity, efficacy, and recovery from desensitization. J Neurosci 25, 3752-3762.

Robert A & Howe JR. (2003). How AMPA receptor desensitization depends on receptor occupancy. J Neurosci 23, 847-858.

Robert A, Irizarry SN, Hughes TE & Howe JR. (2001). Subunit interactions and AMPA receptor desensitization. J Neurosci 21, 5574-5586.

Roche KW, Raymond LA, Blackstone C & Huganir RL. (1994). Transmembrane topology of the glutamate receptor subunit GluR6. The journal of biological chemistry 269, 11679-11682.

Rodriguez-Moreno A, Herreras O & Lerma J. (1997). Kainate receptors presynaptically downregulate GABAergic inhibition in the rat hippocampus. Neuron 19, 893-901.

Rodriguez-Moreno A & Lerma J. (1998). Kainate receptor modulation of GABA release involves a metabotropic function. Neuron 20, 1211-1218.

Rogers SW, Hughes TE, Hollmann M, Gasic GP, Deneris ES & Heinemann S. (1991). The characterization and localization of the glutamate receptor subunit GluR1 in the rat brain. J Neurosci 11, 2713-2724.

Rosenmund C, Stern-Bach Y & Stevens CF. (1998). The tetrameric structure of a glutamate receptor channel. Science 280, 1596-1599.

Rossmann M, Sukumaran M, Penn AC, Veprintsev DB, Babu MM & Greger IH. (2011). Subunit-selective N-terminal domain associations organize the formation of AMPA receptor heteromers. The EMBO journal 30, 959-971.

Roth S, Neuman-Silberberg FS, Barcelo G & Schupbach T. (1995). cornichon and the EGF receptor signaling process are necessary for both anterior-posterior and dorsal-ventral pattern formation in Drosophila. Cell 81, 967-978.

Rouach N, Byrd K, Petralia RS, Elias GM, Adesnik H, Tomita S, Karimzadegan S, Kealey C, Bredt DS & Nicoll RA. (2005). TARP gamma-8 controls hippocampal AMPA receptor number, distribution and synaptic plasticity. Nature neuroscience 8, 1525-1533.

Rousset M, Cens T, Restituito S, Barrere C, Black JL, 3rd, McEnery MW & Charnet P. (2001). Functional roles of gamma2, gamma3 and gamma4, three new Ca2+ channel subunits, in P/Q-type Ca2+ channel expressed in Xenopus oocytes. J Physiol 532, 583-593.

Rozov A & Burnashev N. (1999). Polyamine-dependent facilitation of postsynaptic AMPA receptors counteracts paired-pulse depression. Nature 401, 594-598.

Rozov A, Zilberter Y, Wollmuth LP & Burnashev N. (1998). Facilitation of currents through rat Ca2+-permeable AMPA receptor channels by activity-dependent relief from polyamine block. J Physiol 511 (Pt 2), 361-377.

Ryan TJ, Emes RD, Grant SG & Komiyama NH. (2008). Evolution of NMDA receptor cytoplasmic interaction domains: implications for organisation of synaptic signalling complexes. BMC neuroscience 9, 6.

Safferling M, Tichelaar W, Kummerle G, Jouppila A, Kuusinen A, Keinanen K & Madden DR. (2001). First images of a glutamate receptor ion channel: oligomeric state and molecular dimensions of GluRB homomers. Biochemistry 40, 13948-13953.

Saglietti L, Dequidt C, Kamieniarz K, Rousset MC, Valnegri P, Thoumine O, Beretta F, Fagni L, Choquet D, Sala C, Sheng M & Passafaro M. (2007). Extracellular interactions between GluR2 and N-cadherin in spine regulation. Neuron 54, 461-477.

Sakimura K, Morita T, Kushiya E & Mishina M. (1992). Primary structure and expression of the gamma 2 subunit of the glutamate receptor channel selective for kainate. Neuron 8, 267-274.

Sakmann B, Patlak J & Neher E. (1980). Single acetylcholine-activated channels show burst-kinetics in presence of desensitizing concentrations of agonist. Nature 286, 71-73.

Sali A & Blundell TL. (1993). Comparative protein modelling by satisfaction of spatial restraints. Journal of molecular biology 234, 779-815.

Saller B, Fink H & Mann K. (1998). Kinetics of acute and chronic iodine excess. Experimental and clinical endocrinology & diabetes: official journal, German Society of Endocrinology [and] German Diabetes Association 106 Suppl 3, S34-38.

Salussolia CL, Corrales A, Talukder I, Kazi R, Akgul G, Bowen M & Wollmuth LP. (2011). Interaction of the M4 segment with other transmembrane segments is required for surface expression of mammalian alpha-amino-3-hydroxy-5-methyl-4-isoxazolepropionic acid (AMPA) receptors. The journal of biological chemistry 286, 40205-40218.

Salussolia CL, Gan Q, Kazi R, Singh P, Allopenna J, Furukawa H & Wollmuth LP. (2013). A eukaryotic specific transmembrane segment is required for tetramerization in AMPA receptors. J Neurosci 33, 9840-9845.

Sanacora G, Zarate CA, Krystal JH & Manji HK. (2008). Targeting the glutamatergic system to develop novel, improved therapeutics for mood disorders. Nature reviews Drug discovery 7, 426-437.

Santangelo RM, Acker TM, Zimmerman SS, Katzman BM, Strong KL, Traynelis SF & Liotta DC. (2012). Novel NMDA receptor modulators: an update. Expert opinion on therapeutic patents 22, 1337-1352.

Saunders R, Nahorski SR & Challiss RA. (1998). A modulatory effect of extracellular Ca2+ on type 1alpha metabotropic glutamate receptor-mediated signalling. Neuropharmacology 37, 273-276.

Sauvageau E, Rochdi MD, Oueslati M, Hamdan FF, Percherancier Y, Simpson JC, Pepperkok R & Bouvier M. (2014). CNIH4 interacts with newly synthesized GPCR and controls their export from the endoplasmic reticulum. Traffic 15, 383-400.

Savic N, Luthi A, Gahwiler BH & McKinney RA. (2003). N-methyl-D-aspartate receptor blockade during development lowers long-term potentiation threshold without affecting dynamic range of CA3-CA1 synapses. Proc Natl Acad Sci U S A 100, 5503-5508.

Schauder DM, Kuybeda O, Zhang J, Klymko K, Bartesaghi A, Borgnia MJ, Mayer ML & Subramaniam S. (2013). Glutamate receptor desensitization is mediated by changes in quaternary structure of the ligand binding domain. Proc Natl Acad Sci U S A 110, 5921-5926.

Schmitz D, Frerking M & Nicoll RA. (2000). Synaptic activation of presynaptic kainate receptors on hippocampal mossy fiber synapses. Neuron 27, 327-338.

Schmitz D, Mellor J & Nicoll RA. (2001). Presynaptic kainate receptor mediation of frequency facilitation at hippocampal mossy fiber synapses. Science 291, 1972-1976.

Schnell E, Sizemore M, Karimzadegan S, Chen L, Bredt DS & Nicoll RA. (2002). Direct interactions between PSD-95 and stargazin control synaptic AMPA receptor number. Proc Natl Acad Sci U S A 99, 13902-13907.

Schwenk J, Baehrens D, Haupt A, Bildl W, Boudkkazi S, Roeper J, Fakler B & Schulte U. (2014). Regional diversity and developmental dynamics of the AMPA-receptor proteome in the mammalian brain. Neuron 84, 41-54.

Schwenk J, Harmel N, Brechet A, Zolles G, Berkefeld H, Muller CS, Bildl W, Baehrens D, Huber B, Kulik A, Klocker N, Schulte U & Fakler B. (2012). High-resolution proteomics unravel architecture and molecular diversity of native AMPA receptor complexes. Neuron 74, 621-633.

Schwenk J, Harmel N, Zolles G, Bildl W, Kulik A, Heimrich B, Chisaka O, Jonas P, Schulte U, Fakler B & Klocker N. (2009). Functional proteomics identify cornichon proteins as auxiliary subunits of AMPA receptors. Science 323, 1313-1319.

Seeburg PH. (1993). The TINS/TiPS Lecture. The molecular biology of mammalian glutamate receptor channels. Trends Neurosci 16, 359-365.

Sekiguchi M, Fleck MW, Mayer ML, Takeo J, Chiba Y, Yamashita S & Wada K. (1997). A novel allosteric potentiator of AMPA receptors: 4--2-(phenylsulfonylamino)ethylthio--2,6-difluoro-phenoxyaceta mide. J Neurosci 17, 5760-5771.

Sekiguchi M, Nishikawa K, Aoki S & Wada K. (2002). A desensitization-selective potentiator of AMPA-type glutamate receptors. British journal of pharmacology 136, 1033-1041.

Sekiguchi M, Yamada K, Jin J, Hachitanda M, Murata Y, Namura S, Kamichi S, Kimura I & Wada K. (2001). The AMPA receptor allosteric potentiator PEPA ameliorates post-ischemic memory impairment. Neuroreport 12, 2947-2950.

Semenov A, Moykkynen T, Coleman SK, Korpi ER & Keinanen K. (2012). Autoinactivation of the stargazin-AMPA receptor complex: subunit-dependency and independence from physical dissociation. PloS one 7, e49282.

Sensi SL, Paoletti P, Koh JY, Aizenman E, Bush AI & Hershfinkel M. (2011). The neurophysiology and pathology of brain zinc. J Neurosci 31, 16076-16085.

Shanks NF, Cais O, Maruo T, Savas JN, Zaika EI, Azumaya CM, Yates JR, 3rd, Greger I & Nakagawa T. (2014). Molecular dissection of the interaction between the AMPA receptor and cornichon homolog-3. J Neurosci 34, 12104-12120.

Shanks NF, Savas JN, Maruo T, Cais O, Hirao A, Oe S, Ghosh A, Noda Y, Greger IH, Yates JR, 3rd & Nakagawa T. (2012). Differences in AMPA and kainate receptor interactomes facilitate identification of AMPA receptor auxiliary subunit GSG1L. Cell reports 1, 590-598.

Shelley C & Cull-Candy SG. (2010). Desensitization and models of receptor-channel activation. J Physiol 588, 1395-1397.

Shen L, Liang F, Walensky LD & Huganir RL. (2000). Regulation of AMPA receptor GluR1 subunit surface expression by a 4. 1N-linked actin cytoskeletal association. J Neurosci 20, 7932-7940.

Shi Y, Lu W, Milstein AD & Nicoll RA. (2009). The stoichiometry of AMPA receptors and TARPs varies by neuronal cell type. Neuron 62, 633-640.

Shi Y, Suh YH, Milstein AD, Isozaki K, Schmid SM, Roche KW & Nicoll RA. (2010). Functional comparison of the effects of TARPs and cornichons on AMPA receptor trafficking and gating. Proc Natl Acad Sci U S A 107, 16315-16319.

Shinozaki H & Konishi S. (1970). Actions of several anthelmintics and insecticides on rat cortical neurones. Brain research 24, 368-371.

Sia GM, Beique JC, Rumbaugh G, Cho R, Worley PF & Huganir RL. (2007). Interaction of the N-terminal domain of the AMPA receptor GluR4 subunit with the neuronal pentraxin NP1 mediates GluR4 synaptic recruitment. Neuron 55, 87-102.

Sirrieh RE, MacLean DM & Jayaraman V. (2013). Amino-terminal domain tetramer organization and structural effects of zinc binding in the N-methyl-D-aspartate (NMDA) receptor. The journal of biological chemistry 288, 22555-22564.

Sirrieh RE, MacLean DM & Jayaraman V. (2015). A conserved structural mechanism of NMDA receptor inhibition: A comparison of ifenprodil and zinc. The journal of general physiology 146, 173-181.

Sladeczek F, Pin JP, Recasens M, Bockaert J & Weiss S. (1985). Glutamate stimulates inositol phosphate formation in striatal neurones. Nature 317, 717-719.

Smith TC & Howe JR. (2000). Concentration-dependent substate behavior of native AMPA receptors. Nature neuroscience 3, 992-997.

Sobolevsky AI, Rosconi MP & Gouaux E. (2009). X-ray structure, symmetry and mechanism of an AMPA-subtype glutamate receptor. Nature 462, 745-756.

Sommer B, Burnashev N, Verdoorn TA, Keinanen K, Sakmann B & Seeburg PH. (1992). A glutamate receptor channel with high affinity for domoate and kainate. The EMBO journal 11, 1651-1656.

Sommer B, Keinanen K, Verdoorn TA, Wisden W, Burnashev N, Herb A, Kohler M, Takagi T, Sakmann B & Seeburg PH. (1990). Flip and flop: a cell-specific functional switch in glutamate-operated channels of the CNS. Science 249, 1580-1585.

Sommer B, Kohler M, Sprengel R & Seeburg PH. (1991). RNA editing in brain controls a determinant of ion flow in glutamate-gated channels. Cell 67, 11-19.

Soto D, Coombs ID, Kelly L, Farrant M & Cull-Candy SG. (2007). Stargazin attenuates intracellular polyamine block of calcium-permeable AMPA receptors. Nature neuroscience 10, 1260-1267.

Soto F, Garcia-Guzman M, Gomez-Hernandez JM, Hollmann M, Karschin C & Stuhmer W. (1996). P2X4: an ATP-activated ionotropic receptor cloned from rat brain. Proc Natl Acad Sci U S A 93, 3684-3688.

Sourkes TL. (1991). Early clinical neurochemistry of CNS-active drugs. Bromides. Molecular and chemical neuropathology / sponsored by the International Society for Neurochemistry and the World Federation of Neurology and research groups on neurochemistry and cerebrospinal fluid 14, 131-142.

Srivastava M, Simakov O, Chapman J, Fahey B, Gauthier ME, Mitros T, Richards GS, Conaco C, Dacre M, Hellsten U, Larroux C, Putnam NH, Stanke M, Adamska M, Darling A, Degnan SM, Oakley TH, Plachetzki DC, Zhai Y, Adamski M, Calcino A, Cummins SF, Goodstein DM, Harris C, Jackson DJ, Leys SP, Shu S, Woodcroft BJ, Vervoort M, Kosik KS, Manning G, Degnan BM & Rokhsar DS. (2010). The Amphimedon queenslandica genome and the evolution of animal complexity. Nature 466, 720-726.

Standley S & Baudry M. (2000). The role of glycosylation in ionotropic glutamate receptor ligand binding, function, and trafficking. Cellular and molecular life sciences: CMLS 57, 1508-1516.

Stephenson RP. (1956). A modification of receptor theory. British journal of pharmacology and chemotherapy 11, 379-393.

Stern-Bach Y, Bettler B, Hartley M, Sheppard PO, O'Hara PJ & Heinemann SF. (1994). Agonist selectivity of glutamate receptors is specified by two domains structurally related to bacterial amino acid-binding proteins. Neuron 13, 1345-1357.

Stern-Bach Y, Russo S, Neuman M & Rosenmund C. (1998). A point mutation in the glutamate binding site blocks desensitization of AMPA receptors. Neuron 21, 907-918.

Stevens CF. (1972). Inferences about membrane properties from electrical noise measurements. Biophysical journal 12, 1028-1047.

Straub C, Hunt DL, Yamasaki M, Kim KS, Watanabe M, Castillo PE & Tomita S. (2011). Distinct functions of kainate receptors in the brain are determined by the auxiliary subunit Neto1. Nature neuroscience 14, 866-873.

Straub C, Zhang W & Howe JR. (2011). Neto2 modulation of kainate receptors with different subunit compositions. J Neurosci 31, 8078-8082.

Stuart GJ & Spruston N. (2015). Dendritic integration: 60 years of progress. Nature neuroscience 18, 1713-1721.

Stuhmer W, Conti F, Suzuki H, Wang XD, Noda M, Yahagi N, Kubo H & Numa S. (1989). Structural parts involved in activation and inactivation of the sodium channel. Nature 339, 597-603.

Sucher NJ, Akbarian S, Chi CL, Leclerc CL, Awobuluyi M, Deitcher DL, Wu MK, Yuan JP, Jones EG & Lipton SA. (1995). Developmental and regional expression pattern of a novel NMDA receptor-like subunit (NMDAR-L) in the rodent brain. J Neurosci 15, 6509-6520.

Sugiyama H, Ito I & Watanabe M. (1989). Glutamate receptor subtypes may be classified into two major categories: a study on Xenopus oocytes injected with rat brain mRNA. Neuron 3, 129-132.

Sumioka A, Brown TE, Kato AS, Bredt DS, Kauer JA & Tomita S. (2011). PDZ binding of TARP gamma-8 controls synaptic transmission but not synaptic plasticity. Nature neuroscience 14, 1410-1412.

Sun Y, Olson R, Horning M, Armstrong N, Mayer M & Gouaux E. (2002). Mechanism of glutamate receptor desensitization. Nature 417, 245-253.

Sun YJ, Rose J, Wang BC & Hsiao CD. (1998). The structure of glutamine-binding protein complexed with glutamine at 1.94 A resolution: comparisons with other amino acid binding proteins. Journal of molecular biology 278, 219-229.

Suzuki Y, Goetze TA, Stroebel D, Balasuriya D, Yoshimura SH, Henderson RM, Paoletti P, Takeyasu K & Edwardson JM. (2013). Visualization of structural changes accompanying activation of N-methyl-D-aspartate (NMDA) receptors using fast-scan atomic force microscopy imaging. The journal of biological chemistry 288, 778-784.

Swanson GT, Feldmeyer D, Kaneda M & Cull-Candy SG. (1996). Effect of RNA editing and subunit co-assembly single-channel properties of recombinant kainate receptors. J Physiol 492 (Pt 1), 129-142.

Swanson GT, Green T, Sakai R, Contractor A, Che W, Kamiya H & Heinemann SF. (2002). Differential activation of individual subunits in heteromeric kainate receptors. Neuron 34, 589-598.

Swanson GT, Kamboj SK & Cull-Candy SG. (1997). Single-channel properties of recombinant AMPA receptors depend on RNA editing, splice variation, and subunit composition. J Neurosci 17, 58-69.

Sweatt JD. (2016). Neural Plasticity & Behavior - Sixty Years of Conceptual Advances. Journal of neurochemistry (in press).

Tajima N, Karakas E, Grant T, Simorowski N, Diaz-Avalos R, Grigorieff N & Furukawa H. (2016). Activation of NMDA receptors and the mechanism of inhibition by ifenprodil. Nature 534, 63-68.

Tanabe Y, Masu M, Ishii T, Shigemoto R & Nakanishi S. (1992). A family of metabotropic glutamate receptors. Neuron 8, 169-179.

Tang CM, Dichter M & Morad M. (1989). Quisqualate activates a rapidly inactivating high conductance ionic channel in hippocampal neurons. Science 243, 1474-1477.

Tapken D, Anschutz U, Liu LH, Huelsken T, Seebohm G, Becker D & Hollmann M. (2013). A plant homolog of animal glutamate receptors is an ion channel gated by multiple hydrophobic amino acids. Science signaling 6, ra47.

Taschenberger H & von Gersdorff H. (2000). Fine-tuning an auditory synapse for speed and fidelity: developmental changes in presynaptic waveform, EPSC kinetics, and synaptic plasticity. J Neurosci 20, 9162-9173.

Terwilliger TC, Grosse-Kunstleve RW, Afonine PV, Moriarty NW, Zwart PH, Hung LW, Read RJ & Adams PD. (2008). Iterative model building, structure refinement and density modification with the PHENIX AutoBuild wizard. Acta crystallographica Section D, Biological crystallography 64, 61-69.

Tichelaar W, Safferling M, Keinanen K, Stark H & Madden DR. (2004). The Three-dimensional Structure of an Ionotropic Glutamate Receptor Reveals a Dimer-of-dimers Assembly. Journal of molecular biology 344, 435-442.

Tomita S. (2010). Regulation of ionotropic glutamate receptors by their auxiliary subunits. Physiology 25, 41-49.

Tomita S, Adesnik H, Sekiguchi M, Zhang W, Wada K, Howe JR, Nicoll RA & Bredt DS. (2005). Stargazin modulates AMPA receptor gating and trafficking by distinct domains. Nature 435, 1052-1058.

Tomita S, Chen L, Kawasaki Y, Petralia RS, Wenthold RJ, Nicoll RA & Bredt DS. (2003). Functional studies and distribution define a family of transmembrane AMPA receptor regulatory proteins. J Cell Biol 161, 805-816.

Tomita S, Shenoy A, Fukata Y, Nicoll RA & Bredt DS. (2007). Stargazin interacts functionally with the AMPA receptor glutamate-binding module. Neuropharmacology 52, 87-91.

Tovar KR, McGinley MJ & Westbrook GL. (2013). Triheteromeric NMDA receptors at hippocampal synapses. J Neurosci 33, 9150-9160.

Traynelis SF & Cull-Candy SG. (1990). Proton inhibition of N-methyl-D-aspartate receptors in cerebellar neurons. Nature 345, 347-350.

Traynelis SF, Hartley M & Heinemann SF. (1995). Control of proton sensitivity of the NMDA receptor by RNA splicing and polyamines. Science 268, 873-876.

Traynelis SF & Jaramillo F. (1998). Getting the most out of noise in the central nervous system. Trends Neurosci 21, 137-145.

Traynelis SF, Wollmuth LP, McBain CJ, Menniti FS, Vance KM, Ogden KK, Hansen KB, Yuan H, Myers SJ & Dingledine R. (2010). Glutamate receptor ion channels: structure, regulation, and function. Pharmacol Rev 62, 405-496.

Trimmer JS. (2015). Subcellular localization of K+ channels in mammalian brain neurons: remarkable precision in the midst of extraordinary complexity. Neuron 85, 238-256.

Trussell LO, Thio LL, Zorumski CF & Fischbach GD. (1988). Rapid desensitization of glutamate receptors in vertebrate central neurons. Proc Natl Acad Sci U S A 85, 4562-4566.

Trussell LO, Zhang S & Raman IM. (1993). Desensitization of AMPA receptors upon multiquantal neurotransmitter release. Neuron 10, 1185-1196.

Turetsky D, Garringer E & Patneau DK. (2005). Stargazin modulates native AMPA receptor functional properties by two distinct mechanisms. J Neurosci 25, 7438-7448.

Twomey EC, Yelshanskaya MV, Grassucci RA, Frank J & Sobolevsky AI. (2016). Elucidation of AMPA receptor-stargazin complexes by cryo-electron microscopy. Science 353, 83-86.

Unwin N, Toyoshima C & Kubalek E. (1988). Arrangement of the acetylcholine receptor subunits in the resting and desensitized states, determined by cryoelectron microscopy of crystallized Torpedo postsynaptic membranes. J Cell Biol 107, 1123-1138.

Ursby T, Unge J, Appio R, Logan DT, Fredslund F, Svensson C, Larsson K, Labrador A & Thunnissen MM. (2013). The macromolecular crystallography beamline I911-3 at the MAX IV laboratory. Journal of synchrotron radiation 20, 648-653.

Vandenberghe W, Nicoll RA & Bredt DS. (2005). Stargazin is an AMPA receptor auxiliary subunit. Proc Natl Acad Sci U S A 102, 485-490.

Venskutonyte R, Frydenvang K, Hald H, Rabassa AC, Gajhede M, Ahring PK & Kastrup JS. (2012). Kainate induces various domain closures in AMPA and kainate receptors. Neurochemistry international 61, 536-545.

Veran J, Kumar J, Pinheiro PS, Athane A, Mayer ML, Perrais D & Mulle C. (2012). Zinc potentiates GluK3 glutamate receptor function by stabilizing the ligand binding domain dimer interface. Neuron 76, 565-578.

Verdoorn TA, Burnashev N, Monyer H, Seeburg PH & Sakmann B. (1991). Structural determinants of ion flow through recombinant glutamate receptor channels. Science 252, 1715-1718.

Vicini S, Wang JF, Li JH, Zhu WJ, Wang YH, Luo JH, Wolfe BB & Grayson DR. (1998). Functional and pharmacological differences between recombinant N-methyl-D-aspartate receptors. Journal of neurophysiology 79, 555-566.

Vignes M & Collingridge GL. (1997). The synaptic activation of kainate receptors. Nature 388, 179-182.

Vijayan R, Plested AJ, Mayer ML & Biggin PC. (2009). Selectivity and cooperativity of modulatory ions in a neurotransmitter receptor. Biophysical journal 96, 1751-1760.

Villarroel A, Burnashev N & Sakmann B. (1995). Dimensions of the narrow portion of a recombinant NMDA receptor channel. Biophysical journal 68, 866-875.

Villarroel A, Regalado MP & Lerma J. (1998). Glycine-independent NMDA receptor desensitization: localization of structural determinants. Neuron 20, 329-339.

Volgraf M, Gorostiza P, Numano R, Kramer RH, Isacoff EY & Trauner D. (2006). Allosteric control of an ionotropic glutamate receptor with an optical switch. Nature chemical biology 2, 47-52.

Volianskis A, France G, Jensen MS, Bortolotto ZA, Jane DE & Collingridge GL. (2015). Long-term potentiation and the role of N-methyl-D-aspartate receptors. Brain research 1621, 5-16.

von Engelhardt J, Mack V, Sprengel R, Kavenstock N, Li KW, Stern-Bach Y, Smit AB, Seeburg PH & Monyer H. (2010). CKAMP44: a brain-specific protein attenuating short-term synaptic plasticity in the dentate gyrus. Science 327, 1518-1522.

Vyklicky L, Jr., Benveniste M & Mayer ML. (1990). Modulation of N-methyl-D-aspartic acid receptor desensitization by glycine in mouse cultured hippocampal neurones. J Physiol 428, 313-331.

Vyklicky L, Jr., Patneau DK & Mayer ML. (1991). Modulation of excitatory synaptic transmission by drugs that reduce desensitization at AMPA/kainate receptors. Neuron 7, 971-984.

Walch-Liu P, Liu LH, Remans T, Tester M & Forde BG. (2006). Evidence that L-glutamate can act as an exogenous signal to modulate root growth and branching in Arabidopsis thaliana. Plant & cell physiology 47, 1045-1057.

Watanabe S, Kusama-Eguchi K, Kobayashi H & Igarashi K. (1991). Estimation of polyamine binding to macromolecules and ATP in bovine lymphocytes and rat liver. The journal of biological chemistry 266, 20803-20809.

Watkins JC & Evans RH. (1981). Excitatory amino acid transmitters. Annual review of pharmacology and toxicology 21, 165-204.

Werner P, Voigt M, Keinanen K, Wisden W & Seeburg PH. (1991). Cloning of a putative high-affinity kainate receptor expressed predominantly in hippocampal CA3 cells. Nature 351, 742-744.

Westbrook GL & Mayer ML. (1987). Micromolar concentrations of Zn2+ antagonize NMDA and GABA responses of hippocampal neurons. Nature 328, 640-643.

Weston MC, Schuck P, Ghosal A, Rosenmund C & Mayer ML. (2006). Conformational restriction blocks glutamate receptor desensitization. Nature structural & molecular biology 13, 1120-1127.

Whitlock JR, Heynen AJ, Shuler MG & Bear MF. (2006). Learning induces long-term potentiation in the hippocampus. Science 313, 1093-1097.

Wilding TJ, Chai YH & Huettner JE. (1998). Inhibition of rat neuronal kainate receptors by cis-unsaturated fatty acids. J Physiol 513 (Pt 2), 331-339.

Wilding TJ, Fulling E, Zhou Y & Huettner JE. (2008). Amino acid substitutions in the pore helix of GluR6 control inhibition by membrane fatty acids. The journal of general physiology 132, 85-99.

Wilding TJ & Huettner JE. (1995). Differential antagonism of alpha-amino-3-hydroxy-5-methyl-4- isoxazolepropionic acid-preferring and kainate-preferring receptors by 2,3-benzodiazepines. Molecular pharmacology 47, 582-587.

Wilding TJ, Zhou Y & Huettner JE. (2005). Q/R site editing controls kainate receptor inhibition by membrane fatty acids. J Neurosci 25, 9470-9478.

Williams K. (1993). Ifenprodil discriminates subtypes of the N-methyl-D-aspartate receptor: selectivity and mechanisms at recombinant heteromeric receptors. Molecular pharmacology 44, 851-859.

Williams K. (1996). Separating dual effects of zinc at recombinant N-methyl-D-aspartate receptors. Neuroscience letters 215, 9-12.

Winn MD, Ballard CC, Cowtan KD, Dodson EJ, Emsley P, Evans PR, Keegan RM, Krissinel EB, Leslie AG, McCoy A, McNicholas SJ, Murshudov GN, Pannu NS, Potterton EA, Powell HR, Read RJ, Vagin A & Wilson KS. (2011). Overview of the CCP4 suite and current developments. Acta crystallographica Section D, Biological crystallography 67, 235-242.

Wisden W & Seeburg PH. (1993). A complex mosaic of high-affinity kainate receptors in rat brain. J Neurosci 13, 3582-3598.

Wo ZG & Oswald RE. (1995). Unraveling the modular design of glutamate-gated ion channels. Trends Neurosci 18, 161-168.

Wollmuth LP & Sakmann B. (1998). Different mechanisms of Ca2+ transport in NMDA and Ca2+-permeable AMPA glutamate receptor channels. The journal of general physiology 112, 623-636.

Wollmuth LP & Sobolevsky AI. (2004). Structure and gating of the glutamate receptor ion channel. Trends Neurosci 27, 321-328.

Wong AY, Fay AM & Bowie D. (2006). External ions are coactivators of kainate receptors. J Neurosci 26, 5750-5755.

Wong AY, MacLean DM & Bowie D. (2007). Na+/Cl- dipole couples agonist binding to kainate receptor activation. J Neurosci 27, 6800-6809.

Wu TY, Liu CI & Chang YC. (1996). A study of the oligomeric state of the alpha-amino-3-hydroxy-5-methyl-4-isoxazolepropionic acid-preferring glutamate receptors in the synaptic junctions of porcine brain. The Biochemical journal 319 (Pt 3), 731-739.

Yamada KA, Hill MW, Hu Y & Covey DF. (1998). The diazoxide derivative 7-chloro-3-methyl-3,4-dihydro-2H-1,2,4-benzothiadiazine-S,S-dioxide augments AMPA- and GABA-mediated synaptic responses in cultured hippocampal neurons. Neurobiology of disease 5, 196-205.

Yamada KA & Tang CM. (1993). Benzothiadiazides inhibit rapid glutamate receptor desensitization and enhance glutamatergic synaptic currents. J Neurosci 13, 3904-3915.

Yamazaki M, Ohno-Shosaku T, Fukaya M, Kano M, Watanabe M & Sakimura K. (2004). A novel action of stargazin as an enhancer of AMPA receptor activity. Neuroscience research 50, 369-374.

Yan D & Tomita S. (2012). Defined criteria for auxiliary subunits of glutamate receptors. J Physiol 590, 21-31.

Yan S, Sanders JM, Xu J, Zhu Y, Contractor A & Swanson GT. (2004). A C-terminal determinant of GluR6 kainate receptor trafficking. J Neurosci 24, 679-691.

Yelshanskaya MV, Li M & Sobolevsky AI. (2014). Structure of an agonist-bound ionotropic glutamate receptor. Science 345, 1070-1074.

Yelshanskaya MV, Saotome K, Singh AK & Sobolevsky AI. (2016). Probing Intersubunit Interfaces in AMPA-subtype Ionotropic Glutamate Receptors. Scientific reports 6, 19082.

Yelshanskaya MV, Singh AK, Sampson JM, Narangoda C, Kurnikova M & Sobolevsky AI. (2016). Structural Bases of Noncompetitive Inhibition of AMPA-Subtype Ionotropic Glutamate Receptors by Antiepileptic Drugs. Neuron 91, 1305-1315.

Yu A, Alberstein R, Thomas A, Zimmet A, Grey R, Mayer ML & Lau AY. (2016). Molecular lock regulates binding of glycine to a primitive NMDA receptor. Proc Natl Acad Sci U S A 113, E6786-E6795.

Yuan H, Hansen KB, Vance KM, Ogden KK & Traynelis SF. (2009). Control of NMDA receptor function by the NR2 subunit amino-terminal domain. J Neurosci 29, 12045-12058.

Yuan H, Myers SJ, Wells G, Nicholson KL, Swanger SA, Lyuboslavsky P, Tahirovic YA, Menaldino DS, Ganesh T, Wilson LJ, Liotta DC, Snyder JP & Traynelis SF. (2015). Context-dependent GluN2B-selective inhibitors of NMDA receptor function are neuroprotective with minimal side effects. Neuron 85, 1305-1318.

Yuzaki M. (2003). The delta2 glutamate receptor: 10 years later. Neuroscience research 46, 11-22.

Yuzaki M. (2012). The ins and outs of GluD2--why and how Purkinje cells use the special glutamate receptor. Cerebellum 11, 438-439.

Zhang W, Cho Y, Lolis E & Howe JR. (2008). Structural and single-channel results indicate that the rates of ligand binding domain closing and opening directly impact AMPA receptor gating. J Neurosci 28, 932-943.

Zhang W, Devi SP, Tomita S & Howe JR. (2014). Auxiliary proteins promote modal gating of AMPA- and kainate-type glutamate receptors. Eur J Neurosci 39, 1138-1147.

Zhang W, Robert A, Vogensen SB & Howe JR. (2006). The relationship between agonist potency and AMPA receptor kinetics. Biophysical journal 91, 1336-1346.

Zhang W, St-Gelais F, Grabner CP, Trinidad JC, Sumioka A, Morimoto-Tomita M, Kim KS, Straub C, Burlingame AL, Howe JR & Tomita S. (2009). A transmembrane accessory subunit that modulates kainate-type glutamate receptors. Neuron 61, 385-396.

Zhang Y, Nayeem N, Nanao MH & Green T. (2006). Interface interactions modulating desensitization of the kainate-selective ionotropic glutamate receptor subunit GluR6. J Neurosci 26, 10033-10042.

Zhao H, Berger AJ, Brown PH, Kumar J, Balbo A, May CA, Casillas E, Jr., Laue TM, Patterson GH, Mayer ML & Schuck P. (2012). Analysis of high-affinity assembly for AMPA receptor amino-terminal domains. The journal of general physiology 139, 371-388.

Zhao Y, Chen S, Yoshioka C, Baconguis I & Gouaux E. (2016). Architecture of fully occupied GluA2 AMPA receptor-TARP complex elucidated by cryo-EM. Nature (in press).

Zheng CY, Seabold GK, Horak M & Petralia RS. (2011). MAGUKs, synaptic development, and synaptic plasticity. The Neuroscientist 17, 493-512.

Zhu S, Stein RA, Yoshioka C, Lee CH, Goehring A, McHaourab HS & Gouaux E. (2016). Mechanism of NMDA Receptor Inhibition and Activation. Cell 165, 704-714.

Zivkovic I, Thompson DM, Bertolino M, Uzunov D, DiBella M, Costa E & Guidotti A. (1995). 7-Chloro-3-methyl-3-4-dihydro-2H-1,2,4 benzothiadiazine S,S-dioxide (IDRA 21): a benzothiadiazine derivative that enhances cognition by attenuating DL-alpha-amino-2,3-dihydro-5-methyl-3-oxo-4-isoxazolepropanoic acid (AMPA) receptor desensitization. The journal of pharmacology and experimental therapeutics 272, 300-309.

Zuo J, De Jager PL, Takahashi KA, Jiang W, Linden DJ & Heintz N. (1997). Neurodegeneration in Lurcher mice caused by mutation in delta2 glutamate receptor gene. Nature 388, 769-773.

PART IV:

APPENDICES

APPENDIX I:

Retour aux sources:

defining the structural basis of glutamate

receptor activation

FOREWORD TO APPENDIX ONE

In his position as an Editor at the *Journal of Physiology*, Derek helped put together a special issue of the journal with several review articles detailing different aspects of iGluR biophysics. A catalyst for the issue was the first annual glutamate receptor retreat in 2013, where many notable researchers within the field had a chance to share their perspectives. Given the recent publications from our lab on the role of KAR dimer interface in activation (Daniels et al., 2013; Dawe et al., 2013, results chapter 1) we decided to prepare our own review article, highlighting advances in the structural understanding of iGluR gating processes. The article starts as a historical narrative, featuring many of the same ideas relayed in the literature review at the start of this thesis. The latter half of the article focusses more on work from our lab, though it concludes by referencing some ongoing questions generated by structural studies of intact AMPARs and KARs (i.e. Durr et al., 2014; Meyerson et al., 2014), which had just been published as we were about to submit the manuscript. Ultimately, the review is not a definitive guide to iGluR structure and function, but it certainly touches upon many important ideas that have motivated the experiments I performed throughout my PhD studies.

Appendix I, Article Title:

Retour aux sources:

defining the structural basis of glutamate receptor activation

JPn Neuroscience

The Journal of Physiology

J Physiol 0.0 (2014) pp 1–14

TOPICAL REVIEW

Retour aux sources: defining the structural basis of glutamate receptor activation

G. Brent Dawe[1,3], Mark R. Aurousseau[2,3], Bryan A. Daniels[3] and Derek Bowie[3]

[1] *Integrated Program in Neuroscience, McGill University, Montréal, Québec, Canada*
[2] *Graduate Program in Pharmacology, McGill University, Montréal, Québec, Canada*
[3] *Department of Pharmacology and Therapeutics, McGill University, Montréal, Québec, Canada*

Abstract Ionotropic glutamate receptors (iGluRs) are the major excitatory neurotransmitter receptor in the vertebrate CNS and, as a result, their activation properties lie at the heart of much of the neuronal network activity observed in the developing and adult brain. iGluRs have also been implicated in many nervous system disorders associated with postnatal development (e.g. autism, schizophrenia), cerebral insult (e.g. stroke, epilepsy), and disorders of the ageing brain (e.g. Alzheimer's disease, Parkinsonism). In view of this, an emphasis has been placed on understanding how iGluRs activate and desensitize in functional and structural terms. Early structural models of iGluRs suggested that the strength of the agonist response was primarily governed by the degree of closure induced in the ligand-binding domain (LBD). However, recent studies have suggested a more nuanced role for the LBD with current evidence identifying the iGluR LBD interface as a "hotspot" regulating agonist behaviour. Such ideas remain to be consolidated with recently solved structures of full-length iGluRs to account for the global changes that underlie channel activation and desensitization.

(Received 20 May 2014; accepted after revision 5 September 2014; first published online 12 September 2014)
Corresponding author D. Bowie: Department of Pharmacology and Therapeutics, Bellini Building, Room 164, McGill University, 3649 Promenade Sir William Osler, Montreal, Québec, Canada H3G 0B1. Email: derek.bowie@mcgill.ca

Abbreviations AMPA, α-amino-3-hydroxy-5-methyl-4-isoxazolepropionic acid; AMPAR, AMPA receptor; ATD, amino terminal domain; ED, extracellular domain; GlnBP, glutamine binding protein; iGluR, ionotropic glutamate receptor; KA, kainate; KAR, kainate receptor; LBD, ligand binding domain; L-Glu, L-glutamate; mGluR, metabotropic glutamate receptor; NMDA, *N*-methyl D-aspartate; NMDAR, NMDA receptor; QA, quisqualate; TARP, transmembrane AMPA receptor regulatory protein; TM, transmembrane domain.

Introduction

Fast excitatory neurotransmission in the vertebrate CNS is mediated by a class of plasma membrane-bound, multimeric proteins called ionotropic glutamate receptors (iGluRs). iGluRs assemble as tetramers from subunits encoded by eighteen genes that are divided into three major subgroups, based on their differential sensitivities to the agonists *N*-methyl D-aspartate (NMDAs), α-amino-3-hydroxy-5-methyl-4-isoxazolepropionic acid (AMPAs) and kainate (KAs) (Nakanishi, 1992; Seeburg, 1993; Hollmann & Heinemann, 1994; Collingridge *et al.*

Derek Bowie is the Director of the FRQS (Fonds de recherche du Québec – Santé) research group GEPROM and has been a professor at McGill University in Montréal since 2002. His lab focuses on the structure–function properties of ionotropic glutamate receptors and $GABA_A$ receptors, as well as their role in neuronal circuit behaviour. Dr Bowie completed his doctoral work at the University of London followed by postdoctoral training in France (Université Louis Pasteur), Switzerland (University of Zurich) and the USA (National Institutes of Health) before holding a faculty position at Emory University in Atlanta. **G. Brent Dawe** is a PhD candidate in McGill's Integrated Program in Neuroscience and recipient of an NSERC doctoral scholarship. He obtained his BSc in Biology at the University of Ontario Institute of Technology, where he completed an Honours thesis project with Dr Sean Forrester. His research in the Bowie lab concerns the mechanisms of glutamate receptor activation and desensitization.

DOI: 10.1113/jphysiol.2014.277921

2009), while a fourth, orphan group, comprising the δ subunits, does not appear to form functional ion-conducting channels (Yuzaki, 2003).

At central synapses, iGluRs respond to the transient presence of the neurotransmitter L-glutamate (L-Glu) in the synaptic cleft through a series of binding and conformational steps that lead to membrane depolarization by the opening of a cation-permeable transmembrane pore (Dingledine *et al.* 1999; Traynelis *et al.* 2010; Huettner, 2014). Although iGluRs are often found together in the postsynaptic membrane, their global distribution and specific functions differ. The rapid millisecond activation of AMPA receptors (AMPARs) allows them to facilitate postsynaptic depolarization, which is also a necessary first step in relieving tonic Mg^{2+} block of NMDA receptors (NMDARs) (MacDonald & Nowak, 1990). Once unblocked, NMDARs affect neuronal signalling by transporting extracellular Ca^{2+} into the cytoplasm, a process prolonged by the slow intrinsic gating properties of these receptors (Qian & Johnson, 2002; Paoletti *et al.* 2013). In contrast, kainate receptors (KARs) are thought to fulfil more of a modulatory role on synaptic transmission, acting from both pre- and postsynaptic locales via ionotropic and metabotropic signalling mechanisms (Huettner, 2003; Contractor *et al.* 2011; Lerma & Marques, 2013). Curiously, the orphan-class δ iGluRs exhibit a much restricted expression pattern in the CNS with their most notable role in cerebellar Purkinje cells, where they regulate synaptic plasticity and synaptogenesis via a non-ionotropic pathway (Yuzaki, 2012).

Over the past decade, a wealth of structural information on iGluRs has emerged, describing the topology and assembly of domains (Gouaux, 2004; Mayer, 2011; Sobolevsky, 2013). Importantly, insight into their structural properties is expected to have a significant impact in the long term, as we start to unravel how iGluRs are implicated in several prominent CNS disorders (Bowie, 2008) and continue the rational design of therapeutic compounds (Lipton, 2006; Sanacora *et al.* 2008; Santangelo *et al.* 2012; Pirotte *et al.* 2013). Despite this, our understanding of the basic events that lead to iGluR activation is still emerging. In this review, we re-examine this issue and highlight recent studies that place a greater emphasis on the iGluR ligand binding domain (LBD) dimer interface as a 'hotspot' of channel activation. Particular emphasis will be placed on AMPARs and KARs, as more structural information is available for these families than NMDARs. With the recent elucidation of (near) full-length, tetrameric AMPAR structures in several conformations (Dürr *et al.* 2014; Meyerson *et al.* 2014; Yelshanskaya *et al.* 2014), a more complete understanding of iGluRs will require a multidisciplinary approach that brings together functional and structural data with dynamic simulations of protein movement.

iGluR pharmacology and channel activation

By the mid-1980s it was accepted that iGluRs exist as pharmacologically distinct receptor families (for reviews see Watkins & Evans, 1981; McLennan, 1983; Mayer & Westbrook, 1987; Collingridge & Lester, 1989), though their rapid, millisecond time course of activation and inactivation was only fully appreciated with the application of the concentration-clamp technique (reviewed in Akaike, 1995). The use of the concentration-clamp permitted the first detailed kinetic analysis of iGluR channel kinetics in response to rapid agonist application. Typical exchange rates in whole-cell recording conditions were about 10 ms using stepper motors (Vyklicky *et al.* 1990), while sub-millisecond (300–500 μs) exchange was achieved in outside-out patch recordings with the help of a piezo translator (Jonas, 1995). Since exchange rates in whole-cell recordings are markedly slower than AMPAR or KAR gating kinetics, peak agonist responses can only be measured with accuracy in excised patches (see discussion in Bowie *et al.* 2003).

Using concentration-clamp recordings, it was demonstrated that native AMPAR/KARs expressed by rodent hippocampal neurons exhibited two distinct kinetic phenotypes in response to agonists: rapid desensitization with the neurotransmitter L-Glu or quisqualate (QA) and a non-desensitizing or non-decaying profile with kainate (KA) (Kiskin *et al.* 1986). Kinetic models developed to explain this behaviour proposed that KA binds to the desensitized state of AMPAR/KARs with lower affinity than L-Glu, QA or AMPA (Patneau & Mayer, 1991) (Fig. 1*A* and *B*). In keeping with this, the use of the benzothiadiazine diuretic, cyclothiazide, to attenuate receptor desensitization potentiated equilibrium responses elicited by KA much less than L-Glu (Patneau *et al.* 1993). Analysis of a more extensive range of receptor ligands, including sulfur-containing amino acids and willardiine derivatives, further established that neuronal AMPAR/KARs responded in an agonist-dependent manner (Patneau & Mayer, 1990; Patneau *et al.* 1992), presumably due to the varying degrees of desensitization (Fig. 1*C*). To complicate matters further, single-channel recordings demonstrated that KA primarily activated a low conductance open state, whereas L-Glu or QA gated channels with a much larger unitary conductance(s) (Ascher & Nowak, 1988; Cull-Candy & Usowicz, 1989; Tang *et al.* 1989). Although it was debated whether KA may activate distinct receptor families from L-Glu and QA (Cull-Candy & Usowicz, 1987; Jahr & Stevens, 1987), cross-desensitization experiments on native receptors (Kiskin *et al.* 1986; Patneau & Mayer, 1991) and the cloning of AMPAR receptor subunits (Hollmann *et al.* 1989; Keinanen *et al.* 1990) confirmed that different agonists gate the AMPAR channel pore in quite distinct ways. At NMDARs, gating

behaviour was revealed to be more complicated in that the binding of not one but two neurotransmitters, namely L-Glu as well as the inhibitory transmitter glycine, were required for activation (Johnson & Ascher, 1987; Kleckner & Dingledine, 1988). In this regard, KARs were more comparable to AMPARs, though studies of native receptors (Huettner, 1990; Lerma *et al.* 1993) and receptor clones (Egebjerg *et al.* 1991) revealed that KA elicited a strongly desensitizing response. As discussed below, an ongoing challenge has been to develop structural models of iGluR activation that can account for many of these complications. The first steps in this process began with the study of recombinant iGluRs.

Early insights into the topology of the agonist binding site

The cloning of the many genes that encode iGluR subunits (Nakanishi, 1992; Seeburg, 1993; Hollmann & Heinemann, 1994) permitted a detailed characterization not only of their functional properties, but also led the way to obtaining structural information (Madden, 2002; Gouaux, 2004; Mayer & Armstrong, 2004). Sequence analysis of the earliest cloned iGluRs revealed a large (approximately 500 amino acid) extracellular domain (ED), while overall amino acid sequence identity ranged from about 70% between AMPARs (Keinanen *et al.* 1990), down to 40% and 25% when they were compared to KARs and NMDARs, respectively (Bettler *et al.* 1990; Moriyoshi *et al.* 1991). Interestingly, a 100 amino acid segment of the ED just prior to the first predicted transmembrane domain (TM 1) shared 30% sequence identity with the bacterial periplasmic glutamine binding protein (GlnBP) (Nakanishi *et al.* 1990; Moriyoshi *et al.* 1991). The cloning of the first metabotropic glutamate receptors (mGluRs) revealed that these proteins also possess an approximately 500–600 residue ED (Masu *et al.* 1991; Tanabe *et al.* 1992), but retained significant homology within only two shorter, discontinuous segments (Masu *et al.* 1991). Through more refined sequence analysis techniques, it was later appreciated that iGluRs have two distinct EDs. The first, now referred to as the amino terminal domain (ATD), is homologous to the mGluR ED and the bacterial leucine-isoleucine-valine binding protein (LIVBP), while the second, now referred to as the ligand binding domain (LBD), is homologous to the GlnBP (O'Hara *et al.* 1993). At the time, X-ray crystal structural information was available for LIVBP (Adams & Oxender, 1989; Quiocho, 1990).

Drawing upon this structural information led research groups to use distinct, but complementary approaches to conclude that the agonist specificity of iGluRs and mGluRs is governed by two discontinuous segments of amino acid residues located in the extracellular domain (ED). For mGluRs, molecular modelling techniques were used to construct a homology model of mGluR1, which was then validated by assessing the impact of mutating conserved residues on agonist selectivity (O'Hara *et al.* 1993). For iGluRs, the replacement of native glycosylation sites with mutant sites was exploited to determine a topology of three membrane-spanning domains (TM 1, 3 and 4) with a re-entrant loop (TM 2) in between (Hollmann *et al.* 1994). From this framework, chimeric receptors (generated by swapping extracellular regions of GluA3 AMPARs and GluK2 KARs) were used to verify that two separate domains confer agonist selectivity (Stern-Bach *et al.* 1994). These domains were subsequently named S1 for the amino acid residues prior to transmembrane region 1 (TM 1) and S2 for residues between TM 3 and 4. The structural elucidation of an *E. coli* GlnBP (Hsiao *et al.* 1996) further established the unexpected link between the structural motifs of bacterial periplasmic transport proteins and neurotransmitter receptors expressed in the vertebrate CNS (Paas, 1998).

Two final observations led the way in permitting the resolution of the iGluR agonist/ligand binding site at

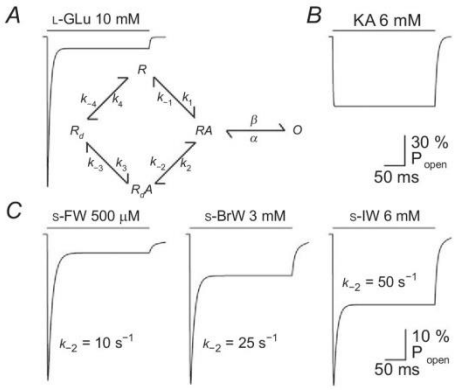

Figure 1. A cyclic gating model recreates AMPAR responses to willardiine series agonists
A, simulated response of AMPARs to L-Glu, generated from a five-state cyclic gating model (Patneau & Mayer, 1991). R, RA, R_d, and O represent resting, agonist-bound, desensitized, and open-channel states of the receptor, respectively. The rate constants for state transitions with L-Glu are adapted from values in another study (Vyklicky *et al.* 1991). *B* and *C*, simulated responses of AMPARs to KA (*B*), as well as to the willardiine series agonists, *S*-5-fluorowillardiine (s-FW), *S*-5-bromowillardiine (s-BrW), and *S*-5-iodowillardiine (s-IW) (*C*). As the halogen substituent increases in size, the equilibrium to peak current ratio recorded from AMPAR/KARs in hippocampal neurons also increases. To recapitulate this effect, the rate constant k_{-2} was increased, while k_{-1} and k_{-3} were adjusted to maintain microscopic reversibility. The rate constants are adapted from published values (Patneau *et al.* 1992), except for the s-BrW simulation, in which values were assigned to reproduce experimental observations.

atomic-level resolution. First, a truncated fusion protein consisting of the S1 and S2 domains of the GluA4 AMPAR, separated by a linker peptide, was shown to exhibit near-identical pharmacological properties to its wild-type counterpart (Kuusinen *et al.* 1995); a strategy that was exploited to obtain large quantities of the GluA2 AMPAR LBD for crystallographic analysis (Chen & Gouaux, 1997). Second, the upper and lower lobes were proposed to act in a 'Venus flytrap' arrangement (Mano *et al.* 1996), which helped further conceptualization of how the iGluR ligand binding cleft might trigger the process of channel activation.

A structural model of agonist efficacy

A new era in the study of iGluRs was heralded when Armstrong and colleagues solved the first high-resolution structure of a LBD; in this case it was the GluA2 AMPAR in complex with KA (Armstrong *et al.* 1998). As anticipated from earlier studies, the GluA2 structure was remarkably similar to that of the *E. coli* GlnBP (Sun *et al.* 1998), with the ligand binding cleft formed between two α-helix- and β-sheet-containing domains that were subsequently named D1 and D2 for the upper and lower lobes, respectively. Appreciating this structural similarity, the authors concluded that the GluA2–KA complex represented a partially closed structure, since the degree of domain closure was intermediate relative to GlnBP's open and closed conformations (Armstrong *et al.* 1998). Given this, they correctly predicted that further domain closure would be possible with different ligands, such as AMPA, with the rearrangement of a few key residues being required to accommodate the ligand. Interestingly, despite the overall low degree of sequence homology amongst iGluR family members, all seven residues that form direct contacts with KA in the structure were shown to be either identical or conservatively substituted, further underlining the importance of keeping these contact points as functionally diverse iGluR subtypes emerged during evolution.

Following this initial study, additional structures of the GluA2 AMPAR LBD in either apo, antagonist-bound (6,7-dinitroquinoxaline-2,3-dione, or DNQX), or agonist-bound (e.g. glutamate, AMPA and kainate) (Fig. 2*A*) conformations were described, which enabled comparisons to be made concerning what rearrangements of the LBD occur for different ligands (Armstrong & Gouaux, 2000; Hogner *et al.* 2002; Jin *et al.* 2002; Armstrong *et al.* 2003). Specifically, what distinguishes an agonist that opens the channel pore from an antagonist that does not? One measure that appeared to correlate well with agonist responsiveness was the angle of LBD closure formed by lobes D1 and D2 around the ligand binding cleft (relative to the apo structure), ranging from about 20 deg for the full agonist L-Glu to 5 deg for the antagonist DNQX (Armstrong & Gouaux, 2000). In support of the cleft closure hypothesis, a relationship between LBD closure, efficacy, and agonist response (in the presence of cyclothiazide, but see below for more details) held for a series of willardiine agonists, each with a different halogen-substituted group at the same position (Jin *et al.* 2003) (Fig. 2*B* and *C*). As predicted, the larger the halogen atom, the less closure around the agonist could be observed in structures, accounting for the lower weighted channel conductance and reduced efficacy seen in electrophysiological experiments (Jin *et al.* 2003). Taken together, all of these studies helped establish the idea that the degree of agonist-induced domain closure determines the extent of receptor activation and thus may represent the structural basis of agonist efficacy.

The need for a revised model of agonist efficacy

In subsequent years, high resolution structures of the LBD of KARs, NMDARs and orphan-class iGluRs were also described, in almost all cases, using the same approach as successfully applied to GluA2 AMPARs (Furukawa & Gouaux, 2003; Mayer, 2005; Naur *et al.* 2007) (though see Nanao *et al.* 2005). However, additional structural analyses of the three functional iGluR families has shown that full cleft closure can in fact be induced by partial agonists, and even antagonists. Structures of a GluA2 mutant for which AMPA becomes a partial agonist captured the AMPA-bound LBD cleft in intermediate, as well as fully closed conformations (Armstrong *et al.* 2003). Concurrently, the first structures of the GluN1 NMDAR subunit (Furukawa & Gouaux, 2003; Inanobe *et al.* 2005) indicated similar cleft closure for full and partial agonists, contrary to the model of agonist behaviour proposed for AMPARs. Moreover, although the initial structural analysis of GluK1 KARs suggested a close correlation between the degree of LBD closure and agonist behaviour (Mayer, 2005), subsequent work suggested that a more complicated relationship was at play (Fay *et al.* 2009; Frydenvang *et al.* 2009). This finding was not entirely surprising since earlier work had already established that external Na^+ and Cl^- ions profoundly affected the KAR agonist response (Bowie, 2002; Bowie & Lange, 2002; Wong *et al.* 2006) by binding to discrete sites at the interface between subunits (Plested & Mayer, 2007; Plested *et al.* 2008; Bowie, 2010) (see below). Taken together, these studies suggested that the structural basis of agonist behaviour was different between iGluR family members and/or that the initial structural model of agonist action at AMPARs needed further refinement.

On that note, Robert and colleagues addressed this issue through a series of structural and functional experiments that examined the impact of mutating a single amino-acid

residue (i.e. T686A) that was expected to destabilize the closed conformation of the GluA2 AMPAR ligand binding cleft (Robert *et al.* 2005). Importantly, the authors were later able to more directly examine agonist efficacy by studying AMPARs at the single-channel level, taking into account sub-conductance levels. These studies suggested a model whereby more efficacious agonists can better stabilize the closed conformation of a dynamic ligand binding cleft (Zhang *et al.* 2008), an idea that has also been used to explain agonist behaviour at KARs (Maclean *et al.* 2011). In agreement, spectroscopic measurements of the willardiine-bound GluA2 S1S2 constructs pinpointed specific residues in the cleft that undergo dynamic motions correlated with agonist potency (Fenwick & Oswald, 2008). Thus, variations in cleft stability could potentially explain why crystal structures might capture this domain in multiple – and sometimes unexpected – conformations given the nature of the agonist or antagonist being examined. Such structures capture low energy states and poorly reflect stochastic processes that underlie channel gating (Lau & Roux, 2007). An alternative to the cleft closure paradigm proposed in recent studies is that other movements influence efficacy. In particular, the need to evaluate ligand-induced conformational changes in three dimensions has been emphasized (Birdsey-Benson *et al.* 2010) and at multiple locations, including the LBD dimer interface (Nayeem *et al.* 2011). As explained below, there has been a renewed focus on the dimer interface in determining agonist efficacy, particularly in KARs, where a novel role for the cation binding pocket has been identified.

Agonist efficacy, desensitization, and the LBD dimer interface

Although much emphasis was placed on relating conformations of iGluR LBDs to activation, it was also appreciated that subunits assemble back-to-back as a dimer of dimers (Armstrong & Gouaux, 2000; Tichelaar *et al.* 2004). Interactions between subunits along the LBD dimer interface are thought to remodel upon activation

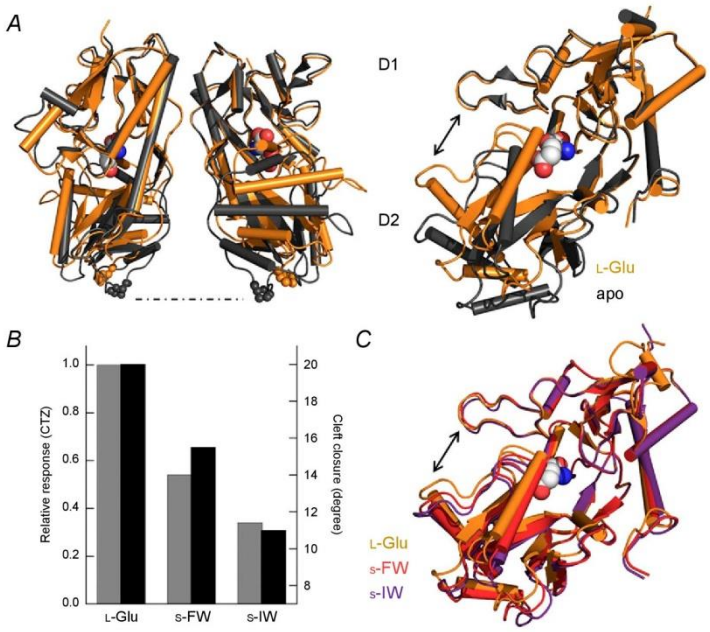

Figure 2. Agonist efficacy correlates with closure of the GluA2 ligand binding cleft
A, side view of the GluA2 LBD with apo (protein data bank (PDB) 1FTO) and L-Glu-bound (PDB 1FTJ) structures overlaid (left). The residue P632, found at the base of the D2 domain, is emphasized to illustrate how this region lifts up and separates upon agonist binding. Visualization of a single subunit highlights how the cleft between D1 and D2 is narrowed in the L-Glu-bound structure (right). *B* and *C*, in the presence of the allosteric modulator cyclothiazide (CTZ) to attenuate desensitization, agonist responsiveness correlates to the degree of closure between D1 and D2 at the ligand binding cleft. For example, willardiine series agonists with smaller halogen substituents were more efficacious and produced a greater degree of cleft closure. (Jin *et al.* 2003).

and desensitization (Fig. 3). Activation is proposed to lift apart the lower D2 lobes of the interface, while desensitization is proposed to reflect the rupture of cross-interface interactions as the upper D1 lobes separate (Sun *et al.* 2002) (Fig. 3). This structural arrangement is also significant from a functional perspective, since it helps explain the onset and recovery from AMPAR desensitization, which occurs in two sequential, kinetic steps (Robert *et al.* 2001; Bowie & Lange, 2002). This model emerged in part because the binding site for the cyclothiazide, and location of the leucine to tyrosine (L–Y) mutation, both of which strongly attenuate AMPAR desensitization (Patneau *et al.* 1993; Stern-Bach *et al.* 1998), are situated where subunits are predicted to come together. Accordingly, studies of the LBD dimer interface have often examined how individual residues affect the kinetics of desensitization (Horning & Mayer, 2004), with less attention paid to their role in agonist efficacy. However, other studies show that mutations along the KAR interface affect the relative efficacies of L-Glu and KA (Fleck *et al.* 2003; Zhang *et al.* 2006; Maclean *et al.* 2011), in addition to the time course of desensitization. Comparisons of agonist behaviour at GluA2 AMPARs in conditions with desensitization present or attenuated (in the presence of cyclothiazide or atop the L–Y mutation) even suggested that desensitization generally inverts the rank order of efficacy (Jin *et al.* 2003; Holm *et al.* 2005).

In light of evidence linking the LBD dimer interface to desensitization, experiments were designed to directly test if it was possible to trap AMPARs or KARs into specific conformational states (i.e. active or desensitized) by introducing disulphide bonds via cysteine residues on opposing sides of the dimer interface to restrict protein movement (Armstrong *et al.* 2006; Priel *et al.* 2006; Weston *et al.* 2006) (Fig. 4*A*). As anticipated, the rapidly decaying response elicited by L-Glu was converted into a non-decaying phenotype via crosslinking of the D1 interface, suggesting that restricting dimer movement in this region locks the AMPAR or KAR into the activated state (Priel *et al.* 2006; Weston *et al.* 2006) (Fig. 4*B*). Despite this, it was surprising that responses elicited by the crosslinked GluA2 AMPAR were potentiated by cyclothiazide to a greater extent than the wild-type receptor (Weston *et al.* 2006). In principle, if desensitization is blocked, the agonist response would be expected to be unaffected by cyclothiazide unless a more complicated mechanism of cyclothiazide action is at play (see Mitchell & Fleck, 2007). Similarly, GluK2 KARs crosslinked to restrict dimer movement (Priel *et al.* 2006; Weston *et al.* 2006) elicited responses that were more consistent with the equilibrium

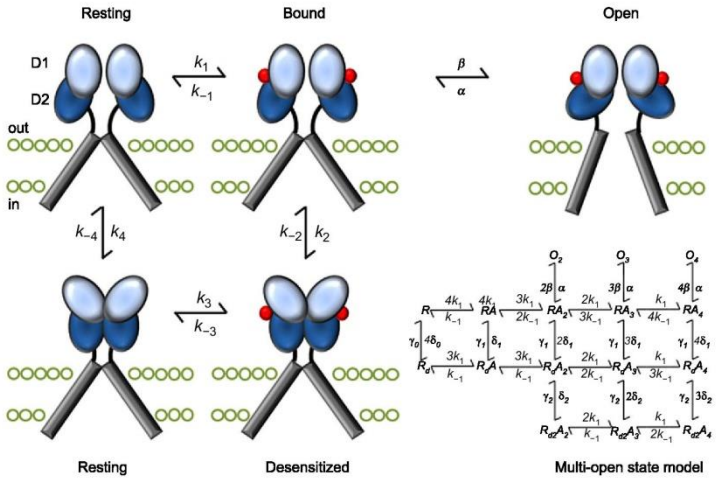

Figure 3. Early structural model of iGluR activation and desensitization
The binding of agonist molecules (red) to the LBD dimer permits subsequent rearrangement to one of two conformations: activated or desensitized. The activated state occurs when the two D2 lobes (dark blue) are lifted apart, generating forces on the transmembrane domains (grey bars) to open the channel pore. Alternatively, the desensitized state stems from the separation of the two D1 domains (light blue) at the dimer interface, relaxing the LBD such that the energy provided by ligand binding cannot open the pore. The structural states are arranged according to the cyclic gating model described in Fig. 1, although to better account for the complex functional behaviour of iGluRs, more advanced kinetic models (Robert & Howe, 2003) have been developed, into which the four agonist binding sites are incorporated (bottom right). Moreover, is not clear to what extent movements of LBD dimers occur in the absence of bound ligands. The ATD has also been excluded for simplicity.

response of wild-type receptors, where the occurrence of desensitization accounts for the slow decay kinetics and the higher apparent agonist affinity (Bowie *et al.* 2003). A clue to the unexpected behaviour of these cysteine mutants could be found in the GluK2 Y521C/L783C crystal structure (Weston *et al.* 2006), which showed the dimer interface to be in a relaxed conformation, in between an activated arrangement and the pseudo-desensitized arrangement of GluA2 S729C (Armstrong *et al.* 2006) (Fig. 5*A*). An important caveat in these studies is that the authors relied on macroscopic responses to infer the absence or presence of desensitization. However, given that desensitization represents long-lived inactive states of the channel (Sakmann *et al.* 1980), its occurrence can only be truly confirmed by single-channel analysis. As explained below, unitary measurements of crosslinked iGluRs revealed an unappreciated importance of the LBD dimer interface in governing the degree of activation.

Single-channel measurements of the GluN1/GluN2A NMDAR crosslinked at equivalent positions to those in AMPARs and KARs demonstrated that restraining dimer movement had a profound effect on activation (i.e. P_{open}), whereas desensitization was still present (Borschel *et al.* 2011). The authors' findings suggested two possibilities: (i) the structural basis of NMDAR desensitization is distinct from that of AMPARs and KARs and/or (ii) earlier studies implicating the dimer interface with AMPAR and KAR desensitization had overlooked the impact of cross-linking on the activation process. In keeping with the latter possibility, single-channel recordings comparing wild-type GluK2 receptor responses to the crosslinked receptor (i.e. GluK2 Y521C/L783C) showed that the mutant receptor activated poorly (Daniels *et al.* 2013) (Fig. 5*B*). Specifically, the crosslinked GluK2 receptor is effectively locked out of the main open-state, rather than having a preference for it, which would be expected if desensitization was abolished (Fig. 5*C*). Preliminary single-channel data on crosslinked GluA2 receptors (B. A. Daniels & D. Bowie, unpublished observations) reveals that channel activation is similarly disrupted. Taken together, these data suggest that the architecture of the LBD dimer interface of all iGluR subtypes is a key location for channel activation.

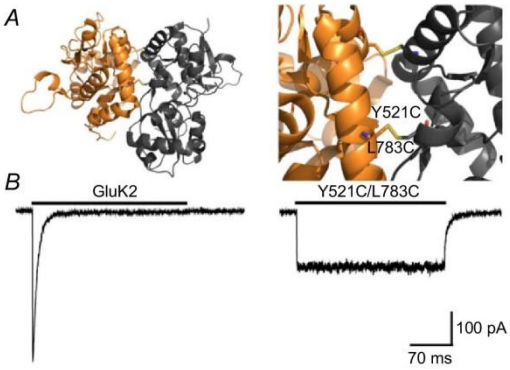

Figure 4. Crosslinking of the GluK2 LBD dimer interface yields non-decaying current responses
A, side views of the LBD dimer interface of GluK2 Y521C/L783C (PDB 2I0C), in its entirety (left) and close-up (right), detailing the inter-protomer disulphide bond (yellow). *B*, activation profiles of wild-type GluK2 and Y521C/L783C receptors in response to 10 mM L-Glu (holding potential –60 mV). Adapted from Daniels *et al.* (2013) with permission.

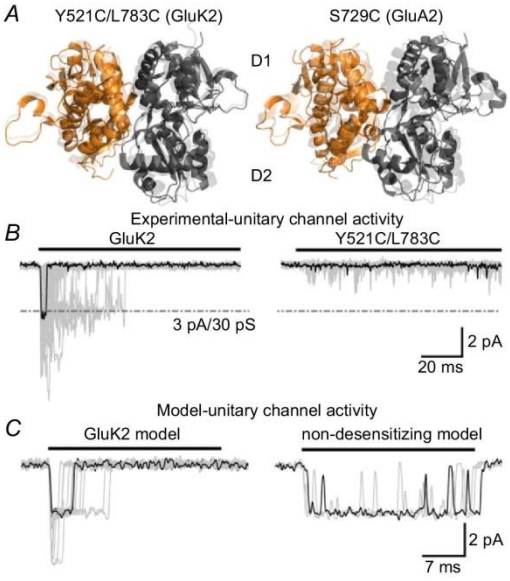

Figure 5. Cysteine crosslinking of the GluK2 LBD dimer interface disrupts activation
A, side views of the LBD dimer interface of GluK2 Y521C/L783C (left, PDB 2I0C) and GluA2 S729C (right, PDB 2I3W) in front of the corresponding L-Glu-bound wild-type receptors (transparent, PDB 3G3F and 1FTJ). For both mutants the distance across the interface between the D1 domains is increased. *B*, activation profiles of wild-type GluK2 and Y521C/L783C receptors at the single-channel level with a typical unitary response highlighted (black) for both receptors. *C*, simulations of GluK2 unitary channel activity in the presence (left) or absence (right) of desensitization, generated from a cyclic gating model (Bowie *et al.* 1998). When a single channel is simulated with desensitized states removed, the open channel probability is much greater than observed experimentally for the double cysteine mutant. Responses were recorded or simulated using 10 mM L-Glu and a holding potential of −100 mV, and experimental data were filtered at 1 kHz. Adapted from Daniels *et al.* (2013) with permission.

The cation binding pocket of KARs acts as an on/off switch

Although the strategy of covalent crosslinking did not lock KARs into the main activated state as expected, another GluK2 receptor mutant, namely GluK2 D776K, had also been proposed to eliminate macroscopic desensitization (Nayeem *et al.* 2009), but had yet to be studied at the single-channel level. Encouragingly, structural data showed that the positively charged Lys776 established a new inter-protomer contact across the dimer interface by tethering to the cation binding pocket (Nayeem *et al.* 2011) and thus affected KARs through a different mechanism from the Cys521/Cys783 disulphide bridge (Fig. 6*A*). This observation was also intriguing given the fact that earlier functional data had shown that occupancy of the cation binding pocket by external cations, such as Na^+, was an absolute requirement for KAR activation (Wong *et al.* 2006; Bowie, 2010). Consequently, it was possible that Lys776 mimicked the effect of external cations and, by near-permanent occupancy of the cation binding pocket, was able to sustain activation and thus eliminate desensitization. In keeping with this, single channel recordings of individual GluK2 D776K receptors activated to the main conductance state of approximately 20 pS and remained there in the continued presence of the agonist (Dawe *et al.* 2013) (Fig. 6*B* and *C*). Using a combination of molecular dynamics simulations and electrophysiological recordings, it was shown that the cation binding pocket acts like an on/off switch with cation binding priming the KAR for activation, whereas desensitization proceeds when the cation site is unoccupied (Dawe *et al.* 2013). From this perspective, GluK2 D776K maximizes agonist efficacy and sustains the agonist response by keeping the KAR in the activated state rather than affecting the process of desensitization directly. Curiously, GluA1 AMPARs contain many of the residues that make up the cation binding pocket in KARs, but remain insensitive to modulation by external cations (Bowie, 2002). Previous studies have explained cation insensitivity of AMPARs by speculating that the Lys residue that lies in the pocket acts as a surrogate cation (Wong *et al.* 2006, 2007). This idea has yet to be tested experimentally; however, given that the Lys residue is conserved amongst some NMDARs, the KAR 'cation binding pocket' may prove to be a hotspot for activation of all iGluR families.

New insights from full-length iGluR structures

Despite the identification of several discrete sites that regulate iGluR activation, the structural domains (ATD and LBD) to which they belong have been studied largely in isolation, making it difficult to ascribe a role to them during any global protein rearrangements that may accompany channel gating. Part of the problem has been the difficulty of obtaining full-length structures at atomic resolution (Mayer, 2011; Sobolevsky, 2013), though lower resolution, single particle electron microscopy (EM) images have actually been available for some time (Nakagawa, 2010). The first 'image' of a tetrameric iGluR was obtained following large-scale expression of recombinant GluA2 (Safferling *et al.* 2001), followed by a more refined three-dimensional reconstruction of the receptor at 20 Å resolution (Tichelaar *et al.* 2004). Native AMPAR complexes, with and without associated transmembrane AMPA receptor regulatory proteins (TARPs), were later imaged in multiple conformations at 30–40 Å

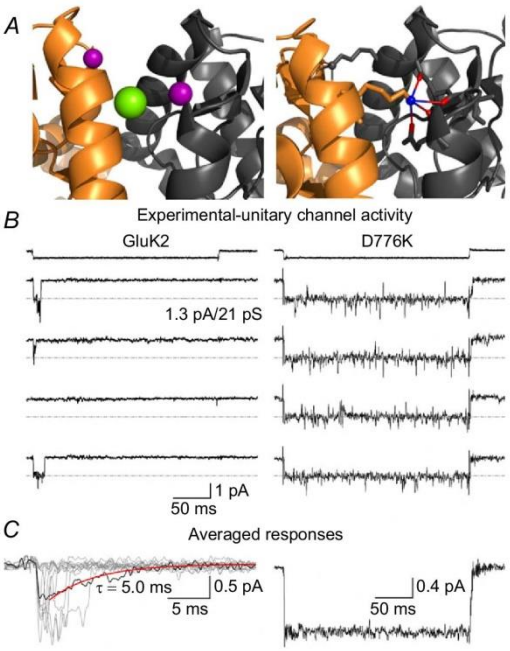

Figure 6. Occupancy of the GluK2 cation binding pocket sustains activation
A, side views of the LBD dimer interface of wild-type GluK2 (left, PDB 3G3F) and the D776K mutant (right, PDB 2XXX). The former includes two allosteric sodium ions (purple) and a chloride ion (green) bound at the apex of the interface, while the latter possesses a charged amino group (blue) on residue 776 tethering into the electronegative pocket (red) normally occupied by sodium. *B*, representative single-channel responses of GluK2 (left) and D776K (right) to 10 mM L-Glu (holding potential −60 mV, filtered at 1 kHz). *C*, averaged responses of individual sweeps taken from the same patch recordings as shown in *B*, which mimic the phenotype exhibited by a large population of receptors. For wild-type GluK2 several individual responses (grey) are overlaid behind the average response, while a fit of the current decay (red) suggests the unitary events are representative of those that contribute to macroscopic decay kinetics, which occur over a similar time course. (Dawe *et al.* 2013).

using cryo-EM techniques (Nakagawa *et al.* 2005, 2006). The AMPARs were sorted into two major classes: a resting and/or activated class possessing a more compact extracellular region, and a desensitized class notable for separation of lobes at the ATD level (Nakagawa *et al.* 2005). This arrangement contrasts with an unliganded GluA2 receptor comprising a compact ATD and separate LBD lobes reported elsewhere (Midgett & Madden, 2008; Midgett *et al.* 2012), and suggests that protein purification conditions may heavily influence the resulting structure. Full-length tetrameric crystal structures have since supported the notion of a Y-shaped structure with a twofold axis of symmetry for apo and antagonist-bound GluA2 AMPARs (Sobolevsky *et al.* 2009; Dürr *et al.* 2014) (Fig. 7*A*). Meanwhile, crystallization in the presence of agonists and allosteric modulators or toxins that increase channel open probability suggest an activated state not too structurally dissimilar from the resting state: amongst many interesting movements, these structures reveal greater closure of the ligand binding cleft, opening between pairs of LBD dimers around the axis of symmetry, and an increase in inter-subunit LBD–TM linker distances (Fig. 7*B*), indicative of a pulling force that precedes channel opening (Chen *et al.* 2014; Dürr *et al.* 2014). These results were largely corroborated by cryo-EM data published simultaneously in which GluA2 is characterized in resting, activated and desensitized states, and contrasted with GluK2 in a desensitized conformation (Meyerson *et al.* 2014). Through improved image-processing techniques, resolution approaching 7 Å was achieved, in contrast to earlier images of apo and desensitized GluK2 receptors of around 20 Å (Schauder *et al.* 2013). Perhaps the most intriguing finding from the later EM study was an asymmetric rearrangement of the LBD during desensitization (Fig. 7*C*), in which the two subunits of each dimer rotate 125 deg and 13 deg in a horizontal plane (Meyerson *et al.* 2014), a movement captured to some extent in an fluorowillardiine-bound crystal structure (Dürr *et al.* 2014), but possibly constrained due to the extensive mutagenesis required for crystallization. GluA2 was also crystallized with nitrowillardiine in another study, but the LBD did not exhibit any drastic

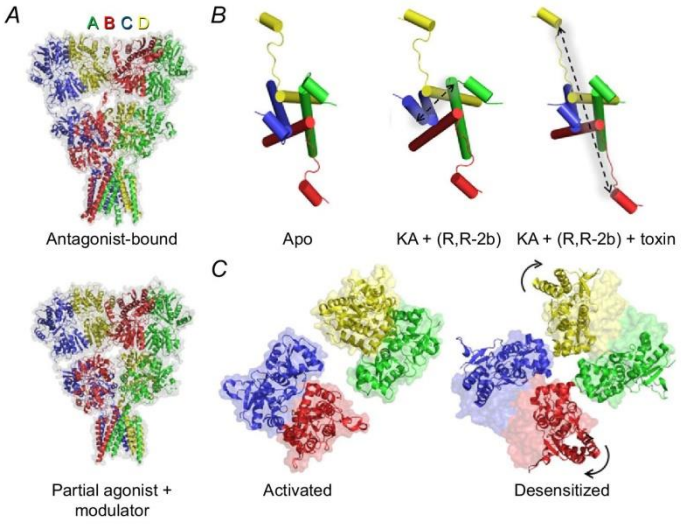

Figure 7. Structural rearrangements of full-length iGluRs during activation and desensitization
A, full-length GluA2 receptor bound by the competitive antagonist ZK200775 (top, PDB 3KG2) or KA and the allosteric modulator R,R-2b (bottom, PDB 4U1W), which potentiates GluA2 current responses in equilibrium conditions (Kaae *et al.* 2007). Both structures retain a twofold axis of symmetry, with the A/C and B/D subunits having distinct arrangements. The latter structure is thought to represent a 'pre-open' state of the receptor during the activation process. *B*, in contrast to the unliganded, apo state of GluA2 (left, PDB 4U2P), the binding of an agonist with positive modulator (centre, PDB 4U1W) causes separation between A/C subunits at the level of the LBD–TM 3 linker, generating forces that could open the pore. Addition of the con-ikot-ikot snail toxin further increases the B/D distance (right, PDB 4U5D). *C*, the tetrameric LBD of GluA2 bound by L-Glu and the allosteric modulator LY451646 (left, PDB 4UQK), a potentiator of AMPAR equilibrium currents (Gates *et al.* 2001), believed to be in an activated state. In contrast, the LBD of GluK2 bound by 2*S*,4*R*-4-methylglutamate (right, PDB 4UQQ) is believed to be in a desensitized state, characterized by large horizontal rotation of the B/D subunits.

rearrangements relative to an antagonist-bound structure of the same, modified receptor (Yelshanskaya *et al.* 2014). Differences in agonist-bound structures are difficult to interpret, since it is unknown whether such structures represent closed or desensitized states, and to what extent mutagenesis of the GluA2 crystal construct or crystal lattice contacts affect the conformations adopted by these proteins (Yelshanskaya *et al.* 2014). Ultimately, the ideas presented in these structural studies remain to be consolidated, yet they will certainly generate many testable hypotheses concerning the mechanisms of AMPAR/KAR gating.

Conclusion

Although we have witnessed great advances in our understanding of iGluR activation in the last three decades, the way forward faces two interrelated obstacles. First, we still do not have a detailed kinetic model of iGluRs that explains the relationship between different activated (i.e. channel conductance(s)) and desensitized states. This obstacle could be addressed with computational approaches that take into account the hierarchical structure of the iGluR (Ollivier *et al.* 2010). However, to provide an accurate starting template for the rule-based modelling of iGluRs, we require a clearer understanding of the stoichiometry of their activation and desensitization. The use of photo-switchable ligands tethered to the iGluR ligand binding cleft (Volgraf *et al.* 2006) could help address this problem, particularly if certain subunits are selectively stimulated (Reiner & Isacoff, 2014), although receptor modification and difficulty replicating response kinetics observed with rapid solution exchange will complicate interpretations made from this technique.

The second major roadblock to understanding iGluR activation is the scarcity of structural correlates for functional states. Despite the recent determination of the full-length structures of AMPARs in a range of agonist and antagonist-induced states (Dürr *et al.* 2014; Meyerson *et al.* 2014), it remains to be seen if these few 'snapshots' can account for the diversity of functional behaviour exhibited by iGluRs. It is also worth noting that no crystal structure has yet shown the pore in an open configuration. Consequently, there is still much to study regarding the signal transduction pathway that allows agonist binding to promote conformational changes that gate the channel pore. In NMDARs, where full-length structures are now available (Karakas & Furukawa, 2014; Lee *et al.* 2014), recent work has shown that the LBD–TM linker provides a mechanical force that increases the likelihood of channel opening (Kazi *et al.* 2014). In AMPARs and KARs, which have a low open probability in equilibrium conditions (e.g. Zhang *et al.* 2008), carrying out such investigations remains difficult. Molecular dynamics simulations of the GluA2 receptor have suggested that small increases in pore diameter can be achieved through rearrangement in the LBD (Dong & Zhou, 2011), but whether this mechanism can permit ion permeation is unclear. In the short term, full-length iGluR structures will provide more insight into which micro-domains may be critically linked to channel activation. But as an alternative approach, recent work on Cys-loop receptors suggests that insight into the allosteric nature of the ligand-gated ion channels may be achieved by mapping out the energy contributions of different structural domains during gating (Purohit *et al.* 2013). In either case, the identification of regions which contribute to the activation and desensitization of intact iGluRs opens up several new avenues of investigation. For instance, it is presently uncertain how dynamic the interactions are between auxiliary proteins (known to affect receptor trafficking and gating kinetics) and iGluRs at the synapse (Jackson & Nicoll, 2011), but having a three-dimensional model of AMPAR activation could shed light on state-dependent modulatory effects. In addition, such models might reveal previously unappreciated sites as new targets for therapeutic compounds. While it is clear that many secrets of glutamate receptor physiology remain to be uncovered, we have learned a great deal from 30 years of research on this neurotransmitter receptor.

References

Adams MD & Oxender DL (1989). Bacterial periplasmic binding protein tertiary structures. *J Biol Chem* **264**, 15739–15742.

Akaike N (1995). Concentration clamp technique. In *Neuromethods, Patch-Clamp Applications and Protocols*, ed. Boulton A, Baker G & Walz W, pp. 141–154. Humana Press Inc.

Armstrong N & Gouaux E (2000). Mechanisms for activation and antagonism of an AMPA-sensitive glutamate receptor: crystal structures of the GluR2 ligand binding core. *Neuron* **28**, 165–181.

Armstrong N, Jasti J, Beich-Frandsen M & Gouaux E (2006). Measurement of conformational changes accompanying desensitization in an ionotropic glutamate receptor. *Cell* **127**, 85–97.

Armstrong N, Mayer M & Gouaux E (2003). Tuning activation of the AMPA-sensitive GluR2 ion channel by genetic adjustment of agonist-induced conformational changes. *Proc Natl Acad Sci U S A* **100**, 5736–5741.

Armstrong N, Sun Y, Chen GQ & Gouaux E (1998). Structure of a glutamate-receptor ligand-binding core in complex with kainate. *Nature* **395**, 913–917.

Ascher P & Nowak L (1988). Quisqualate- and kainate-activated channels in mouse central neurones in culture. *J Physiol* **399**, 227–245.

Bettler B, Boulter J, Hermans-Borgmeyer I, O'Shea-Greenfield A, Deneris ES, Moll C, Borgmeyer U, Hollmann M & Heinemann S (1990). Cloning of a novel glutamate receptor subunit, GluR5: expression in the nervous system during development. *Neuron* **5**, 583–595.

Birdsey-Benson A, Gill A, Henderson LP & Madden DR (2010). Enhanced efficacy without further cleft closure: reevaluating twist as a source of agonist efficacy in AMPA receptors. *J Neurosci* **30**, 1463–1470.

Borschel WF, Murthy SE, Kasperek EM & Popescu GK (2011). NMDA receptor activation requires remodelling of intersubunit contacts within ligand-binding heterodimers. *Nat Commun* **2**, 498.

Bowie D (2002). External anions and cations distinguish between AMPA and kainate receptor gating mechanisms. *J Physiol* **539**, 725–733.

Bowie D (2008). Ionotropic glutamate receptors and CNS disorders. *CNS Neurol Disord Drug Targets* **7**, 129–143.

Bowie D (2010). Ion-dependent gating of kainate receptors. *J Physiol* **588**, 67–81.

Bowie D, Garcia EP, Marshall J, Traynelis SF & Lange GD (2003). Allosteric regulation and spatial distribution of kainate receptors bound to ancillary proteins. *J Physiol* **547**, 373–385.

Bowie D & Lange GD (2002). Functional stoichiometry of glutamate receptor desensitization. *J Neurosci* **22**, 3392–3403.

Bowie D, Lange GD & Mayer ML (1998). Activity-dependent modulation of glutamate receptors by polyamines. *J Neurosci* **18**, 8175–8185.

Chen GQ & Gouaux E (1997). Overexpression of a glutamate receptor (GluR2) ligand binding domain in *Escherichia coli*: application of a novel protein folding screen. *Proc Natl Acad Sci U S A* **94**, 13431–13436.

Chen L, Dürr KL & Gouaux E (2014). X-ray structures of AMPA receptor–cone snail toxin complexes illuminate activation mechanism. *Science* **345**, 1021–1026.

Collingridge GL & Lester RA (1989). Excitatory amino acid receptors in the vertebrate central nervous system. *Pharmacol Rev* **41**, 143–210.

Collingridge GL, Olsen RW, Peters J & Spedding M (2009). A nomenclature for ligand-gated ion channels. *Neuropharmacology* **56**, 2–5.

Contractor A, Mulle C & Swanson GT (2011). Kainate receptors coming of age: milestones of two decades of research. *Trends Neurosci* **34**, 154–163.

Cull-Candy SG & Usowicz MM (1987). Multiple-conductance channels activated by excitatory amino acids in cerebellar neurons. *Nature* **325**, 525–528.

Cull-Candy SG & Usowicz MM (1989). On the multiple-conductance single channels activated by excitatory amino acids in large cerebellar neurones of the rat. *J Physiol* **415**, 555–582.

Daniels BA, Andrews ED, Aurousseau MR, Accardi MV & Bowie D (2013). Crosslinking the ligand-binding domain dimer interface locks kainate receptors out of the main open state. *J Physiol* **591**, 3873–3885.

Dawe GB, Musgaard M, Andrews ED, Daniels BA, Aurousseau MR, Biggin PC & Bowie D (2013). Defining the structural relationship between kainate-receptor deactivation and desensitization. *Nat Struct Mol Biol* **20**, 1054–1061.

Dingledine R, Borges K, Bowie D & Traynelis SF (1999). The glutamate receptor ion channels. *Pharmacol Rev* **51**, 7–61.

Dong H & Zhou HX (2011). Atomistic mechanism for the activation and desensitization of an AMPA-subtype glutamate receptor. *Nat Commun* **2**, 354.

Dürr KL, Chen L, Stein RA, De Zorzi R, Folea IM, Walz T, McHaourab HS & Gouaux E (2014). Structure and dynamics of AMPA receptor GluA2 in resting, pre-open, and desensitized states. *Cell* **158**, 778–792.

Egebjerg J, Bettler B, Hermans-Borgmeyer I & Heinemann S (1991). Cloning of a cDNA for a glutamate receptor subunit activated by kainate but not AMPA. *Nature* **351**, 745–748.

Fay AM, Corbeil CR, Brown P, Moitessier N & Bowie D (2009). Functional characterization and in silico docking of full and partial GluK2 kainate receptor agonists. *Mol Pharmacol* **75**, 1096–1107.

Fenwick MK & Oswald RE (2008). NMR spectroscopy of the ligand-binding core of ionotropic glutamate receptor 2 bound to 5-substituted willardiine partial agonists. *J Mol Biol* **378**, 673–685.

Fleck MW, Cornell E & Mah SJ (2003). Amino-acid residues involved in glutamate receptor 6 kainate receptor gating and desensitization. *J Neurosci* **23**, 1219–1227.

Frydenvang K, Lash LL, Naur P, Postila PA, Pickering DS, Smith CM, Gajhede M, Sasaki M, Sakai R, Pentikainen OT, Swanson GT & Kastrup JS (2009). Full domain closure of the ligand-binding core of the ionotropic glutamate receptor iGluR5 induced by the high affinity agonist dysiherbaine and the functional antagonist 8,9-dideoxyneodysiherbaine. *J Biol Chem* **284**, 14219–14229.

Furukawa H & Gouaux E (2003). Mechanisms of activation, inhibition and specificity: crystal structures of the NMDA receptor NR1 ligand-binding core. *EMBO J* **22**, 2873–2885.

Gates M, Ogden A & Bleakman D (2001). Pharmacological effects of AMPA receptor potentiators LY392098 and LY404187 on rat neuronal AMPA receptors *in vitro*. *Neuropharmacology* **40**, 984–991.

Gouaux E (2004). Structure and function of AMPA receptors. *J Physiol* **554**, 249–253.

Hogner A, Kastrup JS, Jin R, Liljefors T, Mayer ML, Egebjerg J, Larsen IK & Gouaux E (2002). Structural basis for AMPA receptor activation and ligand selectivity: crystal structures of five agonist complexes with the GluR2 ligand-binding core. *J Mol Biol* **322**, 93–109.

Hollmann M & Heinemann S (1994). Cloned glutamate receptors. *Annu Rev Neurosci* **17**, 31–108.

Hollmann M, Maron C & Heinemann S (1994). *N*-glycosylation site tagging suggests a three transmembrane domain topology for the glutamate receptor GluR1. *Neuron* **13**, 1331–1343.

Hollmann M, O'Shea-Greenfield A, Rogers SW & Heinemann S (1989). Cloning by functional expression of a member of the glutamate receptor family. *Nature* **342**, 643–648.

Holm MM, Naur P, Vestergaard B, Geballe MT, Gajhede M, Kastrup JS, Traynelis SF & Egebjerg J (2005). A binding site tyrosine shapes desensitization kinetics and agonist potency at GluR2. A mutagenic, kinetic, and crystallographic study. *J Biol Chem* **280**, 35469–35476.

Horning MS & Mayer ML (2004). Regulation of AMPA receptor gating by ligand binding core dimers. *Neuron* **41**, 379–388.

Hsiao CD, Sun YJ, Rose J & Wang BC (1996). The crystal structure of glutamine-binding protein from *Escherichia coli*. *J Mol Biol* **262**, 225–242.

Huettner JE (1990). Glutamate receptor channels in rat DRG neurons: activation by kainate and quisqualate and blockade of desensitization by Con A. *Neuron* **5**, 255–266.

Huettner JE (2003). Kainate receptors and synaptic transmission. *Prog Neurobiol* **70**, 387–407.

Huettner JE (2014). Glutamate receptor pores. *J Physiol* (in press; DOI: 10.1113/jphysiol.2014.272724).

Inanobe A, Furukawa H & Gouaux E (2005). Mechanism of partial agonist action at the NR1 subunit of NMDA receptors. *Neuron* **47**, 71–84.

Jackson AC & Nicoll RA (2011). The expanding social network of ionotropic glutamate receptors: TARPs and other transmembrane auxiliary subunits. *Neuron* **70**, 178–199.

Jahr CE & Stevens CF (1987). Glutamate activates multiple single channel conductances in hippocampal neurons. *Nature* **325**, 522–525.

Jin R, Banke TG, Mayer ML, Traynelis SF & Gouaux E (2003). Structural basis for partial agonist action at ionotropic glutamate receptors. *Nat Neurosci* **6**, 803–810.

Jin R, Horning M, Mayer ML & Gouaux E (2002). Mechanism of activation and selectivity in a ligand-gated ion channel: structural and functional studies of GluR2 and quisqualate. *Biochemistry* **41**, 15635–15643.

Johnson JW & Ascher P (1987). Glycine potentiates the NMDA response in cultured mouse brain neurons. *Nature* **325**, 529–531.

Jonas P (1995). Fast application of agonists to isolated membrane patches. In *Single-Channel Recording*, ed. Sakmann B & Neher E, pp. 231–243. Plenum Press, New York.

Kaae BH, Harpsoe K, Kastrup JS, Sanz AC, Pickering DS, Metzler B, Clausen RP, Gajhede M, Sauerberg P, Liljefors T & Madsen U (2007). Structural proof of a dimeric positive modulator bridging two identical AMPA receptor-binding sites. *Chem Biol* **14**, 1294–1303.

Karakas E & Furukawa H (2014). Crystal structure of a heterotetrameric NMDA receptor ion channel. *Science* **344**, 992–997.

Kazi R, Dai J, Sweeney C, Zhou HX & Wollmuth LP (2014). Mechanical coupling maintains the fidelity of NMDA receptor-mediated currents. *Nat Neurosci* **17**, 914–922.

Keinanen K, Wisden W, Sommer B, Werner P, Herb A, Verdoorn TA, Sakmann B & Seeburg PH (1990). A family of AMPA-selective glutamate receptors. *Science* **249**, 556–560.

Kiskin NI, Krishtal OA & Tsyndrenko A (1986). Excitatory amino acid receptors in hippocampal neurons: kainate fails to desensitize them. *Neurosci Lett* **63**, 225–230.

Kleckner NW & Dingledine R (1988). Requirement for glycine in activation of NMDA-receptors expressed in *Xenopus* oocytes. *Science* **241**, 835–837.

Kuusinen A, Arvola M & Keinanen K (1995). Molecular dissection of the agonist binding site of an AMPA receptor. *EMBO J* **14**, 6327–6332.

Lau AY & Roux B (2007). The free energy landscapes governing conformational changes in a glutamate receptor ligand-binding domain. *Structure* **15**, 1203–1214.

Lee CH, Lu W, Michel JC, Goehring A, Du J, Song X & Gouaux E (2014). NMDA receptor structures reveal subunit arrangement and pore architecture. *Nature* **511**, 191–197.

Lerma J & Marques JM (2013). Kainate receptors in health and disease. *Neuron* **80**, 292–311.

Lerma J, Paternain AV, Naranjo JR & Mellström B (1993). Functional kainate-selective glutamate receptors in cultured hippocampal neurons. *Proc Natl Acad Sci U S A* **90**, 11688–11692.

Lipton SA (2006). Paradigm shift in neuroprotection by NMDA receptor blockade: memantine and beyond. *Nat Rev Drug Discov* **5**, 160–170.

MacDonald JF & Nowak LM (1990). Mechanisms of blockade of excitatory amino acid receptor channels. *Trends Pharmacol Sci* **11**, 167–172.

Maclean DM, Wong AY, Fay AM & Bowie D (2011). Cations but not anions regulate the responsiveness of kainate receptors. *J Neurosci* **31**, 2136–2144.

McLennan H (1983). Receptors for the excitatory amino acids in the mammalian central nervous system. *Prog Neurobiol* **20**, 251–271.

Madden DR (2002). The structure and function of glutamate receptor ion channels. *Nat Rev Neurosci* **3**, 91–101.

Mano I, Lamed Y & Teichberg VI (1996). A venus flytrap mechanism for activation and desensitization of α-amino-3-hydroxy-5-methyl-4-isoxazole propionic acid receptors. *J Biol Chem* **271**, 15299–15302.

Masu M, Tanabe Y, Tsuchida K, Shigemoto R & Nakanishi S (1991). Sequence and expression of a metabotropic glutamate receptor. *Nature* **349**, 760–765.

Mayer ML (2005). Crystal structures of the GluR5 and GluR6 ligand binding cores: molecular mechanisms underlying kainate receptor selectivity. *Neuron* **45**, 539–552.

Mayer ML (2011). Emerging models of glutamate receptor ion channel structure and function. *Structure* **19**, 1370–1380.

Mayer ML & Armstrong N (2004). Structure and function of glutamate receptor ion channels. *Annu Rev Physiol* **66**, 161–181.

Mayer ML & Westbrook GL (1987). The physiology of excitatory amino acids in the vertebrate central nervous system. *Prog Neurobiol* **28**, 197–276.

Meyerson JR, Kumar J, Chittori S, Rao P, Pierson J, Bartesaghi A, Mayer ML & Subramaniam S (2014). Structural mechanism of glutamate receptor activation and desensitization. *Nature* (in press; DOI: 10.1038/nature13603).

Midgett CR, Gill A & Madden DR (2012). Domain architecture of a calcium-permeable AMPA receptor in a ligand-free conformation. *Front Mol Neurosci* **4**, 56.

Midgett CR & Madden DR (2008). The quaternary structure of a calcium-permeable AMPA receptor: conservation of shape and symmetry across functionally distinct subunit assemblies. *J Mol Biol* **382**, 578–584.

Mitchell NA & Fleck MW (2007). Targeting AMPA receptor gating processes with allosteric modulators and mutations. *Biophys J* **92**, 2392–2402.
Moriyoshi K, Masu M, Ishii T, Shigemoto R, Mizuno N & Nakanishi S (1991). Molecular cloning and characterization of the rat NMDA receptor. *Nature* **354**, 31–37.
Nakagawa T (2010). The biochemistry, ultrastructure, and subunit assembly mechanism of AMPA receptors. *Mol Neurobiol* **42**, 161–184.
Nakagawa T, Cheng Y, Ramm E, Sheng M & Walz T (2005). Structure and different conformational states of native AMPA receptor complexes. *Nature* **433**, 545–549.
Nakagawa T, Cheng Y, Sheng M & Walz T (2006). Three-dimensional structure of an AMPA receptor without associated stargazin/TARP proteins. *Biol Chem* **387**, 179–187.
Nakanishi N, Shneider NA & Axel R (1990). A family of glutamate receptor genes: evidence for the formation of heteromultimeric receptors with distinct channel properties. *Neuron* **5**, 569–581.
Nakanishi S (1992). Molecular diversity of glutamate receptors and implications for brain function. *Science* **258**, 597–603.
Nanao MH, Green T, Stern-Bach Y, Heinemann SF & Choe S (2005). Structure of the kainate receptor subunit GluR6 agonist-binding domain complexed with domoic acid. *Proc Natl Acad Sci U S A* **102**, 1708–1713.
Naur P, Hansen KB, Kristensen AS, Dravid SM, Pickering DS, Olsen L, Vestergaard B, Egebjerg J, Gajhede M, Traynelis SF & Kastrup JS (2007). Ionotropic glutamate-like receptor δ2 binds D-serine and glycine. *Proc Natl Acad Sci U S A* **104**, 14116–14121.
Nayeem N, Mayans O & Green T (2011). Conformational flexibility of the ligand-binding domain dimer in kainate receptor gating and desensitization. *J Neurosci* **31**, 2916–2924.
Nayeem N, Zhang Y, Schweppe DK, Madden DR & Green T (2009). A nondesensitizing kainate receptor point mutant. *Mol Pharmacol* **76**, 534–542.
O'Hara PJ, Sheppard PO, Thogersen H, Venezia D, Haldeman BA, McGrane V, Houamed KM, Thomsen C, Gilbert TL & Mulvihill ER (1993). The ligand-binding domain in metabotropic glutamate receptors is related to bacterial periplasmic binding proteins. *Neuron* **11**, 41–52.
Ollivier JF, Shahrezaei V & Swain PS (2010). Scalable rule-based modelling of allosteric proteins and biochemical networks. *PLoS Comput Biol* **6**, e1000975.
Paas Y (1998). The macro- and microarchitectures of the ligand-binding domain of glutamate receptors. *Trends Neurosci* **21**, 117–125.
Paoletti P, Bellone C & Zhou Q (2013). NMDA receptor subunit diversity: impact on receptor properties, synaptic plasticity and disease. *Nat Rev Neurosci* **14**, 383–400.
Patneau DK & Mayer ML (1990). Structure-activity relationships for amino acid transmitter candidates acting at *N*-methyl-D-aspartate and quisqualate receptors. *J Neurosci* **10**, 2385–2399.
Patneau DK & Mayer ML (1991). Kinetic analysis of interactions between kainate and AMPA: evidence for activation of a single receptor in mouse hippocampal neurons. *Neuron* **6**, 785–798.
Patneau DK, Mayer ML, Jane DE & Watkins JC (1992). Activation and desensitization of AMPA/kainate receptors by novel derivatives of willardiine. *J Neurosci* **12**, 595–606.
Patneau DK, Vyklicky L Jr & Mayer ML (1993). Hippocampal neurons exhibit cyclothiazide-sensitive rapidly desensitizing responses to kainate. *J Neurosci* **13**, 3496–3509.
Pirotte B, Francotte P, Goffin E & de Tullio P (2013). AMPA receptor positive allosteric modulators: a patent review. *Expert Opin Ther Pat* **23**, 615–628.
Plested AJ & Mayer ML (2007). Structure and mechanism of kainate receptor modulation by anions. *Neuron* **53**, 829–841.
Plested AJ, Vijayan R, Biggin PC & Mayer ML (2008). Molecular basis of kainate receptor modulation by sodium. *Neuron* **58**, 720–735.
Priel A, Selak S, Lerma J & Stern-Bach Y (2006). Block of kainate receptor desensitization uncovers a key trafficking checkpoint. *Neuron* **52**, 1037–1046.
Purohit P, Gupta S, Jadey S & Auerbach A (2013). Functional anatomy of an allosteric protein. *Nat Commun* **4**, 2984.
Qian A & Johnson JW (2002). Channel gating of NMDA receptors. *Physiol Behav* **77**, 577–582.
Quiocho FA (1990). Atomic structures of periplasmic binding proteins and the high-affinity active transport systems in bacteria. *Philos Trans R Soc Lond B Biol Sci* **326**, 341–351; discussion 351–342.
Reiner A & Isacoff EY (2014). Tethered ligands reveal glutamate receptor desensitization depends on subunit occupancy. *Nat Chem Biol* **10**, 273–280.
Robert A, Armstrong N, Gouaux JE & Howe JR (2005). AMPA receptor binding cleft mutations that alter affinity, efficacy, and recovery from desensitization. *J Neurosci* **25**, 3752–3762.
Robert A & Howe JR (2003). How AMPA receptor desensitization depends on receptor occupancy. *J Neurosci* **23**, 847–858.
Robert A, Irizarry SN, Hughes TE & Howe JR (2001). Subunit interactions and AMPA receptor desensitization. *J Neurosci* **21**, 5574–5586.
Safferling M, Tichelaar W, Kummerle G, Jouppila A, Kuusinen A, Keinanen K & Madden DR (2001). First images of a glutamate receptor ion channel: oligomeric state and molecular dimensions of GluRB homomers. *Biochemistry* **40**, 13948–13953.
Sakmann B, Patlak J & Neher E (1980). Single acetylcholine-activated channels show burst-kinetics in presence of desensitizing concentrations of agonist. *Nature* **286**, 71–73.
Sanacora G, Zarate CA, Krystal JH & Manji HK (2008). Targeting the glutamatergic system to develop novel, improved therapeutics for mood disorders. *Nat Rev Drug Discov* **7**, 426–437.
Santangelo RM, Acker TM, Zimmerman SS, Katzman BM, Strong KL, Traynelis SF & Liotta DC (2012). Novel NMDA receptor modulators: an update. *Expert Opin Ther Pat* **22**, 1337–1352.
Schauder DM, Kuybeda O, Zhang J, Klymko K, Bartesaghi A, Borgnia MJ, Mayer ML & Subramaniam S (2013). Glutamate receptor desensitization is mediated by changes in quaternary structure of the ligand binding domain. *Proc Natl Acad Sci U S A* **110**, 5921–5926.

Seeburg PH (1993). The TINS/TiPS Lecture. The molecular biology of mammalian glutamate receptor channels. *Trends Neurosci* **16**, 359–365.
Sobolevsky AI (2013). Structure and gating of tetrameric glutamate receptors. *J Physiol* (in press; DOI: 10.1113/jphysiol.2013.264911).
Sobolevsky AI, Rosconi MP & Gouaux E (2009). X-ray structure, symmetry and mechanism of an AMPA-subtype glutamate receptor. *Nature* **462**, 745–756.
Stern-Bach Y, Bettler B, Hartley M, Sheppard PO, O'Hara PJ & Heinemann SF (1994). Agonist selectivity of glutamate receptors is specified by two domains structurally related to bacterial amino acid-binding proteins. *Neuron* **13**, 1345–1357.
Stern-Bach Y, Russo S, Neuman M & Rosenmund C (1998). A point mutation in the glutamate binding site blocks desensitization of AMPA receptors. *Neuron* **21**, 907–918.
Sun Y, Olson R, Horning M, Armstrong N, Mayer M & Gouaux E (2002). Mechanism of glutamate receptor desensitization. *Nature* **417**, 245–253.
Sun YJ, Rose J, Wang BC & Hsiao CD (1998). The structure of glutamine-binding protein complexed with glutamine at 1.94 Å resolution: comparisons with other amino acid binding proteins. *J Mol Biol* **278**, 219–229.
Tanabe Y, Masu M, Ishii T, Shigemoto R & Nakanishi S (1992). A family of metabotropic glutamate receptors. *Neuron* **8**, 169–179.
Tang CM, Dichter M & Morad M (1989). Quisqualate activates a rapidly inactivating high conductance ionic channel in hippocampal neurons. *Science* **243**, 1474–1477.
Tichelaar W, Safferling M, Keinanen K, Stark H & Madden DR (2004). The three-dimensional structure of an ionotropic glutamate receptor reveals a dimer-of-dimers assembly. *J Mol Biol* **344**, 435–442.
Traynelis SF, Wollmuth LP, McBain CJ, Menniti FS, Vance KM, Ogden KK, Hansen KB, Yuan H, Myers SJ & Dingledine R (2010). Glutamate receptor ion channels: structure, regulation, and function. *Pharmacol Rev* **62**, 405–496.
Volgraf M, Gorostiza P, Numano R, Kramer RH, Isacoff EY & Trauner D (2006). Allosteric control of an ionotropic glutamate receptor with an optical switch. *Nat Chem Biol* **2**, 47–52.
Vyklicky L Jr, Benveniste M & Mayer ML (1990). Modulation of *N*-methyl-D-aspartic acid receptor desensitization by glycine in mouse cultured hippocampal neurones. *J Physiol* **428**, 313–331.
Vyklicky L Jr., Patneau DK & Mayer ML (1991). Modulation of excitatory synaptic transmission by drugs that reduce desensitization at AMPA/kainate receptors. *Neuron* **7**, 971–984.
Watkins JC & Evans RH (1981). Excitatory amino acid transmitters. *Annu Rev Pharmacol Toxicol* **21**, 165–204.
Weston MC, Schuck P, Ghosal A, Rosenmund C & Mayer ML (2006). Conformational restriction blocks glutamate receptor desensitization. *Nat Struct Mol Biol* **13**, 1120–1127.
Wong AY, Fay AM & Bowie D (2006). External ions are coactivators of kainate receptors. *J Neurosci* **26**, 5750–5755.
Wong AY, MacLean DM & Bowie D (2007). Na^+/Cl^- dipole couples agonist binding to kainate receptor activation. *J Neurosci* **27**, 6800–6809.
Yelshanskaya MV, Li M & Sobolevsky AI (2014). Structure of an agonist-bound ionotropic glutamate receptor. *Science* **345**, 1070–1074.
Yuzaki M (2003). The δ2 glutamate receptor: 10 years later. *Neurosci Res* **46**, 11–22.
Yuzaki M (2012). The ins and outs of GluD2–why and how Purkinje cells use the special glutamate receptor. *Cerebellum* **11**, 438–439.
Zhang W, Cho Y, Lolis E & Howe JR (2008). Structural and single-channel results indicate that the rates of ligand binding domain closing and opening directly impact AMPA receptor gating. *J Neurosci* **28**, 932–943.
Zhang Y, Nayeem N, Nanao MH & Green T (2006). Interface interactions modulating desensitization of the kainate-selective ionotropic glutamate receptor subunit GluR6. *J Neurosci* **26**, 10033–10042.

Additional information

Competing interests

None declared.

Funding

This work was supported by operating grants from the Canadian Institutes of Health Research (CIHR) as well as a personal award from the Canada Research Chair Program in Receptor Pharmacology. G.B.D. is funded by an Alexander Graham Bell Canada Graduate Scholarship (CGS-D) through the Natural Sciences and Engineering Research Council of Canada (NSERC). M.R.A. was funded through the Frederick Banting and Charles Best CGS-D through the CIHR. B.A.D. is funded through the CIHR/Fragile X Research Foundation of Canada (postdoctoral award).

Acknowledgements

We wish to thank members of the Bowie lab for their thoughtful comments on the manuscript.

APPENDIX II:

Discovery of novel small-molecule antagonists for GluK2

FOREWORD TO APPENDIX TWO

Prior to my joining the Bowie lab, former graduate student Anne-Marie Fay had co-authored a paper that reported the response of GluK2 KARs to various partial agonists (Fay et al., 2009). One aspect of this work involved the *in silico* docking of agonists into the GluK2 LBD structure, which was overseen by Nicolas Moitessier, a professor in the Department of Chemistry at McGill. Stemming from the collaboration, a plan was made by the Moitessier group to synthesize novel KAR agonists and/or antagonists that would protrude against a specific contact point in the GluK2 agonist-binding cleft. Because it took several years for the preparation of these compounds to be realized, I was present by the time my lab was asked to test their effects on recombinant GluK2 KARs. Due to the limited quantity of the purified compounds, it was only possible to conduct a limited number of electrophysiological experiments. Nevertheless, these experiments helped to identify antagonistic activity of the compounds, and allowed us to publish the project in a chemical biology journal.

Appendix II, Article Title:

Discovery of novel small-molecule antagonists for GluK2

Bioorganic & Medicinal Chemistry Letters 25 (2015) 2416–2420

Contents lists available at ScienceDirect

Bioorganic & Medicinal Chemistry Letters

journal homepage: www.elsevier.com/locate/bmcl

Discovery of novel small-molecule antagonists for GluK2

Paolo Schiavini [a], G. Brent Dawe [b,c], Derek Bowie [c], Nicolas Moitessier [a,*]

[a] Department of Chemistry, McGill University, 801 Sherbrooke Street West, Montréal, Québec H3A 0B8, Canada
[b] Integrated Program in Neuroscience, McGill University, Canada
[c] Department of Pharmacology, McGill University, 3649 Promenade Sir William Osler, Montréal, Québec H3G 0B1, Canada

ARTICLE INFO

Article history:
Received 20 February 2015
Revised 30 March 2015
Accepted 1 April 2015
Available online 10 April 2015

Keywords:
Kainate receptor
GluK2
Rational design
Flexible docking
Antagonist

ABSTRACT

KA receptors have shown to be potential therapeutic targets in CNS diseases such as schizophrenia, depression, neuropathic pain and epilepsy. Through the use of our docking tool FITTED, we investigated the relationship between ligand activity towards GluK2 and the conformational state induced at the receptor level. By focusing our rational design on the interaction between the ligand and a tyrosine residue in the binding site, we synthesized a series of molecules based on a glutamate scaffold, and carried out electrophysiological recordings. The observed ability of some of these molecules to inhibit receptor activation shows the potential of our design for the development of effective antagonists with a molecular size comparable to that of the endogenous neurotransmitter L-glutamate.

Kainate-selective ionotropic glutamate receptors (KA-type iGluRs) have received substantial attention as potential drug targets due to their modulatory role in several neuropathological disease states.[1] For example, KARs are involved in frontal lobe epilepsy, neuropathic pain, neurodegeneration, and migraines.[2] Despite showing promise in animal models of these conditions, no KA receptor antagonist has yet been approved for therapeutic intervention in humans.[3] This failure is partially attributable to the difficult development of KA receptor subunit-specific antagonists,[4] however, a more general obstacle is a limited knowledge concerning how iGluR structure relates to function.[5] In particular, it is difficult to predict how compounds rationally designed to target KA receptors will modulate channel activity.

An early structural model describing iGluR activation proposed that the degree of closure of the extracellular agonist binding cleft around agonist molecules correlated with increased agonist efficacy.[6] In this sense, the dimeric agonist binding domain (ABD) can be thought of as a clamshell, comprised of an upper lobe (D1) and lower lobe (D2) that both form the agonist cleft (Fig. 1). When an agonist binds to the ABD, it is thought that the D2 lobes are pulled upward, closing the agonist binding cleft and generating tension on residues linking the ABD to the transmembrane pore. This tension has been shown to correlate with channel opening, whereby cations pass through the cell membrane to generate a physiological response.[7] For KA receptors, channel opening is very transient, occurring for just milliseconds before the agonist-bound receptor enters a desensitized state characterized by long duration channel closures.[8,9] Alternatively, deactivation can produce

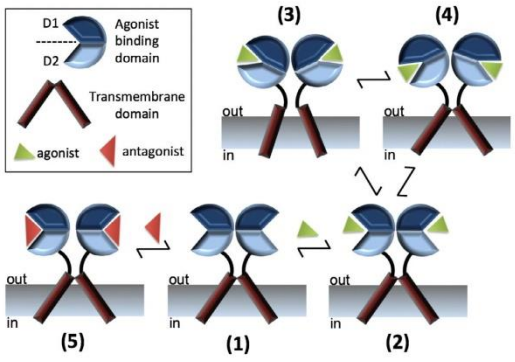

Figure 1. In its resting state (1), the receptor ion channel is closed and the ABD is ready to accept ligands. Binding of agonist molecules (2) favors closure of the ABD, which is correlated with increased frequency of channel opening (3). Receptor activation is in equilibrium with desensitization, where the ABD adopts a different conformation that inhibits opening of the ion channel (4). When binding, an antagonist interferes with closure of the ABD and consequently prevents activation of the receptor (5).

* Corresponding author. Tel.: +1 514 398 5501.
E-mail address: nicolas.moitessier@mcgill.ca (N. Moitessier).

http://dx.doi.org/10.1016/j.bmcl.2015.04.008
0960-894X/

channel closure when agonists unbind from receptor, leading the protein to revert to an unliganded apo state.

Over the last decade, the two most studied KA subunits, GluK1 and GluK2, have been crystallized with many agonists and antagonists. This has permitted extensive investigation of the connections between structural changes and pharmacological responses induced by various ligands.

We previously studied the relationship between closure of the agonist binding cleft and agonist efficacy in GluK2 type KA receptors, by relying on our computational tool Fitted.[10] This software, which is part of our platform Forecaster, can dock ligands to flexible proteins and can therefore predict not only the binding mode of the ligand but also the most favored conformation of the protein.[11,12] In particular, a number of known conformations are given as input files, and the software ranks the likelihood of those conformations induced by a given ligand. In our previous work we identified a series of structurally related amino acids that exhibit the entire range of agonist behavior at GluK2. Then, we applied Fitted to predict the most likely conformation adopted by those ligands. Starting from three input conformations, induced by L-glutamate, kainate and domoate, all new ligands tested were predicted to bind to the same conformation induced by the natural agonist L-glutamate. This particular conformation had been identified as a 'closed' state, as opposed to the 'intermediate' and 'open' state induced by partial agonists kainate and domoate. This observation supported the hypothesis that agonist efficacy might have other structural bases apart from the degree of cleft closure. Instead, it was argued that agonist efficacy was related to the stability of the closed conformation, in other words to the number of favorable interactions in that particular conformational state.

In the same study we could correlate the degree of opening of GluK2 agonist binding cleft to the translational movement of a

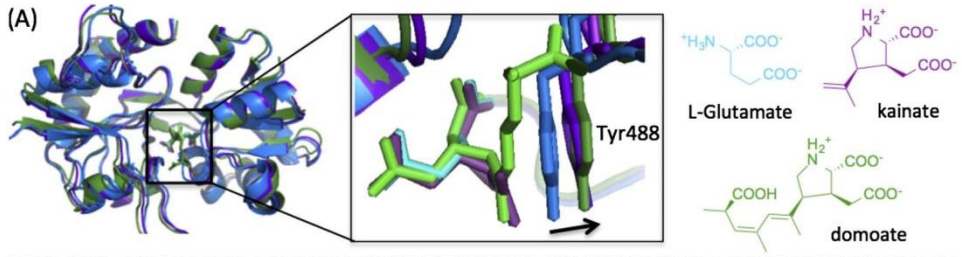

(B)

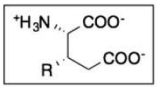

Compound	R	Predicted conformation
L-Glutamate	H	Closed
10	Me	Intermediate
11	Et	Intermediate
12	Pr	Open
13	iBu	Open
14	Ph	Open

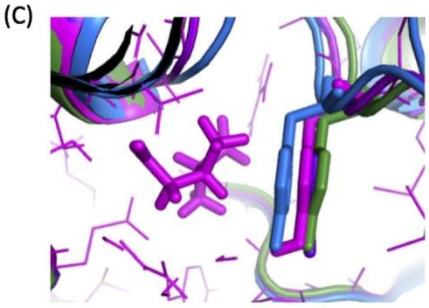

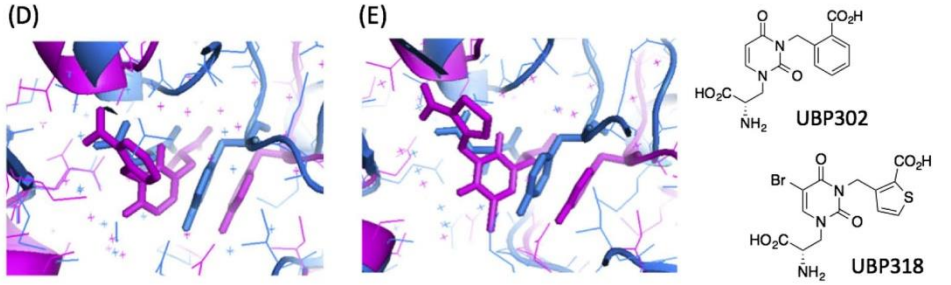

Figure 2. (A) Superimposition of crystal structures of GluK2 ABD bound to glutamate (PDB 1S7Y), kainate (PDB 1TT1) and domoate (PDB 1YAE). The zoom shows the translational movement of Tyr488 in going from a closed state (blue), to intermediate (purple) and open state (green) of GluK2 ABD. Respective ligands are indicated in lighter colors and their structures shown on the right. (B) Series of compounds designed, synthesized and tested. All compounds are predicted by Fitted to induce either an intermediate or an open state of GluK2 ABD. (C) In magenta, predicted conformation induced by **10**, compared to the closed, intermediate and open conformations described in panel A (same color scheme). (D) Superimposition of crystal structures of GluK1 ABD bound to glutamate (in blue, PDB 1TXF) and to antagonist UBP302 (in magenta, PDB 2F35); (E) Superimposition of crystal structures of GluK1 ABD bound to glutamate (in blue) and to antagonist UBP318 (in magenta, PDB 2QS2); On the right, chemical structures of UBP302 and UBP318.

Tyrosine residue (Tyr488) in the orthosteric site.[10] (Fig. 2A). The role of this residue has been also emphasized by Nayeem et al.[13] We hypothesized that the clash between this residue and a bulky group on the nearby ligand could be responsible for hindering full closure of the ABD.

In the study described herein, we wanted to investigate further the effect of ligands that are specifically designed to constrain GluK2 ABD in an intermediate or open state (similar to each other but significantly different from the closed state) through a predicted interaction with the Tyr488. A combination of docking, synthesis and electrophysiological recordings allowed us to collect interesting data for the future design of drugs targeting KA receptors.

In line with traditional structure-based drug design, we started from the visual inspection of the available crystal structures of GluK2. When GluK2 ABD is bound to L-glutamate, it appears that a substituent at the β position of the amino acid would point directly towards Tyr488 (Fig. 2E). To probe this hypothesis, and at the same time minimize the synthetic challenge, we considered the introduction of alkyl groups only. We then relied on our software FITTED to predict which conformational state was favored upon binding of each new potential ligand. Interestingly, the stereochemistry at the β carbon appeared to play an important role in the outcome of the docking. In was found, in fact, that all (3*S*)-β-substituted-glutamates, regardless of the size of the β-substituent, were predicted to induce an intermediate or open state. On the contrary, (3*R*)-analogues showed a less consistent pattern, with some poses being more similar to the closed state. Following our initial interest, only compounds with a (3*S*) stereochemistry were carried forward. Among them, five were successfully synthesized (Fig. 3).

For the synthesis we relied on a procedure that was developed by Wehbe et al. to test β-methylglutamates as EAAT (excitatory amino acid transporters) blockers.[14] In this synthetic methodology the glutamate scaffold is built through a conjugated addition and a chiral auxiliary is used to induce high stereoselectivity at the α carbon (Fig. 3B). The stereoselectivity is not equally high for the β carbon, however we were able to isolate and purify the desired diastereomer. Interestingly, our attempts to introduce secondary or tertiary carbons at the β position (e.g., isopropyl, cyclopropyl, *tert*-butyl) were unproductive. We believe this can be attributed to the high tendency of these β-glutamates to cyclize to pyroglutamic acids in the conditions used for the experiment, a phenomenon reported by Wehbe for methyl analogues. (Fig. 3C).

The five synthesized compounds were tested in a functional assay to determine whether they could competitively bind to GluK2, thereby interfering with L-glutamate binding and the ability of the receptor to activate. Recording pipettes were rapidly switched between background and agonist-containing (typically L-glutamate) external solutions (Fig. 4H), using a piezo-stack driven double-barrelled glass application pipette (details in the Supporting information). The antagonist behaviour of compounds **10**–**14** was assessed by measuring the reduction in GluK2 peak current response. We observed that the first two members of the series, **10** and **11**, when used at 1 mM concentration, inhibited the response of GluK2 to saturating (10 mM) L-Glutamate to 38 ± 3% ($n = 4$) and 46 ± 6% ($n = 4$) of its maximum amplitude (Fig. 4A–B). Compound **12**, when used at the same concentration, slightly inhibited L-glutamate responses to 95 ± 3% of their original amplitude ($n = 4$) (Fig. 4C). The last two bulkier compounds, **13** and **14**, did not affect the current response to glutamate under the same conditions (Fig. 4E–F), indicative of reduced (or minimal) affinity for receptors, relative to their counterparts with smaller substituent groups. Because other trials indicated that the compounds lacked detectable agonist activity at GluK2 receptors (Fig. 4G) our results suggest that the β-methyl, ethyl and propyl glutamates were acting as antagonists.

We also performed an additional experiment to check the absence of artifacts associated with our functional assay set-up. In particular, we wanted to verify that the inhibitor does not have time to unbind from the receptor during the solution exchange (time scale of 100 us). This possibility was indeed ruled out: when compound **11** was present at 1 mM in both the glutamate solution and the background solution, no increase in the inhibition effect was observed. Instead, the response to L-glutamate was reduced to 53 ± 6% ($n = 4$) (data not shown).

Although no experiment definitively confirmed that the molecules under study act as competitive antagonists, their high structural similarity to the natural agonist strongly suggests this is the case. This hypothesis is further supported by the observation that the inhibitory activity decreases with a clear trend in going from more-alike to less-alike analogues of glutamate. Therefore, our assays suggest that compounds **11**, **12** and **13** can compete with the natural ligand for occupancy of the agonist binding cleft.

It also appears that increasing the size of the side chain induces significant clashes of the ligand that is no longer able to compete with the natural ligand under the conditions of the experiments.

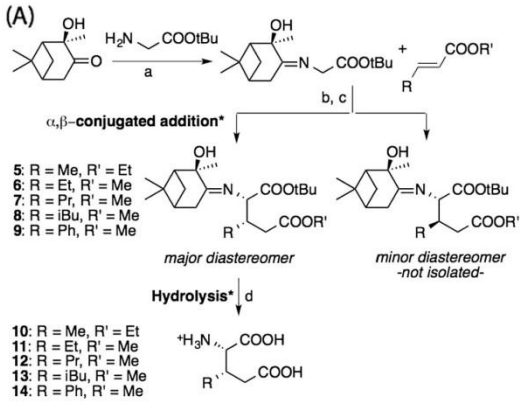

(B)

α,β-conjugated addition*				Hydrolysis*
R	d.r.**	yield (major)		% yield
Me	6:4	34		89
Et	6:4	40		85
Pr	6:4	40		75
iBu	6:4	41		87
Ph	6:4	42		96

** diastereomeric ratio based on ^{1}H NMR analysis

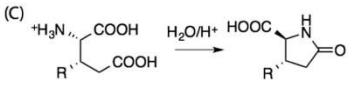

Figure 3. (A) Synthesis of designed ligands: (a) BF_3, benzene, reflux; (b) MeMgBr, THF, −30 °C; (c) DBU, THF, −30 °C; (d) HCl 3 M, reflux; (B) diastereomeric ratios and chemical yields; (C) Proposed reaction of cyclization for β-substituted glutamic acids.

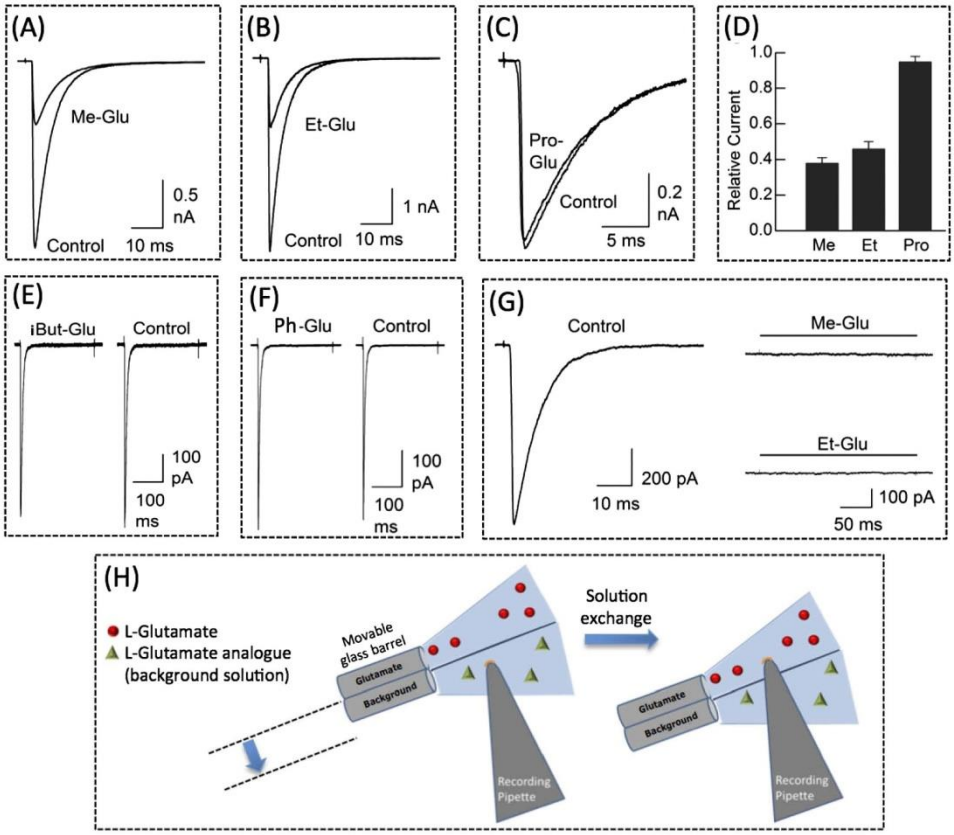

Figure 4. Me-Glu (compound **10**), (B) Et-Glu (compound **11**), and (C) Pro-Glu (compound **12**) inhibition of GluK2 current responses to 10 mM L-glutamate. (D) Summary of inhibition produced by compounds **10**–**12**, shown relative to the L-glutamate induced current measured following a return to the control background solution. (E) In contrast, iBut-Glu (Compound **13**) and (F) Ph-Glu (Compound **14**) did not appear to inhibit responses to 10 mM L-glutamate. (G) When GluK2-expressing patches were exposed to 1 mM Me-Glu ($n = 5$) and Et-Glu ($n = 4$), no current responses were detected, despite the same patches having displayed robust responses to 10 mM L-Glutamate (control). (H) Schematic representation of the functional assay set-up: a membrane patch containing the receptor of interest is first placed on the tip of the recording pipette, and exposed to the antagonist in the background solution prior to L-glutamate application.

The literature contains several reports that can be helpful to rationalize the data. Mayer and colleagues provided insight into the structural basis of KA receptor competitive antagonism by crystallizing GluK1 ABD complexes with novel antagonists. The authors showed that UBP302, UBP310, UBP315, UBP318 and LY466195 induced a similar, generally large opening of the GluK1 agonist binding cleft in comparison to the closed conformation elicited by the full agonist glutamate.[15,16] Although no structural work is available for GluK2 bound to the same or other antagonists, it is reasonable to assume that it behaves similarly to GluK1 from a structural point of view. The two subunits share ~80% peptide sequence, with the most conserved region being around the glutamate binding site. When we look more closely at the available structures of GluK1 ABD bound to L-glutamate and UBP antagonists, and we align the structures, we notice that the tyrosine residue in the ligand proximity undergoes a significant shift (Fig. 2B and C). This indicates that there may be a direct relationship between antagonist behavior and an open conformational state induced at the ABD level.

It must be emphasized that the extent of the movement of the aforementioned tyrosine is based on how structural alignments are performed. In our case, MATCH-UP, a piece of our computational platform FITTED, was used to superimpose the available structures of the ABD without specific structural constraints. Even though current models of iGlu activation predict that the ABD lower domain D2 swings upward relative to D1 when agonists bind, no definitive parallels can be made for GluK1 or GluK2 in the absence of full-length crystal structures of the receptor bound to an antagonist. It is possible that in the receptor physiological state the positions of some binding site residues are more or less constrained than in the isolated ABD, therefore causing unpredicted movements.

Furthermore, based on our observations, it is perplexing that kainate and domoate do not act as GluK2 antagonists, since they induce an intermediate and open conformation, respectively. Even though for most structures the trend remains 'greater closure, greater efficacy', no definitive connection can be made. Indeed, there are examples of antagonists inducing full closure in KAR structures,[17] and of partial agonists inducing varying degrees of closure.[18] One must remember that crystal structures are only snapshots of the receptor at one point in time and do not display other conformations that may be entered less frequently but that are critical for functional behavior. KAR receptors are thought to

be very dynamic and one must take into account the weighted time the receptor spends in closed cleft versus open cleft conformations in regulating efficacy.

Despite the uncertainty that is always correlated with docking studies based on crystal structures, this study refines the existing knowledge about structure-activity relationships for KA inhibition. Most of the antagonists reported so far have a molecular weight significantly higher than glutamate, which agrees with the theory that an effective antagonist must hinder full closure of the ABD acting like a jamming object. Our study reveals that smaller molecules could be as effective, if properly designed. In particular, we showed that targeting Tyr488 in the ABD could be important in the development of effective antagonists. Ensuring that this interaction takes place, while focusing on decreasing the molecular weight, could represent a new potential approach to develop molecules that are able to efficiently reach KA receptors across the blood brain barrier and eventually be useful in the treatment of neuropathological disease states.

Acknowledgments

We thank Eric Therrien for his help and technical support. P.S. was supported by a scholarship from McGill CIHR Drug Discovery Training Program. G.B.D. is funded by an Alexander Graham Bell Canada Graduate Scholarship (CGS-D) through the Natural Sciences and Engineering Research Council of Canada (NSERC). DB is supported by an operating grant from the Canadian Institutes of Health Research (CIHR, FRN: 82804). NM is supported by an discovery grant from NSERC.

Supplementary data

Supplementary data (chemicals and methods used, as well as characterization of compounds) associated with this article can be found, in the online version, at http://dx.doi.org/10.1016/j.bmcl.2015.04.008.

References and notes

1. Jane, D. E.; Lodge, D.; Collingridge, G. L. *Neuropharmacology* **2009**, *56*, 90.
2. Bowie, D. *CNS Neurol. Disord.: Drug Targets* **2008**, *7*, 129.
3. Lerma, J.; Marques, J. M. *Neuron* **2013**, *80*, 292.
4. Larsen, A. M.; Bunch, L. *ACS Chem. Neurosci.* **2011**, *2*, 60.
5. Dawe, G. B. et al *J. Physiol.* **2014**, *593*, 97.
6. Armstrong, N.; Gouaux, E. *Neuron* **2000**, *28*, 165.
7. Kazi, R. et al *Nat. Neurosci.* **2014**, *17*, 914.
8. Zhang, W. et al *Neuron* **2009**, *61*, 385.
9. Dawe, G. B. et al *Nat. Struct. Mol. Biol.* **2013**, *20*, 1054.
10. Fay, A. M. et al *Mol. Pharmacol.* **2009**, *75*, 1096.
11. Corbeil, C. E.; Englebienne, P.; Moitessier, N. *J. Chem. Inf. Model.* **2007**, *47*, 435.
12. Therrien, E. et al *J. Chem. Inf. Model.* **2012**, *52*, 210.
13. Nayeem, N.; Mayans, O.; Green, T. *J. Neurosci.* **2011**, *31*, 2916.
14. Wehbe, J. et al *Tetrahedron: Asymmetry* **2003**, *14*, 1123.
15. Mayer, M. L. et al *J. Neurosci.* **2006**, *26*, 2852.
16. Alushin, G. M.; Jane, D.; Mayer, M. L. *Neuropharmacology* **2011**, *60*, 126.
17. Frydenvang, K. et al *J. Biol. Chem.* **2009**, *284*, 14219.
18. Venskutonyte, R. et al *Neurochem. Int.* **2012**, *61*, 536.

APPENDIX III:

Reprints of published results chapters

nature
structural &
molecular biology

Defining the structural relationship between kainate-receptor deactivation and desensitization

G Brent Dawe[1,2,4], Maria Musgaard[3,4], Elizabeth D Andrews[2], Bryan A Daniels[2], Mark R P Aurousseau[2], Philip C Biggin[3,4] & Derek Bowie[2,4]

Desensitization is an important mechanism curtailing the activity of ligand-gated ion channels (LGICs). Although the structural basis of desensitization is not fully resolved, it is thought to be governed by physicochemical properties of bound ligands. Here, we show the importance of an allosteric cation-binding pocket in controlling transitions between activated and desensitized states of rat kainate-type (KAR) ionotropic glutamate receptors (iGluRs). Tethering a positive charge to this pocket sustains KAR activation, preventing desensitization, whereas mutations that disrupt cation binding eliminate channel gating. These different outcomes explain the structural distinction between deactivation and desensitization. Deactivation occurs when the ligand unbinds before the cation, whereas desensitization proceeds if a ligand is bound without cation pocket occupancy. This sequence of events is absent from AMPA-type iGluRs; thus, cations are identified as gatekeepers of KAR gating, a role unique among even closely related LGICs.

Structural and functional biologists have long sought to understand the mechanisms by which LGICs respond to small chemical ligands and modulators. Seminal work established the general principle that LGICs not only are activated by biologically derived molecules, such as the neurotransmitter acetylcholine[1], but also are inactivated by prolonged exposure to these molecules through a process universally known as desensitization[2]. Since this work, almost all LGICs have been shown to desensitize. For example, desensitization is thought to shape signaling within the vertebrate central nervous system by affecting the fast chemical transmission mediated by iGluRs along with $GABA_A$ and glycine receptors[3]. From all of this work, it has been concluded that the conformational events that lead to the occurrence of deactivation and the onset of desensitization are governed by the physicochemical properties of the bound ligand[4]. In support of this, pioneering work on native AMPA-type iGluRs (AMPARs) has shown that even modest changes to the ligand structure have profound effects on the rates and degree of desensitization[5].

During the last decade, structural and functional analyses of LGICs have revealed that the molecular basis of channel gating may be quite distinct for different ion-channel families[6–8]. For the iGluR family, numerous mechanistic details of activation and desensitization have been identified and extensively commented upon[9–11]. After the elucidation of the ligand-binding domain (LBD) structure[12], a mechanism of iGluR desensitization was proposed, involving the separation of subunits that are assembled as dimers at the LBD[13]. This mechanism has been supported by additional crystal structures that captured AMPARs in different functional states[14]. Accordingly, efforts to engineer iGluR receptors that lack desensitization have focused on constraining movement at the LBD dimer interface. From this, covalent cross-linking of the dimer interface has been shown to generate AMPARs and KARs that yield nondecaying currents upon sustained agonist application[15,16]. Similar experiments on NMDA-type iGluRs have offered a more nuanced explanation of LBD function by uncovering the structural[17] and single-channel effects[18] of dimer cross-linking. Specifically, they propose that constriction of the dimer interface primarily affects open-channel probability and not desensitization[18]. This observation suggests that a more in-depth single-channel analysis of the mechanism of AMPAR and KAR desensitization is warranted.

Here, we set out to study the molecular basis of KAR desensitization by evaluating mutants that are proposed to block it[15,19]. In both cases, the mutations are located in the GluK2 KAR LBD dimer interface, which not only is implicated in receptor desensitization but also contains binding pockets for both sodium and chloride ions[20,21]. Prior work from our laboratory shows that external ions are an absolute requirement for GluK2 receptor activation[22], yet their precise role in desensitization is unresolved[21,23]. Our present data identify that desensitization of KARs proceeds only if a ligand is bound without cation pocket occupancy, whereas deactivation occurs when the ligand unbinds before the cation. This sequence of events identifies external cations as pivotal in directing KARs into active states or long-lived desensitized states.

RESULTS

KARs desensitize with or without prior channel activation

To observe the microscopic behavior of KAR desensitization, we excised outside-out patches from transfected mammalian cells

[1]Integrated Program in Neuroscience, McGill University, Montréal, Québec, Canada. [2]Department of Pharmacology and Therapeutics, McGill University, Montréal, Québec, Canada. [3]Department of Biochemistry, University of Oxford, Oxford, UK. [4]These authors contributed equally to this work. Correspondence should be addressed to P.C.B. (philip.biggin@bioch.ox.ac.uk) or D.B. (derek.bowie@mcgill.ca).

Received 19 March; accepted 17 July; published online 18 August 2013; doi:10.1038/nsmb.2654

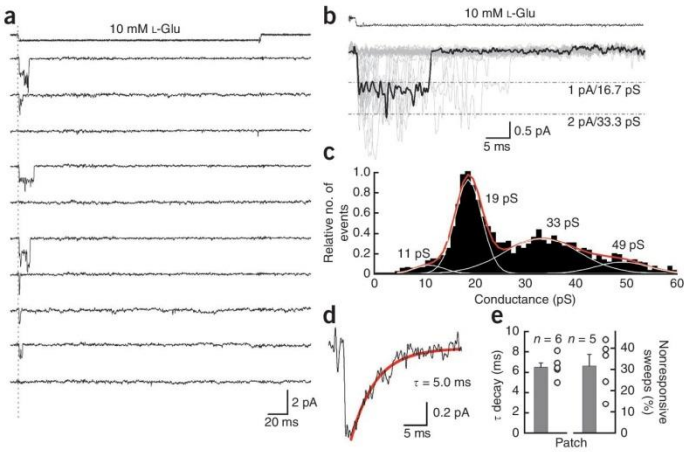

Figure 1 Kainate-receptor desensitization occurs with or without channel activation. (**a**) Typical GluK2 receptor unitary current events elicited by 10 mM L-glutamate (L-Glu; 250-ms pulse duration) in an outside-out patch recording (patch no. 12212p1, –60 mV). (**b**) Overlay of 45 individual current records from the same patch shown in **a**. A typical opening elicited by L-glutamate is shown in thick line. (**c**) GluK2 conductance distributions plotted after time-course fitting. (**d**) Averaged individual current records from the patch in **a** and **b**, showing an ensemble response with a decay fit by a single exponential function whose time constant, τ, is shown. (**e**) Left, decay time constants of ensemble responses from several patches. Right, fraction of L-glutamate applications that did not elicit a measureable response from receptors. Error bars, s.e.m. from five or six independent patch experiments as indicated.

expressing homomeric GluK2 receptors (Online Methods). Using an ultrafast agonist-perfusion system, we recorded single-channel events and then selected, for analysis, recordings in which most responses corresponded to the conductance expected of a single channel[24]. Although the actual number of active receptors per patch is not known, these single-channel recordings nevertheless reveal the different routes taken by KARs before entering into desensitization. In most cases, rapid application of saturating glutamate (10 mM L-glutamate) activated GluK2 receptors, which open to one of several conductance levels (**Fig. 1a–c**). Once in the open state, KAR channels typically closed within tens of milliseconds and did not reopen for any measurable duration of time afterwards, thus indicating that the receptor desensitized. Because desensitization is not thought to occur directly from the open state, it presumably proceeded shortly after channel closure. In agreement with this latter point, ensemble averages of single-channel sweeps exhibited decay time constants (6.49 ± 0.41 ms, $n = 6$; **Fig. 1d,e**) that were statistically indistinguishable from decay rates of macroscopic responses (6.28 ± 0.43 ms, $n = 9$, $P = 0.74$), thus reaffirming that the onset of KAR desensitization is approximated by the duration of channel activity.

In some cases, 10 mM L-glutamate failed to elicit a measurable response during the entire 250-ms application (**Fig. 1a**) corresponding to about 31.7 ± 5.5% of the 525 total sweeps from five patches (**Fig. 1e**). The apparent failure to respond to the agonist may reflect an intrinsic inability of L-glutamate to reliably convert its energy of binding to activation. If this was the case, however, channel opening would eventually be observed, as the continued presence of L-glutamate would ensure that the energy threshold for activation would be overcome. Consequently, the inability of L-glutamate to activate GluK2 receptors must represent the onset of desensitization without prior passage through the open state(s).

The discrete molecular events that bring about desensitization are currently unresolved. Several studies, however, identify the LBD dimer interface[15] and the cation-binding site[19,25] as taking part in the conformational events that initiate KAR macroscopic desensitization. Whether one site or the other has a more direct effect on desensitization has yet to be directly studied. As discussed below, we examined this by studying the single-channel properties of two apparently nondesensitizing GluK2 receptors, namely the mutants D776K and Y521C L783C.

The D776K mutation abolishes GluK2 receptor desensitization

The LBD dimer interface of wild-type GluK2 receptors contains binding sites for two sodium ions and a single chloride ion (**Fig. 2a**)[20,21]. Both GluK2 receptor mutations (D776K and Y521C L783C) are also located at the LBD dimer interface (**Fig. 2b,c**), where they are proposed to eliminate desensitization by constraining subunit movement. The positively charged lysine of D776K establishes new interprotomer contacts by tethering to the cation-binding pocket (**Fig. 2b**)[25], whereas the cysteine residues of Y521C L783C are thought to achieve this through the formation of covalent disulfide bridges between subunits (**Fig. 2c**)[15]. Because both mutant receptors are expected to affect the functional properties of KARs similarly, we were surprised to observe that their single-channel behavior was quite different.

Like wild-type receptors, single D776K channels were rapidly activated by 10 mM L-glutamate. However, instead of opening only briefly before desensitization, agonist binding led to sustained activation of the 21–22 pS main open state (i.e., most frequented) (**Fig. 2d**). In support of this, repetitive applications of 10 mM L-glutamate to patches containing a single D776K receptor elicited activity in every case, thus demonstrating that this mutant GluK2 receptor displays close to the maximum probability of opening. Averaged ensemble responses were nondecaying in nature with rapid off kinetics of ~2–3 ms due to L-glutamate removal (**Fig. 2d**). These persistent openings were nevertheless interrupted by transient closures too brief to represent long-lived desensitized states and which, consequently, must represent sojourns to lower conductance levels or closed or ligand-free states.

Unlike the D776K receptor, the double-cysteine mutant did not yield persistent channel activity in saturating L-glutamate. Instead, recordings were dominated by submillisecond openings that were separated by longer apparent closures (**Fig. 2e**)[26]. Given the infrequent nature of gating, we concluded that responses observed in the excised patches were likely to originate from multiple channels. Despite the transient openings, averaging sweeps from many agonist applications generated a nondecaying ensemble response. The decay kinetics of the ensemble average current of Y521C L783C receptors were nevertheless at least five times slower (14.8 ± 2.9 ms, $n = 4$) than those of D776K receptors (**Fig. 2e**).

For GluK2 D776K, its consistent gating behavior allowed us to make additional inferences. Time-course fitting of resolvable single-channel events estimated conductance levels of 21, 35 and 40 pS, which were

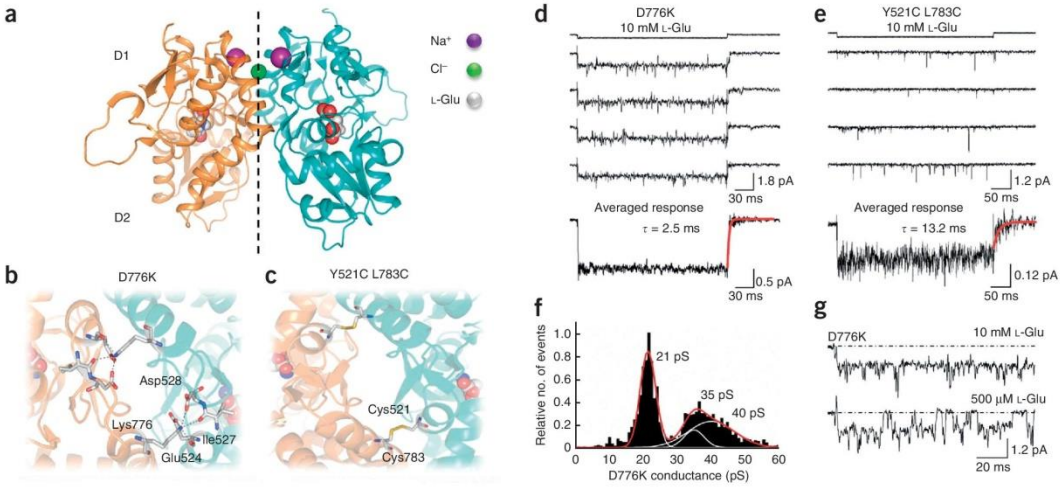

Figure 2 Mutation D776K eliminates GluK2 receptor desensitization. (**a**) Crystal structure of the wild-type GluK2 LBD dimer (PDB 3G3F[42]), including the upper (D1) and lower (D2) domains. (**b**) Top view of the GluK2 D776K LBD dimer interface showing electrostatic interactions between Lys776 and the adjacent subunit (PDB 2XXX[25]). (**c**) Top view of the GluK2 Y521C L783C LBD dimer interface showing covalent cross-linking between subunits (PDB 2I0C[15]). (**d**) Typical current responses elicited by L-glutamate acting on a single D776K channel (patch no. 12127p2, −60 mV). (**e**) Unitary current events elicited by L-glutamate acting on Y521C L783C channels (patch no. 12322p3, −100 mV). In **d** and **e**, averaged ensemble responses were taken from 20 or 95 individual current records, respectively. Time constants of deactivation were obtained by fitting agonist-off current responses with a single exponential function. (**f**) GluK2 D776K conductance distributions plotted after time-course fitting. (**g**) Individual current responses of a single GluK2 D776K receptor to 10 mM and 500 μM L-glutamate (patch no. 12124p1).

calculated by a measured reversal potential of 0 mV (**Fig. 2f**). The open level most frequently visited was 21–22 pS, closely matching the predominant 19-pS conductance level of wild-type receptors, with the two largest conductance levels corresponding to brief sojourns from this state (i.e., 35 and 40 pS). Fitting Gaussian functions to an all-points histogram of D776K data further shows that >90% of the analyzed records corresponded to the main open state (**Supplementary Fig. 1**). These conductance levels are likely to originate from single channels rather than from several channels opening simultaneously, as lowering the concentration of L-glutamate interrupted openings to the 21- to 22-pS state with clear closures to baseline (**Fig. 2g**).

In summary, our single-channel data reveal that GluK2 D776K exhibits all the hallmarks expected of a nondesensitizing KAR: sustained activation, high unitary conductance and an absence of long-duration closures. GluK2 Y521C L783C responds quite differently, and therefore we could conclude that the structural basis of its functional behavior must be different. Because the Lys776 residue is proposed to act as a tethered cation[25], we reasoned that occupancy of the ion-binding pocket might be the key structural event that prevents the onset of desensitization. If true, cation interactions at the Y521C L783C receptor might therefore be unstable, and this would account for differences observed at the single-channel level. As explained below, we tested this hypothesis by using molecular dynamics (MD) simulations to estimate the residency time of sodium bound to the cation-binding pockets of both D776K and Y521C L783C receptors.

Lys776 substitutes for sodium at the cation-binding pocket

We used MD simulations to explore how electrostatic interactions affect occupancy of the cation-binding pocket, a relationship that cannot be clarified with X-ray crystal structures or electrophysiology. Over the course of each of two 100-ns simulations, the cation pockets of the D776K receptor first released both sodium ions and then formed new contact points with the amino groups of Lys776 (**Fig. 3a–d** and **Supplementary Movie 1**). Consequently, the cation-binding pocket was nearly continuously occupied by a positive charge during the entire simulation period, a result consistent with previous structural data[25]. In contrast, simulations of the Y521C L783C receptor predict that these mutations destabilize sodium- and chloride-ion binding, thus facilitating rapid ion release in both simulations performed (**Supplementary Fig. 2a**,**b** and **Supplementary Movie 2**). There was also a tendency for water molecules to more readily occupy the cation pockets of Y521C L783C, and this may explain the instability in sodium- and chloride-ion binding. Measurements of the surface area accessible to solvent indicated a much higher propensity for water molecules to interact with residues lining the cation pocket in the double-cysteine mutant compared to wild-type GluK2 receptors (**Supplementary Fig. 2c**,**d**). If these simulations reflect the physiological behavior of kainate receptors, then activation could depend on the occupancy of the cation pocket, and cation unbinding would promote channel closure and/or desensitization.

GluK2 D776K receptors activate without external cations

If occupancy of the cation-binding pocket is a prerequisite for wild-type KAR activation, removal of all external ions should result in the absence of any detectable current. Although such recordings have already been shown to abolish wild-type KAR activity[22], this original finding has been disputed by more recent work claiming residual channel activity in ion-free conditions[21]. To re-examine this issue, we repeated experiments comparing GluK2 receptors in the presence and absence of external ions. If Lys776 acts as a tethered cation, as suggested by MD simulations (**Fig. 3**) and structural data[25], we reasoned that the GluK2 D776K would gate in the absence of

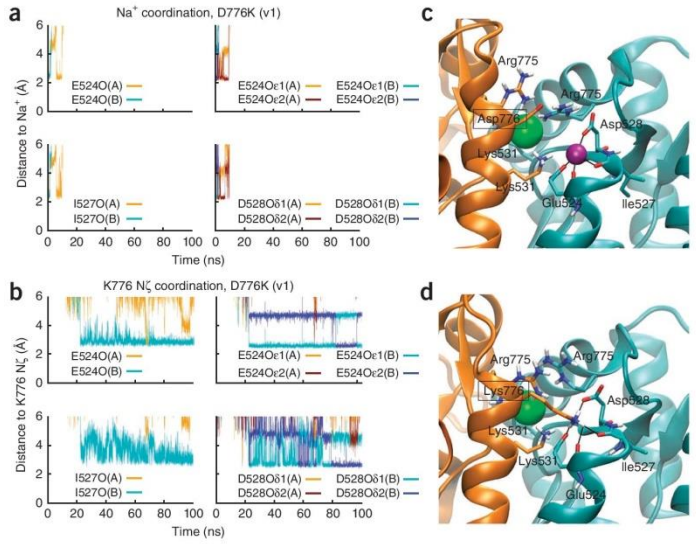

Figure 3 Lys776 can act as a tethered ion at the GluK2 cation-binding pocket. (**a**) Coordination distances between sodium ions (bound to chains A and B) and several oxygen atoms found on residues lining the cation-binding pocket (E524, I527 and D528) during a 100-ns MD simulation (version or repeat 1, v1) of the D776K mutant. (**b**) Coordination distances for the positively charged Nζ of Lys776 (simulation repeat 1, v1). Distances were measured from oxygen atoms normally involved in sodium ion coordination. (**c**) Sodium ion coordination in the crystal structure of wild-type GluK2 LBD. (**d**) Snapshot after 100 ns of MD simulation of the D776K mutant. Orange, chain A and its residues; cyan, chain B and its residues; purple, sodium ion; green, chloride ion. Coordination distances are indicated with black lines for the sodium ion (**c**) and the Lys776 amine (**d**). Water molecules and nonpolar hydrogen atoms are omitted. Black boxes surround mutated residues.

external cations. In contrast, the instability of cation binding to GluK2 Y521C L783C suggests that this mutant would fail to gate in the absence of ions unless cross-linking of the LBD dimer interface permits activation through a different mechanism. Consistent with the above predictions, wild-type GluK2 receptor activity was completely abolished by the removal of external monovalent ions (**Fig. 4a**,**b**), whereas the D776K receptor continued to gate (**Fig. 4c**,**d**), thus demonstrating that the wild-type GluK2 receptor gating mechanism has an absolute requirement for external cations. These data also further support the idea that the Lys776 residue acts as a tethered cation, thus accounting for the ability of the D776K receptor to gate in the absence of external ions.

Interestingly, the Y521C L783C receptor was also able to gate in the absence of external cations (**Fig. 4e**,**f**). This finding is in agreement with a prior study[21] but is inconsistent with the lack of responsiveness of wild-type GluK2 receptors in ion-free conditions (**Fig. 4a**,**b**), thus suggesting the need for an alternative explanation. With this in mind, we considered the possibility that cross-linking of the dimer interface of the GluK2 receptor may eliminate the requirement of external cations for activation. We tested this possibility by identifying mutations in the LBD dimer interface that would disrupt cation binding without forming interprotomer cross-links.

Destabilizing cation binding impairs GluK2 activation

We studied disruption of the cation-binding pocket by examining two mutant receptors, namely GluK2 E524G and L783C, which MD simulations suggest destabilize sodium binding to the cation-binding pocket. Importantly, these mutations do not affect receptor surface expression (**Supplementary Fig. 3a**,**b**). For E524G, which has a less electronegative cation pocket, two 50-ns simulations of sodium coordination both estimated that sodium is released within 5 ns. In contrast, the wild-type receptor retained sodium for the duration of two 100-ns

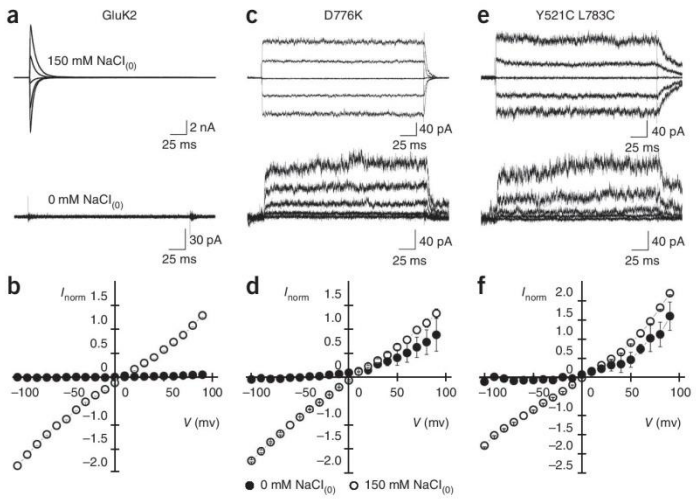

Figure 4 GluK2 D776K receptors gate in the absence of external ions. (**a**,**c**,**e**) Membrane currents evoked by L-glutamate acting on wild-type GluK2 (**a**), D776K (**c**) and Y521C L783C (**e**) receptors, in either 150 mM NaCl (top) or in nominal ion-free (bottom) external solution (V_m = –60, –30, 0, 30 and 60 mV). For wild-type GluK2, the same patch was recorded in both ionic conditions (patch no. 121106p2). Mutant responses were taken from different patches (D776K ion, patch no. 11510 p1; ion free, patch no. 12925p5; Y521C L783C ion, patch no. 121002p2; ion free, patch no. 121023p2). (**b**,**d**,**f**) Averaged current (I_{norm})-voltage (V) plots in 0 mM (filled circles) and 150 mM (open circles) NaCl for wild-type GluK2 (**b**), D776K (**d**) and Y521C L783C (**f**) receptors. Currents were normalized to responses at –60 mV in 150 mM NaCl. Error bars, s.e.m. from three independent experiments for each receptor.

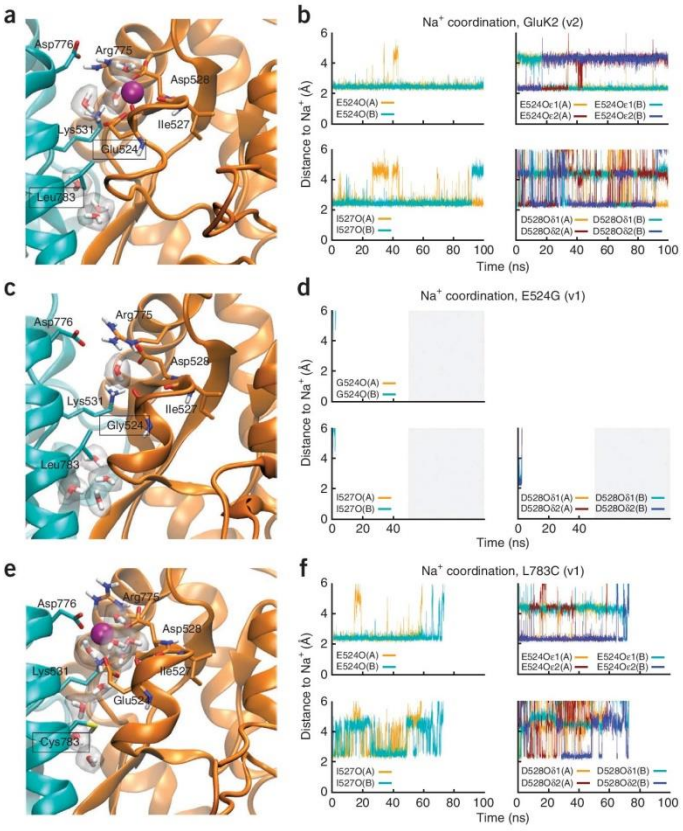

Figure 5 Occupancy of the GluK2 cation-binding pocket is predicted to be disrupted by targeted mutation of the dimer interface. (**a**,**c**,**e**) Snapshots of sodium coordination in the wild-type GluK2 receptor (**a**), as well as mutants E524G (**c**) and L783C (**e**), all taken ~15 ns after the start of the MD simulation. Black boxes surround mutated residues. (**b**,**d**,**f**) Sodium coordination plotted from MD simulations of the LBD dimer in the wild-type GluK2 receptor, repeat 2, v2 (**b**) and mutants E524G, repeat 1, v1 (**d**) and L783C, repeat 1, v1 (**f**).

simulations (**Fig. 5a–d** and **Supplementary Movies 3** and **4**). In this respect, E524G mimics the Y521C L783C receptor; however, it differs in that 10 mM L-glutamate fails to elicit a measurable response in most excised patches (**Supplementary Fig. 3c**). We did observe responses in 3 out of the 18 patches tested, but they were small (<10 pA at −60 mV) in amplitude and thus consistent with the E524G mutation acting to destabilize cation binding.

Interestingly, when only one of the cross-linking residues (i.e., L783C) was mutated, 10 mM L-glutamate failed to elicit a response in all cases, whether we examined whole-cell recordings (B.A.D. and D.B., unpublished data) or excised patches (n = 15) (**Supplementary Fig. 3c**). MD simulations suggested that the L783C mutant has a less pronounced effect than does E524G on sodium stability, yet the ions managed to dissociate from their binding pockets within 100 ns in one of two simulations (**Fig. 5e**,**f**). One potential explanation for the sodium dissociation is that the L783C mutant permits access of additional water molecules into the cation-binding pocket (**Supplementary Movie 5**), as observed in simulations of Y521C L783C. In comparison to the wild-type GluK2 receptor, the sodium ions in L783C interacted more frequently with water molecules and less frequently with residues of the cation pocket (M.M. and P.C.B., unpublished data). In both mutants, our data point to the lack of responsiveness of E524G and L783C arising from their disruptive effects on the cation-binding pocket, a condition that may be similar to desensitization in a wild-type receptor. Because mutant receptors that disrupt L-glutamate binding are retained within mammalian cells[27], we do not think that an inability to bind agonists can account for the phenotypes of E524G and L783C. As a result, an explanation is required to account for an additional cysteine (Y521C) restoring channel gating when introduced atop the L783C mutation. We conclude that the cation-independent activation of GluK2 Y521C L783C is due to its covalent cross-linking of the dimer interface circumventing the normal gating requirements of the wild-type receptor (additional information in ref. 26).

KAR desensitization proceeds after cation unbinding

MD simulations and single-channel data suggest that GluK2 D776K receptors are nondesensitizing, because Lys776 becomes tethered to the cation-binding pocket. We therefore conclude that cation binding primes KARs for activation by the agonist. We also conclude that cation-unbound states are not primed for activation, and thus agonist binding promotes entry into desensitized states, as observed with the L783C and E524G mutant receptors. These different outcomes are important because they will determine the degree to which desensitization, and by implication cation unbinding, contributes to the wild-type KAR response. For example, during long agonist applications routinely used to measure desensitization rates, most receptors should desensitize because cations will eventually unbind with the agonist still bound. In contrast, with brief applications of L-glutamate used to measure deactivation rates, fewer GluK2 receptors should desensitize, because the agonist will unbind before the cation. Importantly, this sequence of events can be tested experimentally. Specifically, we predict that deactivation rates estimated with a brief agonist application should be minimally affected by the presence or absence of desensitization because decay from the peak response corresponds to agonist unbinding from the cation-bound state(s).

To examine the impact of desensitization on deactivation rates, we compared the relaxation kinetics observed after a brief application (i.e., 1 ms) of 10 mM L-glutamate onto wild-type and nondesensitizing D776K KARs (**Fig. 6a**). For comparison, we also performed a similar analysis of wild-type and a mutant GluA1 AMPA receptor (i.e., L497Y) in which single-channel desensitization is strongly inhibited[28] (**Fig. 6b**). Wild-type GluK2 receptors exhibited a fast exponential time constant of deactivation of 2.3 ± 0.1 ms (n = 7) (**Fig. 6a**), which was statistically indistinguishable from the off kinetics of

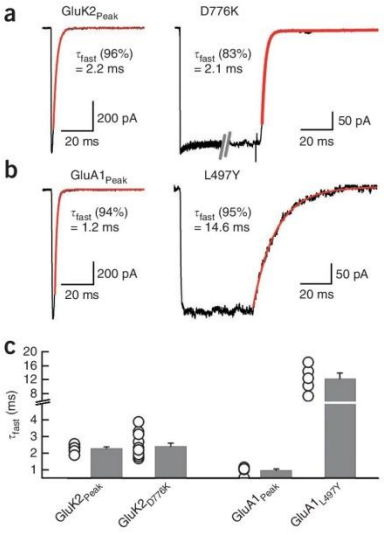

Figure 6 Desensitization and deactivation are uncoupled in GluK2 KARs. (**a**) Typical current decay observed after removal of 10 mM L-glutamate from wild-type GluK2 (1-ms application, patch no. 00327p3) and GluK2 D776K (250-ms application, patch no. 11506p1) receptors. (**b**) Typical current decay observed after removal of 10 mM L-glutamate from wild-type GluA1 (1-ms application, patch no. 00404p1, −55 mV) and GluA1 L497Y (50-ms application, patch no. 99608p1, −55 mV) receptors. For **a** and **b**, decay kinetics from saturating L-glutamate were fit with a second-order exponential function (red) with representative values of the fast, dominant component displayed. (**c**) Distribution of off-kinetic rates show that the τ_{fast} values for the GluK2 peak response and D776K were statistically indistinguishable (described in text), whereas the values for the GluA1 peak response and L497Y were statistically different ($P < 0.001$ by two-tailed Student's t test ($\alpha = 0.05$)). Error bars, s.e.m. from seven (GluK2), twelve (D776K), six (GluA1) or five (L497Y) independent experiments.

D776K receptors regardless of whether 1-ms (2.0 ± 0.2 ms, $n = 9$; $P = 0.63$) or 250-ms agonist pulses (2.4 ± 0.2 ms, $n = 12$; $P = 0.82$) were applied (**Fig. 6a**,**c**). These observations support our assertion that KAR desensitization proceeds after cation unbinding. Accordingly, deactivation and desensitization can therefore be viewed as being structurally distinct and separable processes. In contrast, the decay time constant observed after a 1-ms application of 10 mM L-glutamate to GluA1 AMPARs had a fast exponential time constant of 1.0 ± 0.1 ms ($n = 6$) (**Fig. 6b**), which was about 10 times faster than the off kinetics of the nondesensitizing L497Y mutant (12.4 ± 1.6 ms, $n = 5$; **Fig. 6b**,**c**). This finding is consistent with the effect of the allosteric modulator cyclothiazide, which also attenuates AMPAR desensitization[29].

To further test the impact of desensitization on the activation process, we compared the dose-response relationships of GluK2 D776K and wild-type receptors. We reasoned that because the absence of desensitization had little to no effect on GluK2 deactivation kinetics, rates of L-glutamate unbinding should be high relative to rates of cation unbinding, which equate with desensitization. Under such circumstances, receptors would tend to enter desensitized states only during sustained L-glutamate application. As such, the dose-response relationship of the peak response, occurring less than 1 ms after L-glutamate exposure, should exhibit little change in the absence of desensitization.

In agreement with our predictions, the half-maximal effective concentration (EC_{50}) (and Hill coefficient, n_H) estimated from peak dose-response curves to L-glutamate acting on wild-type GluK2 receptors

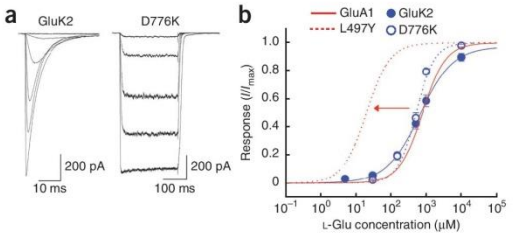

Figure 7 Desensitization does not substantially shift peak agonist potency of GluK2 KARs. (**a**) Typical current responses elicited by L-glutamate (10 μM–10 mM) acting on wild-type GluK2 (patch no. 091204p2) and GluK2 D776K (patch no. 11610p1) receptors. (**b**) L-glutamate dose-response relationships for KARs, normalized to the maximal current (I_{max}) of each patch, as well as simulated dose-response curves of wild-type and GluA1 L497Y receptors taken from previously reported values[29]. Error bars, s.e.m. from seven (GluK2) and eight (D776K) independent experiments.

was 652 ± 47 μM ($n_H = 0.87$, $n = 7$), which closely matched that of D776K receptors, whose EC_{50} values were estimated to be 520 ± 91 μM ($n_H = 1.6$, $n = 8$) (**Fig. 7a**,**b**). These data differ from past work on AMPARs, which has shown that mutations and allosteric modulators that reduce or eliminate desensitization cause progressive leftward shifts in the wild-type dose-response curve[28,29]. For example, one study noted a leftward shift of over an order of magnitude from the wild-type EC_{50} to that of GluA1 L497Y[29] (**Fig. 7b**). Our observations comparing wild-type and D776K receptors support the idea that desensitization has little impact on the time GluK2 receptors remain activated. This is, of course, to be expected if desensitization can proceed only after cation unbinding. Indeed, MD simulations reported here suggest that LBD dimer separation, a structural correlate of desensitization, is promoted for wild-type receptors in the absence of bound sodium ions (**Supplementary Fig. 4**). Our findings also suggest that desensitization affects the time course of AMPAR activation, and this explains the effect of desensitization on both deactivation kinetics and agonist potency.

DISCUSSION

The present study advances the understanding of iGluR gating in several ways. First, we show that cation occupancy is the central requirement in keeping agonist-bound KARs in the activated state and out of desensitization. Second, we propose a structural model for the sequence of events that give rise to deactivation and desensitization. Deactivation is observed when the ligand unbinds from cation-bound states, whereas desensitization proceeds when the ligand is bound to cation-unbound states. Third, and finally, closely related AMPARs do not share this reliance on cation-dependent gating; as a result, desensitization appears able to curtail AMPAR channel activation. As discussed below, this unique property of KARs may provide clues as to how subunit composition and/or auxiliary proteins affect native receptors at glutamatergic synapses.

The KAR dimer interface is a multifaceted structure

It is remarkable that subunit cross-linking at two neighboring sites (residues 776 and 783) along the GluK2 LBD dimer interface produces

very different functional consequences. The Y521C L783C mutation bridges opposing subunits, yet the crystal structure of its LBD suggests a separation of the upper D1 segment of the dimer interface[15]. Although separation of the dimer interface is thought to underlie both KAR and AMPAR desensitization[13], it is not clear how much separation would be tolerable before channel activation could no longer be maintained. Given microscopic recordings showing that Y521C L783C channels cannot stably access the main open state of wild-type GluK2 (ref. 26), we propose that this mutant is a mostly desensitized receptor typified by an open interface and/or a poorly activating receptor by virtue of its sporadic channel openings.

Targeted slightly higher along the LBD interface, the mutant residue Lys776 occupies the GluK2 cation-binding pocket and has two related consequences on receptor function: it increases open-channel probability to such an extent that no failures are observed, and it sustains activation for the duration of agonist application. The latter effect supports the idea that the molecular events leading to desensitization are triggered at the apex of the interface rather than being coordinated through the interface as a whole. Whether these interactions are further complicated according to an emerging idea that KAR subunits desensitize with a tetrameric symmetry and not as a dimer of dimers[30,31] awaits future study.

The cation-binding pocket and its relation to gating events

Although structural rearrangements of the LBD accompany iGluR desensitization[13], it is presently unknown how such conformational changes are initiated. The matter is further complicated in KARs, in which bound ions have been proposed to stabilize the LBD dimer interface[20]. Here, we establish a framework to specify when KARs activate and desensitize by identifying the cation-binding pocket as the molecular switch between these processes. In short, cation pocket occupancy maintains KAR activation, and by implication desensitization cannot occur until cations unbind. The link between cation binding and activation is based on several key observations reported above: the sustained single-channel activation in the GluK2 D776K mutation (**Fig. 2**), in which the cation-binding pocket is thought to be continuously occupied; the inability of GluK2 to activate in the absence of external ions (**Fig. 4**); and the gating deficiencies among mutants designed to disrupt cation binding (**Fig. 5** and **Supplementary Fig. 3**). Furthermore, the assertion that cation unbinding precedes desensitization can be deduced from other observations we reported. Specifically, we showed that deactivation kinetics of wild-type KARs were unaffected by desensitization, thus confirming our assertion that the decay of the KAR peak response corresponds to agonist unbinding from the cation-bound state(s) (**Fig. 6a**,**c**). This conclusion is consistent with previous work showing that GluK2 deactivation kinetics are made faster by lowering of the external cation concentration or replacement of sodium with another cation[32]. With long agonist applications (i.e., 250 ms), we propose that the decline in KAR activity is due to cation unbinding because besides the presence of the agonist, the only other known requirement of KARs to activate is allosteric ions[22]. Given this, we concluded that their departure was the most plausible explanation to trigger the onset of desensitization. In accordance with this notion, MD simulations reported here (**Supplementary Fig. 4**) predict that removal of cations from the LBD dimer interface can induce structural changes associated with the desensitized state(s).

An alternative explanation for the observations above is that KAR desensitization is triggered by intrinsic rearrangements to the LBD structure, which are countered through the occupancy of bound cations. From this perspective, the relation between bound cations and decay kinetics is attributable to a direct modulation of the intrinsic rate of desensitization (by stabilization of LBD dimers), as has been suggested previously[21]. This interpretation, however, is difficult to reconcile with several observations. To begin with, if desensitization is merely opposed but not blocked by the presence of bound cations, some residual activation should be detected in solutions lacking external ions, but this is not the case. Furthermore, from this perspective, the effect of cation species on deactivation kinetics would have to be explained by desensitization rates overlapping with those of deactivation. Experiments reported here show that deactivation kinetics are unaffected by desensitization (i.e., comparison of D776K to wild-type GluK2 receptors) (**Fig. 6**), meaning that desensitization must therefore occur on a slower time scale. Thus, the two processes do not overlap, and activation must be directly regulated by cations.

Ion channels use different strategies to desensitize

Desensitization of LGICs has been classically thought to arise from agonist molecules converting receptor complexes into nonreactive forms[33], in much the same way that even earlier work linked changes in membrane potential to voltage-gated ion-channel inactivation[34]. Since then, structural explanations have emerged to account for how the processes of inactivation and desensitization occur at the amino acid level. Some of the first insights came from work on voltage-gated sodium and potassium channels, which were shown to possess intracellular inactivation gates[35,36], whereas work on cysteine-loop LGICs hinted at a broader rearrangement of quaternary structure[37]. Pioneering studies also identified coupling between activation and inactivation of voltage-gated channels[38], although this coupling has been more difficult to establish at LGICs. Such coupling might be expected to occur at iGluRs because closure in the agonist-binding domain initiated by ligand binding is thought to bring about both activation and subsequent desensitization, as the agonist becomes entrapped in a stable yet inactive conformation[12,39]. In keeping with this, data presented in this study suggest a tight coupling between these structural events in AMPARs. Interestingly, this is not the case for KARs, which uncouple the process of activation from desensitization through cation-dependent gating. This unique aspect of KAR gating provides an ideal target by which native receptor responses could be modulated at central synapses. For example, alterations in cation affinity through protein-protein interactions could explain how heteromeric subunits[40] and/or auxiliary proteins[24] regulate the duration of synaptic KAR activity[41]. Clearly, much still remains to be examined in future studies, including how this allosteric cation-binding pocket might be exploited to regulate KAR signaling within the vertebrate central nervous system.

METHODS

Methods and any associated references are available in the online version of the paper.

Note: Any Supplementary Information and Source Data files are available in the online version of the paper.

ACKNOWLEDGMENTS

This work was supported by operating grants from the Canadian Institutes of Health Research (CIHR) FRN-82804 (D.B.) and by the Leverhulme Trust RPG-059 (P.C.B.). G.B.D. and E.D.A. were supported by Natural Sciences and Engineering Research Council of Canada graduate fellowships, B.A.D. by a Chemical Biology CIHR postdoctoral award and M.R.P.A. by a CIHR Best & Banting doctoral award. D.B. is supported by a Canada Research Chair award. We thank the Oxford Supercomputing Centre for computer time. Finally, we wish to thank J. Johnson for comments on the manuscript and M. Fleck for discussions on AMPA receptors.

AUTHOR CONTRIBUTIONS

G.B.D. designed and performed experiments, analyzed data and wrote the paper; M.M., B.A.D. and M.R.P.A. designed and performed experiments and analyzed

data; E.D.A. analyzed data; P.C.B. designed experiments; and D.B. designed and performed experiments, analyzed data and wrote the paper.

COMPETING FINANCIAL INTERESTS
The authors declare no competing financial interests.

1. Katz, B. & Thesleff, S. A study of the desensitization produced by acetylcholine at the motor end-plate. *J. Physiol.* (*Lond.*) **138**, 63–80 (1957).
2. Shelley, C. & Cull-Candy, S.G. Desensitization and models of receptor-channel activation. *J. Physiol.* (*Lond.*) **588**, 1395–1397 (2010).
3. Jones, M.V. & Westbrook, G.L. The impact of receptor desensitization on fast synaptic transmission. *Trends Neurosci.* **19**, 96–101 (1996).
4. Hille, B. *Ion Channels of Excitable Membranes* 169–200 (Sinauer Associates, 2001).
5. Patneau, D.K., Mayer, M.L., Jane, D.E. & Watkins, J.C. Activation and desensitization of AMPA/kainate receptors by novel derivatives of willardiine. *J. Neurosci.* **12**, 595–606 (1992).
6. Traynelis, S.F. *et al.* Glutamate receptor ion channels: structure, regulation, and function. *Pharmacol. Rev.* **62**, 405–496 (2010).
7. Corringer, P.J. *et al.* Structure and pharmacology of pentameric receptor channels: from bacteria to brain. *Structure* **20**, 941–956 (2012).
8. Flynn, G.E., Johnson, J.P. Jr. & Zagotta, W.N. Cyclic nucleotide-gated channels: shedding light on the opening of a channel pore. *Nat. Rev. Neurosci.* **2**, 643–651 (2001).
9. Hansen, K.B., Yuan, H. & Traynelis, S.F. Structural aspects of AMPA receptor activation, desensitization and deactivation. *Curr. Opin. Neurobiol.* **17**, 281–288 (2007).
10. Wollmuth, L.P. & Sobolevsky, A.I. Structure and gating of the glutamate receptor ion channel. *Trends Neurosci.* **27**, 321–328 (2004).
11. Madden, D.R. The structure and function of glutamate receptor ion channels. *Nat. Rev. Neurosci.* **3**, 91–101 (2002).
12. Armstrong, N., Sun, Y., Chen, G.Q. & Gouaux, E. Structure of a glutamate-receptor ligand-binding core in complex with kainate. *Nature* **395**, 913–917 (1998).
13. Sun, Y. *et al.* Mechanism of glutamate receptor desensitization. *Nature* **417**, 245–253 (2002).
14. Armstrong, N., Jasti, J., Beich-Frandsen, M. & Gouaux, E. Measurement of conformational changes accompanying desensitization in an ionotropic glutamate receptor. *Cell* **127**, 85–97 (2006).
15. Weston, M.C., Schuck, P., Ghosal, A., Rosenmund, C. & Mayer, M.L. Conformational restriction blocks glutamate receptor desensitization. *Nat. Struct. Mol. Biol.* **13**, 1120–1127 (2006).
16. Priel, A., Selak, S., Lerma, J. & Stern-Bach, Y. Block of kainate receptor desensitization uncovers a key trafficking checkpoint. *Neuron* **52**, 1037–1046 (2006).
17. Gielen, M. *et al.* Structural rearrangements of NR1/NR2A NMDA receptors during allosteric inhibition. *Neuron* **57**, 80–93 (2008).
18. Borschel, W.F., Murthy, S.E., Kasperek, E.M. & Popescu, G.K. NMDA receptor activation requires remodelling of intersubunit contacts within ligand-binding heterodimers. *Nat. Commun.* **2**, 498 (2011).
19. Nayeem, N., Zhang, Y., Schweppe, D.K., Madden, D.R. & Green, T. A nondesensitizing kainate receptor point mutant. *Mol. Pharmacol.* **76**, 534–542 (2009).
20. Plested, A.J. & Mayer, M.L. Structure and mechanism of kainate receptor modulation by anions. *Neuron* **53**, 829–841 (2007).
21. Plested, A.J., Vijayan, R., Biggin, P.C. & Mayer, M.L. Molecular basis of kainate receptor modulation by sodium. *Neuron* **58**, 720–735 (2008).
22. Wong, A.Y., Fay, A.M. & Bowie, D. External ions are coactivators of kainate receptors. *J. Neurosci.* **26**, 5750–5755 (2006).
23. Bowie, D. Ion-dependent gating of kainate receptors. *J. Physiol.* (*Lond.*) **588**, 67–81 (2010).
24. Zhang, W. *et al.* A transmembrane accessory subunit that modulates kainate-type glutamate receptors. *Neuron* **61**, 385–396 (2009).
25. Nayeem, N., Mayans, O. & Green, T. Conformational flexibility of the ligand-binding domain dimer in kainate receptor gating and desensitization. *J. Neurosci.* **31**, 2916–2924 (2011).
26. Daniels, B.A., Andrews, E.D., Aurousseau, M.R., Accardi, M.V. & Bowie, D. Crosslinking the ligand-binding domain dimer interface locks kainate receptors out of the main open state. *J. Physiol.* (*Lond.*) http://dx.doi.org/10.1113/jphysiol.2013.253666 (27 May 2013).
27. Mah, S.J., Cornell, E., Mitchell, N.A. & Fleck, M.W. Glutamate receptor trafficking: endoplasmic reticulum quality control involves ligand binding and receptor function. *J. Neurosci.* **25**, 2215–2225 (2005).
28. Stern-Bach, Y., Russo, S., Neuman, M. & Rosenmund, C. A point mutation in the glutamate binding site blocks desensitization of AMPA receptors. *Neuron* **21**, 907–918 (1998).
29. Mitchell, N.A. & Fleck, M.W. Targeting AMPA receptor gating processes with allosteric modulators and mutations. *Biophys. J.* **92**, 2392–2402 (2007).
30. Bowie, D. & Lange, G.D. Functional stoichiometry of glutamate receptor desensitization. *J. Neurosci.* **22**, 3392–3403 (2002).
31. Schauder, D.M. *et al.* Glutamate receptor desensitization is mediated by changes in quaternary structure of the ligand binding domain. *Proc. Natl. Acad. Sci. USA* **110**, 5921–5926 (2013).
32. Bowie, D. External anions and cations distinguish between AMPA and kainate receptor gating mechanisms. *J. Physiol.* (*Lond.*) **539**, 725–733 (2002).
33. Del Castillo, J. & Katz, B. Interaction at end-plate receptors between different choline derivatives. *Proc. R. Soc. Lond. B Biol. Sci.* **146**, 369–381 (1957).
34. Hodgkin, A.L. & Huxley, A.F. The dual effect of membrane potential on sodium conductance in the giant axon of *Loligo*. *J. Physiol.* (*Lond.*) **116**, 497–506 (1952).
35. Hoshi, T., Zagotta, W.N. & Aldrich, R.W. Biophysical and molecular mechanisms of Shaker potassium channel inactivation. *Science* **250**, 533–538 (1990).
36. Stühmer, W. *et al.* Structural parts involved in activation and inactivation of the sodium channel. *Nature* **339**, 597–603 (1989).
37. Unwin, N., Toyoshima, C. & Kubalek, E. Arrangement of the acetylcholine receptor subunits in the resting and desensitized states, determined by cryoelectron microscopy of crystallized Torpedo postsynaptic membranes. *J. Cell Biol.* **107**, 1123–1138 (1988).
38. Armstrong, C.M. & Bezanilla, F. Inactivation of the sodium channel: II. gating current experiments. *J. Gen. Physiol.* **70**, 567–590 (1977).
39. Mano, I., Lamed, Y. & Teichberg, V.I. A venus flytrap mechanism for activation and desensitization of α-amino-3-hydroxy-5-methyl-4-isoxazole propionic acid receptors. *J. Biol. Chem.* **271**, 15299–15302 (1996).
40. Barberis, A., Sachidhanandam, S. & Mulle, C. GluR6/KA2 kainate receptors mediate slow-deactivating currents. *J. Neurosci.* **28**, 6402–6406 (2008).
41. Copits, B.A. & Swanson, G.T. Dancing partners at the synapse: auxiliary subunits that shape kainate receptor function. *Nat. Rev. Neurosci.* **13**, 675–686 (2012).
42. Miesenböck, G., De Angelis, D.A. & Rothman, J.E. Visualizing secretion and synaptic transmission with pH-sensitive green fluorescent proteins. *Nature* **394**, 192–195 (1998).

ONLINE METHODS

Cell culture and transfection. HEK293T cells were transiently cotransfected with cDNA encoding wild-type or mutant GluK2(Q) KAR or GluA1(Q) AMPAR subunits and enhanced GFP ($eGFP_{S65T}$), as previously described[32], or transfected with iGluR-subunit cDNA on plasmids also encoding eGFP behind an internal ribosomal entry site. The cDNA for the mutant receptors was generated in two steps from wild-type plasmid with QuikChange II XL site-directed mutagenesis (Stratagene). After transfection for 4–8 h with the calcium phosphate precipitation method, cells were washed twice with divalent cation–containing PBS and maintained in fresh medium (MEM containing Glutamax and 10% FBS). Electrophysiological recordings were performed 24–48 h later.

GluK2 receptor surface expression. To test for possible trafficking defects in mutants used in this study, we measured the fluorescence emitted by an ecliptic $_{pH}$GFP genetically fused to the extracellular N-termini of mutant or wild-type GluK2 receptors (**Supplementary Fig. 3a**,**b**). Unlike that of eGFP, the fluorescence emission of $_{pH}$GFP is almost entirely quenched at pH 5.45 (ref. 42), which we used to evaluate the cellular location of the fluorophores[43]. With this approach, a substantial but reversible attenuation in the fluorescence signal emitted by wild-type $_{pH}$GFP-GluK2 was observed ($n = 17$ cells) after acidification of the external milieu (**Supplementary Fig. 3a**,**b**), thus demonstrating that most of the fluorescence signal was emitted by tagged GluK2 receptors on the plasma membrane. In contrast, acidification of the external solution had little effect on the weak fluorescence emitted by $_{pH}$GFP-GluK2 R523A receptors ($n = 6$ cells) (**Supplementary Fig. 3a**,**b**), consistent with previous work showing that this mutant has poor surface expression[27]. Fluorescence emitted by $_{pH}$GFP-GluK2 E524G and L783C receptors ($n = 10$ and 6 cells respectively) was robust, much like that of wild-type GluK2, and was reversibly attenuated by acidification (**Supplementary Fig. 3a**,**b**), thus suggesting that trafficking to the plasma membrane is not substantially perturbed for either mutant.

Electrophysiological solutions and recordings. External recording solutions typically contained 150 mM NaCl, 5 mM HEPES, 0.1 mM $CaCl_2$, 0.1 mM $MgCl_2$ and 2% phenol red. The internal recording solution contained 115 mM NaCl, 10 mM NaF, 5 mM HEPES, 5 mM Na_4BAPTA, 0.5 mM $CaCl_2$, 1 mM $MgCl_2$ and 10 mM Na_2ATP to chelate endogenous polyamines. The osmotic pressure was set to 295–300 mOsm with sucrose and the pH adjusted to 7.35 with 5 N NaOH. Agonist solutions were prepared by dissolving the agonist in external solution and adjusting the pH appropriately. In the case of recordings conducted in nominal external ions, the solution contained 100 µM of $CaCl_2$ and $MgCl_2$ to improve patch stability, sucrose to maintain the osmotic pressure at 295–300 mOsm, and 5 mM Tris to buffer pH. The pH was adjusted to 7.3–7.4 with 10 N HCl. To optimize recording stability in solutions of nominal ions, quartz electrodes were used to excise some outside-out patches. The outward current conveyed by receptors in such conditions was due to the efflux of sodium ions from the patch pipette. The lack of inward current in response to L-Glu confirmed that all cations were removed from the external milieu of the membrane patch.

All experiments were performed on excised membrane patches in the outside-out configuration. We used thin-walled borosilicate glass pipettes (3–5 MΩ, King Precision Glass) coated with dental wax for macroscopic experiments. To obtain low-noise or single-channel recordings, we used quartz glass (3–15 MΩ, King Precision Glass) coated with Sylgard (Dow Corning). Agonist solutions were rapidly applied to outside-out patches for 250 ms at −60 mV (unless otherwise stated) with a piezo-stack–driven perfusion system. Sufficient time between applications of L-Glu was allowed for complete recovery from macroscopic desensitization. Solution exchange time was determined routinely at the end of each experiment by measurement of the liquid junction current (10–90% rise time = 100–400 µs). Series resistances (3–15 MΩ) were routinely compensated by 95%. For microscopic recordings, the headstage was set to the capacitive feedback recording mode. All recordings were performed at room temperature with an Axopatch 200B amplifier (Axon Instruments). Current records were filtered at 5 kHz for macroscopic responses and digitized at 25–50 kHz. Single-channel currents were all acquired at 50–100 kHz, low-pass filtered by an eight-pole Bessel filter at 10 kHz and digitally filtered offline at 1–3 kHz. The reference electrode was connected to the bath through an agar bridge of 3 M KCl. Data were acquired with pClamp9 software (Axon Instruments) and illustrated with Origin 7 (OriginLab).

Macroscopic response analysis. Data were analyzed with Clampfit 9.0 and tabulated with Microsoft Excel. Curve fittings for determining the off-kinetic rates were performed with first- or second-order exponential functions: $y = A_i \times \exp(-x/t_i)$. Dose-response data to L-Glu were normalized, pooled across patches and fit with the logistic equation of the following form: $I = I_{max}/(1 + (EC_{50}/[Glu])^{n_H})$, where I is the normalized current at any agonist concentration, I_{max} is the interpolated maximal response, EC_{50} is the concentration of L-Glu that elicits the half-maximal response, and n_H is the slope or Hill coefficient.

Single-channel analysis. For wild-type GluK2 receptors, analysis was conducted on patches ($n = 5$) from which 50 or more agonist applications were made at 15-s intervals. For GluK2 D776K, which displayed uniform current responses, analysis was limited to 58 agonist applications, which were divided among four patches. Single-channel data were subjected to digital low-pass filtering at 3 kHz (or 1 kHz for presentation in figures), which resulted in r.m.s. baseline noise values that averaged 0.22 ± 0.024 pA ($n = 5$) and 0.22 ± 0.043 pA ($n = 4$) for wild-type and D776K receptors, respectively. These noise values corresponded to <50% of the smallest difference between adjacent conductance levels in the wild-type receptor. The 3-kHz frequency was chosen on account of our data containing many rapid transitions between conductance levels, as described previously for AMPARs[44]. Accordingly, a resolution of two filter rise times (2 × 111 µs) was imposed to detect and account for brief events while maintaining resolution of small conductances. Digitally filtered data were exported to Signal 5.0 (Cambridge Electronic Design) for time-course fitting analysis with SCAN[45]. The idealized records were then used to provide information on response amplitudes, which could be fit with Gaussian functions whose peaks reflect discrete conductance levels: $y = \Sigma_{i=1,n} (A_i/w_i \times \mathrm{sqrt}(\pi/2))) \times \exp(-2 \times ((x-xc_i)/w_i)^2$ where A = area, xc = center of the peak, and w = error associated with xc. From this analysis, the distribution and amplitude of single-channel events observed in patches containing a few channels (**Fig. 2f**) were similar to events measured at equilibrium in multichannel patches (**Supplementary Fig. 5**).

Molecular dynamics simulations. All crystal structures used in this manuscript were obtained from the Research Collaboratory for Structural Bioinformatics (RCSB) protein data bank. Two protein structures were used for building models for the MD simulations: an L-Glu–bound GluK2 LBD dimer (PDB 3G3F (resolution 1.38 Å (ref. 46)) and an L-Glu–bound GluK2 Y521C L783C LBD dimer (PDB 2I0C (resolution 2.25 Å (ref. 15)), which was used only for simulations concerning the double-cysteine mutant. Together with the crystallographically resolved water molecules, L-Glu ligands and ions were retained in the simulation setup, whereas two bound isopropyl alcohol molecules were deleted. In simulations of GluK2 without bound sodium ions (**Supplementary Fig. 4**), these were removed before system setup. The protein was solvated in water in a (90 Å) (ref. 43) box with the TIP3P water model[47], whereafter the system was neutralized and 150 mM NaCl was added. Mutations, except for Y521C L783C, were imposed manually before simulation setup, either by editing or deleting atoms in the PDB file or by using the mutate function of PyMOL (http://www.pymol.org/) and adjusting the side chain rotamer. For the double-cysteine mutant, the GluK2 double-cysteine (Y521C L783C) mutant structure was used. This structure had no ions bound, so the interface-bound ions from the wild-type structure were added, and rotamers for side chains surrounding the ion sites were optimized in PyMOL before solvation, neutralization and ionization as described above.

The MD simulations were performed in Gromacs 4.5 (ref. 48) with the OPLS all-atom force field[49,50]. The systems were first energy minimized until the maximum force on an atom was <100 kJ/mol/nm. After energy minimization, a 200-ns restrained simulation with position restraints on protein heavy atoms and on bound ions with a force constant of 1,000 kJ mol^{-1} nm^{-2} was performed in the NVT ensemble with a temperature of 300 K maintained by a Berendsen thermostat[51]. Periodic boundary conditions were used, and van der Waals interactions were cut off at 10 Å. Long-range electrostatics were accounted for by the Particle-Mesh Ewald method[52]. All bonds were treated as constraints with the LINCS algorithm, allowing a time step of 2 fs. Subsequently, 100 ns of production run were performed (only 30–50 ns for E524G). The NPT ensemble was used with the temperature retained at 300 K and the pressure at 1 bar by the Berendsen thermostat and barostat, respectively[51]. Two repeats for each

mutational variant were produced. Analyses were performed with VMD[53] and analysis tools of GROMACS[48].

Statistical methods. Results are expressed as mean ± s.e.m. Statistical analyses of sample means were performed with two-tailed Student's *t* tests. $P < 0.05$ was considered to be statistically significant.

43. Khiroug, S.S. *et al.* Dynamic visualization of membrane-inserted fraction of pHluorin-tagged channels using repetitive acidification technique. *BMC Neurosci.* **10**, 141 (2009).
44. Zhang, W., Cho, Y., Lolis, E. & Howe, J.R. Structural and single-channel results indicate that the rates of ligand binding domain closing and opening directly impact AMPA receptor gating. *J. Neurosci.* **28**, 932–943 (2008).
45. Colquhoun, D. & Sigworth, F.J. in *Single Channel Recording* (eds. Sakmann, B. & Neher, E.) 483–587 (Plenum Press, 1995).
46. Chaudhry, C., Weston, M.C., Schuck, P., Rosenmund, C. & Mayer, M.L. Stability of ligand-binding domain dimer assembly controls kainate receptor desensitization. *EMBO J.* **28**, 1518–1530 (2009).
47. Jorgensen, W.L., Chandrasekhar, J., Madura, J.D., Impey, R.W. & Klein, M.L. Comparison of simple potential functions for simulating liquid water. *J. Chem. Phys.* **79**, 926–935 (1983).
48. Hess, B., Kutzner, C., Van Der Spoel, D. & Lindahl, E. GROMACS 4: algorithms for highly efficient, load-balanced, and scalable molecular simulation. *J. Chem. Theory Comput.* **4**, 435–447 (2008).
49. Jorgensen, W.L., Maxwell, D.S. & Tirado-Rives, J. Development and testing of the OPLS all-atom force field on conformational energetics and properties of organic liquids. *J. Am. Chem. Soc.* **118**, 11225–11236 (1996).
50. Kaminski, G.A., Friesner, R.A., Tirado-Rives, J. & Jorgensen, W.L. Evaluation and reparametrization of the OPLS-AA force field for proteins via comparison with accurate quantum chemical calculations on peptides. *J. Phys. Chem. B* **105**, 6474–6487 (2001).
51. Berendsen, H.J.C., Postma, J.P.M., Van Gunsteren, W.F., Dinola, A. & Haak, J.R. Molecular dynamics with coupling to an external bath. *J. Chem. Phys.* **81**, 3684–3690 (1984).
52. Darden, T., York, D. & Pedersen, L. Particle mesh Ewald: an *N*·log(*N*) method for Ewald sums in large systems. *J. Chem. Phys.* **98**, 10089–10092 (1993).
53. Humphrey, W., Dalke, A. & Schulten, K. VMD: visual molecular dynamics. *J. Mol. Graph.* **14**, 33–38 (1996).

Article

Neuron

Distinct Structural Pathways Coordinate the Activation of AMPA Receptor-Auxiliary Subunit Complexes

Highlights

- Two distinct structural motifs control the time course of AMPA receptor gating
- Intraprotein electrostatic interactions govern gating by pore-forming subunits
- Auxiliary subunits act at a distinct site to prolong channel activity
- Intra- and interprotein interactions coordinate signaling by AMPA receptor complexes

Authors

G. Brent Dawe, Maria Musgaard, Mark R.P. Aurousseau, Naushaba Nayeem, Tim Green, Philip C. Biggin, Derek Bowie

Correspondence

tpgreen@liverpool.ac.uk (T.G.), philip.biggin@bioch.ox.ac.uk (P.C.B.), derek.bowie@mcgill.ca (D.B.)

In Brief

Combining electrophysiology, molecular dynamics simulations, and X-ray crystallography, Dawe et al. identify two distinct structural motifs that coordinate the gating of AMPA receptor-auxiliary subunit complexes, highlighting the importance of intra- and interprotein interactions in fast excitatory signaling.

Accession Numbers

5FTH
5FTI

Dawe et al., 2016, Neuron *89*, 1264–1276
March 16, 2016 ©2016 The Authors
http://dx.doi.org/10.1016/j.neuron.2016.01.038

CellPress

Neuron
Article

Distinct Structural Pathways Coordinate the Activation of AMPA Receptor-Auxiliary Subunit Complexes

G. Brent Dawe,[1,2,5] Maria Musgaard,[3,5] Mark R.P. Aurousseau,[2,5] Naushaba Nayeem,[4] Tim Green,[4,6,*] Philip C. Biggin,[3,6,*] and Derek Bowie[2,6,*]
[1]Integrated Program in Neuroscience, McGill University, Montréal, QC H3A 2B4, Canada
[2]Department of Pharmacology and Therapeutics, McGill University, Montréal, QC H3G 1Y6, Canada
[3]Department of Biochemistry, University of Oxford, Oxford OX1 3QU, UK
[4]Department of Pharmacology, University of Liverpool, Liverpool L69 3BX, UK
[5]Co-first author
[6]Co-senior author
*Correspondence: tpgreen@liverpool.ac.uk (T.G.), philip.biggin@bioch.ox.ac.uk (P.C.B.), derek.bowie@mcgill.ca (D.B.)
http://dx.doi.org/10.1016/j.neuron.2016.01.038

SUMMARY

Neurotransmitter-gated ion channels adopt different gating modes to fine-tune signaling at central synapses. At glutamatergic synapses, high and low activity of AMPA receptors (AMPARs) is observed when pore-forming subunits coassemble with or without auxiliary subunits, respectively. Whether a common structural pathway accounts for these different gating modes is unclear. Here, we identify two structural motifs that determine the time course of AMPAR channel activation. A network of electrostatic interactions at the apex of the AMPAR ligand-binding domain (LBD) is essential for gating by pore-forming subunits, whereas a conserved motif on the lower, D2 lobe of the LBD prolongs channel activity when auxiliary subunits are present. Accordingly, channel activity is almost entirely abolished by elimination of the electrostatic network but restored via auxiliary protein interactions at the D2 lobe. In summary, we propose that activation of native AMPAR complexes is coordinated by distinct structural pathways, favored by the association/dissociation of auxiliary subunits.

INTRODUCTION

Voltage- and ligand-gated ion channels are signaling complexes that are often assembled from both regulatory and pore-forming subunits (Catterall et al., 2006; Jackson and Nicoll, 2011; Trimmer, 2015). AMPA-type (AMPAR) ionotropic glutamate receptors (iGluRs) are composed of pore-forming GluA1–GluA4 subunits (Dingledine et al., 1999) that coassemble with a variety of auxiliary proteins, including the transmembrane AMPAR receptor regulatory protein (TARP) and cornichon (CNIH) families (Jackson and Nicoll, 2011; Schwenk et al., 2009; Tomita et al., 2003), as well as CKAMP44 (von Engelhardt et al., 2010) and SynDIG1 (Kalashnikova et al., 2010), among others (Haering et al., 2014). Each pore-forming subunit possesses four principal domains, with the extracellular amino-terminal domain (ATD) controlling assembly and trafficking (Gan et al., 2015; Greger et al., 2007) and the ligand-binding domain (LBD) providing a bilobed agonist-binding pocket (Dawe et al., 2015). Meanwhile, the three transmembrane helices and re-entrant loop form the central pore domain, which governs cation selectivity and channel block (Huettner, 2015) and connects to the short, intracellular carboxyl-terminal domain (CTD). Once assembled, the native AMPAR is a homo- or heteromeric tetramer (Sobolevsky et al., 2009) with a variable stoichiometry of TARPs (Hastie et al., 2013) that may include additional CNIH subunits (Herring et al., 2013; Jackson and Nicoll, 2011). Understanding these interactions has been an area of intense study in recent years, especially as TARPs and CNIHs have been shown to directly affect the functional behavior of native AMPARs as well as synaptic plasticity mechanisms (Jackson and Nicoll, 2011). Exactly how pore-forming and auxiliary subunits work together to achieve this, however, remains to be established.

Since TARPs and CNIHs are transmembrane proteins, interactions with AMPARs are expected to rely upon their proximity in the plasma membrane. Interestingly, protein-protein interactions of this nature can be short- and long-lived. Autoinactivation of neuronal AMPARs is thought to reflect the rapid, millisecond-scale dissociation of AMPAR-TARP complexes mediated by receptor desensitization (Constals et al., 2015; Morimoto-Tomita et al., 2009). In contrast, single-channel analysis of AMPAR-TARP fusion proteins has revealed less frequent transitions between distinct gating modes of high and low open-channel probability (P_{open}) (Zhang et al., 2014) that are also thought to represent TARP-coupled and TARP-uncoupled forms of the receptor complex, respectively (Howe, 2015). The occurrence of distinct gating behavior raises the question as to how auxiliary subunits mediate their effects on AMPAR gating. One possibility is that agonist-binding triggers channel activation through a single set of structural interactions that is modulated when pore-forming subunits are associated with auxiliary subunits.

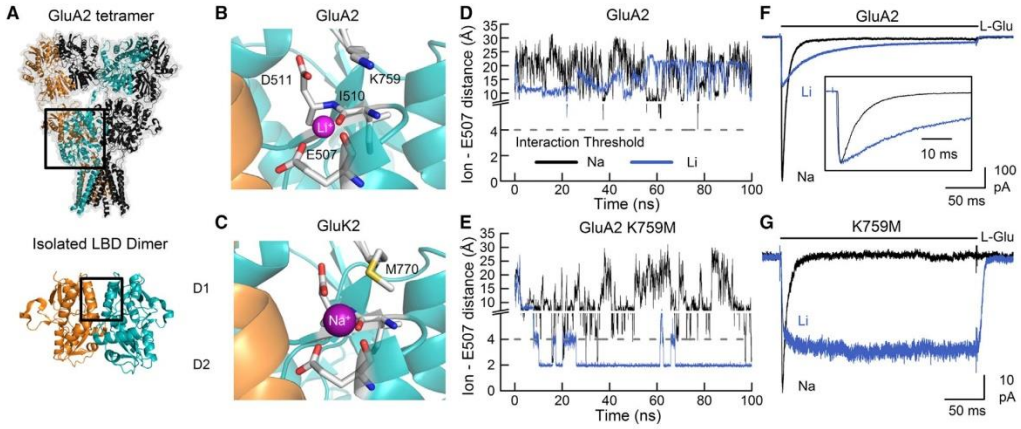

Figure 1. Lithium Modulates GluA2 Responses by Binding at the LBD Apex

(A) Crystal structure of the wild-type GluA2 tetramer (top, PDB: 3KG2; Sobolevsky et al., 2009) and isolated LBD dimer (bottom, PDB: 1FTJ; Armstrong and Gouaux, 2000).

(B and C) Illustration of the GluA2 (B) (PDB: 4IGT; Assaf et al., 2013) and GluK2 (C) (PDB: 2XXR; Nayeem et al., 2011) LBD dimer interfaces showing lithium and sodium ions, respectively, bound at a conserved electronegative pocket.

(D and E) Minimum distance between the nearest sodium or lithium ion and either sidechain oxygen atom found on residue Glu507 of chain A of wild-type GluA2 (D) or the K759M mutant (E). An interaction was deemed to occur when the cation was within 4 Å of an oxygen atom. In total, two 100 ns simulations were conducted in LiCl for each receptor, as well as three or four 100 ns simulations in NaCl for K759M and wild-type GluA2, respectively.

(F and G) Typical current responses elicited by 10 mM L-Glu on wild-type GluA2 (F) (patch number 140225p10) or K759M mutant (G) (patch number 140314p4) receptors in external solutions comprised of either NaCl or LiCl. Responses were also scaled to the same peak amplitude (inset).

Alternatively, auxiliary subunits may integrate other allosteric sites into the activation process, depending on how they are functionally coupled to AMPAR complexes.

Here, we have designed experiments to delineate between these two possibilities. Our data identify a network of intersubunit atomic bonds at the apex of the LBD that are critical to channel activation with pore-forming AMPAR subunits. This network can be stabilized by occupancy of an electronegative pocket that is conserved between AMPARs and kainate-type iGluRs (KARs). Disruption of the apical network abolishes almost all AMPAR gating, though coassembly with auxiliary subunits rescues function because of interactions relayed through the lower, D2 lobe of the LBD. Thus, while it is likely that a common mechanism ultimately triggers opening of the channel pore, we propose that channel activation of native AMPAR complexes is coordinated by pathways originating from distinct structural interactions. One interaction is LBD apex dependent and contained within pore-forming subunits, while the other is apex independent, stemming from the association of AMPARs and auxiliary subunits.

RESULTS

A Conserved Cation Pocket at the AMPAR and KAR LBD Dimer Interface

The topology of the iGluR tetramer is highly conserved between the AMPAR and KAR subfamilies, including the LBD, whose upper (D1) and lower (D2) lobes form the agonist-binding cleft (Figure 1A). AMPARs and KARs also possess an extensive network of electrostatic and hydrophobic interactions along the D1-D1 interface between subunits (Horning and Mayer, 2004) (Figures 1B and 1C), raising the question of their role in iGluR gating. In addition, KARs possess both sodium and chloride ion-binding pockets at the apex of this interface, which are critical for channel gating (Bowie, 2010). In GluK2 KARs, occupancy of the cation-binding pocket (Figure 1C) is required for activation (Wong et al., 2006), with the time course of channel activity regulated by the residence time of bound sodium (Dawe et al., 2013). Curiously, although AMPARs have been considered cation independent (Bowie, 2002), lithium has been modeled at this site in two X-ray crystal structures of the GluA2 LBD, including one determined at 1.24 Å resolution (Figure 1B) (Assaf et al., 2013) that exhibits many of the structural hallmarks of the KAR cation-binding pocket (Figure 1C). Because lithium is frequently present in crystallization buffers for the GluA2 LBD (Green and Nayeem, 2015), we sought to determine if the lithium site is artifactual, with little impact on AMPAR gating, or whether lithium binding under experimental conditions can modulate gating behavior.

To determine whether occupancy of the putative cation pocket affects AMPAR gating, molecular dynamics (MD) simulations were first performed to determine the residence time of lithium ions at wild-type GluA2 AMPARs (Figure 1D). Simulations were performed in either 150 mM NaCl or LiCl without initial occupancy of the pocket, enabling a prediction of whether cations readily bind to the site. When the distance between Glu507

(Figure 1B) and the closest sodium or lithium ion was monitored over a 100 ns simulation, little meaningful interaction occurred (Figure 1D). The average frequency of interactions below 4 Å, taken as the cutoff value for intermolecular electrostatic interactions, was 0.4% in NaCl and 5.2% in LiCl, when the two binding sites of the dimer were considered. One factor that might explain the low propensity for cation binding is the contribution of Lys759 (Figure 1B), which often makes an intrasubunit projection toward the pocket and may compete with lithium ions for contact with electronegative residues. We therefore repeated the MD simulations, incorporating a mutation that replaced the positively charged Lys with a Met residue, as found in GluK2 KARs. As anticipated, lithium resided in the putative cation pocket for much longer periods of time (Figure 1E), confirming that removal of Lys759 impacts the ability of lithium to bind. Contact frequency between lithium and Glu507 averaged 52.1% of simulation time, while sodium binding remained infrequent at 1.9% (Movies S1 and S2, available online). Together, these data make the prediction that lithium binding to the apex of the GluA2 LBD would have measurable consequences on AMPAR gating, which would be more pronounced for GluA2 K759M receptors.

Accordingly, we performed cation substitution experiments during patch-clamp recordings to determine whether lithium modulates the gating behavior of wild-type and mutant GluA2 AMPARs. Membrane currents elicited by L-Glu in 150 mM NaCl at wild-type GluA2 and K759M receptors decayed rapidly with time constants of 6.9 ± 0.2 ms (n = 7; Figure 1F) and 9.9 ± 0.6 ms (n = 8; Figure 1G), consistent with MD simulations showing that sodium ions interact little with the electronegative residues of the cation pocket. The substitution of external NaCl with LiCl caused a dramatic slowing in the onset of desensitization ($\tau = 50.0 \pm 3.4$ ms; n = 7; $p < 0.0001$) for wild-type GluA2 (Figure 1F) and yielded a nondecaying phenotype (n = 6) in GluA2 K759M receptors (Figure 1G). In contrast, substitution with the larger monovalent cation potassium had minimal effect on decay kinetics of both wild-type and mutant GluA2 receptors (Figure S1). This suggests that access to the electronegative, "cation" pocket of AMPARs is restricted to ions of smaller ionic radius. Moreover, single-channel recordings revealed that external lithium prolongs the occurrence of channel openings prior to desensitization (Figure S1). Because the duration of this activity is affected by microscopic rates of channel opening and closing, as well as agonist unbinding and/or desensitization, we refer to channel activation/activity as the sum of these processes.

Taken together, our observations corroborate the idea that in 150 mM LiCl external solution, lithium ions can bind to an electronegative pocket in wild-type and mutant GluA2 AMPARs, sustaining channel activity in an analogous manner to sodium binding at KARs (Dawe et al., 2013). However, unlike sodium, the presence of lithium in the nervous system is typically negligible, and even during lithium treatment for bipolar disorder, effective serum concentrations range from 0.4 to 1.2 mM (Severus et al., 2008). When we supplemented our standard external recording solution with 1.5 mM LiCl, there was no significant change in GluA2 decay kinetics ($p = 0.82$; n = 5; data not shown), meaning we could not ascribe a physiological role to cation binding at the GluA2 LBD. Instead, we used lithium as an experimental tool to interrogate the structural interactions modulated by its binding and how these interactions shape the overall functional output of AMPARs.

GluA2 Activation Does Not Require Electronegative Pocket Occupancy

One question not addressed by the cation substitution experiments is whether wild-type GluA2 or K759M AMPARs gate in the absence of external ions, as described previously for GluK2 KARs (Dawe et al., 2013; Wong et al., 2006). The issue is especially relevant for K759M receptors, where our data already establish that removal of the positively charged Lys provides a favorable binding site for external lithium ions (Figures 1E and 1G). The idea that AMPARs with the K-M mutation may be rendered cation sensitive has been considered previously for GluA1 receptors, but it was not pursued further due to poor expression of the mutant (Wong et al., 2006). Using TIRF microscopy of GFP-tagged AMPARs, we confirmed that the equivalent K759M mutation in GluA2 did not prevent receptor expression at the plasma membrane (Figure S2). We therefore repeated experiments in external ion-free conditions for wild-type and mutant GluA2 receptors to determine their agonist responsiveness (Figure 2). In agreement with observations on GluA1 receptors, GluA2 AMPARs continued to be activated by L-Glu, even in the absence of external NaCl, establishing that GluA2 AMPAR gating is not dependent on external cations, unlike GluK2 KARs (Figures 2A and 2B). GluA2 K759M also continued to elicit membrane currents when external NaCl was removed (Figure 2C), and in this condition, both AMPARs produced outwardly rectifying current-voltage (I-V) plots that contrasted with the loss of the GluK2 response (Figures 2D–2F). These data demonstrate that while KARs require external cations to activate, GluA2 AMPARs require neither interactions with Lys759 in the wild-type receptor nor occupancy by cations in the K759M mutant. As such, additional interactions modulated by lithium binding at the electronegative pocket must be able to profoundly affect GluA2 AMPAR activation.

The Electronegative Pocket Acts through Intersubunit Contacts

Since the lithium binding site is quite distant from the channel pore, it remained unclear how lithium might influence LBD structure to stabilize the activated state of the receptor. To address this, we used MD simulations, which revealed that cation binding promotes rearrangements in the GluA2 K759M LBD dimer interface. Specifically, increasing the number of bound lithium ions shifted the distribution of predicted distances across the interface in a negative direction (Figures 3A and 3B). Because these distances were measured between two points at the apex of each D1 lobe, they are referred to as D1-D1 interface distances (Figure 3B). Nevertheless, lithium binding sites are fully contained within single subunits on each side of the interface, making it unlikely that lithium acts directly as an adhesive force between subunits. However, the ion is coordinated by Glu507, which forms electrostatic interactions across the interface with both Lys514 and Asn768 (Figure 3A). This prompted us to explore whether lithium modulates GluA2 current decay kinetics

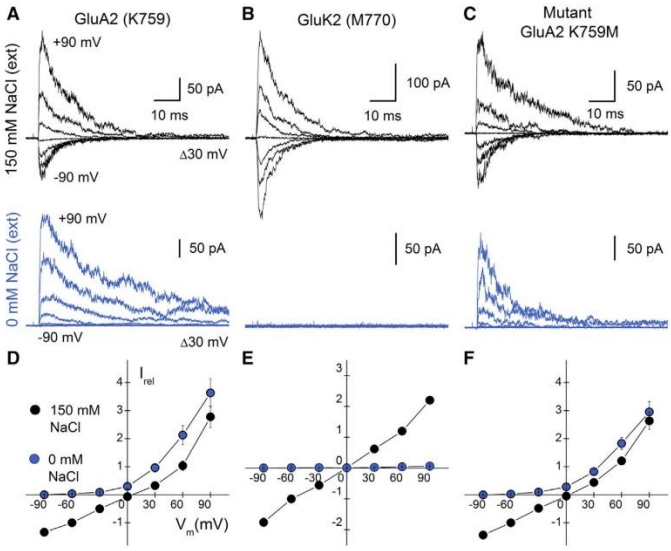

Figure 2. GluA2 K759M Exhibits Robust Activation in the Absence of External NaCl

(A–C) Membrane currents evoked by 1 (for KARs) or 10 mM (for AMPARs) L-Glu acting on wild-type GluA2 (A) and GluK2 (B), as well as GluA2 K759M mutant (C) receptors, in either 150 mM NaCl (top) or NaCl-free, sucrose-based (bottom) external solution (V_m = −90 to +90 mV, at 30 mV increments). For each receptor, the same patch was recorded in both ionic conditions. For wild-type GluA2 (patch number 140417p4) and the K759M mutant (patch number 140502p1), outward currents persisted at positive holding potentials, whereas GluK2 responses (patch number 140904p3) were abolished.

(D–F) Current-voltage plots in 0 mM (blue) and 150 mM (black) NaCl for wild-type GluA2 (D), GluK2 (E), and GluA2 K759M (F) receptors. Currents were normalized to responses at −60 mV in 150 mM NaCl. Data are mean ± SEM, from four (GluA2), three (GluK2), or six (K759M) independent experiments for each receptor.

by stabilizing intersubunit electrostatic interactions. We therefore removed these interactions in a K514M/N768T double mutant, where the mutated residues retain approximately the same bulkiness but lose their charge or ability to form the same crossdimer hydrogen bonds. This mutant exhibited currents that decayed with time constants of 8.4 ± 1.2 ms (n = 5) in NaCl and 6.9 ± 1.1 ms (n = 5) in LiCl (Figures 3C and 3D). The observation that decay kinetics were not significantly different between cation species (p = 0.26) stands in marked contrast to wild-type GluA2 (Figure 3D) and confirms that lithium modulation was abolished. Since it is possible that lithium binding was disrupted in GluA2 K514M/N768T, we used MD simulations to evaluate this possibility. MD data revealed no gross conformational changes to the LBD dimer and, moreover, reported that lithium ions interact with the pocket with a frequency similar to or greater than with wild-type GluA2 (Figure S3). Taken together, our data indicate that experimental concentrations of external LiCl (i.e., 150 mM) influence intersubunit electrostatic contacts at the apex of the LBD dimer interface, thereby stabilizing the activated conformation of the receptor. To explore this idea further, we investigated whether strengthening the apex of the LBD dimer interface could sustain AMPAR activation.

Engineering an Intersubunit Tether to Sustain Channel Activation

In order to incorporate an additional electrostatic interaction across the D1-D1 interface, we used a Thr765 to Lys mutation to introduce a charged tether onto residues forming the opposing electronegative pocket (for additional rationale, see Figure S4). Alone, this mutation had little functional effect, but coupled with the K759M mutation (K759M/T765K), current decay slowed several fold, and the additional mutation N768T (creating K759M/T765K/N768T, or MKT) yielded nondecaying current responses (Figure 4A). Consistent with this, single-channel events of GluA2 MKT were sustained throughout the 250 ms period of agonist application, in contrast to wild-type channels (Figures 4B and 4C). In both cases, current records were fit with four conductance levels of approximately 6, 12, 24, and 40 pS, with the P_{open} of GluA2 MKT estimated to be 0.62 ± 0.14 (n = 4) (Figure 4D). The occurrence of MKT channel closures in these conditions could be explained by the failure of the mutant Lys residue to form a sustained, crossdimer tether, enabling the LBD dimer to rupture.

In order to verify that a Lys tether had been introduced across the GluA2 LBD dimer, we attempted structural analysis of the MKT mutant. However, protein expression levels were too low to obtain diffracting crystals. In contrast, crystals of the GluA2 K759M/T765K LBD were successfully grown in the presence of zinc, and a dataset was collected from a single crystal at 2.9 Å resolution (Table S1). Three protomers were present in the asymmetric unit, of which chains A and B formed a canonical dimer, and the third, C, formed a dimer with its symmetry-related counterpart. In each dimer (A:B and C:C′) electron density was visible for both the mutant Met and Lys residues, and the latter residue was spanning the dimer interface as predicted (Figures 4E and S5). Electrostatic interactions were formed between the amine group on residue 765 (i.e., T765K) and the sidechain carboxyl group of Asp511, as well as the backbone oxygen atom of Ile510 (Figure 4E). In addition to these contacts, there was a general shift in the dimer conformation, with the apical residues having moved closer together relative to structures of wild-type GluA2, forming a more extensive, contiguous interface (Figure 4F).

Consistent with functional recordings of GluA2 K759M/T765K (Figure 4A), our structural data also suggest that the crossdimer tether does not persist indefinitely. First, an additional crystal structure grown in the presence of lithium (Table S1) revealed

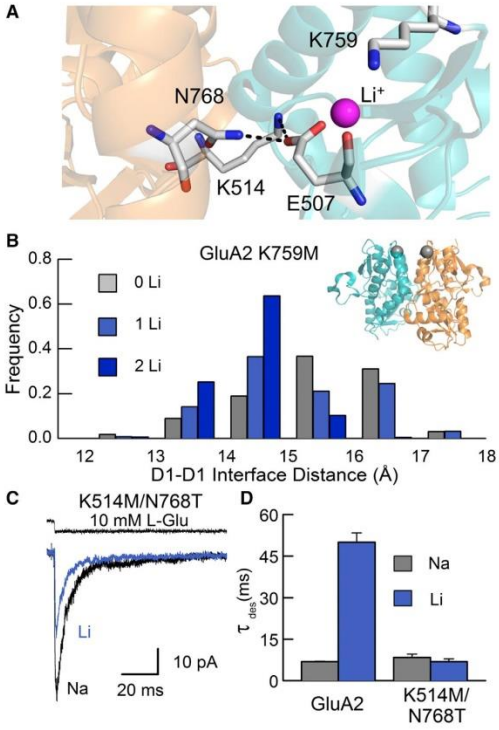

Figure 3. Lithium Modulation Is Mediated by Crossdimer Electrostatic Contacts

(A) Image of an intersubunit salt bridge and hydrogen bond adjacent to the lithium binding site (PDB: 4IGT; Assaf et al., 2013). Residues Lys514 and Asn768 are from chain A, while Glu507 and Lys759 are from chain B.

(B) Intersubunit distance across the apex of the GluA2 LBD, relative to the number of lithium ions occupying the two cation pockets, measured during 100 ns MD simulations (two repeats) of GluA2 K759M in LiCl. Distances were measured between the gray spheres (inset, right), which represent a center of mass for Cα atoms of residues 508–510 and 759–765.

(C) Typical current responses to L-Glu obtained from the GluA2 K514M/N768T mutant (patch number 140718p4), recorded in external NaCl and LiCl. The top trace (black) shows the junction current, recorded with an open patch pipette after the experiment to monitor the profile of solution exchange.

(D) Plot of current decay time constants (τ_{des}) for wild-type GluA2 and K514M/N768T receptors. Data are mean ± SEM, from seven (wild-type GluA2) or five (K514M/N768T) independent patch experiments for each receptor.

that the electronegative pocket was partially occupied by a lithium ion (Figures S4 and S5) and not the opposing Lys residue. Second, in MD simulations of both the double- and triple-mutant receptors, the T765K residue failed to make continuous contact with the electronegative pocket (Figures 4G and 4H; Movies S3 and S4). Overall, these structural and functional data support the premise that the Lys tether is not a permanent feature of the T765K mutant series. However, the MKT mutation makes tethering more favorable, likely because the replacement of Asn by the smaller Thr at position 768 reduces steric block, thereby allowing subunits within each LBD dimer to come closer together. As explained below, we explored the opposite effect of dimer crosslinking by determining if elimination of electrostatic interactions at the apex of the LBD dimer interface would disrupt GluA2 AMPAR functionality.

Removal of an Electrostatic Network Disrupts Gating by Pore-Forming Subunits

Although the addition of new crossdimer interactions (e.g., GluA2 MKT) can sustain GluA2 gating, the mutation of other interface residues has been shown to curtail channel activity. For example, the individual conversion of residues Glu507, Lys514, and Asn768 at the apex of the dimer interface (Figure 5A) to Ala speeds desensitization (Horning and Mayer, 2004). Of these residues, Glu507 and Lys514 form a salt bridge (Figure 5A). Interestingly, the two residues are conserved in AMPARs and KARs, but not NMDARs (Figure S6), suggesting that different sets of interactions regulate their slow time course of activation. However, because both Asn768 and Phe512 (via a backbone oxygen atom) can also contribute to the electrostatic network in GluA2, we evaluated the effect of completely disrupting this network using the triple-mutant GluA2 E507A/K514A/N768A (i.e., GluA2 AAA). On this note, mean peak current responses elicited by GluA2 AAA (94.5 ± 28.5 pA; n = 7) were depressed by almost 10-fold compared to wild-type GluA2 receptors (928 pA ± 317 pA; n = 12) (Figures 5B and 5C). In addition, the onset of desensitization was almost 10-fold faster for GluA2 AAA (τ = 0.74 ± 0.06 ms; n = 7) versus wild-type GluA2 (τ = 6.1 ± 0.2 ms; n = 7) (Figure 5D). The diminished functionality of the GluA2 AAA mutant demonstrates that the network of electrostatic interactions at the apex of the LBD dimer interface is a key structural element mediating channel gating by pore-forming AMPAR subunits.

Appreciating that the positive allosteric modulator cyclothiazide (CTZ) binds to the bottom of the D1-D1 interface (Sun et al., 2002), we tested whether AMPAR functionality could be recovered when CTZ was present. CTZ restored the responsiveness of the GluA2 AAA mutant, causing an 8.5 ± 1.0-fold (n = 7) increase in the peak response. In marked contrast, CTZ potentiated wild-type GluA2 currents to a significantly lesser extent of 1.3 ± 0.03-fold (n = 11; $p < 0.001$; Figures 5B, 5C, and 5E). However, since functionality can be restored by CTZ, we conclude that, under certain circumstances, other interactions are capable of coordinating channel gating independent of the LBD apex region. To explore this further, we tested whether the functionality of GluA2 AAA could be rescued by coexpression with auxiliary subunits.

Auxiliary Subunits Rescue Functionality of the GluA2 AAA Mutant

To test the effect of TARP or CNIH protein association on GluA2 AAA, we coexpressed the mutant receptor with either γ2 or γ7 TARP subunits or CNIH-3 (Figure 6). To control for the effect of TARPs and/or CNIHs on AMPAR trafficking (Jackson and Nicoll, 2011), we used the potentiation of peak L-Glu responses by CTZ as an estimate of P_{open} (Cho et al., 2007), or gating ability, in each

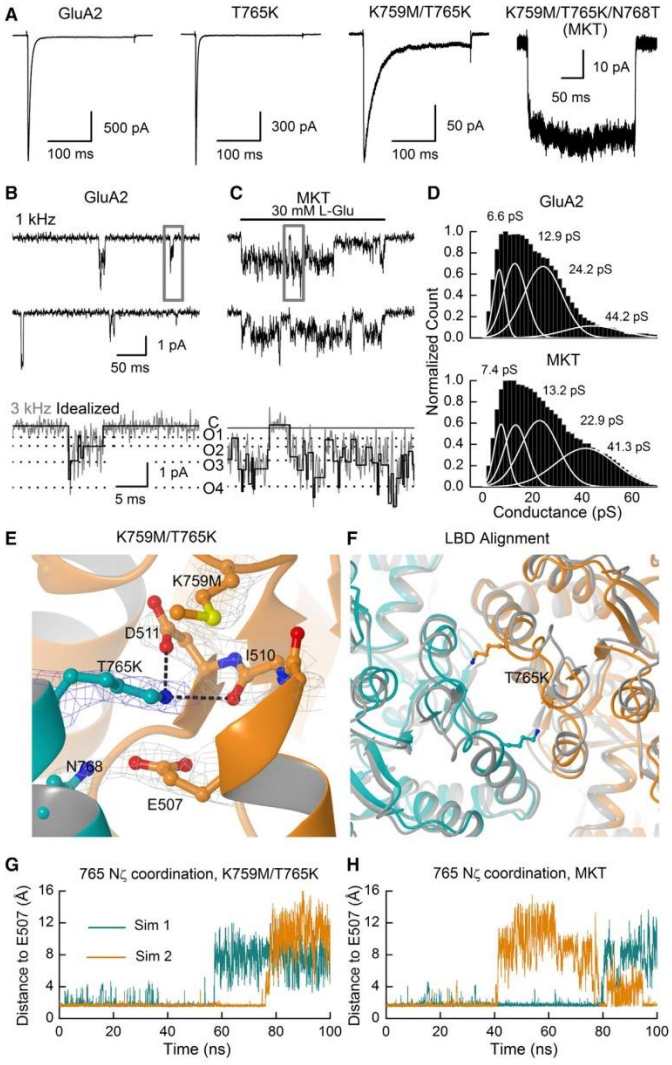

Figure 4. Structural and Functional Data Show T765K Can Act as a Crossdimer Tether

(A) Typical current responses to 10 mM L-Glu for a series of GluA2 mutants engineered to form a crossdimer tether. Wild-type GluA2 (patch number 130221p5) and mutants T765K (patch number 130617p4), K759M/T765K (patch number 130618p6), and K759M/T765K/N768T, or MKT (patch number 130917p6), are shown left to right.

(B and C) Unitary channel activity evoked by 30 mM L-Glu for wild-type GluA2 receptors in equilibrium conditions (B) (patch number 131212p7) and the triple-mutant MKT (C) (patch number 140124p1) during a 250 ms agonist application. Typical records are shown low-pass filtered at 1 kHz (top) or the 3 kHz threshold used to fit channel openings (bottom), expanded from gray box above. Horizontal dotted lines correspond to the conductance levels of open states (O1–O4) fit in (D).

(D) Distributions of conductance levels from idealized records of wild-type GluA2 (top) or GluA2 MKT (bottom) fit with four Gaussian functions (white lines). Openings were analyzed using four patch recordings for each receptor.

(E) View of protomers A (orange) and B (teal) from the K759M/T765K structure, zinc form, showing T765K tethering onto electronegative residues on the opposing subunit. Electron density ($|2F_{obs} - F_{calc}|\alpha_{calc}$, contoured at 1.3σ) is shown around the displayed side chains only. Interactions between the sidechain amine group of residue 765 and atoms in protomer A are shown as dashed lines.

(F) Top view of an alignment between wild-type GluA2 (gray; PDB: 1FTJ; Armstrong and Gouaux, 2000) and K759M/T765K (orange/teal) LBD dimers.

(G and H) Minimum distance between the amine-group nitrogen atom on the mutant Lys (introduced on chain B) and either sidechain oxygen atom found on residue Glu 507 (on chain A) for K759M/T765K (G) and the MKT mutant (H). Simulations were performed using the GluA2 K759M/T765K LBD dimer, while the N768T mutation was introduced atop this structure to simulate GluA2 MKT. Two repeats are shown for each mutant.

condition. Large membrane currents were elicited from GluA2 AAA receptors when coexpressed with either TARP or CNIH subunits, contrasting with the AAA mutant expressed alone (Figures 6A–6D). Moreover, peak current potentiation of GluA2 AAA responses by CTZ was significantly reduced to 1.5- to 3-fold when receptors were coexpressed with γ2, γ7, or CNIH-3 subunits ($p < 0.002$ in all cases), though still higher than observed with wild-type receptors (Figure 6E). This finding reaffirms our hypothesis that auxiliary subunits are capable of coordinating channel gating of pore-forming subunits, independent of the network of electrostatic interactions at the LBD apex region. Also, desensitization kinetics of GluA2 AAA were markedly faster than wild-type receptors when coexpressed with TARPs γ2 and γ7 (Figures 6F and 6G). Auxiliary subunits therefore do not fully rescue the gating deficits of GluA2 AAA and most likely coordinate channel gating in synchrony with the apex region of the AMPAR LBD dimer interface. As a consequence, AMPAR channel gating is coordinated by apex-dependent and apex-independent interactions. The former are comprised of an intraprotein electrostatic network that mediates the activation of pore-forming subunits, while the latter depends upon interactions that become available upon the association of auxiliary subunits.

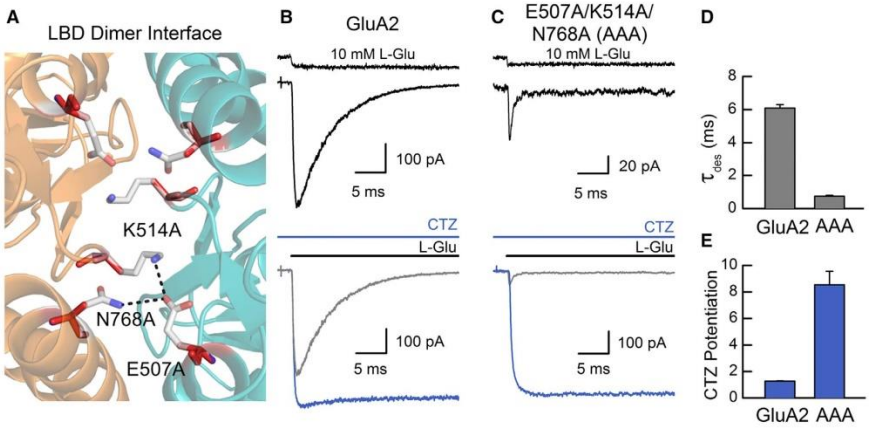

Figure 5. Truncation of Key Residues at the LBD Apex Produces Poorly Functioning Receptors

(A) Top view of the GluA2 LBD dimer interface (PDB: 1FTJ; Armstrong and Gouaux, 2000), showing charged and polar residues (faint gray) that were mutated to Ala (red). Labeled residues Lys514 and Asn768 are from chain A, while Glu507 is from chain B.

(B and C) Typical current responses of wild-type GluA2 (B) (patch number 130305p7) and the E507A/K514A/N768A, or AAA, mutant (C) (patch number 151005p6) to L-Glu before (top, black; bottom, gray) and during (bottom, blue) exposure to cyclothiazide (CTZ), which attenuates desensitization. The uppermost trace (black) shows the junction current, recorded with an open patch pipette after the experiment to monitor the profile of solution exchange.

(D) Average time constants of current decay (τ_{des}) for wild-type GluA2 and the AAA mutant. Data are mean ± SEM, from seven (wild-type GluA2 and GluA2 AAA) independent patch experiments.

(E) CTZ potentiation of wild-type GluA2 and AAA mutant peak currents. Data are mean ± SEM, from eleven (wild-type GluA2) or seven (GluA2 AAA) independent patch experiments.

TARPs Modulate the Duration of AMPAR Gating by Interactions on the D2 Lobe

In order to pinpoint the site(s) where auxiliary proteins modulate AMPAR gating, we first compared the sequence of AMPAR and KAR LBDs. Since KARs do not bind TARPs (Chen et al., 2003), we reasoned that a sequence alignment would identify residues unique to AMPARs that may form functional interactions with auxiliary subunits. The most promising site was a Lys-Gly-Lys, or KGK motif (residues 718–720), situated on the lower, D2 lobe of the GluA2 LBD, which is conserved among all AMPAR subunits (Figures 7A and 7B). The KGK motif faces outward, where an auxiliary subunit might be expected to reside, based on previous cryo-EM (electron microscopy) images of native AMPARs (Nakagawa et al., 2005). These three amino acids were therefore substituted with the single Asp residue (termed "3D" mutation) found in GluK1-3 KARs, where two residues are lost (Figure 7B). Importantly, the GluA2 3D mutant receptor had similar kinetic properties to wild-type GluA2, with deactivation and desensitization time constants of 0.53 ± 0.05 ms (n = 5) and 6.2 ± 0.5 ms (n = 5), respectively, demonstrating that this site has a minimal effect on channel gating mediated solely by pore-forming subunits.

To study the functional impact of the 3D mutant on TARP-dependent gating, we used a GluA2/γ2 fusion protein to constrain subunit stoichiometry and also to prevent any confounding effect of disrupting AMPAR-TARP association. We then evaluated the 3D mutant by investigating three sets of AMPAR properties known to be regulated by TARP association: the time course of channel activation (Priel et al., 2005), apparent agonist efficacy (Turetsky et al., 2005), and the degree of polyamine channel block (Soto et al., 2007). First, we examined the time course of L-Glu-induced channel activation by measuring both deactivation and desensitization kinetics (Figures 7C and 7D). We also assessed the degree of equilibrium desensitization by measuring the equilibrium/peak response ratio (Figure 7E). Second, we examined apparent agonist efficacy by using CTZ potentiation as an indicator of peak P_{open} (Cho et al., 2007) and measuring the KA/L-Glu current ratio (Figure S7). Finally, we analyzed the affinity and voltage dependency of polyamine channel block, which was determined using 100 μM internal spermine (Figure S7).

When incorporated into the wild-type GluA2/γ2 fusion receptor, the 3D mutation accelerated deactivation and desensitization kinetics from 3.2 ± 0.4 ms (n = 9) and 45.7 ± 6.8 ms (n = 11), respectively, to 1.1 ± 0.1 ms (n = 8) and 12.7 ± 1.2 ms (n = 8), respectively (Figures 7C and 7D). Notably, the deactivation (τ = 0.67 ± 0.07 ms; n = 7) and desensitization (τ = 9.5 ± 0.4 ms; n = 7) time constants of GluA2 3D coexpressed with γ2 were statistically indistinguishable from GluA2 expressed alone (p = 0.95 and p = 0.29, respectively; Figures 7F and 7G), suggesting that the 3D mutant almost completely abolishes the effects of γ2 on the time course of GluA2 channel activity. Likewise, the equilibrium/peak response (%) was also reduced from 16.7% ± 2.9% (n = 11) with GluA2/γ2 to 5.1% ± 1.2% (n = 8) with GluA2 3D/γ2 (Figure 7E), which was much closer to the equilibrium/peak response of GluA2 alone (Figures 7E and 7H). The reverse mutation in GluK2 KARs (i.e., Asp732 to Lys-Gly-Lys)

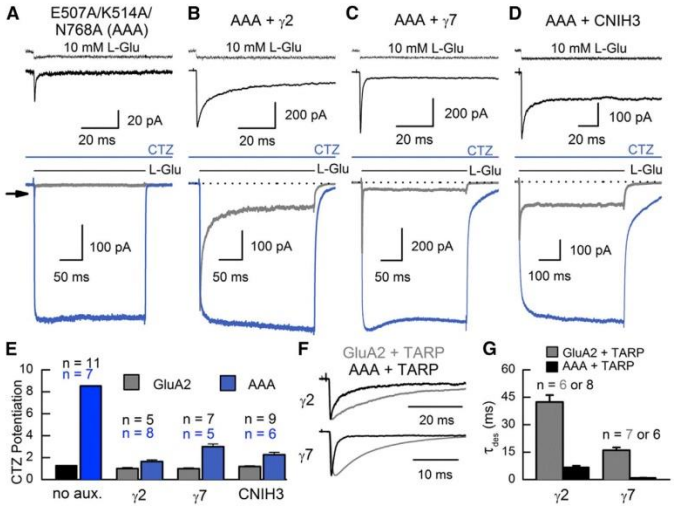

Figure 6. Coexpression of Auxiliary Subunits Rescues Function of the GluA2 AAA Mutant

(A–D) Behavior of GluA2 E507A/K514A/N768A, or AAA, receptors when expressed alone (A) (patch number 151008p10) or coexpressed with the TARP subunits γ2 (B) (patch number 140731p3) or γ7 (C) (patch number 141006p8), as well as the CNIH subunit CNIH-3 (D) (patch number 140926p5). Traces correspond to L-Glu-evoked responses prior to CTZ application (top, black; bottom, gray) or responses during (blue) CTZ exposure. The uppermost trace (black) shows the junction current, recorded with an open patch pipette after the experiment to monitor the profile of solution exchange. Arrow indicates the peak response of GluA2 AAA.

(E) CTZ potentiation of wild-type GluA2 and AAA mutant currents, tabulated in the presence or absence (no aux.) of different auxiliary subunits. Data are mean ± SEM, from the number of independent patch experiments indicated. Values with auxiliary subunits absent are as reported in Figure 5.

(F) Scaled comparison of wild-type GluA2 (gray) and AAA mutant (black) responses when coexpressed with TARP subunits γ2 (wild-type patch number 141006p3, AAA patch number 140721p3) and γ7 (wild-type patch number 141013p4, AAA patch number 141006p8).

(G) Time constants of current decay (τ_{des}) for wild-type GluA2 and GluA2 AAA coexpressed with TARP subunits γ2 or γ7. Data are mean ± SEM, from the number of independent patch experiments indicated.

produced no significant change in channel kinetics between the mutant receptor expressed alone or as a GluK2/γ2 fusion protein (data not shown), suggesting that these residues in the D2 lobe are not sufficient to confer functional TARP modulation of KARs. Taken together, our data identify the KGK motif as the critical structural element by which TARP γ2 prolongs the time course of AMPAR channel activation.

Interestingly, other functional properties of AMPARs modulated by TARPs, such as CTZ potentiation, KA/L-Glu current ratio, and polyamine channel block, were unchanged in the GluA2 3D/γ2 mutant receptor (for details, see Figure S7). These findings demonstrate that TARPs are still able to associate with the 3D mutant GluA2 subunits, despite the reduced modulation of channel decay kinetics. Importantly, these findings also show that the 3D site only accounts for a subset of all properties by which TARPs regulate AMPARs.

LBD Dimer Apex and the D2 Lobes Coordinate Channel Activation Independently

Because the 3D site profoundly attenuates the prolongation of channel activation by TARPs, we examined whether functional coupling between the D2 lobe and the TARP γ2 could account for the rescue of GluA2 AAA receptors by auxiliary subunits (Figure 6). To do this, the time course of channel activation of the double-site mutant, GluA2 AAA/3D, was compared in the presence and absence of TARP γ2 (Figure 8). In the absence of TARP subunits, there was no significant difference between desensitization time constants for GluA2 AAA and GluA2 AAA/3D (τ = 0.68 ± 0.10 ms; n = 6; p = 0.56; Figures 8A and 8B). Consistent with the phenotype of GluA2 AAA, the mean peak response of GluA2 AAA/3D was also small in amplitude (29.8 ± 8.6 pA; n = 7) and greatly potentiated by CTZ (17.0 ± 2.2-fold; n = 7; Figure 8B). However, when coexpressed with the γ2 subunit, the time constant of desensitization was about 3-fold faster (τ = 2.4 ± 0.3 ms; n = 7) for GluA2 AAA/3D than GluA2 AAA (τ = 6.6 ± 0.9 ms; n = 8; p = 0.002; Figures 8C–8E). The attenuation in γ2 modulation of the AAA mutant demonstrates that the 3D site is largely responsible for rescuing the time course of channel activation. Figure 8E summarizes how the coexpression of γ2 affects desensitization rates of the AAA and/or 3D mutant GluA2 receptors. Whether LBD apex interactions are present (i.e., wild-type GluA2) or absent (i.e., GluA2 AAA), the 3D mutation reduces TARP modulation of desensitization kinetics approximately 3-fold (Figure 8E). This suggests an independence of the LBD apex and D2 lobe in regulating the gating behavior of TARP-associated AMPARs. In summary, our data support a model where different sets of structural interactions determine the time course of activation of AMPAR-auxiliary subunit complexes (Figure 8F).

DISCUSSION

This study advances our understanding of AMPARs in two fundamental ways. First, we demonstrate that an evolutionarily conserved electrostatic network within the LBD apex is critical for the activation of pore-forming AMPAR subunits, which use it to generate rapid, millisecond-scale gating at central synapses. This network can be stabilized by the occupancy of an adjacent cation pocket, sustaining channel activation by a similar mechanism to sodium binding at KARs (Dawe et al., 2013).

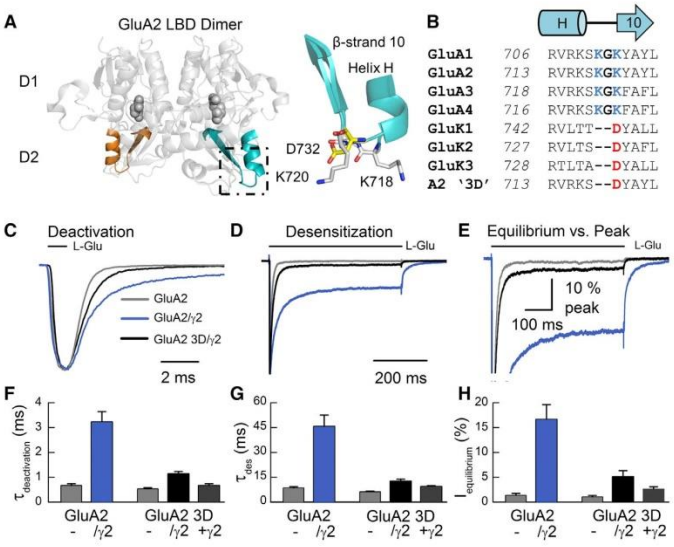

Figure 7. A Single D2 Mutation Attenuates TARP γ2 Modulation of GluA2 Current Decay

(A) View of the GluA2 LBD dimer (PDB: 1FTJ; Armstrong and Gouaux, 2000), highlighting the site of the 718–720 KGK to D (3D) mutation (in color, at left), between helix H and β strand 10 on the D2 lobe (at right). Mutated residues appear as in GluA2 (gray stick) or GluK2 (yellow stick) structures (PDB: 1FTJ or 2XXR; Nayeem et al., 2011).

(B) Sequence alignment of the 3D mutation site for rat AMPAR and KAR subunits.

(C and D) Scaled current responses of wild-type GluA2 (patch number 150317p2, gray), as well as GluA2/γ2 (patch number 150316p3, blue) and GluA2 3D/γ2 (patch number 150511p6, black) AMPAR-TARP fusion proteins to 1 ms (C) and 500 ms (D) applications of 10 mM L-Glu.

(E) Scaled equilibrium responses of wild-type GluA2 (patch number 150317p3, gray), as well as GluA2/γ2 (patch number 150316p3, blue) and GluA2 3D/γ2 (patch number 150511p6, black) AMPAR-TARP fusion proteins during a 500 ms L-Glu application.

(F–H) Mean time constants of current decay after a 1 ms L-Glu application ($\tau_{deactivation}$) (F) or in the continued presence of L-Glu (τ_{des}) (G), as well as mean equilibrium current amplitude, as a percentage of the peak response (H). Data are mean ± SEM, from the number of independent patch experiments that follows: eight (F) or nine (G and H) for GluA2, nine (F) or eleven (G and H) for GluA2/γ2, five (F–H) for GluA2 3D, eight (F–H) for GluA2 3D/γ2, and seven (F–H) for coexpressed GluA2 3D + γ2.

Although physiological cation species do not appear to regulate the GluA2 LBD apex, the near loss of channel activity after elimination of the electrostatic network indicates this region is one of the most important structural determinants of AMPAR gating. Accordingly, our observations reveal that for both KAR and AMPAR families, changes in only a few critical atomic interactions can drastically alter the time course of channel activation. Second, we show that pore-forming AMPAR subunits use different gating pathways when associated with and without auxiliary proteins. Although TARPs have been the focus of numerous studies in recent years, the structural interactions underpinning their modulation of AMPARs have remained largely unknown. Our data identify an important site at the D2 lobe of the GluA2 LBD, which mediates TARP prolongation of channel gating independently of interactions at the LBD apex. Because this motif does not affect other properties modulated by TARPs (i.e., agonist efficacy and permeation), we conclude that several discrete sites must act together to bring about the ensemble behavior of TARP-bound AMPARs.

An Evolutionarily Conserved Hotspot Governing KAR and AMPAR Activation

A key difference between KARs and other iGluRs subfamilies is that external cations are required for KAR activation, in addition to modulating their gating behavior (Bowie, 2002; Wong et al., 2006). Although AMPAR and KAR protein architecture is very similar, the ability of cations to modulate AMPARs has not been thoroughly studied. In part, this was due to the discrepancy between the KAR cation-binding pocket, which can bind monovalent cations of various sizes (Bowie, 2002; Plested et al., 2008), and the equivalent AMPAR site, where lithium binding was only recently observed (Assaf et al., 2013). Moreover, the gating kinetics of GluA1 AMPAR subunits lack modulation by cations (Bowie, 2002) and perhaps cannot bind lithium. It should be noted that a potentiation of GluA2 and GluA3 equilibrium currents by external lithium was reported in oocytes (Karkanias and Papke, 1999), and later experiments characterized an increase in native AMPAR P_{open} under similar conditions (Gebhardt and Cull-Candy, 2010). These observations are consistent with the behavior we observed in outside-out patch recordings; however, no structural mechanism was then ascribed to them.

By combining recordings of full-length GluA2 receptors with simulations of the LBD dimer, we were able to show that high experimental concentrations of external LiCl permit lithium to occupy an electronegative pocket in the apical dimer interface, thereby sustaining channel activation. Furthermore, we identified an intersubunit electrostatic bridge adjacent to the pocket that mediates lithium effects on gating. Because LBD dimer pairs appear to be intact in unliganded and preopen, but not desensitized, GluA2 structures (Dürr et al., 2014; Meyerson et al., 2014), the rupture of this bridge might be a key trigger for desensitization. In this sense, lithium acts upon GluA2 as we proposed sodium does for GluK2, serving as a gatekeeper to prevent desensitization (Dawe et al., 2013).

Auxiliary Subunits Rewire the AMPAR Gating Pathway

There is a substantial body of literature describing to what extent TARP and CNIH proteins modulate or, typically, slow AMPAR desensitization and deactivation kinetics (e.g., Priel et al., 2005; Schwenk et al., 2009). Nevertheless, it is presently

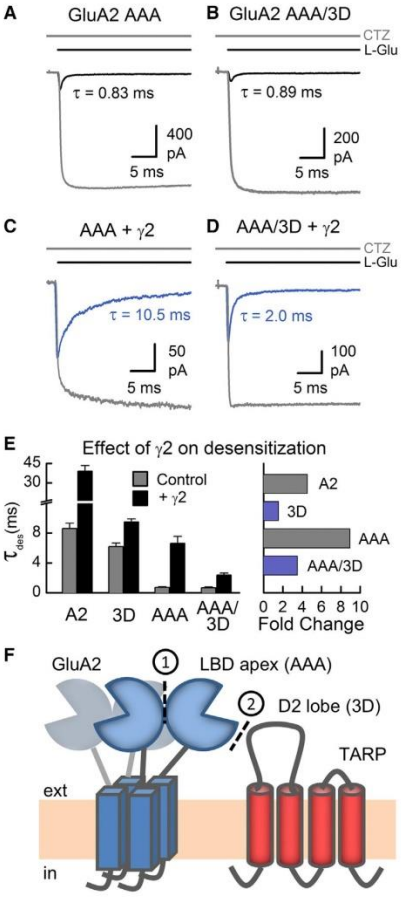

Figure 8. Intra- and Interprotein Interactions Independently Regulate GluA2 Gating

(A–D) Typical current responses of GluA2 AAA (A) (patch number 151005p12), AAA/3D (B) (patch number 151001p11), AAA + γ2 (C) (patch number 140721p3), and AAA/3D + γ2 (D) (patch number 150924p11) mutant receptors to a 250 ms application of 10 mM L-Glu, shown before (black, or blue with γ2) and during (gray) CTZ exposure. Time constants of current decay during desensitization are indicated.

(E) Mean time constants of current decay (τ_{des}, left) for several GluA2 receptors, which were expressed alone (gray bar) or coexpressed with the TARP subunit γ2 (black bar). The ratio of the time constants for each receptor (γ2: no TARP) is also shown, expressed as a fold change (right). Data are mean ± SEM, from the number of independent patch experiments that follows: nine (GluA2), ten (GluA2 + γ2), five (GluA2 3D), seven (GluA2 3D + γ2), seven (GluA2 AAA), eight (GluA2 AAA + γ2), six (GluA2 AAA/3D), and seven (GluA2 AAA/3D + γ2).

(F) Illustration of two distinct LBD regions (apex and D2 lobe) critical for regulating the time course of GluA2 activation, which were disrupted by the AAA and 3D mutations, respectively.

debated whether such effects are mediated primarily through increasing the rate of channel opening, pregating rearrangements of the agonist-binding cleft, or other kinetic transitions. Our observation that the coexpression of auxiliary subunits rescued gating deficits in the GluA2 AAA mutant receptor brings new perspective to how they modulate AMPAR behavior. The Ala mutations were predicted to weaken affinity between individual LBDs, leading dimers to more readily move apart, as is proposed to occur during the structural transition to desensitization (Meyerson et al., 2014; Sun et al., 2002). Because the binding site for CTZ has been well characterized, its rescue of GluA2 AAA could be attributed to the molecule acting as an adhesive in the LBD dimer interface, interfering with the separation of subunits (Sun et al., 2002). In contrast, TARPs and CNIHs are large transmembrane proteins and unlikely to brace the LBD dimer from within, meaning another mechanism should account for their rescue of the AAA mutant.

Cryo-EM experiments have resolved TARP and CNIH proteins situated beside the AMPAR transmembrane domain (TMD), tucked underneath the LBD (Nakagawa et al., 2005; Shanks et al., 2014). More recent assays using antibody labeling of GluA2 peptide arrays have identified several discrete sites to which TARP γ2 may bind, within both the TMD and LBD but also the more distal ATD (Cais et al., 2014). That being said, the LBD appears to be the principle extracellular site where TARPs modulate gating, since removal of the ATD still allows them to promote AMPAR trafficking and modulate decay kinetics (Cais et al., 2014). Specific sites of γ2 interaction identified at the GluA2 LBD include residues that comprise the LBD-TMD linker, segments abutting the agonist-binding cleft, and helices along the D1 dimer interface (Cais et al., 2014). The linker region has been shown to regulate P_{open} of NMDAR channels (Kazi et al., 2014) and could mediate TARP-dependent increases in AMPAR P_{open} (Cho et al., 2007; Tomita et al., 2005). Likewise, more extensive closure of the agonist-binding cleft with γ2 (MacLean et al., 2014) may underlie changes in the relative efficacy of agonists such as KA. Nevertheless, the structural basis for TARP prolongation of channel gating has remained a matter of speculation.

Our identification of a site on the lower, D2 lobe (i.e., the KGK motif) responsible for γ2 modulation of GluA2 deactivation and desensitization kinetics sheds new light on the functional interaction between TARP and AMPAR subunits. Specifically, we propose that TARP auxiliary subunits provide external stabilization at the base of the LBD dimer, interfering with the turning apart and/or separation of receptor subunits that characterizes desensitization (Meyerson et al., 2014; Dürr et al., 2014). The low, outward-facing orientation of the KGK motif is also consistent with the predicted location of TARP subunits in native AMPAR complexes (Nakagawa et al., 2005). Moreover, the continued importance of the KGK residues for γ2 coexpression to rescue gating of GluA2 AAA receptors demonstrates that interprotein interactions relayed through the basal D2 lobe operate independently of the electrostatic interactions at the LBD apex. Given that the KGK motif did not affect TARP modulation of agonist efficacy or polyamine block, it is likely that several other discrete interactions are required to achieve the full set of TARP effects. As such, auxiliary proteins add additional branches to

the intrinsic gating machinery of pore-forming AMPAR subunits, coordinating receptor activation through distinct structural pathways.

EXPERIMENTAL PROCEDURES

Molecular Biology, Electrophysiology, and Surface Expression

HEK293T cells were used to recombinantly express KAR or AMPAR subunits for outside-out patch recordings and surface-expression assays. For AMPARs, the Q/R unedited, flip variant of subunits was used, and residue numbering includes the signal peptide. Mutant receptors were generated using site-directed mutagenesis. Auxiliary subunits and AMPARs were coexpressed at a 2:1 cDNA ratio. External and internal recording solutions typically contained 150 mM XCl (X = alkali metal), 5 mM HEPES, 0.1 mM $CaCl_2$, 0.1 mM $MgCl_2$, and 2% phenol red at pH 7.4; and 115 mM NaCl, 10 mM NaF, 5 mM HEPES, 5 mM Na_4BAPTA, 0.5 mM $CaCl_2$, 1 mM $MgCl_2$, and 10 mM Na_2ATP at pH 7.4, respectively. L-Glu was typically applied at 10 mM and CTZ at 100 μM. Agonist solutions were applied using a piezo-stack-driven perfusion system, and measured solution exchange time was under 400 μs. The recording, acquisition, and analysis of electrophysiological data are detailed in Supplemental Experimental Procedures. Membrane trafficking was assessed from the fluorescence emitted by an ecliptic, pH-sensitive superfolder GFP genetically fused to the extracellular amino terminal of AMPARs, as described previously for KARs (Dawe et al., 2013). Additional details are described in Supplemental Experimental Procedures.

MD Simulations

The GluA2 flip (PDB: 2UXA; Greger et al., 2006) and K759M/T765K LBD dimers were used for constructing models for MD simulations. Proteins were solvated, ions were introduced, and mutations were imposed prior to simulation. MD simulations were performed using Gromacs 4.6 (Hess et al., 2008) with the OPLS all-atom force field (Jorgensen et al., 1996; Kaminski et al., 2001). Periodic boundary conditions were employed, while electrostatic interactions and bonds were accounted for as described previously (Dawe et al., 2013). Simulations of 100 ns were performed in the NPT ensemble at 300 K and 1 bar pressure using the Berendsen thermostat and barostat, respectively (Berendsen et al., 1984). Two to four repeats for each wild-type or mutant dimer were produced. Analyses were performed using VMD (Humphrey et al., 1996) and Gromacs (Hess et al., 2008). Additional details are described in Supplemental Experimental Procedures.

X-Ray Crystallography

The GluA2 (flip) K759M/T765K LBD construct was generated from the wild-type GluA2 LBD (provided by Ingo Greger) using the QuikChange protocol (Stratagene). Induction and expression (1 mM IPTG, 20 hr at 24°C) were followed by protoplast formation and freeze-thaw lysis. Purification of the resulting supernatant on nickel-affinity and HiTrap-Q columns was performed as described previously (Nayeem et al., 2011). Crystals were grown as described in Supplemental Experimental Procedures. Diffraction data were collected at 100 K on Diamond beamline I03 at an energy of 12,700 eV (Pilatus3 6M detector). Data processing was performed using either XDS/XSCALE (lithium form) or XDS/AIMLESS (zinc form). Molecular replacement was performed in PHASER, and refinement was performed using a combination of REFMAC5 (Murshudov et al., 1997) and PHENIX.REFINE (Adams et al., 2002). For the zinc structure, PHASER was used for SAD-MR to locate the five zinc ions, and for map generation, either map sharpening (REFMAC5) or feature-enhanced maps (PHENIX.REFINE) were used. TLS groups were identified using the TLSMD server (Painter and Merritt, 2006). In all cases, model visualization and manipulation were done using COOT (Emsley et al., 2010), and figures were generated using CCP4MG (McNicholas et al., 2011). Additional details are described in Supplemental Experimental Procedures.

Statistical Methods

Results are expressed as mean ± SEM. Statistical analyses of sample means were performed using two-tailed paired or two-sample (assuming unequal variance) t tests. $p < 0.05$ was considered to be statistically significant.

ACCESSION NUMBERS

Model coordinates and diffraction data for the GluA2 K759M/T765K structures have been deposited in the Protein Data Bank under ID codes PDB: 5FTH (zinc form) and 5FTI (lithium form).

SUPPLEMENTAL INFORMATION

Supplemental Information includes Supplemental Experimental Procedures, seven figures, three tables, and four movies and can be found with this article online at http://dx.doi.org/10.1016/j.neuron.2016.01.038.

AUTHOR CONTRIBUTIONS

Conceptualization, G.B.D., M.R.P.A., and D.B. Investigation and Analysis–Electrophysiology, G.B.D.; Investigation and Analysis–Molecular Biology, G.B.D. and M.R.P.A.; Investigation and Analysis–Surface Expression, M.R.P.A.; Investigation and Analysis–MD Simulations, M.M.; Investigation and Analysis–Crystallography, N.N. and T.G. Writing, G.B.D. and D.B. Review and Editing, all authors.

ACKNOWLEDGMENTS

This work was supported by operating grants from the Canadian Institutes of Health Research (FRN: 82804, D.B.), the Leverhulme Trust (RPG-059, P.C.B. and M.M.), and the Medical Research Council (MR/M0004331, P.C.B.). G.B.D. is supported by a Canada Graduate Scholarship (CGS-D) from the Natural Sciences and Engineering Research Council of Canada. M.M. held a postdoctoral fellowship from the Alfred Benzon Foundation. D.B. was a Canada Research Chair. We thank the Advanced Research Computing (ARC) facility, the Blue Joule facility at the Hartree Centre, the National Service for Computational Chemistry Software, the IRIDIS High Performance Computing facility, and the HECTOR and ARCHER UK National Supercomputing Services for computer time through the EPSRC-funded HECBioSim consortium (www.hecbiosim.ac.uk), as well as the Diamond Synchrotron for beam time (provided through the Manchester/Liverpool BBSRC BAG). We also thank Jennifer Flemming for collecting the P2 21 21 dataset at Diamond and Dr. Gergely Lukacs for use of his TIRF microscope.

Received: July 30, 2015
Revised: December 1, 2015
Accepted: January 13, 2016
Published: February 25, 2016

REFERENCES

Adams, P.D., Grosse-Kunstleve, R.W., Hung, L.W., Ioerger, T.R., McCoy, A.J., Moriarty, N.W., Read, R.J., Sacchettini, J.C., Sauter, N.K., and Terwilliger, T.C. (2002). PHENIX: building new software for automated crystallographic structure determination. Acta Crystallogr. D Biol. Crystallogr. *58*, 1948–1954.

Armstrong, N., and Gouaux, E. (2000). Mechanisms for activation and antagonism of an AMPA-sensitive glutamate receptor: crystal structures of the GluR2 ligand binding core. Neuron *28*, 165–181.

Assaf, Z., Larsen, A.P., Venskutonytė, R., Han, L., Abrahamsen, B., Nielsen, B., Gajhede, M., Kastrup, J.S., Jensen, A.A., Pickering, D.S., et al. (2013). Chemoenzymatic synthesis of new 2,4-syn-functionalized (S)-glutamate analogues and structure-activity relationship studies at ionotropic glutamate receptors and excitatory amino acid transporters. J. Med. Chem. *56*, 1614–1628.

Berendsen, H.J.C., Postma, J.P.M., Vangunsteren, W.F., Dinola, A., and Haak, J.R. (1984). Molecular-dynamics with coupling to an external bath. J. Chem. Phys. *81*, 3684–3690.

Bowie, D. (2002). External anions and cations distinguish between AMPA and kainate receptor gating mechanisms. J. Physiol. *539*, 725–733.

Bowie, D. (2010). Ion-dependent gating of kainate receptors. J. Physiol. *588*, 67–81.

Cais, O., Herguedas, B., Krol, K., Cull-Candy, S.G., Farrant, M., and Greger, I.H. (2014). Mapping the interaction sites between AMPA receptors and TARPs reveals a role for the receptor N-terminal domain in channel gating. Cell Rep. *9*, 728–740.

Catterall, W.A., Hulme, J.T., Jiang, X., and Few, W.P. (2006). Regulation of sodium and calcium channels by signaling complexes. J. Recept. Signal Transduct. Res. *26*, 577–598.

Chen, L., El-Husseini, A., Tomita, S., Bredt, D.S., and Nicoll, R.A. (2003). Stargazin differentially controls the trafficking of alpha-amino-3-hydroxyl-5-methyl-4-isoxazolepropionate and kainate receptors. Mol. Pharmacol. *64*, 703–706.

Cho, C.H., St-Gelais, F., Zhang, W., Tomita, S., and Howe, J.R. (2007). Two families of TARP isoforms that have distinct effects on the kinetic properties of AMPA receptors and synaptic currents. Neuron *55*, 890–904.

Constals, A., Penn, A.C., Compans, B., Toulmé, E., Phillipat, A., Marais, S., Retailleau, N., Hafner, A.S., Coussen, F., Hosy, E., and Choquet, D. (2015). Glutamate-induced AMPA receptor desensitization increases their mobility and modulates short-term plasticity through unbinding from Stargazin. Neuron *85*, 787–803.

Dawe, G.B., Musgaard, M., Andrews, E.D., Daniels, B.A., Aurousseau, M.R., Biggin, P.C., and Bowie, D. (2013). Defining the structural relationship between kainate-receptor deactivation and desensitization. Nat. Struct. Mol. Biol. *20*, 1054–1061.

Dawe, G.B., Aurousseau, M.R., Daniels, B.A., and Bowie, D. (2015). Retour aux sources: defining the structural basis of glutamate receptor activation. J. Physiol. *593*, 97–110.

Dingledine, R., Borges, K., Bowie, D., and Traynelis, S.F. (1999). The glutamate receptor ion channels. Pharmacol. Rev. *51*, 7–61.

Dürr, K.L., Chen, L., Stein, R.A., De Zorzi, R., Folea, I.M., Walz, T., Mchaourab, H.S., and Gouaux, E. (2014). Structure and dynamics of AMPA receptor GluA2 in resting, pre-open, and desensitized states. Cell *158*, 778–792.

Emsley, P., Lohkamp, B., Scott, W.G., and Cowtan, K. (2010). Features and development of Coot. Acta Crystallogr. D Biol. Crystallogr. *66*, 486–501.

Gan, Q., Salussolia, C.L., and Wollmuth, L.P. (2015). Assembly of AMPA receptors: mechanisms and regulation. J. Physiol. *593*, 39–48.

Gebhardt, C., and Cull-Candy, S.G. (2010). Lithium acts as a potentiator of AMPAR currents in hippocampal CA1 cells by selectively increasing channel open probability. J. Physiol. *588*, 3933–3941.

Green, T., and Nayeem, N. (2015). The multifaceted subunit interfaces of ionotropic glutamate receptors. J. Physiol. *593*, 73–81.

Greger, I.H., Akamine, P., Khatri, L., and Ziff, E.B. (2006). Developmentally regulated, combinatorial RNA processing modulates AMPA receptor biogenesis. Neuron *51*, 85–97.

Greger, I.H., Ziff, E.B., and Penn, A.C. (2007). Molecular determinants of AMPA receptor subunit assembly. Trends Neurosci. *30*, 407–416.

Haering, S.C., Tapken, D., Pahl, S., and Hollmann, M. (2014). Auxiliary subunits: shepherding AMPA receptors to the plasma membrane. Membranes (Basel) *4*, 469–490.

Hastie, P., Ulbrich, M.H., Wang, H.L., Arant, R.J., Lau, A.G., Zhang, Z., Isacoff, E.Y., and Chen, L. (2013). AMPA receptor/TARP stoichiometry visualized by single-molecule subunit counting. Proc. Natl. Acad. Sci. USA *110*, 5163–5168.

Herring, B.E., Shi, Y., Suh, Y.H., Zheng, C.Y., Blankenship, S.M., Roche, K.W., and Nicoll, R.A. (2013). Cornichon proteins determine the subunit composition of synaptic AMPA receptors. Neuron *77*, 1083–1096.

Hess, B., Kutzner, C., van der Spoel, D., and Lindahl, E. (2008). GROMACS 4: algorithms for highly efficient, load-balanced, and scalable molecular simulation. J. Chem. Theory Comput. *4*, 435–447.

Horning, M.S., and Mayer, M.L. (2004). Regulation of AMPA receptor gating by ligand binding core dimers. Neuron *41*, 379–388.

Howe, J.R. (2015). Modulation of non-NMDA receptor gating by auxiliary subunits. J. Physiol. *593*, 61–72.

Huettner, J.E. (2015). Glutamate receptor pores. J. Physiol. *593*, 49–59.

Humphrey, W., Dalke, A., and Schulten, K. (1996). VMD: visual molecular dynamics. J. Mol. Graph. *14*, 33–38.

Jackson, A.C., and Nicoll, R.A. (2011). The expanding social network of ionotropic glutamate receptors: TARPs and other transmembrane auxiliary subunits. Neuron *70*, 178–199.

Jorgensen, W.L., Maxwell, D.S., and Tirado-Rives, J. (1996). Development and testing of the OPLS all-atom force field on conformational energetics and properties of organic liquids. J. Am. Chem. Soc. *118*, 11225–11236.

Kalashnikova, E., Lorca, R.A., Kaur, I., Barisone, G.A., Li, B., Ishimaru, T., Trimmer, J.S., Mohapatra, D.P., and Díaz, E. (2010). SynDIG1: an activity-regulated, AMPA- receptor-interacting transmembrane protein that regulates excitatory synapse development. Neuron *65*, 80–93.

Kaminski, G.A., Friesner, R.A., Tirado-Rives, J., and Jorgensen, W.L. (2001). Evaluation and reparametrization of the OPLS-AA force field for proteins via comparison with accurate quantum chemical calculations on peptides. J. Phys. Chem. B *105*, 6474–6487.

Karkanias, N.B., and Papke, R.L. (1999). Lithium modulates desensitization of the glutamate receptor subtype gluR3 in Xenopus oocytes. Neurosci. Lett. *277*, 153–156.

Kazi, R., Dai, J., Sweeney, C., Zhou, H.X., and Wollmuth, L.P. (2014). Mechanical coupling maintains the fidelity of NMDA receptor-mediated currents. Nat. Neurosci. *17*, 914–922.

MacLean, D.M., Ramaswamy, S.S., Du, M., Howe, J.R., and Jayaraman, V. (2014). Stargazin promotes closure of the AMPA receptor ligand-binding domain. J. Gen. Physiol. *144*, 503–512.

McNicholas, S., Potterton, E., Wilson, K.S., and Noble, M.E. (2011). Presenting your structures: the CCP4mg molecular-graphics software. Acta Crystallogr. D Biol. Crystallogr. *67*, 386–394.

Meyerson, J.R., Kumar, J., Chittori, S., Rao, P., Pierson, J., Bartesaghi, A., Mayer, M.L., and Subramaniam, S. (2014). Structural mechanism of glutamate receptor activation and desensitization. Nature *514*, 328–334.

Morimoto-Tomita, M., Zhang, W., Straub, C., Cho, C.H., Kim, K.S., Howe, J.R., and Tomita, S. (2009). Autoinactivation of neuronal AMPA receptors via glutamate-regulated TARP interaction. Neuron *61*, 101–112.

Murshudov, G.N., Vagin, A.A., and Dodson, E.J. (1997). Refinement of macromolecular structures by the maximum-likelihood method. Acta Crystallogr. D Biol. Crystallogr. *53*, 240–255.

Nakagawa, T., Cheng, Y., Ramm, E., Sheng, M., and Walz, T. (2005). Structure and different conformational states of native AMPA receptor complexes. Nature *433*, 545–549.

Nayeem, N., Mayans, O., and Green, T. (2011). Conformational flexibility of the ligand-binding domain dimer in kainate receptor gating and desensitization. J. Neurosci. *31*, 2916–2924.

Painter, J., and Merritt, E.A. (2006). Optimal description of a protein structure in terms of multiple groups undergoing TLS motion. Acta Crystallogr. D Biol. Crystallogr. *62*, 439–450.

Plested, A.J., Vijayan, R., Biggin, P.C., and Mayer, M.L. (2008). Molecular basis of kainate receptor modulation by sodium. Neuron *58*, 720–735.

Priel, A., Kolleker, A., Ayalon, G., Gillor, M., Osten, P., and Stern-Bach, Y. (2005). Stargazin reduces desensitization and slows deactivation of the AMPA-type glutamate receptors. J. Neurosci. *25*, 2682–2686.

Schwenk, J., Harmel, N., Zolles, G., Bildl, W., Kulik, A., Heimrich, B., Chisaka, O., Jonas, P., Schulte, U., Fakler, B., and Klöcker, N. (2009). Functional proteomics identify cornichon proteins as auxiliary subunits of AMPA receptors. Science *323*, 1313–1319.

Severus, W.E., Kleindienst, N., Seemüller, F., Frangou, S., Möller, H.J., and Greil, W. (2008). What is the optimal serum lithium level in the long-term treatment of bipolar disorder—a review? Bipolar Disord. *10*, 231–237.

Shanks, N.F., Cais, O., Maruo, T., Savas, J.N., Zaika, E.I., Azumaya, C.M., Yates, J.R., 3rd, Greger, I., and Nakagawa, T. (2014). Molecular dissection of the interaction between the AMPA receptor and cornichon homolog-3. J. Neurosci. *34*, 12104–12120.

Sobolevsky, A.I., Rosconi, M.P., and Gouaux, E. (2009). X-ray structure, symmetry and mechanism of an AMPA-subtype glutamate receptor. Nature *462*, 745–756.

Soto, D., Coombs, I.D., Kelly, L., Farrant, M., and Cull-Candy, S.G. (2007). Stargazin attenuates intracellular polyamine block of calcium-permeable AMPA receptors. Nat. Neurosci. *10*, 1260–1267.

Sun, Y., Olson, R., Horning, M., Armstrong, N., Mayer, M., and Gouaux, E. (2002). Mechanism of glutamate receptor desensitization. Nature *417*, 245–253.

Tomita, S., Chen, L., Kawasaki, Y., Petralia, R.S., Wenthold, R.J., Nicoll, R.A., and Bredt, D.S. (2003). Functional studies and distribution define a family of transmembrane AMPA receptor regulatory proteins. J. Cell Biol. *161*, 805–816.

Tomita, S., Adesnik, H., Sekiguchi, M., Zhang, W., Wada, K., Howe, J.R., Nicoll, R.A., and Bredt, D.S. (2005). Stargazin modulates AMPA receptor gating and trafficking by distinct domains. Nature *435*, 1052–1058.

Trimmer, J.S. (2015). Subcellular localization of K+ channels in mammalian brain neurons: remarkable precision in the midst of extraordinary complexity. Neuron *85*, 238–256.

Turetsky, D., Garringer, E., and Patneau, D.K. (2005). Stargazin modulates native AMPA receptor functional properties by two distinct mechanisms. J. Neurosci. *25*, 7438–7448.

von Engelhardt, J., Mack, V., Sprengel, R., Kavenstock, N., Li, K.W., Stern-Bach, Y., Smit, A.B., Seeburg, P.H., and Monyer, H. (2010). CKAMP44: a brain-specific protein attenuating short-term synaptic plasticity in the dentate gyrus. Science *327*, 1518–1522.

Wong, A.Y., Fay, A.M., and Bowie, D. (2006). External ions are coactivators of kainate receptors. J. Neurosci. *26*, 5750–5755.

Zhang, W., Devi, S.P., Tomita, S., and Howe, J.R. (2014). Auxiliary proteins promote modal gating of AMPA- and kainate-type glutamate receptors. Eur. J. Neurosci. *39*, 1138–1147.

APPENDIX IV:

A personal perspective on MD simulations

FOREWORD TO APPENDIX FOUR

A common line of questioning I have faced at advisory committee meetings, as well as other presentations, concerns the usefulness of MD simulations. Typically, the questioner will ask whether such simulations are worthwhile, particularly in cases where they are accompanied, or superseded by "real" electrophysiological data. Even the use of MD data as a predictive tool has been challenged; on the basis that recombinant electrophysiology can be performed just as rapidly under the right circumstances. Therefore, in light of these inquiries, I have added a brief appendix to my thesis, outlining a personal perspective on MD simulations. Without having a background in computational biochemistry myself, I can appreciate the skepticism of experimental scientists toward simulations. That being said, I hope my experience demonstrates that the synergy of theoretical and experimental data strengthens new ideas beyond what either approach is capable of alone.

Appendix IV, Title:

A personal perspective on MD simulations

From the introduction of this thesis, it is evident that the study of iGluR complexes shifted focus from function to structure as different research techniques became available or were optimized (i.e. X-ray crystallography). Along these lines, MD methodologies have become increasingly influential over the past decade as an expanding array of atomic-resolution protein structures can now serve as templates for dynamic simulations. At the same time, it might not be clear to those outside the biophysical realm why such efforts are needed, since experimental techniques like electrophysiology and FRET continue to build upon the current structural dataset to provide greater insight into the mechanism of iGluR gating. In the paragraphs below, I have outlined four cases where MD simulations can provide some additional value when examining LGICs, and connect each case with an example from my own research.

1-Predicting the binding of allosteric molecules

Though patch-clamp recordings offer great resolution of ion flux through the channel pore, they cannot directly measure the binding of allosteric ions. This poses a problem, in the sense that I have often tried to assign allosteric ion binding or unbinding as an explanation for some electrophysiological phenomenon. For example, I have proposed that sodium binding at the GluK2 LBD is necessary for channels to avoid becoming desensitized in the presence of glutamate. Although patch-clamp experiments in different external sodium concentrations have resulted in an estimate for the EC_{50} of the peak response amplitude (110 mM Na^+, see Plested et al., 2008), such values do not necessarily reflect ion affinity, which may vary between different kinetic states of the receptor. In contrast, MD simulations can be used to "predict" the tendency of an allosteric molecule to interact with a protein surface over time, albeit on a much shorter time scale than channel gating processes -though advances in computing power will likely see

that deficit diminish in the near future, as microsecond-scale simulations are becoming more readily attainable (reviewed in Johnston & Filizola, 2011).

1a-Determining the structural consequences of mutations for which no specific structural data are available

Throughout Chapter 1 of this thesis, several MD simulations reported the relative occupancy of the GluK2 sodium binding pocket. Amongst these were trials that followed the introduction of mutations (E524G and L783C) into the simulation environment of the wildtype LBD dimer. While it could be argued that rapid sodium unbinding from E524G was an obvious outcome determined by the electrostatic nature of the cation pocket, the similar behaviour of the nonfunctional L783C receptor was not intuitive based on its position alone. As a result, the observation with the latter mutant was used to account for the sodium-unbound, open interface in the crystal structure of Y521C/L783C. On the whole, these findings suggest that MD simulations can provide plausible atomic-level explanations for the functional phenotype imparted by point mutations for which experimental structural data are lacking.

Whether differences observed during MD simulations over tens or hundreds of nanoseconds can be extrapolated to variability in gating kinetics is less clear. Though I have proposed that the latency of sodium unbinding from activated receptors reflects the onset of desensitization (Dawe et al., 2013, results chapter 1), small current responses were occasionally observed from GluK2 E524G receptors, which would be inconsistent with MD data depicting the ion unbind within 10 ns. In other words, channel opening should never have been detected if sodium unbound that quickly and necessitated desensitization. Likewise, sodium failed to remain bound throughout longer 500 ns simulations of wildtype GluK2 performed recently (Musgaard & Biggin, 2016), though of course it is a perfectly functional receptor when applying glutamate

over milliseconds. Assuming these MD data are not in error by many orders of magnitude, the instability of sodium binding would actually be consistent with the low apparent affinity estimated using electrophysiological methods. As such, a more nuanced explanation for ion regulation of GluK2 KAR gating than proposed in Chapter 1 could be as follows: sodium may very rapidly bind and unbind from the resting-state and activated LBD apex, but the conformational changes leading to desensitization occur when the ion is absent longer than some critical period.

2-Developing structural mechanisms to account for functional data

Atomic resolution crystal structures provide great snapshots to compare proteins in the presence or absence of different agonists, antagonists, and modulatory molecules. From these structures, one can speculate regarding the conformational changes that occur between different functional states. For example, the transition of intact AMPARs from a "pre-activated" to desensitized arrangement appears to involve profound rotation of certain subunits in the LBD layer (Durr et al., 2014). Unfortunately, structures of the isolated LBD tend to crystallize in the same dimeric arrangement (Pohlsgaard et al., 2011), largely independent of the functional properties expected to be conferred on intact receptors. For example, the prototypical glutamate-bound GluA2 LBD dimer (Armstrong & Gouaux, 2000) appears to align almost identically with the glutamate and lithium-bound dimer (Assaf et al., 2013). Based solely on a comparison of the two structures, it would therefore be quite difficult to develop a mechanism accounting for lithium effects on desensitization.

In Chapter 2 of this thesis, MD simulations were useful in demonstrating a relationship between bound lithium ions and a closer apical LBD interface. These results had the benefit of

being obtained from sampling over many time points, and not just two individual snapshots. In addition, the simulations relied on a single structural template to compare moments when lithium was bound versus unbound, reducing the uncertainty introduced by comparing structures obtained in different conditions and perhaps prone to different crystal packing.

Considered on its own, the effect of the K514M/N768T mutation to eliminate lithium modulation is also supportive of a mechanism whereby bound cations hold together the LBD dimer interface. However, the electrophysiological data merely point to some involvement of those residues, and cannot be used as direct evidence for their structural contribution. Because of this shortcoming, MD simulations served to bridge the gap between structural and functional data to explain the effects of allosteric lithium at GluA2 receptors.

3- Assessing whether a protein interaction is plausible in the context of atomic-level physics

A recurring theme throughout the first two chapters of my thesis was the occupancy of a conserved electronegative pocket in GluK2 KARs and GluA2 AMPARs. In some cases, previously published crystal structures lent support to the idea of occupancy by either cations or the amino groups from lysine residues tethering across the dimer interface (Plested et al., 2008; Nayeem et al., 2011; Assaf et al., 2013). However, ion binding in crystals has the potential to be artifactual in nature, owing to high solvent concentrations in the crystallization buffer (Green & Nayeem, 2015). With this in mind, the occupancy of ion binding sites in a crystal may not reflect that of physiological ion concentrations, and could even lead to the incorrect assignment of a binding site that simply does not exist. Moreover, the ionic environment can also affect how amino acids behave, as evidenced by Lys759 pointing away from the GluA2 cation pocket in the lithium-bound structure, instead of into the pocket.

To ensure that static structures do not give a biased representation of the electrostatic interactions along protein surfaces and interfaces, MD simulations offer the chance to test how such interactions hold up in typical aqueous solutions. Indeed, MD data suggested that lithium may bind poorly at the wildtype GluA2 LBD dimer interface, potentially explaining why the cation induces slower desensitization, rather than eliminating desensitization (as observed for the more consistently lithium-bound K759M mutant). If one assumed from the original crystal structure that (at 150 mM) lithium was always bound to wildtype GluA2 receptors, there would not be an obvious reason to expect the K759M mutation to enhance functional ion modulation.

In a similar vein to the example above, MD simulations also give the crystal structure a chance to "relax" over the simulation time. This becomes important if crystal packing leads to abnormal or energetically unfavourable arrangements between subunits. Although the GluA2 K759M/T765K crystal structure possessed a cross-dimer lysine tether nearly identical to that of GluK2 D776K (Nayeem et al., 2011), the former mutation marginally slowed desensitization, while the latter abolished it completely. If the AMPAR tether actually remained in place during channel gating, how could desensitization proceed, assuming that the LBD dimer interface must rupture at some point to initiate the process? As it turned out, Lys765 unhooked from the cation pocket during MD simulations of the K759M/T765K mutant receptor, suggesting the cross-dimer interaction was not that stable, despite being crystallized.

Whether analyzing lithium or Lys765, it is important to note that representations of binding site occupancy derived from MD simulations may not be indicative of what actually happens in intact proteins. Nevertheless, simulations in these instances can provide a sort of insurance that the structural interactions (or lack thereof) being described are consistent with the physical forces expected to occur in the atomic-level protein environment. This insurance is

important when interpreting electrophysiological experiments, since the dynamic structural processes that occur during channel gating are not necessarily revealed or capable of being hypothesized from static protein structures.

4-Bringing clarity to an idea

The final rationale for the incorporation of MD simulations into primarily experimentally-driven manuscripts stems from the use of visual information to communicate complex ideas. Electrophysiological data are inherently abstract, often comprised of a series of lines (current traces) meant to relay the function of ion channel proteins. It can be even more difficult to navigate this type of data when they are used to make inferences about protein structure. Here, MD simulations can augment electrophysiology to provide a visual framework for thinking about the structure/function relations of proteins. I have often been aided during presentations by showing video representations of MD runs to set the scene for upcoming slides of electrophysiological experiments. For instance, movies capturing infrequent lithium binding at the wildtype GluA2 LBD, then persistent binding at the K759M LBD, highlight that some key structural difference exists between the two receptors, preparing the audience to expect additional variability in functional behaviour afterward. Using this type of approach can reduce lengthy, after-the-fact conjecture, regarding the basis of an electrophysiological phenotype. Consequently, if a wider audience is able to appreciate a new finding, then the fusion of multiple techniques can been thought of as aiding the dissemination of science.